

Development of Lectin
directed Theranostics against
Pseudomonas aeruginosa

Dissertation

Zur Erlangung des Grades der Doktorin der Naturwissenschaften der
Naturwissenschaftlich-Technischen Fakultät der Universität des Saarlandes

von

Mgr. Eva Zahorska, MSc

Saarbrücken

2021

Tag des Kolloquiums: 08. December 2021

Dekan: Prof. Dr. Jörn Eric Walter

Berichterstatter: Prof. Dr. Alexander Titz
Prof. Dr. Anna K. H. Hirsch

Akad. Mitarbeiter: PD Dr. Martin Frotscher

Vorsitz: Prof. Dr. Claus-Michael Lehr

Die vorliegende Arbeit wurde von April 2017 bis August 2021 unter Anleitung von Herrn Prof. Dr. Alexander Titz in der Fachrichtung Pharmazie der Naturwissenschaftlich-Technischen Fakultät der Universität des Saarlandes sowie am Helmholtz-Institut für Pharmazeutische Forschung Saarland (HIPS) in der Arbeitsgruppe Chemische Biologie der Kohlenhydrate angefertigt.

Acknowledgments

I am very grateful to Prof. Dr. Alexander Titz for giving me the possibility to work in his research group leading to this thesis. Thank you, Alex, for your understanding, guidance and support over the years!

I would like to thank Prof. Dr. Anna Hirsch for being my second supervisor, her kindness and support. Furthermore, I would like to express gratitude to the last member of my PhD committee - Dr. Jennifer Herrmann.

I would like to acknowledge all collaborators for their input – it was an honor to work with you.

A special thank you goes to CBCH and DDOP group members for amazing working atmosphere and cooperation. I am extremely lucky that I did not only had good colleagues during PhD, but at the same time many became close friends – like a second family. Friends who I could always rely for both professional and personal aid. Namely, I would like to thank Ghamdan who was always there for me – was it for weekly grocery shopping or introducing me to FP assay. I am grateful to Dirk for unlimited technical aid and for keeping the chemistry lab in such a good but still fun shape. Furthermore, there were many unforgettable evenings with board games with Eike, Sandra, Joscha and many others. Thanks!

I would like to mention Tijmen, Tessy, Haocheng, Auore and Bianca with whom I had a great pleasure to share a flat in Saarbrücken.

Last but not least, I would like to thank my family for their continuous support.

Table of Contents

Acknowledgments.....	V
Summary	VIII
Zusammenfassung.....	IX
Publications included in the thesis.....	X
Contributions report.....	XII
Abbreviations.....	XIV
1. Introduction	1
1.1 <i>Pseudomonas aeruginosa</i> and its lectins LecA and LecB	1
1.1.1 <i>Pseudomonas aeruginosa</i>	1
1.1.2 LecA and LecB.....	2
1.2 Lectin antagonists in infection, immunity, and inflammation	5
1.3 Design of multivalent ligands	23
2. Aim of the thesis.....	26
3. Results.....	28
3.1 Development of LecA and LecB targeting imaging probes for <i>Pseudomonas aeruginosa</i> biofilms.....	28
3.2 A rapid synthesis of low-nanomolar divalent LecA inhibitors in four linear steps from D-galactose pentaacetate.....	44
3.3 Isosteric substitution of acylhydrazones yields highly potent divalent LecA inhibitors with excellent solubility and metabolic stability.....	49
3.4 Divalent fluorescent LecA ligands.....	60
4. Conclusion and Outlook.....	69
5. References	74
6. Appendix.....	82
6.1 Supplementary information for chapter 3.1	83
6.2 Supplementary information for chapter 3.2.....	161
6.3 Supplementary information for chapter 3.3.....	203

6.4	Supplementary information for chapter 3.4.....	268
6.5	Directing Drugs to Bugs: Antibiotic-Carbohydrate Conjugates Targeting Biofilm-Associated Lectins of <i>Pseudomonas aeruginosa</i>	291
6.6	Curriculum vitae.....	310

The references for chapters 1.2, 3.2, 6.2 and 6.5 are listed at the end of each chapter.

Summary

The gram-negative bacterium *Pseudomonas aeruginosa* is one of the major causes of hospital-acquired infections and a leading cause of death in cystic fibrosis patients. Rapid emergence of multidrug resistant strains calls for urgent development of novel treatment options. In this work, *P. aeruginosa* carbohydrate binding proteins LecA and LecB were explored as extracellular targets for lectin-directed theranostics. LecA and LecB ligands were synthetically modified to allow conjugation to imaging moieties in order to enable the detection of an infection site. Fluorescein-carbohydrate conjugates showed good affinities to LecA and LecB and were used to stain *P. aeruginosa* biofilm aggregates *in vitro*. Furthermore, rapidly accessible divalent LecA ligands were designed and synthesised and low nanomolar affinities were achieved. Optimization of these divalent ligands yielded highly potent LecA inhibitors with excellent solubility and good ADME properties *in vitro*. Finally, this design of divalent LecA inhibitors allowed the development of highly potent LecA-targeting imaging probes.

Zusammenfassung

Das Gram-negative Bakterium *Pseudomonas aeruginosa* ist mit hauptverantwortlich für Krankenhausinfektionen und eine der Haupttodesursachen für Patienten mit zystischer Fibrose. Das vermehrte Aufkommen multiresistenter Keime fordert dringend die Erforschung neuartiger Therapiestrategien. In dieser Arbeit wurden zwei Kohlenhydrat-bindende Proteine von *P. aeruginosa*, LecA und LecB, als extrazelluläre Zielstrukturen für neuartige Lektin-bindende Theranostika erforscht. Liganden von LecA und LecB wurden synthetisch so modifiziert, dass eine Konjugation mit Fluoreszenzfarbstoffen die Erkennung von Infektionsherden ermöglichen soll. Diese Fluorescein-Kohlenhydrat-Konjugate zeigten gute Affinitäten gegenüber LecA und LecB und wurden verwendet um Biofilm-Aggregate von *P. aeruginosa in vitro* zu färben. Weiterhin konnten schnell zugängliche divalente LecA-Liganden mit niedrig nanomolaren Affinitäten designt und synthetisiert werden. Weitere Optimierungen dieser Verbindungen ergaben hochpotente LecA-Inhibitoren mit exzellenter Löslichkeit und guten ADME-Parametern *in vitro*. Schließlich ermöglichten diese divalenten LecA-Inhibitoren die Entwicklung hochpotenter LecA-spezifischer Kontrastmittel.

Publications included in the thesis

Lectin antagonists in infection, immunity, and inflammation

Joscha Meiers, Eike Siebs, Eva Zahorska and Alexander Titz

Current Opinion in Chemical Biology, 2019, **53**, 51–67.

DOI: 10.1016/j.cbpa.2019.07.005

Development of LecA and LecB targeting imaging probes for *Pseudomonas aeruginosa* biofilms

Eva Zahorska, Varvara Verkhova, Dirk Hauck, Stefanie Wagner and Alexander Titz

Manuscript in preparation

A rapid synthesis of low-nanomolar divalent LecA inhibitors in four linear steps from D-galactose pentaacetate

Eva Zahorska, Sakonwan Kuhaudomlarp, Saverio Minervini, Sultaan Yousaf, Martin Lepsik, Thorsten Kinsinger, Anna K. H. Hirsch, Anne Imberty and Alexander Titz

Chemical Communications, 2020, **56**, 8822–8825.

DOI: 10.1039/d0cc03490h

Isosteric substitution of acylhydrazones yields highly potent divalent LecA inhibitors with excellent solubility and metabolic stability

Eva Zahorska, Sakonwan Kuhaudomlarp, Joscha Meiers, Dirk Hauck, Emilie Gillon, Katharina Rox, Anne Imberty and Alexander Titz

Manuscript in preparation

Divalent fluorescent LecA ligands

Eva Zahorska, Saverio Minervini, Sakonwan Kuhaudomlarp, Emilie Gillon, Anne Imberty and Alexander Titz

Further work

Directing Drugs to Bugs: Antibiotic-Carbohydrate Conjugates Targeting Biofilm-Associated Lectins of *Pseudomonas aeruginosa*

Joscha Meiers, Eva Zahorska, Teresa Röhrig, Dirk Hauck, Stefanie Wagner and Alexander Titz
Journal of Medicinal Chemistry, 2020, **63**, 11707–11724.

DOI: 10.1021/acs.jmedchem.0c00856

Bivalent LecA inhibitors targeting biofilm formation of *Pseudomonas aeruginosa*

Eva Zahorska, Sakonwan Kuhadomlarp, Saverio Minervini, Anne Imberty and Alexander Titz
European patent application EP19306432.6

Contributions report

Lectin antagonists in infection, immunity, and inflammation

Joscha Meiers, Eike Siebs, [Eva Zahorska](#) and Alexander Titz

Current Opinion in Chemical Biology, 2019, **53**, 51–67.

DOI: 10.1016/j.cbpa.2019.07.005

All authors contributed equally and wrote parts of the review.

Development of LecA and LecB targeting imaging probes for *Pseudomonas aeruginosa* biofilms

[Eva Zahorska](#), Varvara Verkhova, Dirk Hauck, Stefanie Wagner and Alexander Titz

Manuscript in preparation

EZ designed and synthesized imaging probes and their precursors. DH synthesized compound **23** and **24**. EZ performed competitive and direct binding assays based on fluorescence polarization. VV and SW provided mCherry expressing *P. aeruginosa* strains (PAO1 w.t. pMP7605, PAO1 Δ lecA pMP7605 and PAO1 Δ lecB pMP7605). EZ performed biofilm staining experiments with assistance of SW. AT conceived the study. EZ and AT wrote the manuscript with input from all co-authors.

A rapid synthesis of low-nanomolar divalent LecA inhibitors in four linear steps from D-galactose pentaacetate

[Eva Zahorska](#), Sakonwan Kuhaudomlarp, Saverio Minervini, Sultaan Yousaf, Martin Lepsik, Thorsten Kinsinger, Anna K. H. Hirsch, Anne Imberty and Alexander Titz

Chemical Communications, 2020, **56**, 8822–8825.

DOI: 10.1039/d0cc03490h

LecA ligands were designed by EZ and synthesised together with SM (Master thesis) and SY (internship). TK synthesised building blocks **1m** and **1p** for DCC. DCC was performed by EZ with conceptual advice from AH. EZ and SM performed competitive LecA binding assay and ITC measurements. SK designed, performed and analysed SPR experiments with conceptual advice from AI. ML performed and analysed molecular dynamics simulations. AT conceived the study. EZ and AT wrote the paper with input from all co-authors.

Isosteric substitution of acylhydrazones yields highly potent divalent LecA inhibitors with excellent solubility and metabolic stability

Eva Zahorska, Sakonwan Kuhaudomlarp, Joscha Meiers, Dirk Hauck, Emilie Gillon, Katharina Rox, Anne Imberty and Alexander Titz

Manuscript in preparation

EZ designed and synthesised LecA ligands. DH synthesised bis-aniline building blocks **C–F** and monovalent ligands **G2** and **K2**. EZ performed competitive LecA binding assay and ITC measurements. EZ and JM performed solubility determinations. KR obtained and analysed metabolic stability data. SK and EG performed and analysed SPR experiments with conceptual advice from AI. EZ and AT conceived the study. EZ and AT wrote the manuscript with input from all co-authors.

Divalent fluorescent LecA ligands

Eva Zahorska, Saverio Minervini, Sakonwan Kuhaudomlarp, Emilie Gillon, Anne Imberty and Alexander Titz

EZ and SM (Master thesis) designed and synthesised divalent fluorescent ligand **9**. EZ designed and synthesised fluorescent ligand **15**. SK and EG performed and analysed SPR experiments with conceptual advice from AI. EZ and AT conceived the study. EZ and AT wrote this chapter with input from all co-authors.

Abbreviations

ΔG	Change in Gibbs free energy
3WJ	Three-way junction
AMR	Antimicrobial resistance
BSA	Bovine serum albumin
BODIPY	4,4-Difluoro-1,3,5,7,8-Pentamethyl-4-Bora-3a,4a-Diaza-s-Indacene
BDP-FL-Azide	7-[3-[(3-Azidopropyl)amino]-3-oxopropyl]-5,5-difluoro-1,3-dimethyl-5H-dipyrrolo[1,2-c:2',1'-f] [1,3,2]diazaborinin-4-ium-5-uide
CD	Crohn's disease
CF	Cystic fibrosis
CHES	N-Cyclohexyl-2-aminoethanesulfonic acid
CL_{MIC} , CL_{int}	Microsomal clearance, intrinsic microsomal clearance
COSY	Homonuclear correlation spectroscopy
CTB	Cholera toxin B-subunit
CuAAC	Copper-catalyzed alkyne-azide cycloaddition
DAMP/PAMP	Damage-associated or pathogen-associated molecular patterns
DCC	Dynamic combinatorial chemistry
DCL	Dynamic combinatorial library
DCM	Dichloromethane
DEPT	Distortionless enhancement by polarization transfer
DIPEA	N-Ethyldiisopropylamine, Hünigs Base
DMF	Dimethylformamide
DMSO	Dimethylsulfoxide
DNA	Deoxyribonucleic acid
DSMZ	German collection of microorganisms and cell cultures
DTT	Dithiothreitol
EC_{90}	90% maximal effective concentration
ECDC	European Centre for Disease Prevention and Control
EDC	1-ethyl-3(3-dimethylaminopropyl)carbodiimide hydrochloride
EDTA	Ethylenediaminetetraacetic acid
EHEC	Enterohemorrhagic <i>Escherichia coli</i>

ESKAPE	<i>Enterococcus faecium</i> , <i>Staphylococcus aureus</i> , <i>Klebsiella pneumoniae</i> , <i>Acinetobacter baumannii</i> , <i>Pseudomonas aeruginosa</i> , and <i>Enterobacter</i> species
FDA	Food and drug administration
FL	Fucosyl lactose
FP	Fluorescence polarization
Fuc	Fucose
Gal	Galactose
GalNAc	N-Acetylgalactosamine
Gb3	Globotriaosylceramide
Glc	Glucose
GlcNAc	N-Acetylglucosamine
HBGA	Human blood group antigens
HBTU	O-(Benzotriazol-1-yl)-N,N,N,N-tetramethyluronium-hexafluorophosphate
HEK cells	Human embryonic kidney cells
HIV	Human immunodeficiency virus
HLM	Human liver microsomes
HMBC	Heteronuclear multiple bond correlation spectroscopy
HPLC	High pressure liquid chromatography
HRMS	High resolution mass spectrometry
HSQC	Heteronuclear single-quantum correlation spectroscopy
IC ₅₀	Half maximal inhibitory concentration
ITC	Isothermal titration microcalorimetry
K _d	Dissociation equilibrium constant, binding constant
LB	Lysogeny broth
MAG	Myelin-associated glycoprotein
Man	Mannose
MBEC	Minimum biofilm eradication concentration
MDCK cells	Madin-Darby canine kidney cells
MDR	Multidrug resistant
β-ME	β-Mercaptoethanol
MHB II	Müller-Hinton broth II
MIC	Minimum inhibitory concentration

MLM	Mouse liver microsomes
MPLC	Medium pressure liquid chromatography
MRI	Magnetic resonance imaging
MS	Mass spectrometry
MST	Microscale thermophoresis
Neu5Ac	N-Acetylneuraminic acid
NHS	N-hydroxysuccinimide
NMR	Nuclear magnetic resonance spectroscopy
OD	Optical density
PBS	Phosphate buffered saline
PCR	Polymerase chain reaction
PDB	Protein data bank
PDR	Pan-drug resistant, pan-antibiotic resistant
PE	Petroleum ether
PET	Positron emission tomography
PMBN	Polymyxin B nonapeptide
PRR	Pattern recognition receptors
PPB	Plasma protein binding
PyBOP	Benzotriazole-1-yl-oxy-tris-pyrrolidino-phosphonium hexafluorophosphate
RNA	Ribonucleic acid
RU	Response unit
SAR	Structure activity relationship
s.d.	Standard deviation
SL	Sialyl lactose
SPR	Surface plasmon resonance
TAMRA	Carboxytetramethylrhodamine
5-TAMRA-Azide	<i>N</i> -(3-Azidopropyl)-3',6'-bis(dimethylamino)-3-oxo-3 <i>H</i> - spiro[isobenzofuran-1,9'-xanthene]-5-carboxamide
TBS	Tris buffered saline
TCEP	Tris(2-carboxyethyl)phosphine hydrochloride
TEER	Transepithelial electrical resistance
TLC	Thin layer chromatography
TNF	Tumour necrosis factor

Tol	Toluene
UTI	Urinary tract infection
UV	Ultraviolet
QS	Quorum sensing
WHO	World Health Organization
XDR	Extensively drug resistant

1. Introduction

1.1 *Pseudomonas aeruginosa* and its lectins LecA and LecB

1.1.1 *Pseudomonas aeruginosa*

The rise of antimicrobial resistance (AMR) is considered to be one of the biggest threats to public health world-wide.¹ In 2019, the European Centre for Disease Prevention and Control (ECDC) reported 17.6% of the clinical *Pseudomonas aeruginosa* isolates to be resistant to two or more antimicrobial agents.² Furthermore, *P. aeruginosa* is one of the major causes of hospital-acquired infections, predominantly affecting immunocompromised patients (e.g. burn victims, HIV and cancer patients, patients suffering from respiratory diseases and diabetes).³⁻⁵ It is a leading cause of death in cystic fibrosis patients.⁶ *P. aeruginosa* is a rod-shaped opportunistic gram-negative bacterium with ability to colonize almost any part of human body. It belongs to the group of ESKAPE pathogens (*Enterococcus faecium*, *Staphylococcus aureus*, *Klebsiella pneumoniae*, *Acinetobacter baumannii*, *P. aeruginosa*, and *Enterobacter* species) that are characterized with high AMR and an urgent call to action was issued for development of novel treatment options.^{7,8}

The current treatment of *P. aeruginosa* infections depends on administration of antimicrobial agents such as aminoglycosides (e.g., gentamicin, tobramycin), fluoroquinolones (e.g. ciprofloxacin, levofloxacin), polymyxins (e.g., colistin), β -lactam antibiotics cephalosporins (e.g., ceftazidime), monobactams (aztreonam), carbapenems (e.g. imipenem) and novel β -lactam/ β -lactamase inhibitor combinations.^{9,10} Low permeability of outer membrane together with its efflux pumps are responsible for high intrinsic resistance of *P. aeruginosa*.¹⁰⁻¹² *P. aeruginosa* acquires antimicrobial resistance via horizontal gene transfer or mutations in a rather short time, leading to the emergence of multidrug resistant (MDR), extensively drug resistant (XDR) or even pan-antibiotic resistant (PDR) strains.^{13,14} Chronic *Pseudomonas* infections are often associated with bacterial biofilms that form highly impermeable barriers against host immune system and antibiotics, increasing resistance up to 1000-fold.^{15,16}

The alternative treatment strategies focus on blocking pathogenicity instead on inhibition of essential cellular functions that increase the selection pressure and lead to the rise of AMR.^{17,18} The concept of antivirulence therapy is based on disarming the pathogen by inhibition of its virulence factors. *P. aeruginosa* possess a plethora of virulence factors responsible for host infection and tissue damage.¹⁹ Consequently, proteins playing an important

roles in quorum sensing (e.g. PqsR), bacterial toxins (e.g. LasB) or proteins mediating bacterial adhesion and biofilm formation (e.g. LecA) have been investigated as potential drug targets.^{18,20} Quorum sensing (QS) is a bacterial cell-to-cell communication system utilizing small signal molecules (autoinducers) to collectively modify community behaviour.²¹ *P. aeruginosa* has three main interconnected QS pathways - las, rhl, and pqs.²² At high bacterial densities, the concentration of signal molecules reaches a threshold that triggers expression of wide range of pathogenicity-associated genes.²³ Inhibition of QS signalling cascades can be achieved by blocking the biosynthesis of autoinducer molecules, inactivation of the signal compounds or interference with the receptors (e.g. LasR) and showed promising *in-vivo* results.^{18,22,24,25} Among important targets to combat bacterial virulence is the multifunctional elastase LasB (known also as pseudolysin), the most prominent protease in the *P. aeruginosa* secretome.^{26,27} LasB is a zinc-metalloprotease that is able to cleave the host's extracellular matrix components (e.g. elastin) and inactivate several components of the host immune system.²⁸⁻³⁰ Various metal-chelating inhibitors of LasB are reported in the literature.³¹⁻³³ Another targets for antivirulence therapy are the quorum system regulated carbohydrate binding proteins LecA and LecB.³⁴ These lectins are essential biofilm structural components and play important roles in the infection process.³⁵⁻⁴⁰ Numerous glycomimetic inhibitors of LecA and LecB are under development.⁴¹⁻⁴⁷ Furthermore, targeting LecA and LecB by inhalation of simple monosaccharides (D-galactose and L-fucose) was able to reduce bacterial burden in cystic fibrosis patients.⁴⁸ Over the past decade, extensive research attention was paid to the development of antivirulence drugs. Inhibitors targeting *P. aeruginosa* virulence factors are being actively explored, some have reached preclinical development, but none have yet been approved for clinical use.

1.1.2 LecA and LecB

LecA and LecB, formerly known as PA-IL and PA-IIL, are two soluble lectins produced by *P. aeruginosa*.⁴⁹ LecA and LecB were initially isolated from heat resistant *P. aeruginosa* and exhibit extremely high resistance towards thermal denaturation ($T_m \geq 90$ °C).⁵⁰⁻⁵² *lecA* and *lecB* genes are encoded in the *P. aeruginosa* core genome.^{53,54} While *lecA* is highly conserved, *lecB* varies across clinical isolates and can serve as a family marker for PA14- or PAO1-like *Pseudomonas* strains.⁵⁵ Expression of LecA and LecB is regulated by *rhl* and quinolone signal of the quorum sensing system.³⁴ LecA is a planar homotetramer arranged around a pseudo C222 axis (Figure 1) with each subunit consisting of 121 amino acids (12.8 kDa).⁵⁶ Similarly,

tetrameric LecB (Figure 1) shows 222 point group symmetry with each monomer made of 114 amino acids (11.7 kDa).⁵⁷

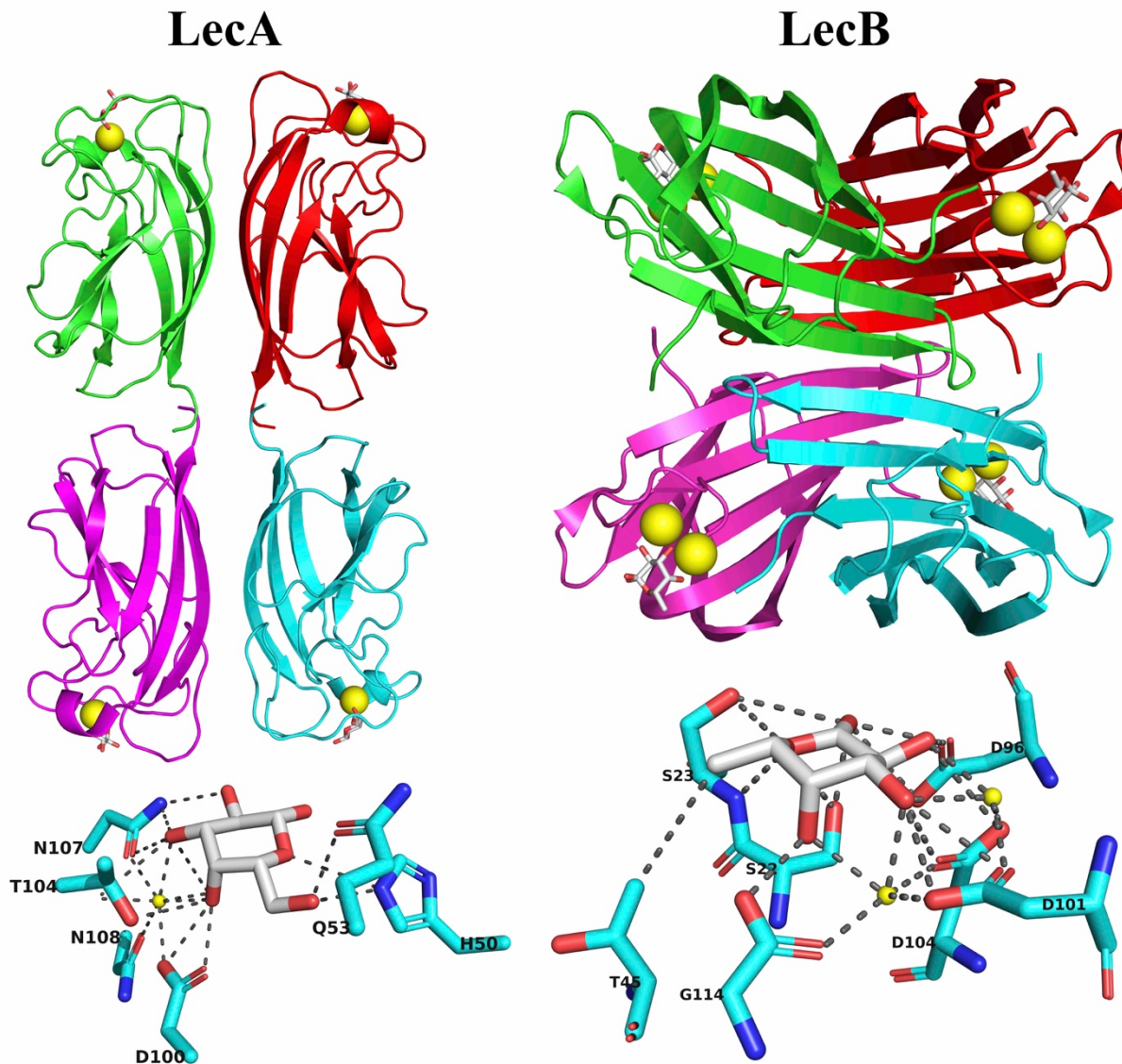


Figure 1: *P. aeruginosa* homotetrameric lectins LecA (top left, PDB code 1OKO) and LecB (top right, PDB code 1OXC) with their monosaccharide ligands (cartoons coloured by chain). Calcium ions (yellow spheres) mediate binding of the LecA to D-galactose (bottom right) and of the LecB to L-fucose (bottom left).

Each carbohydrate recognition domain of LecA contains one calcium ion and is specific towards terminal galactoside-containing glycoconjugates.⁵⁸ LecB binding is mediated by two calcium ions and recognizes L-fucose/D-mannose structures.⁴⁹ Binding affinity of LecA towards monovalent galactosides is in micromolar range (D-galactose $K_d = 88 \mu\text{M}$), whereas monovalent fucosides targeting LecB can reach nanomolar potencies.^{43,47,59–62} In general, two- to three-fold higher affinities were observed for PA14 LecB compared to the more studied PAO1 LecB (methyl α -L-fucoside $\text{IC}_{50,\text{PA14}} = 0.27 \mu\text{M}$, $\text{IC}_{50,\text{PAO1}} = 0.84 \mu\text{M}$).⁵⁵

Primary functions of LecA and LecB are to facilitate bacterial adhesion and biofilm formation. Both lectins showed ability to agglutinate various types of human cells.⁵⁰ LecA plays a role in host cell invasion and mediates host cell signalling processes upon binding to its cellular receptor globotriaosylceramide (Gb3).^{39,40} LecB is known to impair lung ciliary beating, can activate B-cells and affect wound healing.^{37,38,63} Both lectins are crucial for biofilm formation and maintenance.^{35,36} It was demonstrated, that their inhibition can prevent biofilm growth or disperse existing biofilms.^{41,45} Biofilm is a mucoid layer consisting of bacterial cells surrounded by self-produced biopolymeric substances such as extracellular DNA, polysaccharides, rhamnolipids and proteins.⁶⁴ Multivalent nature of LecA and LecB is thought to be responsible for biofilm structural integrity via crosslinking biofilm exopolysaccharides as well as glycans present on host and bacterial cells. It was demonstrated that LecB binds to exopolysaccharide Psl and they colocalize in the biofilm matrix.⁶⁵

1.2 Lectin antagonists in infection, immunity, and inflammation

Authors: Joscha Meiers, Eike Siebs, Eva Zahorska and Alexander Titz

Published in: *Current Opinion in Chemical Biology*, 2019, **53**, 51–67.

DOI: 10.1016/j.cbpa.2019.07.005



ELSEVIER

Lectin antagonists in infection, immunity, and inflammation

Joscha Meiers^{1,2,3,4}, Eike Siebs^{1,2,3,4}, Eva Zahorska^{1,2,3,4} and Alexander Titz^{1,2,3}

Lectins are proteins found in all domains of life with a plethora of biological functions, especially in the infection process, immune response, and inflammation. Targeting these carbohydrate-binding proteins is challenged by the fact that usually low affinity interactions between lectin and glycoconjugate are observed. Nature often circumvents this process through multivalent display of ligand and lectin. Consequently, the vast majority of synthetic antagonists are multivalently displayed native carbohydrates. At the cost of disadvantageous pharmacokinetic properties and possibly a reduced selectivity for the target lectin, the molecules usually possess very high affinities to the respective lectin through ligand epitope avidity. Recent developments include the advent of glycomimetic or allosteric small molecule inhibitors for this important protein class and their use in chemical biology and drug research. This evolution has culminated in the transition of the small molecule GMI-1070 into clinical phase III. In this opinion article, an overview of the most important developments of lectin antagonists in the last two decades with a focus on the last five years is given.

Addresses

¹ Chemical Biology of Carbohydrates, Helmholtz Institute for Pharmaceutical Research Saarland (HIPS), Helmholtz Centre for Infection Research, D-66123 Saarbrücken, Germany

² Deutsches Zentrum für Infektionsforschung (DZIF), Standort Hannover-Braunschweig, Germany

³ Department of Pharmacy, Saarland University, D-66123 Saarbrücken, Germany

Corresponding author: Titz, Alexander (alexander.titz@helmholtz-hzi.de)

⁴ These authors contributed equally.

Current Opinion in Chemical Biology 2019, 53:51–67

This review comes from a themed issue on **Mechanistic biology**

Edited by **Hermen S Overkleeft** and **David J Vocadlo**

<https://doi.org/10.1016/j.cbpa.2019.07.005>

1367-5931/© 2019 Elsevier Ltd. All rights reserved.

Introduction

Lectins are a highly diverse family of proteins found in all domains of life [1,2]. Various folds and classes have been identified and the common functional feature is their specificity for carbohydrate ligands. These glycan-binding

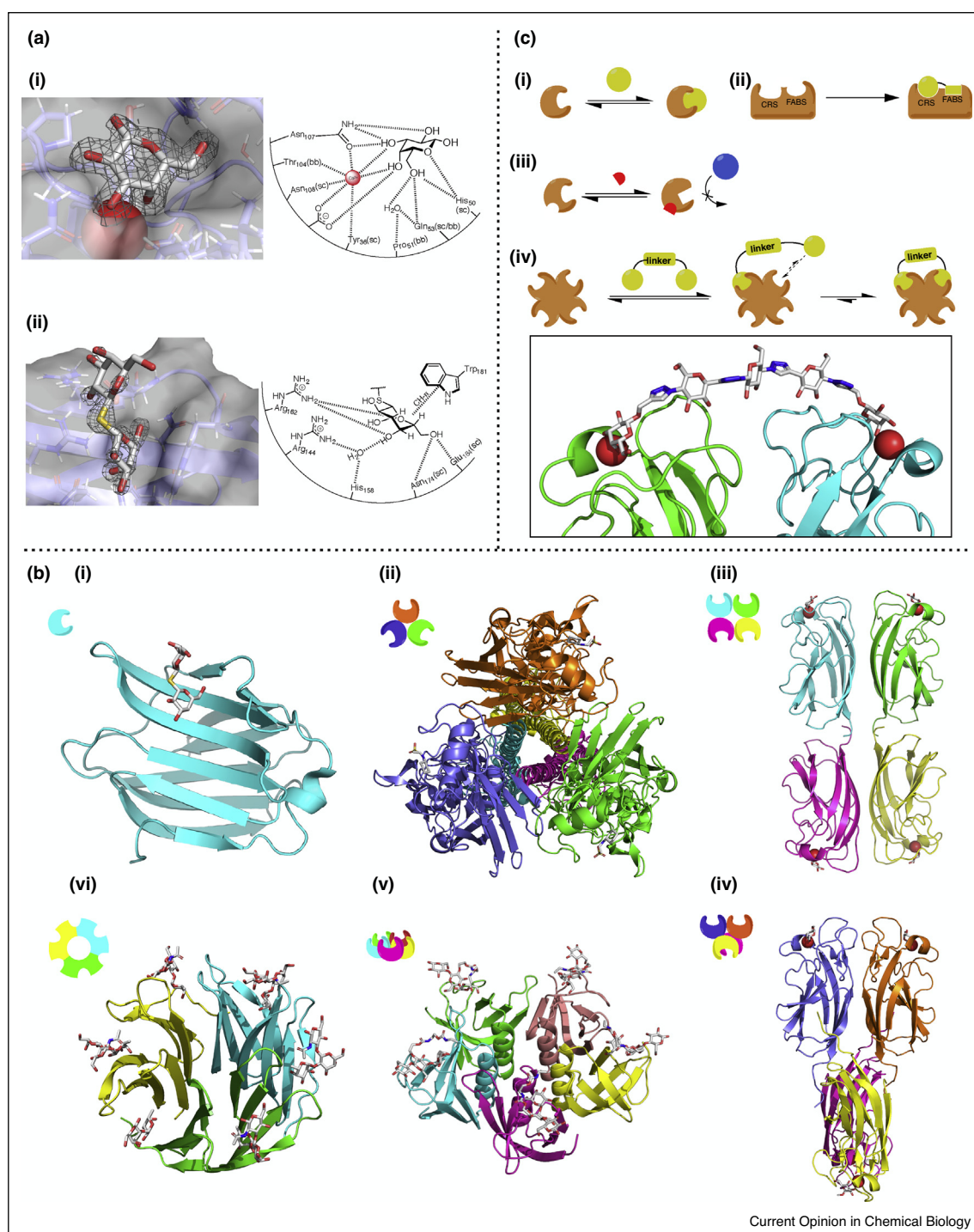
proteins have many important roles in infection, cell recognition, communication and various intracellular processes, such as protein folding and protein targeting.

Numerous viral, bacterial, fungal, and parasitic pathogens employ lectins for initiation and maintenance of an infection by adhering to surface-exposed glycoconjugates of their host organisms [3–5]. In contrast, the mammalian host has developed a plethora of lectin-containing pattern recognition receptors of the innate immune system recognizing glycan structures on intruders [6–8]. In addition to recognizing these non-self structures, other mammalian lectins bind to self-epitopes and thus mediate cell-recognition processes like inflammation and cancer metastasis [9–11].

The natural ligands of lectins are mostly bacterial or fungal polysaccharides, bacterial lipopolysaccharide and peptidoglycan, or eukaryotic glycoconjugates of lipids or proteins [1,12]. Except for bacteria which can have a high diversity among their monosaccharides, generally a relatively small set of different monosaccharide subunits are shared between animals, plants, fungi, parasites, bacteria, and other organisms. These building blocks are assembled into more diverse oligosaccharides where a very high complexity can be achieved due to many possible stereoisomers and regioisomers. In many cases, this leads to organism-specific oligosaccharides, which can then be recognized by innate immunity as non-self antigens and induce neutralization of the intruder [13], or elicit allergic reactions as observed for insect glycans, for example, in bee venom [14]. The opposite phenomenon that pathogen and host have identical glycoconjugates is also observed. The latter has been termed molecular mimicry or glycomimicry, a stealth process of the pathogen believed to be an evolutionary adaptation for evasion of immune surveillance of the host [15,16].

Despite the complexity of those oligosaccharide structures, lectins often recognize terminal monosaccharides or smaller oligosaccharides on a given glycoconjugate. Two common binding modes of carbohydrate ligands are shown in Figure 1a: (i) vicinal hydroxyl groups chelate a Ca^{2+} -ion present in the binding site, or (ii) carbon-bound hydrogen atoms of the carbohydrate ring interact via CH– π stacking with aromatic amino acids in the binding site. Because of the recognition of rather small epitopes, common ligand specificity of different lectins with diverse functional roles often occurs. An example are

Figure 1



Current Opinion in Chemical Biology

(a) Schematic representation of two important recognition modes of carbohydrates by lectins: (i) calcium-ion mediated binding of the ligands, example β -galactoside and LecA (PDB: 1OKO) (ii) tryptophan-mediated stacking on hydrophobic faces of carbohydrates, example galactoside with galectin-3 (PDB: 4JC1). **(b)** Various strategies for domain/binding site orientation: (i) monomeric in galectin-3 (4JC1), (ii) trimeric virus hemagglutinin (6CF5), (iii) tetrameric LecA (1OKO), (iv) tetrameric LecA ortholog PIIA with altered domain orientation (5ODU), (v) pentameric Shiga-like toxin B subunit (1QNU), (vi) trimeric BambL containing 6 carbohydrate binding sites in and between subunits (3ZW2). **(c)** Schematic representation of different lectin inhibition approaches: (i) direct inhibition of carbohydrate binding sites, (ii) growing toward non-carbohydrate binding sites, (iii) allosteric inhibition (iv) multivalent inhibition which refers to clustered binding sites, either multivalent proteins or monovalent lectins clustering on cell membranes.

the functionally different human DC-SIGN and the bacterial lectin LecB with shared specificity for Lewis blood group antigens [17–19]. A large data set for the glycan specificity of many lectins using microarrays is provided by the Consortium for Functional Glycomics (see <http://www.functionalglycomics.org>).

Specificity of the lectins can be further tuned by recognizing functional groups attached to the essential carbohydrate, and, for example, lipids are recognized by a secondary site of the lectin Mincle [20,21], *O*-methylation is required for recognition by the tectonins [22,23], sulfates on nearby amino acids enhance binding of P-selectin to the Lewis-blood groups on glycoproteins [24] and phosphates are required for intracellular trafficking of proteins by the mannose-6-phosphate receptor [25].

Lastly, the spatial presentation of ligands and/or lectin's carbohydrate binding sites (Figure 1b), as well as clustering of several lectin protomers into oligomeric bundles or membrane embedded protein complexes can contribute significantly to specificity by augmentation of apparent binding affinity through avidity [7,26].

Carbohydrate specificity, requirements of additional functional groups and spatial presentation of binding sites are important aspects for the design and success of lectin-targeting probes in chemical biology and drug research. Therefore, the design of lectin antagonists usually follows various approaches from (i) competitive inhibition of a carbohydrate recognition site, (ii) targeting adjacent binding sites, (iii) allosteric inhibition, to (iv) multivalent competitive inhibition of two or more binding sites (Figure 1c).

Consequently, lectins have developed into attractive targets for chemical biology and medicinal chemistry over the past two decades [27,28]. Very active areas of research are the targeting of (i) lectins of pathogenic origin to interfere with mechanisms of infection by viruses and bacteria, and to a smaller extent also fungi and parasites, (ii) the selectins as a family of three closely related proteins crucial for cell migration in inflammation and cancer, as well as (iii) immunotherapeutic or immunomodulatory approaches for the mammalian lectins langerin in vaccine delivery, DC-SIGN in HIV infection or the galectins in cancer and immune modulation. Lectins discussed in this opinion article are summarized in Table 1.

Bacterial lectin antagonists

Bacterial antibiotic resistance is increasing worldwide at an alarming rate. As one consequence, antivirulence drugs have gained considerable research interest as alternative treatment approach with the aim to avoid the rapid onset of resistance [50]. In this context, the inhibition of bacterial lectins to prevent infection and persistence is a newly exploited strategy [3,27]. Targeting lectins involved in

the formation of bacterial biofilms are of particular interest since bacteria embedded in their self-produced biofilm matrix exhibit increased antimicrobial resistance compared to free floating planktonic bacteria. Biofilm-associated bacterial infections are responsible for a broad range of chronic/recurring diseases [51].

The Gram-negative bacterium *Escherichia coli* is the prime pathogen in urinary tract infections (UTIs) and important for intestinal infections as a consequence of Crohn's disease (CD). *E. coli* can build various organelles called pili and fimbriae which are oligomeric cell appendices built up of several proteins. These organelles are often employed for bacterial adhesion. The pilus or fimbria lectins FimH and FmIH, localized on the top of the different organelles, play decisive roles in host colonization, invasion, and biofilm formation [52]. Thus, inhibition of these lectins to antagonize infections presents a viable therapeutic strategy [53,54].

FimH is located on the tip of fimbriae and usually binds to mannosylated glycoconjugates in the bladder endothelium. Pathogenicity of *E. coli* clinical isolates expressing different *fimH* alleles varies, but the mannose binding pocket is invariant [52,55,56]. Hultgren's group demonstrated the activity of a high affinity mannoside FimH inhibitor against different uropathogenic *E. coli* strains [57]. In recent years, several research groups have been developing FimH antagonists for treatment of urinary tract infections and gut inflammations associated with CD. X-ray crystallography guided drug design focused on optimization of interactions with the so-called tyrosine gate adjacent to the mannose binding site. Introduction of aryl and alkyl aglycons increased the binding affinity significantly compared to simple mannose [58–60]. Nanomolar binding affinities were achieved by introducing biaryl aglycons that are tightly coordinated by the tyrosine gate [61–63]. High affinity biaryl mannosides were further optimized to increase metabolic stability by replacing the labile *O*-glycosidic bond with carbon-based linkers to the aglycon [29**,64]. Ester and phosphorylated prodrugs were successfully explored to improve oral bioavailability of both *O*-mannosides and *C*-mannosides [29**,65,66*]. Rational design and optimization of FimH antagonists are summarized in a recent review by Mydock-McGrane *et al.* [67]. The promising preclinical candidate **1** (EC₉₀ = 31 nM, Figure 2) is one example of a highly optimized FimH inhibitor with good metabolic stability and high efficacy in mouse models of acute and chronic UTI [29**]. Recent optimization attempts yielded thiomannosides (e.g. **2**, EC₉₀ = 0.31 μM, Figure 2) with improved metabolic stability compared to respective *O*-mannosides, ability to inhibit biofilm formation *in vitro* and with a prophylactic effect in a mouse UTI model [30]. The first FimH antagonist entering clinical trials was EB8018 from Enterome (Paris, France) designed for the treatment of CD, but its structure has not been

Table 1

Overview of bacterial, viral, and mammalian lectins discussed in this opinion article

	Origin	Binding specificity	Key roles	Status of development/indicator
Bacterial lectins				
FimH	<i>E. coli</i>	Man	Adhesion, biofilm formation	Lead optimization (1, 2) [29**,30], EB8018 in Phase I clinical trials (www.clinicaltrials.gov , NCT03709628)
FmlH	<i>E. coli</i>	Gal, GalNAc	Adhesion, biofilm formation	Hit optimization (3) [31]
LecA	<i>P. aeruginosa</i>	Gal	Adhesion, biofilm formation	Exploratory studies
LecB	<i>P. aeruginosa</i>	Man, Fuc	Adhesion, biofilm formation	First covalent lectin inhibitor (5) [32**] Lead optimization (6, 7) [33,34**]
Shiga toxins	<i>S. dysenteriae</i> , <i>E. coli</i>	Gal, Glc	Toxin	Lead optimization on hold, First peptide-based inhibitor [35]
Cholera toxin	<i>V. cholerae</i>	Gal, Fuc	Toxin	Hit optimization (8) [36]
Viral Lectins				
Hemagglutinin	Human influenza virus	Neu5Ac	Adhesion, cell entry	Hit optimization (12) [37–39] and exploratory studies (10, 11) [40*,41*,42**]
Hemagglutinin–neuraminidase	Human parainfluenza virus	Neu5Ac	Adhesion and detachment, cell entry	Hit optimization [43,44]
Capsid protein P domain	Norovirus	HBGAs	Adhesion, cell entry	Exploratory studies (14, citric acid) [45–47]
Mammalian Lectins				
Langerin	Langerhans cells	Man, Fuc, GlcNAc, sulfated Gal, Glc	Immune response	Exploratory studies First allosteric mammalian lectin inhibitor (15) [48**]
DC-SIGN	Dendritic cells	Man, Fuc, GlcNAc	Immune response	Exploratory studies
Selectins	L-selectin: leukocytes P-selectin: platelets and endothelial cells E-Selectin: endothelial cells	sLe ^x P/L-selectins: Man, Gal and Sulfation [49]	Cell adhesion	GMI-1070 (20) in Phase III clinical trials against vaso-occlusive anemia (www.clinicaltrials.gov , NCT02187003)
Mincle	Immune system	Glycolipids with terminal Glc or Man	Immune response	Exploratory studies
Galectin	Circulating proteins	Gal, for example, <i>N</i> -acetylglucosamine	Regulate cell death	TD139 (24) in Phase II clinical trials against idiopathic pulmonary fibrosis (www.clinicaltrials.gov , NCT03832946)
Siglecs	Immune-cells	Neu5Ac	Cell-cell signaling, immune response and adhesion	Exploratory studies

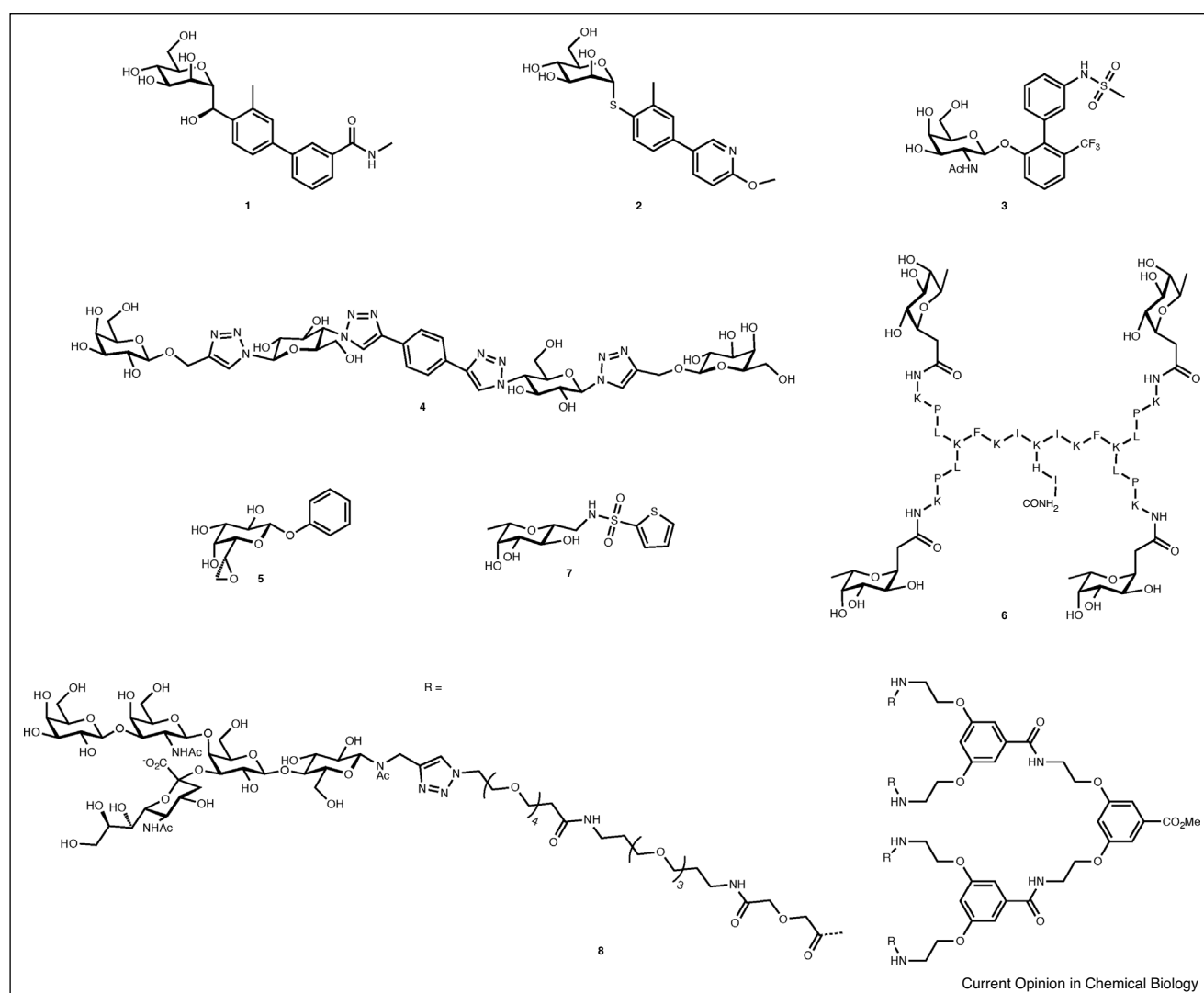
disclosed. In collaboration with Takeda, EB8018 has completed Phase Ia and the Phase Ib trial is ongoing in early 2019 (www.clinicaltrials.gov, NCT03709628). Furthermore, Fimbrion Therapeutics (St. Louis, MO) has announced the selection of a not further specified clinical candidate as antibiotic sparring molecule against UTIs in collaboration with GSK (www.fimbrion.com, press release Dec 06, 2018).

As a secondary target of uropathogenic *E. coli*, the FimH-like adhesin FmlH recognizes Gal(β1-3)GalNAc epitopes on bladder epithelium and enhances *E. coli* urinary tract colonization [54]. Recently, first structure-based inhibitor design approaches for FmlH have been reported [31,68**]. To date, the best FmlH inhibitor 3 (Figure 2) is based on *N*-acetyl galactosamine carrying a further substituted biphenyl aglycon and displays very high binding affinity (IC₅₀ = 34 nM), good aqueous solubility and high metabolic stability. Unfortunately, 3 showed

only low oral bioavailability in rats of less than 1% and further optimization is therefore mandatory [31,68**].

The opportunistic pathogen *Pseudomonas aeruginosa* has two soluble lectins, the extracellularly secreted proteins LecA (Figure 1) and LecB, both mediating bacterial virulence and being crucial components for biofilm formation [69–71]. Consequently, both proteins have been subject to intense research toward biofilm modulators and in drug discovery for antivirulence drugs [27,28,72–74]. LecA binds to various α-galactoside-terminating glycoconjugates with the glycosphingolipid Gb3 as proposed natural ligand [75]. This homotetrameric lectin was later shown to mediate bacterial uptake via Gb3 where it acts as a lipid zipper [76,77]. The affinity of LecA to galactose and simple glycosides thereof is rather weak in the 50–100 μM range. Consequently, development of LecA antagonists mainly focused on multivalent display of galactosides using many different linkers and maximizing

Figure 2



Inhibitors targeting lectins of pathogenic bacteria in *E. coli* (1-3), *P. aeruginosa* (4-7), and toxins of *V. cholerae* (8).

the number of presented epitopes [28,78]. Very potent tetravalent galactoclusters with low nanomolar binding affinities toward LecA have been developed [79^{••},80,81[•],82,83]. In contrast to the high target-binding affinity, they showed only moderate inhibition of biofilm growth in the micromolar range *in vitro*.

The Pieters group has undertaken a different approach and focused on divalent galactosides oriented in a perfect manner to bridge two adjacent binding sites in the LecA tetramer. Several highly potent divalent inhibitors with the rigid spacers consisting of glucose and triazole groups were obtained, including the most potent LecA inhibitor reported so far with a K_d of 12 nM (4, Figure 2) [84^{••},85]. Again, recent optimization of these highly potent molecules on the target revealed a need for additional

multimerization and rather high micromolar concentrations for biofilm blocking [82,86].

Monovalent galactose-derived ligands with binding affinities in low micromolar range could be obtained after introduction of a β -aryl aglycon which establishes a π -stacking interaction with an imidazole-CH of His50 adjacent to the carbohydrate binding site (Figure 1a) [87^{••},88,89]. However, the specificity for further variations appears relaxed and changing substituents at the phenyl aglycon did not lead to significant potency improvements. As an alternative approach to the generally employed glycosides of unmodified galactose residues in LecA ligands, we have embarked on the modification of the galactose residue itself. A cysteine residue in the carbohydrate binding site of LecA was targeted with

the aim to develop a covalent lectin inhibitor using a small electrophilic headgroup in a modified galactose [32**]. Despite the fact that covalent inhibitors are widespread for many other protein classes, epoxide **5** (Figure 2) was established as the first-in-class covalent lectin inhibitor. Because of its moderate affinity toward LecA ($IC_{50} = 64 \mu\text{M}$), the molecule was converted into a tool compound after synthetic derivatization and conjugation to fluorescein enabling the visualization of *P. aeruginosa* biofilm aggregates by confocal fluorescence microscopy [32**].

The second *P. aeruginosa* lectin LecB also forms a homotetrameric quaternary structure, binds broadly to fucosides and mannosides and the highest affinity was determined for Lewis blood group antigens [17,90]. In contrast to LecA, the protein sequence of LecB varies among clinical isolates and two important types occurring in the clinical isolates PAO1 and PA14 have been identified as representative for all studied isolates [18,91]. Despite the observed amino acid sequence differences in LecB between strains, its carbohydrate binding specificity is conserved, underpinning the suitability of LecB as a drug target with conserved specificity among all isolates. Also for LecB, multivalent inhibitors have been the first choice for inhibition [28,78]. However, because of a sterically more distant and less favorable orientation of binding sites in LecB compared to LecA, the obtained multivalent ligands could not achieve a comparable boost in affinity. Nevertheless, two types of multivalent ligands carrying fucosides stand out of the very broad field: tetravalent glycopeptide dendrimer **6** ($IC_{50} = 140 \text{ nM}$, Figure 2) was able to efficiently prevent biofilm formation of *P. aeruginosa* at a concentration of $20 \mu\text{M}$ *in vitro*; [33] furthermore, a calixarene carrying four fucose residues was tested in an infection model in mice [79**]. This compound significantly reduced the number of bacteria colonizing lung and spleen, but was unable to inhibit bacterial biofilms *in vitro* at a concentration of $100 \mu\text{M}$ despite its high affinity at the target ($K_d = 48 \text{ nM}$).

To overcome the intrinsic disadvantages associated with large molecules and multidirectional valency in biofilm formation, we have used the small molecule LecB ligand mannose as a starting point for the rational design of monovalent biofilm targeting glycomimetics [92]. These compounds exhibited rather good target-binding potency ($K_d = 3\text{--}20 \mu\text{M}$) and prevented bacterial adhesion to a glycosylated surface at $100 \mu\text{M}$. Further optimization [93] and removal of the anomeric center [94] finally yielded C-glycosidic inhibitors of LecB (e.g. **7**, Figure 2) with good target-binding potency ($K_d = 290 \text{ nM}$) and very long receptor residence times ($t_{1/2} = 28 \text{ min}$) [34**]. Glycomimetic **7** showed approx. 85% inhibition of biofilm growth *in vitro* at $100 \mu\text{M}$, which contrasts the lack of antibiofilm activity of the natural LecB binder methyl α -L-fucoside, despite its very high target binding affinity ($K_d = 430 \text{ nM}$). Furthermore, glycomimetic **7** is orally

bioavailable which is not possible for large multivalent molecules.

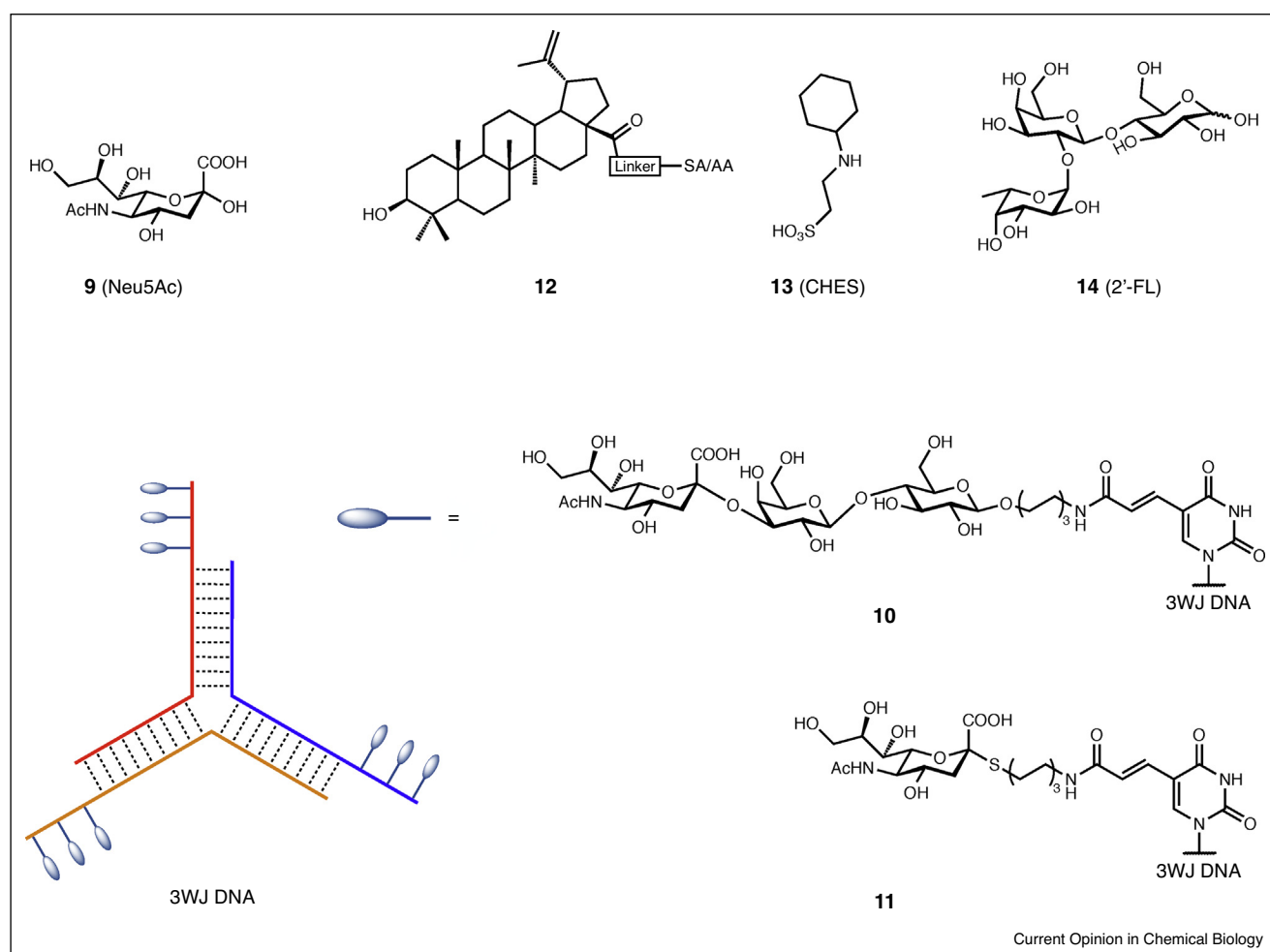
Shiga and cholera toxins are bacterial proteins responsible for severe symptoms in gastrointestinal infections. These so-called AB₅ toxins consist of one catalytic A-subunit and five lectin-like B-subunits (Figure 1b) which are responsible for the binding of the complex to the host cell surface in the gut. Inhibition of the B-subunits and thereby preventing adhesion is a potential treatment strategy [95].

Shiga toxins (Stxs) are produced by *Shigella dysenteriae* and some enteropathogenic *E. coli* strains, for example, enterohemorrhagic *E. coli* (EHEC). Kitov *et al.* designed the pentavalent ligand STARFISH to match the carbohydrate binding sites of the five B-subunits with subnanomolar inhibitory activity against Shiga-like toxins I and II (Stx1 and Stx2) [96]. A modified version of STARFISH, called DAISY, improved the *in vivo* activity and provided full protection against the toxins when administered simultaneously in a mouse model despite its lower target-binding potency [97]. However, further development of DAISY-based inhibitors appears halted (no further publications) since the compound proved ineffective in a treatment scenario, that is, drug administration after infecting mice with the Shiga toxin producing strain *E. coli* O91:H21. Nishikawa *et al.* designed a series of carbosilane dendrimers called SUPERTWIG. The most potent compound of the series was able to completely neutralize Stxs in the blood stream and protect mice against a fatal dose of the Shiga toxin producing strain *E. coli* O157:H7 even when administered after establishment of infection [98]. The rather complex synthesis of multivalent-trisaccharide inhibitors is hindering further clinical development.

From a peptide library, the branched proline and arginine rich high molecular weight peptide Ac-PPP-tet was identified to bind to Stx2 B-subunit and inhibit Stx2 cytotoxicity [35]. This peptide affects the intracellular transport of Stx2 and protected mice from a fatal dose of *E. coli* O157:H7 even when administered after an established infection; this molecule further protected rabbit intestines *ex vivo* against the toxic effect of Stx2 [35,99]. Recent efforts include the synthesis of sugar-amino acid hybrid polymers with highly clustered globotriaosyl residues that showed low micromolar affinities to both Stxs with the ability to neutralize the toxic effects on Vero cells [100].

Vibrio cholerae produces cholera toxin where each B-subunit (CTB) has two binding sites – one primary binding site recognized by the ganglioside GM₁ and a secondary low affinity site recognized by fucosylated glycans [101]. A number of derivatives mimicking the terminal galactose from GM₁ has been screened and m-nitrophenyl α -D-galactoside and 3,5-disubstituted phenylgalactosides were identified as monovalent CTB inhibitors [102,103]. Numerous multivalent inhibitors targeting the primary

Figure 3



Inhibitors of influenza hemagglutinin: Neu5Ac (**9**), macromolecular sialylated three way junctioned DNA **10** and **11** and small molecules **12-13**; or. Norovirus spike protein can be blocked using the trisaccharide 2'-fucosyl lactose **14**. SA: sialic acid, AA: ascorbic acid.

site with down to picomolar binding affinities (e.g. **8**, $IC_{50} = 34 \text{ pM}$, Figure 2) [36] have been developed and were summarized in a recent review by Kumar and Turnbull [104]. Targeting the fucose binding site as new strategy was published by Wands *et al.* who reported inhibition of CTB binding to cell surfaces with 2'-fucosyllactose and a fucosylated polymer [105**].

Viral lectin inhibitors

Viral infections are difficult to treat, control and prevent. Frequent antigen variation, for which the influenza virus is a perfect example, prevents efficient protection and virus clearance by the human immune system. In many viruses, lectin-carbohydrate interactions are crucial for an efficient infection of the host. Hemagglutinin is the sialic acid binding lectin on the surface of the influenza viral envelope and plays a key role in the host cell-virus interaction. Sialic acids are defined as a family of acidic sugars with a nine

carbon atom backbone and the most abundant member found in vertebrates is *N*-acetyl neuraminic acid (**9**, Neu5Ac, Figure 3) [106]. Because the binding interaction of one monomeric hemagglutinin to sialylated glycans is weak ($K_d > 1 \text{ mM}$) [107], trimerization of hemagglutinin on the viral envelope and a high sialic acid density on the host cell lead to an increased avidity. This binding event then triggers the internalization of the virus by endocytosis [108]. Therefore, inhibition of the hemagglutinin-sialic acid interaction could yield prophylactic as well as therapeutic treatments of an influenza virus infection.

For this purpose, Strauch *et al.* [42**] developed a trimeric influenza neutralizing protein, targeting the hemagglutinin receptor binding site. This protein was designed to mimic the key interactions of broadly neutralizing antibodies and its optimization led to a highly avid protein with a trimeric binding mode and nanomolar apparent K_d

values. *In vivo*, using an H3 HK68 influenza infection mouse model, prophylactic and therapeutic treatment significantly protected mice from establishing disease and weight loss. Unfortunately, this designed protein does not show broad spectrum activity since it does not bind to the pathogenic ‘bird flu’ subtype H5N1. Limitations in high scale production and price, together with challenging pharmacokinetic properties will impact on its commercial use as an anti-influenza drug.

A recent review by Li *et al.* describes a wide range of chemical scaffolds and strategies to inhibit the hemagglutinin–host cell interaction. Mostly, trimeric sialosides are presented as binders to the receptor binding site [109].

2,3-Sialyllactose (2,3-SL) conjugated to three way junction (3WJ) DNA, with each DNA strand presenting one, three or five 2,3-SL molecules complementary to the hemagglutinin trimer geometry was reported by Yamabe *et al.* [40,41]. Hemagglutinin inhibition revealed 3WJ DNA with three sialic acid residues per arm in compound **10** as best inhibitor with a $K_i = 0.25 \mu\text{M}$, which corresponds to an 80 000-fold increase compared to monomeric 2,3-SL and an eightfold increase compared to 3WJ DNA with only one sialic acid per strand. Surprisingly, 3WJ DNA presenting five sialic acid per strand led to a reduction in activity ($K_i^{\text{HAI}} > 4.0 \mu\text{M}$) which probably originates from an altered orientation of the carbohydrate epitopes induced by steric hindrance. In contrast to the neuraminidase labile *O*-linked **10**, the more stable thio-linked sialic acid derivative **11** was synthesized as a follow up. For **11**, an increased stability toward influenza neuraminidase present on the viral envelope was observed, while its activity was retained. However, in presence of the full virus both derivatives, that is, *O*-glycoside and *S*-glycoside, were stable under the conditions tested. Another approach using a macromolecular scaffold by Nagao *et al.* yielded a trimeric star-shaped glycopolymer presenting 6'-sialyllactose on each of the three arms, synthesized by reversible addition-fragmentation chain transfer polymerization [110]. The degree of polymerization dictated the length of each arm. Hemagglutinin inhibition clearly depended on the arm-length, resulting in a $K_i = 21 \mu\text{M}$ for their best glycopolymer.

Conjugation of sialic acid or ascorbic acid derivatives onto pentacyclic triterpenes by Zhou and co-workers [37,38] was inspired by the broad antiviral activity of *Dipsacus asperoides* triterpenes and the corresponding synthetic leads [39]. In both cases, conjugation to betulinic acid as in **12** led to a strong reduction of infection by influenza A/WSN/33 in MDCK cells. Cytotoxicity of the triterpenes was also reduced by conjugation to sialic acid or ascorbic acid and a hemagglutination assay and SPR experiments with immobilized hemagglutinin suggested hemagglutinin as the putative target ($K_d = 17 \mu\text{M}$ for the sialic acid conjugate, $K_d = 8.0 \mu\text{M}$ for the ascorbic acid conjugate). Interestingly, the synthetic 2,3-di-*O*-benzyl

ascorbic acid intermediate showed a higher affinity for hemagglutinin ($K_d = 3.78 \mu\text{M}$) and improved inhibition of viral plaque formation (IC_{50} 's of $8.7 \mu\text{M}$ versus $41.3 \mu\text{M}$).

Small molecules possess superior pharmacokinetic properties for drug development than the rather large structures described above. Kadam and Wilson [111] identified the common buffer molecule CHES (**13**) by X-ray crystallography in complex with hemagglutinin. The molecule's binding mode with hemagglutinin mimics the one of sialic acid and its sulfonic acid superimposes with the carboxylate of sialic acid in the complex. Furthermore, the cyclohexyl moiety of CHES forms a CH– π interaction with W153 of hemagglutinin which is normally established by the *N*-acetyl group of sialic acid. As binding of CHES, although in slightly different binding modes, was confirmed for H3-hemagglutinin and H5-hemagglutinin, Kadam and Wilson proposed this non-carbohydrate molecule as a starting point for fragment growing to overcome its very low affinity ($K_d > 20 \text{mM}$) in the discovery of new types of hemagglutinin inhibitors.

The human parainfluenza virus causes respiratory tract diseases in children and elderly patients. In contrast to other influenza viruses, its multifunctional hemagglutinin–neuraminidase protein possesses both receptor-binding (hemagglutinin-function) and receptor-processing (neuraminidase-function) functionalities in one binding site [112]. Usually, lectins are defined as carbohydrate binding proteins without catalytic activity. However, this multifunctionality makes this parainfluenza virus protein an interesting topic for this review. Von Itzstein and co-workers synthesized a set of enzymatic intermediate-like *N*-acylated Neu-2-en and substrate-like *N*-acylated 2,3-difluoro-Neu derivatives to block both functionalities with a single molecule [43,44]. Especially the *N*-isobutyramido Neu-2-en derivatives showed potent hemagglutinin inhibition ($\text{IC}_{50} = 1.15 \mu\text{M}$) as well as inhibition of neuraminidase activity and virus growth.

Norovirus, a worldwide cause of mild to severe acute gastroenteritis, can lead to life-threatening infections for pediatric and geriatric patients and outbreaks, especially in day care centers or nursing homes, which are particularly problematic. To date, therapy of norovirus infections is only supportive and limited to reversal of dehydration and loss of electrolytes [113]. Thus, to control and prevent outbreaks, new drugs are needed. The human norovirus capsid protein P domain interacts with human blood group antigens (HBGA) and plays an important role in infection [114]. This virus–host interaction can be blocked by human milk oligosaccharides such as 2'-fucosyl lactose (**14**, 2'-FL) as shown by Hansman and co-workers [45,46]. The very high concentrations of 2'-FL needed to inhibit the interaction of virus like particles with HBGA *in vitro* ($\text{IC}_{50} = 13\text{--}50 \text{mM}$), could be achieved because of the low toxicity of 2'-FL, its

metabolic stability and low gastrointestinal absorption [115]. Indeed, 2'-FL is a major constituent of human milk with a concentration in the mM range and has been postulated to prevent infections in breast-fed newborns [116]. Another commonly used and safe food supplement, citrate, was shown to bind norovirus in a HBGA-like manner [47].

Mammalian lectin antagonists

There are numerous mammalian lectins and the three important classes, siglecs, galectins and the C-type lectins, are currently addressed in chemical biology and medicinal chemistry. Sialic acid-binding immonoglobulin-like lectins, siglecs, are cell-surface receptors, mainly expressed by cells of the immune system. They are involved in various processes ranging from self-/non-self discrimination to regulating inflammation caused by damage-associated or pathogen-associated molecular patterns (DAMP/PAMP) [117,118]. Galectins, a family of soluble secreted lectins with 14 members, generally bind to β -galactosides [119]. Their functions are diverse and comprise mediation of cell–cell interactions, cell–matrix adhesion and transmembrane signaling [120–122]. C-type lectins are the largest and most diverse lectin family which share a conserved protein fold. The name giving Ca^{2+} -ion present in all carbohydrate recognizing family members directly mediates the binding to the glycan ligand [7]. Only a few examples exist for which Ca^{2+} is dispensable for carbohydrate recognition with dectin-1 being the most prominent example. The C-type lectin receptor family in mammals contains 17 members and many are part of innate immunity [123,124].

Langerin, DC-SIGN

All cells of the innate immune system express a variety of pattern recognition receptors (PRR) such as toll-like receptors, NOD-like receptors and C-type lectin receptors, which allow the orchestration of an appropriate biological response to an incoming microbial threat. These PRRs are specialized to recognize PAMPs such as bacterial cell wall structures, fungal polysaccharides, the viral envelope and foreign RNA/DNA [127,128]. The signaling cascades initiated by these recognition events as well as the antigen uptake and processing pathways eventually lead to activation of cells of the adaptive immune system and hence are central elements bridging these two arms of immunity. For example, PAMPs recognized and processed by dendritic cells can lead to differentiation of CD4^{+} -cells into T-helper cells [123,126]. Important C-type lectin receptors are langerin, DC-SIGN and dectin-1 [123].

The homotrimeric protein langerin is expressed on Langerhans cells in epithelial and mucosal tissues and binds to D-mannose, L-fucose, and D-GlcNAc as well as sulfated D-galactose. Langerin mediates the uptake of *Yersinia pestis* and influenza A virus amongst others in host infection [7,8]. Capitalizing on these carbohydrate-mediated

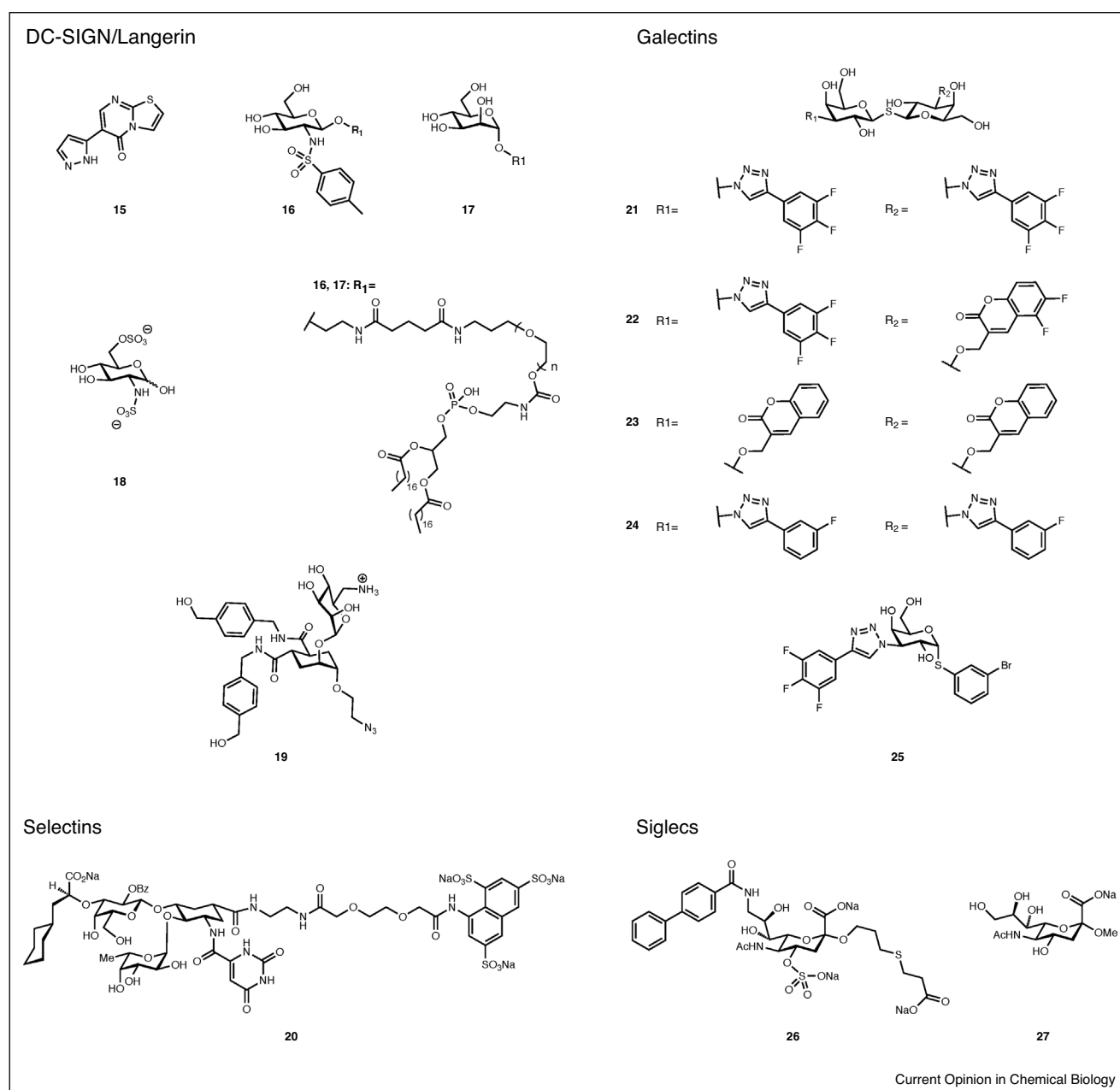
antigen uptake and processing pathways, langerin has also been described as an attractive target for targeted drug-delivery approaches to Langerhans cells [129,130]. This raised the interest in specific langerin ligands and, for example, Aretz *et al.* reported the discovery of thiazolopyrimidines as murine langerin antagonists, revealing the first allosteric inhibition of a mammalian lectin [48^{••}]. Optimization of the initial hit **15** (Figure 4) was found beneficial at position 6 and led to up to 10-fold lower K_d and IC_{50} -values (K_d (**15**) = 0.7 mM; IC_{50} = 0.6 mM). Overall, a large series of langerin inhibitors was presented with IC_{50} values ranging in the two digit micromolar range.

Furthermore, it is well known that langerin has high affinity for sulfated polysaccharides or large oligosaccharides, for example, heparin ($K_d = \sim 2.4$ nM). As the binding affinity is electrostatically driven, no binding was detected with pH values below 4 or at high salt concentrations above 0.5 M [131]. A screening for langerin binding molecules revealed a sulfonamide of glucosamine as weakly binding langerin ligand [132^{••},133^{••}]. Considering this screening hit, the modified phospholipids **16** and **17** were synthesized with the aim to produce glycomimetic modified liposomes for langerin targeting. These were tested against Langerin⁺, DC-SIGN⁺ or Dectin-1⁺ Raji cells. Liposomes consisting of mannosylated phospholipid **17** bound specifically to DC-SIGN⁺ cells and those consisting of sulfonamide **16** specifically to Langerin⁺ cells. Intracellular trafficking of the langerin targeting liposomes consisting of **16** was then observed in Langerin⁺ COS-7 cells by confocal microscopy.

Tetrameric DC-SIGN is expressed by myeloid dendritic cells and macrophages. Since DC-SIGN shares the same EPN amino acid motif with langerin, both proteins recognize similar monosaccharide ligands. While langerin was reported to be protective against HIV infections [134], DC-SIGN promotes viral dissemination via a process called *trans*-infection. Targeting DC-SIGN is therefore of interest to stop the transmission of HIV [135].

One common approach to increase affinity for DC-SIGN is the multivalent presentation of monosaccharide ligands. Following such an avidity-driven strategy, a dodecavalent fuco-dendrimer with a 420-fold potency increase compared to fucose was reported [136]. However, unspecific binding to langerin due to its similar binding specificity imposes a selectivity issue. GlcNAc is recognized by both C-type lectins but sulfation of position six and replacement of the *N*-acetyl group by a *N*-sulfate led to a favored recognition of the negatively charged compound **18** by langerin [125[•]]. The development of positively charged amino species in the pseudo-1,2-mannobioside **19** favored the selectivity toward DC-SIGN ($\text{IC}_{50} = 254$ μM ; (langerin $\text{IC}_{50} > 4400$ μM) [125[•]]. Pseudo-1,2-mannobiosides were shown to bind to the carbohydrate recognition domain in DC-SIGN using X-ray crystallography [137]. As an alternative approach to

Figure 4



Allosteric (**15**) and carbohydrate-binding site directed (**16-27**) mammalian lectin antagonists.

generate specificity, a recent report highlighted the presence of five secondary binding sites on DC-SIGN. These sites recognize drug-like compounds unrelated to carbohydrates, and hence constitute a potential starting point for future development [138*].

Dectin-1, a mammalian lectin of the innate immune system, recognizes β -glucans found on fungal cell walls and is able to function as a PRR in fungal-infection [124]. Liposomes carrying the currently used antifungal drug

amphotericin B intercalated into the lipid membrane reduce the antifungal's toxicity compared to detergent-solubilized drugs. Coating of these liposomes with dectin-1 for the specific targeting toward fungal cells showed a 200-fold higher affinity to those cells than untargeted liposomes [139]. These dectin-modified delivery vehicles also reduced growth and viability of the mold *Aspergillus fumigatus* with higher efficiency and thus provide a new opportunity to fight those resistant and difficult to treat infections.

Selectins

Selectins are a subfamily of the C-type lectins consisting of three single-chain transmembrane glycoproteins, which are found on endothelial cells (E-selectin or CD62E), leukocytes (L-selectin or CD62L) and platelets (P-selectin or CD62P). They are involved in constitutive lymphocyte homing, chronic and acute inflammation processes and their minimal common binding epitope is the blood group antigen sialyl Lewis X (sLe^x). [140]

In accordance with the bioactive conformation of the tetrasaccharide sLe^x for E-selectin, this carbohydrate lead was successively optimized in a series of papers from Ernst and co-workers [141–145]. NMR screening of fragments allowed the identification of a second site binder and upon merging with the first site sLe^x mimic, 30 nM lectin antagonists were obtained from a 1 mM lead [146]. Subsequent addressing of the additional sulfate-binding domain in P-selectins/L-selectins led to the successful pan-selectin antagonist Rivipansel (GMI-1070, **20**) out of the development program by Ernst and Magnani that started in the mid-1990s, despite the common fashion to drop selectin research in pharmaceutical industry in the early 2000s [147]. Since June 2015, Rivipansel is in clinical phase III studies against vaso-occlusive anemia in hospitalized subjects with sickle cell disease (trial end date: June 2019, clinicaltrials.gov Identifier: NCT02187003).

Mincle

Mincle has been identified as a C-type lectin receptor of the innate immune system with glycolipid binding specificity that plays an important role in infection by mycobacteria. Mincle binds the mycobacterial glycolipid trehalose dimycolate [20,21] and has recently been addressed by a number of groups describing synthetic molecules based on the bacterial glycolipid [148^{••},149,150,151].

Galectins

Galectin-3, the best described member of the galectin family, is involved in many biological processes, *inter alia*, cell growth, cell adhesion and apoptosis. Consequently, it plays an important role in many diseases, among them are cancer, inflammation, fibrosis, heart disease and stroke [152–154]. For that reason, galectin-3 became an important drug target, recently reviewed by Cagnoni *et al.* [11].

Symmetric C3-aryltriazolyl-substituted thiodigalactosides have shown high affinities for galectin-3 down to $K_d = 1\text{--}2$ nM. However, most of the compounds also bound to galectin-1 raising concerns about the specificity (e.g.: **21**, K_d (galectin-1) = 69 nM; K_d (galectin-3) = 2.3 nM). After combining C3 aryltriazolyl groups with O3-coumaryl groups into asymmetrical thiodigalactosides the selectivity toward galectin-3 increased: specificity of compound **22** toward galectin-3 was achieved with a high affinity (K_d (galectin-1) = 340 nM; K_d (galectin-3) = 7.5 nM) [155^{••}]. Dicoumaryl digalactoside **23** (K_d (galectin-1) = 16 μ M; K_d (galectin-

3) = 91 nM) was then analyzed *in vivo* in mice against bleomycin-induced lung fibrosis. At a dose of 3.5 mg/kg of digalactoside **23** the fibrosis score could be reduced but no effect on the inflammatory score was observed [156]. TD139 (**24**) is a derivative of **21** with a single fluorine atom in *meta*-position of the phenyl rings which is in clinical trials phase II as a galectin-3 inhibitor in idiopathic pulmonary fibrosis since February 2019 using the pulmonary route of administration (www.clinicaltrials.gov, NCT03832946) [157,158]. Oral administration of these disaccharides is impeded by their poor membrane permeability. Currently, various research groups are optimizing this property and a new galectin-inhibitor class with only one sugar residue and low nanomolar affinity was discovered, for example, **25**, $K_d = 37$ nM [159].

Siglecs

A number of siglecs have attracted the attention in the past decades and several antibodies targeting siglecs are approved drugs or in clinical trials [160,161]. Many publications report the development of antagonists for siglec-4, also called myelin-associated glycoprotein (MAG) [162–164]. This protein is important for glial scar formation after central nervous system lesions and inhibition of MAG is considered one therapeutic approach to prevent scar formation and enable axonal regeneration [165,166].

Siglec-2 (CD22) is a target receptor in anti-cancer therapy of lymphoma, leukemia as well as in the treatment of autoimmune diseases such as lupus and rheumatoid arthritis [167]. Biphenylcarboxamidated sialic acid derivative **26** ($IC_{50} = 2$ nM) was developed with an over 500 000-fold stronger binding affinity compared to the minimal siglec ligand α Me-Neu5Ac (**27**, $IC_{50} = 1.5$ mM) against siglec-2 [168^{••}]. Despite the fact that this protein is a monomeric protein, divalent or trivalent *N*-glycans show a very high affinity in the low nM/high pM range. The group by Paulson suggest that this high affinity in their assays originates from simultaneous binding to several CD22 lectins clustering on the cell surface within 30–50 Å to each other [169^{••}].

Conclusions

Lectins are a large family of proteins that are present in each domain of life. These carbohydrate-binding proteins possess numerous functions, both intracellularly and outside the cell. Research toward lectin antagonists has developed rapidly over the past two decades focusing on lectins from selected fields, mainly related to immunity and infection involving mammalian lectins and those from pathogenic bacteria and viruses. The largest block of literature focusses on the assembly of native carbohydrates onto a plethora of different multivalent scaffolds. With some important exceptions discussed here, these publications usually center around the chemical synthesis and compounds are only evaluated in a target-binding assay and not employed further for questions of chemical biology and drug research.

However, in the last decade, a number of strategies toward glycomimetic lectin antagonists has been published that led to drug-like structures which proved equally useful in chemical biology research and early preclinical drug discovery. Antibacterial glycomimetic drugs applied alone or in combination with conventional antibiotics will provide new effective therapies for multi-resistant bacterial infections. And because of an increasing resistance toward established drugs and the absence of effective drugs against several, so far untreated viruses, viral lectins have become attractive targets in recent years and further research will likely yield new tools for chemical biology and drug therapy. Despite the intrinsic difficulty of developing probes/therapeutics for these low affinity carbohydrate–protein interactions, the field is developing rapidly and the first lectin antagonist currently in phase III clinical trials is GMI-1070 (20, Figure 4).

Many new lectins are being uncovered every year providing a large playground for new lectin antagonists for chemical biology and potentially as therapeutic targets. Lectins from other organisms, such as fungi or bacteria that are not pathogenic to humans are active areas of research. It will be interesting to probe, for example, fungal lectins [22,23,170,171] with a distinct specificity for methylated glycans or those of bacteria [172–174] that live in symbiosis with nematodes and kill invaded insects. Furthermore, a large number of bacterial adhesins in pathogenic bacteria are being uncovered, for example, the *Burkholderia* lectins [175–178] or carbohydrate binding adhesins from *Salmonella enterica* [179], and thus, there is a bright future for the chemical biology of lectin antagonists ahead.

Conflict of interest statement

Nothing declared.

Acknowledgements

The authors thank Dr. Christoph Rademacher for constructive comments on the manuscript. We further acknowledge funding by the Helmholtz Association (VH-NG-934).

References and recommended reading

Papers of particular interest, published within the period of review, have been highlighted as:

- of special interest
- of outstanding interest

1. Cummings RD, Schnaar RL, Esko JD, Drickamer K, Taylor ME: **Principles of glycan recognition**. In *Essentials of Glycobiology*. Edited by Varki A, Cummings RD, Esko JD, Stanley P, Hart GW, Aebi M, Darvill AG, Kinoshita T, Packer NH, Prestegard JH, Schnaar RL, Seeberger PH. Cold Spring Harbor Laboratory Press; 2015.
2. Lis H, Sharon N: **Lectins: carbohydrate-specific proteins that mediate cellular recognition**. *Chem Rev* 1998, **98**:637–674.
3. Sharon N: **Carbohydrates as future anti-adhesion drugs for infectious diseases**. *Biochim Biophys Acta* 2006, **1760**:527–537.
4. Rodrigues JA, Acosta-Serrano A, Aebi M, Ferguson MAJ, Routier FH, Schiller I, Soares S, Spencer D, Titz A, Wilson IBH, Izquierdo L: **Parasite glycobiology: a bittersweet symphony**. *PLoS Pathog* 2015, **11**:e1005169.
5. Thompson AJ, de Vries RP, Paulson JC: **Virus recognition of glycan receptors**. *Curr Opin Virol* 2019, **34**:117–129.
6. van Kooyk Y, Rabinovich GA: **Protein-glycan interactions in the control of innate and adaptive immune responses**. *Nat Immunol* 2008, **9**:593–601.
7. Drickamer K, Taylor ME: **Recent insights into structures and functions of C-type lectins in the immune system**. *Curr Opin Struct Biol* 2015, **34**:26–34.
8. Dam TK, Brewer CF: **Lectins as pattern recognition molecules: the effects of epitope density in innate immunity**. *Glycobiology* 2010, **20**:270–279.
9. McEver RP: **Selectins: initiators of leucocyte adhesion and signalling at the vascular wall**. *Cardiovasc Res* 2015, **107**:331–339.
10. Borsig L: **Selectins in cancer immunity**. *Glycobiology* 2018, **28**:648–655.
11. Cagnoni AJ, Pérez Sáez JM, Rabinovich GA, Mariño KV: **Turning-off signaling by siglecs, selectins, and galectins: chemical inhibition of glycan-dependent interactions in cancer**. *Front Oncol* 2016, **6**:109.
12. Varki A, Gagneux P: **Biological functions of glycans**. In *Essentials of Glycobiology*. Edited by Varki A, Cummings RD, Esko JD, Stanley P, Hart GW, Aebi M, Darvill AG, Kinoshita T, Packer NH, Prestegard JH, Schnaar RL, Seeberger PH. Cold Spring Harbor Laboratory Press; 2015.
13. Fujita T: **Evolution of the lectin–complement pathway and its role in innate immunity**. *Nat Rev Immunol* 2002, **2**:346–353.
14. Hoffmann-Sommergruber K, Paschinger K, Wilson IBH: **Glycomarkers in parasitic infections and allergy**. *Biochem Soc Trans* 2011, **39**:360–364.
15. Moran AP: **Molecular mimicry of host glycosylated structures by bacteria**. In *Microbial Glycobiology*. Edited by Holst O, Brennan PJ, von Itzstein M. Academic Press; 2010:847–870.
16. Comstock LE, Kasper DL: **Bacterial glycans: key mediators of diverse host immune responses**. *Cell* 2006, **126**:847–850.
17. Perret S, Sabin C, Dumon C, Pokorná M, Gautier C, Galanina O, Ilija S, Bovin N, Nicaise M, Desmadril M *et al.*: **Structural basis for the interaction between human milk oligosaccharides and the bacterial lectin PA-IIL of *Pseudomonas aeruginosa***. *Biochem J* 2005, **389**:325–332.
18. Sommer R, Paulson JC, Titz A, Varrot A, Wagner S, Khaledi A, Häussler S, Nycholat CM, Imberty A: **The virulence factor LecB varies in clinical isolates: consequences for ligand binding and drug discovery**. *Chem Sci* 2016, **7**:4990–5001.
19. Guo Y, Feinberg H, Conroy E, Mitchell DA, Alvarez R, Blixt O, Taylor ME, Weis WI, Drickamer K: **Structural basis for distinct ligand-binding and targeting properties of the receptors DC-SIGN and DC-SIGNR**. *Nat Struct Mol Biol* 2004, **11**:591–598.
20. Williams SJ: **Sensing lipids with mincle: structure and function**. *Front Immunol* 2017, **8**:1662.
21. Furukawa A, Kamishikiryō J, Mori D, Toyonaga K, Okabe Y, Toji A, Kanda R, Miyake Y, Ose T, Yamasaki S, Maenaka K: **Structural analysis for glycolipid recognition by the C-type lectins Mincle and MCL**. *Proc Natl Acad Sci U S A* 2013, **110**:17438–17443.
22. Wohlschlagler T, Butschi A, Grassi P, Sutov G, Gauss R, Hauck D, Schmieder SS, Knobel M, Titz A, Dell A, Haslam SM, Hengartner MO, Aebi M, Künzler M: **Methylated glycans as conserved targets of animal and fungal innate defense**. *Proc Natl Acad Sci U S A* 2014, **111**:E2787–E2796.
23. Sommer R, Makshakova ON, Wohlschlagler T, Hutin S, Marsh M, Titz A, Künzler M, Varrot A: **Crystal structures of fungal tectonin in complex with O-methylated glycans suggest key role in innate immune defense**. *Structure* 2018, **26**:391–402.e4.
24. Wilkins PP, Moore KL, McEver RP, Cummings RD: **Tyrosine sulfation of P-selectin glycoprotein ligand-1 is required for**

- high affinity binding to P-selectin.** *J Biol Chem* 1995, **270**:22677-22680.
25. Dahms NM, Olson LJ, Kim J-JP: **Strategies for carbohydrate recognition by the mannose 6-phosphate receptors.** *Glycobiology* 2008, **18**:664-678.
26. Weis WI, Drickamer K: **Structural basis of lectin-carbohydrate recognition.** *Annu Rev Biochem* 1996, **65**:441-473.
27. Ernst B, Magnani JL: **From carbohydrate leads to glycomimetic drugs.** *Nat Rev Drug Discov* 2009, **8**:661-677.
28. Cecioni S, Imberty A, Vidal S: **Glycomimetics versus multivalent glycoconjugates for the design of high affinity lectin ligands.** *Chem Rev* 2015, **115**:525-561.
29. Mydock-McGrane L, Cusumano Z, Han Z, Binkley J, Kostakioti M, Hannan T, Pinkner JS, Klein R, Kalas V, Crowley J et al.: **Antivirulence C-mannosides as antibiotic-sparing, oral therapeutics for urinary tract infections.** *J Med Chem* 2016, **59**:9390-9408.
- Design, synthesis, *in vitro* and *in vivo* evaluation of the new class of C-mannosides as FimH inhibitors. The lead compounds showed improved PK and metabolic stability compared to O-mannosides and high efficacy in mouse UTI model.
30. Sattigeri JA, Garg M, Bhateja P, Soni A, Rauf ARA, Gupta M, Deshmukh MS, Jain T, Alekar N, Barman TK et al.: **Synthesis and evaluation of thiomannosides, potent and orally active FimH inhibitors.** *Bioorg Med Chem Lett* 2018, **28**:2993-2997.
31. Kalas V, Hibbing ME, Maddirala AR, Chugani R, Pinkner JS, Mydock-McGrane LK, Conover MS, Janetka JW, Hultgren SJ: **Structure-based discovery of glycomimetic FimH ligands as inhibitors of bacterial adhesion during urinary tract infection.** *Proc Natl Acad Sci U S A* 2018, **115**:E2819-E2828.
32. Wagner S, Hauck D, Hoffmann M, Sommer R, Joachim I, Müller R, Imberty A, Varrot A, Titz A: **Covalent lectin inhibition and application in bacterial biofilm imaging.** *Angew Chem—Int Ed* 2017, **56**:16559-16564.
- Design and synthesis of the first covalent lectin inhibitor. The covalent inhibitor targeting a cysteine residue of LecA was conjugated to fluorescein and used for LecA-specific staining of *P. aeruginosa* biofilm aggregates.
33. Johansson EMV, Cruz SA, Kolomiets E, Buts L, Kadam RU, Cacciarini M, Bartels KM, Diggle SP, Cámara M, Williams P et al.: **Inhibition and dispersion of *Pseudomonas aeruginosa* biofilms by glycopeptide dendrimers targeting the fucose-specific lectin LecB.** *Chem Biol* 2008, **15**:1249-1257.
34. Sommer R, Wagner S, Rox K, Varrot A, Hauck D, Wamhoff EC, Schreiber J, Ryckmans T, Brunner T, Rademacher C et al.: **Glycomimetic, orally bioavailable lectin inhibitors block biofilm formation of *Pseudomonas aeruginosa*.** *J Am Chem Soc* 2018, **140**:2537-2545.
- Development of small molecule LecB inhibitors with high potency, excellent receptor binding kinetics, thermodynamics, selectivity, and pharmacokinetic properties. These glycomimetic inhibitors showed inhibition of *P. aeruginosa* biofilm formation *in vitro* and are promising leads for drug development.
35. Nishikawa K, Watanabe M, Kita E, Igai K, Omata K, Yaffe MB, Natori Y: **A multivalent peptide library approach identifies a novel Shiga toxin inhibitor that induces aberrant cellular transport of the toxin.** *FASEB J* 2006, **20**:2597-2599.
36. Fu O, Pukin AV, Vanufford HCQ, Branson TR, Thies-Weesie DME, Turnbull WB, Visser GM, Pieters RJ: **Tetra-versus pentavalent inhibitors of cholera toxin.** *Chem Open* 2015, **4**:471-477.
37. Han X, Shi Y, Si L, Fan Z, Wang H, Xu R, Jiao P, Meng K, Tian Z, Zhou X et al.: **Design, synthesis and biological activity evaluation of novel conjugated sialic acid and pentacyclic triterpene derivatives as anti-influenza entry inhibitors.** *MedChemComm* 2016, **7**:1932-1945.
38. Wang H, Xu R, Shi Y, Si L, Jiao P, Fan Z, Han X, Wu X, Zhou X, Yu F et al.: **Design, synthesis and biological evaluation of novel l-ascorbic acid-conjugated pentacyclic triterpene derivatives as potential influenza virus entry inhibitors.** *Eur J Med Chem* 2016, **110**:376-388.
39. Yu M, Si L, Wang Y, Wu Y, Yu F, Jiao P, Shi Y, Wang H, Xiao S, Fu G et al.: **Discovery of pentacyclic triterpenoids as potential entry inhibitors of influenza viruses.** *J Med Chem* 2014, **57**:10058-10071.
40. Yamabe M, Kaihatsu K, Ebara Y: **Sialyllactose-modified three-way junction DNA as binding inhibitor of influenza virus hemagglutinin.** *Bioconjug Chem* 2018, **29**:1490-1494.
- Sialic acid presented on a three-way junction DNA matches the hemagglutinin receptor binding site. The authors studied the structure activity relationship and showed highly active hemagglutinin inhibitors.
41. Yamabe M, Fujita A, Kaihatsu K, Ebara Y: **Synthesis of neuraminidase-resistant sialoside-modified three-way junction DNA and its binding ability to various influenza viruses.** *Carbohydr Res* 2019, **474**:43-50.
- As a follow-up study of Ref. 40, the introduction of a S-glycosidic bond instead of an O-glycosidic bond increased the stability against neuraminidase.
42. Strauch E-M, Bernard SM, La D, Bohn AJ, Lee PS, Anderson CE, Nieuwsma T, Holstein CA, Garcia NK, Hooper KA et al.: **Computational design of trimeric influenza-neutralizing proteins targeting the hemagglutinin receptor binding site.** *Nat Biotechnol* 2017, **35**:667-671.
- A highly avid trimeric protein, specifically *in silico* designed to match the binding site architecture of hemagglutinin. The resulting hemagglutinin inhibitor shows prophylactic and therapeutic activity against H3N2 in a mouse model.
43. Guillon P, Dirr L, El-Deeb IM, Winger M, Bailly B, Haselhorst T, Dyason JC, Von Itzstein M: **Structure-guided discovery of potent and dual-acting human parainfluenza virus haemagglutinin-neuraminidase inhibitors.** *Nat Commun* 2014, **5**:5268.
44. Dirr L, El-Deeb IM, Chavas LMG, Guillon P, Von Itzstein M: **The impact of the butterfly effect on human parainfluenza virus haemagglutinin-neuraminidase inhibitor design.** *Sci Rep* 2017, **7**.
45. Koromyslova A, Tripathi S, Morozov V, Schroten H, Hansman GS: **Human norovirus inhibition by a human milk oligosaccharide.** *Virology* 2017, **508**:81-89.
46. Weichert S, Koromyslova A, Singh BK, Hansman S, Jennewein S, Schroten H, Hansman GS: **Structural basis for norovirus inhibition by human milk oligosaccharides.** *J Virol* 2016, **90**:4843-4848.
47. Koromyslova AD, White PA, Hansman GS: **Treatment of norovirus particles with citrate.** *Virology* 2015, **485**:199-204.
48. Aretz J, Anumala UR, Fuchsberger FF, Molavi N, Ziebart N, Zhang H, Nazaré M, Rademacher C: **Allosteric inhibition of a mammalian lectin.** *J Am Chem Soc* 2018, **140**:14915-14925.
- The first allosteric inhibition of a mammalian lectin (langerin) using thiazolopyrimidines to binding affinities in a double-digit micromolar range.
49. Mcever RP: **Selectins: initiators of leucocyte adhesion and signalling at the vascular wall.** *Cardiovasc Res* 2015, **107**:331-339.
50. Clatworthy AE, Pierson E, Hung DT: **Targeting virulence: a new paradigm for antimicrobial therapy.** *Nat Chem Biol* 2007, **3**:541-548.
51. Davies D: **Understanding biofilm resistance to antibacterial agents.** *Nat Rev Drug Discov* 2003, **2**:114-122.
52. Hung C, Bouckaert J, Hung D, Pinkner J, Widberg C, Defusco A, Auguste CG, Strouse R, Langermann S, Waksman G, Hultgren SJ: **Structural basis of tropism of *Escherichia coli* to the bladder during urinary tract infection.** *Mol Microbiol* 2002, **44**:903-915.
53. Hartmann M, Lindhorst TK: **The bacterial lectin FimH, a target for drug discovery – carbohydrate inhibitors of Type 1 fimbriae-mediated bacterial adhesion.** *Eur J Org Chem* 2011, **2011**:3609.
54. Conover MS, Ruer S, Taganna J, Kalas V, De Greve H, Pinkner JS, Dodson KW, Remaut H, Hultgren SJ: **Inflammation-induced adhesin-receptor interaction provides a fitness advantage to uropathogenic *E. coli* during chronic infection.** *Cell Host Microbe* 2016, **20**:482-492.

55. Chen SL, Hung CS, Pinkner JS, Walker JN, Cusumano CK, Li Z, Bouckaert J, Gordon JI, Hultgren SJ: **Positive selection identifies an *in vivo* role for FimH during urinary tract infection in addition to mannose binding.** *Proc Natl Acad Sci U S A* 2009, **106**:22439-22444.
56. Schwartz DJ, Kalas V, Pinkner JS, Chen SL, Spaulding CN, Dodson KW, Hultgren SJ: **Positively selected FimH residues enhance virulence during urinary tract infection by altering FimH conformation.** *Proc Natl Acad Sci U S A* 2013, **110**:15530-15537.
57. Spaulding CN, Klein RD, Ruer S, Kau AL, Schreiber IVHL, Cusumano ZT, Dodson KW, Pinkner JS, Fremont DH, Janetka JW *et al.*: **Selective depletion of uropathogenic *E. coli* from the gut by a FimH antagonist.** *Nature* 2017, **546**:528-532.
58. Firon N, Ashkenazi S, Mirelman D, Ofek I, Sharon N: **Aromatic alpha-glycosides of mannose are powerful inhibitors of the adherence of type 1 fimbriated *Escherichia coli* to yeast and intestinal epithelial cells.** *Infect Immun* 1987, **55**:472-476.
59. Bouckaert J, Berglund J, Schembri M, De Genst E, Cools L, Wührer M, Hung CS, Pinkner J, Slättegård R, Zavialov A *et al.*: **Receptor binding studies disclose a novel class of high-affinity inhibitors of the *Escherichia coli* FimH adhesin.** *Mol Microbiol* 2005, **55**:441-455.
60. Sivignon A, Yan X, Dorta DA, Bonnet R, Bouckaert J, Fleury E, Bernard J, Gouin SG, Darfeuille-Michaud A, Barnich N: **Development of heptylmannoside-based glycoconjugate antiadhesive compounds against adherent-invasive *Escherichia coli* bacteria associated with crohn's disease.** *mBio* 2015, **6**:1-9.
61. Chalopin T, Alvarez Dorta D, Sivignon A, Caudan M, Dumych TI, Bilyy RO, Deniaud D, Barnich N, Bouckaert J, Gouin SG: **Second generation of thiazolymannosides, FimH antagonists for *E. coli*-induced Crohn's disease.** *Org Biomol Chem* 2016, **14**:3913-3925.
62. Jarvis C, Han DZ, Kalas V, Klein R, Pinkner JS, Ford B, Binkley J, Cusumano CK, Cusumano Z, Mydock-McGrane L *et al.*: **Antivirulence isoquinolone mannosides: optimization of the biaryl aglycone for FimH lectin binding affinity and efficacy in the treatment of chronic UTI.** *ChemMedChem* 2016, **11**:367-373.
63. Schönemann W, Cramer J, Mühlethaler T, Fiege B, Silbermann M, Rabbani S, Dätwyler P, Zihlmann P, Jakob RP, Sager CP *et al.*: **Improvement of aglycone π -stacking yields nanomolar to sub-nanomolar FimH antagonists.** *ChemMedChem* 2019, **14**:749-757.
64. Alvarez Dorta D, Sivignon A, Chalopin T, Dumych TI, Roos G, Bilyy RO, Deniaud D, Krammer EM, De Ruyck J, Lensink MF *et al.*: **The antiadhesive strategy in crohn's disease: orally active mannosides to decolonize pathogenic *Escherichia coli* from the gut.** *ChemBioChem* 2016, **17**:936-952.
65. Schönemann W, Kleeb S, Dätwyler P, Schwardt O, Ernst B: **Prodruggability of carbohydrates — oral FimH antagonists.** *Can J Chem* 2016, **94**:909-919.
66. Kleeb S, Jiang X, Frei P, Sigl A, Bezençon J, Bamberger K, Schwardt O, Ernst B: **FimH antagonists: phosphate prodrugs improve oral bioavailability.** *J Med Chem* 2016, **59**:3163-3182.
- Phosphate-prodrugs have been synthesized and increased drug availability at the site of infection.
67. Mydock-McGrane LK, Hannan TJ, Janetka JW: **Rational design strategies for FimH antagonists: new drugs on the horizon for urinary tract infection and Crohn's disease.** *Expert Opin Drug Discov* 2017, **12**:711-731.
68. Maddirala AR, Klein R, Pinkner JS, Kalas V, Hultgren SJ, Janetka JW: **Biphenyl Gal and GalNAc FmIH lectin antagonists of uropathogenic *E. coli* (UPEC): optimization through iterative rational drug design.** *J Med Chem* 2019, **62**:467-479.
- Structure-guided optimization was used to develop very potent FmIH inhibitors with excellent metabolic stability and good PK, but low oral bioavailability. This represents a good starting point for drug development for the recently identified target FmIH.
69. Tielker D, Hacker S, Loris R, Strathmann M, Wingender J, Wilhelm S, Rosenau F, Jaeger KE: ***Pseudomonas aeruginosa* lectin LecB is located in the outer membrane and is involved in biofilm formation.** *Microbiology* 2005, **151**:1313-1323.
70. Diggie SP, Stacey RE, Dodd C, Cámara M, Williams P, Winzer K: **The galactophilic lectin, LecA, contributes to biofilm development in *Pseudomonas aeruginosa*.** *Environ Microbiol* 2006, **8**:1095-1104.
71. Gilboa-Garber N: ***Pseudomonas aeruginosa* lectins.** *Methods Enzymol* 1982, **83**:378-385.
72. Wagner S, Sommer R, Hinsberger S, Lu C, Hartmann RW, Empting M, Titz A: **Novel strategies for the treatment of *Pseudomonas aeruginosa* infections.** *J Med Chem* 2016, **59**:5929-5969.
73. Calvert MB, Jumde VR, Titz A: **Pathoblockers or antivirulence drugs as a new option for the treatment of bacterial infections.** *Beilstein J Org Chem* 2018, **14**:2607-2617.
74. Titz A: **Carbohydrate-based anti-virulence compounds against chronic *Pseudomonas aeruginosa* infections with a focus on small molecules.** *Top Med Chem* 2014, **12**:169-186.
75. Blanchard B, Nurisso A, Hollville E, Tétaud C, Wiels J, Pokorná M, Wimmerová M, Varrot A, Imberty A: **Structural basis of the preferential binding for globo-series glycosphingolipids displayed by *Pseudomonas aeruginosa* Lectin I.** *J Mol Biol* 2008, **383**:837-853.
76. Eierhoff T, Bastian B, Thuenauer R, Madl J, Audfray A, Aigal S, Juillot S, Rydell GE, Muller S, de Bentzmann S *et al.*: **A lipid zipper triggers bacterial invasion.** *Proc Natl Acad Sci U S A* 2014, **111**:12895-12900.
77. Imberty A, Wimmerová M, Mitchell EP, Gilboa-Garber N: **Structures of the lectins from *Pseudomonas aeruginosa*: insights into the molecular basis for host glycan recognition.** *Microbes Infect* 2004, **6**:221-228.
78. Bernardi A, Jiménez-Barbero J, Casnati A, De Castro C, Darbre T, Fieschi F, Finne J, Funken H, Jaeger K-E, Lahmann M *et al.*: **Multivalent glycoconjugates as anti-pathogenic agents.** *Chem Soc Rev* 2013, **42**:4709-4727.
79. Boukerb AM, Rousset A, Galanos N, Méar JB, Thépaut M, Grandjean T, Gillon E, Cecioni S, Abderrahmen C, Faure K *et al.*: **Antiadhesive properties of glycoclusters against *Pseudomonas aeruginosa* lung infection.** *J Med Chem* 2014, **57**:10275-10289.
- Lectin-targeting clusters show beneficial effects in a *Pseudomonas aeruginosa* co-institution mouse model of acute lung infection.
80. Kadam RU, Bergmann M, Hurley M, Garg D, Cacciarini M, Swiderska MA, Nativi C, Sattler M, Smyth AR, Williams P *et al.*: **A Glycopeptide dendrimer inhibitor of the galactose-specific lectin LecA and of *Pseudomonas aeruginosa* biofilms.** *Angew Chem Int Ed* 2011, **50**:10631-10635.
81. Michaud G, Visini R, Bergmann M, Salerno G, Bosco R, Gillon E, Richichi B, Nativi C, Imberty A, Stocker A *et al.*: **Overcoming antibiotic resistance in *Pseudomonas aeruginosa* biofilms using glycopeptide dendrimers.** *Chem Sci* 2016, **7**:166-182.
- Lectin-antagonistic peptide dendrimers targeting LecB restored efficacy of the antibiotic tobramycin in biofilms of *Pseudomonas aeruginosa*.
82. Visini R, Jin X, Bergmann M, Michaud G, Pertici F, Fu O, Pukin A, Branson TR, Thies-Weesie DME, Kemmink J *et al.*: **Structural insight into multivalent galactoside binding to *Pseudomonas aeruginosa* Lectin LecA.** *ACS Chem Biol* 2015, **10**:2455-2462.
83. Ligeour C, Vidal O, Dupin L, Casoni F, Gillon E, Meyer A, Vidal S, Vergoten G, Lacroix J, Souteyrand E *et al.*: **Mannose-centered aromatic galactoclusters inhibit the biofilm formation of *Pseudomonas aeruginosa*.** *Org Biomol Chem* 2015, **13**:8433-8444.
84. Pertici F, Pieters RJ: **Potent divalent inhibitors with rigid glucose click spacers for *Pseudomonas aeruginosa* lectin LecA.** *Chem Commun* 2012, **48**:4008-4010.
- Synthesis of divalent LecA inhibitors using azide-alkyne click chemistry. The most potent divalent inhibitor showed 545-fold increased potency compared to the monovalent alkyne ligand.
85. Yu G, Vicini AC, Pieters RJ: **Assembling of divalent ligands and their effect on divalent binding to *Pseudomonas aeruginosa* lectin LecA.** *J Org Chem* 2019, **84**:2470-2488.

86. Yu G, Thies-Weesie DME, Pieters RJ: **Tetravalent *Pseudomonas aeruginosa* adhesion lectin leca inhibitor for enhanced biofilm inhibition.** *Helv Chim Acta* 2019, **102**:e1900014.
87. Kadam RU, Garg D, Schwartz J, Visini R, Sattler M, Stocker A, Darbre T, Reymond JL: **CH- π “t-shape” interaction with histidine explains binding of aromatic galactosides to *Pseudomonas aeruginosa* lectin LecA.** *ACS Chem Biol* 2013, **8**:1925-1930.
- CH- π interaction between galactoside aryl aglycon and His50 increases ligand binding potency. Identification and exploiting such interactions may help with design of small molecule inhibitors.
88. Rodrigue J, Ganne G, Blanchard B, Saucier C, Giguère D, Shiao TC, Varrot A, Imberty A, Roy R: **Aromatic thioglycoside inhibitors against the virulence factor LecA from *Pseudomonas aeruginosa*.** *Org Biomol Chem* 2013, **11**:6906-6918.
89. Joachim I, Rikker S, Hauck D, Ponader D, Boden S, Sommer R, Hartmann L, Titz A: **Development and optimization of a competitive binding assay for the galactophilic low affinity lectin LecA from: *Pseudomonas aeruginosa*.** *Org Biomol Chem* 2016, **14**:7933-7948.
90. Mitchell E, Houles C, Sudakevitz D, Wimmerova M, Gautier C, Pérez S, Wu AM, Gilboa-Garber N, Imberty A: **Structural basis for oligosaccharide-mediated adhesion of *Pseudomonas aeruginosa* in the lungs of cystic fibrosis patients.** *Nat Struct Biol* 2002, **9**:918-921.
91. Boukerb AM, Decor A, Ribun S, Tabaroni R, Rousset A, Commin L, Buff S, Doléans-Jordheim A, Vidal S, Varrot A et al.: **Genomic rearrangements and functional diversification of lecA and lecB lectin-coding regions impacting the efficacy of glycomimetics directed against *Pseudomonas aeruginosa*.** *Front Microbiol* 2016, **7**:1-16.
92. Hauck D, Joachim I, Frommeyer B, Varrot A, Philipp B, Möller HM, Imberty A, Exner TE, Titz A: **Discovery of two classes of potent glycomimetic inhibitors of *Pseudomonas aeruginosa* LecB with distinct binding modes.** *ACS Chem Biol* 2013, **8**:1775-1784.
93. Sommer R, Hauck D, Varrot A, Wagner S, Audfray A, Prestel A, Möller HM, Imberty A, Titz A: **Cinnamide derivatives of d-mannose as inhibitors of the bacterial virulence factor LecB from *Pseudomonas aeruginosa*.** *ChemistryOpen* 2015, **4**:756-767.
94. Sommer R, Exner TE, Titz A: **A biophysical study with carbohydrate derivatives explains the molecular basis of monosaccharide selectivity of the *Pseudomonas aeruginosa* lectin lecB.** *PLoS One* 2014, **9**:1-22.
95. Fan E, Merritt EA, Verlinde CLMJ, Hol WGJ: **AB5 toxins: structures and inhibitor design.** *Curr Opin Struct Biol* 2000, **10**:680-686.
96. Kitov PI, Sadowska JM, Mulvey G, Armstrong GD, Ling H, Pannu NS, Read RJ, Bundle DR: **Shiga-like toxins are neutralized by tailored multivalent carbohydrate ligands.** *Nature* 2000, **403**:669-672.
97. Mulvey GL, Marcato P, Kitov PI, Sadowska J, Bundle DR, Armstrong GD: **Assessment in mice of the therapeutic potential of tailored, multivalent shiga toxin carbohydrate ligands.** *J Infect Dis* 2003, **187**:640-649.
98. Nishikawa K, Matsuoka K, Kita E, Okabe N, Mizuguchi M, Hino K, Miyazawa S, Yamasaki C, Aoki J, Takashima S et al.: **A therapeutic agent with oriented carbohydrates for treatment of infections by Shiga toxin-producing *Escherichia coli* O157:H7.** *Proc Natl Acad Sci U S A* 2002, **99**:7669-7674.
99. Watanabe-Takahashi M, Sato T, Dohi T, Noguchi N, Kano F, Murata M, Hamabata T, Natori Y, Nishikawa K: **An orally applicable Shiga toxin neutralizer functions in the intestine to inhibit the intracellular transport of the toxin.** *Infect Immun* 2010, **78**:177-183.
100. Matsuoka K, Nishikawa K, Goshu Y, Koyama T, Hatano K, Matsushita T, Watanabe-Takahashi M, Natori Y, Terunuma D: **Synthetic construction of sugar-amino acid hybrid polymers involving globotriaose or lactose and evaluation of their biological activities against Shiga toxins produced by *Escherichia coli* O157:H7.** *Bioorg Med Chem* 2018, **26**:5792-5803.
101. Cervin J, Wands AM, Casselbrant A, Wu H, Krishnamurthy S, Cvjetkovic A, Estelius J, Dedic B, Sethi A, Wallom KL et al.: **GM1 ganglioside-independent intoxication by Cholera toxin.** *PLoS Pathog* 2018, **14**:e1006862.
102. Merritt EA, Sarfaty S, Feil IK, Hol WGJ: **Structural foundation for the design of receptor antagonists targeting *Escherichia coli* heat-labile enterotoxin.** *Structure* 1997, **5**:1485-1499.
103. Mitchell DD, Pickens JC, Korotkov K, Fan E, Hol WGJ: **3,5-Substituted phenyl galactosides as leads in designing effective cholera toxin antagonists: synthesis and crystallographic studies.** *Bioorg Med Chem* 2004, **12**:907-920.
104. Kumar V, Turnbull WB: **Carbohydrate inhibitors of cholera toxin.** *Beilstein J Org Chem* 2018, **14**:484-498.
105. Wands AM, Cervin J, Huang H, Zhang Y, Youn G, Brautigam CA, Matson Dzebo M, Björklund P, Wallenius V, Bright DK et al.: **Fucosylated molecules competitively interfere with cholera toxin binding to host cells.** *ACS Infect Dis* 2018, **4**:758-770.
- Inhibition of cholera toxin by targeting the neglected fucose binding site compared to the well studied GM1 primary binding site. For the first time, the fucosylated polymers were used to inhibit cholera toxin binding to human cells *in vitro*.
106. Varki A, Schnaar RL, Schauer R: *Sialic Acids and Other Nonulosonic Acids.* Cold Spring Harbor Laboratory Press; 2015.
107. Sauter NK, Bednarski MD, Wurzburg BA, Hanson JE, Whitesides GM, Skehel JJ, Wiley DC: **Hemagglutinins from two influenza virus variants bind to sialic acid derivatives with millimolar dissociation constants: a 500-MHz proton nuclear magnetic resonance study.** *Biochemistry* 1989, **28**:8388-8396.
108. Nizet V, Varki A, Aebi M: **Microbial lectins: hemagglutinins, adhesins, and toxins.** In *Essentials of Glycobiology.* Edited by Varki A, Cummings RD, Esko JD, Stanley P, Hart GW, Aebi M, Darvill AG, Kinoshita T, Packer NH, Prestegard JH, Schnaar RL, Seeberger PH. Cold Spring Harbor Laboratory Press; 2015.
109. Li F, Ma C, Wang J: **Inhibitors targeting the influenza virus hemagglutinin.** *Curr Med Chem* 2015, **22**.
110. Nagao M, Matsubara T, Hoshino Y, Sato T, Miura Y: **Topological design of star glycopolymers for controlling the interaction with the influenza virus.** *Bioconjug Chem* 2019, **30**:1192-1198 <http://dx.doi.org/10.1021/acs.bioconjchem.9b00134>.
111. Kadam RU, Wilson IA: **A small-molecule fragment that emulates binding of receptor and broadly neutralizing antibodies to influenza A hemagglutinin.** *Proc Natl Acad Sci U S A* 2018, **115**:4240-4245.
112. Moscona A: **Entry of parainfluenza virus into cells as a target for interrupting childhood respiratory disease.** *J Clin Invest* 2005, **115**:1688-1698.
113. Robilotti E, Deresinski S, Pinsky BA: **Norovirus.** *Clin Microbiol Rev* 2015, **28**:134-164.
114. Taube S, Mallagaray A, Peters T: **Norovirus, glycans and attachment.** *Curr Opin Virol* 2018, **31**:33-42.
115. Coulet M, Phoithirath P, Allais L, Schilter B: **Pre-clinical safety evaluation of the synthetic human milk, nature-identical, oligosaccharide 2'-O-Fucosyllactose (2'FL).** *Regul Toxicol Pharmacol* 2014, **68**:59-69.
116. Morrow AL, Ruiz-Palacios GM, Altaye M, Jiang X, Lourdes Guerrero M, Meinen-Derr JK, Farkas T, Chaturvedi P, Pickering LK, Newburg DS: **Human milk oligosaccharides are associated with protection against diarrhea in breast-fed infants.** *J Pediatr* 2004, **145**:297-303.
117. Pillai S, Netravali IA, Cariappa A, Mattoo H: **Siglecs and immune regulation.** *Annu Rev Immunol* 2012, **30**:357-392.
118. Macauley MS, Crocker PR, Paulson JC: **Siglec-mediated regulation of immune cell function in disease.** *Nat Rev Immunol* 2014, **14**:653-666.
119. Barondes SH, Cooper DN, Gitt MA, Leffler H: **Galectins. Structure and function of a large family of animal lectins.** *J Biol Chem* 1994, **269**:20807-20810.

120. Thiemann S, Baum LG: **Galectins and immune responses—just how do they do those things they do?** *Annu Rev Immunol* 2016, **34**:243-264.
121. Compagno D, Jaworski FM, Gentilini L, Contrufo G, González Pérez I, Elola MT, Pregi N, Rabinovich GA, Laderach DJ: **Galectins: major signaling modulators inside and outside the cell.** *Curr Mol Med* 2014, **14**:630-651.
122. Rabinovich GA, Toscano MA: **Turning “sweet” on immunity: galectin-glycan interactions in immune tolerance and inflammation.** *Nat Rev Immunol* 2009, **9**:338-352.
123. van den Berg LM, Gringhuis SI, Geijtenbeek TBH: **An evolutionary perspective on C-type lectins in infection and immunity.** *Ann N Y Acad Sci* 2012, **1253**:149-158.
124. Brown GD, Willment JA, Whitehead L: **C-type lectins in immunity and homeostasis.** *Nat Rev Immunol* 2018, **18**:374-389.
125. Porkolab V, Chabrol E, Varga N, Ordanini S, Sutkevičiūtė I, Thépaut M, García-Jiménez MJ, Girard E, Nieto PM, Bernardi A, Fieschi F: **Rational-differential design of highly specific glycomimetic ligands: targeting DC-SIGN and excluding langerin recognition.** *ACS Chem Biol* 2018, **13**:600-608.
- GlcNAc is recognized by both lectins— langerin and DC-SIGN. Selectivity toward langerin was achieved by sulfation on position six.
126. Wilson NJ, Boniface K, Chan JR, McKenzie BS, Blumenschein WM, Mattson JD, Basham B, Smith K, Chen T, Morel F *et al.*: **Development, cytokine profile and function of human interleukin 17-producing helper T cells.** *Nat Immunol* 2007, **8**:950-957.
127. Yang K, Park CG, Cheong C, Bulgheresi S, Zhang S, Zhang P, He Y, Jiang L, Huang H, Ding H *et al.*: **Host Langerin (CD207) is a receptor for *Yersinia pestis* phagocytosis and promotes dissemination.** *Immunol Cell Biol* 2015, **93**:815-824.
128. Ng WC, Londrigan SL, Nasr N, Cunningham AL, Turville S, Brooks AG, Reading PC: **The C-type lectin langerin functions as a receptor for attachment and infectious entry of Influenza A virus.** *J Virol* 2016, **90**:206-221.
129. Idoyaga J, Suda N, Suda K, Park CG, Steinman RM: **Antibody to Langerin/CD207 localizes large numbers of CD8alpha+ dendritic cells to the marginal zone of mouse spleen.** *Proc Natl Acad Sci U S A* 2009, **106**:1524-1529.
130. Flacher V, Tripp CH, Stoitzner P, Haid B, Ebner S, Del Frari B, Koch F, Park CG, Steinman RM, Idoyaga J, Romani N: **Epidermal Langerhans cells rapidly capture and present antigens from C-type lectin-targeting antibodies deposited in the dermis.** *J Invest Dermatol* 2010, **130**:755-762.
131. Zhao J, Liu X, Kao C, Zhang E, Li Q, Zhang F, Linhardt RJ: **Kinetic and structural studies of interactions between glycosaminoglycans and langerin.** *Biochemistry* 2016, **55**:4552-4559.
132. Wamhoff E-C, Schulze J, Bellmann L, Bachem G, Fuchsberger FF, Rademacher J, Hermann M: **A specific, glycomimetic Langerin ligand for human Langerhans cell targeting.** *bioRxiv* 2018 <http://dx.doi.org/10.1101/286021>.
- Intracellular trafficking of synthesized langerin targeting liposomes was observed in Langerin+ COS-7 cells by confocal microscopy. It paves the way for trans-cutaneous vaccinations using these liposomes in therapeutic applications.
133. Wamhoff E-C, Schulze J, Bellmann L, Rentsch M, Bachem G, Fuchsberger FF, Rademacher J, Hermann M, Del Frari B, van Dalen R *et al.*: **A specific, glycomimetic langerin ligand for human langerhans cell targeting.** *ACS Cent Sci* 2019, **5**:808-820 <http://dx.doi.org/10.1021/acscentsci.9b00093>.
- Intracellular trafficking of synthesized langerin targeting liposomes was observed in Langerin+ COS-7 cells by confocal microscopy. It paves the way for trans-cutaneous vaccinations using these liposomes in therapeutic applications.
134. de Witte L, Nabatov A, Pion M, Fluitsma D, de Jong MAWP, de Gruijl T, Piguat V, van Kooyk Y, Geijtenbeek TBH: **Langerin is a natural barrier to HIV-1 transmission by Langerhans cells.** *Nat Med* 2007, **13**:367-371.
135. Geijtenbeek TB, Kwon DS, Torensma R, van Vliet SJ, van Duijnhoven GC, Middel J, Cornelissen IL, Nottet HS, KewalRamani VN, Littman DR *et al.*: **DC-SIGN, a dendritic cell-specific HIV-1-binding protein that enhances trans-infection of T cells.** *Cell* 2000, **100**:587-597.
136. Bertolotti B, Sutkevičiūtė I, Ambrosini M, Ribeiro-Viana R, Rojo J, Fieschi F, Dvořáková H, Kašáková M, Parkan K, Hlaváčková M *et al.*: **Polyvalent C-glycomimetics based on l-fucose or d-mannose as potent DC-SIGN antagonists.** *Org Biomol Chem* 2017, **15**:3995-4004.
137. Thépaut M, Guzzi C, Sutkevičiūtė I, Sattin S, Ribeiro-Viana R, Varga N, Chabrol E, Rojo J, Bernardi A, Angulo J *et al.*: **Structure of a glycomimetic ligand in the carbohydrate recognition domain of C-type Lectin DC-SIGN. Structural requirements for selectivity and ligand design.** *J Am Chem Soc* 2013, **135**:2518-2529.
138. Aretz J, Baukmann H, Shanina E, Hanske J, Wawrzinek R, Zapol'skii VA, Seeberger PH, Kaufmann DE, Rademacher C: **Identification of multiple druggable secondary sites by fragment screening against DC-SIGN.** *Angew Chem Int Ed* 2017, **56**:7292-7296.
- Increased number of druggable pockets on DC-SIGN allows the development of new multivalent compounds with higher binding affinities. The inhibition of the cell-surface receptor DC-SIGN is important due to pathogenic threats.
139. Ambati S, Ferraro AR, Kang SE, Lin J, Lin X, Momany M, Lewis ZA, Meagher RB: **Dectin-1-targeted antifungal liposomes exhibit enhanced efficacy.** *mSphere* 2019, **4**:e00025-19.
140. Ley K: **The role of selectins in inflammation and disease.** *Trends Mol Med* 2003, **9**:263-268.
141. Peters T, Scheffler K, Ernst B, Katopodis A, Magnani JL, Wang WT, Weisemann R: **Determination of the bioactive conformation of the carbohydrate ligand in the E-selectin/Sialyl LewisX complex.** *Angew Chem Int Ed Engl* 1995, **34**:1841-1844.
142. Thoma G, Magnani JL, Patton JT, Ernst B, Jahnke W: **Preorganization of the bioactive conformation of Sialyl LewisX analogues correlates with their affinity to E-selectin.** *Angew Chem Int Ed* 2001, **40**:1941-1945.
143. Norman KE, Anderson GP, Kolb HC, Ley K, Ernst B: **Sialyl Lewis (x) (sLe(x)) and an sLe(x) mimetic, CGP69669A, disrupt E-selectin-dependent leukocyte rolling in vivo.** *Blood* 1998, **91**:475-483.
144. Schwizer D, Patton JT, Cutting B, Smieško M, Wagner B, Kato A, Weckerle C, Binder FPC, Rabbani S, Schwardt O, Magnani JL, Ernst B: **Pre-organization of the core structure of E-selectin antagonists.** *Chem – A Eur J* 2012, **18**:1342-1351.
145. Kolb HC, Ernst B: **Development of tools for the design of selectin antagonists.** *Chem – A Eur J* 1997, **3**:1571-1578.
146. Egger J, Weckerle C, Cutting B, Schwardt O, Rabbani S, Lemme K, Ernst B: **Nanomolar E-selectin antagonists with prolonged half-lives by a fragment-based approach.** *J Am Chem Soc* 2013, **135**:9820-9828.
147. Chang J, Patton JT, Sarkar A, Ernst B, Magnani JL, Frenette PS: **GMI-1070, a novel pan-selectin antagonist, reverses acute vascular occlusions in sickle cell mice.** *Blood* 2010, **116**:1779-1786.
148. Decout A, Silva-Gomes S, Drocourt D, Barbe S, André I, Cueto FJ, Lioux T, Sancho D, Pérouzel E, Vercellone A *et al.*: **Rational design of adjuvants targeting the C-type lectin Mincle.** *Proc Natl Acad Sci U S A* 2017, **114**:2675-2680.
- Structure-based design of mincle inhibitors as promising vaccine adjuvants.
149. Feinberg H, Rambaruth NDS, Jégouzo SAF, Jacobsen KM, Djurhuus R, Poulsen TB, Weis WI, Taylor ME, Drickamer K: **Binding sites for acylated trehalose analogs of glycolipid ligands on an extended carbohydrate recognition domain of the macrophage receptor mincle.** *J Biol Chem* 2016, **291**:21222-21233.
150. Matsumaru T, Ikeno R, Shuchi Y, Iwamatsu T, Tadokoro T, Yamasaki S, Fujimoto Y, Furukawa A, Maenaka K: **Synthesis of glycerolipids containing simple linear acyl chains or aromatic rings and evaluation of their Mincle signaling activity.** *Chem Commun (Camb)* 2019, **55**:711-714.

151. Bird JH, Khan AA, Nishimura N, Yamasaki S, Timmer MSM, Stocker BL: **Synthesis of branched trehalose glycolipids and their mincle agonist activity.** *J Org Chem* 2018, **83**:7593-7605.
152. Dumić J, Dabelić S, Flögel M: **Galectin-3: an open-ended story.** *Biochim Biophys Acta – Gen Subj* 2006, **1760**:616-635.
153. Sharma UC, Pokharel S, van Brakel TJ, van Berlo JH, Cleutjens JPM, Schroen B, Andre' S, Crijs HJGM, Gabius H-J, Maessen J, Pinto YM: **Galectin-3 marks activated macrophages in failure-prone hypertrophied hearts and contributes to cardiac dysfunction.** *Circulation* 2004, **110**:3121-3123128.
154. Raimond J, Zimonjic DB, Mignon C, Mattei M-G, Popescu NC, Monsigny M, Legrand A: **Mapping of the galectin-3 gene (LGALS3) to human chromosome 14 at region 14q21-22.** *Mamm Genome* 1997, **8**:706-707.
155. Peterson K, Kumar R, Stenström O, Verma P, Verma PR, Håkansson M, Kahl-Knutsson B, Zetterberg F, Leffler H, Akke M et al.: **Systematic tuning of fluoro-galectin-3 interactions provides thiodigalactoside derivatives with single-digit nM affinity and high selectivity.** *J Med Chem* 2018, **61**:1164-1175.
Selectivity for galectin-3 inhibitors over galectin-1 is important for the targeting of galectin-3, for example, in cancer, inflammation and fibrosis. Asymmetric thiodigalactosides were designed and synthesized for the selective inhibition of galectin-3.
156. Rajput VK, MacKinnon A, Mandal S, Collins P, Blanchard H, Leffler H, Sethi T, Schambye H, Mukhopadhyay B, Nilsson UJ: **A selective galactose-coumarin-derived Galectin-3 inhibitor demonstrates involvement of Galectin-3-glycan interactions in a pulmonary fibrosis model.** *J Med Chem* 2016, **59**:8141-8147.
157. Delaine T, Collins P, MacKinnon A, Sharma G, Stegmayr J, Rajput VK, Mandal S, Cumpstey I, Larumbe A, Salameh BA et al.: **Galectin-3-binding glycomimetics that strongly reduce bleomycin-induced lung fibrosis and modulate intracellular glycan recognition.** *ChemBioChem* 2016, **17**:1759-1770.
158. Chen W-S, Cao Z, Leffler H, Nilsson UJ, Panjwani N: **Galectin-3 inhibition by a small-molecule inhibitor reduces both pathological corneal neovascularization and fibrosis.** *Invest Ophthalmol Vis Sci* 2017, **58**:9.
159. Zetterberg FR, Peterson K, Johnsson RE, Brimert T, Håkansson M, Logan DT, Leffler H, Nilsson UJ: **Monosaccharide derivatives with low-nanomolar lectin affinity and high selectivity based on combined fluorine-amide, phenyl-arginine, sulfur- π , and halogen bond interactions.** *ChemMedChem* 2018, **13**:133-137.
160. Angata T, Nycholat CM, Macauley MS: **Therapeutic targeting of siglecs using antibody- and glycan-based approaches.** *Trends Pharmacol Sci* 2015, **36**:645-660.
161. O'Reilly MK, Paulson JC: **Siglecs as targets for therapy in immune cell mediated disease.** *Trends Pharmacol Sci* 2009, **30**:240.
162. Schwardt O, Kelm S, Ernst B: **SIGLEC-4 (MAG) antagonists: from the natural carbohydrate epitope to glycomimetics.** *Top Curr Chem* 2013:151-200.
163. Zaccai NR, Maenaka K, Maenaka T, Crocker PR, Brossmer R, Kelm S, Jones EY: **Structure-guided design of sialic acid-based Siglec inhibitors and crystallographic analysis in complex with sialoadhesin.** *Structure* 2003, **11**:557-567.
164. Zeng Y, Rademacher C, Nycholat CM, Futakawa S, Lemme K, Ernst B, Paulson JC: **High affinity sialoside ligands of myelin associated glycoprotein.** *Bioorg Med Chem Lett* 2011, **21**:5045-5049.
165. Lopez PHH: **Role of myelin-associated glycoprotein (Siglec-4a) in the nervous system.** *Adv Neurobiol* 2014:245-262.
166. Schnaar RL, Collins BE, Wright LP, Kiso M, Tropak MB, Roder JC, Crocker PR: **Myelin-associated glycoprotein binding to gangliosides. Structural specificity and functional implications.** *Ann N Y Acad Sci* 1998, **845**:92-105.
167. Macauley MS, Crocker PR, Paulson JC: **Siglec-mediated regulation of immune cell function in disease.** *Nat Rev Immunol* 2014, **14**:653-666.
168. Prescher H, Schweizer A, Kuhfeldt E, Nitschke L, Brossmer R: **Discovery of multifold modified sialosides as Human CD22/Siglec-2 ligands with nanomolar activity on B-cells.** *ACS Chem Biol* 2014, **9**:1444-1450.
Modified sialoside inhibitors against CD22 were synthesized and showed increased binding affinities. These compounds are useful for further investigation of the function of CD22.
169. Peng W, Paulson JC: **CD22 ligands on a natural N-glycan scaffold efficiently deliver toxins to B-lymphoma cells.** *J Am Chem Soc* 2017, **139**:12450-12458.
A chemically defined natural N-linked glycan scaffold showed 1500-fold increase in potency compared to the monovalent ligand. Conjugates of auristatin and saporin toxins with this scaffold resulted in efficient killing of the B-cell lymphoma cells. This represents an alternative strategy to the antibody and nanoparticle mediated approaches for drug delivery.
170. Cabanettes A, Perkams L, Spies C, Unverzagt C, Varrot A: **Recognition of complex core-fucosylated N-glycans by a mini lectin.** *Angew Chem Int Ed Engl* 2018, **57**:10178-10181.
171. Varrot A, Basheer SM, Imberty A: **Fungal lectins: structure, function and potential applications.** *Curr Opin Struct Biol* 2013, **23**:678-685.
172. Kumar A, Sýkorová P, Demo G, Dobeš P, Hyršl P, Wimmerová M: **A novel fucose-binding lectin from *Photorhabdus luminescens* (PLL) with an unusual heptabladed β -propeller tetrameric structure.** *J Biol Chem* 2016, **291**:25032-25049.
173. Jančaříková G, Houser J, Dobeš P, Demo G, Hyršl P, Wimmerová M: **Characterization of novel bangle lectin from *Photorhabdus asymbiotica* with dual sugar-binding specificity and its effect on host immunity.** *PLoS Pathog* 2017, **13**: e1006564.
174. Beshr G, Sikandar A, Jemiller E-M, Klymiuk N, Hauck D, Wagner S, Wolf E, Koehnke J, Titz A: ***Photorhabdus luminescens* lectin A (PLIA): a new probe for detecting α -galactoside-terminating glycoconjugates.** *J Biol Chem* 2017, **292**:19935-19951.
175. Lameignere E, Malinová L, Sláviková M, Duchaud E, Mitchell EP, Varrot A, Sedo O, Imberty A, Wimmerová M: **Structural basis for mannose recognition by a lectin from opportunistic bacteria *Burkholderia cenocepacia*.** *Biochem J* 2008, **411**:307-318.
176. Beshr G, Sommer R, Hauck D, Siebert DCB, Hofmann A, Imberty A, Titz A: **Development of a competitive binding assay for the *Burkholderia cenocepacia* lectin BC2L-A and structure activity relationship of natural and synthetic inhibitors.** *MedChemComm* 2016, **7**:519-530.
177. Šulák O, Cioci G, Delia M, Lahmann M, Varrot A, Imberty A, Wimmerová M: **A TNF-like trimeric lectin domain from *Burkholderia cenocepacia* with specificity for fucosylated human histo-blood group antigens.** *Structure* 2010, **18**:59-72.
178. Šulák O, Cioci G, Lameignère E, Balloy V, Round A, Gutsche I, Malinová L, Chignard M, Kosma P, Aubert DF et al.: ***Burkholderia cenocepacia* BC2L-C is a super lectin with dual specificity and proinflammatory activity.** *PLoS Pathog* 2011, **7**: e1002238.
179. Wagner C, Barlag B, Gerlach RG, Deiwick J, Hensel M: **The *Salmonella enterica* giant adhesin SiiE binds to polarized epithelial cells in a lectin-like manner.** *Cell Microbiol* 2014, **16**:962-975.

1.3 Design of multivalent ligands

Multivalency describes the simultaneous interactions between a multivalent ligand and one or more receptors. Strong but reversible interactions achieved with multivalent bindings are found in all biological systems. Despite monovalent drugs rule the current market, significant investigations of multivalent scaffolds were carried out in the past decades, especially in the field of glycobiology.^{66–69} Multivalent interactions between carbohydrate ligands and their receptors (i.e. lectins) are of prime importance to overcome the rather weak monovalent sugar binding (mM to μ M range).⁷⁰ Protein-carbohydrate interactions are essential for numerous biological processes, such as fertilization, B-cell activation, inflammation or pathogen virulence.^{71–74}

The average free energy (ΔG) of ligand-receptor interactions in a multivalent system can be higher than (cooperative effect), equal to (additive effect), or lower (interfering effect) than the free energy of its analogous monovalent interaction.^{75,76} Multivalent ligands can engage their targets with number of binding modes (Figure 1).^{68,77} The chelate effect is commonly associated with binding of a multivalent ligand to a multivalent receptor, when the first binding event results in increase of apparent binding affinity for subsequent binding interactions (also known as avidity) due to the reduced translational entropy costs. Subsite binding occurs in presence of a secondary binding site with different affinity and specificity. High density of binding epitopes presented by a multivalent ligand (their high local concentration) can compete against the complete ligand dissociation from its receptor and increase the apparent affinity through statistical reassociation. Multivalent ligands can cause clustering of receptors anchored in cell membrane due to their motility (diffusion) in the lipid bilayer and can lead to the activation of signalling pathways.⁷⁸

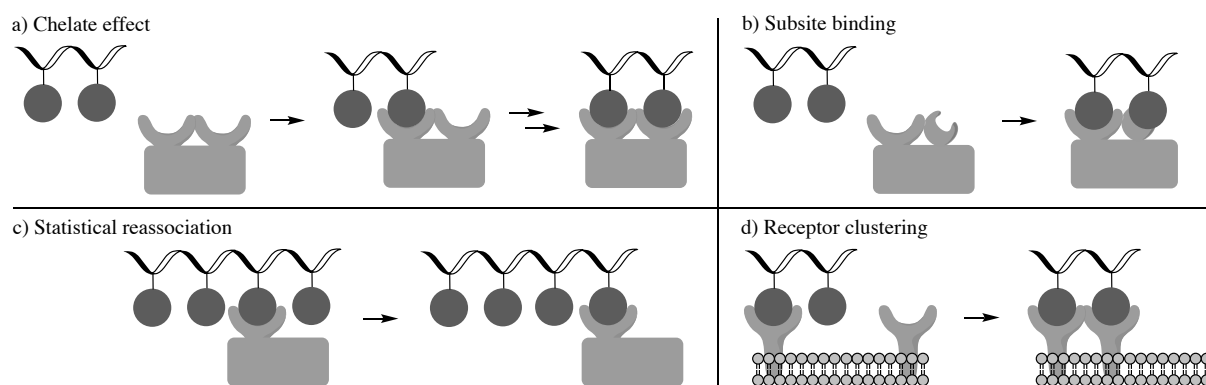


Figure 1: Mechanisms of multivalent binding: a) Multivalent ligands binding to multivalent receptors occupying multiple binding sites (Chelate effect). b) Binding of multivalent ligands to primary and secondary sites of a receptor (Subsite binding). c) Statistical reassociation through high density of ligands in proximity of the receptor

binding pocket. d) Cell surface receptor diffusion through the lipid bilayer due to the presence of multivalent ligand (Receptor clustering). Adapted from Kiessling *et. al.*.⁷⁷

Different scaffolds have been explored for multivalent glycoconjugates, such as calixarenes, fullerenes, dendrimers, polymers, proteins, nanoparticles, peptides, etc.⁶⁸ The architecture of spacers plays an important role by controlling the number of displayed ligands, their distance from each other and their spatial orientation. Selectivity can be modulated through densities of the displayed carbohydrates and their spatial preorganization.^{79,80} The flexible linker structures increase the likelihood of optimal ligand-receptor interactions at the cost of conformational entropy loss in the backbone (Figure 2a). Non-negligible entropy contribution/penalty can arise from the changes in linker solvation in bound and unbound state. On the other hand, rigid spacers must display the ligands in an ideal fashion to avoid the binding enthalpy penalties (Figure 2b). Since such precision is rare, usually a combined approach with limited flexibility allowing the optimal ligand fit to the binding pocket is applied in the design of multivalent inhibitors (Figure 2c). Furthermore, the linkers themselves can introduce additive interactions with a receptor surface.

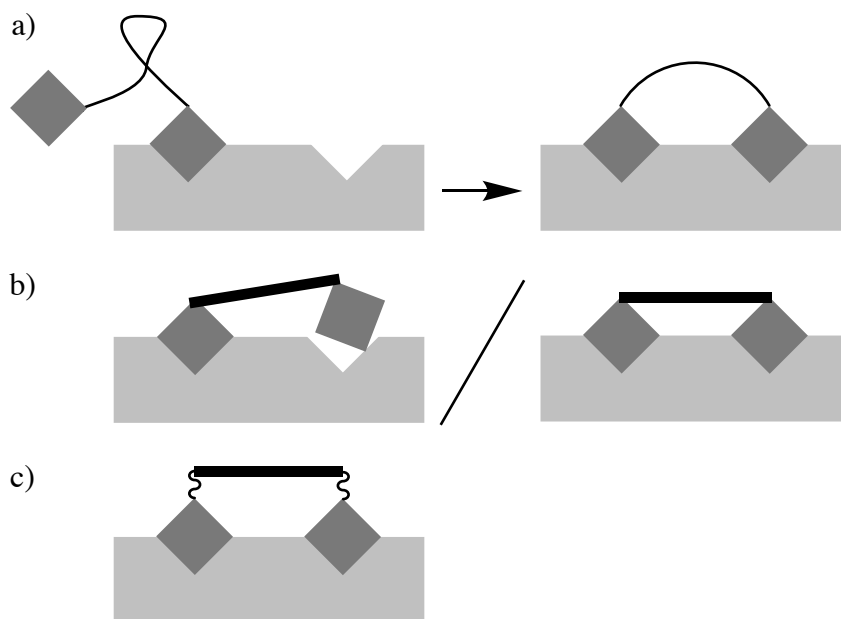


Figure 2: Influence of linker flexibility on divalent binding. a) A flexible linker allows great number of different conformations and entropy is lost upon divalent binding. b) Imperfect rigid spacer does not allow an ideal fit of a ligand to a binding pocket and thus result in loss of enthalpy binding contribution (left). Optimal divalent binding is achieved only with a perfectly fitting rigid spacer (right). c) Divalent ligand with a rigid linker containing flexible regions allows slight adjustment of ligands and achieve optimal divalent binding without severe entropy penalty.

The most extensively studied multivalent inhibitors are targeting viral and bacterial adhesins and toxins. For instance, the multivalent display of sialic acid groups is used to inhibit

hemagglutinin mediated endocytosis of influenza virus⁸¹ or the neutralization of cholera toxin from *Vibrio cholera* with divalent to polyvalent carbohydrate ligands.⁸² Pieters and co-workers developed highly potent divalent ligands against *P. aeruginosa* lectin LecA using rigid spacers made of repeating glucose-triazole units (Figure 3). Notably, divalent ligand **1** with three glucose-triazole units in the linker reached binding affinity of 28 nM and its structure was fully visible in co-crystal structure with LecA, confirming its binding to two neighbouring binding sites.^{42,83} No beneficial interactions with the protein surface were achieved with functionalization of the glucose moiety in the linker (**2–4**, $K_d = 57–89$ nM).⁸⁴ Replacement of one of the glucose-bistriazole unit with cyclohexyl bistiourea moiety simplified the spacer synthesis to 7 steps and compound **5** ($K_d = 30$ nM) was equipotent to **1**.⁸⁵ The most potent divalent ligand from the optimization campaign around the rigid spacer connecting two galactosides was compound **6** ($K_d = 12$ nM) with the phenyl ring instead of the central glucose unit.⁸⁶ Despite the cumbersome multi-step synthesis of multivalent glycoconjugates, they provide potent pharmaceutical agents.

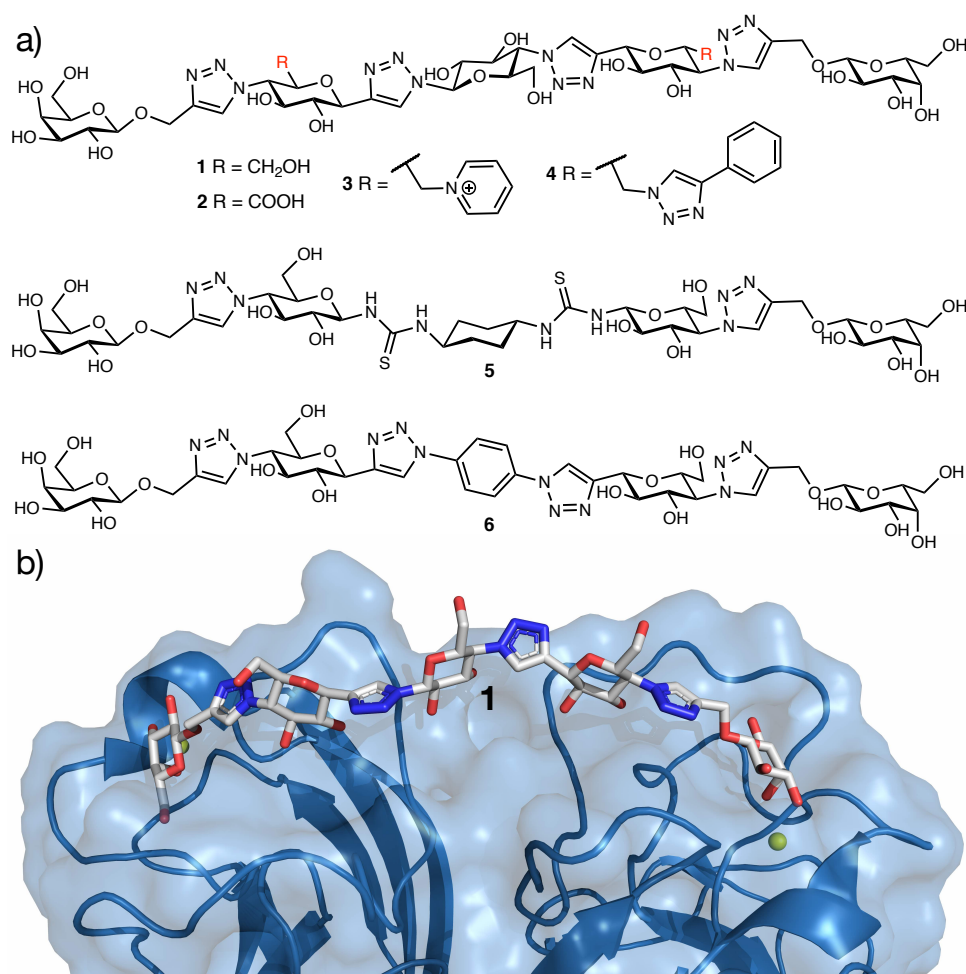


Figure 3: Divalent galactose ligands with rigid, rod-shaped spacer with low nanomolar binding affinities towards LecA. a) Structures of divalent LecA inhibitors. b) Co-crystal structure of LecA and compound **1** (PDB code 4YWA).

2. Aim of the thesis

Since the discovery of penicillin in the early 20th century,⁸⁷ more than 20 different classes of antibiotics have reached the market.⁸⁸ However, only two new classes have been successfully developed in the last 30 years (the oxazolidinone linezolid and the lipopeptide daptomycin). It has been estimated, that infections caused by antimicrobial resistant pathogens will lead to more than 10 million deaths per year by 2050.⁸⁹ The alarming lack of development of novel antimicrobial agents by the pharmaceutical industry combined with the current AMR crisis calls for urgent innovation. Additionally, modern healthcare faces a high demand for rapid and accurate diagnostic tools. In the field of infection medicine, early identification and localization of a pathogen is vital for an appropriate treatment, reducing the unnecessary use of broad-spectrum antimicrobial agents, preventing toxicity and rise of multi-drug resistance bacteria.^{90,91} Over the past century, the most frequent diagnostic method has been slow and error-prone pathogen detection and characterization via conventional microbiological methods (microscopic examination, pure culture isolation, etc.). Other common methods include serology, molecular and radiology techniques. Despite technological advances in latest decade, pathogen identification remains time-consuming, often accompanied with invasive procedures required for sample collection (i.e. biopsies) and unable to provide information about extent and location of the infection.⁹²

The objective of this thesis was to develop lectin-directed theranostics targeting *Pseudomonas aeruginosa* extracellular carbohydrate-binding proteins LecA and LecB (Chapters 3.1). LecA and LecB are *P. aeruginosa* adhesins and essential biofilm structural components^{35,36} and thus conjugation of imaging moieties or antibiotic cargo to the lectin binders shall lead to their accumulation at the infection site. Increasing the local drug concentration with lectin-targeted antibiotic conjugates could overcome antimicrobial resistance and/or lower drug side effects and could lead to a so much needed alternative treatment strategy. The lectin directed imaging probes could serve as a fast, non-surgical, pathogen-specific diagnostics tools. Development of pathogen-specific imaging tools may enable localization and real-time monitoring of infection. Positive blood cultures (except in highly immunocompromised hosts) and conclusive radiology findings are rare in *Pseudomonas pneumonia* and clinicians mostly rely on time-consuming bacterial culture-based techniques.^{93,94} Therefore, development of fast and sensitive detection method for this pathogen is of prime importance.

The second part of this work was aimed to develop highly active divalent LecA ligands with a focus on their drug-like properties and synthetic accessibility (Chapters 3.2 and 3.3).

Since LecA plays important role in *P. aeruginosa* infections,^{36,39,40} potent LecA inhibitors could be used as anti-virulence drugs and decrease the pathogenicity of *P. aeruginosa*. The best monovalent LecA inhibitors have potencies only in low micromolar range, but an increase in activity down to low nanomolar range have been reported with multivalent ligands.^{43,60,61,83} Unfortunately, the lengthy synthesis required for multivalent inhibitors hinders their drug development. Simplification of the multivalent ligand scaffold and reducing the number of synthesis steps shall result in faster lead optimization.

In the last section of this work (Chapters 3.4), we aimed to merge both projects by transferring the divalent LecA inhibitors into highly potent divalent LecA targeting imaging probes.

3. Results

3.1 Development of LecA and LecB targeting imaging probes for *Pseudomonas aeruginosa* biofilms

In this chapter, conjugation of LecA and LecB inhibitors to a signal compound, i.e. fluorophore, was explored in order to develop diagnostic tools for *P. aeruginosa* infections. Similar concept for development of non-invasive diagnostic method for bacterial infection based on siderophore targeting with first successful *in vitro* and *in vivo* imaging studies is under development.^{95,96} However, carbohydrate-binding protein LecA and LecB are extracellular targets. A proof-of-concept study was reported by Wagner *et al.*, using the covalent LecA inhibitor with fluorescein label **1** (Figure 1) for LecA-specific staining of *P. aeruginosa* biofilms.⁴⁴ The covalent LecA inhibition was based on an epoxygalactoheptoside warhead that targeted a cysteine residue in the LecA carbohydrate binding domain (Cys62). The alkyne precursor of **1** showed moderate binding affinity ($IC_{50} = 109 \mu\text{M}$). Due to a challenging synthesis, potential non-specific reactivity and toxicity of the epoxide-based probe **1**, we decided to address the LecA binding pocket with conventional galactose-based ligands. Glycosidase susceptible O-glycosidic linkage was replaced with a glycosidase resistance S-linkage to improve metabolic stability. The galactose phenyl aglycon was equipped with an alkyne handle to enable future substitution of the fluorescein signalling moiety with other fluorophores, MRI dyes or PET tracers. A small SAR study around the clickable handle was carried out by varying position, length and chemical nature (ether or amine) of the linker.

The design of LecB targeting imaging probes was based on a conjugation of a fluorophore moiety to the highly optimized LecB C-glycoside inhibitor **2** (Figure 1).⁴⁷ Compound **2** showed high binding affinity ($K_d = 290 \text{ nM}$), long receptor residence, excellent *in vivo* pharmacokinetic properties and ability to block *P. aeruginosa* biofilm formation *in vitro*. The alkyne handle for conjugation to an imaging moiety was installed at position 5 of the thiophene ring, since it was identified as a potential growth vector by the analysis of the co-crystal structure of LecB in complex with **2** (PDB code: 5MAY). Substitution of the thiophene moiety of **2** with a benzene, containing terminal alkyne handle on a short flexible linker at *para* position, was also explored.

Xylose is not known to play a role in *P. aeruginosa* infection process and was unable to prevent *P. aeruginosa* adherence to kidney or lung cells.⁹⁷ Furthermore, xylose showed lower metabolism rates in comparison to glucose or fructose,⁹⁸ possibly due to slower active transport across the gram-negative cell wall. Since LecA is specific for D-galactosides⁵⁸ and LecB for

L-fucosides/D-mannosides,⁴⁹ xylose was selected as a negative control monosaccharide targeting moiety. Xylose-based imaging compounds mimicking the design of LecA targeted conjugates were synthesized.

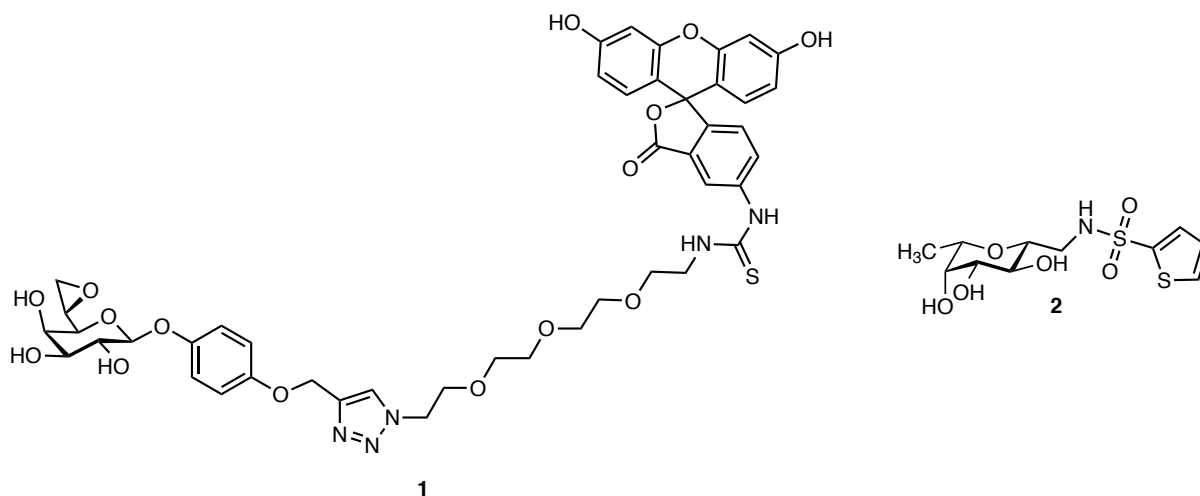
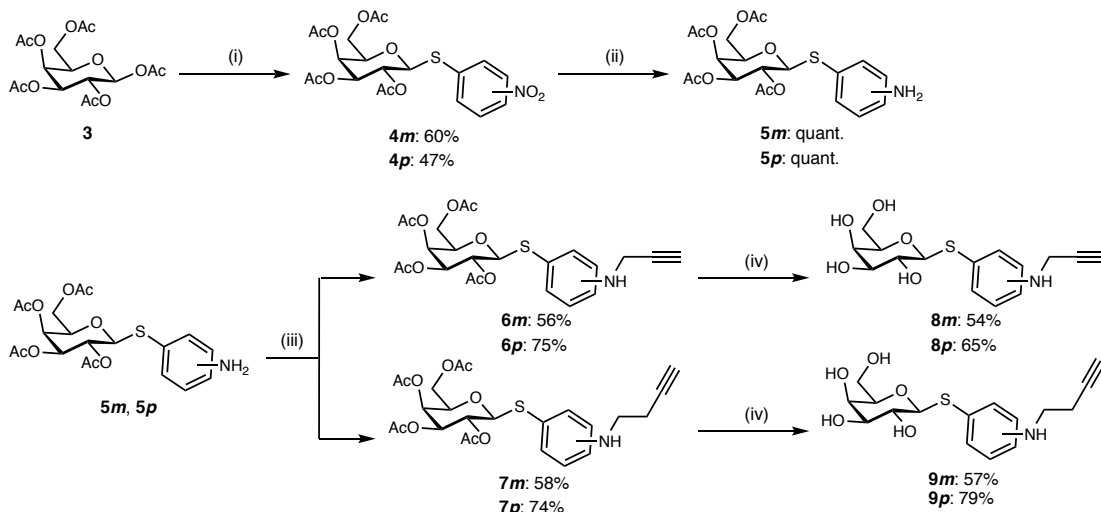


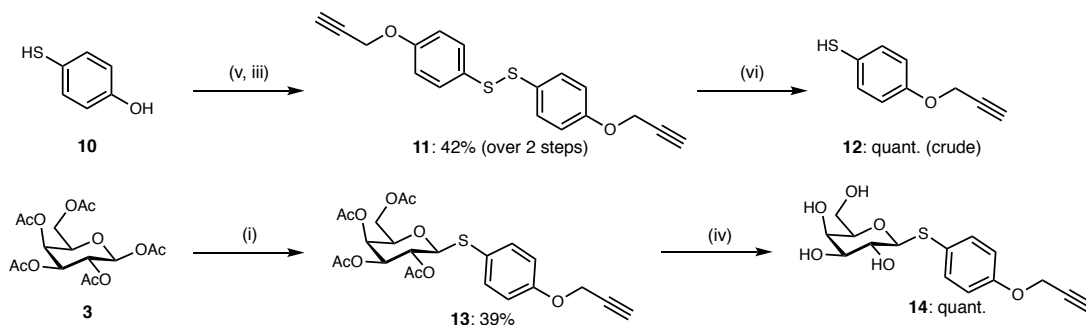
Figure 1: Structures of covalent LecA targeting imaging probe **1** and LecB inhibitor **2**.

Synthesis of galactose- and xylose-based precursors was performed in analogy to each other, starting from the acetylated galactose **3** and xylose **15**, respectively (Scheme 1). Galactosides and xyloside with amine linker (**8m**, **8p**, **9m**, **9p**, **19**) were synthesized in four linear steps, whereas their ether analogues in convergent manner (**14**, **21**). Lewis acid promoted glycosylation of corresponding thiol acceptors gave glycosides **4m**, **4p**, **13**, and **14** in fair yields (39–60%), while xyloside **20** was obtained in a poor isolated yield (12%) due to the limited separation of anomers during normal phase chromatographic purification. Disulphide formation was used as a provisional protecting group for O-alkylation to intermediate **11** during synthesis of the glycosyl acceptor **12**. Disulphide reduction conditions using sodium borohydride or triphenyl phosphine were tested, however the reaction with dithiothreitol was the most successful to obtain thiol **12** (fast and not requiring a chromatographic purification). Palladium catalysed hydrogenation of the nitro intermediates gave anilines **5m**, **5p**, and **17** quantitatively. N-alkylations yielding **6m**, **6p**, **7m**, **7p**, and **18** had to be closely monitored to minimize the production of undesired tertiary amines (SI: **39m**, **39p**, **40p**). Furthermore, carbamate side products were detected during the alkylations with 4-bromo-1-butyne (SI: **41p**), when potassium carbonate base served as a carbon dioxide source. Deprotection under Zemplén conditions gave the desired terminal alkyne containing precursors for imaging probes, galactosides **8m**, **8p**, **9m**, **9p**, **14** and xylosides **19** and **21**.

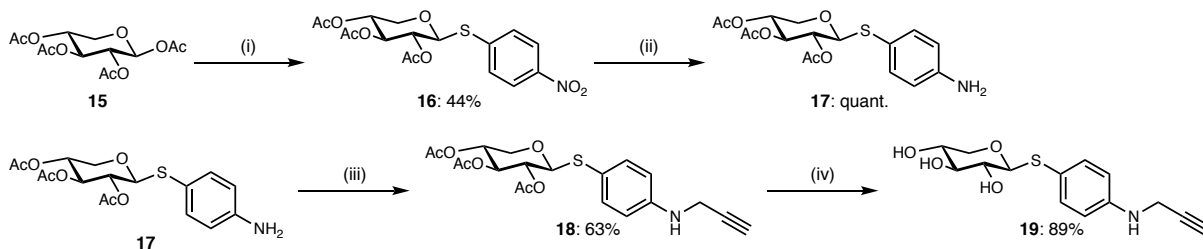
Galactose-based precursors with amine linker



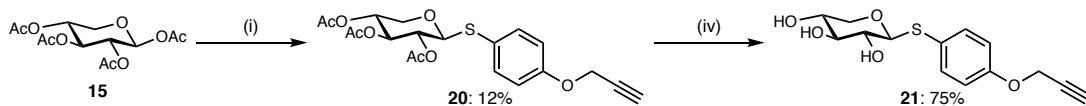
Galactose-based precursors with ether linker



Xylose-based precursors with amine linker



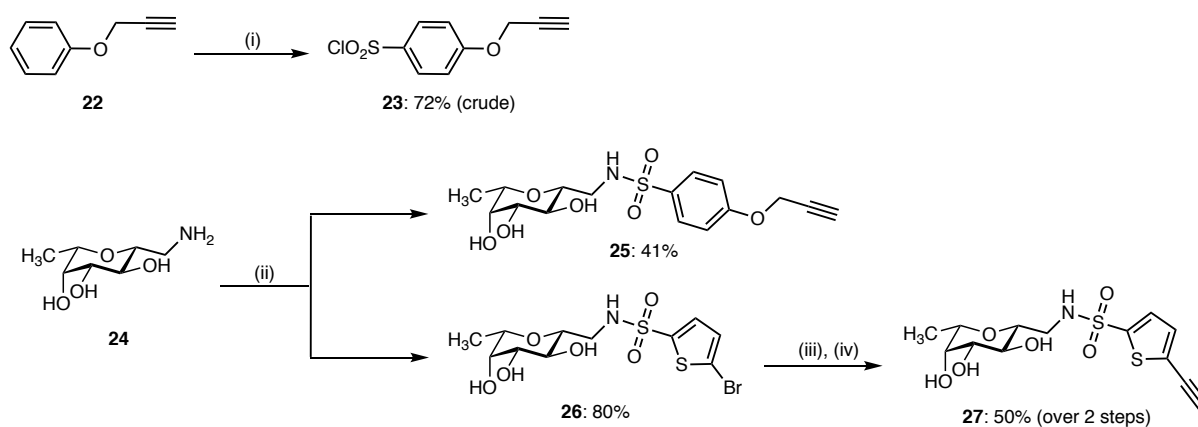
Xylose-based precursors with ether linker



Scheme 1: Synthesis of alkyne precursors for galactose- and xylose-based imaging probes. Reagents and conditions: (i) *m*-nitrothiophenol/*p*-nitrothiophenol/4-prop-2-ynyloxyphenyl thiol (**12**), $\text{BF}_3 \cdot \text{Et}_2\text{O}$, CH_2Cl_2 , 0°C – r.t., o.n.; (ii) H_2 , Pd/C, CH_2Cl_2 , r.t., o.n.; (iii) propargyl bromide/4-bromo-1-butyne, K_2CO_3 , DMF, $0 - 40^\circ\text{C}$ (for **7m** and **7p**: $0 - 70^\circ\text{C}$), 6 h – o.n.; (iv) NaOMe, MeOH, r.t., 1 – 2 h; (v) I_2 , EtOH, r.t., 5 h; (vi) dithiothreitol, *N*-ethyl-diisopropylamine, MeOH, r.t., 3 h.

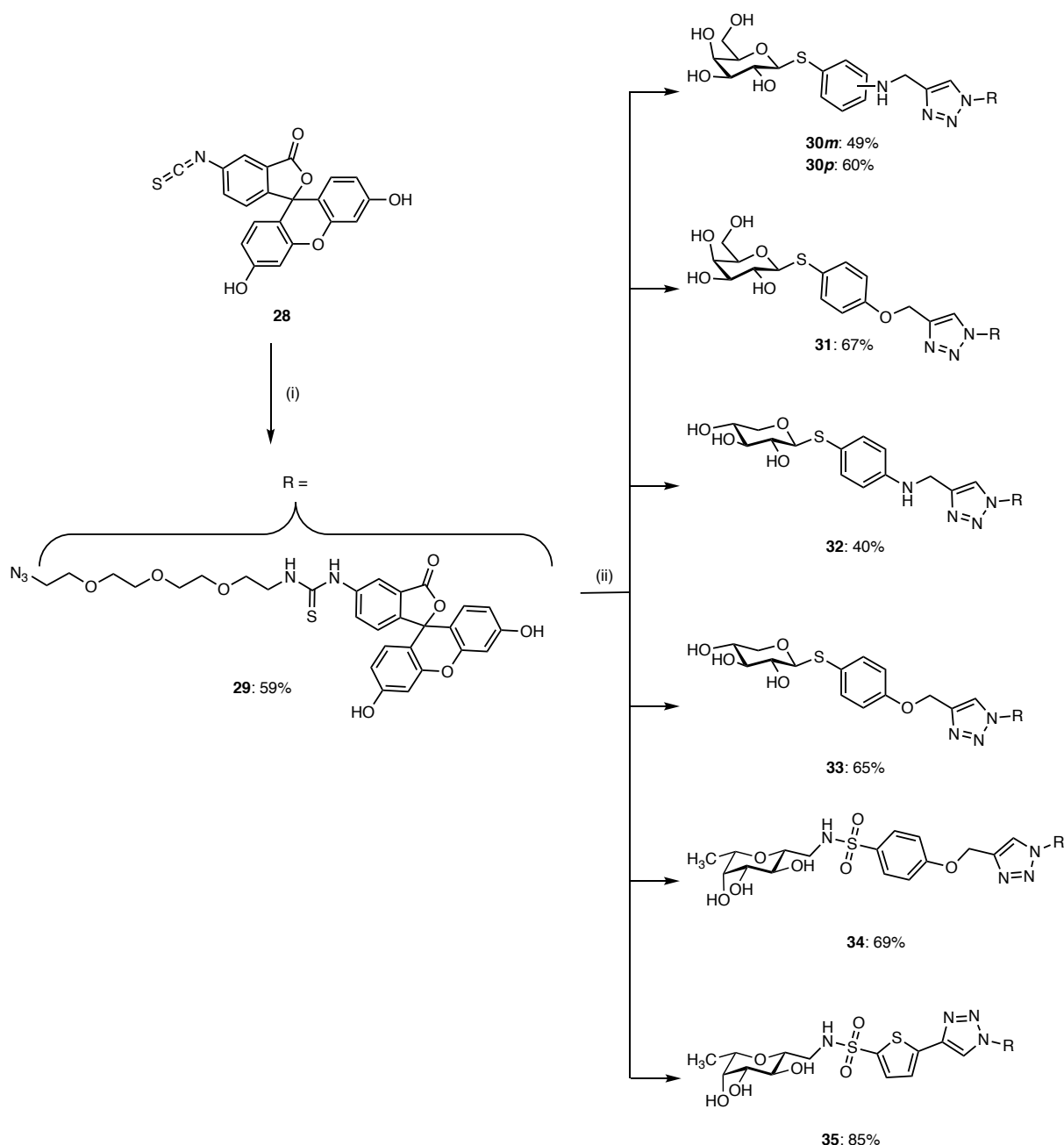
Synthesis of alkyne 1-deoxy-fucose-based precursors started from β -C-glycoside **24**⁹⁹ that was coupled to the corresponding sulfonyl chloride, yielding precursor **25** and intermediate **26** (Scheme 2). Benzenesulfonyl chloride building block **23** was prepared by chlorosulfonation

of propargyl phenyl ether **22**, whereas thiophene building block was commercially available. Palladium-catalysed Sonogashira cross coupling reaction with **26** and the protected acetylene followed by desilylation gave precursor **27** in 50% yield (over 2 steps).



Scheme 2: Synthesis of alkyne precursors for 1-deoxy-fucose-based imaging probes. Reagents and conditions: (i) ClSO_3H , CH_2Cl_2 , $0\text{ }^\circ\text{C}$, 2 h; (ii) 5-bromothiophene-2-sulfonylchloride/4-(propargyloxy)benzenesulfonyl chloride (**23**), Et_3N , DMF, $0\text{ }^\circ\text{C}$ – r.t., 2 – 3 h; (iii) trimethylsilyl acetylene, CuI , $\text{PdCl}_2(\text{PPh}_3)_2$, Et_3N , DMF, $30\text{ }^\circ\text{C}$, 5 h; (iv) K_2CO_3 , MeOH, r.t., 3 h.

Assembly of imaging probes was performed using Huisgen azide-alkyne cycloaddition between alkyne precursors and azide modified fluorescein **29** (Scheme 3). Fluorescein 5-isothiocyanate (**28**) was coupled to the short flexible polyethylene glycol spacer with terminal azide to give **29** in 59% yield. Based on the results of competitive binding assay showing no difference in activity was for galactosides with extended linker **9m** and **9p** (*vide infra*), only the galactose-based compounds bearing a propargyl handle (**8m** and **8p**) were chosen for final conjugation to the fluorophore. High amounts of copper source were necessary for efficient CuAAC reaction turnover, probably due to its coordination to the building blocks. Imaging probes **30–35** were synthesized in fair yields (40–85%).



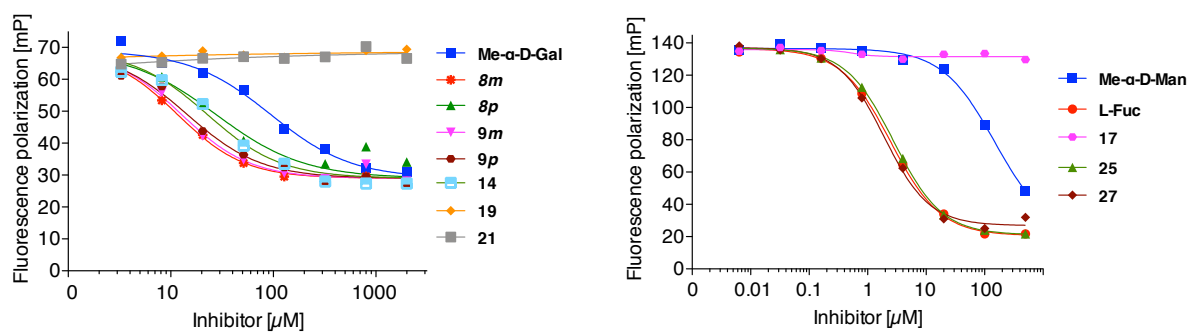
Scheme 3: Conjugation of fluorescein with the alkyne precursors. Reagents and conditions: (i) 11-azido-3,6,9-trioxaundecan-1-amine, Et₃N, DMF, 0 °C – r.t., 1 h; (ii) corresponding terminal alkyne (**8m**, **8p**, **9m**, **9p**, **14**, **19**, **21**, **25** or **27**), CuSO₄, sodium ascorbate, DMF/H₂O (4:1), r.t., overnight.

All synthesized alkyne precursors (**8m**, **8p**, **9m**, **9p**, **14**, **19**, **21**, **25** and **27**) were analysed in the previously established competitive binding assays based on fluorescence polarization (Figure 1).^{61,62} As intended, xylose-based compounds **19** and **21** did not bind to LecA neither LecB in the tested concentration range and served as negative controls. Galactose-based compounds (**8m**, **8p**, **9m**, **9p**, **14**) showed IC₅₀ values between 18–32 μM, that is 3–6 times higher than the positive control Me-α-D-Gal (IC₅₀ = 101.0 ± 19.3 μM). *Meta* substitution on the phenyl aglycon was preferred with compounds **8m** (IC₅₀ = 17.8 ± 8.2 μM) and **9m** (IC₅₀ = 17.8 ± 7.5 μM) being the most potent LecA inhibitors. A minor increase in binding affinity was

achieved by exchanging an amine linker (**8p** $IC_{50} = 31.5 \pm 6.5 \mu\text{M}$) with an ether linker (**14** $IC_{50} = 24.3 \pm 3.8 \mu\text{M}$). No significant effect on binding affinity was observed for increasing the amine linker length by one methylene unit (**8m** vs. **9m**, **8p** vs. **9p** $IC_{50} = 22.3 \pm 9.3 \mu\text{M}$).

Activity of 1-deoxy-fucose-based compounds were assessed against more studied PAO1-like LecB.⁵⁵ Compounds **26** ($IC_{50} = 3.8 \pm 0.9 \mu\text{M}$) and **27** ($IC_{50} = 2.4 \pm 0.5 \mu\text{M}$) showed very similar binding profiles to LecB. Both were more active than natural ligand Me- α -D-Man ($IC_{50} = 166 \pm 22 \mu\text{M}$) and had comparable binding affinities to L-Fuc ($IC_{50} = 2.6 \pm 0.1 \mu\text{M}$).

Binding affinities of imaging probes **30–35** were determined in direct titration experiments based on fluorescence polarization (Figure 3).^{61,62} Galactose-based imaging probes showed binding affinity to LecA in low micromolar range. In analogy to the competitive binding assay, *meta* substituted compound **30m** ($K_d = 5.3 \pm 0.7 \mu\text{M}$) showed the strongest binding. Similarly, ether linked compound **31** ($K_d = 8.5 \pm 0.8 \mu\text{M}$) showed a slight increase in binding potency over compound **30p** with amine linker ($K_d = 11.6 \pm 0.7 \mu\text{M}$). Xylose-based imaging probes (**32** and **33**) and negative control **29** without any sugar moiety did not bind to LecA. Likewise, no binding interaction was observed for xyloside **32** to LecB. 1-deoxy-fucose-based imaging probe **34** ($K_d = 0.84 \pm 0.11 \mu\text{M}$) was twice as active as imaging probe **35** ($K_d = 1.65 \pm 0.14 \mu\text{M}$), demonstrating that a short flexible linker between the LecB inhibitor and triazole moiety is preferable. Titration results were validated with reporter ligands used in competitive binding assays as positive controls – LecA targeting O-galactoside **36** ($K_d = 8.7 \pm 1.0 \mu\text{M}$, lit. $K_d = 7.4 \pm 2.8 \mu\text{M}$)⁶¹ and LecB targeting O-fucoside **37** ($K_d = 0.16 \pm 0.02 \mu\text{M}$, lit. $K_d = 697 \text{ nM}$)⁶² and O-mannoside **38** ($K_d = 27.2 \pm 10.8 \mu\text{M}$, lit. $K_d = 16 \mu\text{M}$).¹⁰⁰ The intensity range of fluorescence polarization varied among compounds probably due to different residual mobility of the fluorophore-protein complexes.



LecA			LecB		
Structure	Compound	IC ₅₀ [μM]	Structure	Compound	IC ₅₀ [μM]
	Me-α-D-Gal	101.0 ± 19.3		Me-α-D-Man	166 ± 22
	8m	17.8 ± 8.2		L-Fuc	2.6 ± 0.1
	8p	31.5 ± 6.5		19	n.b.
	9m	17.8 ± 7.5		25	3.8 ± 0.9
	9p	22.3 ± 9.3		27	2.4 ± 0.5
	14	24.3 ± 3.8			
	19	n.b.			
	21	n.b.			

Figure 2: Ligand evaluation against LecA (left) and LecB (right) in the competitive binding assay. One representative titration is shown for each. Averages and standard deviations from at least three independent titrations of triplicates each. n.b. = not binding.

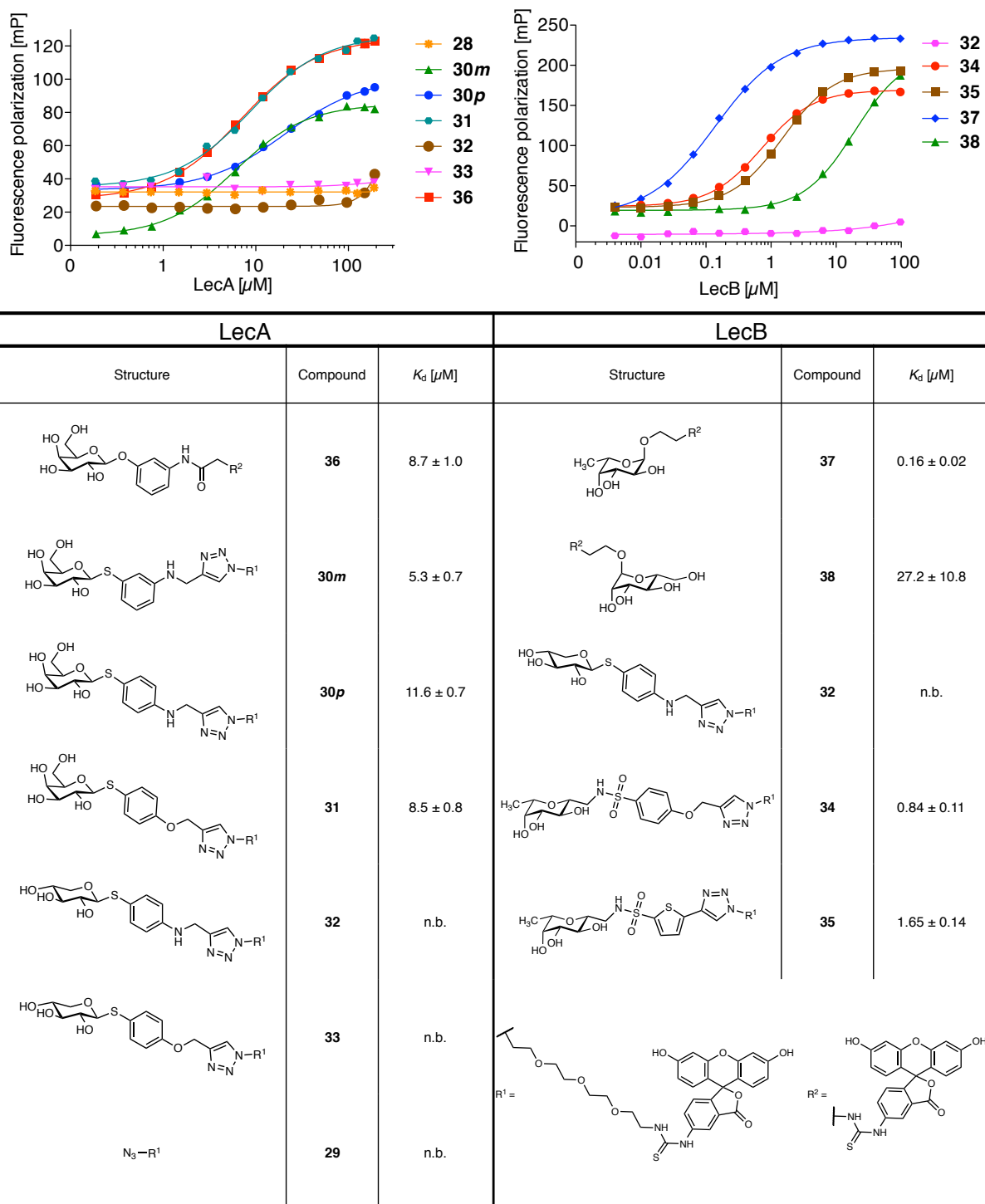


Figure 3: Titrations of imaging probes (10 nM) with LecA (left) or LecB (right). One representative titration is shown for each. Averages and standard deviations from at least three independent titrations of triplicates each. n.b. = not binding.

Since the binding of imaging probes to their lectin targets was confirmed, we proceeded to study their ability to stain *P. aeruginosa* (PAO1) biofilm aggregates *in vitro* under static conditions in analogy to Wagner *et. al.*⁴⁴ Biofilm aggregates were stained with the lectin-targeted imaging probes (10 to 40 μ M), images were recorded with a confocal laser scanning

microscope and analysed using open source image analysis software Fiji¹⁰¹ and then re-analysed with commercial image analysis and visualization software Imaris. Galactose-based and xylose-based imaging probes with ether linker (**31** and **33**) were excluded from the preliminary experiments due to their later synthesis.

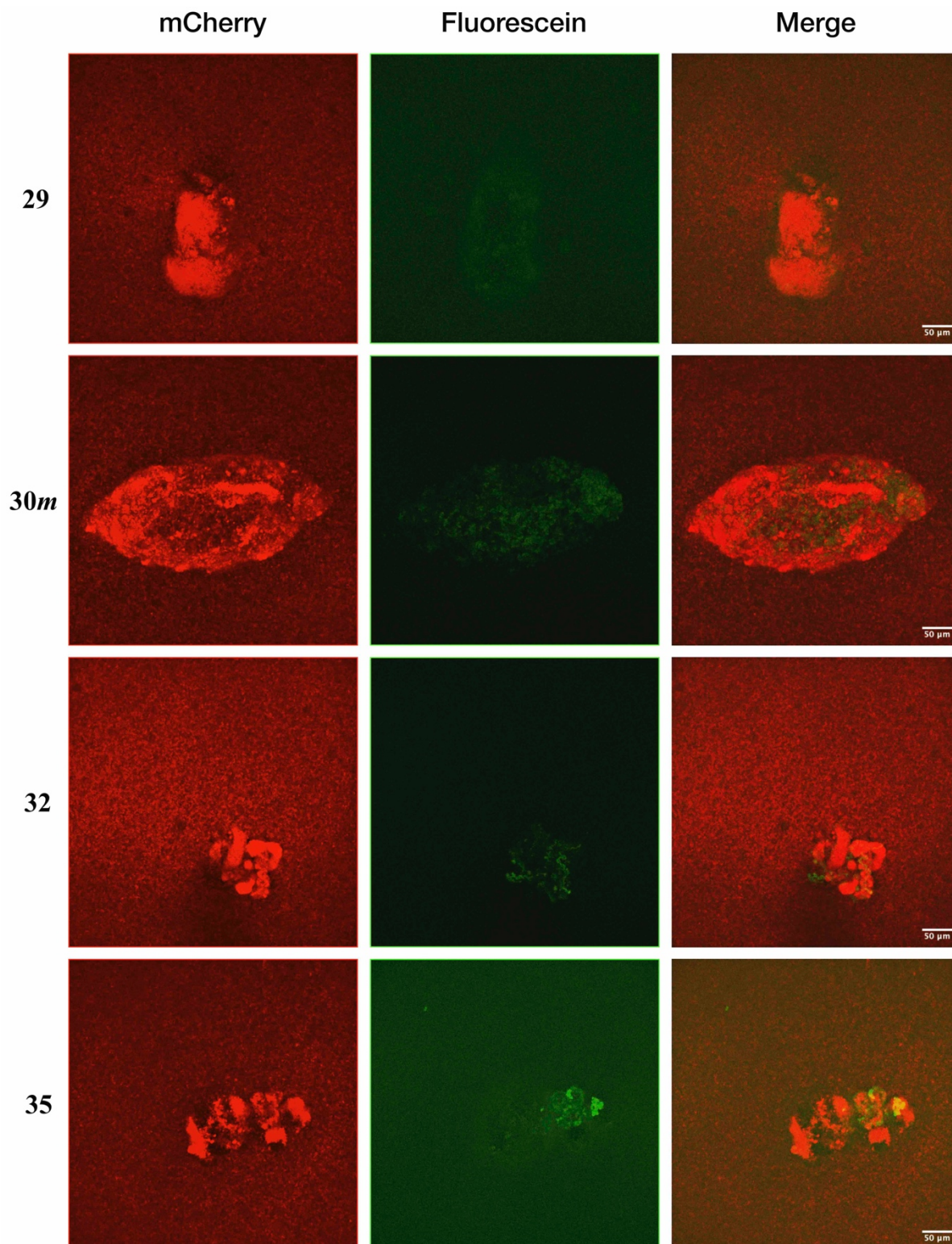


Figure 4: Images of *P. aeruginosa* (PAO1) biofilm aggregates stained with 10 μM of imaging probes and displayed as maximum intensity Z-projections using Fiji. Azide modified fluorescein **29** did not stain

P. aeruginosa biofilm aggregates. Biofilm aggregates were stained with imaging probes bearing a carbohydrate moiety, independent of the identity of the carbohydrate moiety (galactose-based **30m**, 1-deoxy-fucose-based **35**, xylose-based **32**) and rather low staining contrast was observed in all cases (Fluorescein/green channel). One image of stained aggregate is shown for each. *P. aeruginosa* was expressing mCherry (ex.: 561 nm) from pMP7605⁴⁴ and is displayed in red and fluorescein conjugates (ex.: 488 nm) in green. Scale bars = 50 μ m.

At 10 μ M, all imaging probes bearing a carbohydrate moiety showed accumulation at the biofilm aggregates, including xylose-based probe **32** – the intended negative control (Figure 4, Figures S1-S6). In all cases, the green signal corresponding to the fluorescein conjugates was not evenly spread over the entire structure of the biofilm aggregates and rather weak staining contrast with only occasional brighter spots was observed. At 10 μ M, the azide modified fluorescein building block **29** did not show any staining, only very faint green shadows were detected. Therefore, fluorescein derivative **29** served as the negative control in the assay and biofilm staining with imaging probes was carbohydrate dependent.

Additionally, staining of pellicle biofilms was also recorded in few cases (Figure 5), but these results were not statistically validated (reproduced) due to the focus on biofilm aggregates inside liquid cultures. A pellicle is a biofilm that assembles at the air-liquid interface of a liquid culture. The lectin-targeted imaging probes were not always able to stain pellicle biofilms. An increased amount (20 μ M) of imaging probe **30p** did not enhance staining efficiency of pellicles, while the staining was improved with higher amount (20 μ M) of imaging probe **34**. One possible explanation for pellicle staining or lack of it is that upon application of the dyes in some cases the pellicle barrier was disturbed and pellicle was stained, while in other cases the barrier was left intact and the dyes were not able to penetrate through.

Uneven staining of biofilm aggregates together with poor contrast could be a result of insufficient amount of dye present. Therefore, the concentration of imaging probes was increased to 40 μ M in hope of enhancing the staining efficiency (Figure 6, Figures S7-S13). In general, all carbohydrate-fluorescein conjugates showed staining of biofilm aggregates and increase in dye concentrations enhanced the staining intensity. The least efficient staining was observed for 1-deoxy-fucose-based imaging probe **34**, showing only weak accumulation of a green signal at biofilm aggregates. On the other hand, the second LecB targeting imaging probe **35** showed comparable staining efficiency to LecA targeting galactose-based probes (**30m**, **30p** and **31**) or xylose-based probes (**32** and **33**, unknown target). Variations in linker position (**30m** and **30p**) or linker chemistry (**30p** and **31**, **32** and **33**) did not cause any observable staining difference. The imaging probes were able to penetrate inside bacterial aggregates (see 3D cross section views displayed by Imaris). Despite increased dye concentration, a uniform staining of the aggregates was rare (e.g. Figure S10, bottom) and in most cases the fluorescein conjugates

accumulated at the bottom of the aggregates (Figure 6). Unexpectedly, occasional staining was recorded for the negative control **29** at 40 μ M (Figure 7). In some cases, no staining or only a very faint shadow was observed for **29**, similarly to experiments carried at lower concentration. However, weak to strong green signals corresponding to an accumulation of the azide modified fluorescein **29** at biofilm aggregates was also observed. Sometimes, staining efficiency of **29** varied even within the biofilm aggregates found in the same well. This suggest weak unspecific interaction of the modified fluorescein **29** with the *P. aeruginosa* biofilms due to high amount of dye present. We tried to confirm the specific staining of LecA and LecB targeting probes using Δ *lecA* and Δ *lecB* knockout mutant strains. However, these lectins are essential biofilm components^{35,36} and the mutant strains did not form biofilm aggregates at all and only very few and not compact biofilm structures were found (Figure S14-S16). Therefore, staining of Δ *lecA* and Δ *lecB* strains (PAO1) was abandoned.

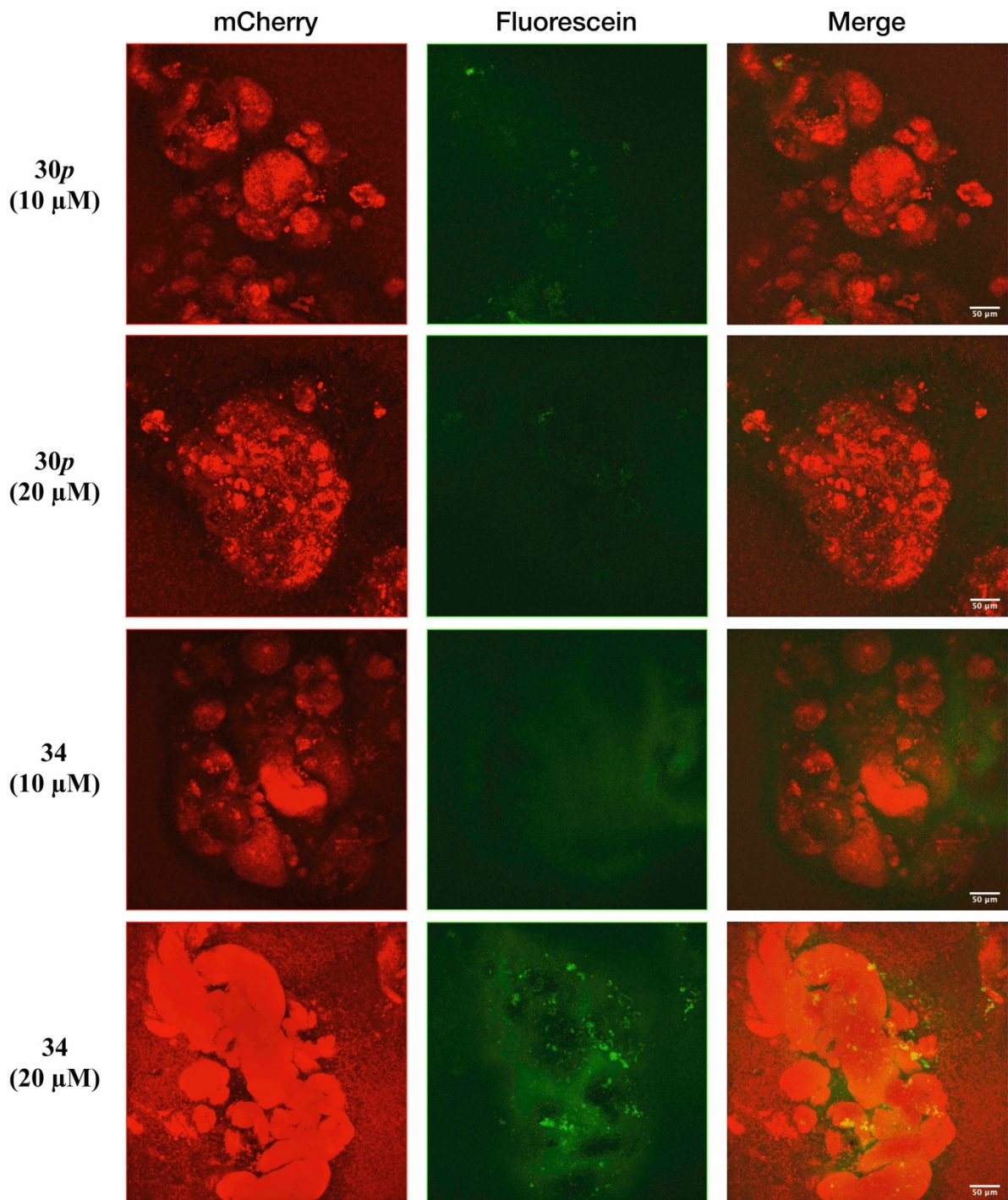


Figure 5: Images of *P. aeruginosa* (PAO1) pellicle stained with galactose-based imaging probe **30p** and 1-deoxy-fucose-based imaging probe **34** displayed as maximum intensity Z-projections using Fiji. *P. aeruginosa* was expressing mCherry (ex.: 561 nm) from pMP7605 and is displayed in red and fluorescein conjugates (ex.: 488 nm) in green. Scale bars = 50 μ m.

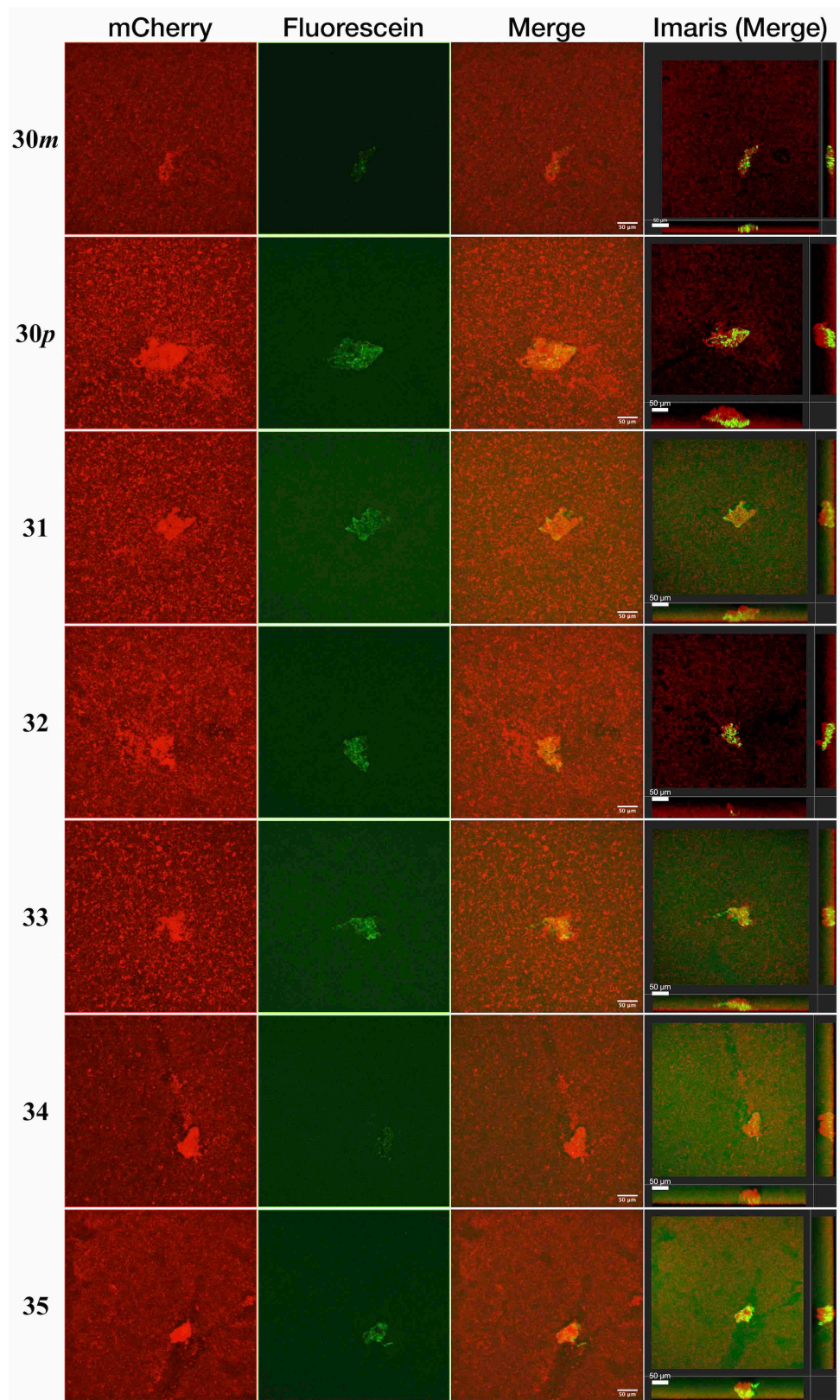


Figure 6: Images of stained *P. aeruginosa* (PAO1) biofilm aggregates stained with 40 μ M of imaging probes and displayed as maximum intensity Z-projections using Fiji and as three-dimensional maximum intensity projection using Imaris. Accumulation of the imaging probes at the biofilm aggregates was observed in all cases. One representative picture is shown for each carbohydrate-fluorescein conjugate. *P. aeruginosa* was expressing mCherry (ex.: 561 nm) from pMP7605 and is displayed in red and fluorescein conjugates (ex.: 488 nm) in green. Scale bars = 50 μ m.

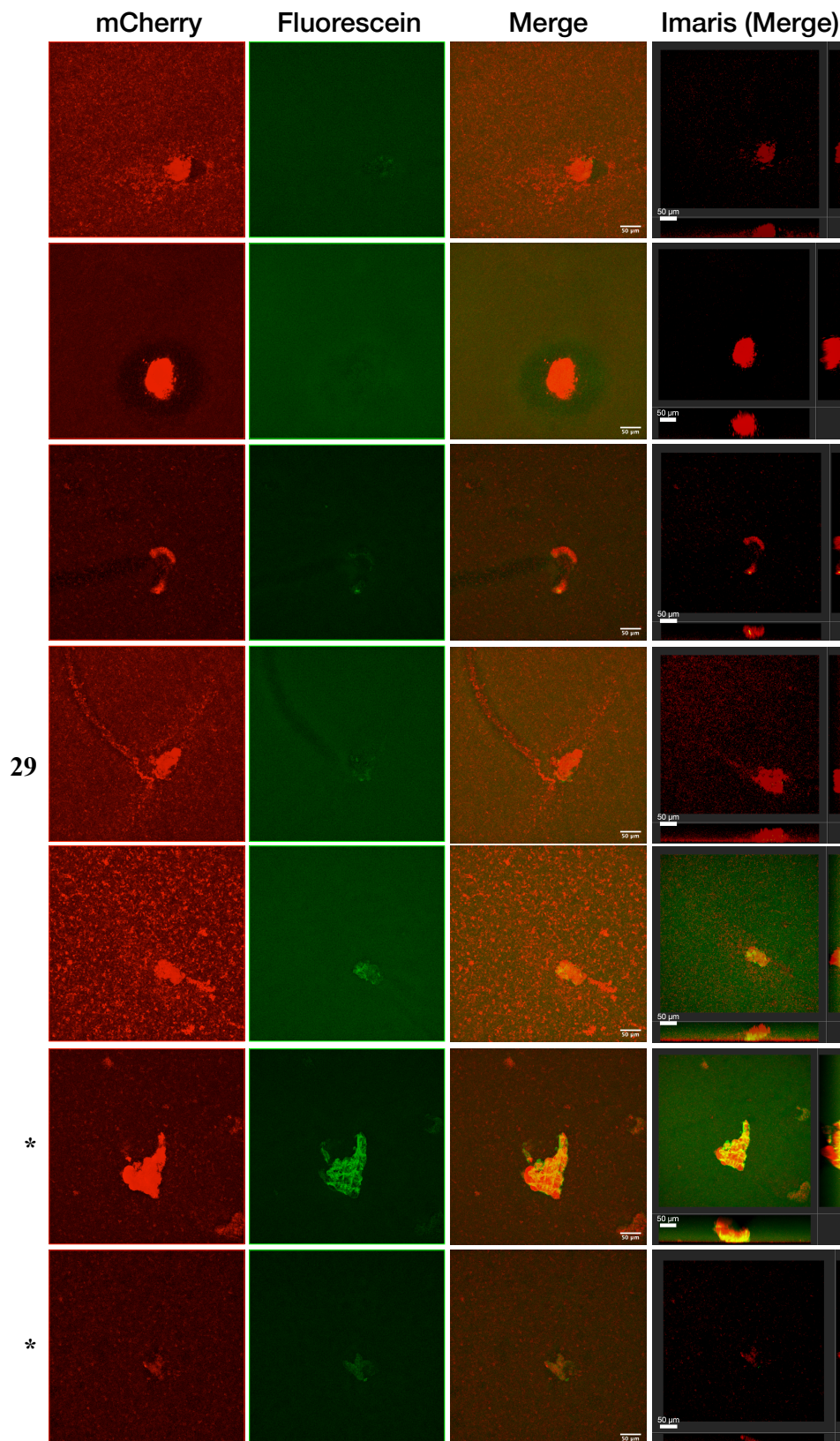


Figure 7: Images of stained *P. aeruginosa* (PAO1) biofilm aggregates stained with 40 μ M of the azide modified fluorescein **29** and displayed as maximum intensity Z-projections using Fiji and as three-dimensional maximum intensity projection using Imaris. Inconsistent staining of **29** was observed. Images showed in two bottom rows marked with star (*) were recorded from the same well. *P. aeruginosa* was expressing mCherry (ex.: 561 nm) from pMP7605 and is displayed in red and fluorescein conjugates (ex.: 488 nm) in green. Scale bars = 50 μ m.

In conclusion, we designed and synthesized fluorescein imaging probes targeting *P. aeruginosa* lectins LecA and LecB. The binding affinities of the alkyne precursors and the final imaging probes were determined to be in low micromolar range for LecA (galactose-based compounds) and low micromolar to sub-micromolar for LecB (1-deoxy-fucose-based compounds). The binding affinities were consistent with literature values of other monovalent ligands of these lectins.^{46,60–62,102} Attachment of the fluorescein moiety was well tolerated by both proteins with negligible influence of the linker, providing a valuable knowledge for synthesis of lectin-targeted conjugates. Staining of *P. aeruginosa* biofilms with epoxygalactoheptoside-based probe **1** targeting LecA reported by Wagner *et al.*⁴⁴ was reproduced with synthetically more accessible galactose-based probes and achieved for the first time with 1-deoxy-fucose probes as well as xylose-based probes. It must be noted, that great variations of biofilm aggregates shapes and sizes were observed but no correlation existed between their physical appearance and staining results. Similar staining efficiency was achieved with all carbohydrate-fluorescein conjugates, except for 1-deoxy-fucose-based imaging probe **34** for which a weaker staining was observed. Since xylose-based imaging probes did not show binding to LecA neither to LecB and nevertheless showed accumulation at the biofilm aggregates, xylose-binding lectin or completely different mode of action had to be responsible. However, there are no reports about *P. aeruginosa* xylose-specific lectin in the literature. Biofilm is a highly complex dense matrix, therefore interactions with other matrix components than lectins could be responsible for accumulation of xylose-based imaging probes in the biofilm aggregates. Indeed, occasional biofilm staining with fluorescein building block **29** (lacking any carbohydrate) only at high concentration (40 μ M) suggest unspecific interactions caused by fluorophore moiety. Substitution of the carboxylic acid containing fluorescein with a positively charged TAMRA dye and/or a neutral BODIPY dye will be explored in the future. Furthermore, weak unspecific interaction of **29** as well as weak staining contrast could be overcome by biofilm imaging assay under flow conditions using flow cell in analogy to M \ddot{u} sken *et al.*¹⁰³ Flow conditions would allow washing away weakly, unspecific bound ligands as well as unbound dyes, thus improving staining contrast. Choice of image visualization software, image processing and display options play an important role as well. In general, analogous processing functions were applied by open source software Fiji and commercial software Imaris, but brighter pictures were displayed by Imaris due to automatic contrast range adjustment. Real-time monitoring technique for *P. aeruginosa* biofilms is needed for the development of antibiofilm drugs as well as for better understanding of biofilm mode of this pathogen. We believe that together with PCR/MS methods,^{92,104} specifically tailored probes for

molecular imaging techniques (e.g. MRI, PET) might provide fast and pathogen specific detection and localization of bacterial infections.

3.2 A rapid synthesis of low-nanomolar divalent LecA inhibitors in four linear steps from D-galactose pentaacetate

Authors: Eva Zahorska, Sakonwan Kuhaudomlarp, Saverio Minervini, Sultaan Yousaf, Martin Lepsik, Thorsten Kinsinger, Anna K. H. Hirsch, Anne Imberty and Alexander Titz

Published in: *Chemical Communications*, 2020, **56**, 8822–8825.

DOI: 10.1039/d0cc03490h


 Cite this: *Chem. Commun.*, 2020, 56, 8822

 Received 15th May 2020,
Accepted 17th June 2020

DOI: 10.1039/d0cc03490h

rsc.li/chemcomm

A rapid synthesis of low-nanomolar divalent LecA inhibitors in four linear steps from D-galactose pentaacetate†

 Eva Zahorska,^{id abc} Sakonwan Kuhaudomlarp,^{id d} Saverio Minervini,^a Sultaan Yousaf,^a Martin Lepsik,^{id d} Thorsten Kinsinger,^a Anna K. H. Hirsch,^{id bce} Anne Imberty,^{id d} and Alexander Titz^{id *abc}

Chronic infections with *Pseudomonas aeruginosa* are associated with the formation of bacterial biofilms. The tetrameric *P. aeruginosa* lectin LecA is a virulence factor and an anti-biofilm drug target. Increasing the overall binding affinity by multivalent presentation of binding epitopes can enhance the weak carbohydrate–ligand interactions. Low-nanomolar divalent LecA ligands/inhibitors with up to 260-fold valency-normalized potency boost and excellent selectivity over human galectin-1 were synthesized from D-galactose pentaacetate and benzaldehyde-based linkers in four linear steps.

Pseudomonas aeruginosa has been classified as a priority-1 pathogen by the World Health Organization due to its high antimicrobial resistance and the lack of new drugs to treat multidrug-resistant strains.¹ New strategies against these bacterial infections are being explored to overcome the current antimicrobial-resistance crisis.² The so-called anti-virulence therapy aims to neutralize bacterial virulence factors instead of increasing the selection pressure imposed by targeting essential cellular functions with antibiotics and thereby circumvents the advent of new resistances whilst preserving commensal bacteria.^{3,4} This strategy is investigated for *P. aeruginosa* infections by targeting its tetravalent lectins LecA and LecB.^{2,5,6} Both proteins are virulence factors regulated by quorum sensing, mediate bacterial host-cell adhesion and are essential structural components of *P. aeruginosa* biofilms.^{7–9} Whereas the best L-fucose/D-mannose-based LecB antagonists bind in the nanomolar range, monovalent D-galactose-based LecA inhibitors only

reach binding affinities in the mid to low micromolar range.^{10–15} In Nature, the rather weak lectin–carbohydrate binding is often overcome by increasing valency, and thus enhancing apparent affinity.^{16,17} Likewise, a boost in target-binding affinity was achieved with multivalent inhibitors of LecA and LecB.^{6,18} Since LecA is a tetramer and pairs of binding sites are geometrically favorably oriented, simultaneously binding divalent inhibitors can boost binding affinity through favorable binding entropy.^{19,20} Notably, Pieters and co-workers have developed divalent LecA inhibitors based on complex and rigid repeating units of carbohydrate-triazole spacers with potent binding affinities ranging from 12 to 220 nM,^{21–23} while a divalent inhibitor with a more flexible linker reaches an affinity of 80 nM.²⁴ In another report, an oligoproline-spaced digalactoside bound to LecA with K_d of 71 nM.²⁵

In this work, we aimed to develop divalent LecA ligands with a focus on drug-like properties, synthetic accessibility and linker simplicity enabling future lead optimization. Spacer length and flexibility are important factors contributing to the overall potency of multivalent inhibitors.⁶ An optimized linker connecting two neighboring binding sites within one LecA tetramer and avoiding unwanted cross-linking between different LecA tetramers is desired (Fig. 1a). β -Linked aryl aglycons increase the binding strength of galactosides to LecA by establishing CH– π interactions with His50.¹⁵ The co-crystal structure of LecA with phenyl β -D-galactoside (PDB code: 5d21) showed possible growth vectors in *meta*- and *para*-position at the phenyl aglycon (Fig. 1b).²⁶

Protein-templated dynamic combinatorial chemistry (DCC) is an elegant method for the identification of potent ligands from a combinatorial library of building blocks with suitable linking chemistry in presence of a given protein.^{27,28} To apply this method to LecA, we introduced hydrazides at the *para*- or *meta*-position of phenyl β -D-galactoside in order to allow for acylhydrazone formation in DCC. For this purpose, we chose two galactoside building blocks with *meta*- or *para*-attached hydrazides, **1m** and **1p**, and varied linker length, rigidity and number of rotatable bonds by systematically increasing the number of methylene units in the corresponding benzaldehyde

^a Chemical Biology of Carbohydrates, Helmholtz Institute for Pharmaceutical Research Saarland, Helmholtz Centre for Infection Research, 66123 Saarbrücken, Germany. E-mail: alexander.titz@helmholtz-hzi.de

^b Deutsches Zentrum für Infektionsforschung (DZIF), Standort Hannover-Braunschweig, 38124 Braunschweig, Germany

^c Department of Pharmacy, Saarland University, 66123 Saarbrücken, Germany

^d Université Grenoble Alpes, CNRS, CERMAV, 38000 Grenoble, France

^e Drug Design and Optimization, Helmholtz Institute for Pharmaceutical Research Saarland, Helmholtz Centre for Infection Research, 66123 Saarbrücken, Germany

† Electronic supplementary information (ESI) available. See DOI: 10.1039/d0cc03490h



Communication

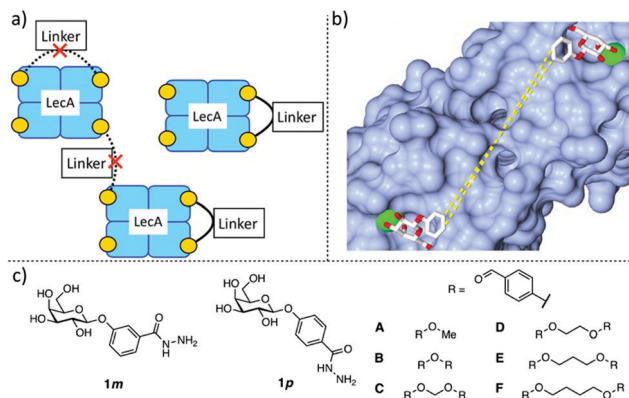
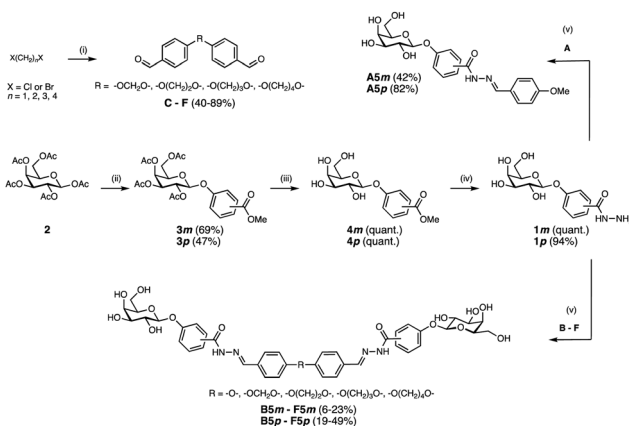


Fig. 1 Design of divalent LecA inhibitors accessible through a short synthetic route with acylhydrazone coupling chemistry. (a) Possible binding modes of divalent LecA inhibitors with desired linkage for two adjacent binding sites. (b) The crystal structure of phenyl β -D-galactoside in complex with LecA (pdb code: 5d21) and distances between two ligands within one pair of binding sites in LecA (from *meta* to *meta*: 23 Å, from *para* to *para*: 25 Å). (c) Building blocks of LecA inhibitors: *m/p*-hydrazinocarboxylphenyl β -D-galactopyranoside (**1m**, **1p**) and benzaldehydes **A–F**. Bis-benzaldehyde linkers **B–F** with systematic variation of length and number of rotatable bonds to optimize distance and flexibility.

spacers **B–F**. The corresponding monovalent control **A** was included (Fig. 1c).

Benzaldehydes **A** and **B** were commercially available and bis-benzaldehydes **C–F** were obtained in one step using 4-hydroxybenzaldehyde in a double nucleophilic substitution reaction on aliphatic α,ω -di-halogenated C1–C4 hydrocarbons under microwave irradiation (Scheme 1). Lewis acid-promoted glycosylation of methyl *meta*- or *para*-hydroxybenzoate with β -D-galactose pentaacetate (**2**) yielded glycosides **3m** and **3p** in 69% and 47% yield, respectively. Removal of the acetates under Zemplén conditions gave galactosides **4m** and **4p** quantitatively. Subsequent ester hydrazinolysis resulted in hydrazides **1m** and **1p** in very good yields. These building blocks were then used in DCC reactions in presence



Scheme 1 Synthesis of divalent LecA ligands and their monovalent analogs. *Reagents and conditions*: (i) 4-hydroxybenzaldehyde, K_2CO_3 , DMF, 70 °C, microwave, 3–10 h; (ii) methyl *m/p*-hydroxybenzoate, $BF_3 \cdot Et_2O$, CH_2Cl_2 , 0 °C – r.t., o.n.; (iii) NaOMe, MeOH, r.t., o.n.; (iv) $NH_2NH_2 \cdot H_2O$, MeOH, 70 °C, o.n.; (v) formic acid, DMSO, r.t., 4 h, for **D5m**: DMSO/MeCN, for **F5m**: H_2O /MeCN.

of LecA: since the addition of LecA to the library caused precipitation, all divalent molecules were individually synthesized in absence of protein. Acylhydrazone formation of aldehydes **A–F** with excess hydrazide **1m** or **1p** under acidic conditions yielded the mono- and divalent LecA ligands **A5m–F5m** and **A5p–F5p**. The reduced solubility of the *meta*-series compared to the *para*-series and more difficult purifications could explain the lower yields despite nearly quantitative turnover during the individual reactions.

All synthesized galactosides, **A5m–F5m** and **A5p–F5p**, were then analyzed in the previously established competitive LecA binding assay based on fluorescence polarization (Fig. 2).¹¹ Monovalent *meta*-ligand **A5m** ($IC_{50} = 21.6 \pm 4.5 \mu M$) was twice as potent as its *para*-isomer **A5p** ($IC_{50} = 55.5 \pm 4.4 \mu M$). The divalent ligands **B5m–F5m** and **B5p–F5p** showed a very similar profile in the competitive binding assay with very similar IC_{50} values in the single-digit micromolar range and a very steep Hill slope of the fit. These observations are likely a result of reaching the lower assay limit since the low affinity of the fluorescent primary ligand ($K_d = 7.4 \mu M$) required a relatively high LecA concentration of 20 μM . Therefore, ligand affinities with orders-of-magnitude higher potencies than the primary competitively displaced ligand cannot be reliably determined.

To overcome the competitive binding assay's limitation, we analyzed all inhibitors in a direct LecA binding experiment using surface plasmon resonance (SPR). In case of the monovalent inhibitors **A5m** and **A5p**, rapid changes in the binding response during the association and dissociation phases were observed, indicating fast association/dissociation kinetics of the monovalent inhibitors to immobilized LecA (Fig. 3a and b). Due to this fast association/dissociation behavior, k_{on} and k_{off} for their interaction with LecA could not be accurately determined and affinity analysis was performed instead of determining K_d at steady-state binding. In SPR, the monovalent ligands **A5m** and **A5p** have K_d values of 4.9 ± 0.1 and $5.6 \pm 0.3 \mu M$, respectively (Table 1). The binding affinities for those monovalent compounds were validated using isothermal titration microcalorimetry (ITC) as an orthogonal method and similar values to SPR data were obtained (ITC: **A5m** $K_d = 2.7 \pm 1.3 \mu M$, **A5p** $K_d = 6.1 \pm 0.5 \mu M$, Table 1 and Fig. S1, ESI[†]). In both analyses, a *meta*-substitution of the phenyl aglycon in **A5m** resulted in higher affinities to LecA compared to the *para*-isomer **A5p**.

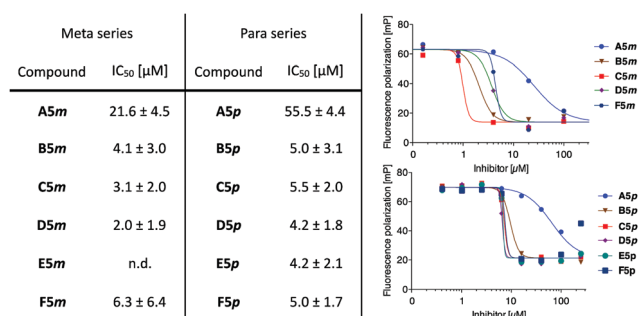
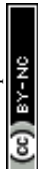


Fig. 2 Evaluation in a competitive binding assay. One representative titration is shown for each series (right) – steep titration slopes for divalent inhibitors indicate the lower assay limit was reached. Aver. and std. dev. from at least 3 independent titrations of triplicates each. n.d. = not determined.



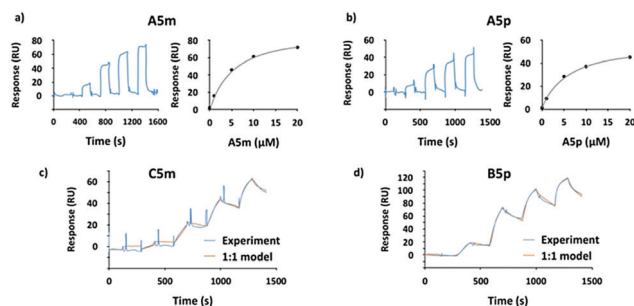


Fig. 3 SPR analyses of the interaction between the monovalent inhibitors (a) **A5m** and (b) **A5p**. The sensorgrams are shown on the left panel and the affinity analyses on the right. (c) Sensorgrams of the most potent divalent inhibitors from *meta*-series (**C5m**) and (d) from *para*-series (**B5p**) at five different concentrations (0, 10, 50, 100, 200 nM).

In contrast to the monovalent hydrazides, the SPR sensorgrams of the divalent inhibitors clearly indicated much slower association/dissociation of the compounds from LecA, demonstrating the benefit of divalent binding and enabling determination of kinetic parameters (k_{on} and k_{off}) as well as K_{d} (calculated from $k_{\text{off}}/k_{\text{on}}$, Fig. 3c, d and Fig. S2, ESI[†]). The divalent inhibitors **B5m–F5m** and **B5p–F5p** showed a strong increase in potency into the low nanomolar range (Table 1). In the *para*-series, compound **B5p** was the most potent ligand ($K_{\text{d}} = 10.8 \pm 1.0$ nM), with a 520-fold increase (260-fold valency-corrected) compared to its monovalent congener **A5p** ($K_{\text{d}} = 5600 \pm 300$ nM). The divalent *para*-ligands showed a slight decrease in potency with increasing spacer length, resulting from gradually decreasing k_{on} and increasing k_{off} (Table 1). In the *meta*-series, similar trends were absent. **C5m** with one central methylene unit had the optimal length and showed a K_{d} of 18.9 ± 1.6 nM. Shortening or increasing spacer length resulted in reduced affinities and surprisingly the second longest compound **E5m** was the least efficient inhibitor (K_{d} of 80.7 ± 11.4 nM). Comparing across the *meta*-series, the k_{on} values were surprisingly 2–4 times smaller for compounds **C5m** and **E5m**. The k_{off} values were gradually increasing going from **C5m–F5m**. The k_{off} for **B5m** was 5-times higher than that of **C5m**.

We then studied compound selectivity in binding experiments towards human galectin-1, a homodimeric lectin that specifically recognizes β -galactoside containing glycans such as Me- β -lactoside ($K_{\text{d}} = 187$ μM).²⁹ The most potent inhibitors

from the *para*- and *meta*-series, **B5p** and **C5m**, together with their respective monovalent counterparts (**A5p** and **A5m**), were analyzed by SPR for their interaction with human galectin-1. Neither the monovalent (at 250 μM) nor the divalent compounds (at 25 μM) had a detectable interaction with the immobilized galectin-1 (Fig. S3, ESI[†]).

Since we did not succeed in obtaining crystal structures of LecA complexed with the divalent inhibitors, we carried out modeling on pairs of *para*- and *meta*-compounds, selecting the high-affinity binder **C5m** and its *para*-counterpart **C5p**; and the longer, less active **E5m** and **E5p**. The dynamics of these four compounds were simulated in the free state and in the modeled complex with LecA. In the free state, the ligands adopted a broad range of semi-extended to fully extended conformations characterized by Gal:C1...Gal:C1 distances ranging from 20 to 31 Å at a cutoff of 5% frequency (Fig. 4a, solid curves). A distance close to the crystallographic value of 29 Å (PDB: 5d21) is desired for optimal divalent binding of LecA. In the longer compounds, **E5m** and **E5p**, there was a small population (around 5%) of folded conformations (see the peaks at 5 Å in Fig. 4a). The unfolding of these conformations prior to LecA binding may be in part responsible for their slower on-rate (k_{on}).

The four ligands modeled in complex with LecA showed a narrow distribution of the Gal:C1...Gal:C1 distances (Fig. 4a, dashed lines). **C5m**, **C5p** and **E5p** sampled distances of 28.9 ± 0.4 Å, 28.1 ± 0.9 Å, and 28.2 ± 0.7 Å, respectively, close to the 29 Å observed in crystal structures, thus indicating that the linker lengths are well-suited to bridge two LecA monomers. The narrow range for **C5m** (28–31 Å) may explain the lower affinity of shorter **B5m**. In contrast, **C5p** and **E5p** have larger range (26–31 Å) and shortening is beneficial such as in **B5p**. **E5m** with LecA displayed a higher mean distance of 30.2 ± 0.8 Å (range of 28 to 33 Å). Such longer *meta* linker pushes the two LecA monomers slightly apart, which is not favourable. The T-shaped CH- π interaction between His50 and the phenyl aglycon was observed with higher frequency for the *meta* compounds **C5m** and **E5m** compared to their *para* analogues **C5p** and **E5p** (Fig. 4b). On the opposite, the *para* ligands, **C5p** and **E5p**, preferentially adopted an inverted V-shape (Fig. 4c and d) in which their phenyl aglycons sampled a variety of arrangements with respect to His50 (parallel, diagonal, T-shape).

To conclude, we designed and synthesized highly potent divalent LecA inhibitors in four linear chemical steps from

Table 1 Affinity and kinetic analyses of the LecA-inhibitor interactions determined by SPR and ITC^a

<i>meta</i> series				<i>para</i> series					
	$k_{\text{on}} (\times 10^3 \text{ M}^{-1} \text{ s}^{-1})$	$k_{\text{off}} (\times 10^{-3} \text{ s}^{-1})$	$K_{\text{d}} (\text{nM})$	r.p.		$k_{\text{on}} (\times 10^3 \text{ M}^{-1} \text{ s}^{-1})$	$k_{\text{off}} (\times 10^{-3} \text{ s}^{-1})$	$K_{\text{d}} (\text{nM})$	r.p.
A5m	—	—	4900 ± 100	1	A5p	—	—	5600 ± 300	1
			2700 ± 1300^b	—				6100 ± 500^b	—
B5m	196 ± 6	5.34 ± 0.28	27.3 ± 1.6	90	B5p	152 ± 3	1.64 ± 0.13	10.8 ± 1.0	259
C5m	59 ± 3	1.11 ± 0.08	18.9 ± 1.6	130	C5p	114 ± 2	2.33 ± 0.02	20.5 ± 0.2	137
D5m	120 ± 41	2.67 ± 0.38	23.8 ± 7.1	103	D5p	121 ± 9	2.57 ± 0.20	21.4 ± 1.0	131
E5m	45 ± 4	3.64 ± 0.35	80.7 ± 11.4	30	E5p	103 ± 2	2.19 ± 0.45	22.5 ± 9.0	124
F5m	104 ± 53	3.39 ± 1.5	33.4 ± 2.3	73	F5p	79 ± 5	3.98 ± 0.16	50.1 ± 1.2	56

^a Averages and std. dev. from three independent experiments. Relative potencies (r.p.) were calculated compared to monovalent compound in each series (**A5m** and **A5p**) and valency-normalized. ^b ITC determination.



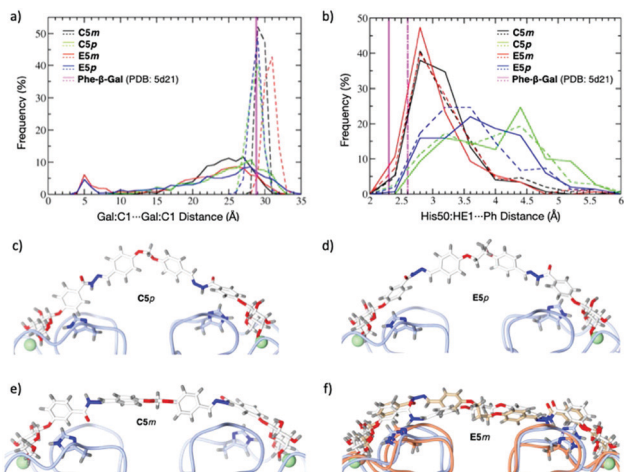


Fig. 4 Molecular dynamics simulations of **C5m**, **E5m**, **C5p**, **E5p**: (a) distribution of Gal:C1...Gal:C1 distances of compounds in the free state (solid lines) and in complex with LecA (dashed lines). (b) Distribution of distances between His50 and the phenyl aglycon of ligands in complex with LecA (solid lines for LecA protein chain A, dashed lines for chain B). (c–f) Snapshot from trajectories of **C5p** (c), **E5p** (d), **C5m** (e), and two snapshots of **E5m** (f) indicating the conformational change of LecA.

galactose pentaacetate. These simple and rapidly accessible divalent inhibitors **B5m–F5m** and **B5p–F5p** have comparable or superior activity to the previously reported and structurally complex di- and multivalent LecA ligands. Monovalent analogs **A5m** and **A5p** showed binding to LecA in SPR and ITC experiments in the low micromolar range ($K_d = 2.7\text{--}6.1\ \mu\text{M}$). Divalent display of these epitopes in **B5m–F5m** and **B5p–F5p** boosted binding affinity with LecA to low nanomolar values. Molecular dynamics simulations gave insights into the interplay of linker geometry and length for an optimal divalent binding. To the best of our knowledge, compound **B5p** with a K_d of 10.8 nM is the most potent divalent LecA ligand reported to date with confirmed selectivity for LecA over galectin-1. Due to the simplicity of our synthetic design and readily accessible building blocks, further fine tuning and optimization of drug-like properties can be readily implemented. Future optimization of these compounds targeting LecA may provide a treatment of biofilm-associated *P. aeruginosa* infections.

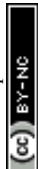
The authors are grateful to Dirk Hauck (HIPS) for excellent technical assistance and Varsha R. Jumde (HIPS) for assisting with DCC. M. L. acknowledges a EU H2020 Marie Skłodowska-Curie grant (795605). Computations were run on GRICAD infrastructure, HPC-EUROPA3 project (H2020-INFRAIA-2016-1-730897), and EPCC at the University of Edinburgh, Scotland, and HPC resources from GENCI-IDRIS (Grant 2019-A0070711040). A. T. thanks the European Research Council (ERC Starting Grant, Sweetbullets) and Deutsche Forschungsgemeinschaft (Ti756/5-1). S. Y. acknowledges a RISE fellowship, German Academic Exchange Service DAAD. The work was supported by the ANR/DFG French-German GLYCOMIME project (ANR-AAPG-2017, DFG Ti756/5-1). A. I. and S. K. acknowledge support from Glyco@Alps (ANR-15-IDEX02), Labex Arcane/CBH-EUR-GS (ANR-17-EURE-0003). A. K. H. gratefully acknowledges the ERC Starting Grant (757913).

Conflicts of interest

There are no conflicts to declare.

Notes and references

- WHO, <https://www.who.int/news-room/detail/27-02-2017-who-publishes-list-of-bacteria-for-which-new-antibiotics-are-urgently-needed>, accessed 9 April 2020.
- S. Wagner, R. Sommer, S. Hinsberger, C. Lu, R. W. Hartmann, M. Empting and A. Titz, *J. Med. Chem.*, 2016, **59**, 5929–5969.
- A. E. Clatworthy, E. Pierson and D. T. Hung, *Nat. Chem. Biol.*, 2007, **3**, 541–548.
- M. B. Calvert, V. R. Jumde and A. Titz, *Beilstein J. Org. Chem.*, 2018, **14**, 2607–2617.
- J. Meiers, E. Siebs, E. Zahorska and A. Titz, *Curr. Opin. Chem. Biol.*, 2019, **53**, 51–67.
- S. Cecioni, A. Imberty and S. Vidal, *Chem. Rev.*, 2015, **115**, 525–561.
- K. Winzer, C. Falconer, N. C. Garber, S. P. Diggle, M. Camara and P. Williams, *J. Bacteriol.*, 2000, **182**, 6401–6411.
- S. P. Diggle, R. E. Stacey, C. Dodd, M. Cámara, P. Williams and K. Winzer, *Environ. Microbiol.*, 2006, **8**, 1095–1104.
- D. Tielker, S. Hacker, R. Loris, M. Strathmann, J. Wingender, S. Wilhelm, F. Rosenau and K. E. Jaeger, *Microbiology*, 2005, **151**, 1313–1323.
- J. Rodrigue, G. Ganne, B. Blanchard, C. Saucier, D. Giguère, T. C. Shiao, A. Varrot, A. Imberty and R. Roy, *Org. Biomol. Chem.*, 2013, **11**, 6906–6918.
- I. Joachim, S. Rikker, D. Hauck, D. Ponader, S. Boden, R. Sommer, L. Hartmann and A. Titz, *Org. Biomol. Chem.*, 2016, **14**, 7933–7948.
- R. Sommer, S. Wagner, K. Rox, A. Varrot, D. Hauck, E. C. Wamhoff, J. Schreiber, T. Ryckmans, T. Brunner, C. Rademacher, R. W. Hartmann, M. Brönstrup, A. Imberty and A. Titz, *J. Am. Chem. Soc.*, 2018, **140**, 2537–2545.
- R. Sommer, K. Rox, S. Wagner, D. Hauck, S. S. Henrikus, S. Newsad, T. Arnold, T. Ryckmans, M. Brönstrup, A. Imberty, A. Varrot, R. W. Hartmann and A. Titz, *J. Med. Chem.*, 2019, **62**, 9201–9216.
- S. Wagner, D. Hauck, M. Hoffmann, R. Sommer, I. Joachim, R. Müller, A. Imberty, A. Varrot and A. Titz, *Angew. Chem., Int. Ed.*, 2017, **56**, 16559–16564.
- R. U. Kadam, D. Garg, J. Schwartz, R. Visini, M. Sattler, A. Stocker, T. Darbre and J.-L. Reymond, *ACS Chem. Biol.*, 2013, **8**, 1925–1930.
- M. Mammen, S.-K. Choi and G. M. Whitesides, *Angew. Chem., Int. Ed.*, 1998, **37**, 2754–2794.
- K. Drickamer and M. E. Taylor, *Curr. Opin. Struct. Biol.*, 2015, **34**, 26–34.
- A. Bernardi, J. Jiménez-Barbero and A. Casnati, *et al.*, *Chem. Soc. Rev.*, 2013, **42**, 4709–4727.
- G. Cioci, E. P. Mitchell, C. Gautier, M. Wimmerová, D. Sudakevitz, S. Pérez, N. Gilboa-Garber and A. Imberty, *FEBS Lett.*, 2003, **555**, 297–301.
- J. E. Gestwicki, C. W. Cairo, L. E. Strong, K. A. Oetjen and L. L. Kiessling, *J. Am. Chem. Soc.*, 2002, **124**, 14922–14933.
- F. Pertici and R. J. Pieters, *Chem. Commun.*, 2012, **48**, 4008–4010.
- G. Yu, A. C. Vicini and R. J. Pieters, *J. Org. Chem.*, 2019, **84**, 2470–2488.
- R. Visini, X. Jin, M. Bergmann, G. Michaud, F. Pertici, O. Fu, A. Pukin, T. R. Branson, D. M. E. Thies-Weesie, J. Kemmink, E. Gillon, A. Imberty, A. Stocker, T. Darbre, R. J. Pieters and J. L. Reymond, *ACS Chem. Biol.*, 2015, **10**, 2455–2462.
- A. Novoa, T. Eierhoff, J. Topin, A. Varrot, S. Barluenga, A. Imberty, W. Römer and N. Winssinger, *Angew. Chem., Int. Ed.*, 2014, **53**, 8885–8889.
- S.-F. Huang, C.-H. Lin, Y.-T. Lai, C.-L. Tsai, T.-J. R. Cheng and S.-K. Wang, *Chem. – Asian J.*, 2018, **13**, 686–700.
- M. Bergmann, G. Michaud, R. Visini, X. Jin, E. Gillon, A. Stocker, A. Imberty, T. Darbre and J. L. Reymond, *Org. Biomol. Chem.*, 2016, **14**, 138–148.
- M. Mondal and A. K. H. Hirsch, *Chem. Soc. Rev.*, 2015, **44**, 2455–2488.
- A. M. Hartman, R. M. Gierse and A. K. H. Hirsch, *Eur. J. Org. Chem.*, 2019, 3581–3590.
- I. Cumpstey, E. Salomonsson, A. Sundin, H. Leffler and U. J. Nilsson, *ChemBioChem*, 2007, **8**, 1389–1398.



3.3 Isosteric substitution of acylhydrazones yields highly potent divalent LecA inhibitors with excellent solubility and metabolic stability

Carbohydrate-protein interactions are essential recognition codes in many biological processes, including microbial and viral infections. Lectins of pathogenic origin involved in host-cell recognition, adhesion and/or biofilm formation are being recognized as new therapeutic targets.^{105,106} *Pseudomonas aeruginosa* is a Gram-negative opportunistic bacterium that belongs to the group of highly resistant ESKAPE pathogens.⁷ Resistance to an antimicrobial treatment can be further enhanced by its ability to grow biofilms – the causative mechanism of chronic infections.¹⁵ *P. aeruginosa* adhesion and biofilm formation are mediated by the tetravalent lectins LecA and LecB, encoded in its core genome and functionally conserved across clinical isolates.^{35,36,55,107} Thus, their inhibition is desired to counteract pathogenicity.¹⁸ Furthermore, it was shown that LecA acts as a lipid zipper upon binding to its cellular receptor Gb3 and triggers bacterial invasion.³⁹ It was demonstrated that inhalation of D-galactose and L-fucose aerosols, the monosaccharide ligands of LecA and LecB, respectively, reduced bacterial burden in cystic fibrosis patients.⁴⁸

Numerous glycomimetics based on D-galactose ($K_d = 88 \mu\text{M}$)⁵⁹ and L-fucose/D-mannose ($K_d = 430 \text{ nM}$ for methyl α -L-fucoside, $K_d = 71 \mu\text{M}$ methyl α -D-mannoside)¹⁰⁸ have been developed for LecA and LecB, respectively.^{18,68,106} Some of these compounds targeting LecB lack carbohydrate character and showed potent inhibition of LecB with beneficial pharmacokinetic properties.^{46,47,62} Numerous monovalent LecA glycomimetic inhibitors have also been reported^{43,60,61} and we have recently introduced the first covalent lectin inhibitor in general⁴⁴ targeting a surface exposed cysteine residue and the first non-carbohydrate lectin inhibitors for bacterial lectins, a catechol motif.⁵² However, all monovalent LecA inhibitors reached at best only moderate potencies in the 5 to 50 μM range.

In contrast to LecB, the quaternary structure of LecA⁵⁶ displays two adjacent binding sites that are optimally oriented in space for simultaneous inhibition with divalent ligands leading to a potency boost. Notably, Pieters and coworkers developed low nanomolar LecA inhibitors (down to $K_d = 12 \text{ nM}$) by connecting two galactosides containing several copies of rigid glucose-triazole linkers.^{42,86} Despite the efficient CuAAC chemistry applied for the final assembly of the divalent ligands, 17 synthetic steps were required to prepare the individual azide and alkyne building blocks and assemble the final compound. Replacement of one of the glucose-bistriazole spacers with cyclohexyl bithiourea moieties somewhat simplified the synthesis to 9 steps and one compound with 30 nM affinity was obtained.⁸⁵ Similarly, rather

complex divalent LecA ligands with peptide-based linkers obtained from a lengthy synthesis were reported by Novoa *et al.* ($K_d = 82$ nM) and Huang *et al.* ($K_d = 71$ nM).^{109,110}

We have recently reported a series of highly active divalent LecA inhibitors based on acylhydrazone linking chemistry ($K_d = 11 - 81$ nM) synthesized in only four chemical steps.¹¹¹ While these molecules showed the highest potency among all published divalent LecA inhibitors, they suffer from an intrinsic hydrolytic lability of the acylhydrazone bond and very low aqueous solubility despite the presence of the two hydrophilic carbohydrate moieties. Furthermore, since acylhydrazones undergo hydrolysis at acidic pH, potentially toxic aldehydes and hydrazides may be formed *in vivo*.

Here, we report the optimization of these highly potent divalent LecA inhibitors by replacing the acylhydrazone motif with a more stable amide bond and varying linker identity and length to increase solubility and stability (Figure 1a). We chose two galactoside building blocks bearing coumaric acid (**1**, Figure 1b) or hydroxyphenyl propionic acid (**2**) as aglycons to investigate the effect of the more rigid olefin in **1**, comparable to the parent acylhydrazones, versus the flexible alkyl motif in **2**. These galactosylated carboxylic acids were intended for coupling to various bisanilines to yield the corresponding divalent LecA inhibitors. Since an optimal length and geometry is important for the divalent ligand to bind simultaneously to two neighbouring LecA sites, linker length was varied by stepwise introduction of methylene units. The aromatic moieties and linker lengths were varied: bisaniline linkers **B–F** and their monovalent control **A** (Figure 1c) were used to mimic previously used bis-benzaldehyde structures;¹¹¹ our rational solubility optimization included the introduction of hydrogen-bonding polar groups or ionizable moieties into bisaminopyridine linkers **H–J** and sulfonated linker **L** and their monovalent controls **G** and **K**, respectively.

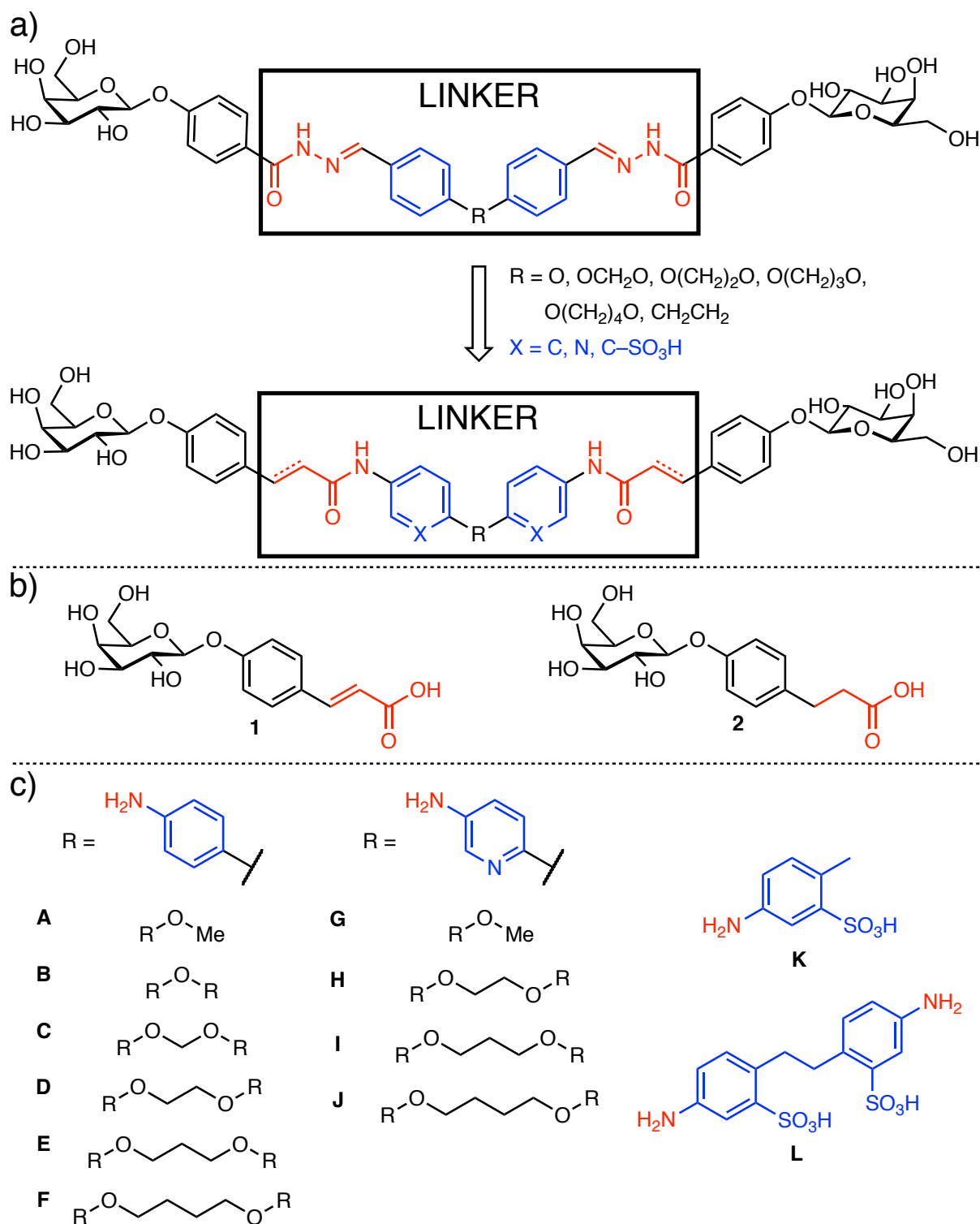
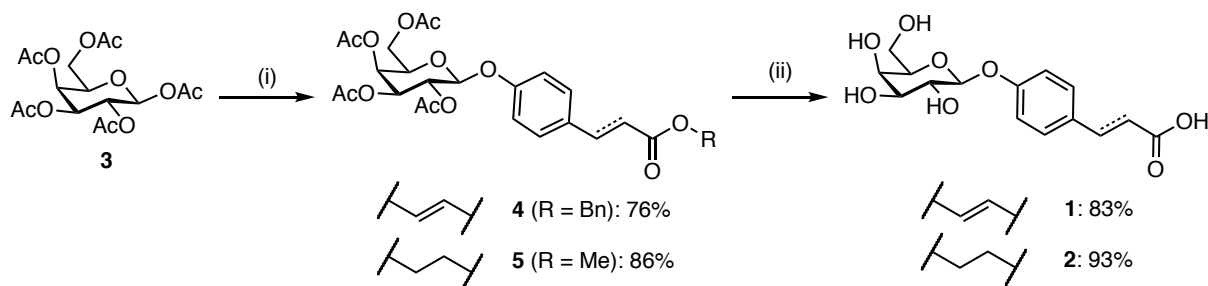


Figure 1: Divalent precision LecA ligands: (a) parent bisacylhydrazone LecA inhibitors (top) and new generation optimized bioisosters (bottom). Proposed chemical modifications are highlighted: amide linkage as acylhydrazone bioisoster in red and linker derivatizations in blue. (b) Galactoside building blocks with terminal α,β -unsaturated carboxylate **1** and its saturated analogue **2**. (c) Linker moieties: anilines **B–F**, aminopyridines **H–J** and sulfonated linker **L**, and their monovalent controls **A**, **G**, and **K**.

Synthesis of the two galactoside building blocks **1** and **2** started with β -selective glycosylation of benzyl coumarate or methyl 3-(4-hydroxyphenyl)propanoate with β -D-galactose pentaacetate (**3**) under Lewis acid catalysis (Scheme 1). β -Glycosides **4** and **5** were obtained in good yields (76-86%) and full saponification of the esters was achieved by treating with aqueous NaOH to give galactosides **1** and **2** in high yields. Synthesis of coumarate **1** was initially attempted using the methyl ester under identical glycosylation conditions as for compound **2**, but this transformation was unsuccessful most probably due to its poor solubility in dichloromethane and only poor yields were achieved when carried out in the more polar solvent chloroform instead. Changing the glycosyl acceptor from methyl to benzyl coumarate improved solubility in those solvents and the glycosylation yielded 76% of compound **4**.

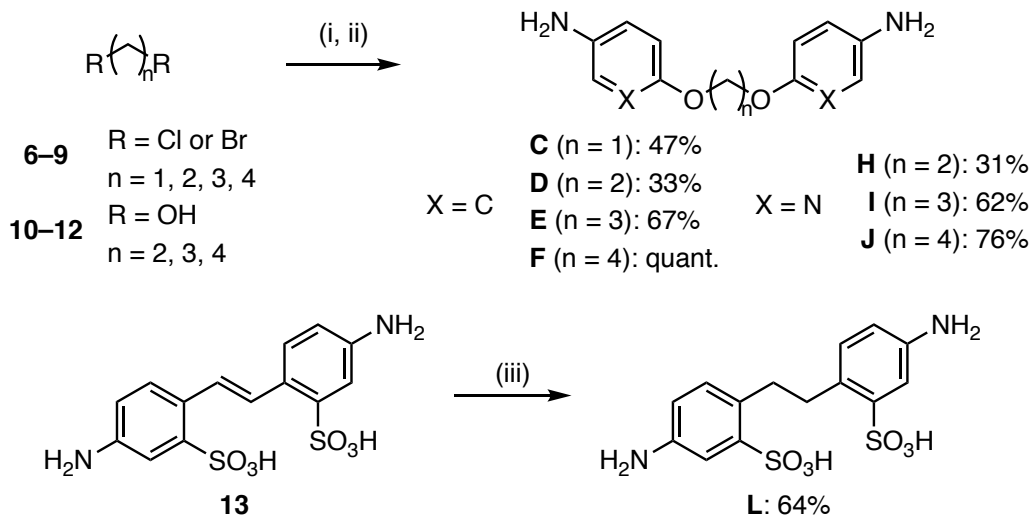


Scheme 1: Synthesis of galactoside building blocks **1** and **2**. Reagents and conditions: (i) benzyl *p*-coumarate/methyl 3-(4-hydroxyphenyl)propanoate, $\text{BF}_3 \cdot \text{Et}_2\text{O}$, CHCl_3 for **4** and CH_2Cl_2 for **5**, 0°C – r.t., overnight; (ii) NaOH, $\text{H}_2\text{O}/\text{MeOH}$ (1:1), 50°C for **1** and r.t. for **2**, 1 h – 2 h.

The linkers needed for assembly of those galactosides into divalent LecA inhibitors were synthesized or purchased. While, anilines **A** and **B**, amino pyridine **G** and sulfonated linker **K** were commercially available, linkers **C–F** and bis-aminopyridine linkers **H–J** were prepared in two steps: a double nucleophilic substitution of the α,ω -alkyldihalides (**6–9**) with 4-nitrophenol or a double nucleophilic aromatic substitution using α,ω -alkyldiols (**10–12**) with 2-chloro-5-nitro-pyridine followed in both cases by palladium-catalyzed hydrogenation to the desired bis-anilines or bis-aminopyridines, respectively (Scheme 2). Ethyl-spaced bissulfonated linker **L** was by obtained by reduction of 4,4'-diaminostilbene-2,2'-disulfonic acid (**13**) with hydrogen on Raney nickel.

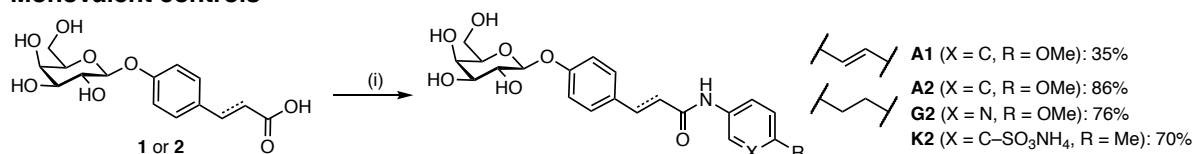
Final assembly of the divalent LecA inhibitors was achieved by coupling of the amino-substituted linkers **A–L** and carboxylate-containing galactosides **1** and **2** using HBTU or PyBOP as peptide coupling reagents (Scheme 3). High reaction turnovers were observed for all coupling reactions, but purification difficulties caused varying yields: lower solubility was responsible for isolated yields in the benzene series (**A1–F1** and **A2–F2**), whereas side product formation was observed in the pyridine series (**H1–I1** and **G2–J2**). After chromatographic

separation, the sulfonic acids induced acid catalysed hydrolysis of the glycosidic linkage upon solvent removal and concentration, thus the sulfonated ligands **K2** and **L2** had to be purified using buffered eluents as ammonium salts.

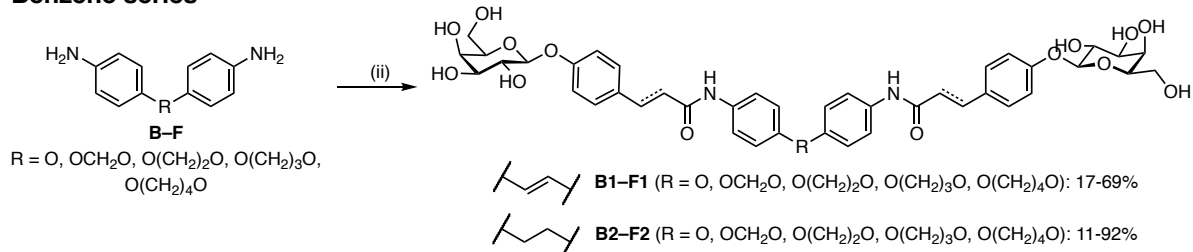


Scheme 2: Synthesis of benzene, pyridine and phenylsulfonate linkers. Reagents and conditions: (i) for **C-F**: 4-nitrophenol, K_2CO_3 , DMF, 70 °C, microwave, 11 h – 4 d (for **C** 10 days, no irradiation), for **H-J**: 2-chloro-5-nitropyridine, NaH, r.t., DMF, 1 h – 2 d (for **H** K_2CO_3 , 65 °C, DMF, 5 d); (ii) H_2 , Pd/C, $\text{CH}_2\text{Cl}_2/\text{MeOH}$ (2:1, 3:1 for **D-F**), r.t., 3h – o.n.; (iii) Raney Ni, H_2 , r.t., H_2O , 6 d.

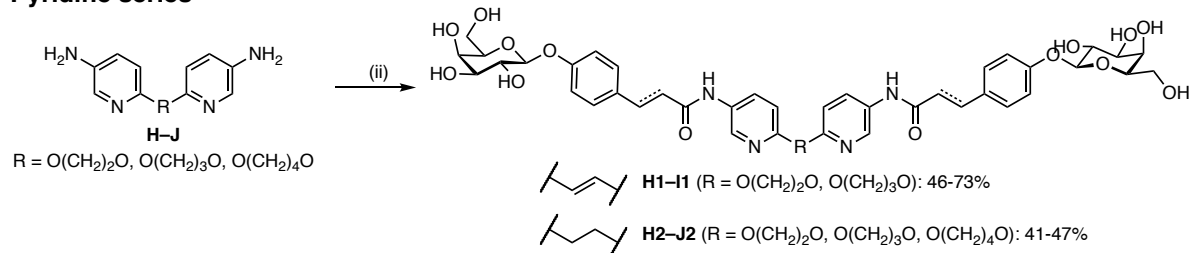
Monovalent controls



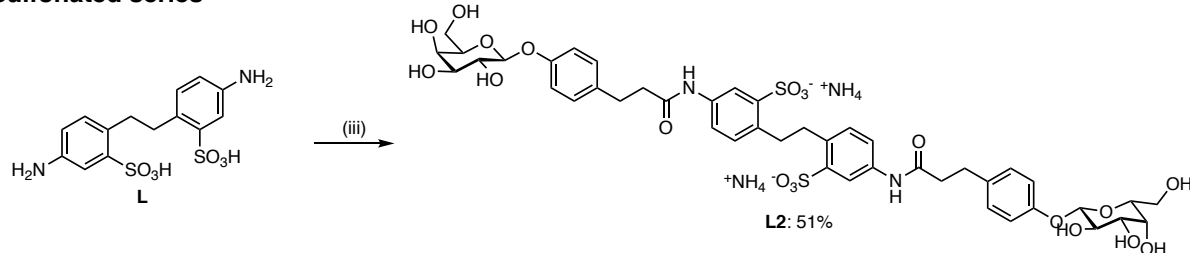
Benzene series



Pyridine series



Sulfonated series



Scheme 3: Synthesis of divalent LecA ligands and their monovalent analogues as controls. Reagents and conditions: (i) for **A** and **G**: HBTU, DIPEA, DMF, r.t., 1 h – overnight, for **K**: PyBOP, N-methylmorpholine, DMF, r.t., overnight; (ii) galactoside **1** or **2**, HBTU, DIPEA, DMF, r.t., 2 h – 2 d, (iii) galactoside **2**, PyBOP, N-methylmorpholine, DMF, r.t., overnight.

Previously, the parent acylhydrazone divalent LecA ligands¹¹¹ (Figure 1) suffered from poor aqueous solubility. Therefore, we tested selected representatives of each new class aiming at higher solubility and one of the parent bisacylhydrazones and quantified their solubility in aqueous media (Table 1). All tested new derivatives showed significantly improved solubility compared to the previous bisacylhydrazone **14**. The very low kinetic solubility of the bis-acylhydrazone **14** ($S < 300$ nM) was increased at least fourfold in its α,β -unsaturated amide analogue **D1** ($S = 1.2 \pm 0.6$ μ M) and at least over 20-fold in the saturated analogue **D2** ($S = 7.5 \pm 4.2$ μ M). Substitution of the benzene ring with a pyridine moiety further increased solubility by 5- to 10-fold enhancement (**H1** $S = 5.5 \pm 1.4$ μ M, **H2** $S = 71.4 \pm 14.9$ μ M) compared to **D1/D2**. Generally, more flexible saturated propanamide divalent ligands **D1** and **H1** were more soluble than their unsaturated acrylamide-based analogues **D2** and **H2**. Excellent solubility was

finally achieved with sulfonated divalent ligand **L2**, which was fully dissolved from its solid form in an aqueous buffer ($S > 1.5$ mM).

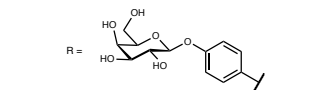
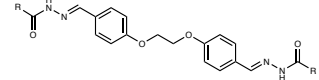
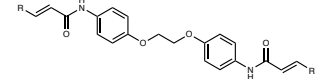
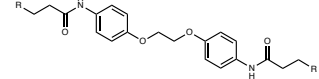
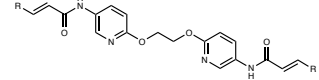
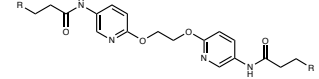
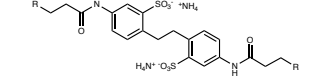
We then set out to determine early *in vitro* ADME properties for a selected subset of the synthesized LecA inhibitors **D1**, **D2**, **H1**, **H2** and **L2** to evaluate their stability in blood plasma and against liver metabolism and compare it to one parent bisacylhydrazone compound **14** (Table 1). The data obtained from microsomal stability tests revealed a low intrinsic clearance by mouse microsomes ($CL_{int} = 6.8 - 23$ $\mu\text{L}/\text{min}/\text{mg}$ protein) for all tested compounds, except of the slightly elevated clearance by **D2** ($CL_{int} = 29.6$ $\mu\text{L}/\text{min}/\text{mg}$ protein) and by the sulfonated ligand **L2** ($CL_{int} = 29.5$ $\mu\text{L}/\text{min}/\text{mg}$ protein). On the other hand, significant differences in metabolic stability were observed in human liver microsomes. Introduction of the pyridine ring decreased the compound stability (**H1** $CL_{int} = 28.6$ $\mu\text{L}/\text{min}/\text{mg}$ protein, **H2** $CL_{int} = 32.5$ $\mu\text{L}/\text{min}/\text{mg}$ protein) compared to their benzene analogues (**D1** $CL_{int} = 21.9$ $\mu\text{L}/\text{min}/\text{mg}$ protein, **D2** $CL_{int} = 21.0$ $\mu\text{L}/\text{min}/\text{mg}$ protein) or even to the parent acylhydrazone ligand **14** ($CL_{int} = 19.6$ $\mu\text{L}/\text{min}/\text{mg}$ protein). The sulfonated ligand **L2** was the most stable compound in human microsomes ($CL_{int} = 9.2$ $\mu\text{L}/\text{min}/\text{mg}$ protein).

In mouse plasma, the parent acylhydrazone ligand **14** was rather quickly degraded ($t_{1/2} = 48.9$ min) and a somewhat slower degradation was observed in human plasma ($t_{1/2} = 123.5$ min). In contrast, the new generation of ligands exhibited high stability in both mouse and human plasma ($t_{1/2} \geq 180$ min), with exception of coumarate-bearing pyridine **H2** in mouse plasma ($t_{1/2} = 81.1$ min) and coumarate-bearing benzene **D2** in human plasma ($t_{1/2} = 132.5$ min), both of which still showed superior stability to the bisacylhydrazone **14**. The observed higher plasma stability of all tested amide derivatives supports the isosteric replacement of the hydrolysis prone bisacylhydrazone linking motif. All tested compounds showed very high to full mouse and human plasma protein binding (PPB) with lowest PPB for saturated pyridyl amide **H2** at 97% except for the sulfonated ligand **L2** which showed remarkably low plasma protein binding in both species, mouse and human (14.48 % and 38.45 %, respectively).

All synthesized galactosides were then evaluated for LecA inhibition in the previously reported competitive binding assay based on fluorescence polarization (Figure S1).⁶¹ Monovalent galactosides (**A1**, **A2**, **G2** and **K2**) showed IC_{50} values between 14 – 19 μM and did not significantly differ from each other. The monovalent ligand carrying the α,β -unsaturated acrylamide motif **A1** ($IC_{50} = 18.8 \pm 6.6$ μM) was equipotent to its saturated and more flexible propanamide analogue **A2** ($IC_{50} = 18.9 \pm 5.5$ μM). Replacement of the benzene ring with pyridine in **G2** ($IC_{50} = 14.3 \pm 7.2$ μM) or addition of the sulfonate solubility tag in **K2** ($IC_{50} = 14.4 \pm 3.6$ μM) were well tolerated by the protein. In contrast to the monovalent controls and

similar to our previous observations for the bisacylhydrazones, the titrations of the fluorescent galactoside-LecA mixture with all divalent LecA ligands exhibited very steep Hill slopes with IC₅₀s in the single digit micromolar range indicating the high potency of divalent compounds reaching the lower assay limit.¹¹¹

Table 1: Aqueous solubility and early ADME data of selected LecA inhibitors. Kinetic solubility was determined in aqueous TBS/Ca²⁺ buffer containing 1% DMSO by LC-MS. Averages and std. dev. from three independent experiments. *Thermodynamic solubility in TBS/Ca²⁺ buffer (w/o DMSO), one replicate. Plasma stability, plasma protein binding and metabolic stability using S9-fractions were performed in triplicates. Data were analysed using LC-MS/MS measurements.

	Compound	Solubility S [μ M]	CL _{int} [μ L/min/mg protein]		Plasma stability t _{1/2} [min]		PPB [%]	
			Mouse	Human	Mouse	Human	Mouse	Human
	14	< 0.3	< 23	19.6	48.9	123.5	100 ± 0	100 ± 0
	D1	1.2 ± 0.6	22.4	21.9	180.1	223.9	99.43 ± 1.0	99.57 ± 0.8
	D2	7.5 ± 4.2	29.6	21.0	182.7	132.5	100 ± 0	99.51 ± 0.8
	H1	5.5 ± 1.4	17.5	28.6	> 180	> 240	100 ± 0	100 ± 0
	H2	71.4 ± 14.9	6.8	32.5	81.1	214.9	97.58 ± 2.1	99.50 ± 0.9
	L2	> 1500*	29.5	9.2	> 240	> 240	14.48 ± 6.8	38.45 ± 12.4

To circumvent the limit of the competitive binding assay for these highly potent inhibitors, direct binding to LecA was quantified using SPR (Figure 2, Figures S2–S3). In agreement with the competitive binding assay, no difference in binding affinity was observed for the monovalent ligands carrying the acrylamide motif **A1** ($K_d = 5.21 \pm 0.60 \mu\text{M}$) compared to the propanamide derivative **A2** ($K_d = 5.38 \pm 0.09 \mu\text{M}$). Interestingly, a striking difference between these structures was observed for the divalent inhibitors. Within the benzene series, the acrylamide-based ligands **B1–F1** showed K_d s in the nanomolar to micromolar range while their propanamide-based analogues **B2–F2** were two- to threefold more active when attached to the shorter linkers **B–D** and 100- to 200-fold more potent for the longest linkers **E** and **F**. With respect to the linker length, the divalent ligands with linker **C** containing one methylene unit were the most potent ones (**C1** $K_d = 37.7 \pm 11 \text{ nM}$, **C2** $K_d = 15.3 \pm 0.6 \text{ nM}$). With increased linker length, the binding potency was decreasing in the acrylamide-based divalent ligands **B1–F1**, with the exception of **C1**. Complete loss of divalent binding boost was observed for the **F1** ligand ($K_d = 2.25 \pm 0.3 \mu\text{M}$). Divalent ligands carrying the propanamide motif **B2–F2** showed

high binding affinity to LecA in 15–23 nM range. K_d values were oscillating based on the number of methylene units present in the linker, possibly as the results of “zig-zag” geometry of the hydrocarbon chain.

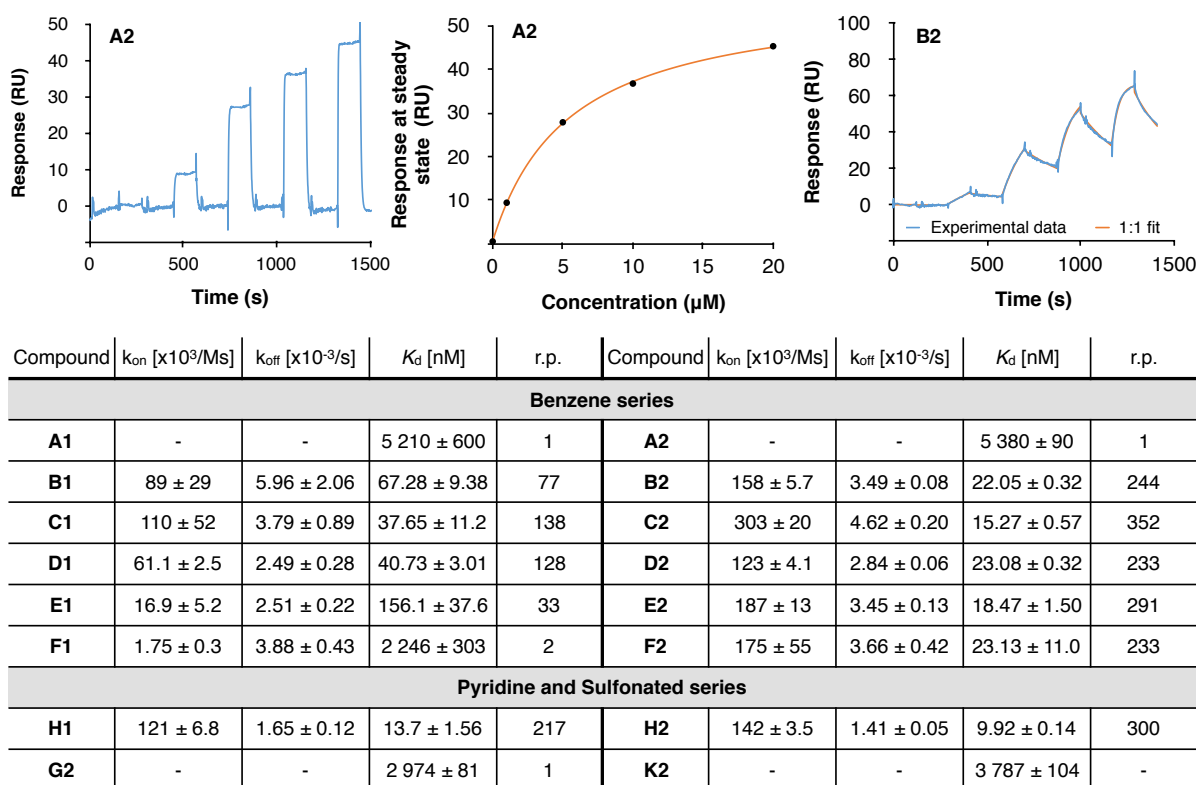


Figure 2: Direct binding of LecA ligands determined by SPR. Sensogram of monovalent ligand **A2** (left) with its affinity analysis (centre) and sensogram of divalent ligand **B2** (right) from single-cycle kinetics experiments (injections of 0, 10, 50, 100, 200 nM) are shown. Averages and std. dev. were calculated from three independent experiments. Relative potencies (r.p.) were calculated compared to respective monovalent compound in each series and valency-normalized.

Compared to **A2**, monovalent ligands from the pyridine series **G2** and sulfonated series **K2** showed only slightly enhanced binding affinity to LecA (**G2** $K_d = 2.97 \pm 0.08 \mu\text{M}$, **K2** $K_d = 3.78 \pm 0.10 \mu\text{M}$). In case of divalent ligands, substitution of the benzene ring with pyridine showed three-fold increase in binding affinity of the shortest divalent acrylamide-based ligand **H1** ($K_d = 13.7 \pm 1.56 \text{ nM}$) and two-fold increase in the shortest divalent propanamide derivative **H2** ($K_d = 9.92 \pm 0.14 \text{ nM}$), when compared to their benzene analogues **D1** and **D2**, respectively. The observed potency boost might be a result of additional interactions of the pyridine rings with the protein surface (e.g. H-bond) or a solvation contribution. Evaluation of the remaining divalent ligands from pyridine series (**I1**, **I2**, **J2**) and the sulfonated ligand **L2** by SPR is in progress. However, due to the superior solubility of the propanamide ligands in the pyridine series and an excellent solubility of the sulfonated ligand **L2**, we were now able to determine their binding affinities using solution phase direct binding to LecA by ITC (Figure 3, Figures

S4–S8). K_d values measured for monovalent ligands **G2** and **K2** by ITC were slightly higher than their SPR values, but were validated to be in low micromolar range (**G2** $K_d = 5.27 \pm 0.03 \mu\text{M}$, **K2** $K_d = 6.23 \pm 0.44 \mu\text{M}$). Comparable binding affinities in low nanomolar range were measured for divalent pyridine-containing ligand **I2** ($K_d = 35.1 \pm 12.5 \text{ nM}$) and divalent sulfonated ligand **L2** ($K_d = 39.9 \pm 3.6 \text{ nM}$). In both cases, enthalpy contributions were roughly doubled (**I2** $\Delta H = -23.9 \pm 1.2 \text{ kcal/mol}$, **L2** $\Delta H = -19.5 \pm 1.3 \text{ kcal/mol}$) compared to their monovalent analogues (**G2** $\Delta H = -11.0 \pm 0.2 \text{ kcal/mol}$, **K2** $\Delta H = -10.3 \pm 0.1 \text{ kcal/mol}$), while the entropy costs were increased at least threefold (**G2** $\Delta S = -12.8 \pm 0.6 \text{ cal/mol/deg}$ vs. **I2** $\Delta S = -45.9 \pm 4.5 \text{ cal/mol/deg}$, **K2** $\Delta S = -10.7 \pm 0.6 \text{ cal/mol/deg}$ vs. **L2** $\Delta S = -31.6 \pm 4.4 \text{ cal/mol/deg}$). Divalent ligand with the longest linker **J2** was less potent, yet still in nanomolar range ($K_d = 79.5 \pm 32.8 \text{ nM}$), with decreased enthalpy contribution ($\Delta H = -13.5 \pm 0.90 \text{ kcal/mol}$) but also lower entropy costs ($\Delta S = -12.6 \pm 1.8 \text{ cal/mol/deg}$), suggesting different binding mode for **J2**.

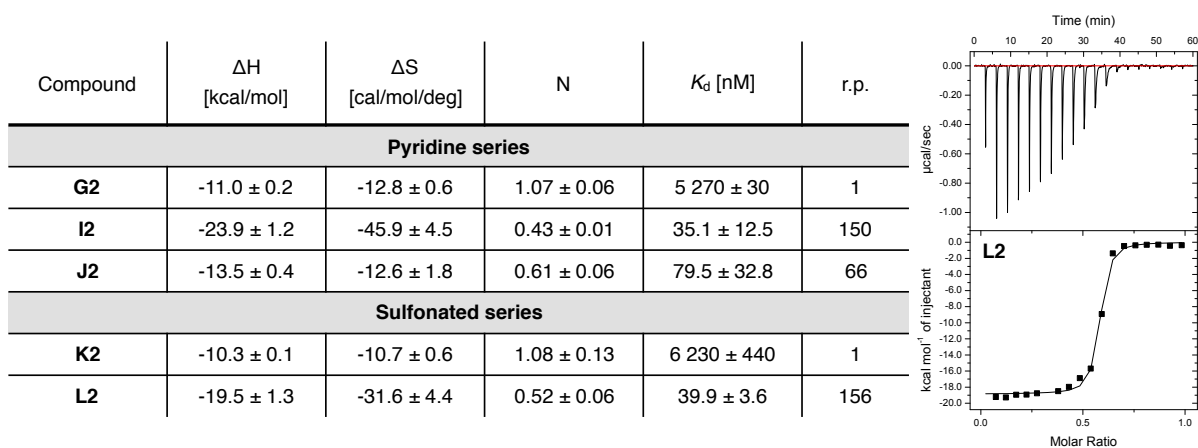


Figure 3: Direct binding of LecA ligands determined by ITC. Titration of LecA ($50 \mu\text{M}$) with divalent sulfonated ligand **L2** ($250 \mu\text{M}$) is shown. Averages and std. dev. Were calculated from three independent experiments. Relative potencies (r.p.) were calculated compared to respective monovalent compound in each series and valency-normalized.

In conclusion, we synthesized a small library of divalent LecA ligands in only three to five chemical steps as bioisosters of the poorly soluble and chemical labile but highly potent bisacylhydrazones reported previously. The aim of this work to increase solubility and stability while maintaining on target activity for LecA was achieved and all modifications (Figure1) lead to an increase in solubility. A remarkable solubility boost over 5000-fold was achieved with the sulfonated ligand **L2** ($S > 1.5 \text{ mM}$). Furthermore, replacement of the chemically labile acylhydrazone linkage with its amide bioisoster enhanced compound stability in plasma. Divalent ligands from the benzene series (**D1**, **D2**) as well as the sulfonated ligand **L2** exhibited high stability in human liver microsomes while the pyridine **H1**, **H2** were slightly less stable.

All ligands showed high plasma protein binding in mouse and human species, whereas the ligand **L2** exhibited remarkably low plasma protein binding properties. Low nanomolar binding affinities associated with a strong divalent potency boost could be retained for all synthesized compounds with a single exception of the longest acrylamide-based ligand **F1** (**I1** not yet measured). Good solubility of propanamide ligands in the pyridine series **H2–J2** and the divalent sulfonated ligand **L2** allowed evaluation of the thermodynamics binding parameters with ITC in addition to kinetic parameters determined by SPR. These highly optimized compounds will be studied in experiments with *P. aeruginosa*. The inhibition of LecA virulence may provide an alternative treatment option for *P. aeruginosa* infections.

3.4 Divalent fluorescent LecA ligands

Conjugation of LecA and LecB inhibitors to fluorophore cargo was explored in order to develop novel diagnostic options for *P. aeruginosa* infections (Chapters 3.1). One of the drawbacks of carbohydrate-based ligands is the weak monovalent sugar binding. Likewise, on-target activity of our lectin-directed fluorescent conjugates bearing only one sugar targeting moiety was only in low micromolar range. However, a boost in activity can be achieved by multivalent display of the binding epitopes. Development of rapidly accessible divalent LecA inhibitors with low nanomolar binding affinities is described in Chapter 3.2.

Here we aimed to modify our divalent LecA inhibitors to allow attachment of various cargo molecules (e.g. fluorophore, antibiotic or photosensitiser), while retaining their high binding affinity. Molecular dynamics simulations of acylhydrazone divalent ligand **1** in complex with LecA showed a possible growth vector at the centre of the ligand (Figure 1). Modification of the compound **1** only its linker core with a side branch was proposed. In a proof-of-concept design, the linker side branch bearing terminal alkyne moiety was used for conjugation to fluorescent signal compound, i.e. fluorescein. High affinity fluorescently labelled LecA ligand could be used to improve the competitive binding assay based on fluorescence polarization⁶¹ or as a diagnostic tool for *P. aeruginosa* infections.

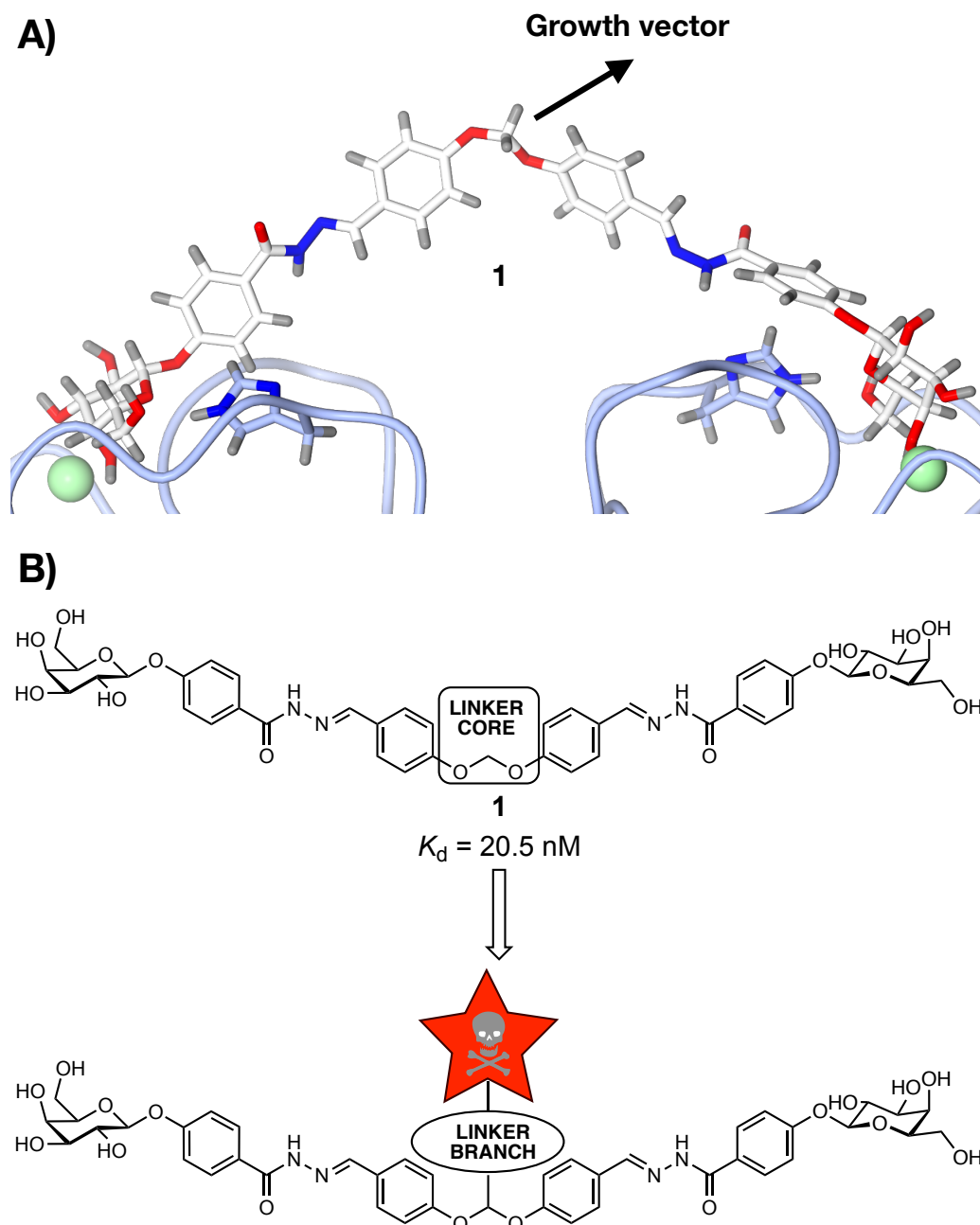
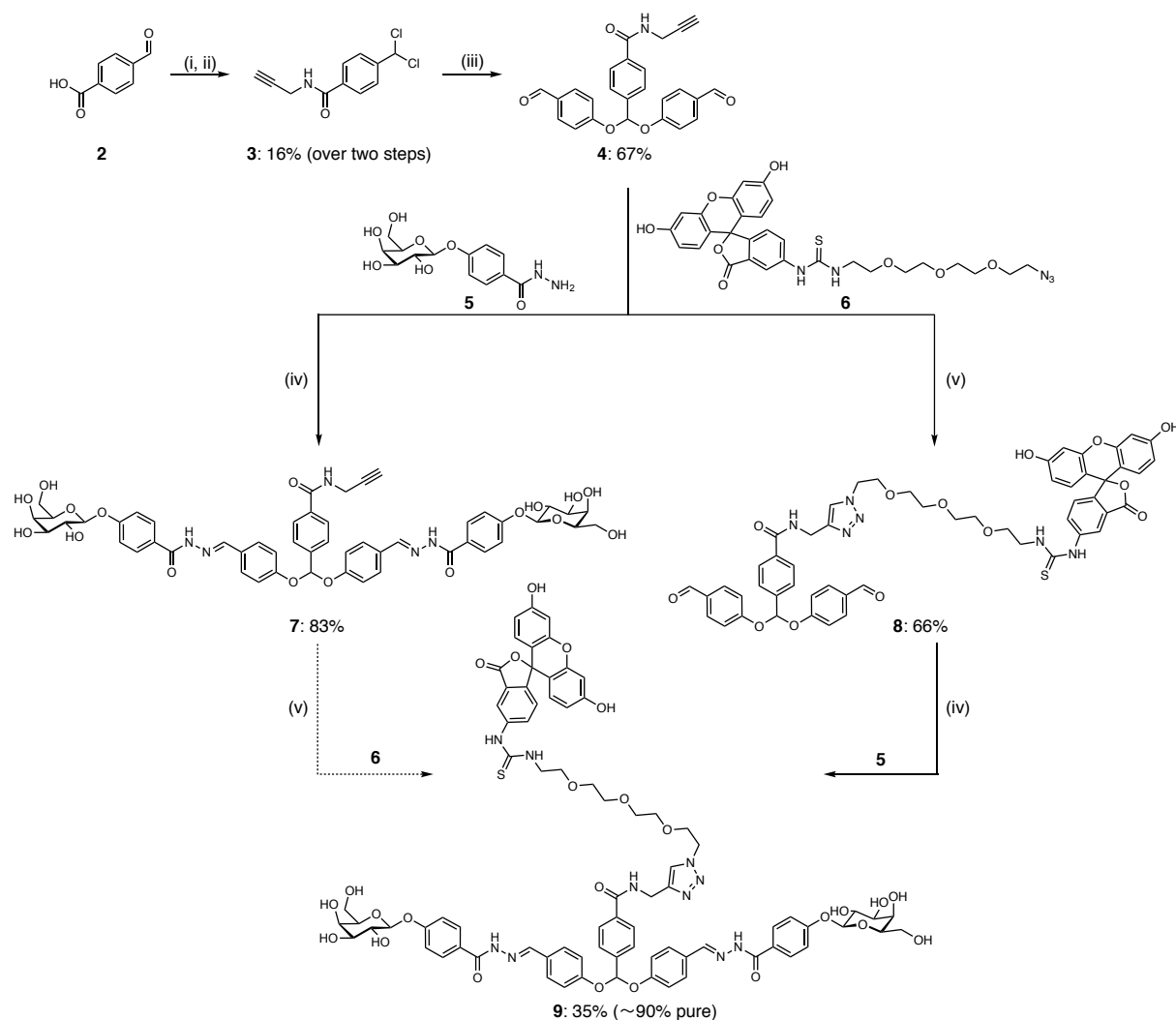


Figure 1: Design of divalent fluorescent LecA ligand. A) A snapshot of molecular dynamics trajectories of compound **1** in complex with LecA. The arrow indicates a possible growth vector for attachment of the cargo molecules. B) Structure of the divalent ligand **1** with the proposed branching site at the linker core for the conjugation to the fluorophore cargo.

Synthesis started with the chlorination of 4-formylbenzoic acid (**2**) followed by an amide formation with propargyl amine yielding the linker core building block **3** (Scheme 1). Next synthesis steps were performed in analogy to synthesis of bis-acylhydrazone divalent LecA ligand **1** (Chapters 3.2). A double nucleophilic substitution reaction on **3** with 4-hydroxybenzaldehyde gave the new branched linker **4** in a moderate yield (67%). The bis-acylhydrazone formation with the hydrazide bearing galactoside **5** under acidic conditions

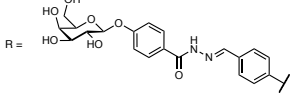
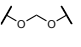
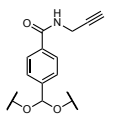
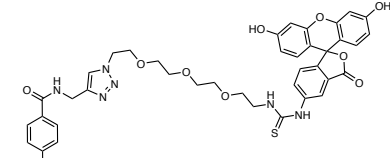
yielded divalent ligand **7**. Huisgen dipolar cycloaddition between crude product **7** and the azide modified fluorescein **6** was not successful – no product peak was detected by LCMS, despite the consumption of the starting material **7**. The click reaction was not attempted with purified bis-acylhydrazone **7**, instead firstly the CuAAC reaction between the azide modified fluorescein **6** and the branched linker **4** was performed to obtain bis-benzaldehyde fluorescent linker **8** and then the chemically labile acylhydrazone bonds were formed. Despite nearly quantitative turnover for the condensation reaction between bis-benzaldehyde **8** and hydrazide bearing galactoside **5**, divalent fluorescent ligand **9** was obtained only in 35% yield. The product loss was probably a result of its poor solubility and chemical instability of the acylhydrazone bond. Unfortunately, partial hydrolysis of the acylhydrazone bond was detected after preparative HPLC purification and accounted for approximately 10% impurity in the final compound **9**.



Scheme 1: Synthesis of divalent fluorescent LecA ligand. Reagents and conditions: (i) SOCl_2 , reflux, 1 d; (ii) propargyl amine, Et_3N , CH_2Cl_2 , 0 °C–r.t., 3 h; (iii) 4-hydroxybenzaldehyde, K_2CO_3 , DMF, reflux, 2 d; (iv) **5**, formic acid, DMSO, r.t., 2.5 h; (v) **6**, CuSO_4 , sodium ascorbate, DMF/ H_2O /DMSO, r.t., 7.5 h.

The divalent bis-acylhydrazone ligand **7** and the divalent fluorescent ligand **9** binding to LecA was evaluated in the previously reported binding assay based on fluorescence polarization (FP)⁶¹ and by SPR (Figure 2). Similarly to the parent divalent ligand **1** ($IC_{50} = 5.5 \pm 2.0 \mu\text{M}$), steep yet slightly shifted titration slope was observed for bis-acylhydrazone ligand **7** ($IC_{50} = 11.3 \pm 1.0 \mu\text{M}$) in the competitive binding assay. Very steep Hill slopes indicated the highly potent divalent compounds reaching the lower assay limit. The direct titration of the divalent fluorescent ligand **9** with LecA gave the K_d of $4.2 \mu\text{M}$. We speculated that the loss of divalent binding boost might be the result of the steric clash between the linker branch carrying the fluorescein moiety and the protein. To our surprise, low nanomolar binding affinity to immobilized LecA on SPR chip was measured for both ligands (**7** $K_d = 30.6 \pm 2.6 \text{ nM}$, **9** $K_d = 37.2 \pm 2.9 \text{ nM}$). SPR results showed that the linker side branch carrying fluorescein cargo is well tolerated by the protein with an acceptable binding penalty when compared to the divalent ligand **1** ($K_d = 20.5 \pm 0.2 \text{ nM}$).

The inconsistency of the binding affinity constants obtained from two different methods was investigated and we discovered that the compound **9** decomposes in aqueous buffers (pH 7.4, Figure S1-S4). The decomposition fragments were not assigned by HPLC-MS (m/z values did not correspond to modelled fragments), but the decomposition in the linker core due to its acetal nature was suspected. On the other hand, no decomposition in Tris buffer was observed for the parent acylhydrazone ligand **1** neither for the divalent bis-acylhydrazone ligand **7** (Figure S5-S6). Therefore, most likely the combination of the acetal core and the carboxylic acid containing fluorescein are responsible for compound degradation in aqueous solutions. The divalent fluorescent ligand **9** was stable when stored frozen as dimethyl sulfoxide solution ($-20 \text{ }^\circ\text{C}$) for over 1 year (not further investigated). High binding affinity constant obtained for **9** by SPR might be explained by better sample quality in this assay, since freshly prepared dilutions from dimethyl sulfoxide stock were used. The direct titration of divalent fluorescent ligand **9** with LecA was not repeated with newly prepared dilution from DMSO stock due to high consumption of the protein in the experiment and already confirmed decomposition. Further biophysical and biological evaluation of the divalent fluorescent ligand **9** was discontinued due to lack of stability in aqueous media.

	 pNO ₂ -Ph-β-D-Gal	 1	 7	 9
FP IC ₅₀ [nM]	62 500 ± 24 700	5 500 ± 2 000	11 300 ± 1 000	-
FP K _d [nM]	-	-	-	4 200 ± 1 200 (decomposed)
SPR K _d [nM]	-	20.5 ± 0.2	30.6 ± 2.6	37.2 ± 2.9

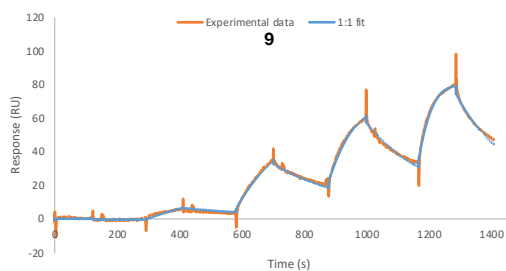
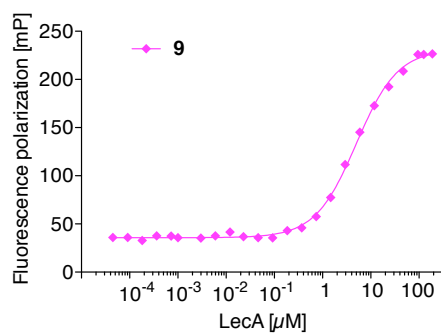
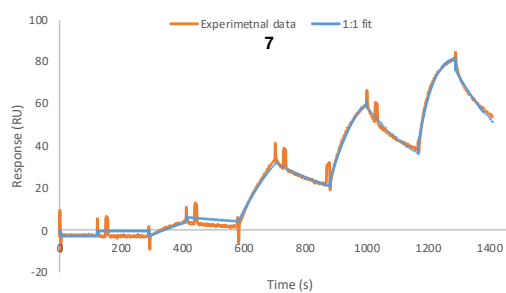
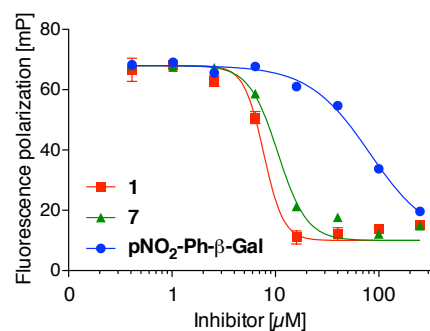


Figure 2: Evaluation of the divalent ligands binding to LecA in fluorescence polarization-based assays and in SPR. Averages and std. dev. from at least three independent experiments. One representative experiment is shown for each. Step Hill slopes of compound **1** and **7** in the competitive binding assay indicate the lower assay limit was reached. Decomposed sample **9** was used in direct titration with LecA.

In order to overcome the synthesis and purification challenges and especially the poor stability of the branched bis-acylhydrazone divalent ligand **9**, the design of a second-generation divalent fluorescent ligand was based on the amide-based divalent ligands described in Chapter 3.3 (Figure 3). Our previous work on divalent LecA inhibitors showed that linker core made by 1 to 5 atoms (oxygen in from of ether linkage and/or carbon in from of methylene units) provided the optimal length for the divalent binding and ether functionality was not essential. A nitrogen atom was incorporated to provide the central branching point.

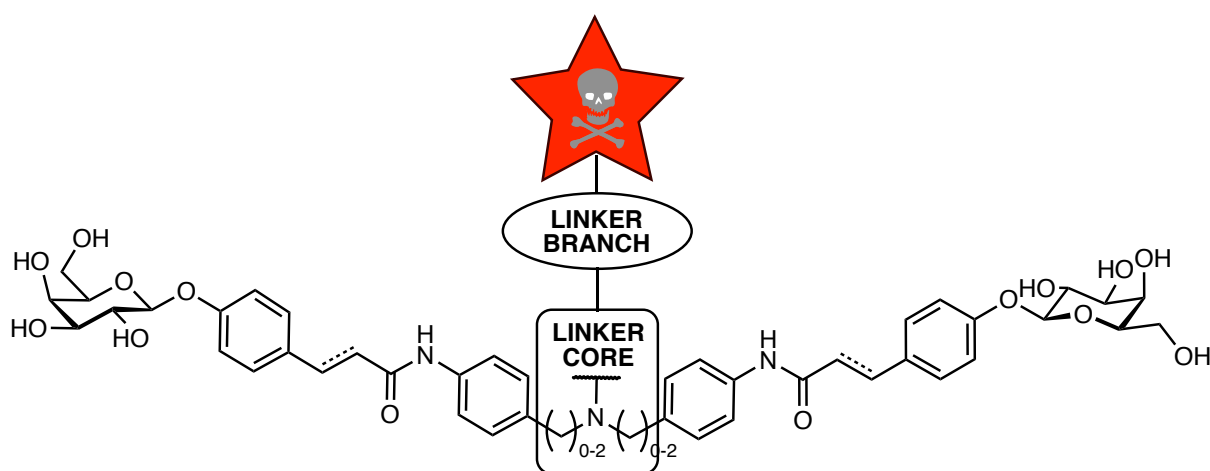
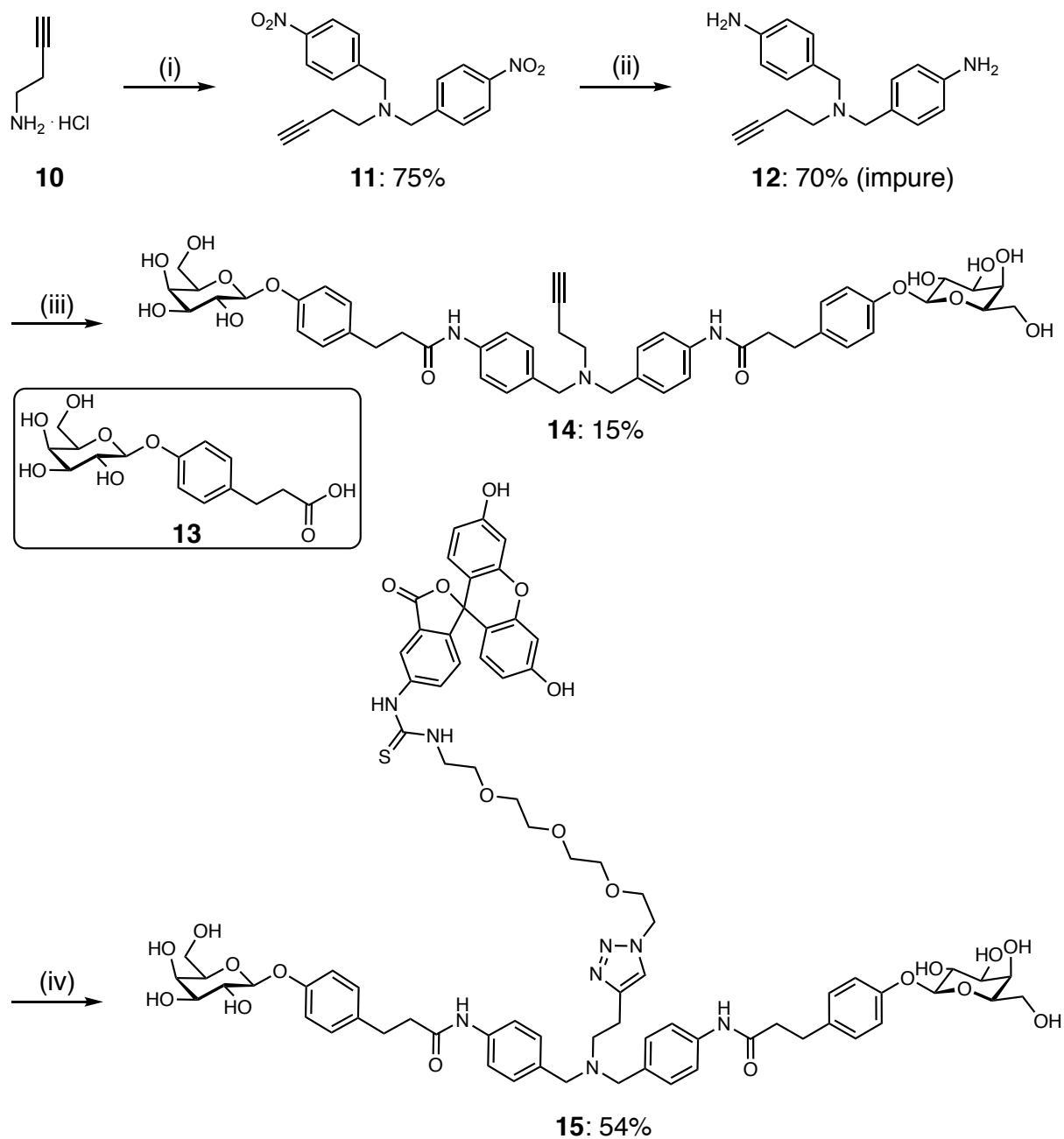
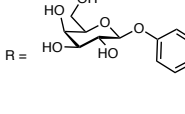
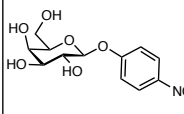
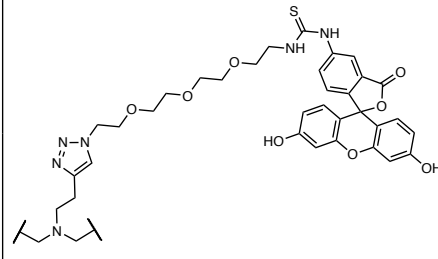


Figure 3: Design of the second generation divalent LecA ligand with attached cargo molecule.

Synthesis of the second generation divalent branched LecA ligand **15** started with a double nucleophilic substitution of the 4-nitrobenzyl bromide with but-3-yn-1-amine (**10**) (Scheme 2). Selective reduction of the bis-nitro intermediate **11** with iron powder gave the desired bis-aniline linker **12** with impurities. The RP chromatography would probably be able to completely purify **12**, but was skipped here and only performed after peptide coupling to the galactoside **13**. Divalent ligand **14** was synthesized in poor yield (15%) due to impure starting material as well as side product formation. Despite slow reaction turnover during Huisgen dipolar cycloaddition between divalent ligand **14** and the azide modified fluorescein **6**, possibly due to copper coordination to the reactants, the second-generation divalent fluorescent ligand **15** was synthesized in 54% yield.



Scheme 2: Synthesis of the second generation divalent fluorescent LecA ligand. Reagents and conditions: (i) 4-nitrobenzyl bromide, K_2CO_3 , r.t., DMF, overnight; (ii) Fe, CaCl_2 , EtOH/ H_2O , 40 °C–r.t., 9 d; (iii) **13**, HBTU, DIPEA, DMF, r.t., 2 d; (iv) **6**, CuSO_4 , sodium ascorbate, DMF/ H_2O , r.t.–35 °C, 6 d.

			
	pNO₂-Ph-β-D-Gal	14	15
FP IC ₅₀ [nM]	62 500 ± 24 700	5 630 ± 2 240	-
FP K _d [nM]	-	-	1 050 ± 120
SPR K _d [nM]	-	9.9 ± 0.5	19.3 ± 10.5

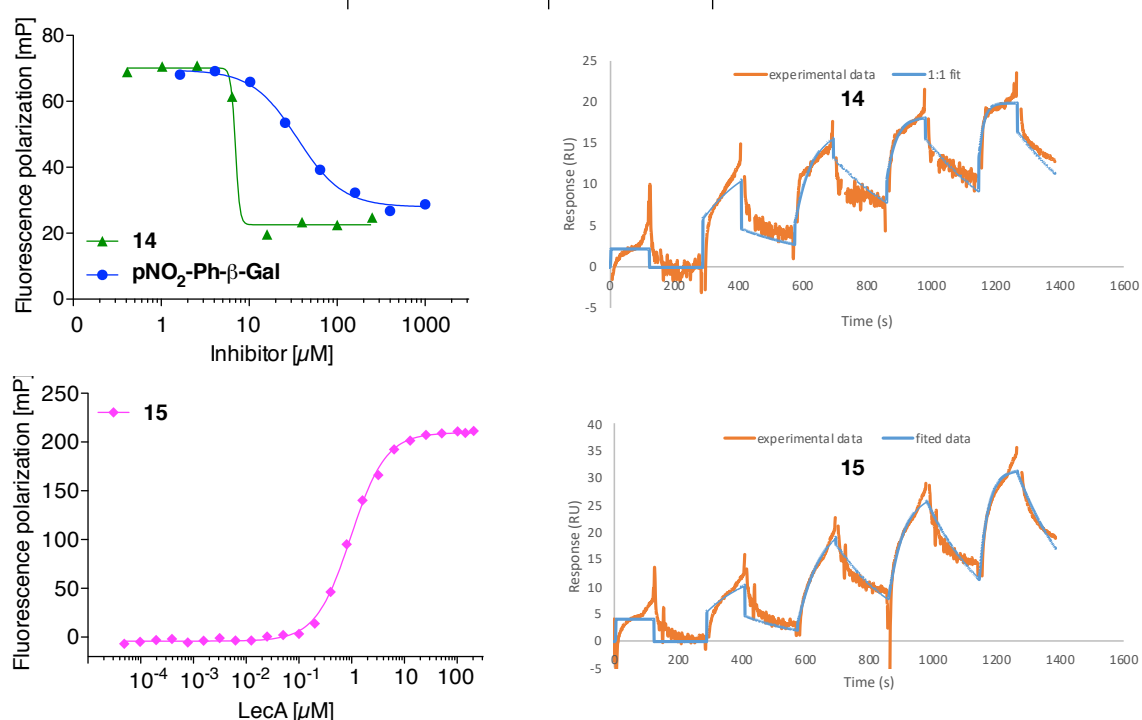


Figure 4: Evaluation of the second-generation divalent ligands binding to LecA in fluorescence polarization-based assays and in SPR. Averages and std. dev. from at least two independent experiments. One representative experiment is shown for each.

Low nanomolar binding affinities for divalent ligands **14** ($K_d = 9.9 \pm 0.5$ nM) and **15** ($K_d = 19.3 \pm 10.5$ nM) were measured by SPR (Figure 4). On the other hand, direct titration of the fluorescent ligand **15** with LecA in FP assay gave K_d of 1.05 μM - that is at least four-times lower than the binding affinity reached with monovalent fluorescent ligands (Chapter 3.1), but fifty-fold higher compared to the SPR result. In analogy to other divalent LecA ligands, compound **14** ($IC_{50} = 5.6 \pm 2.2$ μM) reached the lower assay limit in the competitive binding assay based on FP. Compound **15** did not show any degradation in Tris buffer after 24 h and was considered as stable (Figure S7).

In conclusion, two divalent fluorescent ligands based on previously reported highly potent LecA inhibitors were designed and synthesized. The first-generation divalent fluorescent ligand **9** based on central acetal showed low nanomolar binding affinity to LecA in SPR, but degraded in aqueous buffers and was abandoned. The second-generation divalent fluorescent LecA ligand **15** based on a stable tertiary amine as branching point showed low nanomolar binding in SPR and only low micromolar binding in fluorescence polarization assay. The divalent fluorescent ligands can bind to two neighbouring sites of LecA and/or crosslink LecA tetramers. An impact of these binding modes on fluorescence polarization was not studied and must be further investigated. Binding of **15** to LecA will be further evaluated by orthogonal methods, such as isothermal titration microcalorimetry. This work represents the first step towards high affinity LecA-directed imaging probes that could be used as diagnostics tool for *P. aeruginosa* infections. Furthermore, the design allows modular replacement of the fluorophore moiety with other imaging moieties or antibiotic cargo and thus could be used for their delivery to the site of infection in course of targeted therapy.

4. Conclusion and Outlook

The world-wide rise of antimicrobial resistance combined with the insufficient supply chain of novel antimicrobial agents calls for development of alternative treatment strategies. Antivirulence drugs, such as lectin inhibitors, applied alone or in combination with conventional antibiotics might provide efficient treatment options for multi-resistant bacterial infections. The development of imaging tools for real-time monitoring of *P. aeruginosa* biofilms is desired not only for research purposes, but also as a possible future diagnostic method with clinical application.

The aim of the first part of the thesis was the development of a novel diagnostic method for *P. aeruginosa* infections by targeting its lectins LecA and LecB. A small library of galactose-, xylose- and 1-deoxy-fucose-based compounds were synthesised to established their SAR to LecA and LecB. Attachment of an alkyne handle to LecA and LecB inhibitors as well as subsequent conjugation to fluorescein was well tolerated by both proteins and variations in the linkers caused only minor differences in binding affinities. Since the binding affinities of galactose-fluorescein conjugates to LecA and 1-deoxy-fucose-fluorecein conjugates to LecB corresponded to known affinities of LecA and LecB ligands,^{61,62,100} these imaging probes successfully occupied the flat carbohydrate-binding pockets of these lectins without any steric clash despite significant growth in their size.

In vitro imaging of *P. aeruginosa* biofilm aggregates using the synthesised probes with confocal laser scanning microscopy showed staining of biofilm aggregates independent of the attached sugar identity (galactose, 1-deoxy-fucose or xylose). Successful staining of biofilm aggregates was observed for both tested concentrations of imaging probes (10 μ M and 40 μ M). Only at higher concentration (40 μ M), the azide modified fluorescein lacking any carbohydrate moiety occasionally accumulated at biofilm aggregates as well. Thus, a carbohydrate-dependent staining was observed using 10 μ M of imaging probes, but at 40 μ M the accumulation of the imaging probes at biofilm aggregates might not be solely due to lectin-targeting but also due to interactions caused by a fluorescein moiety. In the future, the unspecific staining due to the fluorescein interactions with the *P. aeruginosa* biofilm will be investigated. Substitution of the carboxylic acid containing fluorescein (ionic or lactone forms possible, pH dependent)^{112,113} with a positively charged TAMRA dye and a neutral BODIPY dye is proposed (Figure 1). Surprising accumulation of the xylose-based imaging probes at the biofilm aggregates even at lower concentration (10 μ M) pointed to the binding of xylose to an unknown target or possible recognition of this sugar moiety as a nutrient source and its uptake, despite other carbon sources available in nutrient rich LB medium. Substitution of D-xylose

with its enantiomer L-xylose or another sugar moiety, e.g. arabinose, might give insights to this mystery. In addition or as an alternative to fluorophore replacement, the conditions of the staining assay should be optimized. For instance, biofilm staining under flow condition using a microfluidic system would be beneficial as the unbound imaging probes could be washed away and improve staining contrast. A washing step was not introduced into the staining assay performed in 24 well-plates as the biofilm aggregates would be washed out too. Initial flow-cell experiments with *P. aeruginosa* biofilms are ongoing in Titz's lab. Furthermore, a collaboration with Dr. Stefan Lienenklaus from Hannover Medical School was established for the *in vivo* imaging study of *P. aeruginosa* in a murine infection model. The best LecA and LecB targeting imaging probes from *in vitro* studies will be selected and their fluorophore moiety will be a near infrared dye allowing whole body imaging of a small animal model.

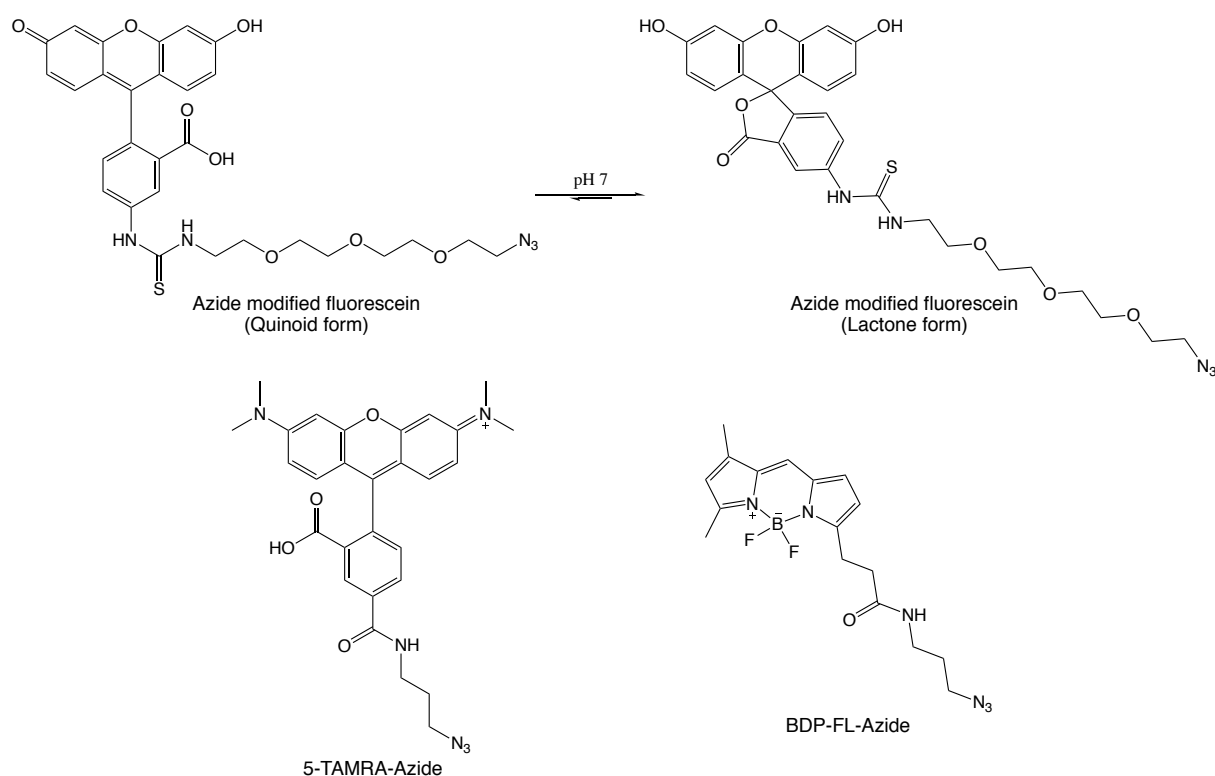


Figure 5: Structures of azide modified fluorescent dyes. Azide modified fluorescein used for synthesis of LecA and LecB targeting imaging probes described in Chapters 3.1 and 3.4 can be substituted with the physicochemically different TAMRA and BDP-FL fluorophores. Lactone form of fluorescein ($pK_{a_s} = 2.4, 3.1-3.4, 6.3$)¹¹³ is the most abundant at neutral pH. Protonated form of TAMRA (bottom left) and TAMRA zwitterion (with carboxylate, not shown) are present at neutral and alkaline pH, while its lactone form exists only at very low pH ($pK_a \sim 3$).¹¹⁴ A neutral BDP-FL-Azide with a boron-dipyromethene core structure.

The second part of this work was dedicated to divalent LecA inhibitors in order to boost the moderate affinity of the monovalent ligands. The obtained high affinity LecA ligands might

be used as antivirulence drugs and after conjugation to an imaging moiety or an antibiotic cargo they might lead to efficient pathogen specific theranostics. The design of divalent LecA inhibitors was tailored initially for use of DCC to enable the protein to select the best binder from the ligand library. Protein-templated DCC is mainly used to identify and optimize monovalent ligands, but it was also successfully used to evaluate multivalent systems in case of ConcanavalinA or for development of divalent inhibitors of glutathione S-transferase.¹¹⁵⁻¹¹⁷ Unfortunately in the present case, addition of LecA caused precipitation of library components – most likely due to the crosslinking of LecA tetramers with divalent ligands and aggregation. LCMS analysis of the library precipitate and supernatant revealed the presence of all library components in both samples at comparable levels. Thus, a specific enrichment was not observed. In the future, DCC might be successful for screening monovalent LecA ligands and more soluble library components are recommended.

The divalent acylhydrazone-based LecA ligands were therefore synthesised individually in absence of the protein. The simplicity of the design was in stark contrast to other structurally complex multivalent LecA inhibitors which required lengthy synthesis.^{42,109,110} In fact, the divalent acylhydrazone-based LecA ligands were synthesised from D-galactose pentaacetate and benzaldehyde-based linkers in only four linear steps. Moreover, low nanomolar binding affinities were reached and divalent ligand **B5p** ($K_d = 10.8$ nM, Chapter 3.2) showed superior activity to all previously reported divalent LecA inhibitors^{42,86,109,110} with confirmed selectivity for LecA over human galactose-binding protein galectin 1 and a selectivity factor over 1000. The divalent ligands' selectivity for LecA compared to other galactophilic lectins likely originates from the presence of β -linked aryl aglycons establishing CH- π stacking interactions with His50 and their optimized length to fit the two neighboring LecA binding sites. The obtained high selectivity and activity of these compounds make them good candidates for lead optimization, while their synthetic accessibility will ease follow-up studies.

Since the biggest drawback of these divalent inhibitors was their poor solubility and lack of chemical stability over a broad pH range, an optimization campaign was carried out. In the first optimization round, acylhydrazones were isosterically replaced with amide linkages improving compounds chemical stability as well as plasma stability. Both acrylamide and propanamide motifs were tolerated, except for the longest acrylamide-based ligand **F1** (Chapter 3.3). The observed SAR emphasizes the relevance of linker length and flexibility in design of multivalent ligands. Afterwards, solubility of the divalent ligands was enhanced by a rational optimization focusing on the linker moiety. The obtained divalent sulfonated ligand **L2** (Chapter 3.3) showed an excellent solubility and good ADME properties, while retaining low

nanomolar on target activity. Divalent ligands with pyridine-based linkers (**H1–I1** and **H2–J2**, Chapter 3.3) also represent important structures with high on target activity, despite slightly inferior solubility and ADME properties compared to the divalent sulfonated ligand **L2**. Taken together, the optimized divalent ligands are excellent candidates for further drug development.

In the future, divalent LecA ligands will be studied in functional biological assays to evaluate their therapeutic potential. Until today, only moderate inhibition of *P. aeruginosa* biofilm growth *in vitro* was reported for multivalent LecA ligands at micromolar concentrations, despite their nanomolar binding affinities.^{41,59,83} A perfect fit to two adjacent LecA binding pockets might be needed to prevent the undesirable crosslinking of LecA tetramers that might strengthen biofilms. Further fine-tuning of the length of the divalent ligands and their drug-like properties might be necessary to achieve efficient biofilm inhibitory effect. Crystal structures with the divalent ligands in complex with LecA may give insights on their binding modes. Since LecA also interferes with *P. aeruginosa* host cell invasion and signalling processes,^{39,40} evaluation of the divalent LecA ligands as inhibitors of bacterial adhesion, invasiveness and virulence in cellular assays is proposed. For this purpose, a collaboration with the group of Prof. Dr. Winfried Römer from Freiburg University was established. Divalent LecA ligands described in Chapter 3.2 and Chapter 3.3 are covered by European patent application (EP19306432.6).

In the last part of this work, the addition of a fluorescent tag to the above mentioned divalent LecA ligands was explored. High affinity divalent fluorescent LecA ligands might be of use for optimized competitive binding assays. Fluorescence polarization assay established by Joachim *et al.* for screening LecA inhibitors relies on monovalent galactose-fluorescein conjugate with K_d of 7.4 μM ,⁶¹ thus rather high concentration of LecA (20 μM) is required and as demonstrated in this work, IC_{50} of compounds with orders-of-magnitude higher potencies cannot be reliably determined because they reach lower assay limit. Furthermore, high affinity divalent fluorescent ligands will be used to stain *P. aeruginosa* biofilms and will likely surpass the performance of the monovalent imaging probes described in Chapter 3.1.

Modified linkers bearing an alkyne handle and galactose building blocks were used for the assembly of divalent fluorescent ligands which were subsequently clicked to the azide modified fluorescein. The first generation acylhydrazone divalent fluorescent ligand (**9**, Chapter 3.4) showed low nanomolar affinity to LecA by SPR, but suffered from instability in aqueous solutions. Since no decomposition of its alkyne precursor was observed, it would be interesting to replace the carboxylic acid containing fluorescein moiety with another fluorophore such as BODIPY (Figure 1). However, due to concerns about stability of the acetal

linker core as well as potential hydrolysis of the acylhydrazones, these compounds were discontinued. In general, the acylhydrazone divalent fluorescent ligand represents the first proof that divalent LecA ligands can be modified to carry a large substituent as a cargo (i.e. fluorophore) without significant loss of binding affinity.

The second generation divalent fluorescent LecA ligand with a central tertiary nitrogen atom as branching point and propanamide motif instead of the acylhydrazones (**15**, Chapter 3.4) was stable and reached nanomolar binding affinity to LecA in SPR. Surprisingly, only micromolar binding affinity was detected in a solution phase binding assay based on fluorescence polarization. It is possible, that crosslinking of LecA tetramers and/or their aggregation caused by the divalent ligand influenced fluorescence polarization and thus a lower binding affinity was observed, whereas crosslinking/aggregation of LecA immobilized on a SPR chip is unlikely. The observed discrepancy between SPR and FP assay results will be further investigated by orthogonal methods (e.g. ITC). Afterwards, solubility and ADME properties of the second generation ligand **15** will be determined and its ability to stain *P. aeruginosa* biofilms will be evaluated.

The above-mentioned designs of divalent fluorescent ligands further allow straightforward replacement of a fluorophore moiety with another cargo (e.g. an antimicrobial agent) at the last synthetic step in a CuAAC reaction. Therefore, this work also represents an important first step towards more efficient delivery scaffolds targeting *P. aeruginosa* not only for diagnostic purposes with imaging probes but also as a lectin-directed therapeutic strategy when conjugated to an antimicrobial agent.

5. References

- 1 World Health Organization, *Antimicrobial Resistance: Global Report on Surveillance*, Geneva, 2014.
- 2 European Centre for Disease Prevention and Control, *Antimicrobial resistance in the EU/EEA (EARS-Net) - Annual Epidemiological Report 2019*, Stockholm, 2020.
- 3 European Centre for Disease Prevention and Control, *Point prevalence survey of healthcare-associated infections and antimicrobial use in European acute care hospitals*, 2013.
- 4 D. Nathwani, G. Raman, K. Sulham, M. Gavaghan and V. Menon, *Antimicrob. Resist. Infect. Control*, 2014, **3**, 1–16.
- 5 J. A. Trubiano and A. A. Padiglione, *Anaesth. Intensive Care Med.*, 2015, **16**, 598–602.
- 6 R. Sordé, A. Pahissa and J. Rello, *Infect. Drug Resist.*, 2011, **4**, 31–41.
- 7 L. B. Rice, *J. Infect. Dis.*, 2008, **197**, 1079–1081.
- 8 H. W. Boucher, G. H. Talbot, J. S. Bradley, J. E. Edwards, D. Gilbert, L. B. Rice, M. Scheld, B. Spellberg and J. Bartlett, *Clin. Infect. Dis.*, 2009, **48**, 1–12.
- 9 M. Bassetti, A. Vena, A. Croxatto, E. Righi and B. Guery, *Drugs Context*, 2018, **7**, 1–18.
- 10 R. E. W. Hancock and D. P. Speert, *Drug Resist. Updat.*, 2000, **3**, 247–255.
- 11 B. L. Angus, A. M. Carey, D. A. Caron, A. M. Kropinski and R. E. Hancock, *Antimicrob. Agents Chemother.*, 1982, **21**, 299–309.
- 12 J. R. Aeschlimann, *Pharmacotherapy*, 2003, **23**, 916–924.
- 13 C. Suarez, C. Peña, O. Arch, M. A. Dominguez, F. Tubau, C. Juan, L. Gavaldá, M. Sora, A. Oliver, M. Pujol and J. Ariza, *BMC Infect. Dis.*, 2011, **11**, 1–8.
- 14 A. P. Magiorakos, A. Srinivasan, R. B. Carey, Y. Carmeli, M. E. Falagas, C. G. Giske, S. Harbarth, J. F. Hindler, G. Kahlmeter, B. Olsson-Liljequist, D. L. Paterson, L. B. Rice, J. Stelling, M. J. Struelens, A. Vatopoulos, J. T. Weber and D. L. Monnet, *Clin. Microbiol. Infect.*, 2012, **18**, 268–281.
- 15 D. Davies, *Nat. Rev. Drug Discov.*, 2003, **2**, 114–122.
- 16 H. C. Flemming and J. Wingender, *Nat. Rev. Microbiol.*, 2010, **8**, 623–633.
- 17 A. E. Clatworthy, E. Pierson and D. T. Hung, *Nat. Chem. Biol.*, 2007, **3**, 541–548.
- 18 S. Wagner, R. Sommer, S. Hinsberger, C. Lu, R. W. Hartmann, M. Empting and A. Titz, *J. Med. Chem.*, 2016, **59**, 5929–5969.
- 19 T. Strateva and I. Mitov, *Ann. Microbiol.*, 2011, **61**, 717–732.
- 20 M. B. Calvert, V. R. Jumde and A. Titz, *Beilstein J. Org. Chem.*, 2018, **14**, 2607–2617.

- 21 K. Papenfort and B. L. Bassler, *Nat. Rev. Microbiol.*, 2016, **14**, 576–588.
- 22 F. Soukarieh, P. Williams, M. J. Stocks and M. Cámara, *J. Med. Chem.*, 2018, **61**, 10385–10402.
- 23 M. B. Miller and B. L. Bassler, *Annu. Rev. Microbiol.*, 2001, **55**, 165–169.
- 24 T. B. Rasmussen and M. Givskov, *Microbiology*, 2006, **152**, 895–904.
- 25 E. Shaw, W. M. Wuest and W. M. Wuest, *RSC Med. Chem.*, 2020, **11**, 358–369.
- 26 E. Kessler and M. Safrin, in *Pseudomonas Methods and Protocols. Methods in Molecular Biology*, ed. R. J. Filloux A., Humana Press, New York, 2014, vol. 1149, pp. 135–169.
- 27 A. C. M. Galdino, M. H. Branquinha, A. L. S. Santos and L. Viganor, *Pseudomonas aeruginosa and its arsenal of proteases: weapons to battle the host*, Springer, Singapore, 2017.
- 28 B. Wretling and O. R. Pavlovskis, *Rev. Infect. Dis.*, 1983, **5**, 998–1004.
- 29 J. Yang, H. L. Zhao, L. Y. Ran, C. Y. Li, X. Y. Zhang, H. N. Su, M. Shi, B. C. Zhou, X. L. Chen and Y. Z. Zhang, *Sci. Rep.*, 2015, **5**, 1–7.
- 30 F. Bastaert, S. Kheir, V. Saint-Criq, B. Villeret, P. M. C. Dang, J. El-Benna, J. C. Sirard, R. Voulhoux and J. M. Sallenave, *Front. Immunol.*, 2018, **9**, 1–18.
- 31 J. Zhu, X. Cai, T. L. Harris, M. Gooyit, M. Wood, M. Lardy and K. D. Janda, *Chem. Biol.*, 2015, **22**, 483–491.
- 32 A. M. Kany, A. Sikandar, S. Yahiaoui, J. Hauptenthal, I. Walter, M. Empting, J. Köhnke and R. W. Hartmann, *ACS Chem. Biol.*, 2018, **13**, 2449–2455.
- 33 J. Konstantinović, S. Yahiaoui, A. Alhayek, J. Hauptenthal, E. Schönauer, A. Andreas, A. M. Kany, R. Müller, J. Koehnke, F. K. Berger, M. Bischoff, R. W. Hartmann, H. Brandstetter and A. K. H. Hirsch, *J. Med. Chem.*, 2020, **63**, 8359–8368.
- 34 K. Winzer, C. Falconer, N. C. Garber, S. P. Diggle, M. Camara and P. Williams, *J. Bacteriol.*, 2000, **182**, 6401–6411.
- 35 D. Tielker, S. Hacker, R. Loris, M. Strathmann, J. Wingender, S. Wilhelm, F. Rosenau and K. E. Jaeger, *Microbiology*, 2005, **151**, 1313–1323.
- 36 S. P. Diggle, R. E. Stacey, C. Dodd, M. Cámara, P. Williams and K. Winzer, *Environ. Microbiol.*, 2006, **8**, 1095–1104.
- 37 E. C. Adam, B. S. Mitchell, D. U. Schumacher, G. Grant and U. Schumacher, *Am. J. Respir. Crit. Care Med.*, 1997, **155**, 2102–2104.
- 38 C. Cott, R. Thuenauer, A. Landi, K. Kühn, S. Juillot, A. Imberty, J. Madl, T. Eierhoff and W. Römer, *Biochim. Biophys. Acta - Mol. Cell Res.*, 2016, **1863**, 1106–1118.

- 39 T. Eierhoff, B. Bastian, R. Thuenauer, J. Madl, A. Audfray, S. Aigal, S. Juillot, G. E. Rydell, S. Muller, S. de Bentzmann, A. Imberty, C. Fleck and W. Romer, *Proc. Natl. Acad. Sci.*, 2014, **111**, 12895–12900.
- 40 S. Zheng, T. Eierhoff, S. Aigal, A. Brandel, R. Thuenauer, S. de Bentzmann, A. Imberty and W. Römer, *Biochim. Biophys. Acta - Mol. Cell Res.*, 2017, **1864**, 1236–1245.
- 41 A. M. Boukerb, A. Rousset, N. Galanos, J. B. Méar, M. Thépaut, T. Grandjean, E. Gillon, S. Cecioni, C. Abderrahmen, K. Faure, D. Redelberger, E. Kipnis, R. Dessen, S. Havet, B. Darblade, S. E. Matthews, S. De Bentzmann, B. Guéry, B. Cournoyer, A. Imberty and S. Vidal, *J. Med. Chem.*, 2014, **57**, 10275–10289.
- 42 F. Pertici and R. J. Pieters, *Chem. Commun.*, 2012, **48**, 4008–4010.
- 43 R. U. Kadam, D. Garg, J. Schwartz, R. Visini, M. Sattler, A. Stocker, T. Darbre and J. L. Reymond, *ACS Chem. Biol.*, 2013, **8**, 1925–1930.
- 44 S. Wagner, D. Hauck, M. Hoffmann, R. Sommer, I. Joachim, R. Müller, A. Imberty, A. Varrot and A. Titz, *Angew. Chemie - Int. Ed.*, 2017, **56**, 16559–16564.
- 45 E. M. V Johansson, S. A. Cruz, E. Kolomiets, L. Buts, R. U. Kadam, M. Cacciarini, K. M. Bartels, S. P. Diggle, M. Cámara, P. Williams, R. Loris, C. Nativi, F. Rosenau, K. E. Jaeger, T. Darbre and J. L. Reymond, *Chem. Biol.*, 2008, **15**, 1249–1257.
- 46 R. Sommer, K. Rox, S. Wagner, D. Hauck, S. S. Henrikus, S. Newsad, T. Arnold, T. Ryckmans, M. Brönstrup, A. Imberty, A. Varrot, R. W. Hartmann and A. Titz, *J. Med. Chem.*, 2019, **62**, 9201–9216.
- 47 R. Sommer, S. Wagner, K. Rox, A. Varrot, D. Hauck, E. C. Wamhoff, J. Schreiber, T. Ryckmans, T. Brunner, C. Rademacher, R. W. Hartmann, M. Brönstrup, A. Imberty and A. Titz, *J. Am. Chem. Soc.*, 2018, **140**, 2537–2545.
- 48 H. P. Hauber, M. Schulz, A. Pforte, D. Mack, P. Zabel and U. Schumacher, *Int. J. Med. Sci.*, 2008, **5**, 371–376.
- 49 N. Gilboa-Garber, *Methods Enzymol.*, 1982, **83**, 378–385.
- 50 N. Gilboa-Garber, *BBA - Gen. Subj.*, 1972, **273**, 165–173.
- 51 R. Sommer, D. Hauck, A. Varrot, S. Wagner, A. Audfray, A. Prestel, H. M. Möller, A. Imberty and A. Titz, *ChemistryOpen*, 2015, **4**, 756–767.
- 52 S. Kuhaudomlarp, E. Siebs, E. Shanina, J. Topin, I. Joachim, S. Figueiredo, C. Gomes, A. Varrot, D. Rognan, A. Imberty and A. Titz, *Angew. Chem. Int. Ed.*, 2021, **60**, 2–13.
- 53 C. K. Stover, X. Q. Pham, A. L. Erwin, S. D. Mizoguchi, P. Warrenner, M. J. Hickey, F. S. L. Brinkman, W. O. Hufnagle, D. J. Kowallk, M. Lagrou, R. L. Garber, L. Goltry, E. Tolentino, S. Westbrook-Wadman, Y. Yuan, L. L. Brody, S. N. Coulter, K. R. Folger,

- A. Kas, K. Larbig, R. Lim, K. Smith, D. Spencer, G. K. S. Wong, Z. Wu, I. T. Paulsen, J. Relzer, M. H. Saler, R. E. W. Hancock, S. Lory and M. V. Olson, *Nature*, 2000, **406**, 959–964.
- 54 D. G. Lee, J. M. Urbach, G. Wu, N. T. Liberati, R. L. Feinbaum, S. Miyata, L. T. Diggins, J. He, M. Saucier, E. Déziel, L. Friedman, L. Li, G. Grills, K. Montgomery, R. Kucherlapati, L. G. Rahme and F. M. Ausubel, *Genome Biol.*, 2006, **7**, 1–14.
- 55 R. Sommer, J. C. Paulson, A. Titz, A. Varrot, S. Wagner, A. Khaledi, S. Häussler, C. M. Nycholat and A. Imberty, *Chem. Sci.*, 2016, **7**, 4990–5001.
- 56 G. Cioci, E. P. Mitchell, C. Gautier, M. Wimmerová, D. Sudakevitz, S. Pérez, N. Gilboa-Garber and A. Imberty, *FEBS Lett.*, 2003, **555**, 297–301.
- 57 R. Loris, D. Tielker, K. E. Jaeger and L. Wyns, *J. Mol. Biol.*, 2003, **331**, 861–870.
- 58 B. Blanchard, A. Nurisso, E. Hollville, C. Tétaud, J. Wiels, M. Pokorná, M. Wimmerová, A. Varrot and A. Imberty, *J. Mol. Biol.*, 2008, **383**, 837–853.
- 59 R. U. Kadam, M. Bergmann, M. Hurley, D. Garg, M. Cacciarini, M. A. Swiderska, C. Nativi, M. Sattler, A. R. Smyth, P. Williams, M. Cámara, A. Stocker, T. Darbre and J. L. Reymond, *Angew. Chemie - Int. Ed.*, 2011, **50**, 10631–10635.
- 60 J. Rodrigue, G. Ganne, B. Blanchard, C. Saucier, D. Giguère, T. C. Shiao, A. Varrot, A. Imberty and R. Roy, *Org. Biomol. Chem.*, 2013, **11**, 6906–6918.
- 61 I. Joachim, S. Rikker, D. Hauck, D. Ponader, S. Boden, R. Sommer, L. Hartmann and A. Titz, *Org. Biomol. Chem.*, 2016, **14**, 7933–7948.
- 62 D. Hauck, I. Joachim, B. Frommeyer, A. Varrot, B. Philipp, H. M. Möller, A. Imberty, T. E. Exner and A. Titz, *ACS Chem. Biol.*, 2013, **8**, 1775–1784.
- 63 I. Wilhelm, E. Levit-Zerdoun, J. Jakob, S. Villringer, M. Frensch, R. Übelhart, A. Landi, P. Müller, A. Imberty, R. Thuenauer, J. Claudinon, H. Jumaa, M. Reth, H. Eibel, E. Hobeika and W. Römer, *Sci. Signal.*, 2019, **12**, 1–18.
- 64 E. E. Mann and D. J. Wozniak, *FEMS Microbiol Rev.*, 2012, **36**, 893–916.
- 65 D. Passos da Silva, M. L. Matwichuk, D. O. Townsend, C. Reichhardt, D. Lamba, D. J. Wozniak and M. R. Parsek, *Nat. Commun.*, 2019, **10**, 1–11.
- 66 W. B. Turnbull and J. F. Stoddart, *Rev. Mol. Biotechnol.*, 2002, **90**, 231–255.
- 67 M. Mammen, S. K. Choi and G. M. Whitesides, *Angew. Chemie - Int. Ed.*, 1998, **37**, 2754–2794.
- 68 S. Cecioni, A. Imberty and S. Vidal, *Chem. Rev.*, 2015, **115**, 525–561.
- 69 B. Ernst and J. L. Magnani, *Nat. Rev. Drug Discov.*, 2009, **8**, 661–677.
- 70 C. Lee and T. Lee, *Acc. Chem. Res.*, 1995, **28**, 321–327.

- 71 P. C. Pang, P. C. N. Chiu, C. L. Lee, L. Y. Chang, M. Panico, H. R. Morris, S. M. Haslam, K. H. Khoo, G. F. Clark, W. S. B. Yeung and A. Dell, *Science*, 2011, **333**, 1761–1764.
- 72 E. Baba, M. Nakamura, Y. Tanaka, M. Kuroki, Y. Itoyama, S. Nakano and Y. Niho, *J Immunol*, 1993, **151**, 1013–1024.
- 73 D. Vestweber and J. E. Blanks, *Physiol. Rev.*, 1999, **79**, 181–213.
- 74 A. Imberty and A. Varrot, *Curr. Opin. Struct. Biol.*, 2008, **18**, 567–576.
- 75 M. Mammen, S.-K. Choi and G. M. Whitesides, *Angew. Chem. Int. Ed.*, 1998, **37**, 2754–2794.
- 76 C. Fasting, C. A. Schalley, M. Weber, O. Seitz, S. Hecht, B. Koksche, J. Dervede, C. Graf, E. Knapp and R. Haag, *Angew. Chem. Int. Ed.*, 2012, **51**, 10472–10498.
- 77 L. L. Kiessling, J. E. Gestwicki and L. E. Strong, *Curr. Opin. Chem. Biol.*, 2000, **4**, 696–703.
- 78 C.-H. Heldin, *Cell*, 1995, **80**, 213–223.
- 79 K. H. Mortell, R. V. Weatherman and L. L. Kiessling, *J. Am. Chem. Soc.*, 1996, **118**, 2297–2298.
- 80 N. Horan, L. Yan, H. Isobe, G. M. Whitesides and D. Kahne, *Proc. Natl. Acad. Sci. U. S. A.*, 1999, **96**, 11782–11786.
- 81 R. Heida, Y. C. Bhide, M. Gasbarri, Ö. Kocabiyik, F. Stellacci, A. L. W. Huckriede, W. L. J. Hinrichs and H. W. Frijlink, *Drug Discov. Today*, 2021, **26**, 122–137.
- 82 V. Kumar and W. B. Turnbull, *Beilstein J. Org. Chem.*, 2018, **14**, 484–498.
- 83 R. Visini, X. Jin, M. Bergmann, G. Michaud, F. Pertici, O. Fu, A. Pukin, T. R. Branson, D. M. E. Thies-Weesie, J. Kemmink, E. Gillon, A. Imberty, A. Stocker, T. Darbre, R. J. Pieters and J. L. Reymond, *ACS Chem. Biol.*, 2015, **10**, 2455–2462.
- 84 O. Fu, A. V. Pukin, H. C. Quarlesvanufford, J. Kemmink, N. J. DeMol and R. J. Pieters, *ChemistryOpen*, 2015, **4**, 463–470.
- 85 A. V. Pukin, A. J. Brouwer, L. Koomen, H. C. Quarles Van Ufford, J. Kemmink, N. J. De Mol and R. J. Pieters, *Org. Biomol. Chem.*, 2015, **13**, 10923–10928.
- 86 G. Yu, A. C. Vicini and R. J. Pieters, *J. Org. Chem.*, 2019, **84**, 2470–2488.
- 87 A. Fleming, *Br J Exp Pathol.*, 1929, **10**, 226–236.
- 88 J. H. Powers, *Clin Microbiol Infect*, 2004, **10**, 23–31.
- 89 J. O'Neill, *Tackling Drug-Resistant Infections Globally: Final Report and Recommendations, Review on Antimicrobial Resistance*, London, 2016.
- 90 A. Kumar, D. Roberts, K. E. Wood, B. Light, J. E. Parrillo, S. Sharma, R. Suppes, D. Feinstein, S. Zanotti, L. Taiberg, D. Gurka, A. Kumar and M. Cheang, *Crit. Care Med.*,

- 2006, **34**, 1589–1596.
- 91 M. H. Kollef, G. Sherman, S. Ward and V. J. Fraser, *Clin. Investig. Crit. Care*, 1999, **115**, 462–474.
- 92 E. L. Tsalik, R. A. Bonomo and V. G. Fowler, *Annu. Rev. Med.*, 2018, **69**, 379–394.
- 93 S. Fujitani, H. Y. Sun, V. L. Yu and J. A. Weingarten, *Chest*, 2011, **139**, 909–919.
- 94 A. Agodi, M. Barchitta, R. Cipresso, L. Giaquinta, M. A. Romeo and C. Denaro, *Intensive Care Med.*, 2007, **33**, 1155–1161.
- 95 K. Ferreira, H. Y. Hu, V. Fetz, H. Prochnow, B. Rais, P. P. Müller and M. Brönstrup, *Angew. Chemie - Int. Ed.*, 2017, **56**, 8272–8276.
- 96 M. Petrik, E. Umlaufova, V. Raclavsky, A. Palyzova, V. Havlicek, H. Haas, Z. Novy, D. Dolezal, M. Hajduch and C. Decristoforo, *Sci. Rep.*, 2018, **8**, 1–9.
- 97 J. Beuth, H. L. Ko, G. Uhlenbruck and G. Pulverer, *Eur. J. Clin. Microbiol.*, 1987, **6**, 591–593.
- 98 R. K. Nelson, V. Poroyko, M. J. Morowitz, D. Liu and J. C. Alverdy, *Surg. Infect. (Larchmt)*, 2013, **14**, 35–42.
- 99 D. Hauck, V. R. Jumde, C. J. Crawford and A. Titz, in *Carbohydrate Chemistry*, eds. P. Kosma, T. M. Wrodnigg and A. Stütz, CRC Press, 2021, pp. 17–21.
- 100 European Patent Office, EP2650289, 2013.
- 101 J. Schindelin, I. Arganda-Carreras, E. Frise, V. Kaynig, M. Longair, T. Pietzsch, S. Preibisch, C. Rueden, S. Saalfeld, B. Schmid, J. Y. Tinevez, D. J. White, V. Hartenstein, K. Eliceiri, P. Tomancak and A. Cardona, *Nat. Methods*, 2012, **9**, 676–682.
- 102 R. U. Kadam, D. Garg, J. Schwartz, R. Visini, M. Sattler, A. Stocker, T. Darbre and J.-L. Reymond, *ACS Chem. Biol.*, 2013, **8**, 1925–1930.
- 103 M. Müsken, V. Pawar, T. Schwebs, H. Bähre, S. Felgner, S. Weiss and S. Häussler, *Antimicrob. Agents Chemother.*, 2018, **62**, 1–13.
- 104 J. W. Chen, Y. Y. Lau, T. Krishnan, K. G. Chan and C. Y. Chang, *Front. Microbiol.*, 2018, **9**, 1–8.
- 105 B. Ernst and J. L. Magnani, *Nat. Rev. Drug Discov.*, 2009, **8**, 661–677.
- 106 J. Meiers, E. Siebs, E. Zahorska and A. Titz, *Curr. Opin. Chem. Biol.*, 2019, **53**, 51–67.
- 107 A. M. Boukerb, A. Decor, S. Ribun, R. Tabaroni, A. Rousset, L. Commin, S. Buff, A. Doléans-Jordheim, S. Vidal, A. Varrot, A. Imberty and B. Cournoyer, *Front. Microbiol.*, 2016, **7**, 1–16.
- 108 C. Sabin, E. P. Mitchell, M. Pokorná, C. Gautier, J. P. Utille, M. Wimmerová and A. Imberty, *FEBS Lett.*, 2006, **580**, 982–987.

- 109 A. Novoa, T. Eierhoff, J. Topin, A. Varrot, S. Barluenga, A. Imberty, W. Römer and N. Winssinger, *Angew. Chemie - Int. Ed.*, 2014, **53**, 8885–8889.
- 110 S. F. Huang, C. H. Lin, Y. T. Lai, C. L. Tsai, T. J. R. Cheng and S. K. Wang, *Chem. - An Asian J.*, 2018, **13**, 686–700.
- 111 E. Zahorska, S. Kuhadomlarp, S. Minervini, S. Yousaf, M. Lepsik, T. Kinsinger, A. K. H. Hirsch, A. Imberty and A. Titz, *Chem. Commun.*, 2020, **56**, 8822–8825.
- 112 V. Zanker and W. Peter, *Chem. Ber.*, 1958, 572–580.
- 113 N. Klonis and W. H. Sawyer, *J. Fluoresc.*, 1996, **6**, 147–157.
- 114 K. Gracie, W. E. Smith, P. Yip, J. U. Sutter, D. J. S. Birch, D. Graham and K. Faulds, *Analyst*, 2014, **139**, 3735–3743.
- 115 M. Mondal and A. K. H. Hirsch, *Chem. Soc. Rev.*, 2015, **44**, 2455–2488.
- 116 O. Ramström, S. Lohmann, T. Bunyapaiboonsri and J. M. Lehn, *Chem. - A Eur. J.*, 2004, **10**, 1711–1715.
- 117 A. J. Clipson, V. T. Bhat, I. McNae, A. M. Caniard, D. J. Campopiano and M. F. Greaney, *Chem. - A Eur. J.*, 2012, **18**, 10562–10570.
- 118 H. E. Gottlieb, V. Kotlyar and A. Nudelman, *J. Org. Chem.*, 1997, **62**, 7512–7515.
- 119 R. B. Cohen, K.-C. Tsou, S. H. Rutenburg and A. M. Seligman, *J. Biol. Chem.*, 1952, **195**, 239–249.
- 120 J. Ramos-Soriano, U. Niss, J. Angulo, M. Angulo, A. J. Moreno-Vargas, A. T. Carmona, S. Ohlson and I. Robina, *Chem. - A Eur. J.*, 2013, **19**, 17989–18003.
- 121 S. Cao, S. J. Meunier, F. O. Andersson, M. Letellier and R. Roy, *Tetrahedron: Asymmetry*, 1994, **5**, 2303–2312.
- 122 V. Kumar, I. Jamie Talisman, O. Bukhari, J. Razzaghy and S. V. Malhotra, *RSC Adv.*, 2011, **1**, 1721–1727.
- 123 A. Bartolozzi, H. M. Foudoulakis and B. M. Cole, *Synthesis (Stuttg.)*, 2008, 2023–2032.
- 124 A. Nakahashi, M. Fujita, E. Miyoshi, T. Umeyama, K. Naka and Y. Chujo, *J. Polym. Sci.*, 2007, **45**, 3580–3587.
- 125 C. S. Hudson and J. M. Johnson, *J. Am. Chem. Soc.*, 1915, **37**, 2748–2753.
- 126 R. Šardžik, G. T. Noble, M. J. Weissenborn, A. Martin, S. J. Webb and S. L. Flitsch, *Beilstein J. Org. Chem.*, 2010, **6**, 699–703.
- 127 H. Driguez and W. Szeja, *Synthesis (Stuttg.)*, 1994, **12**, 1413–1414.
- 128 J. A. H. Inkster, K. Liu, S. Ait-Mohand, P. Schaffer, B. Guérin, T. J. Ruth and T. Storr, *Chem. - A Eur. J.*, 2012, **18**, 11079–11087.
- 129 S. Loison, M. Cottet, H. Orcel, H. Adihou, R. Rahmeh, L. Lamarque, E. Trinquet, E.

- Kellenberger, M. Hibert, T. Durroux, B. Mouillac and D. Bonnet, *J. Med. Chem.*, 2012, **55**, 8588–8602.
- 130 E. P. Mitchell, C. Sabin, L. Šnajdrová, M. Pokorná, S. Perret, C. Gautier, C. Hofr, N. Gilboa-Garber, J. Koča, M. Wimmerová and A. Imberty, *Proteins Struct. Funct. Genet.*, 2005, **58**, 735–746.
- 131 G. Beshr, A. Sikandar, E. M. Jemiller, N. Klymiuk, D. Hauck, S. Wagner, E. Wolf, J. Koehnke and A. Titz, *J. Biol. Chem.*, 2017, **292**, 19935–19951.
- 132 W. Guo, J. Li, N. Fan, W. Wu, P. Zhou and C. Xia, *Synth. Commun.*, 2005, **35**, 145–152.
- 133 N. Takada, E. Kato, K. Ueda, S. Yamamura and M. Ueda, *Tetrahedron Lett.*, 2002, **43**, 7655–7658.
- 134 S. Akimoto, D. Kato, M. Jikei and M. A. Kakimoto, *J. Photopolym. Sci. Technol.*, 1999, **12**, 245–248.
- 135 M. S. Butt, Z. Akhtar, M. Zafar-Uz-Zaman and A. Munir, *Eur. Polym. J.*, 2005, **41**, 1638–1646.
- 136 A. Shiotani and M. Kohda, *J. Appl. Polym. Sci.*, 1999, **74**, 2404–2413.
- 137 I. N. Bazanova, N. V. Kholodkova and V. P. Gostikin, *Russ. J. Appl. Chem.*, 2002, **75**, 436–440.
- 138 W. B. Turnbull and A. H. Daranas, *J. Am. Chem. Soc.*, 2003, **125**, 14859–14866.

6. Appendix

Chemical synthesis

Thin layer chromatography (TLC) was performed using silica gel 60 aluminum plates containing fluorescence indicator (Merck KGaA, Darmstadt, Germany) and developed under UV light (254 nm) and using a molybdate solution (0.02 M solution of $(\text{NH}_4)_4\text{Ce}(\text{SO}_4)_4 \cdot 2 \text{H}_2\text{O}$ and $(\text{NH}_4)_6\text{Mo}_7\text{O}_{24} \cdot 4 \text{H}_2\text{O}$ in aqueous 10% H_2SO_4) or a potassium permanganate solution (3 g of KMnO_4 , 20 g of K_2CO_3 in 5 mL of 5% NaOH and 300 mL of water) with heating.

Medium pressure liquid chromatography (MPLC) was performed on a Teledyne Isco Combiflash Rf200 system using normal phase self-packed silica gel columns (60 Å, 400 mesh particle size, Fluka) or reversed-phase pre-packed silica gel 60 Å columns from Macherey-Nagel (C_{18} ec, endcapped). Preparative high-pressure liquid chromatography (HPLC) was performed on Waters 2545 Binary Gradient Module with a Waters 2489 UV/Vis detector using a RP-18 column (250/21 Nucleodur C18 Gravity SB, 5 μM from Macherey-Nagel, Germany).

Analytical HPLC-MS was performed on a Thermo Dionex Ultimate 3000 HPLC coupled to a Bruker amaZon SL mass spectrometer, with UV detection at 254 nm using a RP-18 column (100/2 Nucleoshell RP18plus, 2.7 μM from Macherey-Nagel, Germany) as stationary phase. High resolution mass spectrometry (HRMS) was performed on an Ultimate 3000 UPLC system coupled to a Q Exactive Focus Orbitrap system with HESI source (Thermo Fisher, Dreieich, Germany). The UPLC was operated with a C18 column (EC 150/2 Nucleodur C18 Pyramid, 3 μm from Macherey-Nagel, Germany).

^1H -NMR and ^{13}C -NMR spectra were recorded on a Bruker Avance III 500 UltraShield spectrometer at 500 MHz and 126 MHz. Chemical shifts (δ) are given in ppm and were calibrated on residual solvent peaks: CDCl_3 (^1H -NMR $\delta = 7.26$ ppm, ^{13}C -NMR $\delta = 77.0$ ppm), MeOH-d_4 (^1H -NMR $\delta = 3.31$ ppm, ^{13}C -NMR $\delta = 49.0$ ppm), DMSO-d_6 (^1H -NMR $\delta = 2.50$ ppm, ^{13}C -NMR $\delta = 39.51$ ppm), D_2O (^1H -NMR $\delta = 4.79$ ppm), acetone- d_6 (^1H -NMR $\delta = 2.05$ ppm, ^{13}C -NMR $\delta = 29.84$ ppm, $\delta = 206.26$ ppm).¹¹⁸ Deuterated solvents were purchased from Eurisotop (Saarbrücken, Germany). Multiplicities are specified as s = singlet, d = doublet, t = triplet, q = quartet, m = multiplet. The spectra were assigned with the help of ^1H , ^1H -COSY; ^1H , ^{13}C -HSQC and ^1H , ^{13}C -HMBC experiments.

6.1 Supplementary information for chapter 3.1

Compounds synthesis

β -D-galactopyranose pentaacetate (3)

β -D-Galactopyranose pentaacetate was obtained following the procedure of Cohen *et al.*¹¹⁹ D-Galactose (100 g, 0.56 mol), acetic anhydride (600 mL, 6.35 mol) and anhydrous sodium acetate (50.08 g, 0.61 mol) were heated to 100 °C for 20 minutes. The mixture was allowed to cooled down to room temperature, poured over 1600 mL ice water and stirred for 1 hour. The product was extracted with dichloromethane, washed with water, dried over anhydrous Na₂SO₄, filtered and evaporated to a syrup. Crude product was purified by crystallisation from ethanol (81.3 g, 0.21 mol, 38%).

¹H NMR (500 MHz, CDCl₃) δ 5.70 (d, J = 8.3 Hz, 1H, H-1), 5.42 (d, J = 3.4, 1H, H-4), 5.33 (dd, J = 10.4, 8.3 Hz, 1H, H-2), 5.07 (dd, J = 10.4, 3.3 Hz, 1H, H-3), 4.19 – 4.08 (m, 2H, H-6), 4.05 (t, J = 6.5 Hz, 1H, H-5), 2.16 (s, 3H, CH₃), 2.12 (s, 3H, CH₃), 2.06 – 2.03 (m, 6H, CH₃), 1.99 (s, 3H, CH₃).

¹³C NMR (126 MHz, CDCl₃) δ 170.50 (C=O), 170.27 (C=O), 170.11 (C=O), 169.57 (C=O), 169.13 (C=O), 92.30 (C-1), 71.85 (C-5), 70.99 (C-3), 67.96 (C-2), 66.94 (C-4), 61.18 (C-6), 20.97 (CH₃), 20.82 (CH₃), 20.81 (CH₃), 20.78 (CH₃), 20.70 (CH₃).

HPLC-MS: [C₁₆H₂₂O₁₁ + Na]⁺ calcd. 413.11, found 413.05.

***m*-Nitrophenyl-thio- β -D-galactopyranose tetraacetate (4m)**

3-Nitrobenzene disulphide (1.28 g, 4.15 mmol) was dissolved in dry tetrahydrofuran (5 mL) and NaBH₄ (0.51 g, 13.39 mmol) was added carefully in small portions. The resulting mixture was stirred for 3 h then cooled to 0 °C. 20 mL of ice-cold water was added and the resulting mixture was acidified with 1M HCl solution. 3-Nitrophenyl thiol (quant.) was extracted to dichloromethane, washed with water and brine, dried over anhydrous Na₂SO₄, filtered and concentrated *in vacuo*.

β -D-Galactopyranose pentaacetate (**3**, 0.88 g, 2.26 mmol) and 3-nitrophenyl thiol (189 mg, 1.22 mmol) were dissolved in dry dichloromethane (5 mL). Reaction mixture was cooled to 0 °C and BF₃·OEt₂ (1 mL, 7.96 mmol) was added dropwise. Mixture was allowed to warm to room temperature and stirred overnight. The reaction was poured over ice cold saturated NaHCO₃ solution and diluted with dichloromethane. Organic phase was washed with saturated NaHCO₃ solution and brine, dried over anhydrous Na₂SO₄, filtered and concentrated *in vacuo*. Purification by normal phase MPLC (toluene/ethyl acetate, 5–20% ethyl acetate) gave

compound **4m** (358 mg, 0.74 mmol, 60%). Synthesis of compound **4m** was first reported by Ramos-Soriano *et. al.*¹²⁰

¹H NMR (300 MHz, CDCl₃) δ 8.43 (t, *J* = 2.0 Hz, 1H, ArH), 8.15 (ddt, *J* = 8.3, 1.9, 0.9 Hz, 1H, ArH), 7.78 (ddt, *J* = 7.9, 1.8, 0.9 Hz, 1H, ArH), 7.49 (t, *J* = 8.0 Hz, 1H, ArH), 5.45 (dd, *J* = 3.3, 1.0 Hz, 1H, H-4), 5.22 (t, *J* = 9.9 Hz, 1H, H-2), 5.07 (dd, *J* = 10.0, 3.3 Hz, 1H, H-3), 4.78 (d, *J* = 9.8 Hz, 1H, H-1), 4.25 – 4.11 (m, 2H, H-6), 4.05 – 3.97 (m, 1H, H-5), 2.11 (s, 3H, CH₃), 2.09 (s, 3H, CH₃), 2.06 (s, 3H, CH₃), 1.96 (s, 3H, CH₃).

¹³C NMR (75 MHz, CDCl₃) δ 170.58 (1C, C=O), 170.19 (1C, C=O), 170.05 (1C, C=O), 169.46 (1C, C=O), 148.50 (1C, ArC), 137.84 (1C, ArCH), 135.10 (1C, ArC), 129.61 (1C, ArCH), 126.56 (1C, ArCH), 122.90 (1C, ArCH), 85.52 (1C, C-1), 75.01 (1C, C-5), 71.89 (1C, C-3), 67.31 (1C, C-4), 66.89 (1C, C-2), 61.93 (1C, C-6), 20.89 (1C, CH₃), 20.77 (1C, CH₃), 20.67 (2C, CH₃).

HPLC-MS: [C₂₀H₂₃NO₁₁S + NH₄]⁺ calcd. 503.13, found 503.06.

***p*-Nitrophenyl-thio-β-D-galactopyranose tetraacetate (4p)**

β-D-Galactopyranose pentaacetate (**3**, 1.06 g, 2.71 mmol) and 4-nitrophenyl thiol (1.20 g, 7.75 mmol) were dissolved in dry dichloromethane (10 mL). Reaction mixture was cooled to 0 °C and BF₃·OEt₂ (1.6 mL, 12.74 mmol) was added dropwise. Mixture was allowed to warm to room temperature and stirred for 8 h. The reaction was poured over ice cold saturated NaHCO₃ solution and diluted with dichloromethane. Organic phase was washed with saturated NaHCO₃ solution and brine, dried over anhydrous Na₂SO₄, filtered and concentrated *in vacuo*. Purification by normal phase MPLC (toluene/ethyl acetate, 5–20% ethyl acetate) gave compound **4p** (0.61 g, 1.26 mmol, 47%). The analytical data of **4p** are in agreement with literature.¹²¹

¹H NMR (300 MHz, CDCl₃) δ 8.20 – 8.12 (m, 2H, ArH), 7.65 – 7.57 (m, 2H, ArH), 5.47 (dd, *J* = 3.4, 1.0 Hz, 1H, H-4), 5.29 (t, *J* = 9.9 Hz, 1H, H-2), 5.10 (dd, *J* = 9.9, 3.3 Hz, 1H, H-3), 4.86 (d, *J* = 9.9 Hz, 1H, H-1), 4.26 – 4.09 (m, 2H, H-6), 4.08 – 4.00 (m, 1H, H-5), 2.16 (s, 3H, CH₃), 2.08 (s, 3H, CH₃), 2.07 (s, 3H, CH₃), 1.98 (s, 3H, CH₃).

¹³C NMR (126 MHz, CDCl₃) δ 170.46 (1C, C=O), 170.16 (1C, C=O), 170.10 (1C, C=O), 169.51 (1C, C=O), 146.97 (1C, ArC), 142.54 (1C, ArC), 130.54 (2C, ArCH), 123.99 (2C, ArCH), 84.98 (1C, C-1), 74.98 (1C, C-5), 71.86 (1C, C-3), 67.20 (1C, C-4), 66.85 (1C, C-2), 61.81 (1C, C-6), 20.88 (1C, CH₃), 20.84 (1C, CH₃), 20.79 (1C, CH₃), 20.68 (1C, CH₃).

HPLC-MS: [C₂₀H₂₃NO₁₁S + NH₄]⁺ calcd. 503.13, found 503.06.

***m*-Aminophenyl-thio- β -D-galactopyranose tetraacetate (**5m**)**

Compound **4m** (1.97 g, 4.06 mmol) was dissolved in dry dichloromethane (40 mL) and 10% Pd/C (100 mg, 0.09 mmol) was added. After three vacuum/H₂ cycles the reaction was stirred under H₂ atmosphere (1 atm) for 2 d. The reaction was filtered over celite and concentrated *in vacuo*. Pure product **5m** was obtained (1.84 g, 4.04 mmol, quant.) without further purification. ¹H NMR (300 MHz, DMSO-d₆) δ 6.98 (t, J = 7.8 Hz, 1H, ArH), 6.64 (t, J = 1.9 Hz, 1H, ArH), 6.59 (ddd, J = 7.6, 1.8, 1.0 Hz, 1H, ArH), 6.48 (ddd, J = 8.0, 2.2, 0.9 Hz, 1H, ArH), 5.31 (dd, J = 3.6, 1.1 Hz, 1H, H-4), 5.26 (dd, J = 9.5, 3.5 Hz, 1H, H-3), 5.19 (s, 2H, NH₂), 5.15 – 4.97 (m, 2H, H-1, H-2), 4.29 (t, J = 6.5 Hz, 1H, H-5), 4.13 – 3.99 (m, 2H, H-6), 2.13 (s, 3H, CH₃), 2.04 (s, 3H, CH₃), 2.00 (s, 3H, CH₃), 1.92 (s, 3H, CH₃).

¹³C NMR (75 MHz, DMSO-d₆) δ 169.97 (1C, C=O), 169.87 (1C, C=O), 169.43 (1C, C=O), 169.21 (1C, C=O), 149.15 (1C, ArC), 133.12 (1C, ArC), 129.44 (1C, ArCH), 117.59 (1C, ArCH), 115.67 (1C, ArCH), 113.13 (1C, ArCH), 84.80 (1C, C-1), 73.33 (1C, C-5), 71.05 (1C, C-3), 67.51 (1C, C-4), 67.18 (1C, C-2), 61.56 (1C, C-6), 20.54 (1C, CH₃), 20.47 (1C, CH₃), 20.41 (1C, CH₃), 20.34 (1C, CH₃).

HPLC-MS: [C₂₀H₂₅NO₉S + H]⁺ calcd. 456.13, found 456.03.

HRMS: [C₂₀H₂₅NO₉S + H]⁺ calcd. 456.1323, found 456.1315.

***p*-Aminophenyl-thio- β -D-galactopyranoside tetraacetate (**5p**)**

Compound **4p** (0.66 g, 1.36 mmol) was dissolved in dry dichloromethane (20 mL) and 10% Pd/C (75 mg, 0.07 mmol) was added. After three vacuum/H₂ cycles the reaction was stirred under H₂ atmosphere (1 atm) overnight. The reaction was filtered over celite and concentrated *in vacuo*. Pure product **5p** was obtained (0.62 g, 1.36 mmol, quant.) without further purification. The analytical data of **5p** are in agreement with literature.¹²²

¹H NMR (300 MHz, DMSO-d₆) δ 7.18 – 7.09 (m, 2H, ArH), 6.57 – 6.48 (m, 2H, ArH), 5.39 (s, 2H, NH₂), 5.25 (dd, J = 3.5, 1.0 Hz, 1H, H-4), 5.18 (dd, J = 9.7, 3.5 Hz, 1H, H-3), 4.93 (t, J = 9.9 Hz, 1H, H-2), 4.78 (d, J = 10.0 Hz, 1H, H-1), 4.21 – 4.13 (m, 1H, H-5), 4.12 – 3.94 (m, 2H, H-6), 2.09 (s, 3H, CH₃), 2.06 (s, 3H, CH₃), 2.00 (s, 3H, CH₃), 1.90 (s, 3H, CH₃).

¹³C NMR (75 MHz, DMSO-d₆) δ 169.93 (1C, C=O), 169.84 (1C, C=O), 169.46 (1C, C=O), 169.17 (1C, C=O), 149.42 (1C, ArC), 135.15 (2C, ArCH), 115.20 (1C, ArC), 114.07 (2C, ArCH), 86.07 (1C, C-1), 73.25 (1C, C-5), 71.20 (1C, C-3), 67.62 (1C, C-4), 67.24 (1C, C-2), 61.66 (1C, C-6), 20.63 (1C, CH₃), 20.51 (1C, CH₃), 20.40 (1C, CH₃), 20.36 (1C, CH₃).

HPLC-MS: [C₂₀H₂₅NO₉S + H]⁺ calcd. 456.13, found 456.04.

Galactoside **6m**

Compound **5m** (308.7 mg, 0.68 mmol) was dissolved in dry dimethylformamide (3 mL) and potassium carbonate (184 mg, 1.33 mmol) was added. The reaction mixture was cooled to 0 °C and propargyl bromide (100 μ L, 1.02 mmol) was added dropwise. The mixture was allowed to warm to room temperature and then heated to 45 °C for 6.5 h. The reaction was cooled to room temperature, poured over cold water and diluted with dichloromethane. Organic phase was washed with water and brine, dried over anhydrous Na₂SO₄, filtered and concentrated *in vacuo*. Purification by normal phase MPLC (toluene/ethyl acetate + 0.25% Et₃N, 5–30% ethyl acetate) gave compound **6m** (188.3 mg, 0.38 mmol, 56%).

¹H NMR (500 MHz, DMSO-d₆) δ 7.12 – 7.05 (m, 1H, ArH), 6.71 – 6.65 (m, 2H, ArH), 6.60 – 6.55 (m, 1H, ArH), 6.15 (t, *J* = 6.1 Hz, 1H, NH), 5.32 (dd, *J* = 3.6, 1.2 Hz, 1H, H-4), 5.26 (dd, *J* = 9.8, 3.5 Hz, 1H, H-3), 5.18 (d, *J* = 10.1 Hz, 1H, H-1), 5.02 (t, *J* = 10.0 Hz, 1H, H-2), 4.34 – 4.28 (m, 1H, H-5), 4.11 – 4.01 (m, 2H, H-6), 3.86 (dd, *J* = 6.2, 2.4 Hz, 2H, CH₂), 3.08 (t, *J* = 2.4 Hz, 1H, C \equiv CH), 2.12 (s, 3H, CH₃), 2.05 (s, 3H, CH₃), 1.99 (s, 3H, CH₃), 1.92 (s, 3H, CH₃).

¹³C NMR (126 MHz, DMSO-d₆) δ 170.02 (1C, C=O), 169.92 (1C, C=O), 169.50 (1C, C=O), 169.30 (1C, C=O), 148.25 (1C, ArC), 133.45 (1C, ArC), 129.41 (1C, ArCH), 118.27 (1C, ArCH), 114.11 (1C, ArCH), 112.06 (1C, ArCH), 84.65 (1C, C-1), 81.92 (1C, C \equiv CH), 73.38 (1C, C-5), 73.15 (1C, C \equiv CH), 71.06 (1C, C-3), 67.53 (1C, C-4), 67.11 (1C, C-2), 61.60 (1C, C-6), 31.96 (1C, CH₂), 20.59 (1C, CH₃), 20.50 (1C, CH₃), 20.44 (1C, CH₃), 20.38 (1C, CH₃).

HPLC-MS: [C₂₃H₂₇NO₉S + H]⁺ calcd. 494.15, found 494.18.

HRMS: [C₂₃H₂₇NO₉S + H]⁺ calcd. 494.1479, found 494.1471.

Galactoside **6p**

Compound **5p** (105.3 mg, 0.23 mmol) was dissolved in dry dimethylformamide (1 mL) and potassium carbonate (64.3 mg, 0.46 mmol) was added. The reaction mixture was cooled to 0 °C and propargyl bromide (29 μ L, 0.30 mmol) was added dropwise. The mixture was allowed to warm to room temperature and then heated to 40 °C. After 20 h, dry dimethylformamide (1 mL), potassium carbonate (81.0 mg, 0.59 mmol) and propargyl bromide (25 μ L, 0.26 mmol at 0 °C) were added and stirred for 6 h at 40 °C. The reaction was cooled to room temperature, poured over cold water and diluted with dichloromethane. Organic phase was washed with water, dried over anhydrous Na₂SO₄, filtered and concentrated *in vacuo*. Purification by normal phase MPLC (toluene/ethyl acetate + 0.25% Et₃N, 5–30% ethyl acetate) gave compound **6p** (85.8 mg, 0.17 mmol, 75%).

^1H NMR (300 MHz, DMSO- d_6) δ 7.24 (d, J = 8.4 Hz, 2H, ArH), 6.66 – 6.57 (m, 2H, ArH), 6.30 (t, J = 6.1 Hz, 1H, NH), 5.26 (d, J = 3.5 Hz, 1H, H-4), 5.19 (dd, J = 9.6, 3.5 Hz, 1H, H-3), 4.95 (t, J = 9.8 Hz, 1H, H-2), 4.84 (d, J = 9.9 Hz, 1H, H-1), 4.19 (t, J = 6.3 Hz, 1H, H-5), 4.13 – 3.94 (m, 2H, H-6), 3.87 (dd, J = 6.2, 2.4 Hz, 2H, CH₂), 3.07 (t, J = 2.2 Hz, 1H, C \equiv CH), 2.09 (s, 3H, CH₃), 2.07 (s, 3H, CH₃), 2.00 (s, 3H, CH₃), 1.90 (s, 3H, CH₃).

^{13}C NMR (75 MHz, DMSO- d_6) δ 169.92 (1C, C=O), 169.84 (1C, C=O), 169.44 (1C, C=O), 169.18 (1C, C=O), 148.27 (1C, ArC), 134.84 (2C, ArCH), 116.56 (1C, ArC), 112.93 (2C, ArCH), 85.84 (1C, C-1), 81.87 (1C, C \equiv CH), 73.25 (1C, C-5), 73.05 (1C, C \equiv CH), 71.17 (1C, C-3), 67.59 (1C, C-4), 67.25 (1C, C-2), 61.66 (1C, C-6), 31.84 (1C, CH₂), 20.62 (1C, CH₃), 20.53 (1C, CH₃), 20.41 (1C, CH₃), 20.35 (1C, CH₃).

HPLC-MS: [C₂₃H₂₇NO₉S + H]⁺ calcd. 494.15, found 494.13.

HRMS: [C₂₃H₂₇NO₉S + H]⁺ calcd. 494.1479, found 494.1475.

Galactoside **7m**

Compound **5m** (337.1 mg, 0.74 mmol) was dissolved in dry dimethylformamide (3 mL) and potassium carbonate (175 mg, 1.26 mmol) was added. The reaction mixture was cooled to 0 °C and 4-bromo-1-butyne (205 μL , 2.12 mmol) was added dropwise. The mixture was allowed to warm to room temperature and then heated to 70 °C. After 48 h, dry dimethylformamide (1 mL), potassium carbonate (120 mg, 0.87 mmol) and 4-bromo-1-butyne (100 μL , 1.07 mmol at 0 °C) were added and stirred for additional 48 h at 70 °C. The reaction was cooled to room temperature, poured over cold water and diluted with dichloromethane. Organic phase was washed with water, dried over anhydrous Na₂SO₄, filtered and concentrated *in vacuo*. Purification by normal phase MPLC (toluene/ethyl acetate + 0.25% Et₃N, 5–30% ethyl acetate) gave compound **7m** (219.4 mg, 0.43 mmol, 58%).

^1H NMR (500 MHz, DMSO- d_6) δ 7.087 – 7.01 (m, 1H, ArH), 6.64 – 6.60 (m, 2H, ArH), 6.53 – 6.50 (m, 1H, ArH), 5.88 (t, J = 6.0 Hz, 1H, NH), 5.31 (dd, J = 3.5, 1.1 Hz, 1H, H-4), 5.27 (dd, J = 9.8, 3.6 Hz, 1H, H-3), 5.18 (d, J = 10.1 Hz, 1H, H-1), 5.02 (t, J = 10.0 Hz, 1H, H-2), 4.31 (td, J = 6.8, 6.4, 1.2 Hz, 1H, H-5), 4.10 – 4.01 (m, 2H, H-6), 3.19 (q, J = 6.9 Hz, 2H, NHCH₂CH₂), 2.85 (t, J = 2.7 Hz, 1H, C \equiv CH), 2.39 (td, J = 7.1, 2.7 Hz, 2H, NHCH₂CH₂), 2.12 (s, 3H, CH₃), 2.04 (s, 3H, CH₃), 1.99 (s, 3H, CH₃), 1.92 (s, 3H, CH₃).

^{13}C NMR (126 MHz, DMSO- d_6) δ 169.97 (1C, C=O), 169.86 (1C, C=O), 169.45 (1C, C=O), 169.22 (1C, C=O), 148.67 (1C, ArC), 133.42 (1C, ArC), 129.50 (1C, ArCH), 117.71 (1C, ArCH), 113.26 (1C, ArCH), 111.54 (1C, ArCH), 84.47 (1C, C-1), 82.62 (1C, C \equiv CH), 73.35 (1C, C-5), 72.21 (1C, C \equiv CH), 71.04 (1C, C-3), 67.55 (1C, C-4), 67.08 (1C, C-2), 61.62 (1C,

C-6), 41.76 (1C, NHCH₂CH₂), 20.56 (1C, CH₃), 20.49 (1C, CH₃), 20.42 (1C, CH₃), 20.35 (1C, CH₃), 18.35 (1C, NHCH₂CH₂).

HPLC-MS: [C₂₄H₂₉NO₉S + H]⁺ calcd. 508.16, found 508.22.

Galactoside **7p**

Compound **5p** (315.8 mg, 0.69 mmol) was dissolved in dry dimethylformamide (3 mL) and potassium carbonate (280 mg, 2.03 mmol) was added. The reaction mixture was cooled to 0 °C and 4-bromo-1-butyne (280 μL, 2.98 mmol) was added dropwise. The mixture was allowed to warm to room temperature and then heated to 65 °C. After 48 h, dry dimethylformamide (1 mL), potassium carbonate (88.7 mg, 0.64 mmol) and 4-bromo-1-butyne (100 μL, 1.07 mmol at 0 °C) were added and stirred for additional 48 h at 65 °C. The reaction was cooled to room temperature, poured over cold water and diluted with dichloromethane. Organic phase was washed with water, dried over anhydrous Na₂SO₄, filtered and concentrated *in vacuo*. Purification by normal phase MPLC (toluene/ethyl acetate + 0.25% Et₃N, 5–30% ethyl acetate) gave compound **7p** (259.3 mg, 0.51 mmol, 74%).

¹H NMR (300 MHz, DMSO-d₆) δ 7.25 – 7.14 (m, 2H, ArH), 6.60 – 6.50 (m, 2H, ArH), 6.05 (t, *J* = 6.0 Hz, 1H, NH), 5.26 (dd, *J* = 3.5, 1.0 Hz, 1H, H-4), 5.19 (dd, *J* = 9.7, 3.5 Hz, 1H, H-3), 4.94 (t, *J* = 9.8 Hz, 1H, H-2), 4.80 (d, *J* = 10.0 Hz, 1H, H-1), 4.21 – 4.12 (m, 1H, H-5), 4.12 – 3.92 (m, 2H, H-6), 3.19 (q, *J* = 6.8 Hz, 2H, NHCH₂CH₂), 2.85 (t, *J* = 2.6 Hz, 1H, C≡CH), 2.38 (td, *J* = 7.0, 2.7 Hz, 2H, NHCH₂CH₂), 2.08 (s, 3H, CH₃), 2.06 (s, 3H, CH₃), 2.00 (s, 3H, CH₃), 1.90 (s, 3H, CH₃).

¹³C NMR (126 MHz, DMSO-d₆) δ 169.97 (1C, C=O), 169.90 (1C, C=O), 169.51 (1C, C=O), 169.23 (1C, C=O), 148.84 (1C, ArC), 135.28 (2C, ArCH), 115.54 (1C, ArC), 112.26 (2C, ArCH), 86.04 (1C, C-1), 82.64 (1C, C≡CH), 73.25 (1C, C-5), 72.29 (1C, C≡CH), 71.19 (1C, C-3), 67.60 (1C, C-4), 67.24 (1C, C-2), 61.67 (1C, C-6), 41.69 (1C, NHCH₂CH₂), 20.67 (1C, CH₃), 20.56 (1C, CH₃), 20.44 (1C, CH₃), 20.40 (1C, CH₃), 18.37 (1C, NHCH₂CH₂).

HPLC-MS: [C₂₄H₂₉NO₉S + H]⁺ calcd. 508.16, found 508.18.

HRMS: C₂₄H₂₉NO₉S + H]⁺ calcd. 508.1636, found 508.1633.

Galactoside precursor **8m**

Compound **6m** (224.5 mg, 0.45 mmol) was suspended in dry methanol (4 mL) and 1M sodium methoxide in methanol (cat.) was added and stirred overnight. The reaction mixture was neutralized with 1M HCl solution and the solvent was removed *in vacuo*. Purification by normal

phase MPLC (dichloromethane/ethanol + 1% NH₄OH, 1–20% ethanol) gave compound **8m** (79.7 mg, 0.24 mmol, 54%).

¹H NMR (500 MHz, MeOH-d₄) δ 7.05 (t, *J* = 7.9 Hz, 1H, ArH), 6.94 (t, *J* = 2.0 Hz, 1H, ArH), 6.86 – 6.81 (m, 1H, ArH), 6.58 (dd, *J* = 8.0, 2.1 Hz, 1H, ArH), 4.60 (d, *J* = 9.8 Hz, 1H, H-1), 3.92 – 3.88 (m, 3H, H-4, CH₂), 3.82 – 3.69 (m, 2H, H-6), 3.65 – 3.57 (m, 2H, H-2, H-5), 3.50 (dd, *J* = 9.2, 3.3 Hz, 1H, H-3), 2.51 (t, *J* = 2.4 Hz, 1H, C≡CH).

¹³C NMR (126 MHz, MeOH-d₄) δ 149.63 (1C, ArC), 136.71 (1C, ArC), 130.19 (1C, ArCH), 120.81 (1C, ArCH), 116.03 (1C, ArCH), 113.46 (1C, ArCH), 90.37 (1C, C-1), 82.40 (1C, C≡CH), 80.58 (1C, C-5), 76.37 (1C, C-3), 71.93 (1C, C≡CH), 70.96 (1C, C-2), 70.44 (1C, C-4), 62.65 (1C, C-6), 33.73 (1C, CH₂).

HPLC-MS: [C₁₅H₁₉NO₅S + H]⁺ calcd. 326.11, found 326.20.

HRMS: [C₁₅H₁₉NO₅S + H]⁺ calcd. 326.1057, found 326.1056.

Galactoside precursor **8p**

Compound **6p** (148.1 mg, 0.30 mmol) was suspended in dry methanol (9 mL) and 1M sodium methoxide in methanol (cat.) was added. After 4 h, the reaction mixture was neutralized with 1M HCl solution. The solvent was removed *in vacuo*. Purification by C18 column HPLC chromatography (water/acetonitrile + 0.1% formic acid, 5–40% acetonitrile) gave compound **8p** (63.5 mg, 0.20 mmol, 65%).

¹H NMR (500 MHz, MeOH-d₄) δ 7.43 – 7.37 (m, 2H, ArH), 6.68 – 6.61 (m, 2H, ArH), 4.32 (d, *J* = 9.5 Hz, 1H, H-1), 3.88 (d, *J* = 2.4 Hz, 2H, CH₂), 3.86 (d, *J* = 3.1 Hz, 1H, H-4), 3.76 – 3.67 (m, 2H, H-6), 3.54 – 3.43 (m, 3H, H-2, H-3, H-5), 2.50 (t, *J* = 2.4 Hz, 1H, C≡CH).

¹³C NMR (126 MHz, MeOH-d₄) δ 149.45 (1C, ArC), 136.20 (2C, ArCH), 120.79 (1C, ArC), 114.59 (2C, ArCH), 91.65 (1C, C-1), 82.21 (1C, C≡CH), 80.46 (1C, C-5), 76.37 (1C, C-3), 71.86 (1C, C≡CH), 70.97 (1C, C-2), 70.42 (1C, C-4), 62.54 (1C, C-6), 33.56 (1C, CH₂).

HPLC-MS: [C₁₅H₁₉NO₅S + H]⁺ calcd. 326.11, found 326.21.

HRMS: [C₁₅H₁₉NO₅S + Na]⁺ calcd. 348.0876, found 348.0875.

Galactoside precursor **9m**

Compound **7m** (214.1 mg, 0.42 mmol) was suspended in dry methanol (4 mL) and 1M sodium methoxide in methanol (cat.) was added and stirred overnight. The reaction mixture was neutralized with 1M HCl solution and the solvent was removed *in vacuo*. Purification by normal phase MPLC (dichloromethane/ethanol + 1% NH₄OH, 1–20% ethanol) gave compound **9m** (81.4 mg, 0.24 mmol, 57%).

^1H NMR (500 MHz, MeOH- d_4) δ 7.03 (t, $J = 7.9$ Hz, 1H, ArH), 6.87 (t, $J = 1.9$ Hz, 1H), 6.81 – 6.78 (m, 1H, ArH), 6.52 (dd, $J = 8.0, 1.9$ Hz, 1H, ArH), 4.58 (d, $J = 9.7$ Hz, 1H, H-1), 3.90 (d, $J = 3.1$ Hz, 1H, H-4), 3.82 – 3.68 (m, 2H, H-6), 3.64 – 3.55 (m, 2H, H-2, H-5), 3.50 (dd, $J = 9.2, 3.3$ Hz, 1H, H-3), 3.28 (t, $J = 7.0$ Hz, 2H, NHCH_2CH_2), 2.44 (td, $J = 7.0, 2.6$ Hz, 2H, NHCH_2CH_2), 2.30 (t, $J = 2.6$ Hz, 1H, $\text{C}\equiv\text{CH}$).

^{13}C NMR (126 MHz, MeOH- d_4) δ 150.01 (1C, ArC), 136.63 (1C, ArC), 130.38 (1C, ArCH), 120.43 (1C, ArCH), 115.72 (1C, ArCH), 113.01 (1C, ArCH), 90.37 (1C, C-1), 82.82 (1C, $\text{C}\equiv\text{CH}$), 80.59 (1C, C-5), 76.36 (1C, C-3), 70.96 (1C, $\text{C}\equiv\text{CH}$), 70.78 (1C, C-2), 70.44 (1C, C-4), 62.67 (1C, C-6), 43.67 (1C, NHCH_2CH_2), 19.62 (1C, NHCH_2CH_2).

HPLC-MS: $[\text{C}_{16}\text{H}_{21}\text{NO}_5\text{S} + \text{H}]^+$ calcd. 340.12, found 340.22.

HRMS: $[\text{C}_{16}\text{H}_{21}\text{NO}_5\text{S} + \text{H}]^+$ calcd. 340.1213, found 340.1215.

Galactoside precursor **9p**

Compound **7p** (232.4 mg, 0.46 mmol) was suspended in dry methanol (5 mL) and 1M sodium methoxide in methanol (cat.) was added and stirred overnight. The reaction mixture was neutralized with 1M HCl solution and the solvent was removed *in vacuo*. Purification by normal phase MPLC (dichloromethane/ethanol + 1% NH_4OH , 1–20% ethanol) gave compound **9p** (118.2 mg, 0.36 mmol, 79%).

^1H NMR (500 MHz, MeOH- d_4) δ 7.41 – 7.35 (m, 2H, ArH), 6.60 – 6.53 (m, 2H, ArH), 4.30 (d, $J = 9.5$ Hz, 1H, H-1), 3.86 (dd, $J = 3.3, 1.1$ Hz, 1H, H-4), 3.77 – 3.65 (m, 2H, H-6), 3.54 – 3.43 (m, 3H, H-2, H-3, H-5), 3.27 (t, $J = 7.1$ Hz, 2H, NHCH_2CH_2), 2.43 (td, $J = 7.1, 2.7$ Hz, 2H, NHCH_2CH_2), 2.30 (t, $J = 2.7$ Hz, 1H, $\text{C}\equiv\text{CH}$).

^{13}C NMR (126 MHz, MeOH- d_4) δ 149.88 (1C, ArC), 136.58 (2C, ArCH), 119.77 (1C, ArC), 113.94 (2C, ArCH), 91.64 (1C, C-1), 82.71 (1C, $\text{C}\equiv\text{CH}$), 80.45 (1C, C-5), 76.37 (1C, C-3), 70.93 (1C, C-2), 70.76 (1C, $\text{C}\equiv\text{CH}$), 70.42 (1C, C-4), 62.54 (1C, C-6), 43.57 (1C, NHCH_2CH_2), 19.61 (1C, NHCH_2CH_2).

HPLC-MS: $[\text{C}_{16}\text{H}_{21}\text{NO}_5\text{S} + \text{H}]^+$ calcd. 340.12, found 340.21.

HRMS: $[\text{C}_{16}\text{H}_{21}\text{NO}_5\text{S} + \text{H}]^+$ calcd. 340.1213, found 340.1215.

Bis(4-prop-2-ynyloxyphenyl) disulphide (**11**)

Iodine solution (satd., 0.5 mL) was added to 4-hydroxy thiophenol (**10**, 187.4 mg, 1.49 mmol) and dissolved in ethanol (5 mL) in air. After 5 h, aqueous $\text{Na}_2\text{S}_2\text{O}_3$ solution was added to remove the residual iodine. Product was extracted to ethyl acetate, organic phase was washed with aqueous $\text{Na}_2\text{S}_2\text{O}_3$ solution and half satd. brine, dried over anhydrous Na_2SO_4 , filtered and

concentrated *in vacuo*. Crude bis(4-hydroxyphenyl) disulfide was purified by crystallization from chloroform (93.6 mg, 0.37 mmol, 50%). The analytical data matched the literature.¹²³

Bis(4-hydroxyphenyl) disulfide (80.4 mg, 0.32 mmol) was dissolved in dry dimethylformamide (3 mL) and potassium carbonate (227.5 mg, 1.65 mmol) was added. Propargyl bromide (185 μ L, 1.89 mmol) was added dropwise and stirred overnight. The reaction was poured over cold water and diluted with dichloromethane. Organic phase was washed half satd. brine, dried over anhydrous Na₂SO₄, filtered and concentrated *in vacuo*. Purification by normal phase MPLC (petrol ether/ethyl acetate, 5–20% ethyl acetate) gave compound **11** (87.3 mg, 0.27 mmol, 83%). The analytical data match the literature.¹²⁴

¹H NMR (500 MHz, CDCl₃) δ 7.44 – 7.39 (m, 4H, ArH), 6.94 – 6.89 (m, 4H, ArH), 4.68 (d, J = 2.4 Hz, 4H, CH₂), 2.53 (t, J = 2.4 Hz, 2H, C \equiv CH).

¹³C NMR (126 MHz, CDCl₃) δ 157.85 (2C, ArC), 132.15 (4C, ArCH), 129.56 (2C, ArC), 115.72 (4C, ArCH), 78.30 (2C, C \equiv CH), 75.99 (2C, C \equiv CH), 56.04 (2C, CH₂).

4-prop-2-ynyloxyphenyl thiol (**12**)

Compound **11** (726 mg, 2.22 mmol) was dissolved in dry methanol (30 mL). 1,4-Dithio-threitol (1.72 g, 11.1 mmol) and DIPEA (1 mL, 5.74 mmol) were added. The reaction was stirred for 3 h at r.t., then concentrated and diluted with EtOAc. The organic phase was washed with 1M HCl solution, half satd. brine, dried over anhydrous Na₂SO₄, filtered and concentrated *in vacuo*. Crude 4-prop-2-ynyloxyphenyl thiol (**12**, quant., with \approx 1 eq. of 1,2-dithiane-4,5-diol impurity) was used without further purification.

¹H NMR (500 MHz, MeOH-d₄) δ 7.26 – 7.21 (m, 2H, ArH), 6.90 – 6.86 (m, 2H, ArH), 4.69 (d, J = 2.4 Hz, 2H, CH₂), 3.49 (d, J = 8.7 Hz, 1H, impurity), 3.03 (d, J = 12.1 Hz, 1H, impurity), 2.93 (t, J = 2.3 Hz, 1H, C \equiv CH), 2.88 (dd, J = 12.9, 9.5 Hz, 1H, impurity).

Galactoside **13**

β -D-Galactopyranose pentaacetate (**3**, 1.49 g, 3.83 mmol) and 4-prop-2-ynyloxyphenyl thiol (**12**, 365 mg, 2.22 mmol) were dissolved in mixture of dry dichloromethane (20 mL) and toluene (15 mL). Reaction mixture was cooled to 0 °C and BF₃·OEt₂ (1 mL, 7.96 mmol) was added dropwise. Mixture was allowed to warm to room temperature and stirred overnight. The reaction was poured over ice cold satd. NaHCO₃ solution and diluted with dichloromethane. Organic phase was washed with satd. NaHCO₃ solution and brine, dried over anhydrous Na₂SO₄, filtered and concentrated *in vacuo*. Purification by normal phase MPLC (toluene/ethyl acetate, 5–25% ethyl acetate) gave compound **13** (736 mg, 1.49 mmol, 39%).

^1H NMR (500 MHz, CDCl_3) δ 7.48 (d, $J = 7.8$ Hz, 2H, ArH), 6.93 (d, $J = 7.9$ Hz, 2H, ArH), 5.38 (s, 1H, H-4), 5.17 (t, $J = 9.9$ Hz, 1H, H-2), 5.05 – 4.98 (m, 1H, H-3), 4.69 (s, 2H, CH_2), 4.58 (d, $J = 9.9$ Hz, 1H, H-1), 4.21 – 4.05 (m, 2H, H-6), 3.89 (t, $J = 6.5$ Hz, 1H, H-5), 2.53 (s, 2H, $\text{C}\equiv\text{CH}$), 2.10 (s, 3H, CH_3), 2.09 (s, 3H, CH_3) 2.03 (s, 3H, CH_3), 1.96 (s, 3H, CH_3).

^{13}C NMR (126 MHz, CDCl_3) δ 170.52 (1C, $\text{C}=\text{O}$), 170.32 (1C, $\text{C}=\text{O}$), 170.22 (1C, $\text{C}=\text{O}$), 169.58 (1C, $\text{C}=\text{O}$), 158.23 (1C, ArC), 135.79 (2C, ArCH), 123.43 (1C, ArC), 115.38 (2C, ArCH), 87.01 (1C, C-1), 78.26 (1C, $\underline{\text{C}}\equiv\text{CH}$), 76.00 (1C, $\text{C}\equiv\text{CH}$), 74.42 (1C, C-5), 72.15 (1C, C-3), 67.40 (1C, C-2), 67.30 (1C, C-4), 61.66 (1C, C-5), 55.93 (1C, CH_2), 21.03 (1C, CH_3), 20.83 (1C, CH_3), 20.78 (1C, CH_3), 20.73 (1C, CH_3).

HPLC-MS: $[\text{C}_{23}\text{H}_{26}\text{O}_{10}\text{S} + \text{NH}_4]^+$ calcd. 512.16, found 512.15.

HRMS: $[\text{C}_{23}\text{H}_{26}\text{O}_{10}\text{S} + \text{Na}]^+$ calcd. 517.1139, found 517.1134.

Galactoside precursor 14

Compound **13** (736 mg, 1.49 mmol) was dissolved in dry methanol (30 mL) and 1M sodium methoxide in methanol (cat.) was added. After 2h, the reaction mixture was neutralized with Amberlite IR 120/ H^+ . The solvent was removed *in vacuo*. Purification by normal phase MPLC (dichloromethane/methanol, 1–20% methanol) gave compound **14** (485 mg, 1.49 mmol, quant.).

^1H NMR (500 MHz, MeOH-d_4) δ 7.54 (d, $J = 7.6$ Hz, 2H, ArH), 6.93 (d, $J = 7.6$ Hz, 2H, ArH), 4.72 (s, 2H, CH_2), 4.42 (d, $J = 9.5$ Hz, 1H, H-1), 3.88 (s, 1H, H-4), 3.80 – 3.66 (m, 2H, H-6), 3.58 – 3.45 (m, 3H, H-2, H-3, H-5), 2.95 (d, $J = 2.1$ Hz, 1H, $\text{C}\equiv\text{CH}$).

^{13}C NMR (126 MHz, MeOH-d_4) δ 159.05 (1C, ArC), 135.47 (2C, ArCH), 126.56 (1C, ArC), 116.37 (2C, ArCH), 91.05 (1C, C-1), 80.47 (1C, C-5), 79.61 (1C, $\underline{\text{C}}\equiv\text{CH}$), 76.90 (1C, $\text{C}\equiv\text{CH}$), 76.31 (1C, C-3), 70.94 (1C, C-2), 70.46 (1C, C-4), 62.62 (1C, C-6), 56.63 (1C, CH_2).

HPLC-MS: $[\text{C}_{15}\text{H}_{18}\text{O}_6\text{S} + \text{NH}_4]^+$ calcd. 344.12, found 344.11.

HRMS: $[\text{C}_{15}\text{H}_{18}\text{O}_6\text{S} + \text{Na}]^+$ calcd. 349.0716, found 349.0714.

β -D-Xylopyranose tetraacetate (15)

β -D-Xylopyranose tetraacetate was prepared in analogy to synthesis of β -D-galactopyranose pentaacetate (**3**) reported by Cohen *et al.*¹¹⁹ D-xylose (1.20 g, 7.99 mmol), acetic anhydride (9.4 mL, 99.4 mmol) and anhydrous sodium acetate (0.85 g, 10.4 mmol) were heated to 100 °C for 20 minutes. The mixture was allowed to cooled down to room temperature, poured over 50 mL of ice water and stirred for 1 hour. The product was extracted with dichloromethane, washed with water, dried over anhydrous Na_2SO_4 , filtered and evaporated to a syrup. Crude product

was purified by crystallisation from ethanol (1.00 g, 3.15 mmol, 39%). Compound **15** was first reported by Hudson and Johnson¹²⁵ and the analytical data match the literature.¹²⁶

¹H NMR (500 MHz, CDCl₃) δ 5.71 (d, *J* = 6.8 Hz, 1H, H-1), 5.20 (t, *J* = 8.3 Hz, 1H, H-3), 5.03 (dd, *J* = 8.4, 6.9 Hz, 1H, H-2), 4.97 (td, *J* = 8.3, 5.0 Hz, 1H, H-4), 4.14 (dd, *J* = 12.0, 5.0 Hz, 1H, Heq-5), 3.52 (dd, *J* = 12.0, 8.4 Hz, 1H, Hax-5), 2.10 (s, 3H, CH₃), 2.05 (s, 3H, CH₃), 2.05 (s, 6H, CH₃).

¹³C NMR (126 MHz, CDCl₃) δ 169.96 (2C, C=O), 169.45 (1C, C=O), 169.18 (1C, C=O), 92.17 (1C, C-1), 71.13 (1C, C-3), 69.61 (1C, C-2), 68.44 (1C, C-4), 62.94 (1C, C-5), 20.95 (1C, CH₃), 20.86 (1C, CH₃), 20.80 (1C, CH₃), 20.74 (1C, CH₃).

HPLC-MS: [C₁₃H₁₈O₉ + Na]⁺ calcd. 341.08, found 341.16.

***p*-Nitrophenyl-thio-β-D-xylopyranose triacetate (16)**

β-D-Xylopyranose tetraacetate (**15**, 1.00 g, 3.15 mmol) and 4-nitrophenyl thiol (1.33 g, 8.55 mmol) were dissolved in dry dichloromethane (12 mL). Reaction mixture was cooled to 0 °C and BF₃·OEt₂ (1.5 mL, 9.45 mmol) was added dropwise. Mixture was allowed to warm to room temperature and stirred for 5 h. The reaction was poured over ice cold saturated NaHCO₃ solution and diluted with dichloromethane. Organic phase was washed with saturated NaHCO₃ solution and brine, dried over anhydrous Na₂SO₄, filtered and concentrated *in vacuo*. Purification by normal phase MPLC (toluene/ethyl acetate, 5–20% ethyl acetate) gave compound **16** (573 mg, 1.39 mmol, 44%). The analytical data match the literature.¹²⁷

¹H NMR (500 MHz, MeOH-d₄) δ 8.19 – 8.13 (m, 2H, ArH), 7.60 – 7.53 (m, 2H, ArH), 5.20 (t, *J* = 7.4 Hz, 1H, H-3), 5.07 (d, *J* = 7.3 Hz, 1H, H-1), 4.99 (t, *J* = 7.3 Hz, 1H, H-2), 4.94 (td, *J* = 7.6, 4.5 Hz, 1H, H-4), 4.35 (dd, *J* = 12.1, 4.5 Hz, 1H, Heq-5), 3.56 (dd, *J* = 12.0, 7.7 Hz, 1H, Hax-5), 2.10 (s, 3H, CH₃), 2.09 (s, 3H, CH₃), 2.08 (s, 3H, CH₃).

HPLC-MS: [C₁₇H₁₉NO₉S + Na]⁺ calcd. 436.07, found 436.11.

***p*-Aminophenyl-thio-β-D-xylopyranose triacetate (17)**

Compound **16** (553 mg, 1.34 mmol) was dissolved in dry dichloromethane (15 mL) and 10% Pd/C (54.7 mg, 0.05 mmol) was added. After three vacuum/H₂ cycles the reaction was stirred under H₂ atmosphere (1 atm) overnight. The reaction was filtered over celite and concentrated *in vacuo*. Pure product **17** was obtained (517 mg, 1.34 mmol, quant.) without further purification.

¹H NMR (500 MHz, DMSO-d₆) δ 7.11 – 7.06 (m, 2H, ArH), 6.54 – 6.49 (m, 2H, ArH), 5.37 (s, 2H, NH₂), 5.19 (t, *J* = 8.9 Hz, 1H, H-3), 4.79 – 4.69 (m, 2H, H-1, H-4), 4.67 (t, *J* = 9.0 Hz, 1H,

H-2), 3.99 (dd, $J = 11.3, 5.3$ Hz, 1H, Heq-5), 3.49 (dd, $J = 11.3, 9.9$ Hz, 1H, Hax-5), 2.04 (s, 3H, CH₃), 1.97 (s, 3H, CH₃), 1.95 (s, 3H, CH₃).

¹³C NMR (126 MHz, DMSO-d₆) δ 169.45 (2C, C=O), 168.92 (1C, C=O), 149.68 (1C, ArC), 135.89 (2C, ArCH), 114.09 (2C, ArCH), 113.87 (1C, ArC), 85.60 (1C, C-1), 72.39 (1C, C-3), 69.67 (1C, C-2), 68.32 (1C, C-4), 64.84 (1C, C-5), 20.51 (1C, CH₃), 20.44 (1C, CH₃), 20.35 (1C, CH₃).

HPLC-MS: [C₁₇H₂₁NO₇S + H]⁺ calcd. 384.11, found 384.16.

HRMS: [C₁₇H₂₁NO₇S + H]⁺ calcd. 384.1111, found 384.1105.

Xyloside 18

Compound **17** (221 mg, 0.58 mmol) was dissolved in dry dimethylformamide (2 mL) and potassium carbonate (159 mg, 1.15 mmol) was added. The reaction mixture was cooled to 0 °C and propargyl bromide (125 μ L, 1.28 mmol) was added dropwise. The mixture was allowed to warm to room temperature and then heated to 40 °C. After 6 h, the reaction was cooled to room temperature, poured over cold water and diluted with dichloromethane. Organic phase was washed with water, dried over anhydrous Na₂SO₄, filtered and concentrated *in vacuo*. Purification by normal phase MPLC (toluene/ethyl acetate + 0.25% Et₃N, 5–20% ethyl acetate) gave compound **18** (152 mg, 0.36 mmol, 63%).

¹H NMR (500 MHz, DMSO-d₆) δ 7.23 – 7.16 (m, 2H, ArH), 6.66 – 6.55 (m, 2H, ArH), 6.33 (t, $J = 6.1$ Hz, 1H, NH), 5.20 (t, $J = 9.0$ Hz, 1H, H-3), 4.82 (d, $J = 9.3$ Hz, 1H, H-1), 4.77 – 4.66 (m, 2H, H-4, H-2), 3.99 (dd, $J = 11.3, 5.3$ Hz, 1H, Heq-5), 3.87 (dd, $J = 6.1, 2.5$ Hz, 2H, CH₂), 3.51 (dd, $J = 11.3, 9.9$ Hz, 1H, Hax-5), 3.10 – 3.05 (m, 1H, C \equiv CH), 2.05 (s, 3H, CH₃), 1.97 (s, 3H, CH₃), 1.95 (s, 3H, CH₃).

¹³C NMR (126 MHz, DMSO-d₆) δ 169.52 (1C, C=O), 169.51 (1C, C=O), 169.03 (1C, C=O), 148.47 (1C, ArC), 135.61 (2C, ArCH), 115.42 (1C, ArC), 113.02 (2C, ArCH), 85.54 (1C, C-1), 81.87 (1C, C \equiv CH), 73.16 (1C, C \equiv CH), 72.34 (1C, C-3), 69.73 (1C, C-2), 68.34 (1C, C-4), 64.85 (1C, C-5), 31.84 (1C, CH₂), 20.56 (1C, CH₃), 20.49 (1C, CH₃), 20.40 (1C, CH₃).

HPLC-MS: [C₂₀H₂₃NO₇S + H]⁺ calcd. 422.13, found 422.14.

HRMS: [C₂₀H₂₃NO₇S + H]⁺ calcd. 422.1268, found 422.1261.

Xyloside precursor 19

Compound **18** (142 mg, 0.34 mmol) was suspended in dry methanol (4 mL) and 1M sodium methoxide in methanol (cat.) was added and stirred overnight. The reaction mixture was neutralized with 1M HCl solution and the solvent was removed *in vacuo*. Purification by normal

phase MPLC (dichloromethane/ethanol + 1% NH₄OH, 1–20% ethanol) gave compound **19** (88.5 mg, 0.30 mmol, 89%).

¹H NMR (500 MHz, MeOH-d₄) δ 7.40 – 7.32 (m, 2H, ArH), 6.68 – 6.59 (m, 2H, ArH), 4.26 (d, *J* = 9.4 Hz, 1H, H-1), 3.92 – 3.86 (m, 3H, Heq-5, CH₂), 3.43 – 3.37 (m, 1H, H-4), 3.31 – 3.28 (m, 1H, H-3), 3.18 – 3.08 (m, 2H, H-2, Hax-5), 2.51 (t, *J* = 2.4 Hz, 1H, C≡CH).
¹³C NMR (126 MHz, MeOH-d₄) δ 149.75 (1C, ArC), 137.06 (2C, ArCH), 119.17 (1C, ArC), 114.49 (2C, ArCH), 90.91 (1C, C-1), 82.15 (1C, C≡CH), 79.42 (1C, C-3), 73.36 (1C, C-2), 71.88 (1C, C≡CH), 70.94 (1C, C-4), 70.62 (1C, C-5), 33.51 (1C, CH₂).

HPLC-MS: [C₁₄H₁₇NO₄S + H]⁺ calcd. 296.10, found 296.14.

HRMS: [C₁₄H₁₇NO₄S + H]⁺ calcd. 296.0951, found 296.0949.

Xyloside **20**

β-D-Xylopyranose triacetate (**15**, 1.21 g, 3.81 mmol) and 4-prop-2-ynoxyphenyl thiol (**12**, 365 mg, 2.22 mmol) were dissolved in mixture of dry dichloromethane (20 mL) and toluene (15 mL). Reaction mixture was cooled to 0 °C and BF₃·OEt₂ (1 mL, 7.96 mmol) was added dropwise. Mixture was allowed to warm to room temperature and stirred for 5 h. The reaction was poured over ice cold saturated NaHCO₃ solution and diluted with dichloromethane. Organic phase was washed with saturated NaHCO₃ solution and brine, dried over anhydrous Na₂SO₄, filtered and concentrated *in vacuo*. Purification by normal phase MPLC (toluene/ethyl acetate, 5–20% ethyl acetate) gave compound **20** (176 mg, 0.42 mmol, 12%).

¹H NMR (500 MHz, CDCl₃) δ 7.43 (d, *J* = 8.5 Hz, 2H, ArH), 6.93 (d, *J* = 8.5 Hz, 2H, ArH), 5.16 (t, *J* = 8.4 Hz, 1H, H-3), 4.92 – 4.83 (m, 2H, H-2, H-4), 4.69 (s, 2H, CH₂), 4.63 (d, *J* = 8.6 Hz, 1H, H-1), 4.23 (dd, *J* = 11.7, 5.0 Hz, 1H, H-5eq.), 3.41 – 3.33 (m, 1H, H-5ax.), 2.54 (s, 1H, C≡CH), 2.10 (s, 3H, CH₃), 2.03 (s, 6H, CH₃).

¹³C NMR (126 MHz, CDCl₃) δ 170.12 (1C, C=O), 169.92 (1C, C=O), 169.49 (1C, C=O), 158.31 (1C, ArC), 136.03 (2C, ArCH), 122.94 (1C, ArC), 115.55 (2C, ArCH), 86.53 (1C, C-1), 78.27 (1C, C≡CH), 76.01 (1C, C≡CH), 72.48 (1C, C-3), 69.95 (1C, C-2), 68.59 (1C, C-4), 65.61 (1C, C-5), 55.95 (1C, CH₂), 20.97 (1C, CH₃), 20.85 (2C, CH₃).

HPLC-MS: [C₂₀H₂₂O₈S + NH₄]⁺ calcd. 440.14, found 440.12.

HRMS: [C₂₀H₂₂O₈S + Na]⁺ calcd. 445.0928, found 445.0918.

Xyloside precursor (**21**)

Compound **20** (157.3 mg, 0.37 mmol) was dissolved in dry methanol (10 mL) and 1M sodium methoxide in methanol (cat.) was added. After 5h, the reaction mixture was neutralized with

Amberlite IR 120/H⁺. The solvent was removed *in vacuo*. Purification by normal phase MPLC (dichloromethane/methanol, 1–20% methanol) gave compound **21** (83.0 mg, 0.28 mmol, 75%). ¹H NMR (500 MHz, MeOH-d₄) δ 7.53 – 7.46 (m, 2H, ArH), 6.97 – 6.92 (m, 2H, ArH), 4.73 (d, *J* = 2.4 Hz, 2H, CH₂), 4.37 (d, *J* = 9.4 Hz, 1H, H-1), 3.91 (dd, *J* = 11.3, 5.2 Hz, 1H, H-5eq.), 3.46 – 3.37 (m, 1H, H-4), 3.34 – 3.29 (m, 1H, H-3), 3.22 – 3.08 (m, 2H, H-2, H-5ax.), 2.96 (t, *J* = 2.4 Hz, 1H, C≡CH).

¹³C NMR (126 MHz, MeOH-d₄) δ 159.41 (1C, ArC), 136.53 (2C, ArCH), 125.15 (1C, ArC), 116.36 (2C, ArCH), 90.56 (1C, C-1), 79.55 (1C, C≡CH), 79.31 (1C, C-3), 76.95 (1C, C≡CH), 73.50 (1C, C-2), 70.91 (1C, C-4), 70.56 (1C, C-5), 56.64 (1C, CH₂).

HPLC-MS: [C₁₄H₁₆O₆S + NH₄]⁺ calcd. 314.11, found 314.06.

HRMS: [C₁₄H₁₆O₆S + Na]⁺ calcd. 319.0610, found 319.0610.

4-(Propargyloxy)benzenesulfonyl chloride (**23**)

Propargyl phenyl ether (**22**, 212.5 mg, 1.61 mmol) was dissolved in dichloromethane (8 mL) and cooled to 0 °C. Chlorosulfonic acid (300 μL, 4.51 mmol) was added dropwise. The reaction was stirred for 2 h at 0 °C and then poured over ice. The product was extracted to chloroform. Organic phase was washed with water and half satd. brine, dried over anhydrous Na₂SO₄, filtered and concentrated *in vacuo*. Crude compound **23** (266.6 mg, 1.56 mmol, 72%) was used without further purification. Synthesis of compound **23** was first reported by Inkster *et. al.*¹²⁸

1-deoxy-fucoside precursor **25**

(1-Aminomethyl)-1-deoxy-β-L-fucopyranoside⁹⁹ (**24**, 194.6 mg, 0.91 mmol) was dissolved in dry dimethylformamide (12 mL) and triethyl amine (190 μL, 1.36 mmol) was added. The reaction was cooled to 0 °C in an ice bath and compound **23** (266.6 mg, 1.56 mmol) in dry dimethylformamide (10 mL) was added slowly. Mixture was allowed to warm to room temperature and stirred for 3 h. The reaction was concentrated *in vacuo*, diluted with ethyl acetate and satd. ammonium chloride solution. Phases were separated, aqueous phase was re-extracted with ethyl acetate. Combined organic phases were washed with half satd. brine, dried over anhydrous Na₂SO₄, filtered and concentrated *in vacuo*. Purification by reverse phase MPLC (water/acetonitrile supplemented with 1% formic acid, 10–20% acetonitrile) gave compound **25** (137.7 mg, 0.37 mmol, 34%).

¹H NMR (500 MHz, MeOH-d₄) δ 7.85 – 7.78 (m, 2H, ArH), 7.17 – 7.10 (m, 2H, ArH), 4.84 (d, *J* = 2.4 Hz, 2H, CH₂C≡CH), 3.61 – 3.57 (m, 1H, H-4), 3.47 – 3.42 (m, 1H, H-5), 3.41 – 3.34 (m, 2H, H-1, H-3), 3.32 – 3.26 (m, 1H, CH_{2,a}NH), 3.11 (td, *J* = 9.0, 8.4, 2.5 Hz, 1H, H-2), 3.02

(t, $J = 2.4$ Hz, 1H, C \equiv CH), 2.98 (dd, $J = 13.0, 7.3$ Hz, 1H, CH_{2,b}NH), 1.18 (d, $J = 6.5$ Hz, 3H, CH₃).

¹³C NMR (126 MHz, MeOH-d₄) δ 162.17 (1C, ArC), 134.28 (1C, ArC), 130.10 (2C, ArCH), 116.18 (2C, ArCH), 79.52 (1C, C-2), 79.01 (1C, C \equiv CH), 77.51 (1C, C \equiv CH), 76.31 (1C, C-5), 75.51 (1C, C-3), 73.56 (1C, C-4), 69.75 (1C, C-1), 56.88 (1C, CH₂C \equiv CH), 45.55 (1C, CH₂NH), 17.06 (1C, CH₃).

HPLC-MS: [C₁₆H₂₁NO₇S + H]⁺ calcd. 372.11, found 372.11.

HRMS: [C₁₆H₂₁NO₇S + H]⁺ calcd. 372.1111, found 372.1111.

1-deoxy-fucoside **26**

(1-Aminomethyl)-1-deoxy- β -L-fucopyranoside⁹⁹ (**24**, 350.5 mg, 1.98 mmol) was dissolved in dry dimethylformamide (20 mL) and triethyl amine (350 μ L, 2.51 mmol) was added. The reaction was cooled to 0 °C in an ice bath and 5-bromothiophene-2-sulfonyl chloride (481.2, 1.84 mmol) in dry dimethylformamide (15 mL) was added slowly. Mixture was allowed to warm to room temperature and stirred for 2 h. The reaction was concentrated *in vacuo*, diluted with ethyl acetate and satd. ammonium chloride solution. Phases were separated, aqueous phase was re-extracted with ethyl acetate. Combined organic phases were washed with half satd. brine, dried over anhydrous Na₂SO₄, filtered and concentrated *in vacuo*. Purification by normal phase MPLC (dichloromethane/methanol, 1–20% methanol) gave compound **26** (635 mg, 1.58 mmol, 80%). The analytical data match the literature.⁴⁶

¹H NMR (500 MHz, MeOH-d₄) δ 7.40 (d, $J = 4.0$ Hz, 1H, ArH), 7.19 (d, $J = 4.0$ Hz, 1H, ArH), 3.61 (d, $J = 1.6$ Hz, 1H, H-4), 3.54 – 3.48 (m, 1H, H-5), 3.41 – 3.37 (m, 3H, H-1, H-3, CH_{2,a}), 3.22 – 3.15 (m, 1H, H-2), 3.08 (dd, $J = 12.9, 7.2$ Hz, 1H, CH_{2,b}), 1.20 (d, $J = 6.5$ Hz, 3H, CH₃).

¹³C NMR (126 MHz, MeOH-d₄) δ 144.15 (1C, ArC), 133.19 (1C, ArCH), 131.91 (1C, ArCH), 119.81 (1C, ArC), 79.48 (1C, C-2), 76.31 (1C, C-3), 75.54 (1C, C-5), 73.56 (1C, C-4), 69.67 (1C, C-1), 45.73 (1C, CH₂), 17.06 (1C, CH₃).

HPLC-MS: [C₁₁H₁₆BrNO₆S₂ + H]⁺ calcd. 401.97, found 401.95.

1-deoxy-fucoside precursor **27**

Compound **26** (112.7 mg, 0.28 mmol) was dissolved in dry degassed dimethylformamide (3 mL). CuI (5.1 mg, 0.03 mmol), PdCl₂(PPh₃)₂ (8.9 mg, 0.01 mmol), triethyl amine (100 μ L, 0.72 mmol) and trimethylsilyl acetylene (350 μ L, 2.53 mmol) were added at r.t.. The reaction was stirred at 30 °C for 5 h, then cooled down to r.t. and diluted with ethyl acetate. Organic phase was washed with satd. ammonium chloride solution and brine, dried over anhydrous

Na₂SO₄, filtered and concentrated *in vacuo*. Silyl protected intermediate was purified by normal phase MPLC (dichloromethane/ethanol, 1–15% ethanol), then dissolved in methanol (10 mL) and powder potassium carbonate (79.4 mg, 57 mmol) was added. After 1 h, the reaction was acidified with 1M HCl solution and concentrated *in vacuo*. The reaction mixture was diluted with ethyl acetate and satd. ammonium chloride solution. Phases were separated, the organic phase was washed with satd. ammonium chloride solution and brine, dried over anhydrous Na₂SO₄, filtered and concentrated *in vacuo*. Purification by reverse phase MPLC (water/acetonitrile with 1% formic acid, 10–20% acetonitrile) gave compound **27** (48.5 mg, 0.14 mmol, 50% over two steps).

¹H NMR (500 MHz, DMSO-d₆) δ 7.96 (s, 1H, NH), 7.49 (d, *J* = 3.9 Hz, 1H, ArH), 7.40 (d, *J* = 3.9 Hz, 1H, ArH), 4.83 (s, 2H, C≡CH, OH-2), 4.62 (s, 1H, OH-3), 4.28 (d, *J* = 3.1 Hz, 1H, OH-4), 3.42 – 3.38 (m, 2H, H-4, H-5), 3.29 (dd, *J* = 13.1, 2.0 Hz, 1H, CH_{2,a}), 3.22 (dd, *J* = 9.1, 2.8 Hz, 1H, H-3), 3.15 (t, *J* = 9.2 Hz, 1H, H-1), 3.03 (td, *J* = 8.9, 2.1 Hz, 1H, H-2), 2.81 (dd, *J* = 13.1, 8.4 Hz, 1H, CH_{2,b}), 1.06 (d, *J* = 6.4 Hz, 3H, CH₃).

¹³C NMR (126 MHz, DMSO-d₆) δ 142.73 (1C, ArC), 133.48 (1C, ArCH), 131.17 (1C, ArCH), 126.30 (1C, ArC), 87.95 (1C, C≡CH), 78.26 (1C, C-2), 75.40 (1C, C≡CH), 74.65 (1C, C-3), 73.69 (1C, C-5), 71.60 (1C, C-4), 68.26 (1C, C-1), 44.80 (1C, CH₂), 16.93 (1C, CH₃).

HPLC-MS: [C₁₃H₁₇NO₆S₂ + H]⁺ calcd. 348.06, found 348.06.

HRMS: [C₁₃H₁₇NO₆S₂ + Na]⁺ calcd. 370.0389, found 370.0387.

5-(3-(2-(2-(2-(2-azidoethoxy)ethoxy)ethoxy)ethyl)thioureido)-2-(6-hydroxy-3-oxo-3H-xanthen-9-yl)benzoic acid (29)

Fluorescein 5-isothiocyanate (**28**, 109.1 mg, 0.25 mmol) was dissolved in dimethylformamide (1 mL) and triethylamine (100 μL, 0.72 mmol) was added. The reaction mixture was cooled to 0 °C and a solution of 11-azido-3,6,9-trioxaundecan-1-amine (68 μL, 0.34 mmol) in dimethylformamide (0.5 mL) was added. The mixture was allowed to warm to r.t. and stirred for 1 h. The reaction mixture was dried *in vacuo*. Purification by normal phase MPLC (dichloromethane/methanol with 1% formic acid, 1–20% methanol) gave the azide modified fluorescein **29** (97.9 mg, 0.16 mmol, 59%). Synthesis of **29** was first described by Loison *et al.*¹²⁹

¹H NMR (500 MHz, MeOH-d₄) δ 8.18 (d, *J* = 1.7 Hz, 1H, ArH), 7.80 (d, *J* = 7.9 Hz, 1H, ArH), 7.17 (d, *J* = 8.2 Hz, 1H, ArH), 6.73 – 6.68 (m, 4H, ArH), 6.57 (dd, *J* = 8.7, 2.4 Hz, 2H, ArH), 3.82 (s, 2H, NHCSNHCH₂), 3.71 (t, *J* = 5.1 Hz, 2H, NHCSNHCH₂CH₂), 3.68 (s, 4H, CH₂), 3.66 – 3.59 (m, 6H, CH₂), 3.36 – 3.32 (m, 2H, CH₂N₃).

^{13}C NMR (126 MHz, MeOH- d_4) δ 182.90 (1C, C=S), 171.01 (1C, C=O), 161.74 (2C, ArCOH), 154.39 (2C, ArC), 142.53 (1C, ArCNH), 131.61 (1C, ArCH), 130.46 (2C, ArCH), 129.06 (1C, ArC), 125.88 (1C, ArCH), 119.90 (1C, ArCH), 113.85 (2C, ArCH), 111.71 (2C, ArC), 103.51 (2C, ArCH), 71.65 (1C, CH₂), 71.56 (1C, CH₂), 71.49 (1C, CH₂), 71.33 (1C, CH₂), 71.09 (1C, CH₂), 70.20 (1C, CH₂), 51.73 (1C, CH₂N₃), 45.51 (1C, NHCSNHCH₂).

HPLC-MS: [C₂₉H₂₉N₅O₈S + H]⁺ calcd. 608.18, found. 608.21.

HRMS: [C₂₉H₂₉N₅O₈S + H]⁺ calcd. 608.1810, found 608.1803.

Imaging probe **30m**

Azide modified fluorescein (**29**, 21.0 mg, 34.7 μmol) and propargylated galactoside **8m** (16.3 mg, 50.1 μmol) were dissolved in dimethylformamide (2 mL). CuSO₄ solution (315 μL , 100 mM in water, 32 μmol) and sodium ascorbate solution (630 μL , 100 mM in water, 63 μmol) were added. The reaction was stirred at r.t. overnight. After lyophilization, product was purified by preparative HPLC (water/acetonitrile with 0.1% formic acid, 20–35% acetonitrile). Compound **30m** was obtained as yellow solid (15.8 mg, 16.9 μmol , 49%).

^1H NMR (500 MHz, DMSO- d_6) δ 10.11 (s, 2H, OH-fluorescein), 8.28 (s, 1H, ArH-fluorescein), 8.17 (s, 1H, NH-thiourea), 7.91 (s, 1H, CH-triazole), 7.74 (d, $J = 7.6$ Hz, 1H, ArH-fluorescein), 7.17 (d, $J = 8.3$ Hz, 1H, ArH-fluorescein), 6.97 (t, $J = 7.9$ Hz, 1H, ArH), 6.74 (s, 1H, ArH), 6.67 (d, $J = 2.2$ Hz, 2H, ArH-fluorescein), 6.63 – 6.58 (m, 3H, ArH, ArH-fluorescein), 6.57 (d, $J = 2.2$ Hz, 1H, ArH-fluorescein), 6.55 (d, $J = 2.3$ Hz, 1H, ArH-fluorescein), 6.48 (dd, $J = 8.1$, 1.7 Hz, 1H, ArH), 6.08 (t, $J = 5.8$ Hz, 1H, NH), 5.08 (s, 1H, OH-2), 4.86 (s, 1H, OH-3), 4.62 (s, 1H, OH-6), 4.53 – 4.44 (m, 4H, H-1, CH₂, OH-4), 4.27 (d, $J = 5.8$ Hz, 2H, NHCH₂), 3.78 (t, $J = 5.2$ Hz, 2H, CH₂), 3.71 (s, 1H, H-4), 3.67 (s, 2H, CH₂), 3.58 (t, $J = 5.4$ Hz, 2H, CH₂), 3.56 – 3.38 (m, 13H, H-2, H-3, H-5, H-6, CH₂).

^{13}C NMR (126 MHz, DMSO- d_6) δ 180.56 (1C, C=S), 168.57 (1C, C=O), 159.68 (2C, ArC-fluorescein), 151.95 (2C, ArC-fluorescein), 148.69 (1C, ArC), 146.92 (2C, ArC-fluorescein), 145.44 (1C, C=CH-triazole), 141.36 (1C, ArC-fluorescein), 136.03 (1C, ArC), 129.35 (4C, ArCH-fluorescein), 129.09 (1C, ArCH), 126.74 (1C, ArCH-fluorescein), 124.14 (1C, ArCH-fluorescein), 123.11 (1C, C=CH-triazole), 116.74 (1C, ArCH), 116.47 (1C, ArCH-fluorescein), 112.72 (1C, ArCH-fluorescein), 112.49 (1C, ArCH), 110.60 (1C, ArCH), 109.80 (2C, ArC-fluorescein), 102.26 (2C, ArCH-fluorescein), 88.01 (1C, C-1), 79.03 (1C, C-5), 74.78 (1C, C-3), 69.75 (1C, CH₂), 69.65 (2C, CH₂), 69.58 (1C, CH₂), 69.28 (1C, CH₂), 68.81 (1C, C-2), 68.42 (1C, CH₂), 68.33 (1C, C-4), 60.54 (1C, C-6), 49.33 (1C, CH₂), 43.70 (1C, CH₂), 38.40 (1C, NHCH₂).

HPLC-MS: [C₄₄H₄₈N₆O₁₃S₂ + H]⁺ calcd. 933.28, found. 933.35.

HRMS: [C₄₄H₄₈N₆O₁₃S₂ + H]⁺ calcd. 933.2794, found 933.2769.

Imaging probe 30p

Azide modified fluorescein (**29**, 22.9 mg, 37.9 μmol) and propargylated galactoside **8p** (19.0 mg, 58.4 μmol) were dissolved in dimethylformamide (2.1 mL). CuSO₄ solution (330 μL, 100 mM in water, 33 μmol) and sodium ascorbate solution (660 μL, 100 mM in water, 66 μmol) were added. The reaction was stirred at r.t. overnight. After lyophilization, product was purified by preparative HPLC (water/acetonitrile with 0.1% formic acid, 20–35% acetonitrile). Compound **30p** was obtained as yellow solid (21 mg, 22.5 μmol, 60%).

¹H NMR (500 MHz, DMSO-d₆) δ 10.09 (s, 2H, OH-fluorescein), 8.26 (s, 1H, ArH-fluorescein), 8.15 (s, 1H, NH-thiourea), 7.92 (s, 1H, CH-triazole), 7.73 (d, *J* = 7.2 Hz, 1H, ArH-fluorescein), 7.23 (d, *J* = 8.6 Hz, 2H, ArH), 7.16 (d, *J* = 8.3 Hz, 1H, ArH-fluorescein), 6.68 – 6.52 (m, 8H, ArH, ArH-fluorescein), 6.23 (t, *J* = 5.7 Hz, 1H, NH), 4.93 (s, 1H, OH-2), 4.78 (s, 1H, OH-3), 4.57 (s, 1H, OH-6), 4.47 (t, *J* = 5.1 Hz, 2H, CH₂), 4.38 – 4.31 (m, 1H, OH-4), 4.27 (d, *J* = 5.7 Hz, 2H, NHCH₂), 4.20 (d, *J* = 8.9 Hz, 1H, H-1), 3.77 (t, *J* = 5.2 Hz, 2H, CH₂), 3.73 – 3.61 (m, 3H, H-4, CH₂), 3.58 (t, *J* = 5.3 Hz, 2H, CH₂), 3.56 – 3.52 (m, 2H, CH₂), 3.52 – 3.41 (m, 8H, H-6, CH₂), 3.32 – 3.24 (m, 3H, H-2, H-3, H-5).

¹³C NMR (126 MHz, DMSO-d₆) δ 180.56 (1C, C=S), 168.59 (1C, C=O), 160.05 (2C, ArC-fluorescein), 152.18 (2C, ArC-fluorescein), 148.15 (1C, ArC), 145.39 (1C, C=CH-triazole), 141.29 (1C, ArC-fluorescein), 134.18 (2C, ArCH) 129.17 (4C, ArC-fluorescein), 124.38 (1C, ArCH-fluorescein), 123.17 (1C, C=CH-triazole), 118.31 (1C, ArC), 116.88 (1C, ArC-fluorescein), 113.09 (1C, ArC-fluorescein), 112.58 (2C, ArCH), 109.97 (2C, ArC-fluorescein), 102.29 (2C, ArCH-fluorescein), 89.71 (1C, C-1), 79.01 (1C, C-5), 74.75 (1C, C-3), 69.76 (1C, CH₂), 69.66 (2C, CH₂), 69.58 (1C, CH₂), 69.28 (1C, CH₂), 68.80 (1C, C-2), 68.42 (1C, CH₂), 68.29 (1C, C-4), 60.51 (1C, C-6), 49.34 (1C, CH₂), 43.71 (1C, CH₂), 38.42 (1C, NHCH₂).

HPLC-MS: [C₄₄H₄₈N₆O₁₃S₂ + H]⁺ calcd. 933.28, found. 933.34.

HRMS: [C₄₄H₄₈N₆O₁₃S₂ + H]⁺ calcd. 933.2794, found 933.2777.

Imaging probe 31

Azide modified fluorescein (**29**, 15.4 mg, 25.3 μmol) and propargylated galactoside **14** (11.0 mg, 33.7 μmol) were dissolved in dimethylformamide (1.5 mL). CuSO₄ solution (125 μL, 100 mM in water, 12.5 μmol) and sodium ascorbate solution (125 μL, 100 mM in water, 12.5 μmol) were added. The reaction was stirred at r.t. overnight. After lyophilization, product was purified

by preparative HPLC (water/acetonitrile with 0.1% formic acid, 20–40% acetonitrile). Compound **31** was obtained as yellow solid (15.9 mg, 17.0 μmol , 67%).

^1H NMR (500 MHz, MeOH-d_4) δ 8.13 (s, 1H, ArH-fluorescein), 8.10 (s, 1H, CH-triazole), 7.77 (d, $J = 7.3$ Hz, 1H, ArH-fluorescein), 7.57 – 7.49 (m, 2H, ArH), 7.16 (d, $J = 8.2$ Hz, 1H, ArH-fluorescein), 6.99 – 6.93 (m, 2H, ArH), 6.75 (d, $J = 8.7$ Hz, 2H, ArH-fluorescein), 6.69 (d, $J = 2.3$ Hz, 2H, ArH-fluorescein), 6.58 (d, $J = 2.3$ Hz, 1H, ArH-fluorescein), 6.56 (d, $J = 2.4$ Hz, 1H, ArH-fluorescein), 6.57 (dd, $J = 8.8, 2.4$ Hz, 2H, ArH-fluorescein), 5.15 (s, 2H, CH_2), 4.57 (t, $J = 4.9$ Hz, 2H, CH_2), 4.44 (d, $J = 9.5$ Hz, 1H, H-1), 3.91 – 3.85 (m, 3H, H-4, CH_2), 3.81 (s, 2H, CH_2), 3.79 – 3.70 (m, 2H, H-6), 3.70 – 3.66 (m, 2H, CH_2), 3.65 – 3.48 (m, 11H, H-2, H-3, H-5, CH_2).

^{13}C NMR (126 MHz, MeOH-d_4) δ 182.73 (1C, C=S), 171.37 (1C, C=O), 159.60 (1C, ArC), 154.76 (2C, ArC-fluorescein), 144.62 (1C, $\text{C}=\text{CH}$ -triazole), 135.59 (2C, ArCH), 130.66 (4C, ArCH-fluorescein), 126.36 (1C, $\text{C}=\underline{\text{C}}\text{H}$ -triazole), 126.24 (1C, ArC), 120.33 (1C, ArCH-fluorescein), 116.35 (2C, ArCH), 114.58 (1C, ArCH-fluorescein), 112.05 (1C, ArC-fluorescein), 103.58 (2C, ArCH-fluorescein), 90.99 (1C, C-1), 80.53 (1C, C-5), 76.31 (1C, C-3), 71.55 (1C, CH_2), 71.42 (1C, CH_2), 71.40 (1C, CH_2), 71.32 (1C, CH_2), 70.96 (1C, C-2), 70.43 (1C, C-4), 70.26 (2C, CH_2), 62.61 (1C, C-6), 62.42 (1C, CH_2), 51.47 (1C, CH_2), 45.48 (1C, CH_2).

HPLC-MS: $[\text{C}_{44}\text{H}_{47}\text{N}_5\text{O}_{14}\text{S}_2 + \text{H}]^+$ calcd. 934.26, found. 934.34.

HRMS: $[\text{C}_{44}\text{H}_{47}\text{N}_5\text{O}_{14}\text{S}_2 + \text{H}]^+$ calcd. 934.2634, found 934.2622.

Imaging probe **32**

Azide modified fluorescein (**29**, 20.02 mg, 32.9 μmol) and propargylated xyloside **19** (15.7 mg, 53.2 μmol) were dissolved in dimethylformamide (2 mL). CuSO_4 solution (330 μL , 100 mM in water, 33 μmol) and sodium ascorbate solution (660 μL , 100 mM in water, 66 μmol) were added. The reaction was stirred at r.t. for 2h. After lyophilization, product was purified by preparative HPLC (water/acetonitrile with 0.1% formic acid, 20–35% acetonitrile). Compound **32** was obtained as yellow solid (11.9 mg, 17.0 μmol , 40%).

^1H NMR (500 MHz, DMSO-d_6) δ 10.16 (s, 2H, OH-fluorescein), 8.27 (s, 1H, ArH-fluorescein), 8.21 (s, 1H, NH-thiourea), 7.93 (s, 1H, CH-triazole), 7.74 (d, $J = 7.1$ Hz, 1H, ArH-fluorescein), 7.20 (d, $J = 8.5$ Hz, 2H, ArH), 7.16 (d, $J = 8.3$ Hz, 1H, ArH-fluorescein), 6.66 (s, 2H, ArH-fluorescein), 6.63 – 6.52 (m, 7H, ArH, ArH-fluorescein), 6.30 (t, $J = 5.7$ Hz, 1H, NH), 5.11 (s, 1H, OH-2), 5.05 (s, 1H, OH-3), 4.95 (s, 1H, OH-4), 4.47 (t, $J = 5.1$ Hz, 2H, CH_2), 4.27 (d, $J = 5.7$ Hz, 2H, NHCH_2), 4.20 (d, $J = 9.2$ Hz, 1H, H-1), 3.78 (t, $J = 5.1$ Hz, 2H, CH_2), 3.74 – 3.62

(m, 3H, H-5eq., CH₂), 3.58 (t, *J* = 5.2 Hz, 2H, CH₂), 3.56 – 3.52 (m, 2H, CH₂), 3.52 – 3.44 (m, 8H, CH₂), 3.23 – 3.14 (m, 2H, H-4), 3.11 (t, *J* = 8.4 Hz, 1H, H-3), 2.99 (t, *J* = 10.6 Hz, 1H, H-5ax.), 2.95 – 2.88 (m, 1H, H-2).

¹³C NMR (126 MHz, DMSO-d₆) δ 180.58 (1C, C=S), 168.60 (1C, C=O), 160.05 (2C, ArC-fluorescein), 152.08 (2C, ArC-fluorescein), 148.54 (1C, ArC), 145.32 (1C, C=CH-triazole), 141.36 (1C, ArC-fluorescein), 135.37 (2C, ArCH), 129.14 (4C, ArCH-fluorescein), 127.10 (1C, ArC-fluorescein), 124.27 (1C, ArCH-fluorescein), 123.18 (1C, C=CH-triazole), 116.58 (1C, ArC), 112.94 (1C, ArCH-fluorescein), 112.54 (2C, ArCH), 109.90 (2C, ArC-fluorescein), 102.28 (2C, ArCH-fluorescein), 89.17 (1C, C-1), 77.84 (1C, C-3), 72.03 (1C, C-2), 69.76 (1C, CH₂), 69.66 (2C, CH₂), 69.59 (1C, CH₂), 69.40 (1C, C-4), 69.25 (1C, C-5), 68.80 (1C, CH₂), 68.42 (1C, CH₂), 49.36 (1C, CH₂), 43.70 (1C, CH₂), 38.35 (1C, NHCH₂).

HPLC-MS: [C₄₃H₄₆N₆O₁₂S₂ + H]⁺ calcd. 903.27, found. 903.33.

HRMS: [C₄₃H₄₆N₆O₁₂S₂ + 2H]²⁺ calcd. 452.1381, found 452.1375.

Imaging probe 33

Azide modified fluorescein (**29**, 15.7 mg, 25.8 μmol) and propargylated xyloside **21** (10.1 mg, 34.1 μmol) were dissolved in dimethylformamide (1.5 mL). CuSO₄ solution (125 μL, 100 mM in water, 12.5 μmol) and sodium ascorbate solution (125 μL, 100 mM in water, 12.5 μmol) were added. The reaction was stirred at r.t. for 2 days. After lyophilization, product was purified by preparative HPLC (water/acetonitrile with 0.1% formic acid, 20–40% acetonitrile). Compound **33** was obtained as yellow solid (15.7 mg, 16.8 μmol, 65%).

¹H NMR (500 MHz, MeOH-d₄) δ 8.12 (s, 1H, ArH-fluorescein), 8.08 (s, 1H, CH-triazole), 7.74 (d, *J* = 6.5 Hz, 1H, ArH-fluorescein), 7.47 (d, *J* = 8.7 Hz, 2H, ArH), 7.14 (d, *J* = 8.2 Hz, 1H, ArH-fluorescein), 6.95 (d, *J* = 8.7 Hz, 2H, ArH), 6.73 – 6.64 (m, 4H, ArH-fluorescein), 6.55 (d, *J* = 2.1 Hz, 1H, ArH-fluorescein), 6.53 (d, *J* = 2.2 Hz, 1H, ArH-fluorescein), 5.14 (s, 2H, CH₂), 4.55 (t, *J* = 4.7 Hz, 2H, CH₂), 4.37 (d, *J* = 9.4 Hz, 1H, H-1), 3.93 – 3.73 (m, 5H, H-5eq, CH₂), 3.70 – 3.52 (m, 10H, CH₂), 4.37 (d, *J* = 9.4 Hz, 1H, H-4), 3.36 – 3.31 (m, 1H, H-3), 3.20 – 3.09 (m, 2H, H-2, H-5ax.).

¹³C NMR (126 MHz, MeOH-d₄) δ 182.77 (1C, C=S), 171.28 (1C, C=O), 159.96 (1C, ArC), 154.52 (2C, ArC-fluorescein), 144.58 (1C, C=CH-triazole), 142.29 (1C, ArC-fluorescein), 136.60 (2C, ArCH), 130.54 (4C, ArCH-fluorescein), 126.24 (1C, C=CH-triazole), 126.15 (1C, ArCH-fluorescein), 125.01 (1C, ArC), 120.14 (1C, ArCH-fluorescein), 116.34 (2C, ArCH), 114.20 (1C, ArCH-fluorescein), 111.84 (1C, ArC-fluorescein), 103.56 (2C, ArCH-fluorescein), 90.53 (1C, C-1), 79.30 (1C, C-3), 73.52 (1C, C-2), 71.55 (1C, CH₂), 71.42 (2C, CH₂), 71.32

(1C, CH₂), 70.92 (1C, C-4), 70.56 (1C, C-), 70.27 (1C, CH₂), 62.42 (1C, CH₂), 51.48 (1C, CH₂), 45.49 (1C, CH₂).

HPLC-MS: [C₄₃H₄₄N₅O₁₃S₂ + H]⁺ calcd. 904.25, found. 904.33.

HRMS: [C₄₃H₄₄N₅O₁₃S₂ + H]⁺ calcd. 904.2529, found 904.2519.

Imaging probe 34

Azide modified fluorescein (**29**, 16.3 mg, 26.8 μmol) and propargylated 1-deoxy fucoside **25** (13.1 mg, 35.3 μmol) were dissolved in dimethylformamide (2 mL). CuSO₄ solution (45 μL, 100 mM in water, 4.5 μmol) and sodium ascorbate solution (95 μL, 100 mM in water, 9.5 μmol) were added. The reaction was stirred at r.t. overnight. After lyophilization, product was purified by preparative HPLC (water/acetonitrile with 0.1% formic acid, 20–40% acetonitrile). Compound **34** was obtained as yellow solid (18.1 mg, 18.5 μmol, 69%).

¹H NMR (500 MHz, DMSO-d₆) δ 10.06 (s, 2H, OH-fluorescein), 8.26 (s, 1H, ArH-fluorescein), 8.22 (s, 1H, CH-triazole), 8.12 (s, 1H, NH-thiourea), 7.73 (d, *J* = 8.9 Hz, 3H, ArH, ArH-fluorescein), 7.37 (s, 1H, NH-thiourea), 7.20 (d, *J* = 8.9 Hz, 2H, ArH), 7.17 (d, *J* = 8.3 Hz, 1H, ArH-fluorescein), 6.67 (d, *J* = 2.2 Hz, 2H, ArH-fluorescein), 6.62 – 6.54 (m, 4H, ArH-fluorescein), 5.23 (s, 2H, PhOCH₂), 4.77 (s, 1H, OH-2), 4.59 (s, 1H, OH-3), 4.53 (t, *J* = 5.2 Hz, 2H, CH₂), 4.27 (d, *J* = 4.9 Hz, 1H, OH-4), 3.82 (t, *J* = 5.2 Hz, 2H, CH₂), 3.67 (s, 2H, CH₂), 3.58 (t, *J* = 5.4 Hz, 2H, CH₂), 3.57 – 3.47 (m, 8H, CH₂), 3.36 (m, 42H, H-4, H-5), 3.23 – 3.08 (m, 3H, H-3, H-1, CH_{2,a}NHSO₂), 2.98 (td, *J* = 8.9, 2.1 Hz, 1H, H-2), 2.69 – 2.62 (m, 1H, CH_{2,b}NHSO₂), 1.06 (d, *J* = 6.4 Hz, 3H, CH₃).

¹³C NMR (126 MHz, DMSO-d₆) δ 180.56 (1C, C=S), 168.57 (1C, C=O), 160.77 (1C, ArC), 159.74 (2C, ArC-fluorescein), 151.98 (2C, ArC-fluorescein), 146.85 (1C, ArC-fluorescein), 141.97 (1C, C=CH-triazole), 141.31 (1C, ArC-fluorescein), 132.79 (1C, ArC), 129.34 (1C, ArCH-fluorescein), 129.10 (4C, ArCH-fluorescein), 128.65 (2C, ArCH), 126.83 (1C, ArC-fluorescein), 125.19 (1C, C=CH-triazole), 124.19 (1C, ArCH-fluorescein), 116.52 (1C, ArCH-fluorescein), 114.89 (2C, ArCH), 112.75 (1C, ArCH-fluorescein), 109.82 (2C, ArC-fluorescein), 102.27 (2C, ArCH-fluorescein), 78.34 (1C, C-2), 74.66 (1C, C-3), 73.63 (1C, C-5), 71.59 (1C, C-4), 69.76 (1C, CH₂), 69.68 (1C, CH₂), 69.65 (3C, CH₂), 69.56 (1C, CH₂), 68.68 (1C, CH₂), 68.42 (1C, CH₂), 68.32 (1C, C-1), 61.44 (1C, PhOCH₂), 49.48 (1C, CH₂), 44.54 (1C, CH₂NHSO₂), 43.71 (1C, CH₂), 16.94 (1C, CH₃).

HPLC-MS: [C₄₅H₅₀N₆O₁₅S₂ + H]⁺ calcd. 979.28, found. 979.36.

HRMS: [C₄₅H₅₀N₆O₁₅S₂ + H]⁺ calcd. 979.2849, found 979.2826.

Imaging probe 35

Azide modified fluorescein (**29**, 21.8 mg, 35.9 μmol) and propargylated 1-deoxy fucoside **27** (15.7 mg, 45.2 μmol) were dissolved in dimethylformamide (2.2 mL). CuSO_4 solution (35 μL , 100 mM in water, 3.5 μmol) and sodium ascorbate solution (85 μL , 100 mM in water, 8.5 μmol) were added. The reaction was stirred at r.t. overnight. After lyophilization, product was purified by preparative HPLC (water/acetonitrile with 0.1% formic acid, 20–40% acetonitrile). Compound **35** was obtained as yellow solid (29.0 mg, 16.8 μmol , 85%).

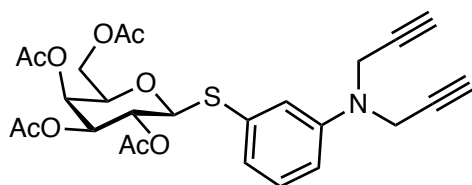
^1H NMR (500 MHz, DMSO-d_6) δ 10.03 (s, 2H, OH-fluorescein), 8.61 (s, 1H, CH-triazole), 8.27 (s, 1H, ArH-fluorescein), 8.09 (s, 1H, NH-thiourea), 7.73 (d, $J = 7.5$ Hz, 1H, ArH-fluorescein), 7.56 (d, $J = 3.9$ Hz, 1H, ArH), 7.46 (d, $J = 3.8$ Hz, 1H, ArH), 7.17 (d, $J = 8.3$ Hz, 1H, ArH-fluorescein), 6.67 (d, $J = 2.2$ Hz, 2H, ArH-fluorescein), 6.63 – 6.53 (m, 4H, ArH-fluorescein), 4.83 (s, 1H, OH-2), 4.61 (s, 1H, OH-3), 4.58 (t, $J = 5.1$ Hz, 2H, CH_2), 4.28 (d, $J = 5.2$ Hz, 1H, OH-4), 3.85 (t, $J = 5.1$ Hz, 2H, CH_2), 3.67 (s, 2H, CH_2), 3.58 (t, $J = 5.4$ Hz, 2H, CH_2), 3.56 – 3.48 (m, 8H, CH_2), 3.42 – 3.38 (m, 2H, H-4, H-5), 3.31 – 3.28 (m, 1H, $\text{CH}_{2,\text{a}}\text{NHSO}_2$), 3.89 – 3.80 (m, 1H, H-3), 3.16 (t, $J = 9.2$ Hz, 1H, H-1), 3.06 (td, $J = 8.9, 2.0$ Hz, 1H, H-2), 2.82 (dd, $J = 13.0, 8.4$ Hz, 1H, $\text{CH}_{2,\text{b}}\text{NHSO}_2$), 1.07 (d, $J = 6.4$ Hz, 3H, CH_3).

^{13}C NMR (126 MHz, DMSO-d_6) δ 180.55 (1C, C=S), 168.55 (1C, C=O), 159.66 (2C, ArC-fluorescein), 151.94 (2C, ArC-fluorescein), 146.95 (1C, ArC-fluorescein), 141.32 (1C, ArC-fluorescein), 140.31 (1C, ArC), 139.78 (1C, C=CH-triazole), 138.55 (1C, ArC), 132.08 (1C, ArCH), 129.37 (1C, ArCH-fluorescein), 129.08 (4C, ArCH-fluorescein), 126.73 (1C, ArC-fluorescein), 124.15 (1C, ArCH-fluorescein), 123.80 (1C, ArCH), 122.44 (1C, C=CH-triazole), 116.49 (1C, ArCH-fluorescein), 112.70 (1C, ArCH-fluorescein), 109.79 (2C, ArC-fluorescein), 102.26 (2C, ArCH-fluorescein), 78.31 (1C, C-2), 74.66 (1C, C-3), 73.67 (1C, C-5), 71.60 (1C, C-4), 69.74 (1C, CH_2), 69.62 (3C, CH_2), 68.52 (1C, CH_2), 68.42 (1C, CH_2), 68.30 (1C, C-1), 49.87 (1C, CH_2), 44.81 (1C, CH_2NHSO_2), 43.69 (1C, CH_2), 16.94 (1C, CH_3).

HPLC-MS: $[\text{C}_{42}\text{H}_{46}\text{N}_6\text{O}_{14}\text{S}_3 + \text{H}]^+$ calcd. 955.23, found. 955.30.

HRMS: $[\text{C}_{42}\text{H}_{46}\text{N}_6\text{O}_{14}\text{S}_3 + \text{H}]^+$ calcd. 955.2307, found 955.2295.

Galactoside side product 39m



Compound **39m** (19.2 mg, 36.1 μmol , 5%) was isolated as side product during the synthesis of compound **6m**.

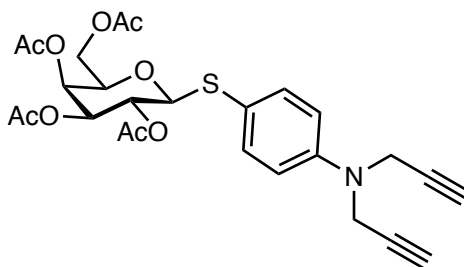
^1H NMR (300 MHz, DMSO- d_6) δ 7.22 (t, J = 8.0 Hz, 1H, ArH), 6.94 (t, J = 2.0 Hz, 1H, ArH), 6.91 – 6.82 (m, 2H, ArH), 5.36 – 5.31 (m, 1H, H-4), 5.30 – 5.22 (m, 2H, H-1, H-3), 5.04 (t, J = 9.9 Hz, 1H, H-2), 4.39 – 4.30 (m, 1H, H-5), 4.16 (d, J = 2.4 Hz, 4H, CH_2), 4.07 (d, J = 6.3 Hz, 2H, H-6), 3.19 – 3.15 (m, 2H, $\text{C}\equiv\text{CH}$), 2.12 (s, 3H, CH_3), 2.05 (s, 3H, CH_3), 1.99 (s, 3H, CH_3), 1.92 (s, 3H, CH_3).

^{13}C NMR (75 MHz, DMSO- d_6) δ 169.96 (1C, C=O), 169.87 (1C, C=O), 169.46 (1C, C=O), 169.29 (1C, C=O), 147.61 (1C, ArC), 133.77 (1C, ArC), 129.40 (1C, ArCH), 120.00 (1C, ArCH), 115.99 (1C, ArCH), 113.94 (1C, ArCH), 84.36 (1C, C-1), 79.65, 75.16, 73.43 (1C, C-5), 71.02 (1C, C-3), 67.54 (1C, C-2), 67.00 (1C, C-4), 61.64 (1C, C-6), 20.57 (1C, CH_3), 20.49 (1C, CH_3), 20.40 (1C, CH_3), 20.34 (1C, CH_3).

HPLC-MS: $[\text{C}_{26}\text{H}_{29}\text{NO}_9\text{S} + \text{H}]^+$ calcd. 532.16, found. 532.19.

HRMS: $[\text{C}_{26}\text{H}_{29}\text{NO}_9\text{S} + \text{H}]^+$ calcd. 532.1636, found. 532.1628.

Galactoside side product **39p**



Compound **39p** (16.5 mg, 31.0 μmol , 13%) was isolated as side product during the synthesis of compound **6p**.

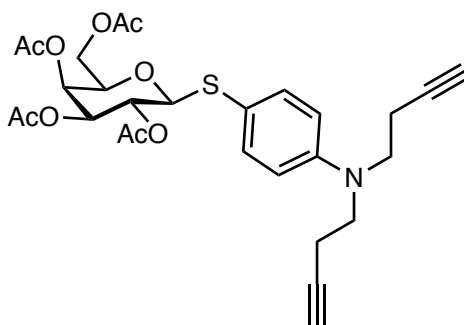
^1H NMR (300 MHz, DMSO- d_6) δ 7.39 – 7.31 (m, 2H ArH), 6.93 – 6.86 (m, 2H, ArH), 5.27 (d, J = 3.4 Hz, 1H, H-4), 5.18 (tt, J = 7.8, 3.4 Hz, 1H, H-3), 5.03 – 4.90 (m, 2H, H-1, H-2), 4.28 – 4.13 (m, 5H, H-5, CH_2), 4.13 – 3.95 (m, 2H, H-6), 3.18 – 3.14 (m, 2H, $\text{C}\equiv\text{CH}$), 2.09 (s, 3H, CH_3), 2.07 (s, 3H, CH_3), 2.01 (s, 3H, CH_3), 1.91 (s, 3H, CH_3).

^{13}C NMR (75 MHz, DMSO- d_6) δ 169.94 (1C, C=O), 169.88 (1C, C=O), 169.44 (1C, C=O), 169.23 (1C, C=O), 147.19 (1C, ArC), 133.97 (2C, ArCH), 119.44 (1C, ArC), 114.85 (2C, ArCH), 85.37 (1C, C-1), 79.72 (2C, $\text{C}\equiv\text{CH}$), 75.03 (2C, $\text{C}\equiv\text{CH}$), 73.31 (1C, C-5), 71.13 (1C, C-3), 67.58 (1C, C-2), 67.22 (1C, C-4), 61.70 (1C, C-6), 20.60 (2C, CH_3), 20.44 (1C, CH_3), 20.35 (1C, CH_3).

HPLC-MS: $[\text{C}_{26}\text{H}_{29}\text{NO}_9\text{S} + \text{H}]^+$ calcd. 532.16, found. 532.17.

HRMS: $[\text{C}_{26}\text{H}_{29}\text{NO}_9\text{S} + \text{H}]^+$ calcd. 532.1636, found. 532.1632.

Galactoside side product 40p



Compound **40p** (23.3 mg, 41.6 μmol , 6%) was isolated as side product during the synthesis of compound **7p**.

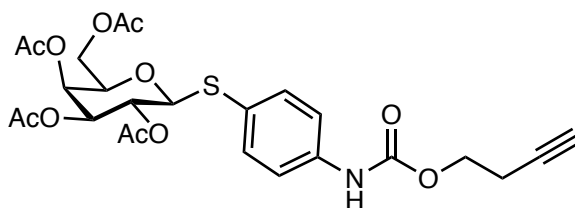
^1H NMR (300 MHz, DMSO-d_6) δ 7.35 – 7.25 (m, 2H ArH), 6.71 – 6.60 (m, 2H, ArH), 5.26 (dd, $J = 3.4, 1.0$ Hz, 1H, H-4), 5.19 (dd, $J = 9.7, 3.5$ Hz, 1H, H-3), 4.96 (t, $J = 9.8$ Hz, 1H, H-2), 4.84 (d, $J = 10.0$ Hz, 1H, H-1), 4.23 – 4.14 (m, 1H, H-5), 4.12 – 3.95 (m, 2H, H-6), 3.54 (t, $J = 7.1$ Hz, 4H, NHCH_2CH_2), 2.87 (t, $J = 2.6$ Hz, 2H, $\text{C}\equiv\text{CH}$), 2.40 (td, $J = 7.1, 2.6$ Hz, 4H, NHCH_2CH_2), 2.08 (s, 3H, CH_3), 2.07 (s, 3H, CH_3), 2.00 (s, 3H, CH_3), 1.91 (s, 3H, CH_3).

^{13}C NMR (126 MHz, DMSO-d_6) δ 169.96 (1C, $\text{C}=\text{O}$), 169.89 (1C, $\text{C}=\text{O}$), 169.51 (1C, $\text{C}=\text{O}$), 169.26 (1C, $\text{C}=\text{O}$), 146.80 (1C, ArC), 135.32 (2C, ArCH), 116.19 (1C, ArC), 111.85 (2C, ArCH), 85.91 (1C, C-1), 82.35 (2C, $\text{C}\equiv\text{CH}$), 73.23 (1C, C-5), 72.61 (2C, $\text{C}\equiv\text{CH}$), 71.15 (1C, C-3), 67.57 (1C, C-2), 67.26 (1C, C-4), 61.64 (1C, C-6), 49.23 (2C, NHCH_2CH_2), 20.67 (1C, CH_3), 20.54 (1C, CH_3), 20.42 (1C, CH_3), 20.40 (1C, CH_3), 16.50 (2C, NHCH_2CH_2).

HPLC-MS: $[\text{C}_{28}\text{H}_{33}\text{NO}_9\text{S} + \text{H}]^+$ calcd. 560.19, found. 560.24.

HRMS: $[\text{C}_{28}\text{H}_{33}\text{NO}_9\text{S} + \text{H}]^+$ calcd. 560.1949, found. 560.1945.

Galactoside side product 41p



Compound **41p** (15.3 mg, 27.7 μmol , 4%) was isolated as side product during the synthesis of compound **7p**.

^1H NMR (300 MHz, DMSO-d_6) δ 9.87 (s, 1H, NH), 7.51 – 7.44 (m, 2H, ArH), 7.42 – 7.35 (m, 2H, ArH), 5.29 (dd, $J = 3.5, 1.0$ Hz, 1H, H-4), 5.22 (dd, $J = 9.4, 3.5$ Hz, 1H, H-3), 5.08 – 4.92 (m, 2H, H-1, H-2), 4.29 – 4.21 (m, 1H, H-5), 4.15 (t, $J = 6.4$ Hz, 2H, NHCH_2CH_2), 4.11 – 3.97 (m, 2H, H-6), 2.90 (t, $J = 2.6$ Hz, 1H, $\text{C}\equiv\text{CH}$), 2.56 (td, $J = 6.4, 2.7$ Hz, 2H, NHCH_2CH_2), 2.10 (s, 3H, CH_3), 2.05 (s, 3H, CH_3), 2.00 (s, 3H, CH_3), 1.91 (s, 3H, CH_3).

^{13}C NMR (126 MHz, DMSO- d_6) δ 169.95 (1C, C=O), 169.88 (1C, C=O), 169.49 (1C, C=O), 169.26 (1C, C=O), 153.17 (1C, NHC=O), 139.13 (1C, ArC), 132.81 (2C, ArCH), 124.80 (1C, ArC), 118.53 (2C, ArCH), 84.73 (1C, C-1), 81.17 (1C, $\underline{\text{C}}\equiv\text{CH}$), 73.44 (1C, C-5), 72.67 (1C, $\text{C}\equiv\underline{\text{C}}\text{H}$), 71.10 (1C, C-3), 67.59 (1C, C-2), 67.04 (1C, C-4), 62.42 (1C, $\text{COO}\underline{\text{C}}\text{H}_2\text{CH}_2$), 61.78 (1C, C-5), 20.60 (1C, CH_3), 20.53 (1C, CH_3), 20.42 (1C, CH_3), 20.38 (1C, CH_3), 18.71 (1C, $\text{COO}\underline{\text{C}}\text{H}_2\text{CH}_2$).

HPLC-MS: $[\text{C}_{25}\text{H}_{29}\text{NO}_{11}\text{S} + \text{H}]^+$ calcd. 552.15, found. 552.08.

HRMS: $[\text{C}_{25}\text{H}_{29}\text{NO}_{11}\text{S} + \text{NH}_4]^+$ calcd. 569.1800, found. 569.1795.

Biophysical evaluation

Expression and purification of LecA^{58,61} and LecB(PAO1)^{62,130} was performed in analogy to the previously published protocols. LecA was purified on melibiose-coupled sepharose CL- 6B affinity column¹³¹ and then dialysed against TBS/ Ca^{2+} buffer (20 mM Tris, 137 mM NaCl, 2.6 mM KCl at pH 7.4 supplemented with 1 mM CaCl_2). Protein concentration was determined by UV spectroscopy at 280 nm using a molar extinction coefficient of 27 960 $\text{M}^{-1} \text{cm}^{-1}$ for LecA and 6 990 $\text{M}^{-1} \text{cm}^{-1}$ for LecB.

LecA competitive binding assay was performed in presence of 2% DMSO, whereas LecB competitive binding assay had less than 0.5% DMSO present. In short, the compound dilution series were prepared in 96 well plates. 10 μL of each dilution in triplicates were mixed with 10 μL of master mix (40 μM LecA, 20 nM **36** or 300 nM LecB and 20 nM **37** in TBS/ Ca^{2+} buffer) in 384-well microtiter plates (Greiner Bio-One, Germany, cat no 781900). The plates were centrifuged (1 min, 500 g), sealed (EASYseal, Greiner Bio-One, cat no 676001) and incubated for 1 h in case of LecA and 6 h in case of LecB in a dark wet chamber under gentle shaking. Fluorescence was measured on a PheraStar FS plate reader (BMG Labtech GmbH, Germany) with excitation filters at 485 nm and emission filters at 535 nm. The measured intensities were reduced by the blank values (protein in TBS/ Ca^{2+} buffer) and analysed with MARS Data Analysis Software (BMG Labtech GmbH, Germany). IC_{50} values were determined by the four-parameter variable slope model with the minimum and maximum limits of the fit fixed according to the controls in each assay (Me- α -D-Gal or L-Fuc).

Direct binding affinity determination of LecA and LecB imaging probes was performed with direct titration of protein and imaging probes in TBS/ Ca^{2+} buffer. Protein dilution series was prepared in 96 well plates and 10 μL of each dilution in triplicates were mixed with 10 μL of fluorescent compound (20 nM) in 384-well microtiter plates (Greiner Bio-One, Germany, cat no 781900). The plates were centrifuged (1 min, 500 g), sealed and incubated for 2 h in dark

wet chamber under gentle shaking. Fluorescence was measured on a PheraStar FS plate reader (BMG Labtech GmbH, Germany) with excitation filters at 485 nm and emission filters at 535 nm. The data were analysed with MARS Data Analysis Software (BMG Labtech GmbH, Germany) to calculate K_d values.

Biofilm experiments

Biofilm staining experiments were performed in analogy to Wagner *et. al.*⁴⁴ Bacterial overnight cultures of mCherry expressing *P. aeruginosa* PAO1 w.t. + pMP7605,⁴⁴ PAO1 Δ lecA + pMP7605⁴⁴ and PAO1 Δ lecB + pMP7605 (courtesy of Stefanie Wagner and Varvara Verkhova, unpublished results) were inoculated from single colonies in 5 mL LB supplemented with gentamicin (120 μ g/mL) and grown at 37 °C and 180 rpm. The bacterial overnight cultures were then diluted to OD₆₀₀ of 0.02 with LB and 500 μ L of culture per well were transferred to 24-well plate (24CG, Art. No. 5231 or 24FC, Art. No. 3231). The biofilm was grown under shaking conditions (180 rpm) at 37 °C for 20 – 24 h. Biofilm aggregates were visualized using a confocal laser scanning microscope (Leica TCS Sp8 CLSM) using a 25 \times numerical-aperture water objective. Z-stacks (463 x 463 μ m) were recorded every 2 μ m for mCherry (ex.: 561 nm, red) and for fluorescein containing imaging compounds (ex.: 488 nm, green). 5 – 20 μ L of 1 mM stock (TBS/Ca²⁺ buffer with 10% DMSO) of imaging compounds were carefully added to the wells containing biofilms ($c = 10 - 40 \mu$ M) and incubated under static conditions for 30 – 190 min. Images were processed using Fiji¹⁰¹ software by subsequently using following functions: subtract background (rolling ball, 50 pixels radius), remove outliers (2 pixels radius, threshold 50) and Z-project max display. Images were later re-analysed with the Imaris software (Bitplane AG An Oxford Instruments Company, Switzerland) by subtracting image backgrounds, applying a median filter and displayed as Maximum Intensity Projections (contrast range automatically adjusted by Imaris). Only one staining experiment was carried out for imaging probes **31** and **32**, all other fluorescein conjugates were analysed in at least three independent experiments.

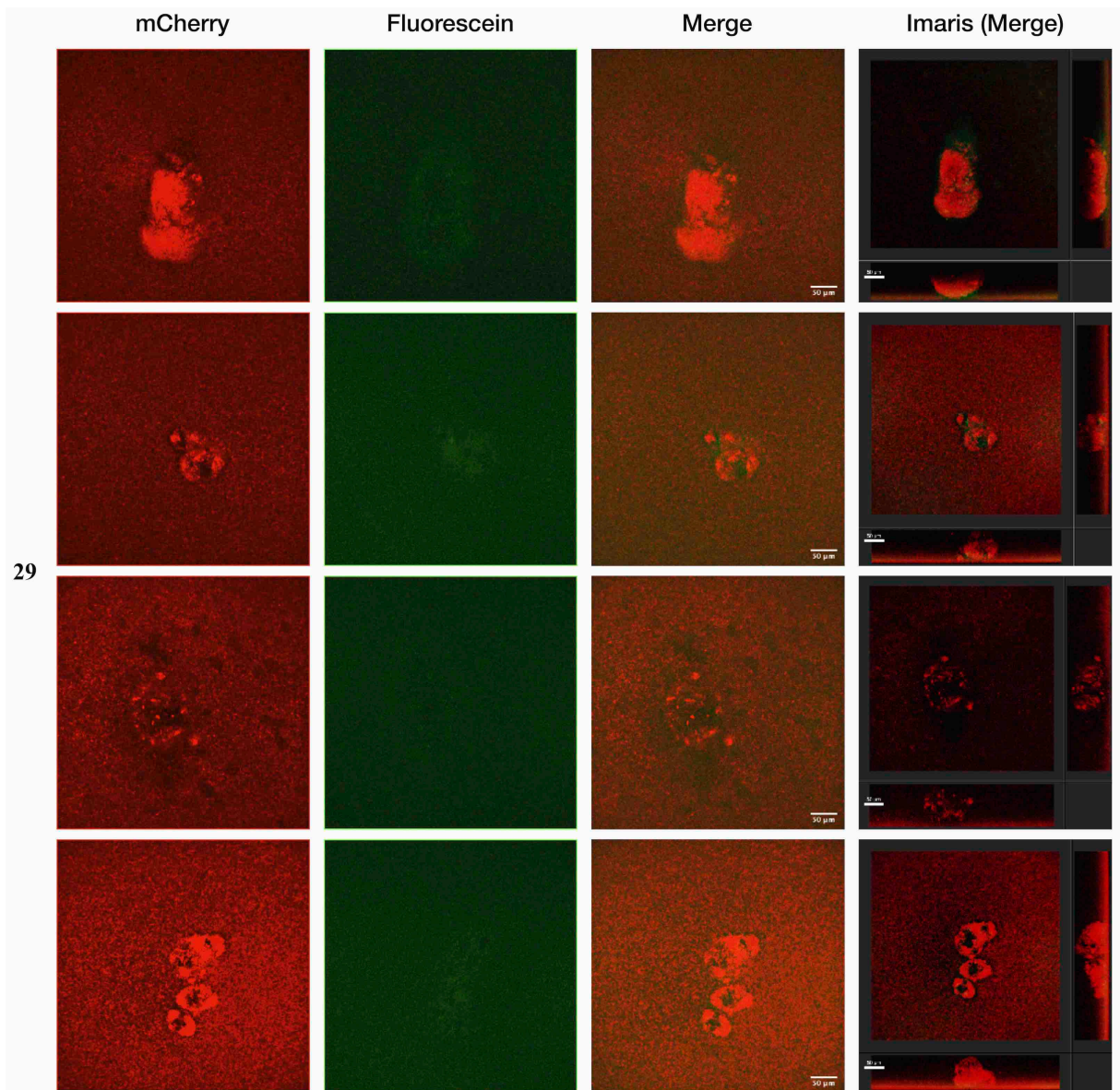


Figure S1: *P. aeruginosa* PAO1wt + pMP7605 biofilm aggregates (in red, from mCherry ex.: 561 nm) stained with 10 μ M of azide modified fluorescein **29** (in green, from fluorescein conjugate ex.: 488 nm) displayed as maximum intensity Z-projections using Fiji and as three-dimensional maximum intensity projection using Imaris. Scale bars = 50 μ m.

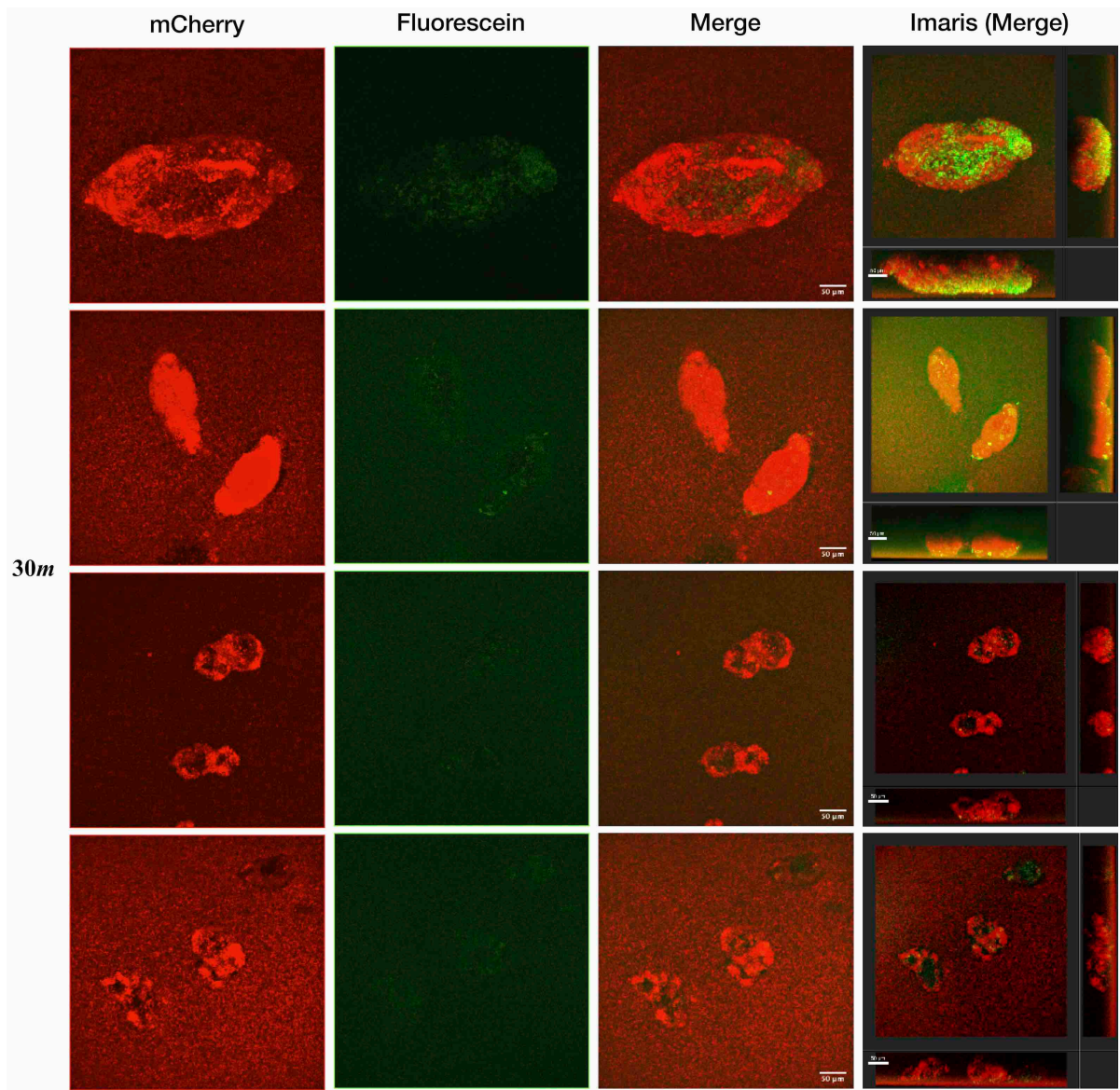


Figure S2: *P. aeruginosa* PAO1wt + pMP7605 biofilm aggregates (in red, from mCherry ex.: 561 nm) stained with 10 μ M of galactose-based imaging probe **30m** (in green, from fluorescein conjugate ex.: 488 nm) displayed as maximum intensity Z-projections using Fiji and as three-dimensional maximum intensity projection using Imaris. Scale bars = 50 μ m.

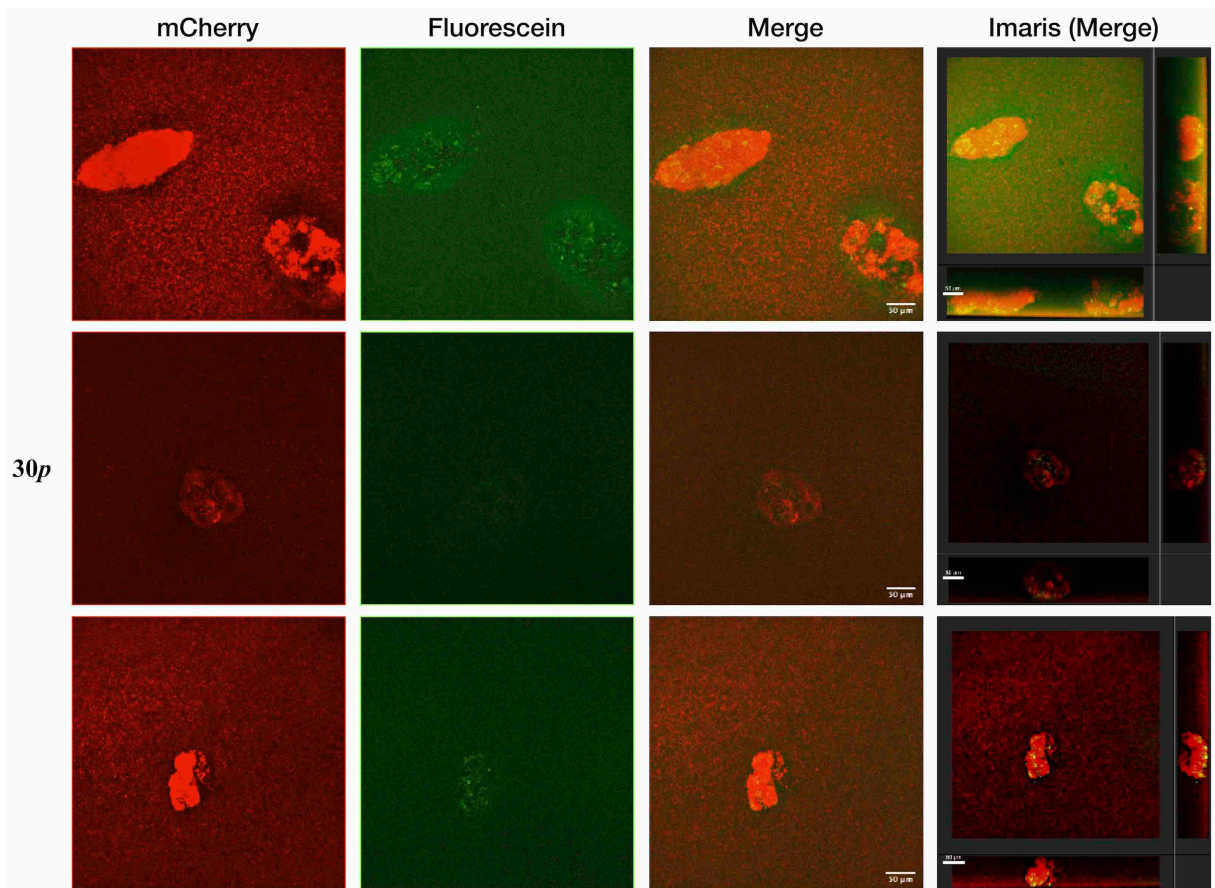


Figure S3: *P. aeruginosa* PAO1wt + pMP7605 biofilm aggregates (in red, from mCherry ex.: 561 nm) stained with 10 μ M of galactose-based imaging probe **30p** (in green, from fluorescein conjugate ex.: 488 nm) displayed as maximum intensity Z-projections using Fiji and as three-dimensional maximum intensity projection using Imaris. Scale bars = 50 μ m.

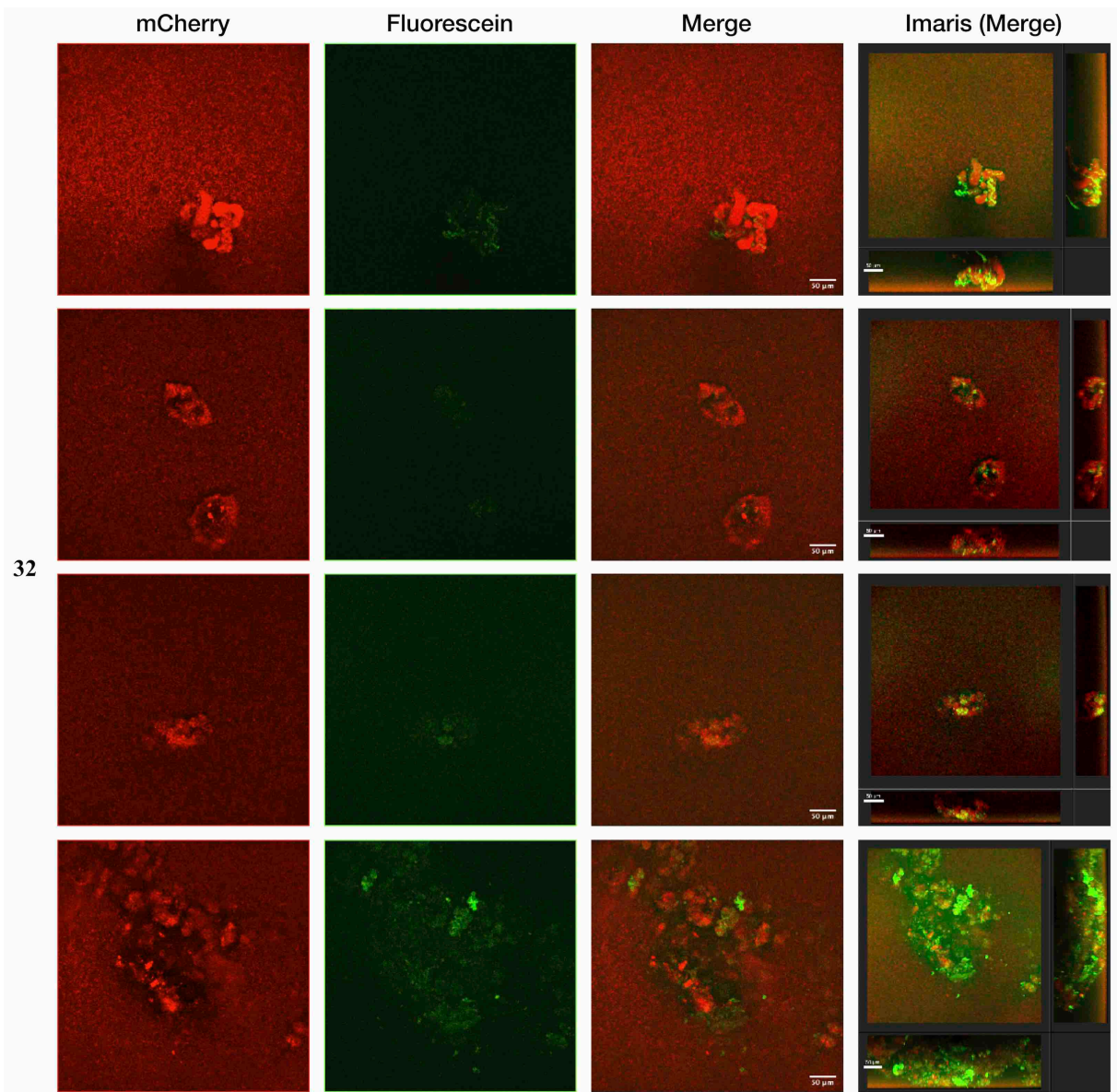


Figure S4: *P. aeruginosa* PAO1wt + pMP7605 biofilm aggregates (in red, from mCherry ex.: 561 nm) stained with 10 µM of xylose-based imaging probe **32** (in green, from fluorescein conjugate ex.: 488 nm) displayed as maximum intensity Z-projections using Fiji and as three-dimensional maximum intensity projection using Imaris. Bottom row shows stained pellicle. Scale bars = 50 µm.

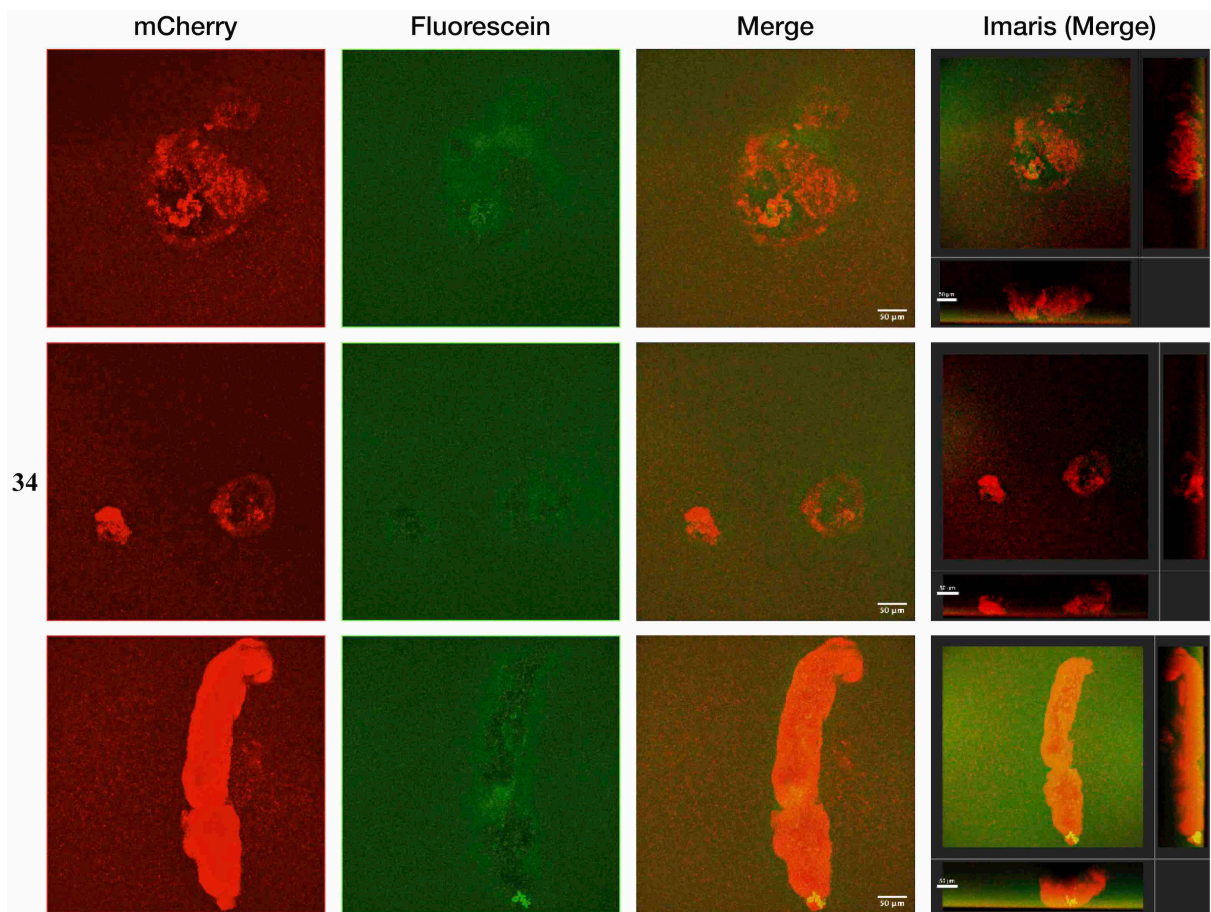
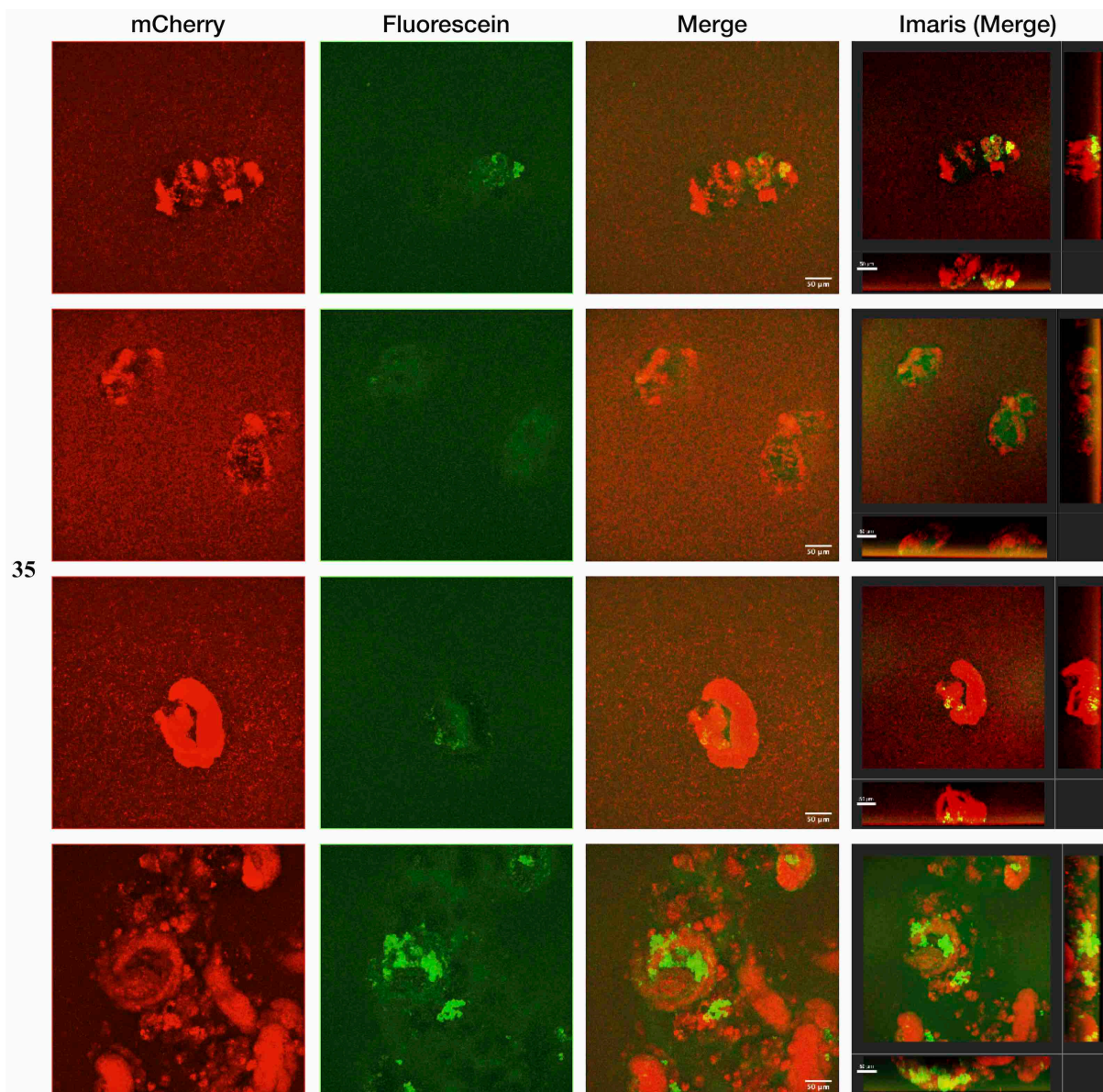


Figure S5: *P. aeruginosa* PAO1wt + pMP7605 biofilm aggregates (in red, from mCherry ex.: 561 nm) stained with 10 μ M of 1-deoxy-fucose-based imaging probe **34** (in green, from fluorescein conjugate ex.: 488 nm) displayed as maximum intensity Z-projections using Fiji and as three-dimensional maximum intensity projection using Imaris. Scale bars = 50 μ m.



35

Figure S6: *P. aeruginosa* PAO1wt + pMP7605 biofilm aggregates (in red, from mCherry ex.: 561 nm) stained with 10 μ M of 1-deoxy-fucose-based imaging probe **35** (in green, from fluorescein conjugate ex.: 488 nm) displayed as maximum intensity Z-projections using Fiji and as three-dimensional maximum intensity projection using Imaris. Bottom row shows stained pellicle. Scale bars = 50 μ m.

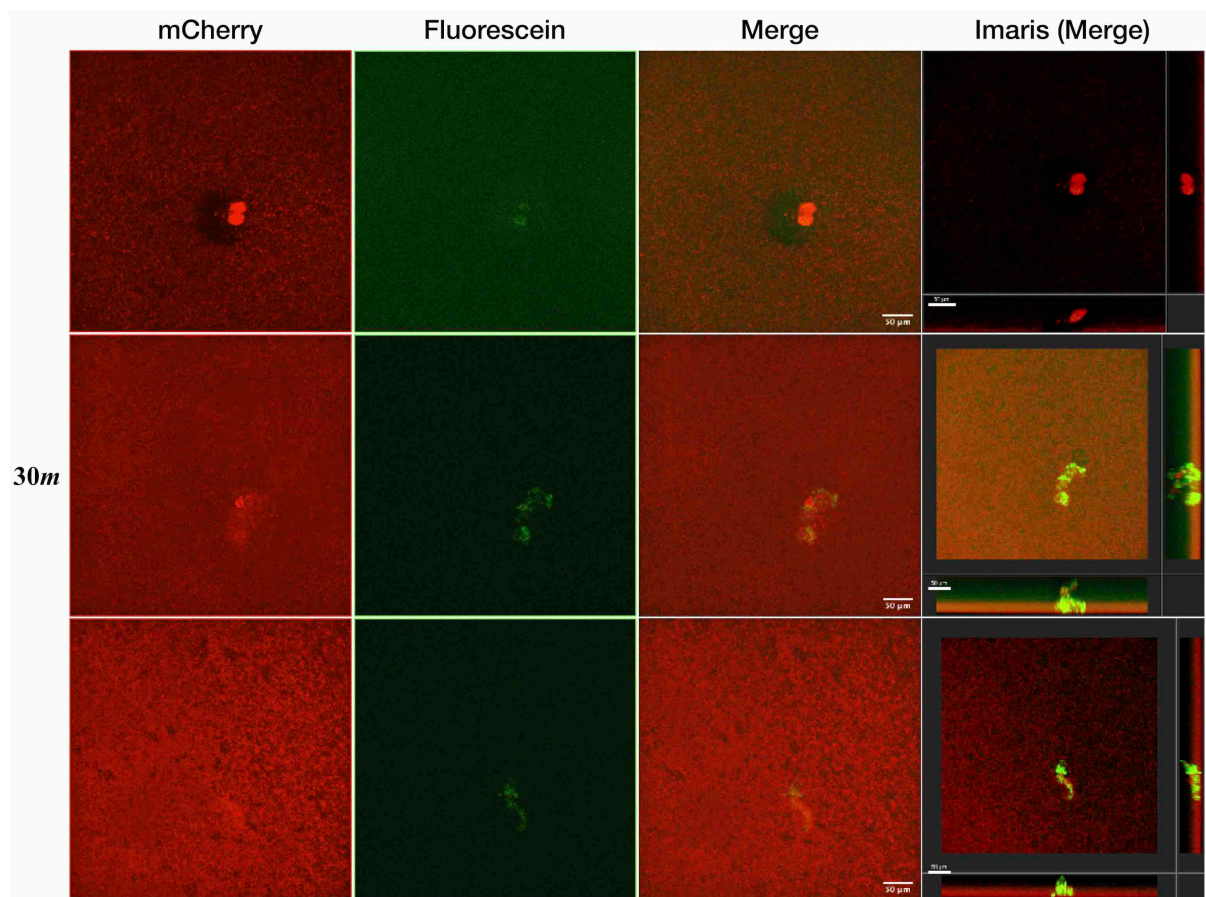


Figure S7: *P. aeruginosa* PAO1wt + pMP7605 biofilm aggregates (in red, from mCherry ex.: 561 nm) stained with 40 μ M of galactose-based imaging probe **30m** (in green, from fluorescein conjugate ex.: 488 nm) displayed as maximum intensity Z-projections using Fiji and as three-dimensional maximum intensity projection using Imaris. Scale bars = 50 μ m.

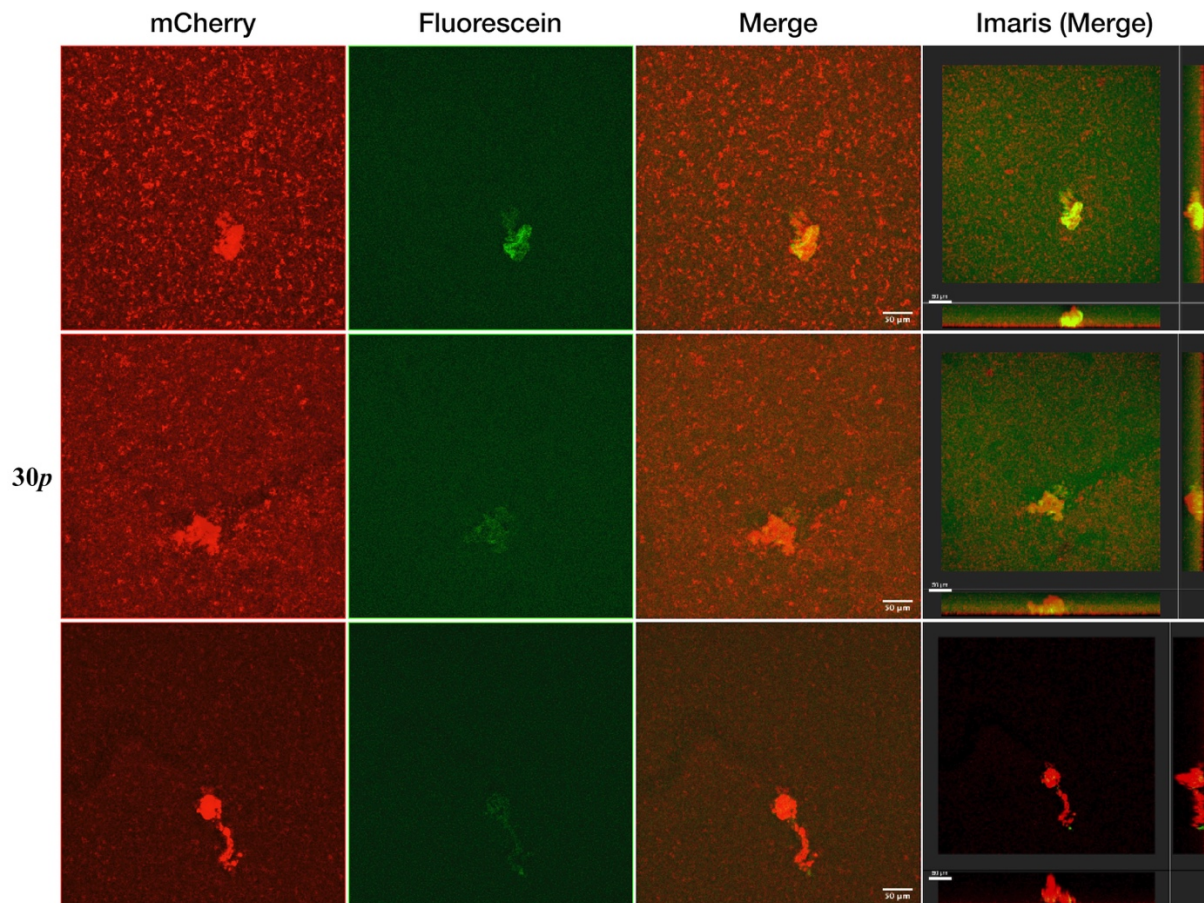


Figure S8: *P. aeruginosa* PAO1wt + pMP7605 biofilm aggregates (in red, from mCherry ex.: 561 nm) stained with 40 μ M of galactose-based imaging probe **30p** (in green, from fluorescein conjugate ex.: 488 nm) displayed as maximum intensity Z-projections using Fiji and as three-dimensional maximum intensity projection using Imaris. Scale bars = 50 μ m.

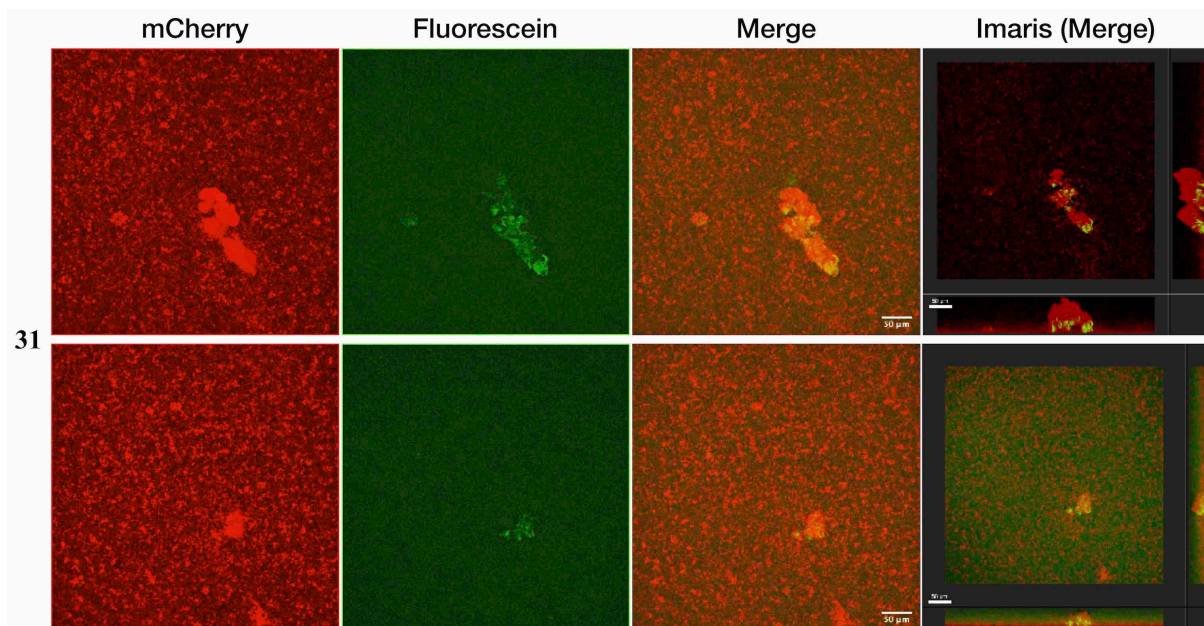


Figure S9: *P. aeruginosa* PAO1wt + pMP7605 biofilm aggregates (in red, from mCherry ex.: 561 nm) stained with 40 μ M of galactose-based imaging probe **31** (in green, from fluorescein conjugate ex.: 488 nm) displayed as

maximum intensity Z-projections using Fiji and as three-dimensional maximum intensity projection using Imaris. Scale bars = 50 μm .

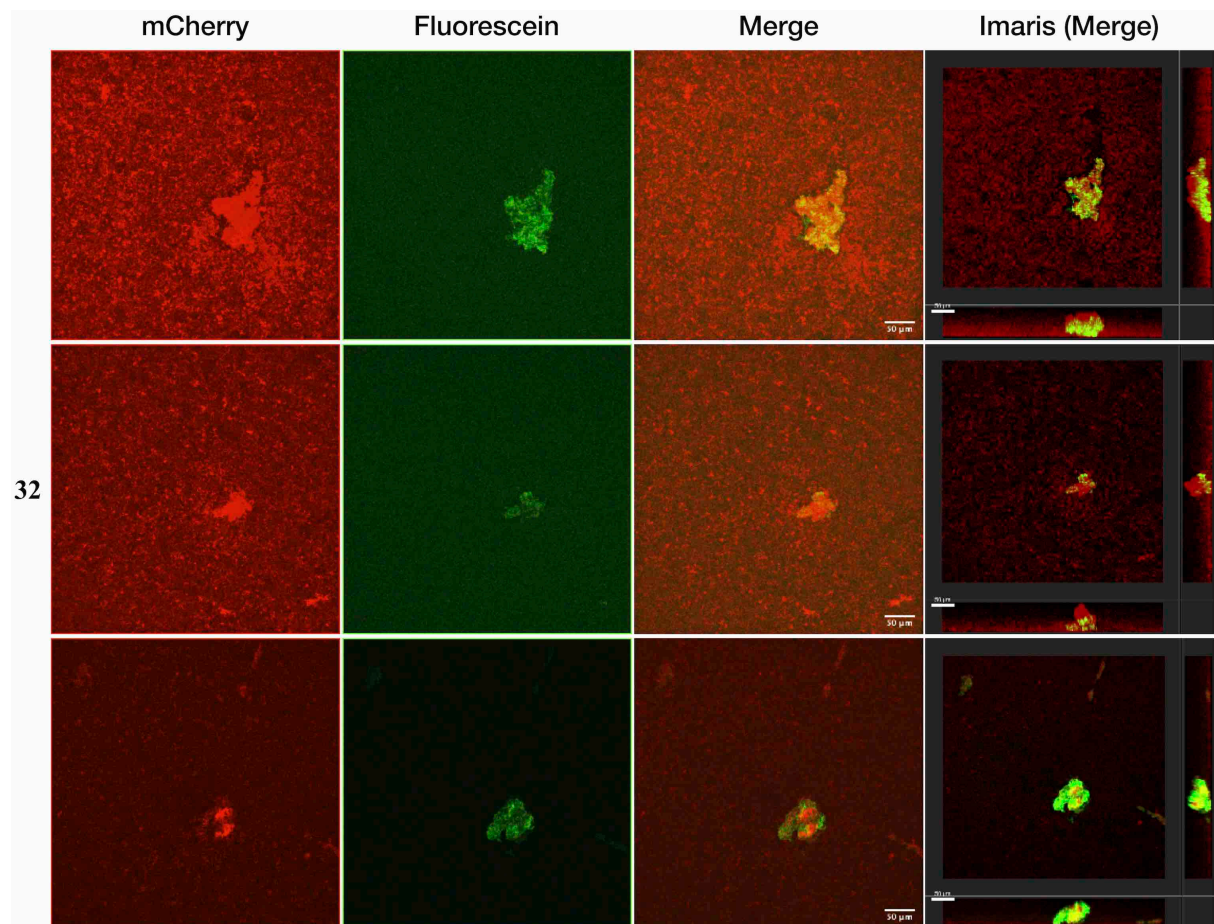


Figure S10: *P. aeruginosa* PAO1wt + pMP7605 biofilm aggregates (in red, from mCherry ex.: 561 nm) stained with 40 μM of xylose-based imaging probe **32** (in green, from fluorescein conjugate ex.: 488 nm) displayed as maximum intensity Z-projections using Fiji and as three-dimensional maximum intensity projection using Imaris. Scale bars = 50 μm .

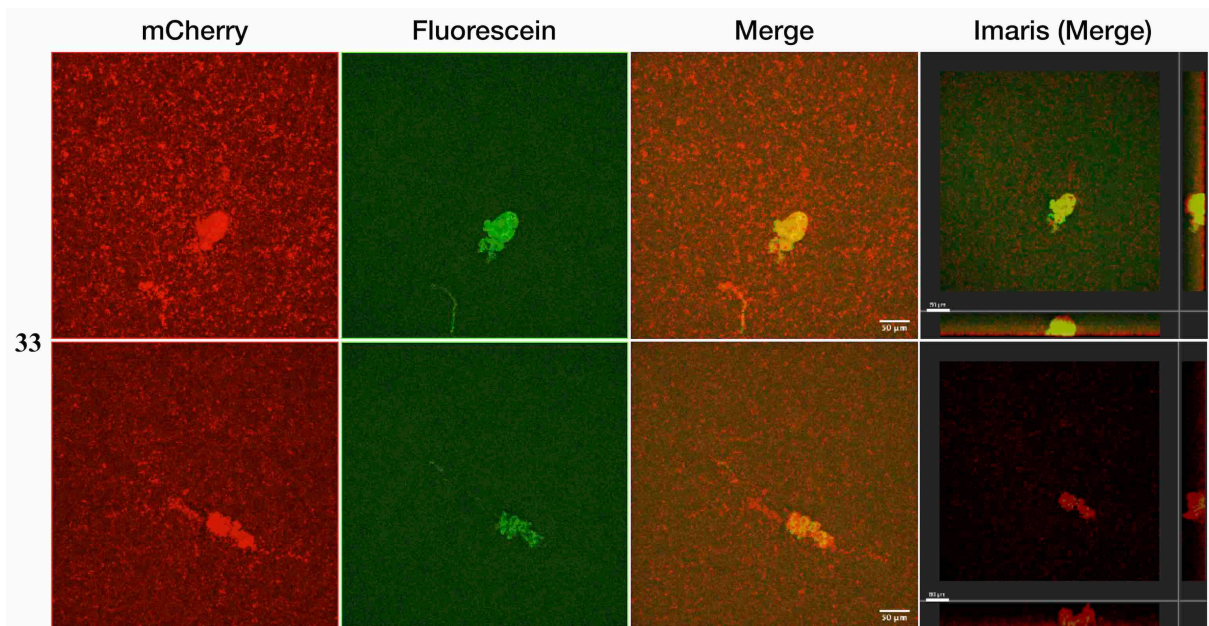


Figure S11: *P. aeruginosa* PAO1wt + pMP7605 biofilm aggregates (in red, from mCherry ex.: 561 nm) stained with 40 µM of xylose-based imaging probe **33** (in green, from fluorescein conjugate ex.: 488 nm) displayed as maximum intensity Z-projections using Fiji and as three-dimensional maximum intensity projection using Imaris. Scale bars = 50 µm.

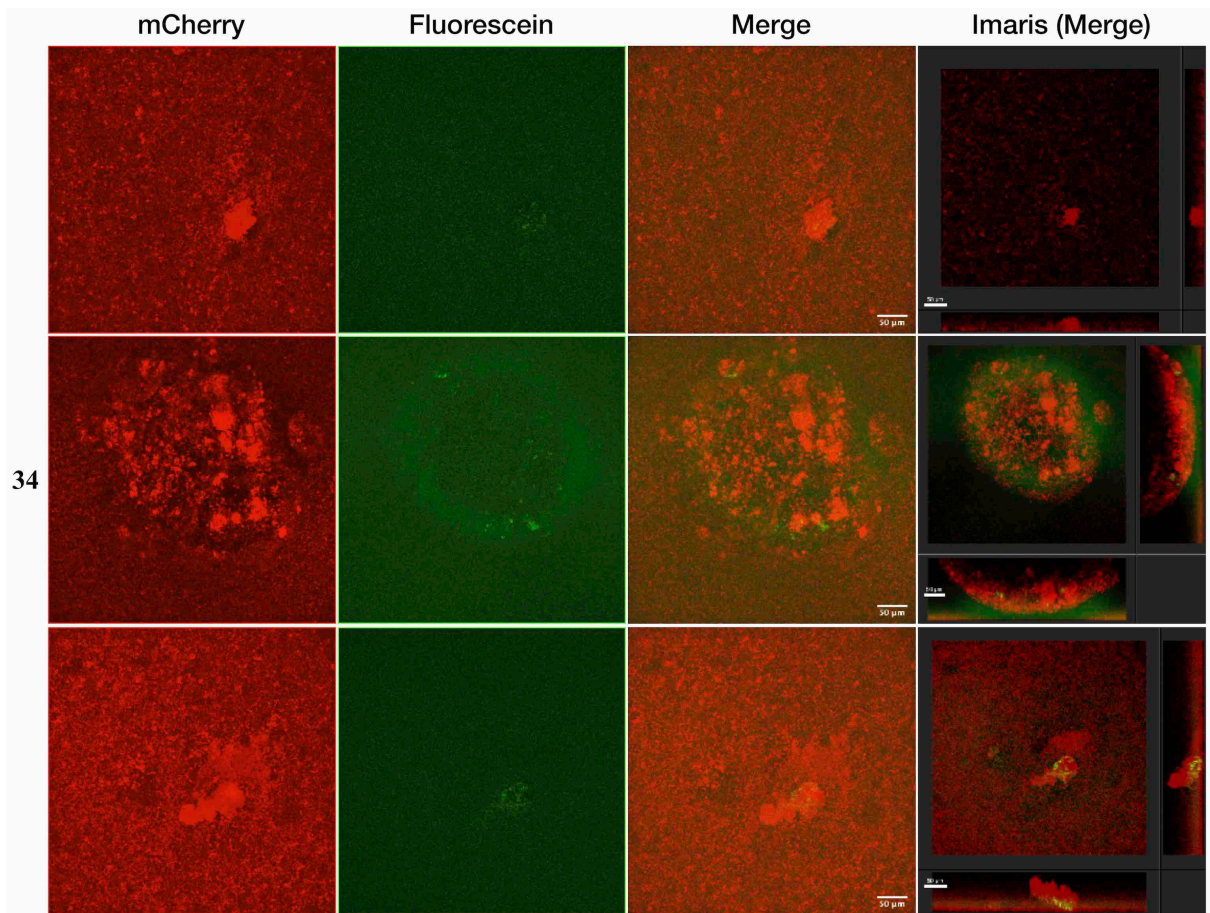


Figure S12: *P. aeruginosa* PAO1wt + pMP7605 biofilm aggregates (in red, from mCherry ex.: 561 nm) stained with 40 µM of 1-deoxy-fucose-based imaging probe **34** (in green, from fluorescein conjugate ex.: 488 nm) displayed as maximum intensity Z-projections using Fiji and as three-dimensional maximum intensity projection using Imaris. Scale bars = 50 µm.

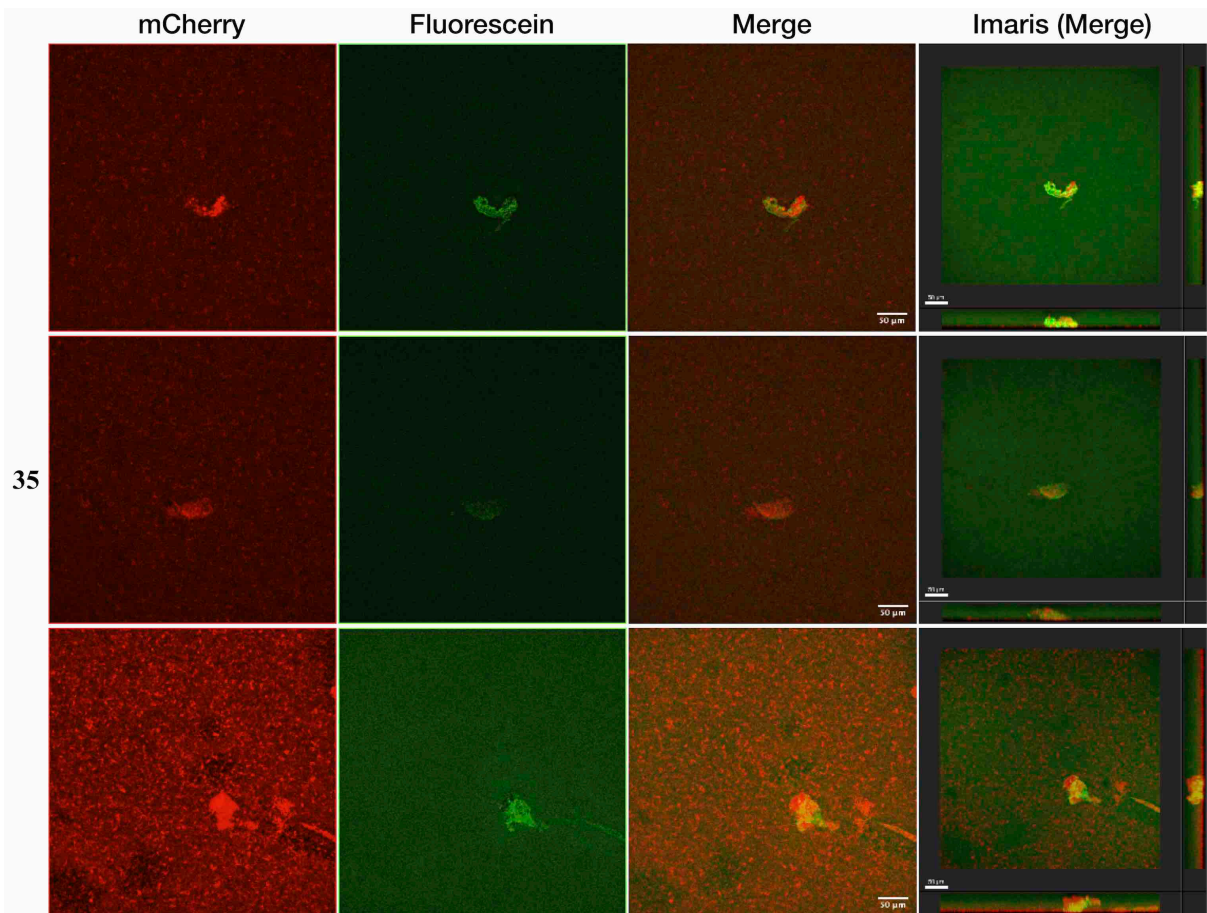


Figure S13: *P. aeruginosa* PAO1wt + pMP7605 biofilm aggregates (in red, from mCherry ex.: 561 nm) stained with 40 μ M of 1-deoxy-fucose-based imaging probe **35** (in green, from fluorescein conjugate ex.: 488 nm) displayed as maximum intensity Z-projections using Fiji and as three-dimensional maximum intensity projection using Imaris. Scale bars = 50 μ m.

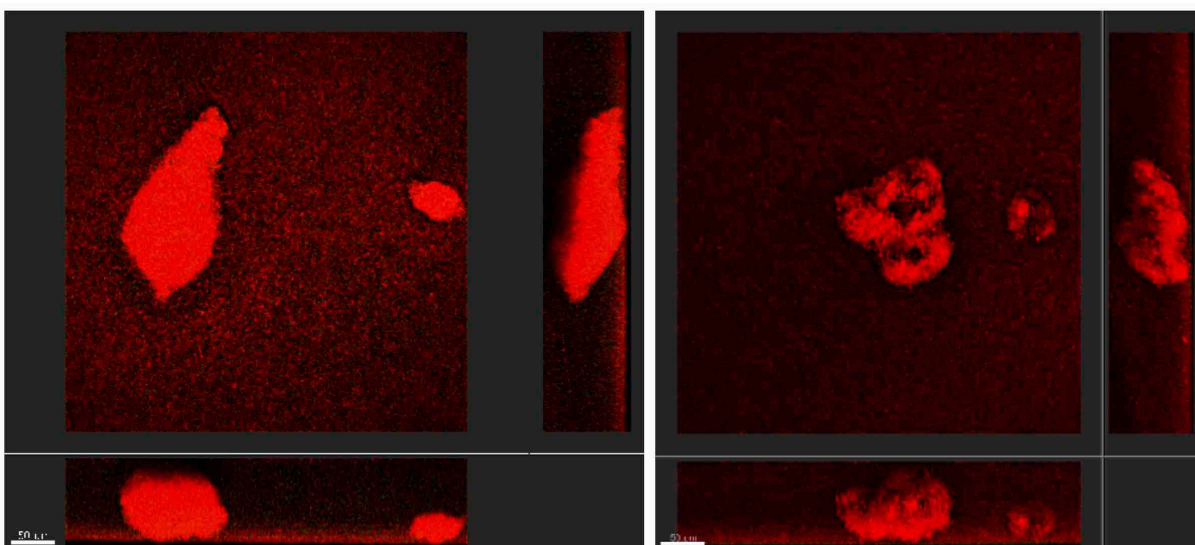


Figure S14: Example of *P. aeruginosa* PAO1wt + pMP7605 biofilm aggregates (in red, from mCherry ex.: 561 nm) before staining displayed as three-dimensional maximum intensity projection using Imaris.

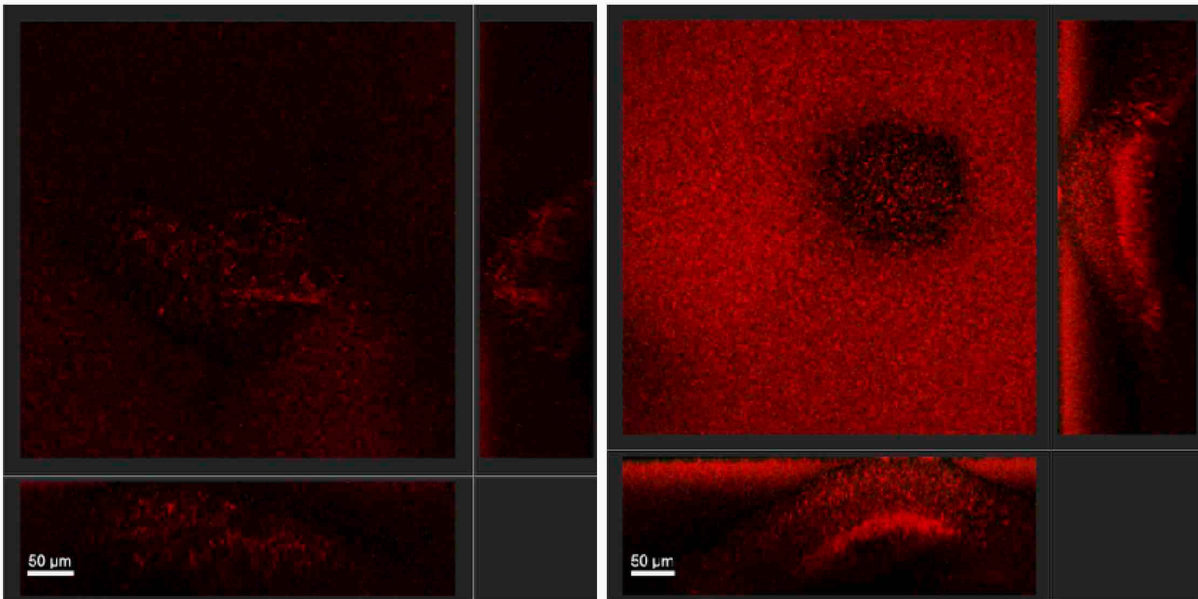


Figure S15: Example of *P. aeruginosa* PAO1ΔlecA + pMP7605 biofilm structures (in red, from mCherry ex.: 561 nm) before staining displayed as three-dimensional maximum intensity projection using Imaris.

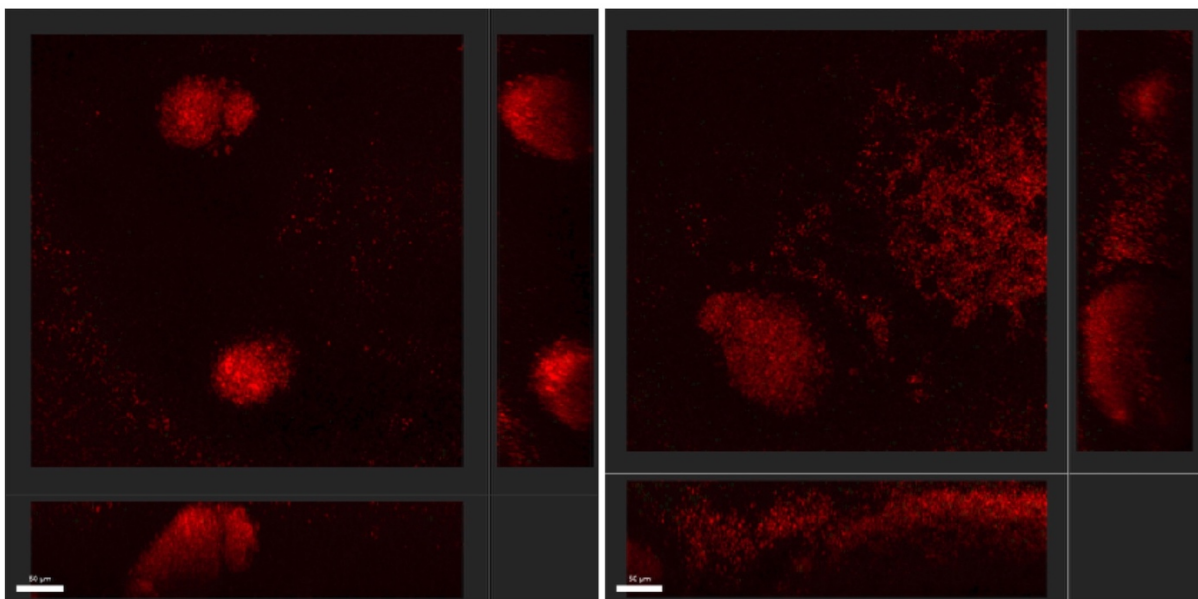
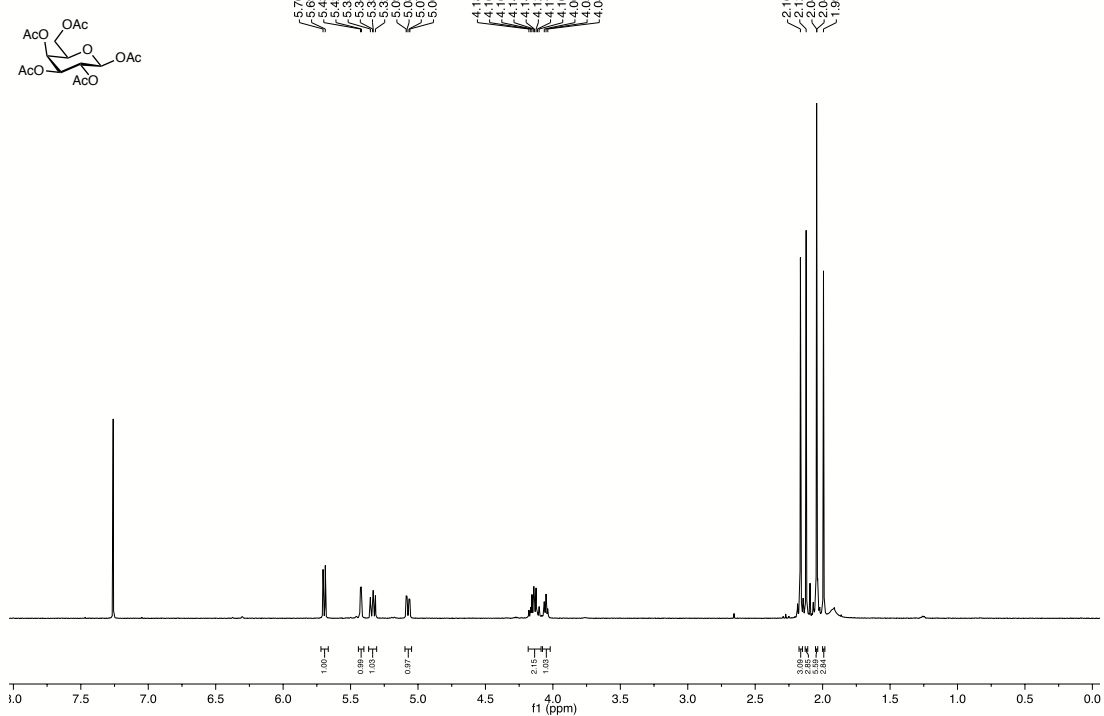
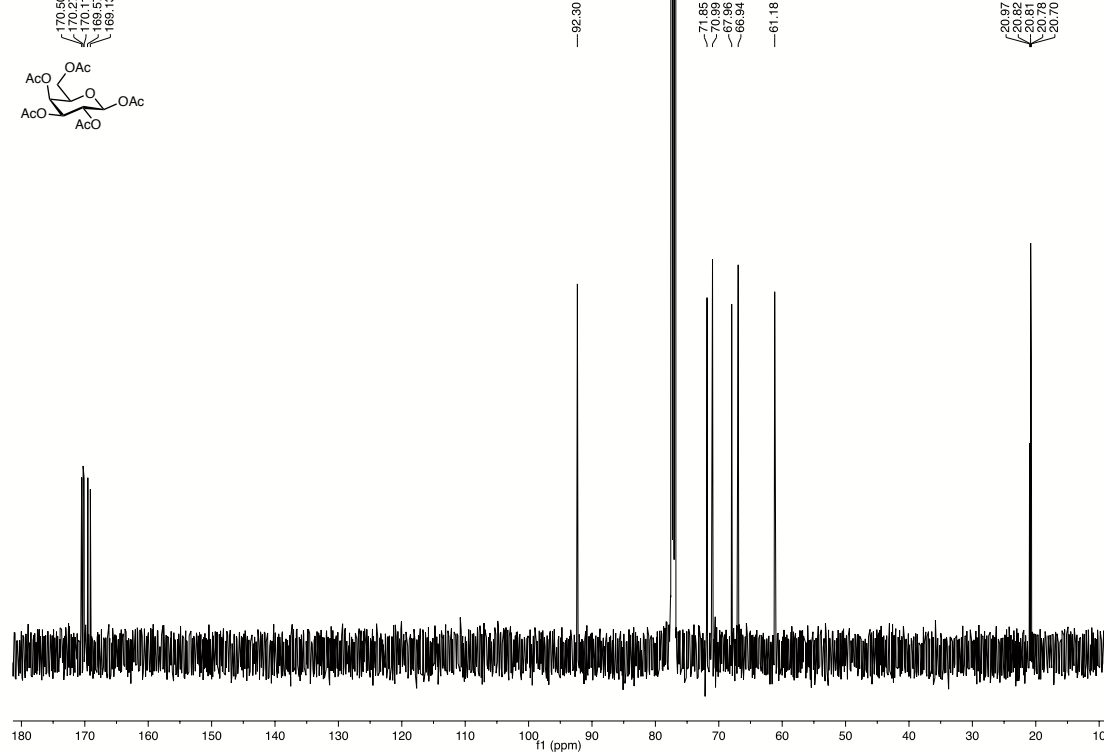


Figure S16: Example of *P. aeruginosa* PAO1ΔlecB + pMP7605 biofilm structures (in red, from mCherry ex.: 561 nm) before staining displayed as three-dimensional maximum intensity projection using Imaris.

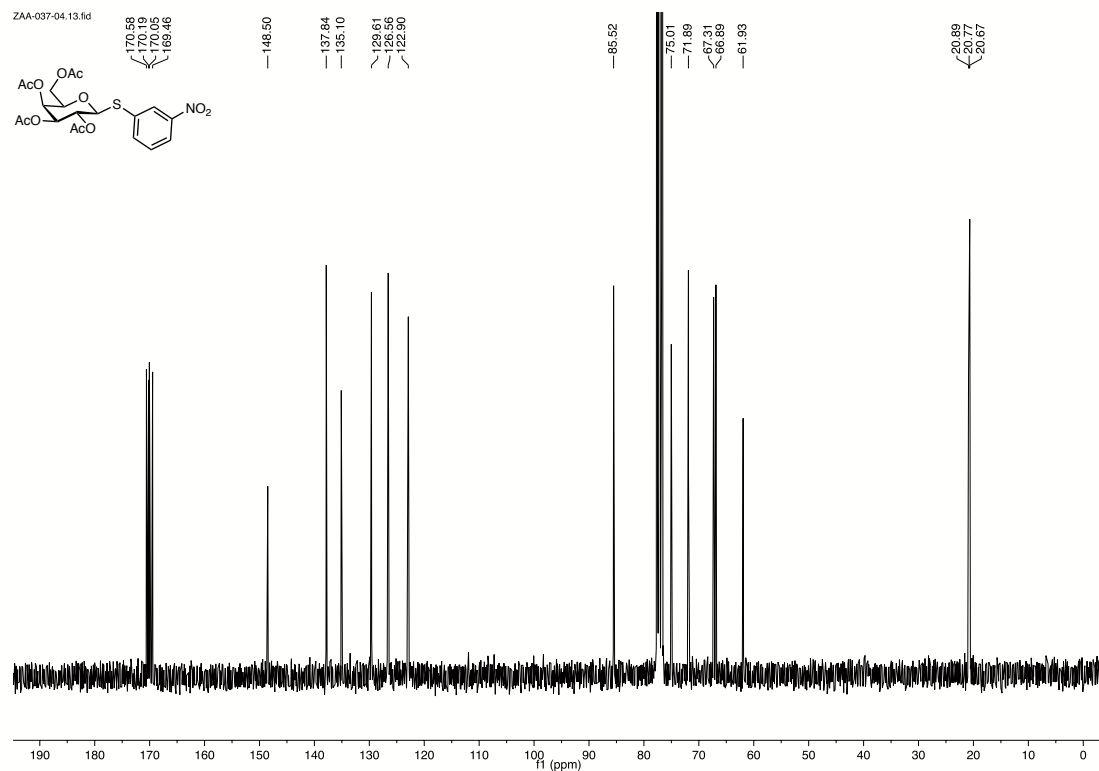
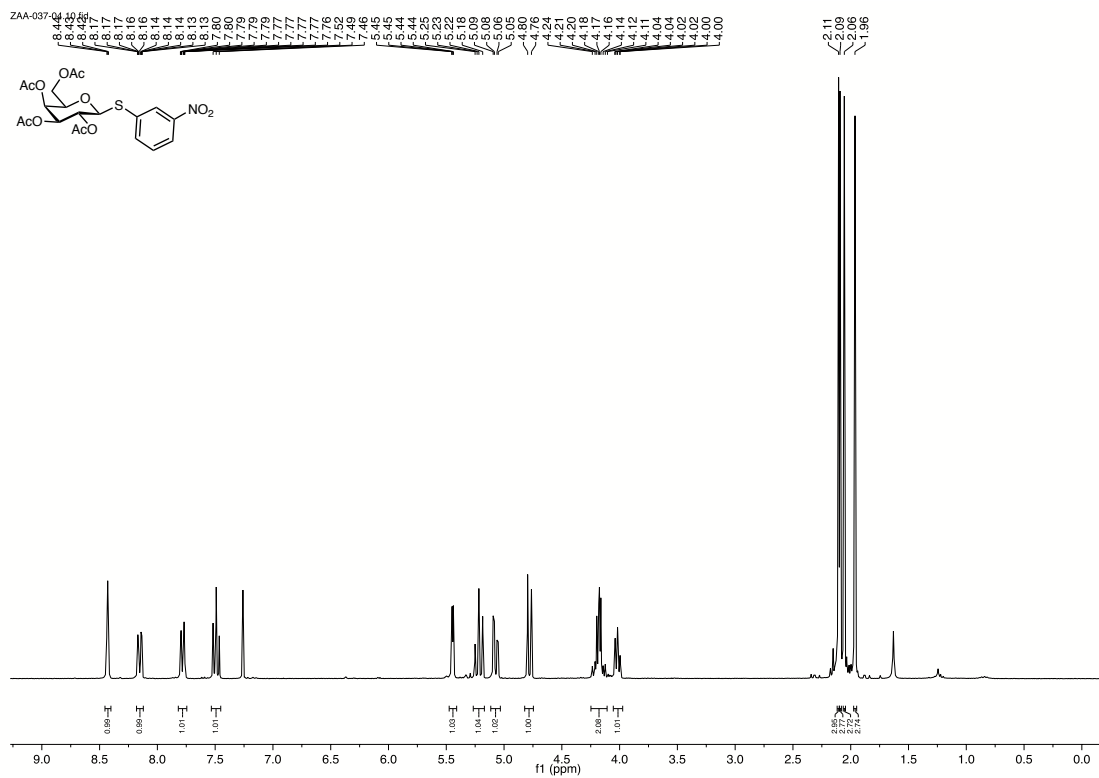
3105zaa_001_05.1.fid



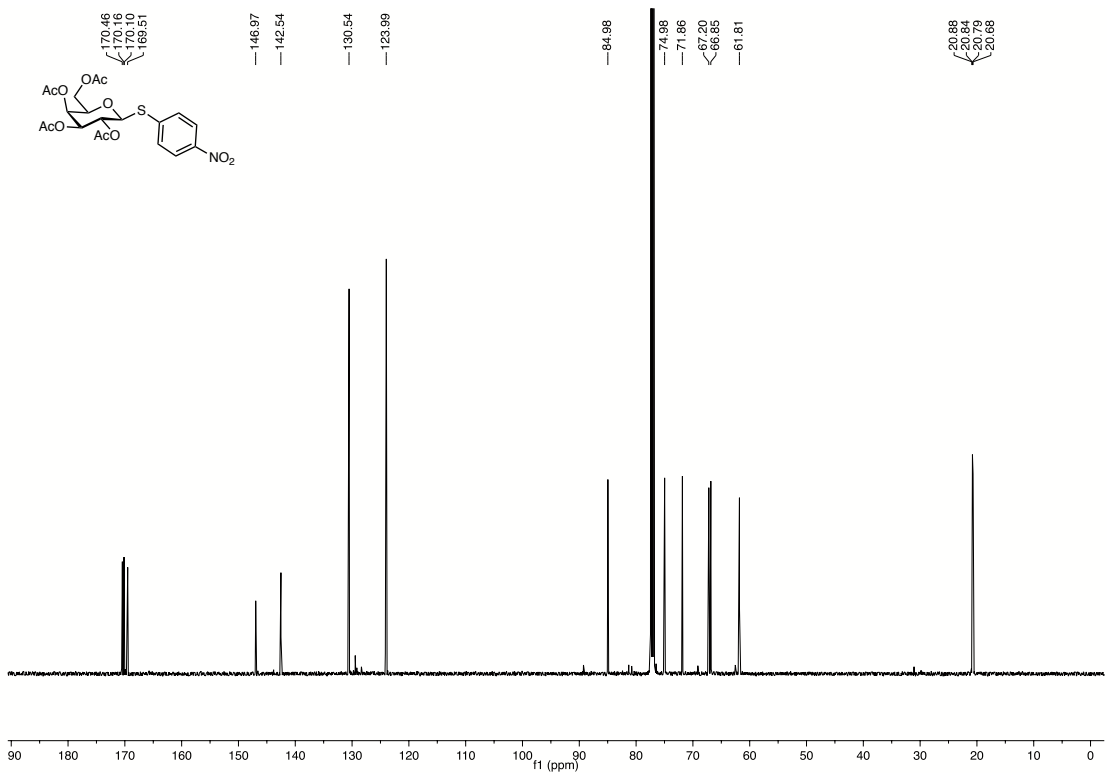
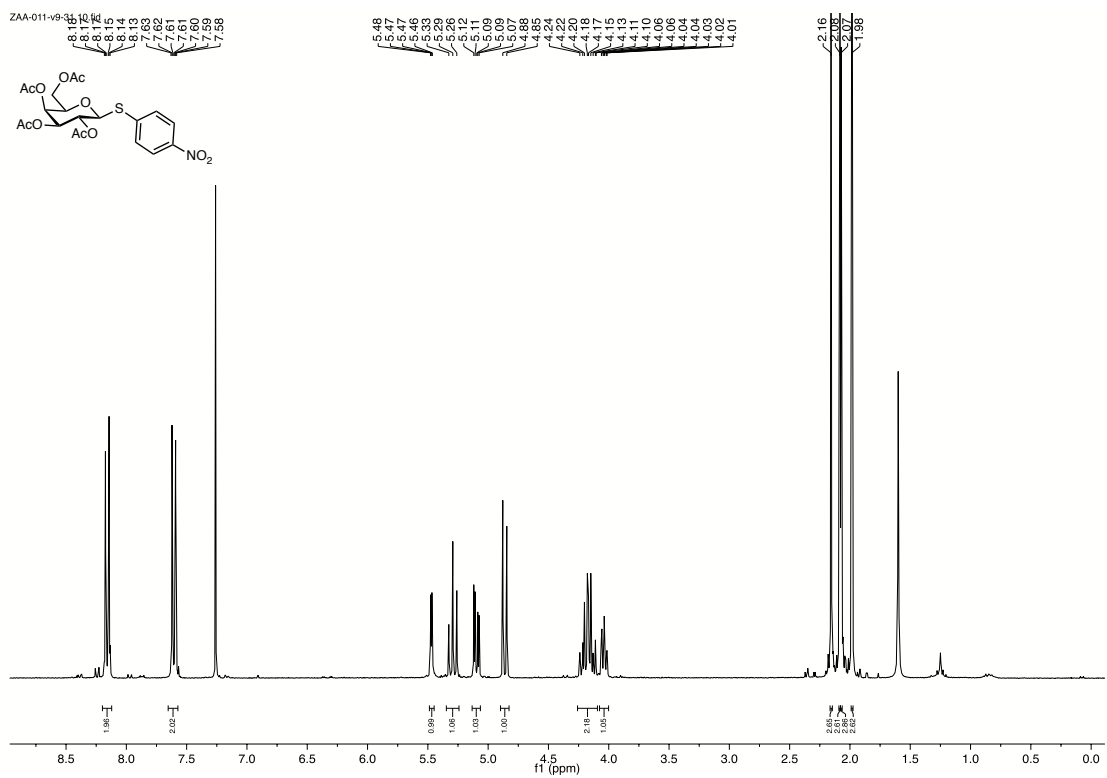
3105zaa_001_05.2.fid



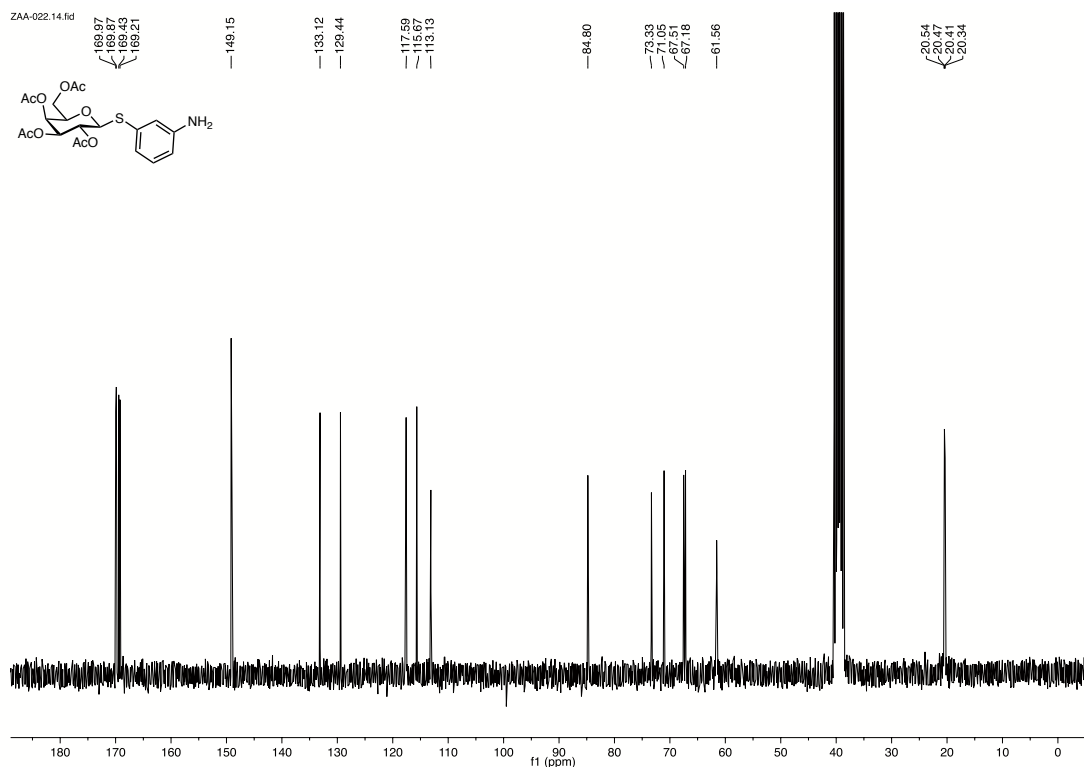
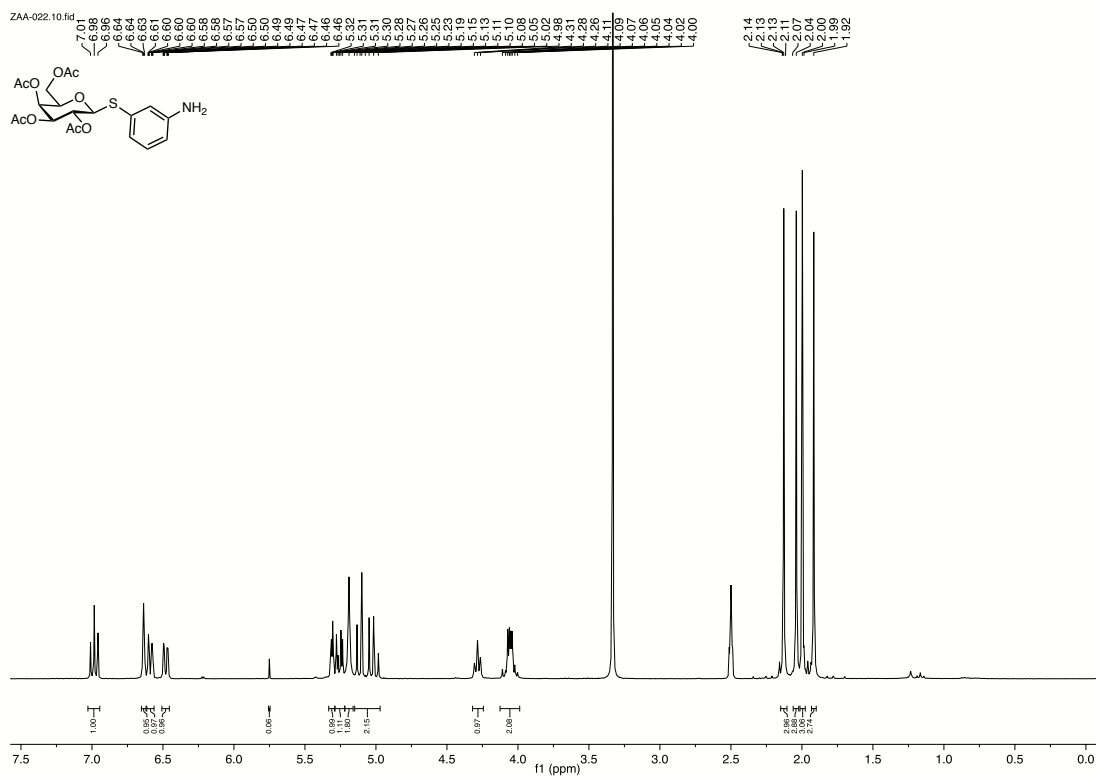
¹H and ¹³C NMR of 3



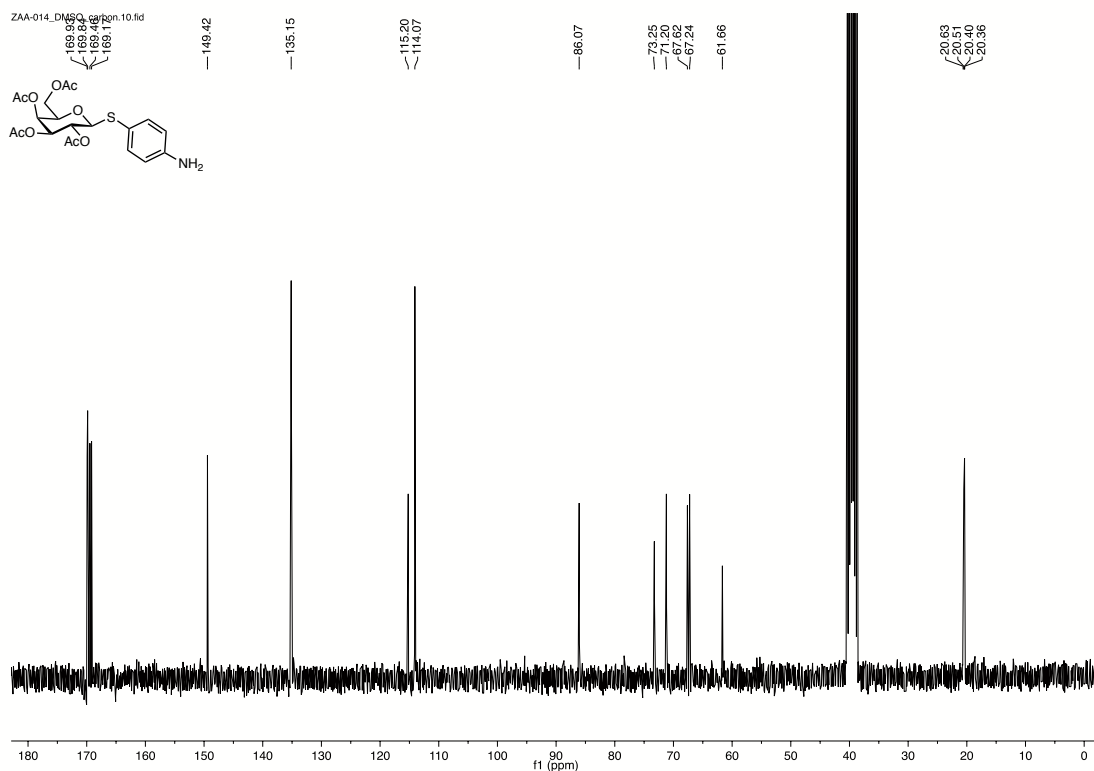
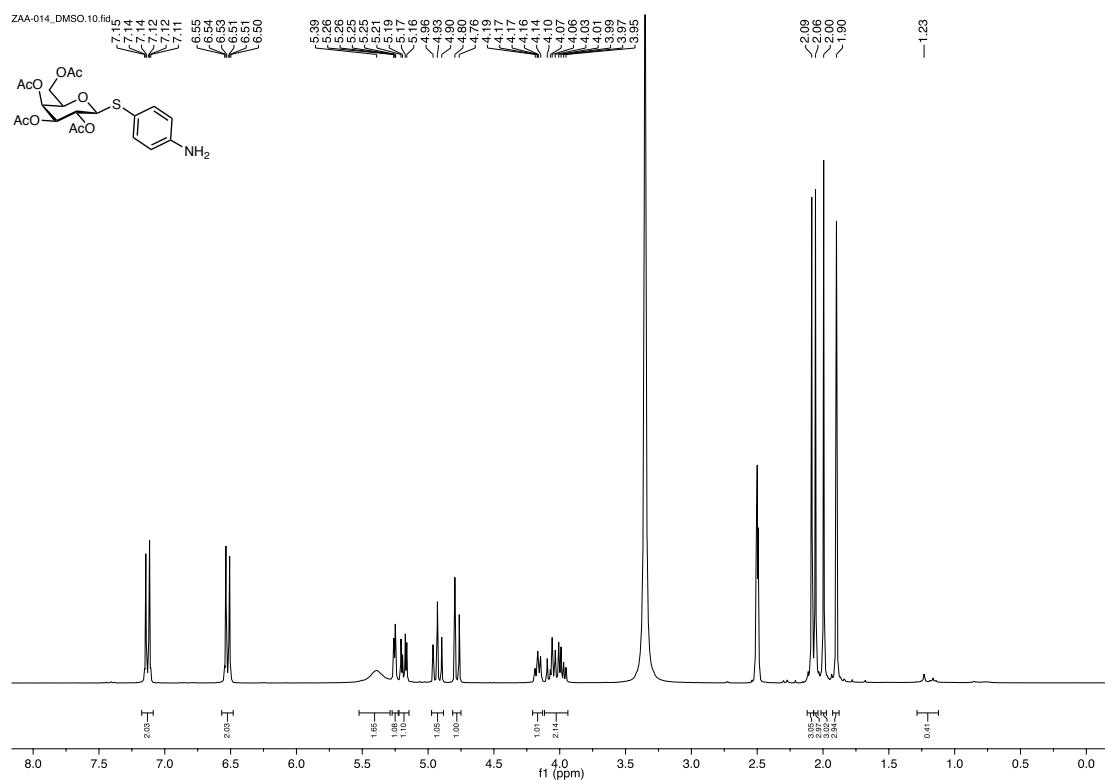
¹H and ¹³C NMR of **4m**



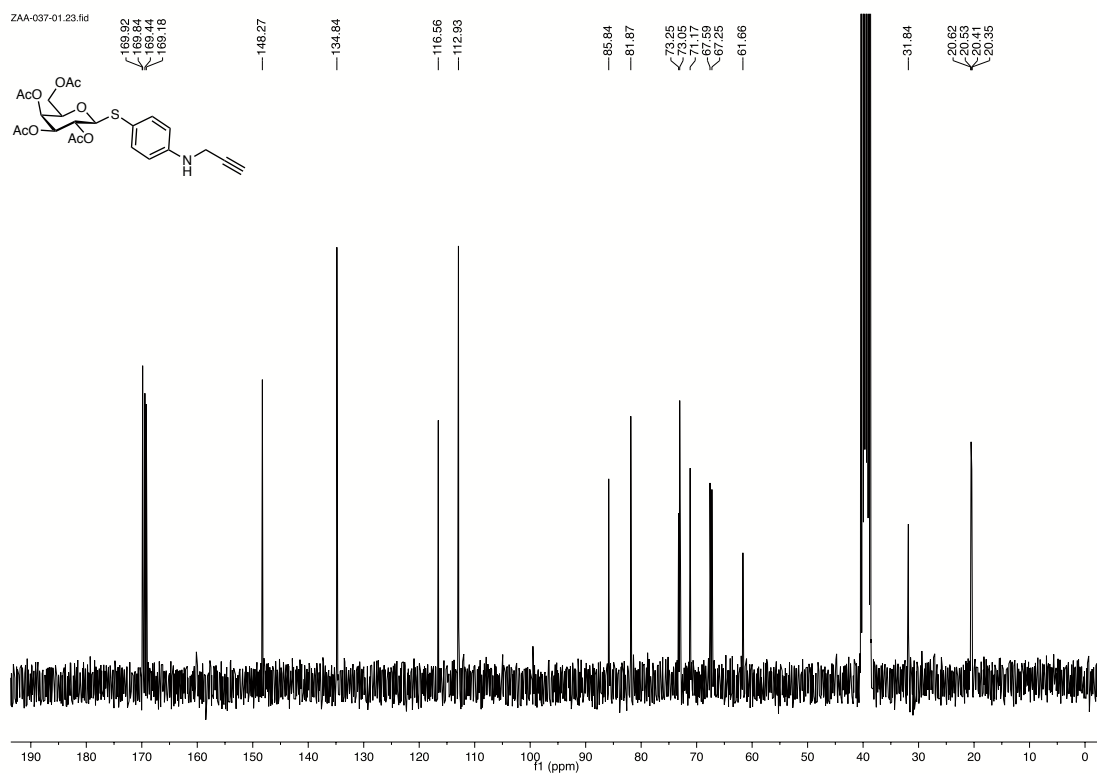
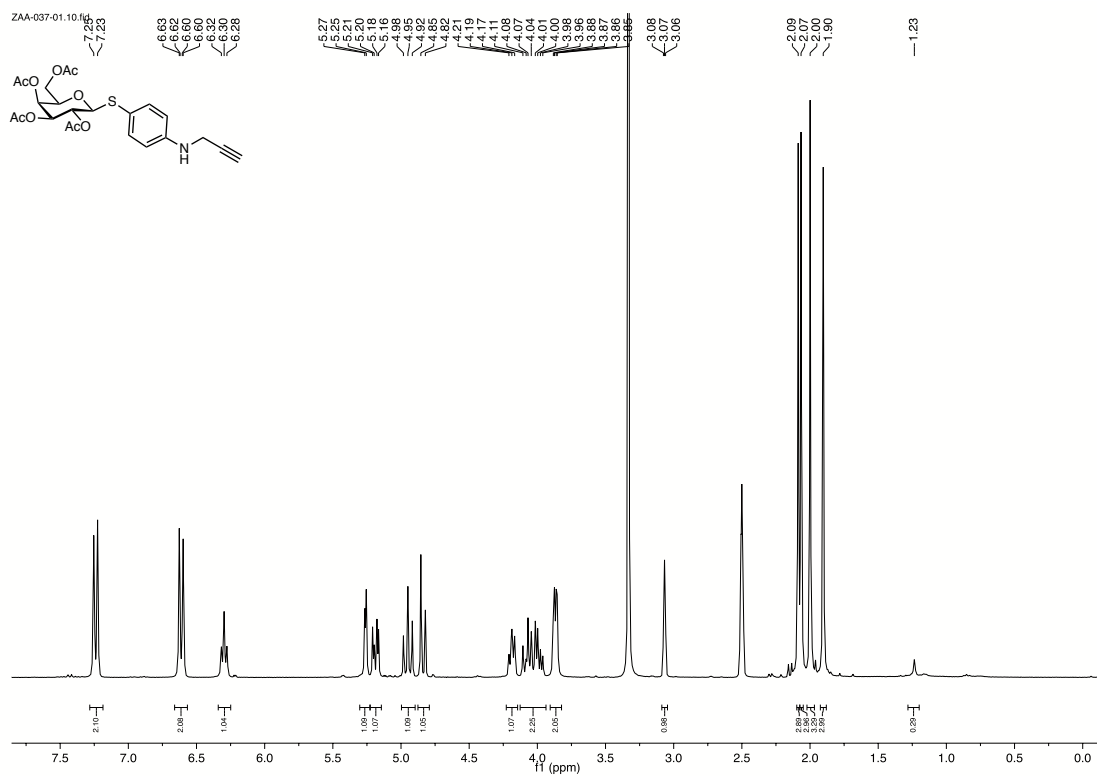
¹H and ¹³C NMR of **4p**



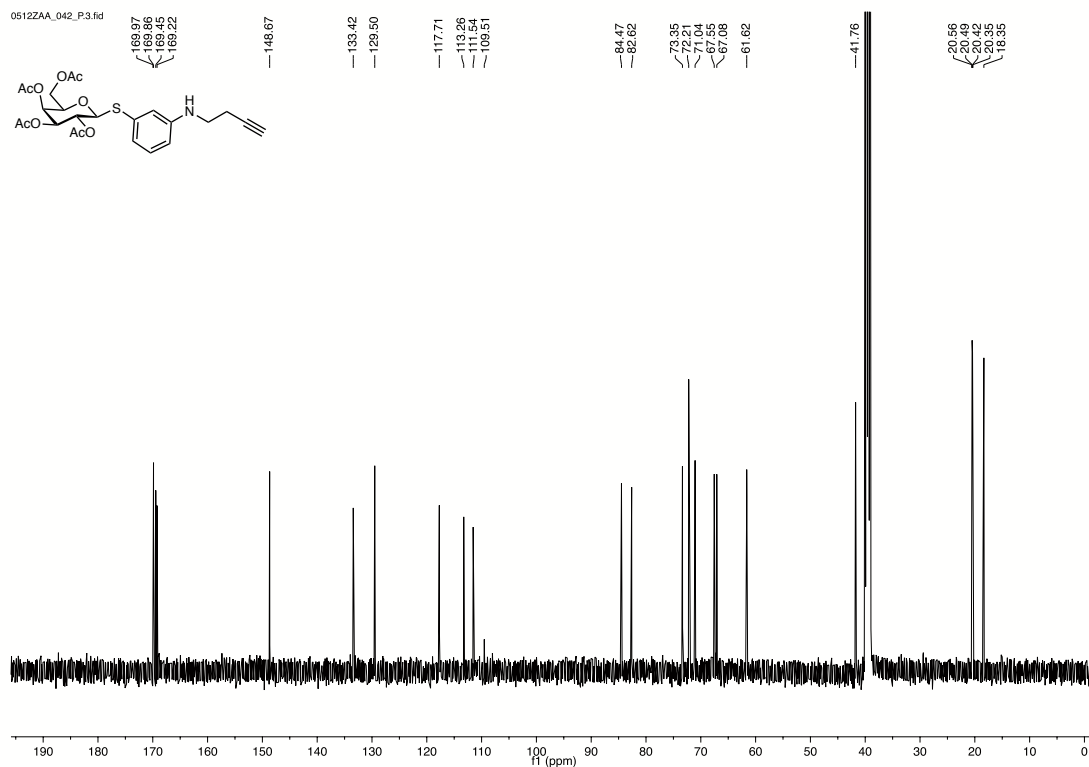
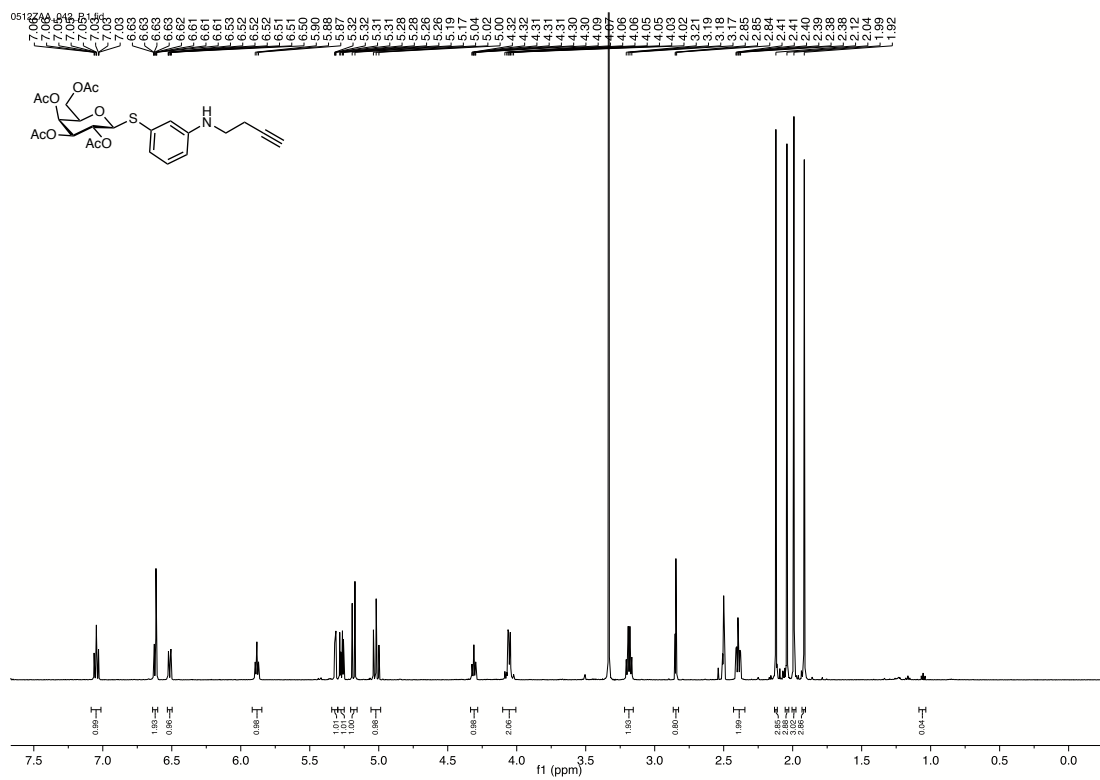
^1H and ^{13}C NMR of **5m**



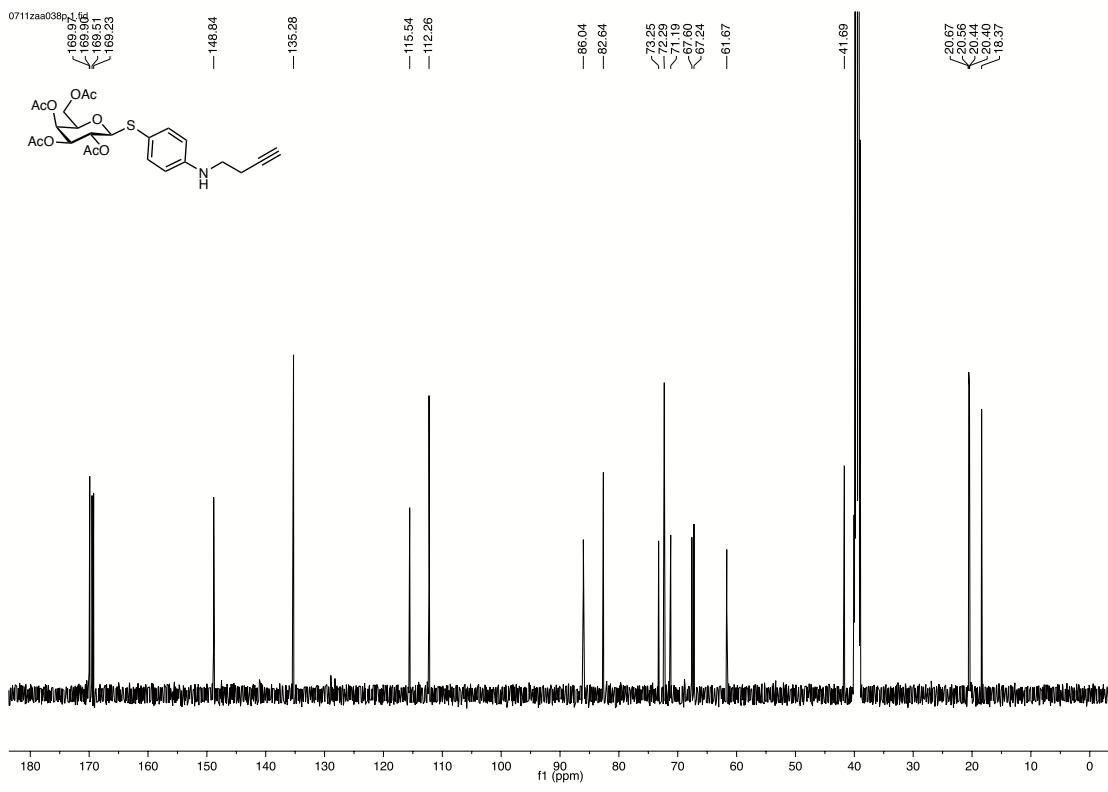
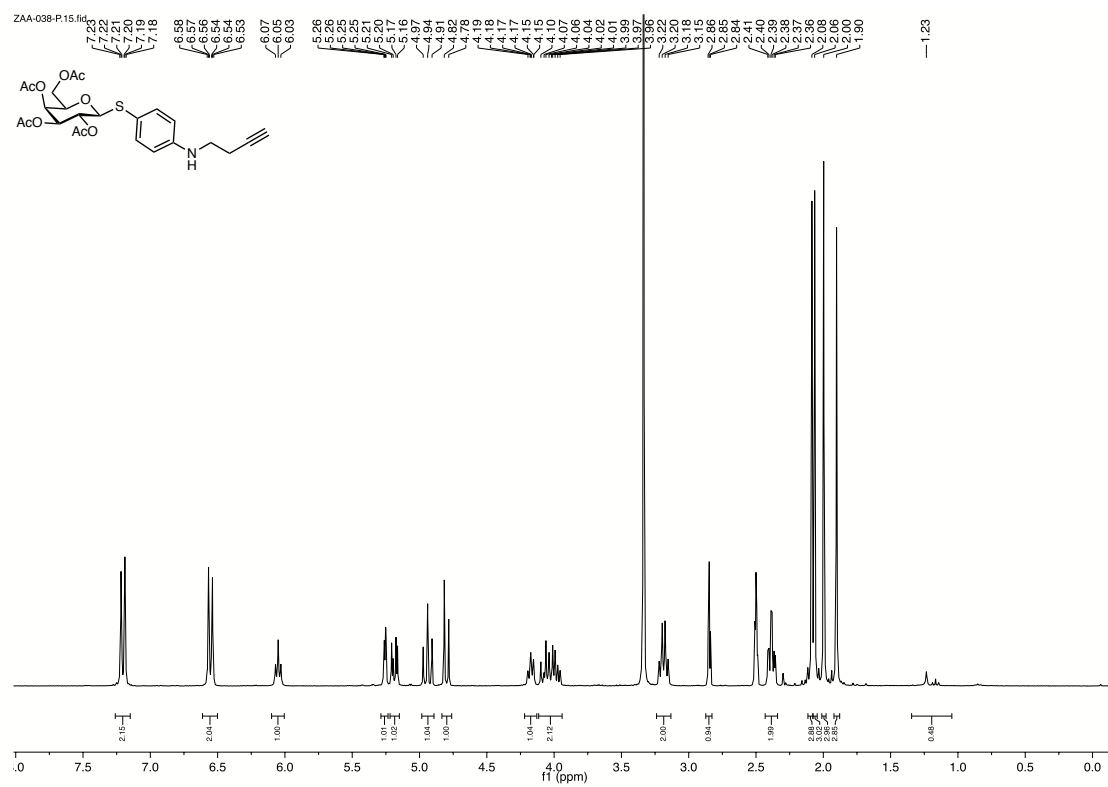
^1H and ^{13}C NMR of **5p**



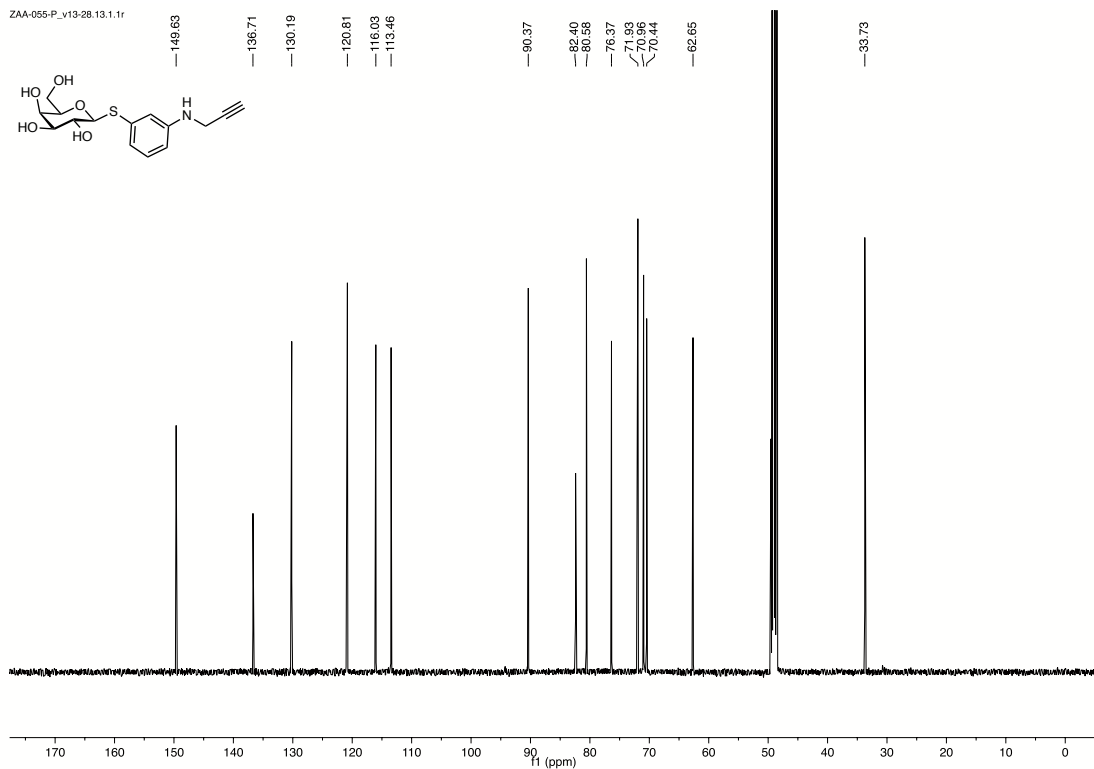
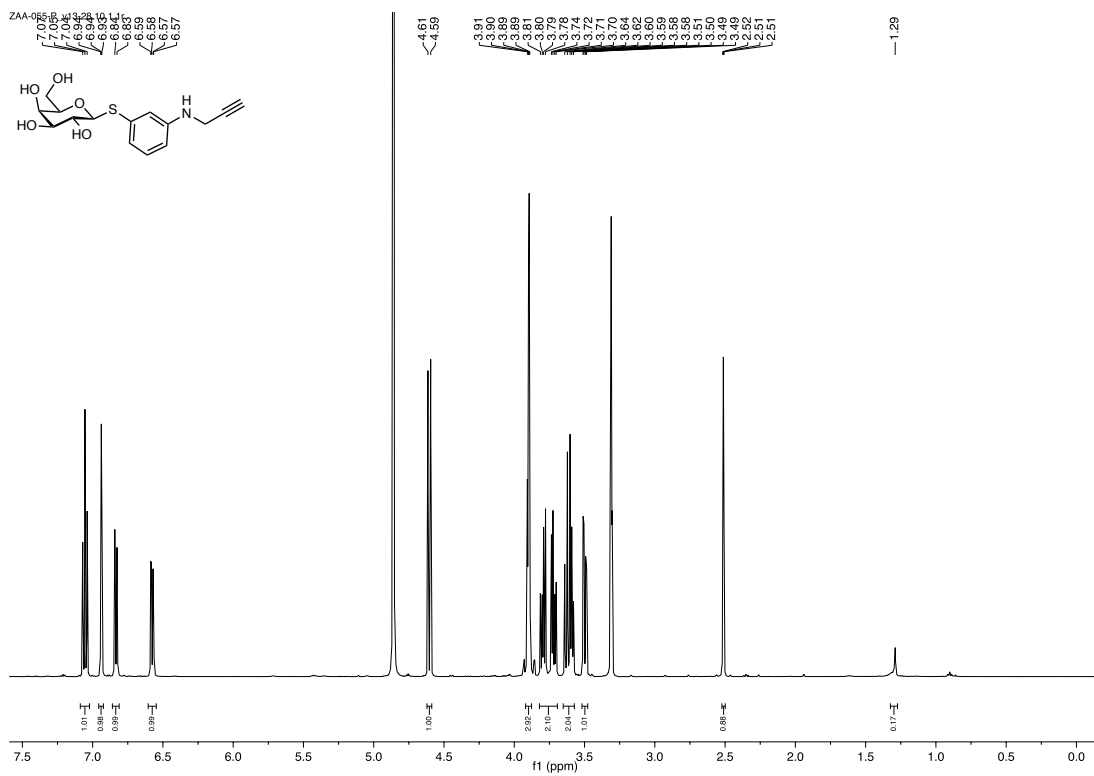
¹H and ¹³C NMR of **6p**



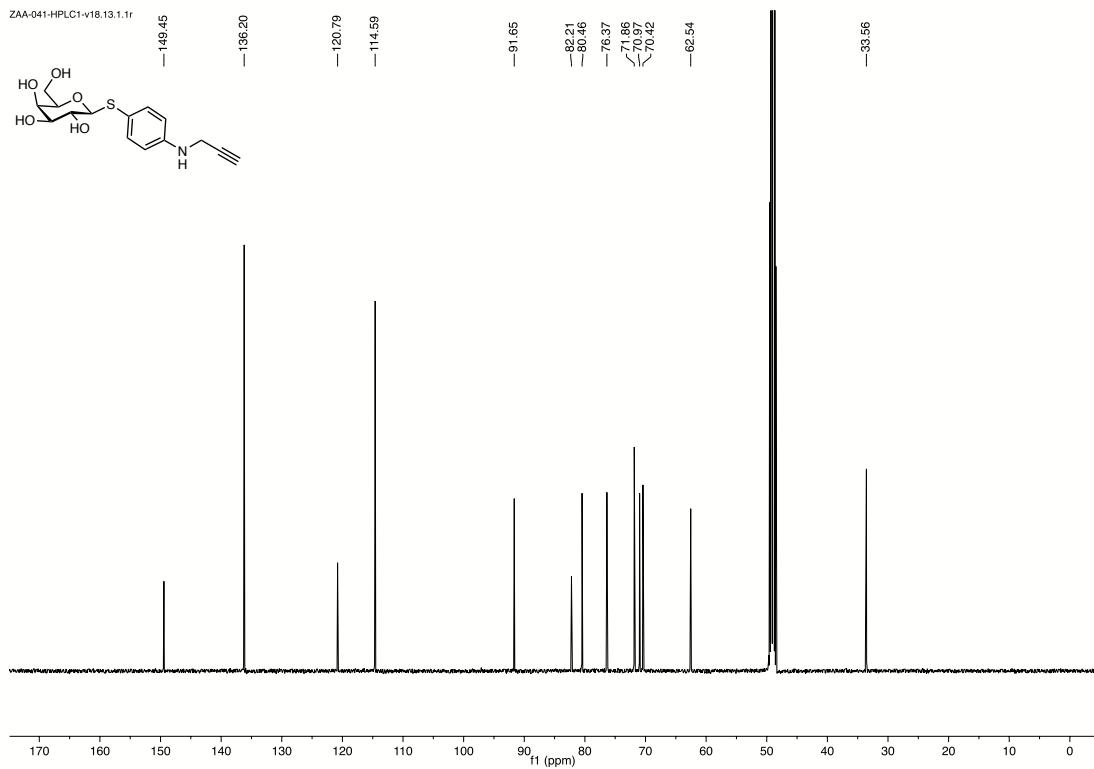
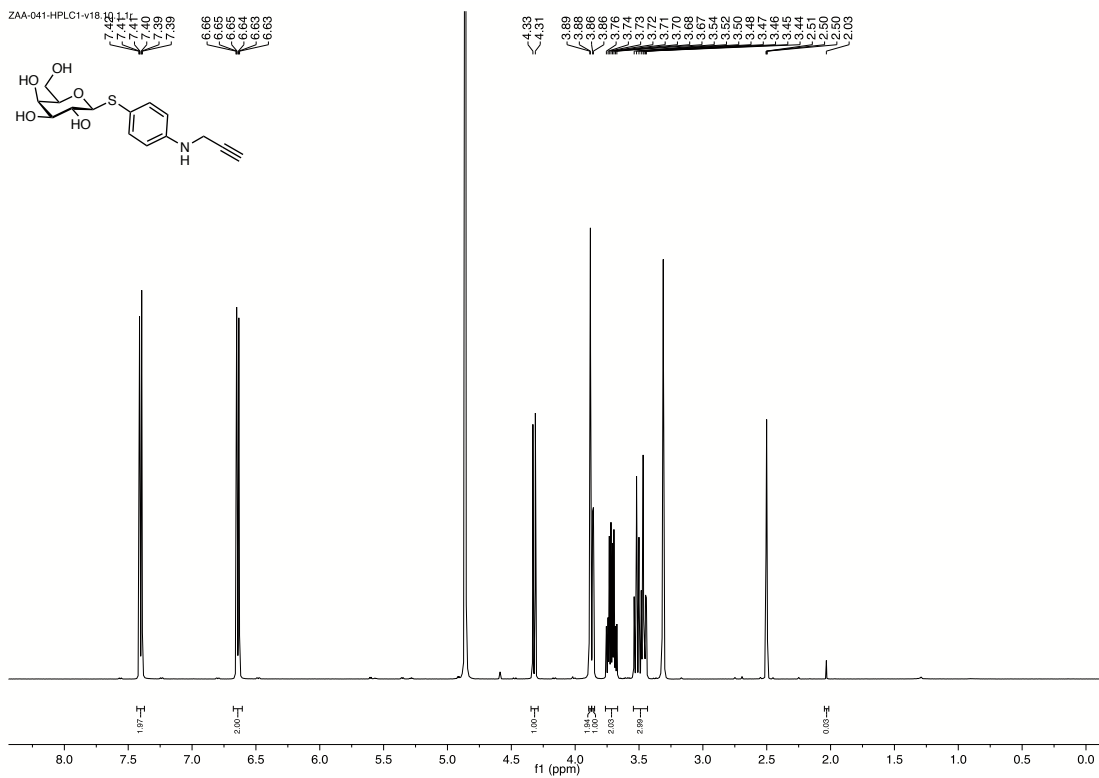
¹H and ¹³C NMR of **7m**



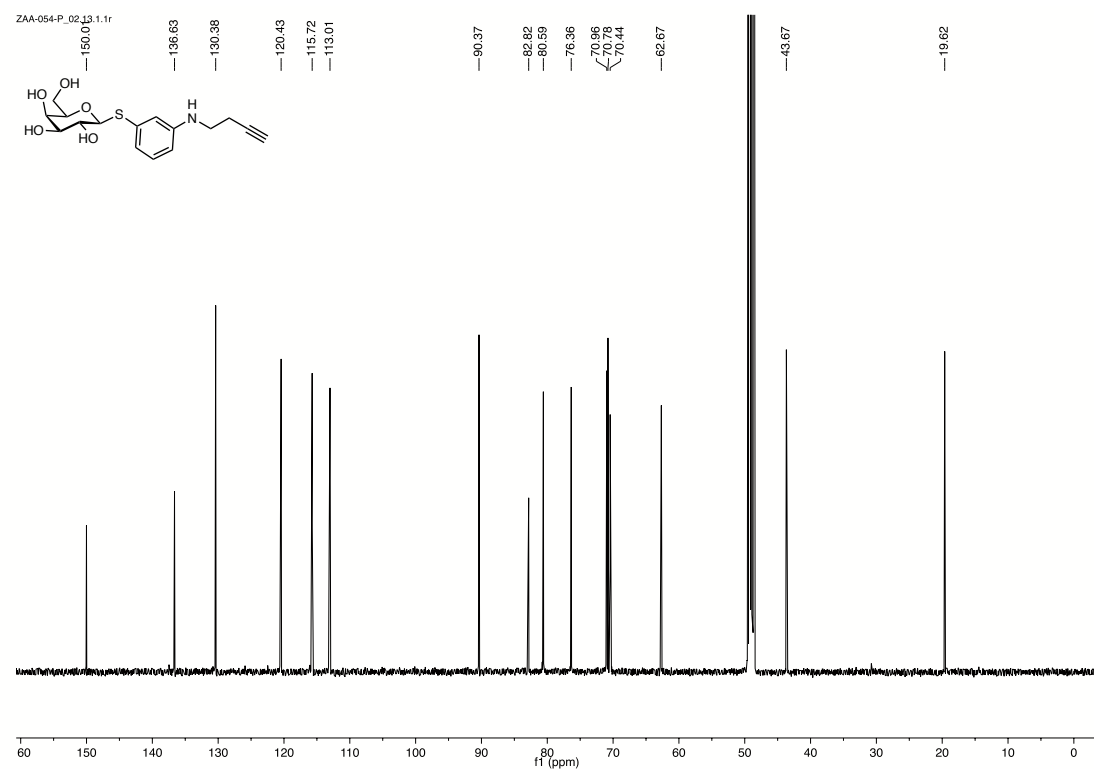
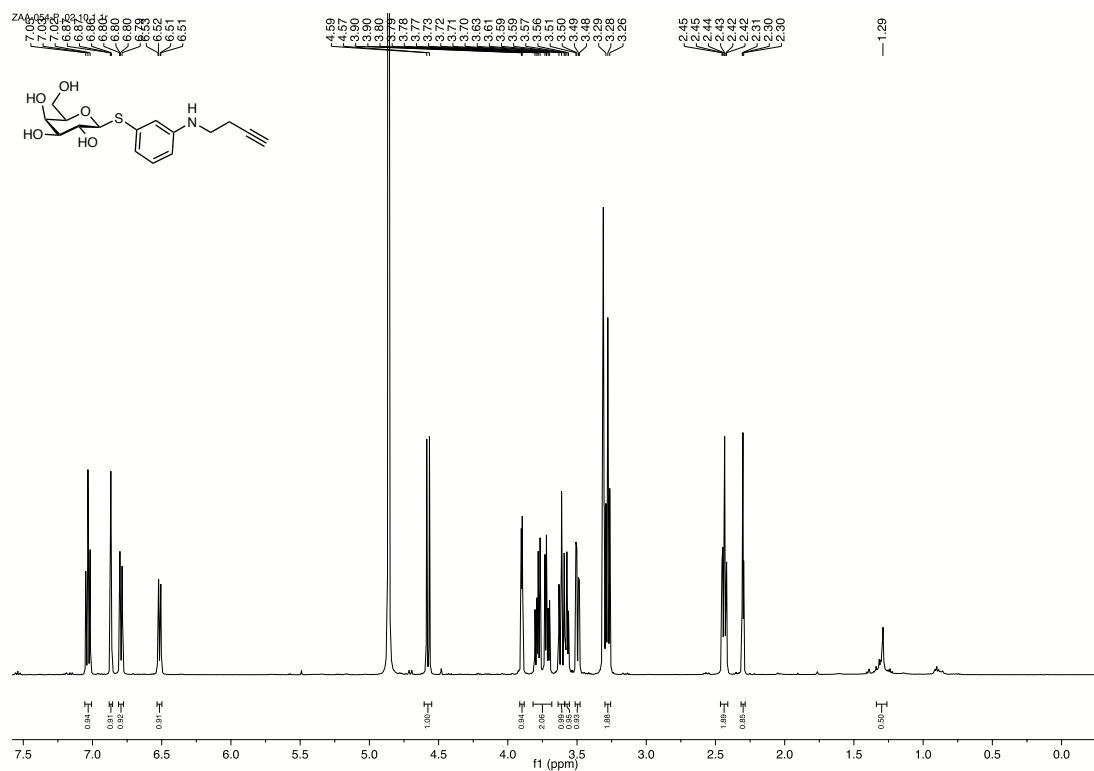
¹H and ¹³C NMR of **7p**



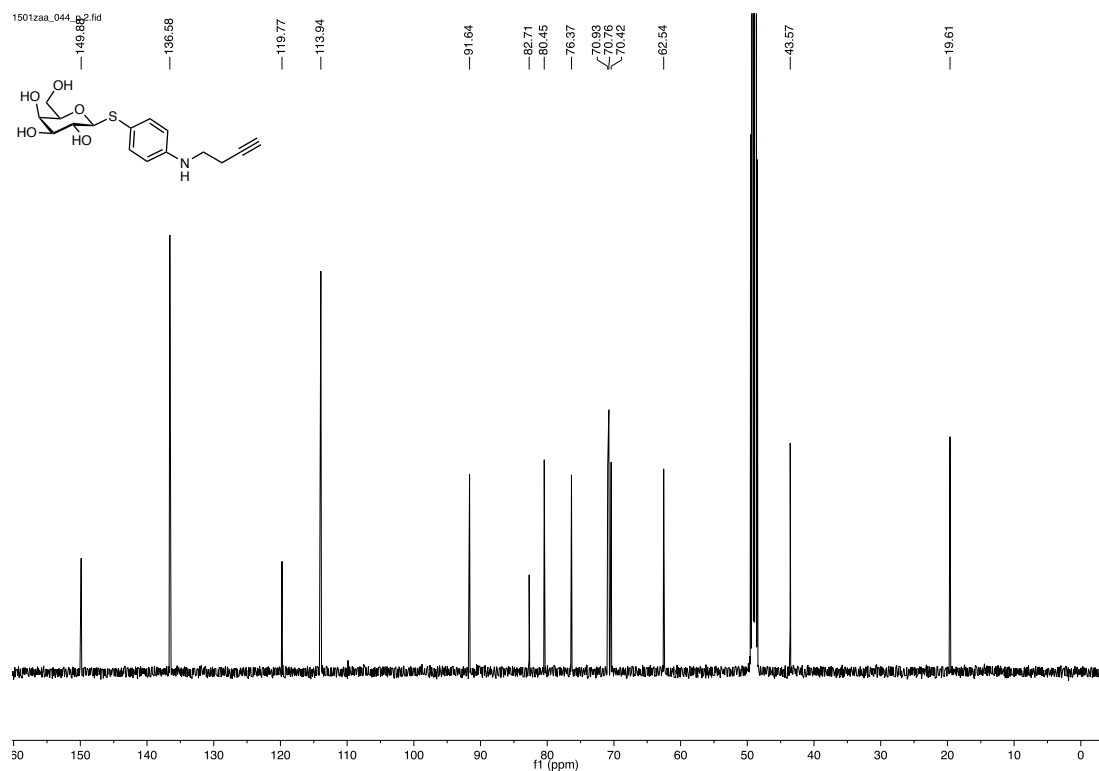
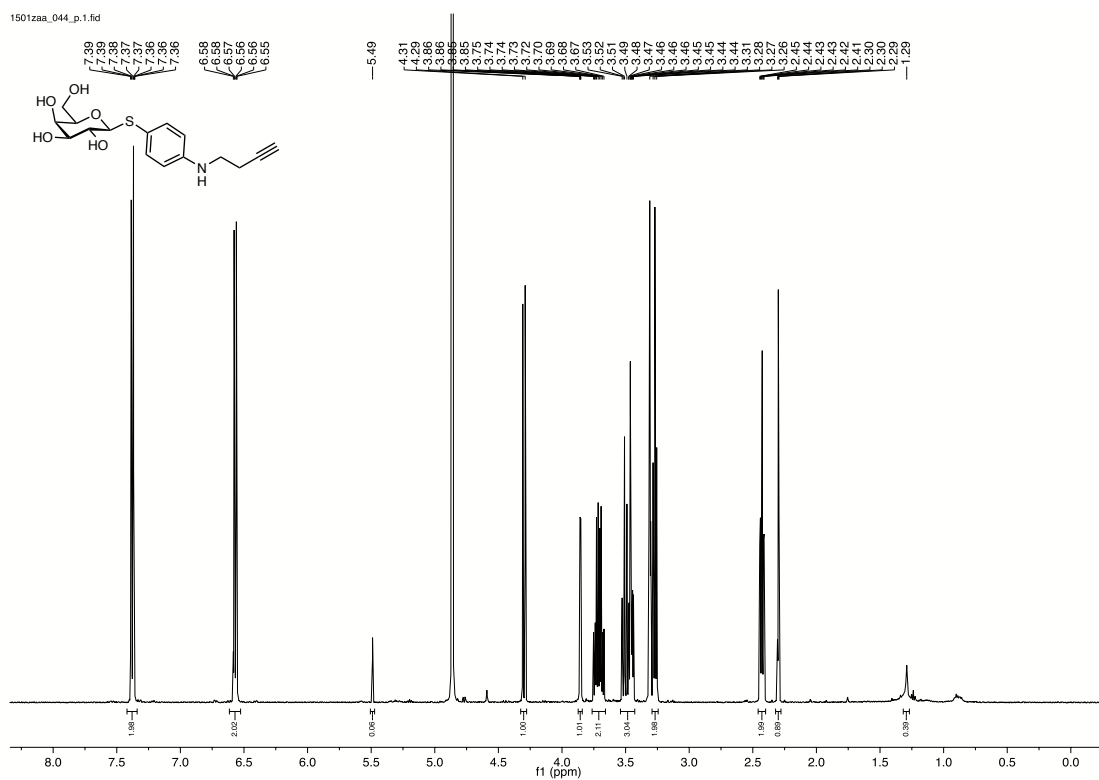
^1H and ^{13}C NMR of **8m**



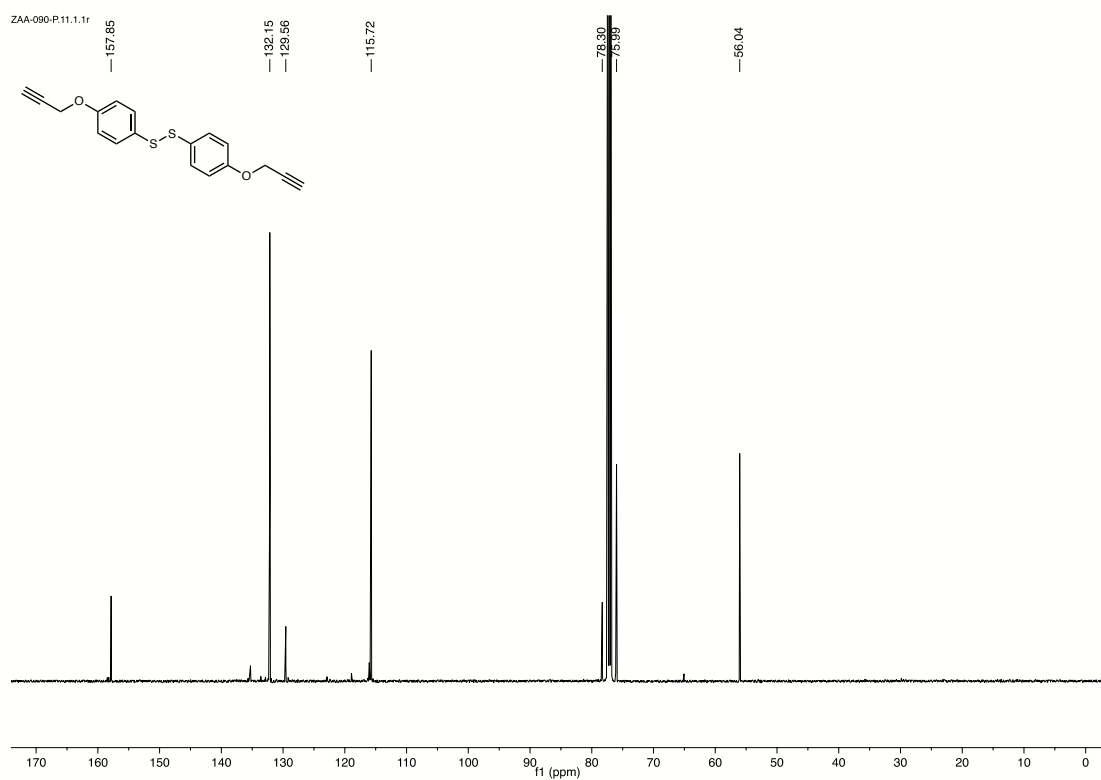
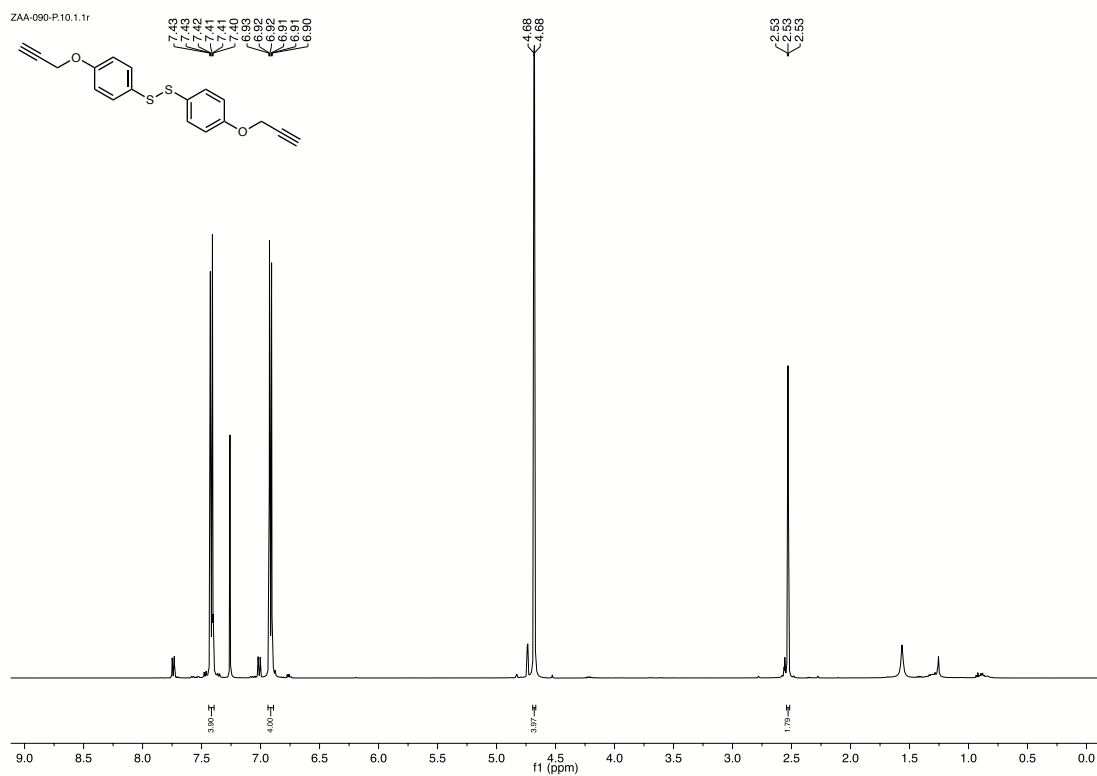
^1H and ^{13}C NMR of **8p**



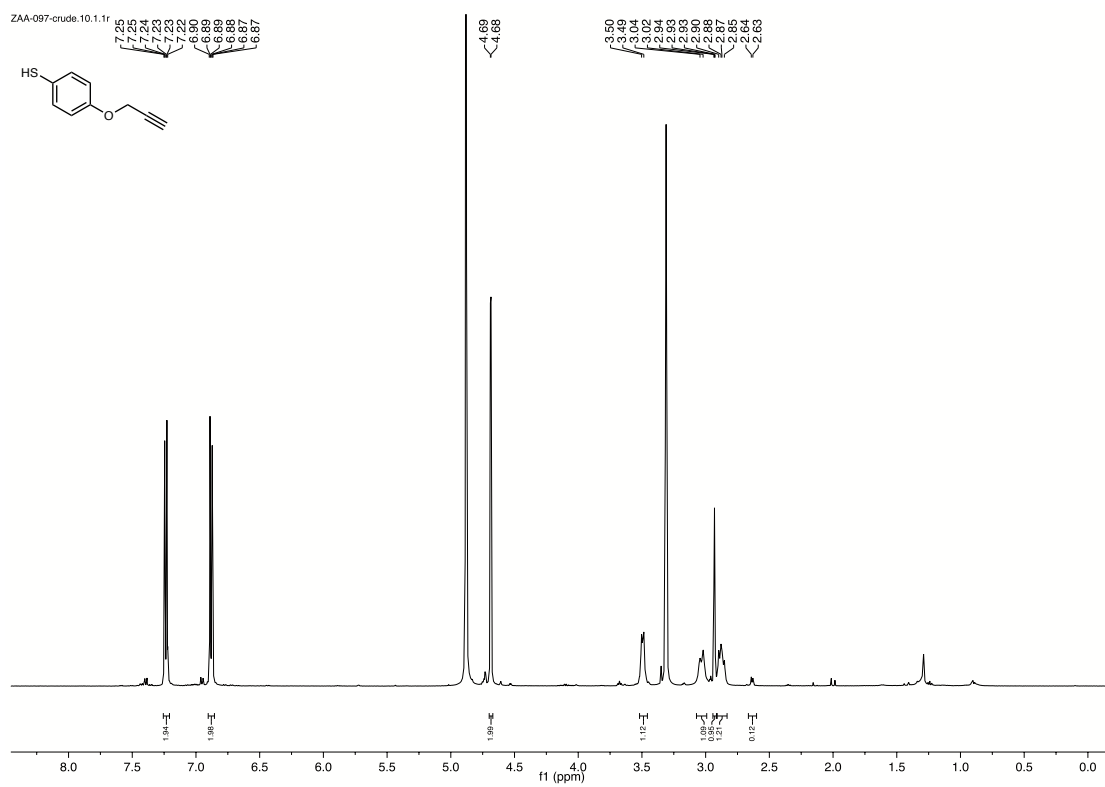
^1H and ^{13}C NMR of **9m**



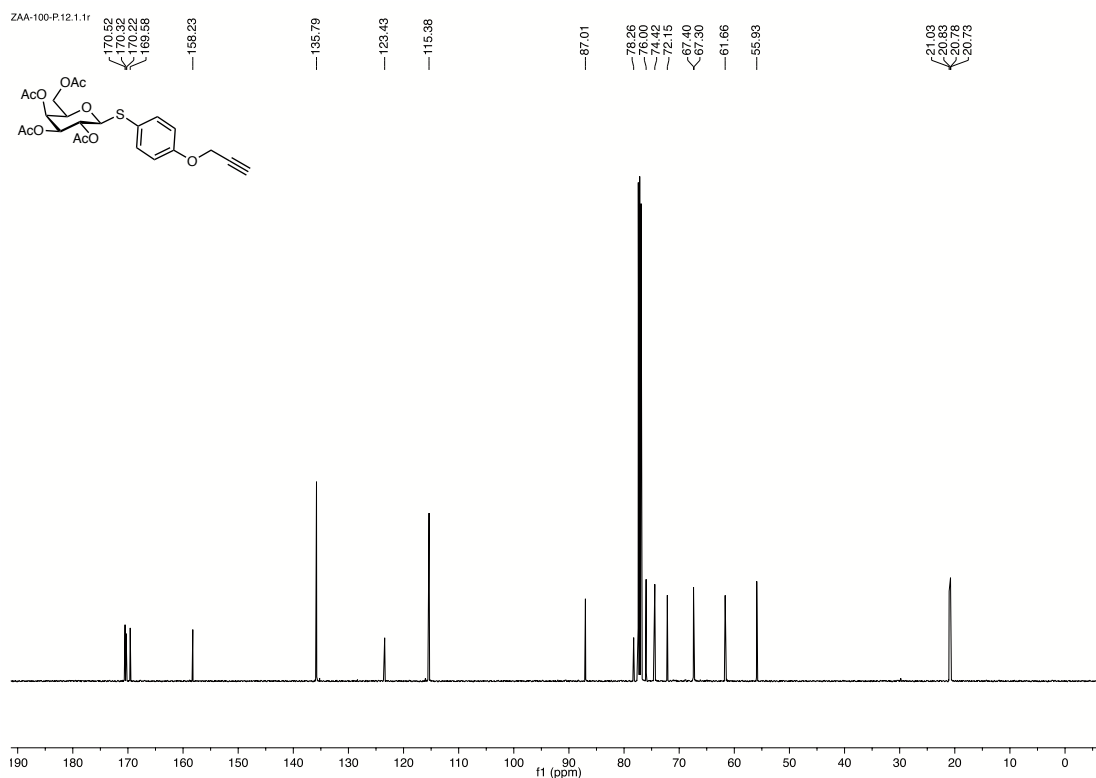
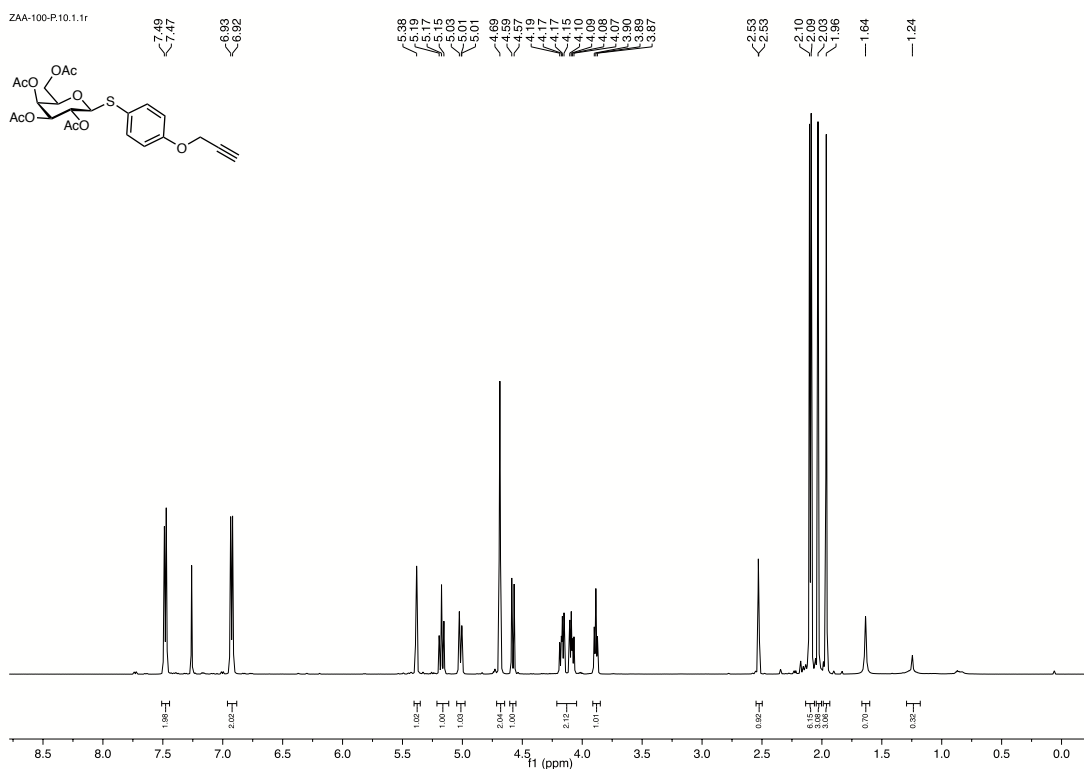
^1H and ^{13}C NMR of **9p**



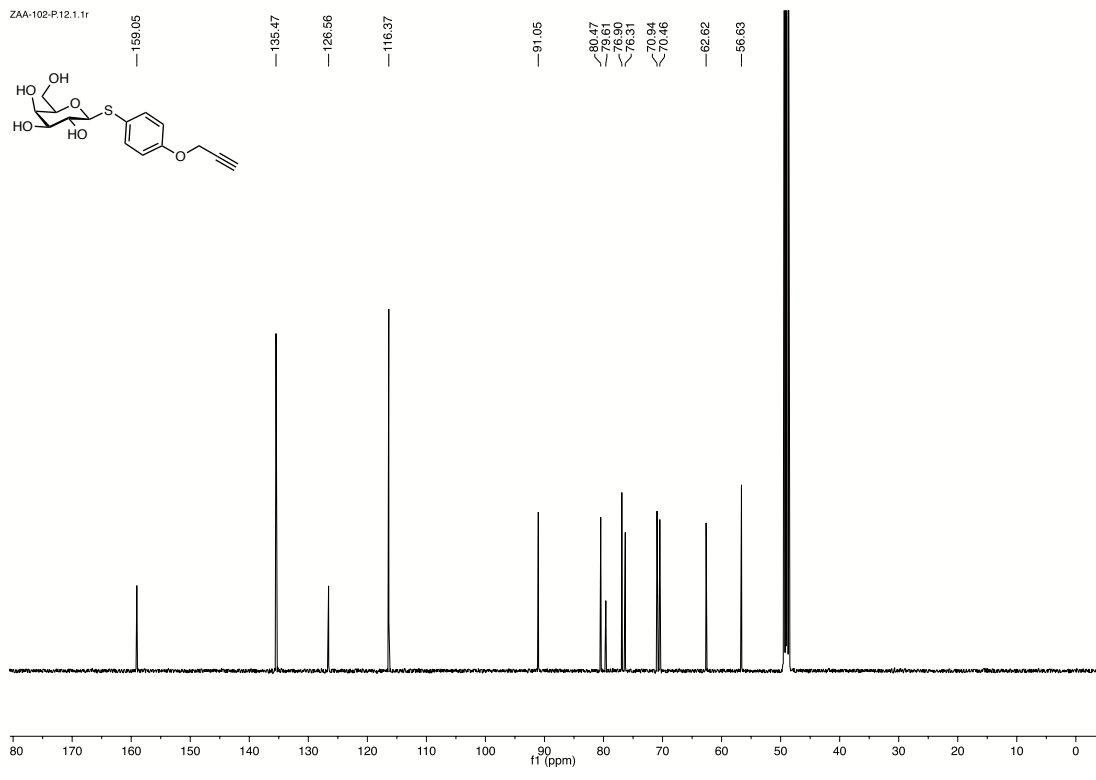
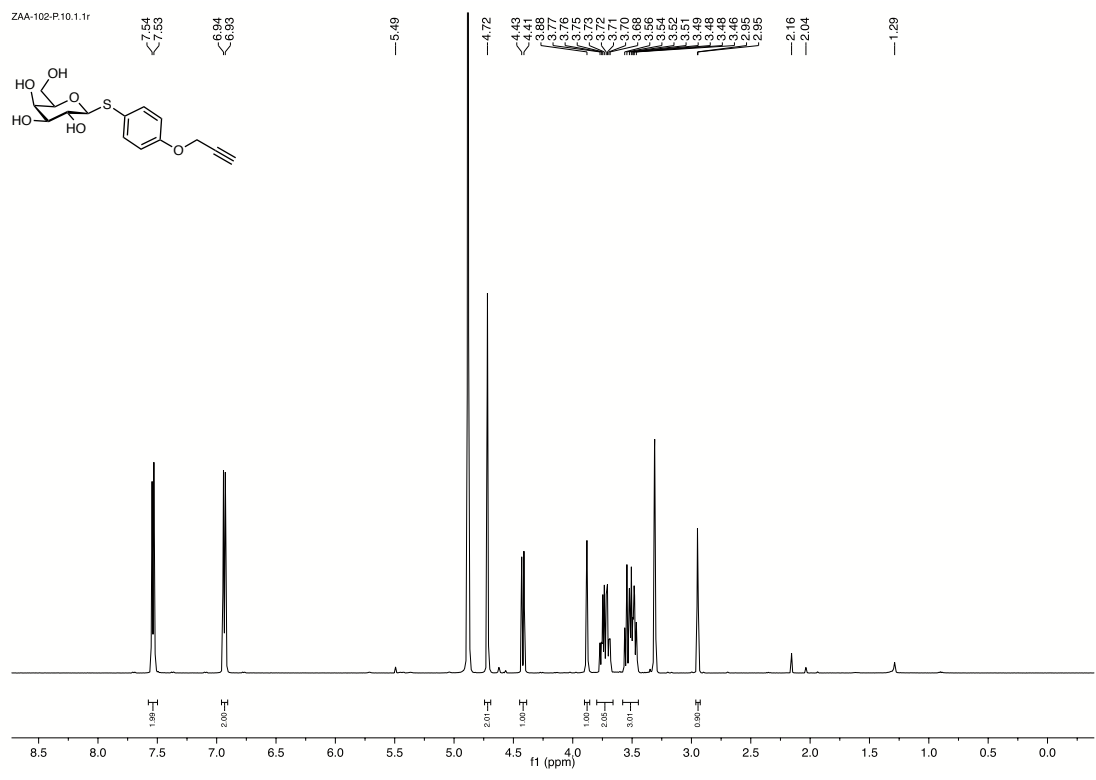
^1H and ^{13}C NMR of **11**



^1H of **12** (crude, impure)

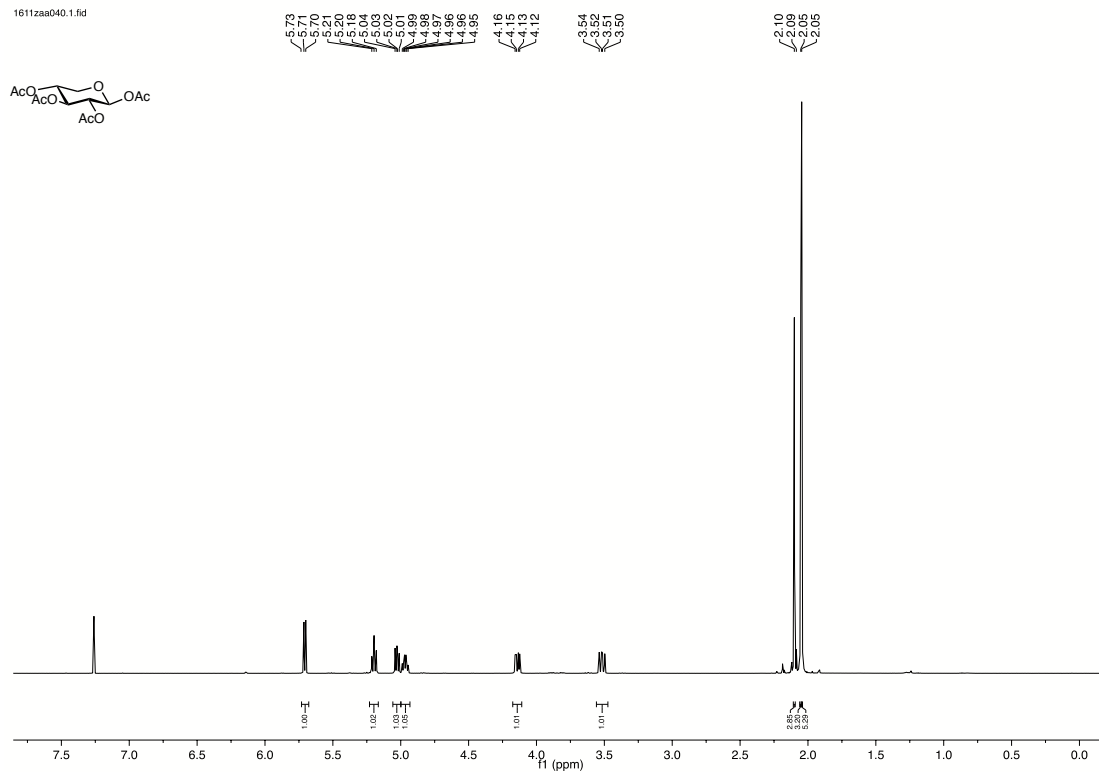


^1H and ^{13}C NMR of **13**

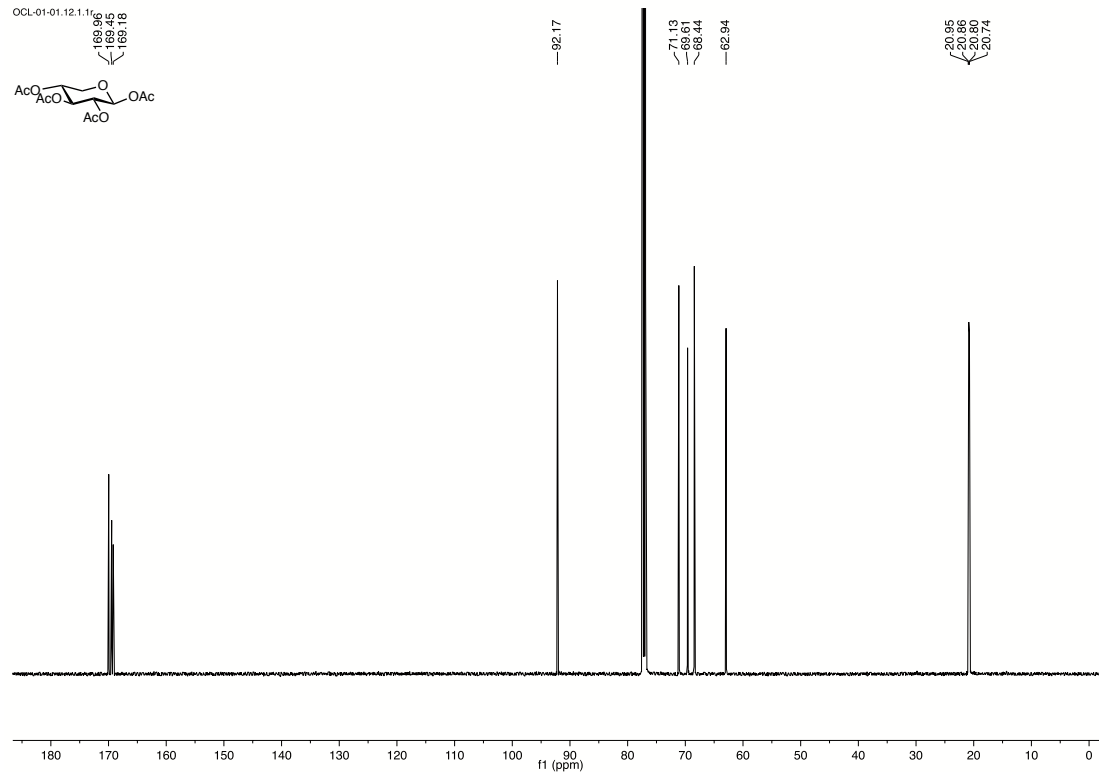


^1H and ^{13}C NMR of **14**

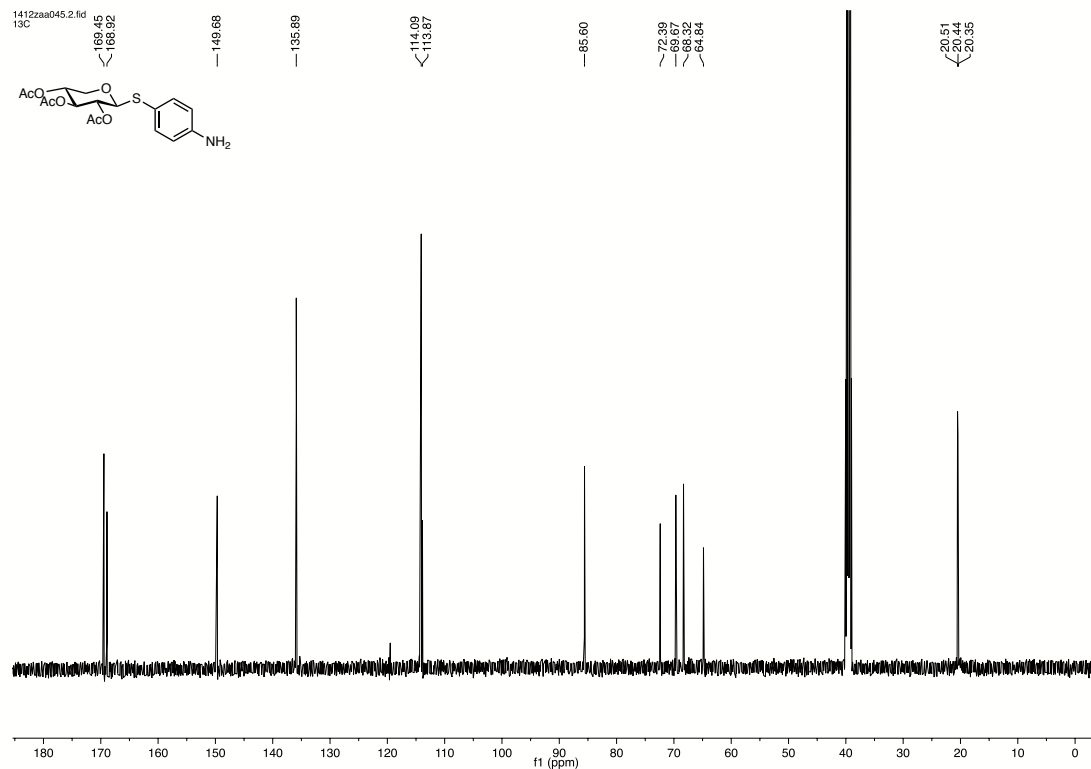
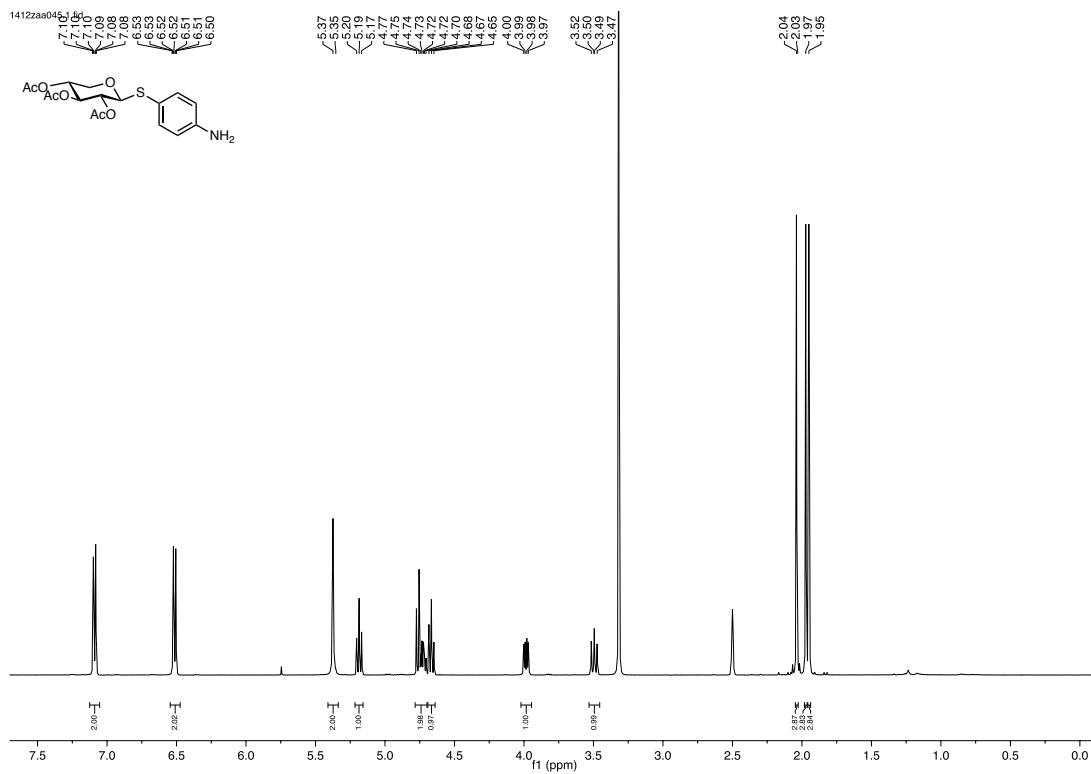
16112aa040.1.fid



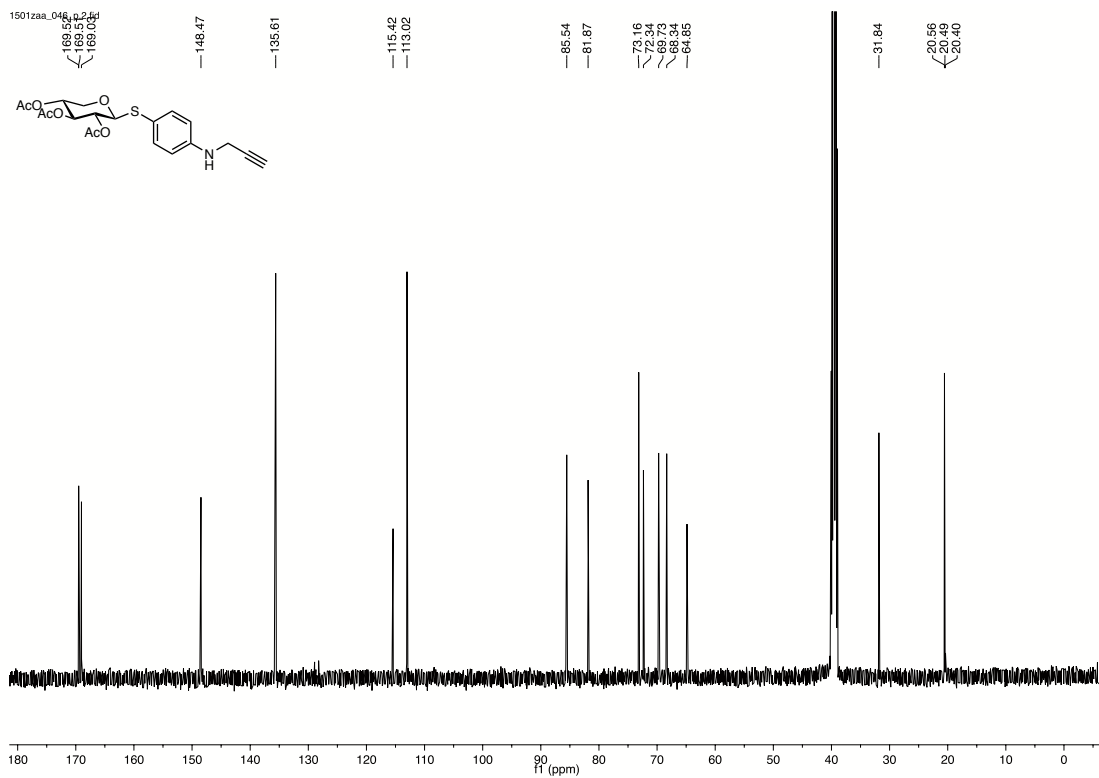
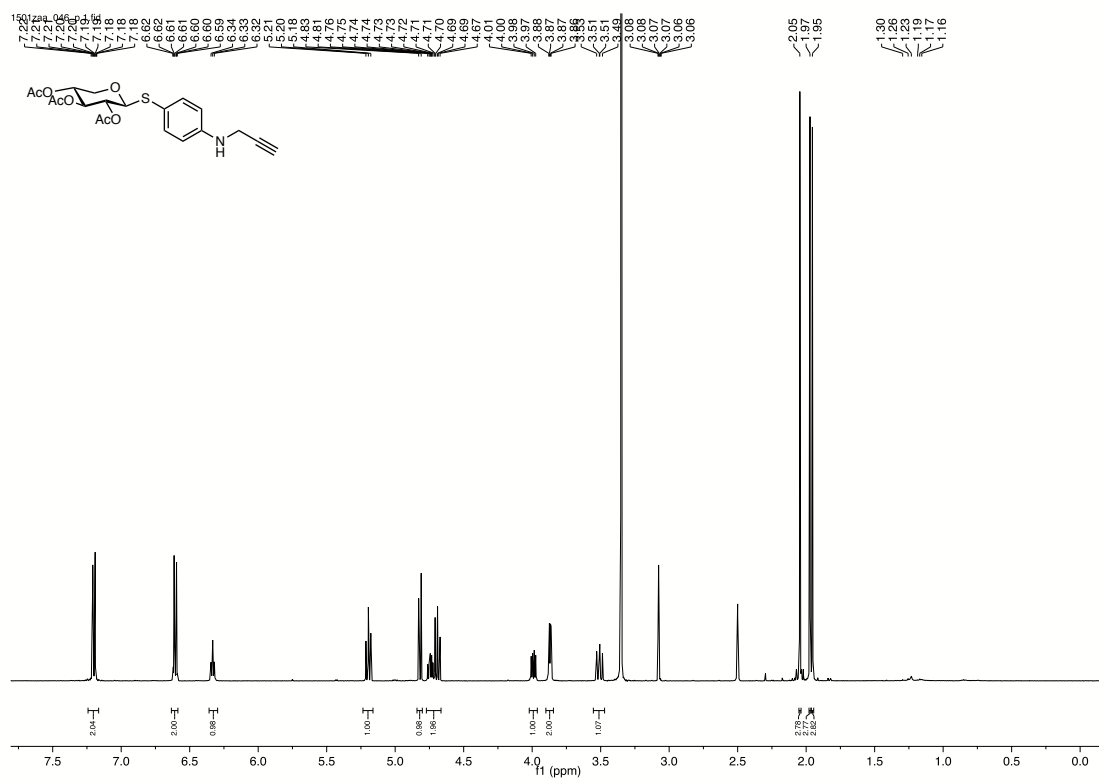
OCL-01-01.12.1-1.fid



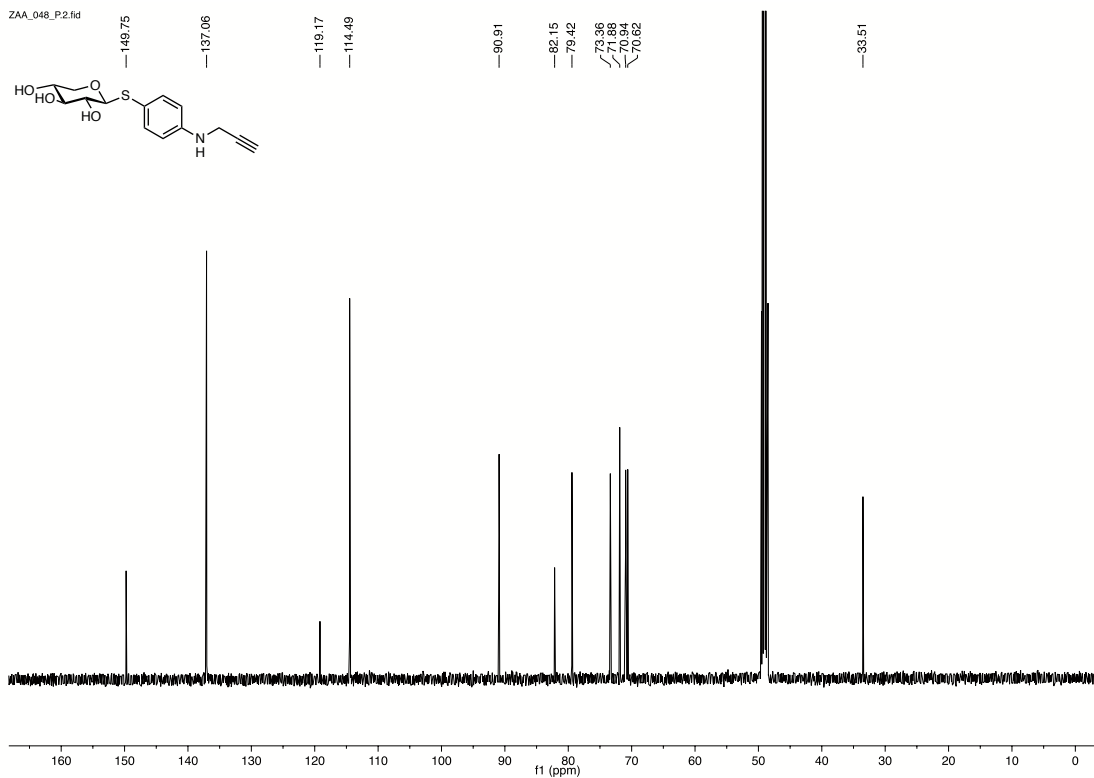
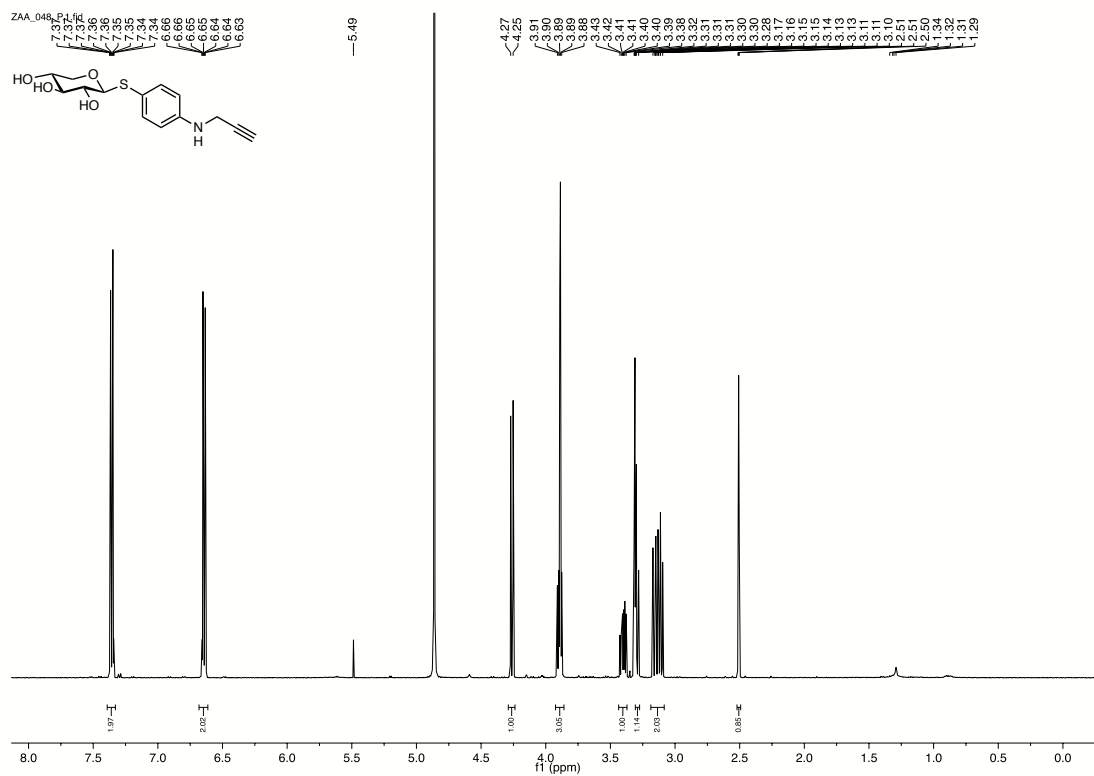
^1H and ^{13}C NMR of **15**



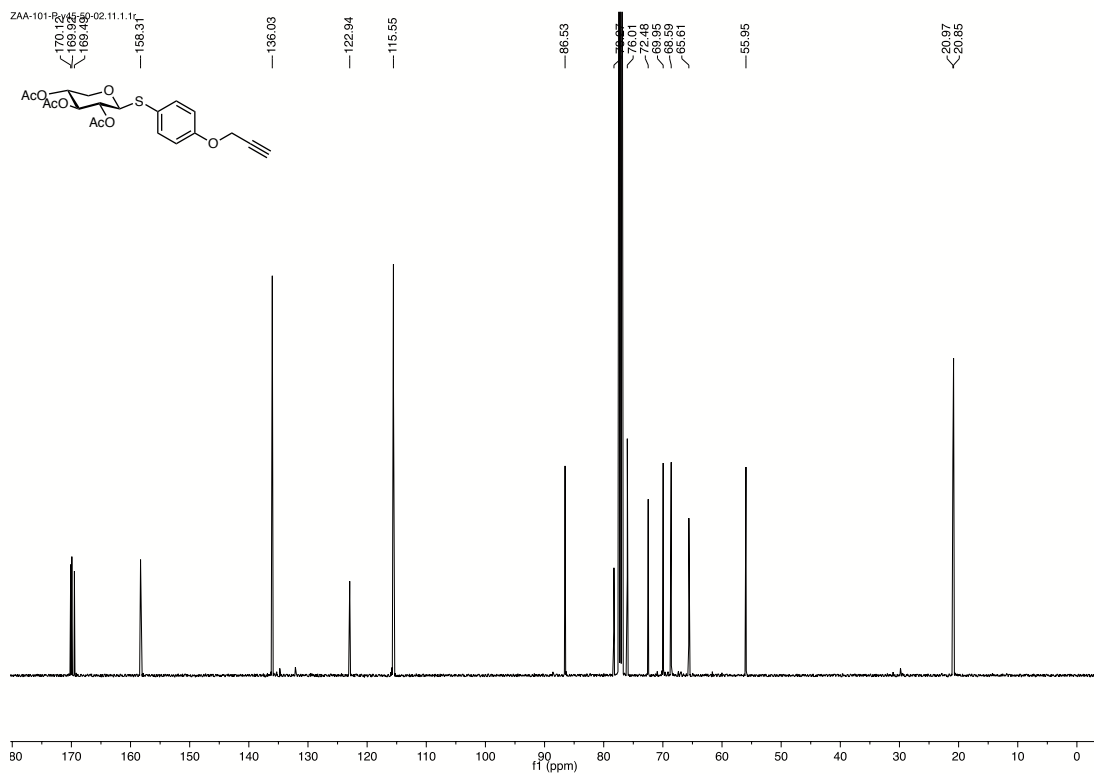
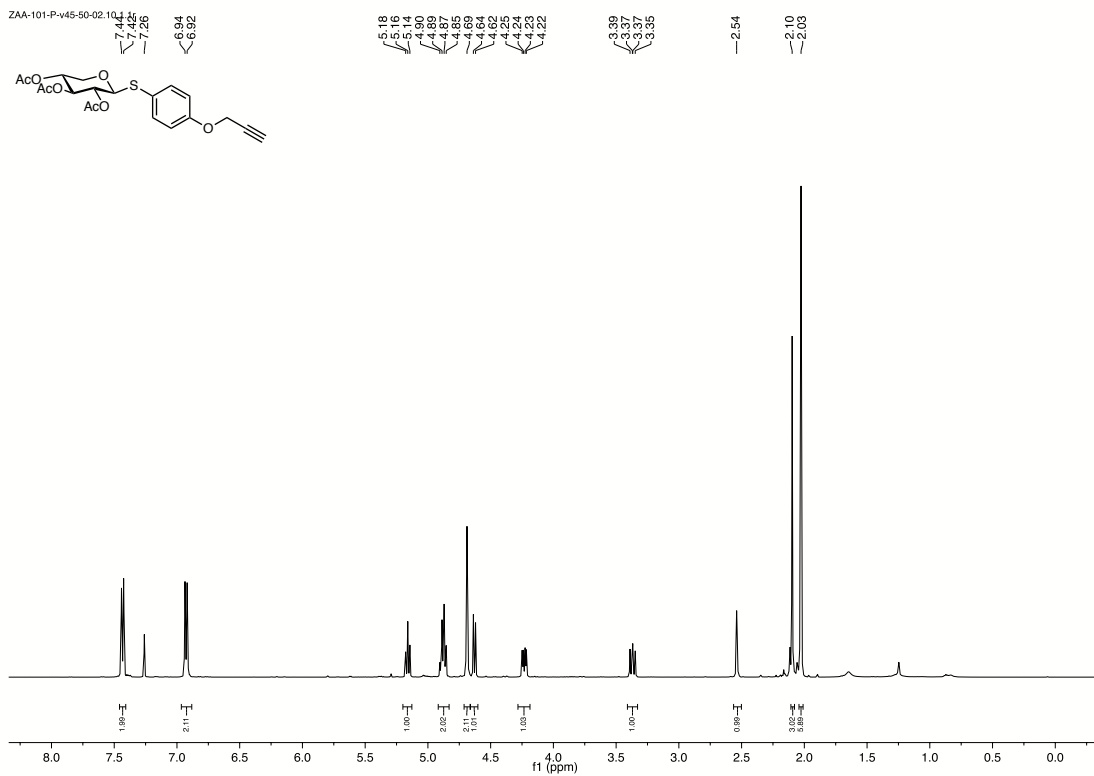
^1H and ^{13}C NMR of 17



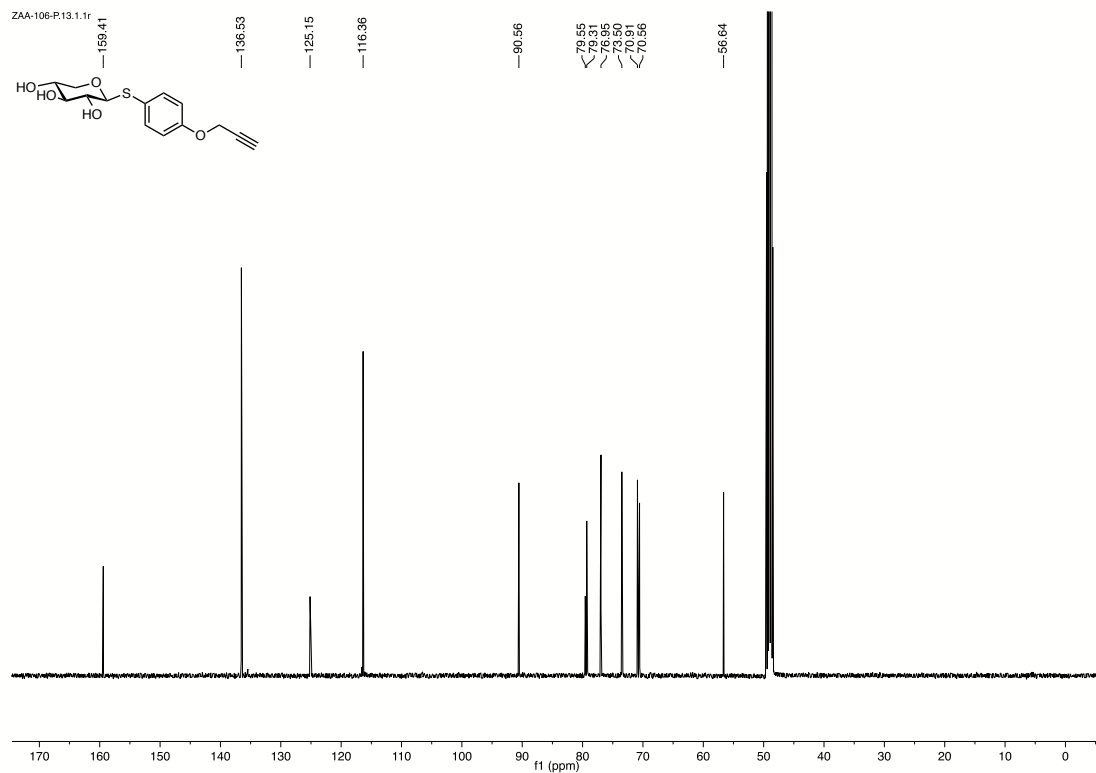
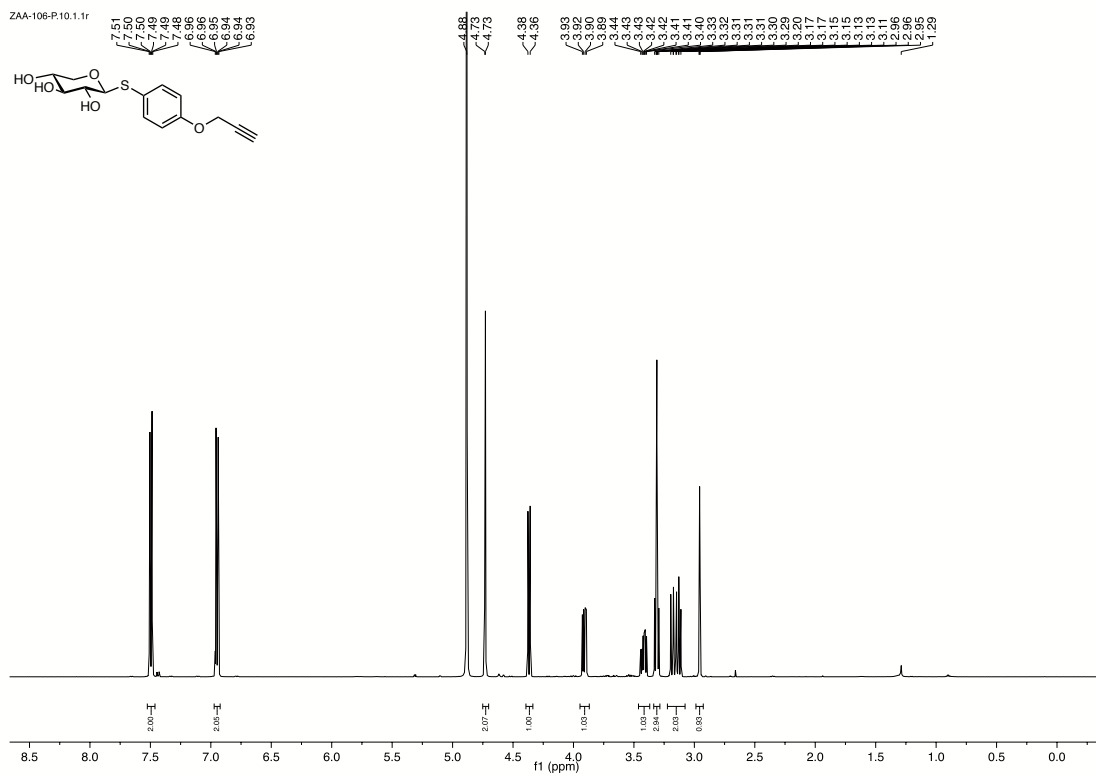
^1H and ^{13}C NMR of 18



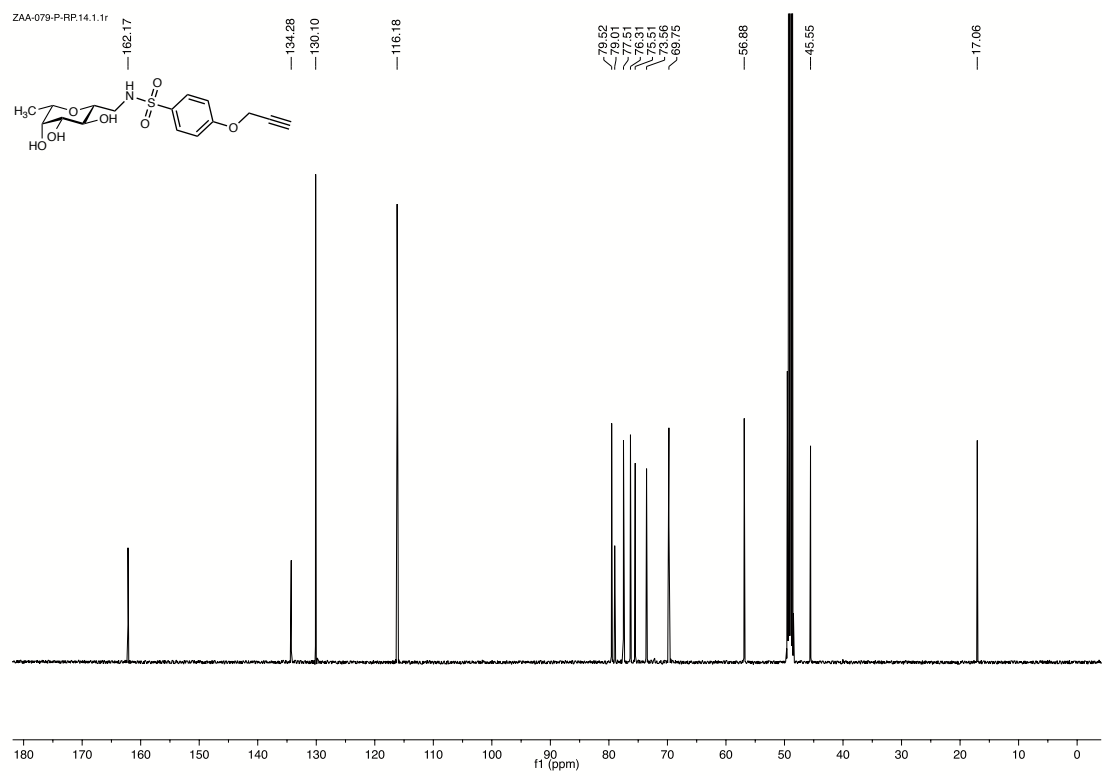
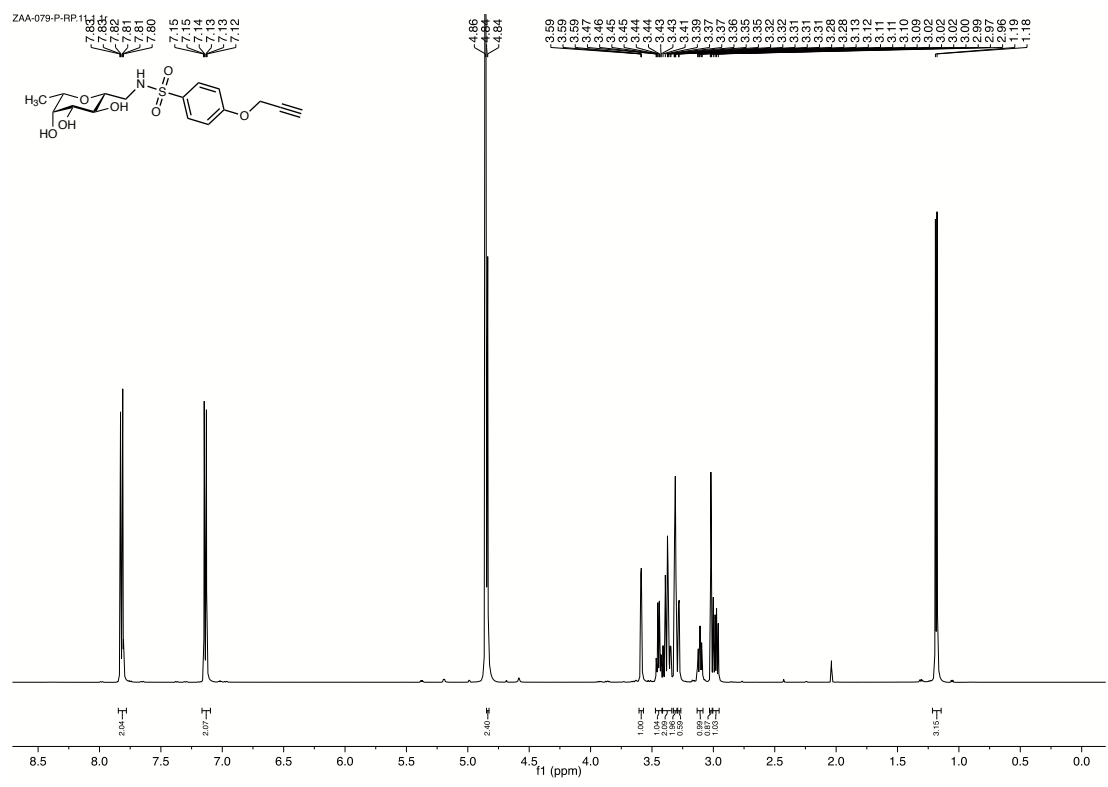
^1H and ^{13}C NMR of **19**



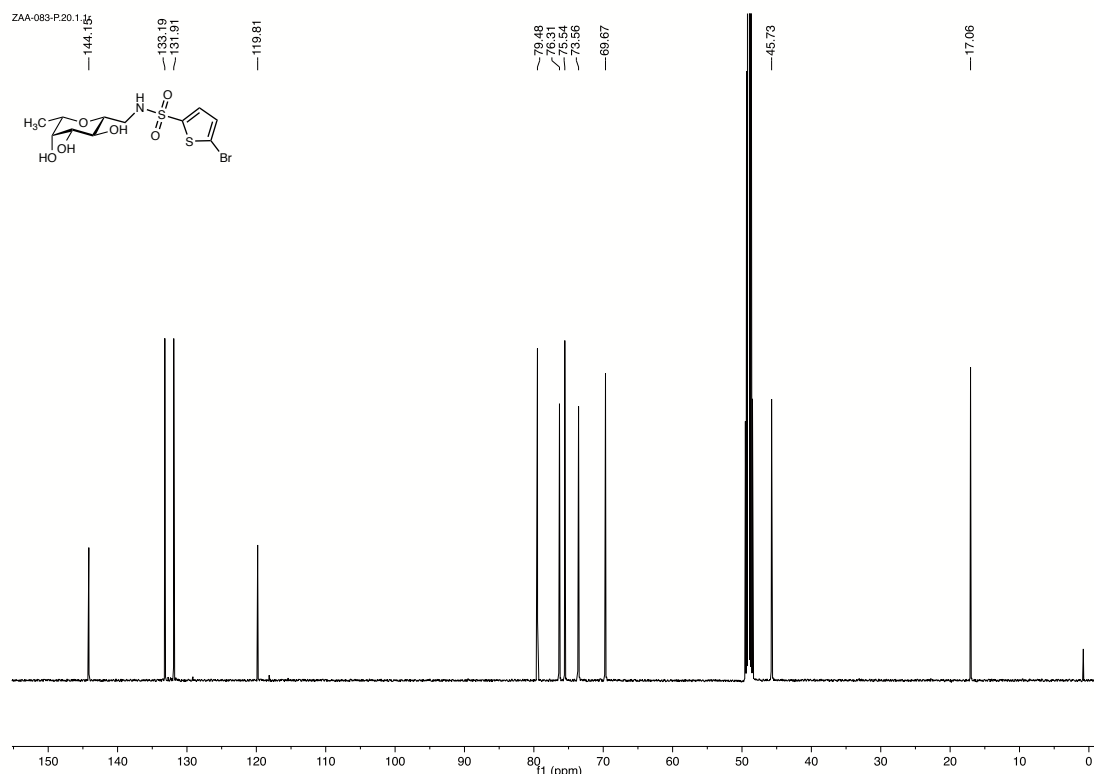
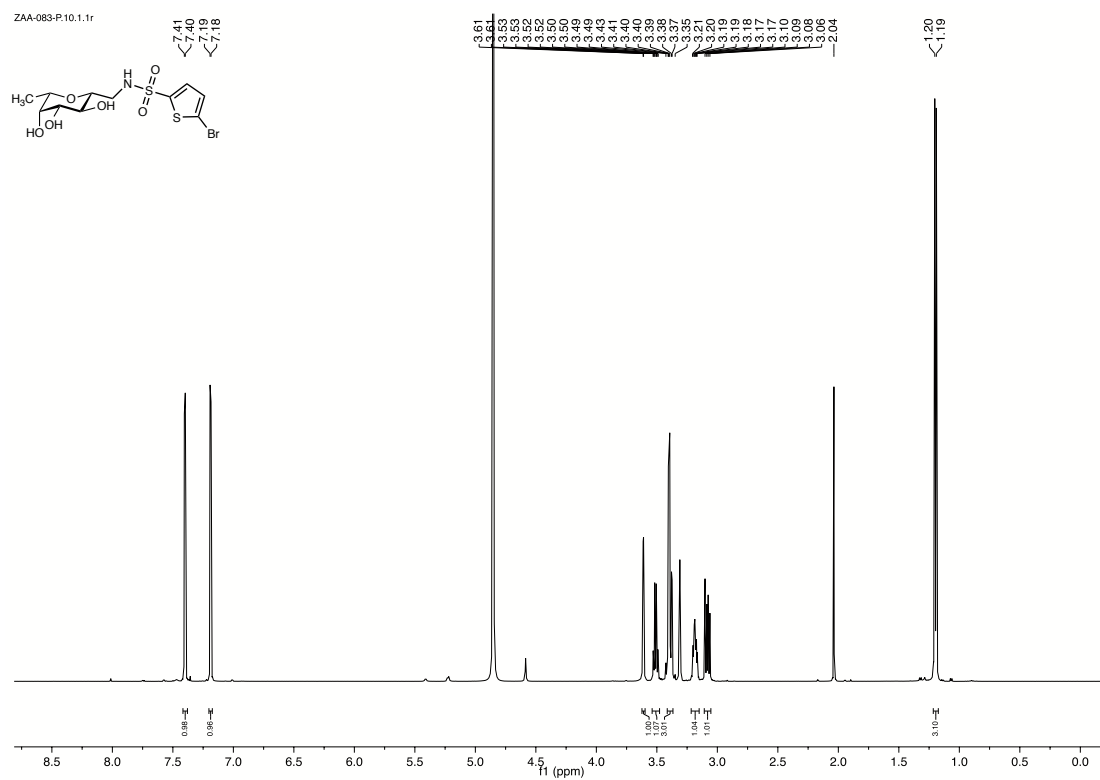
^1H and ^{13}C NMR of **20**



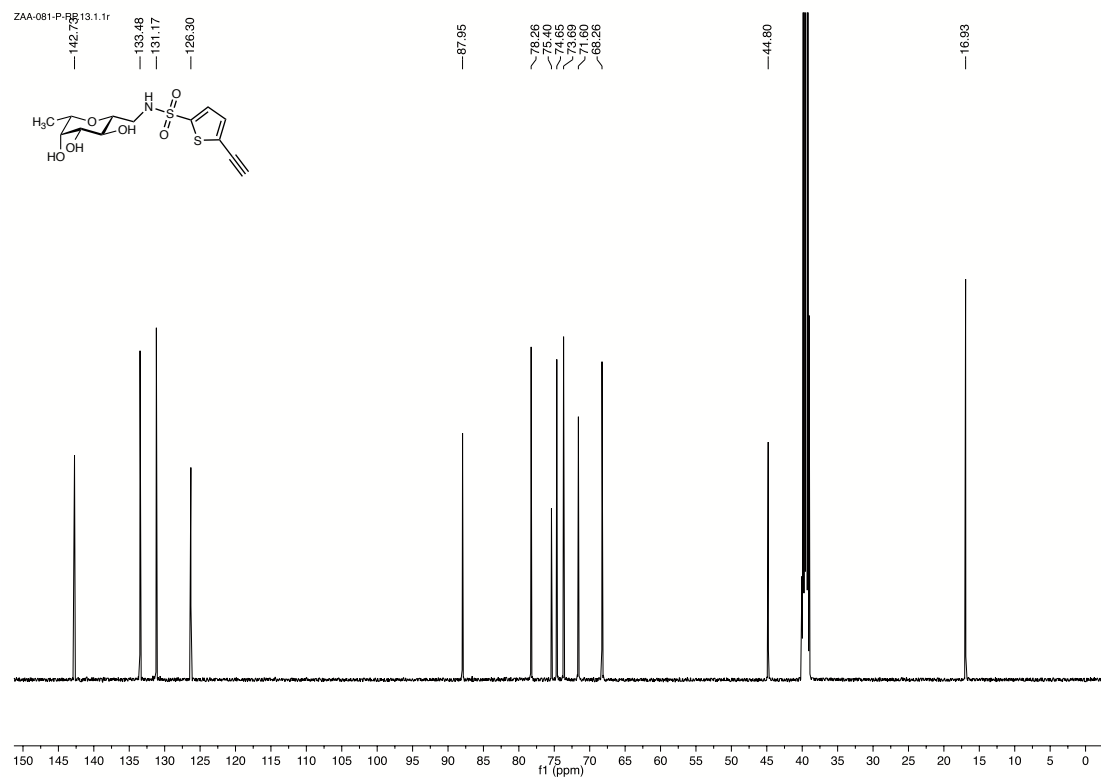
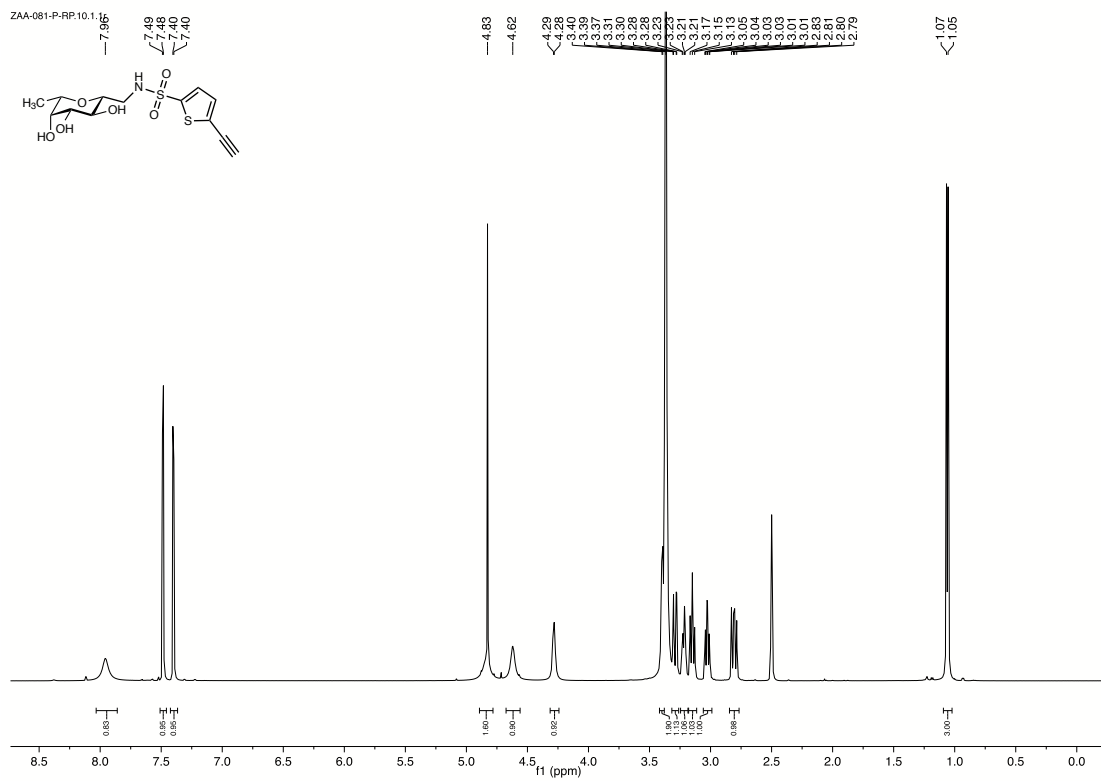
^1H and ^{13}C NMR of **21**



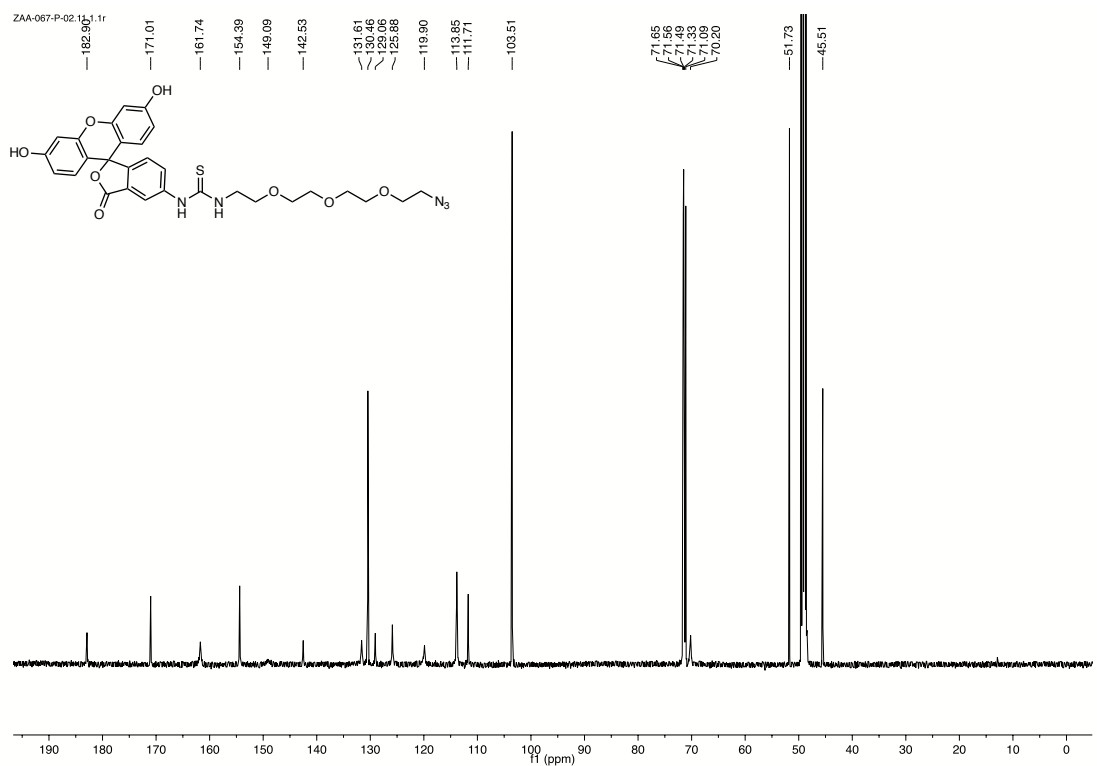
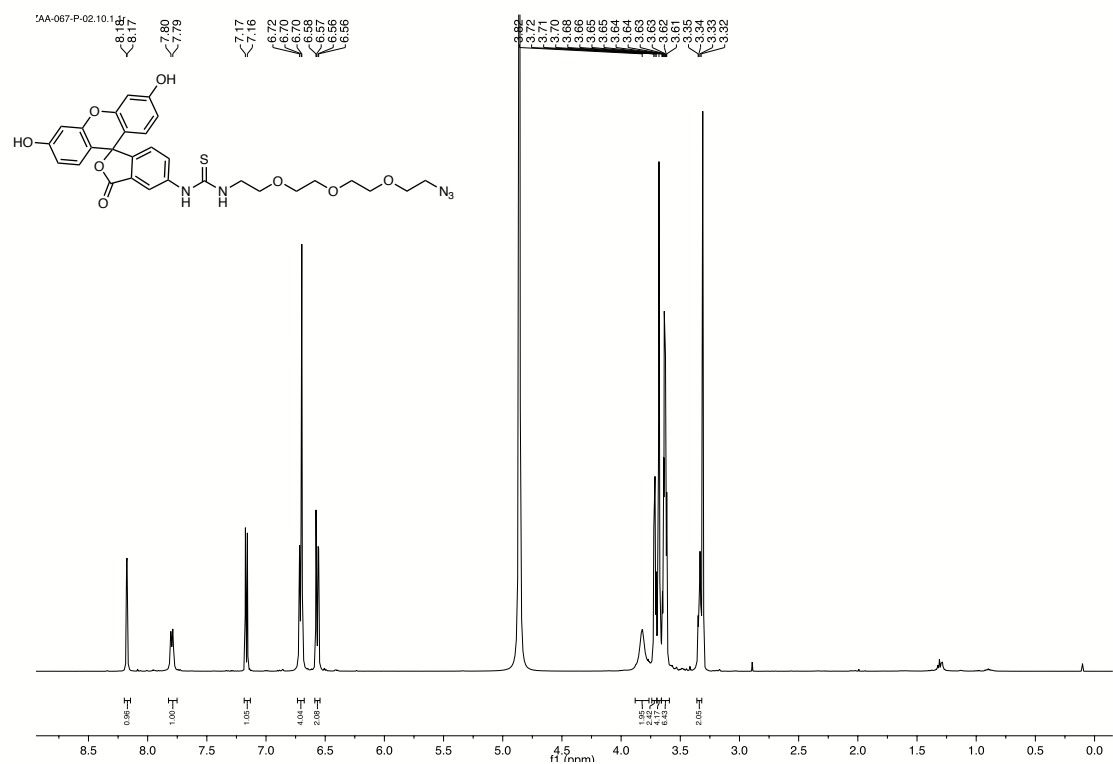
¹H and ¹³C NMR of 25



^1H and ^{13}C NMR of **26**

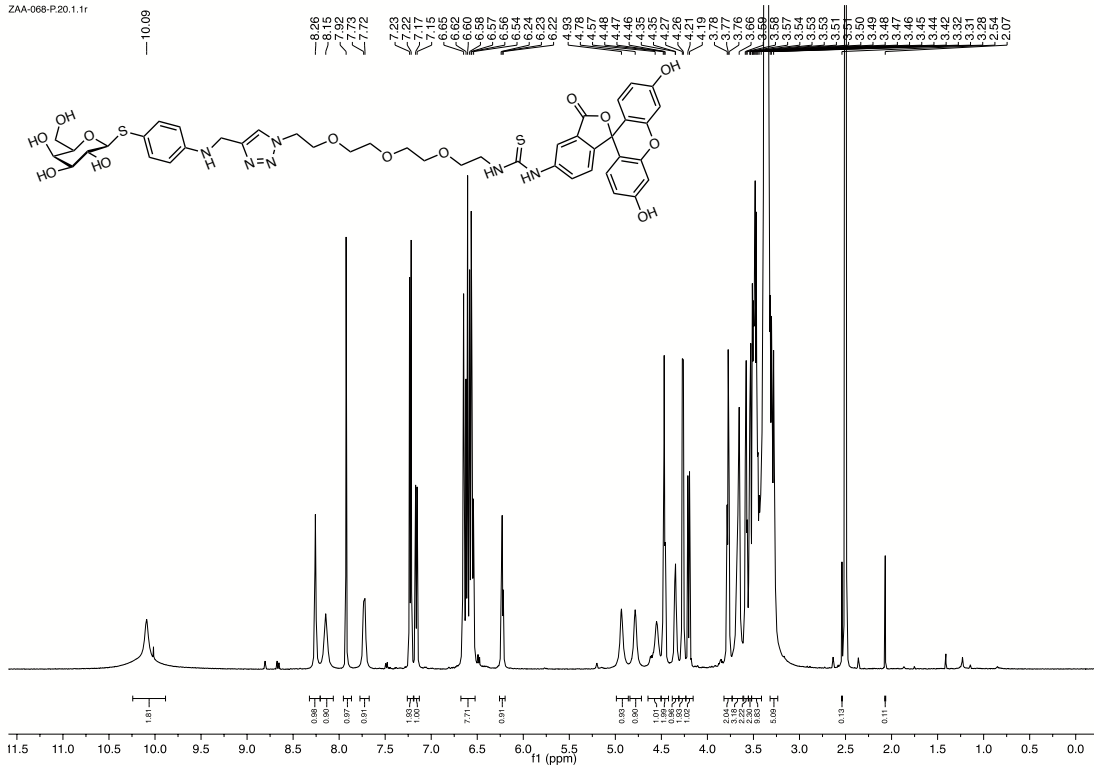


^1H and ^{13}C NMR of **27**

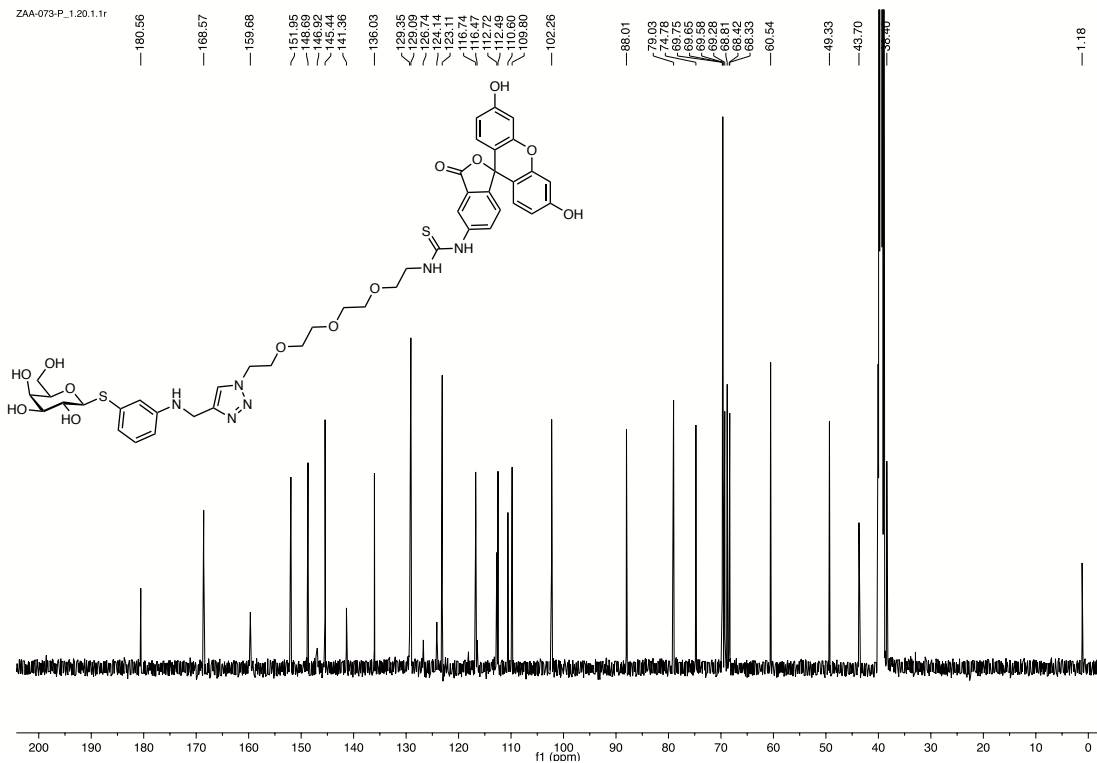


^1H and ^{13}C NMR of **29**

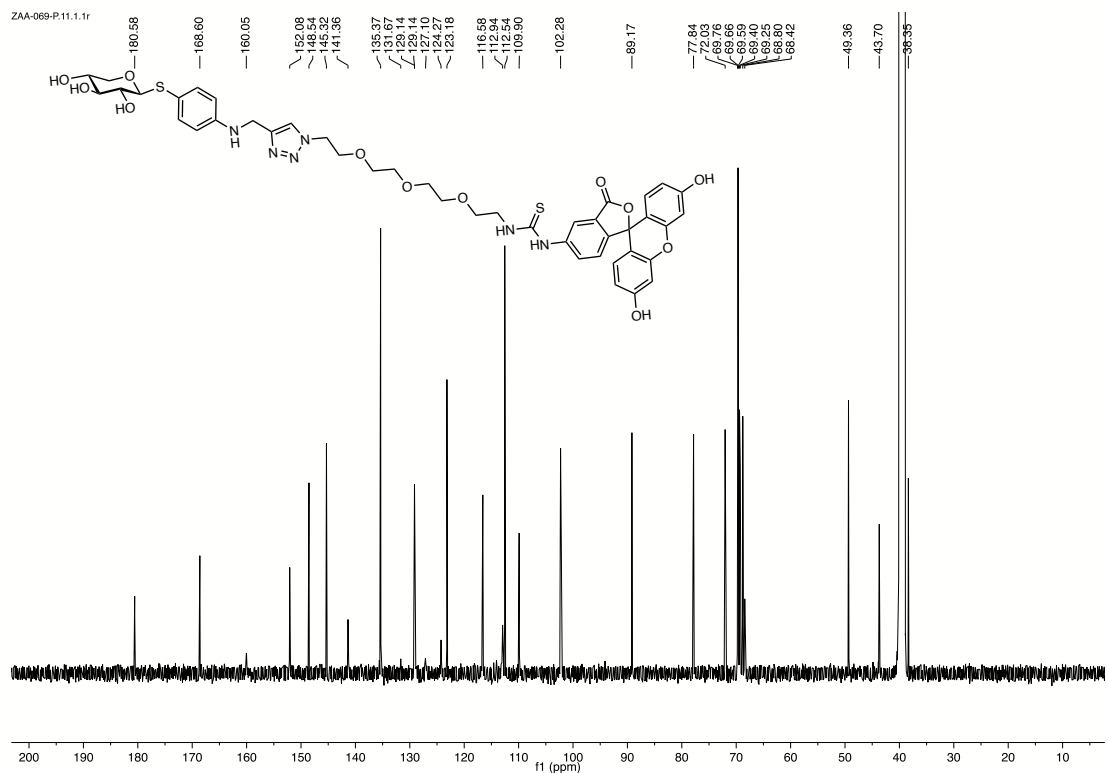
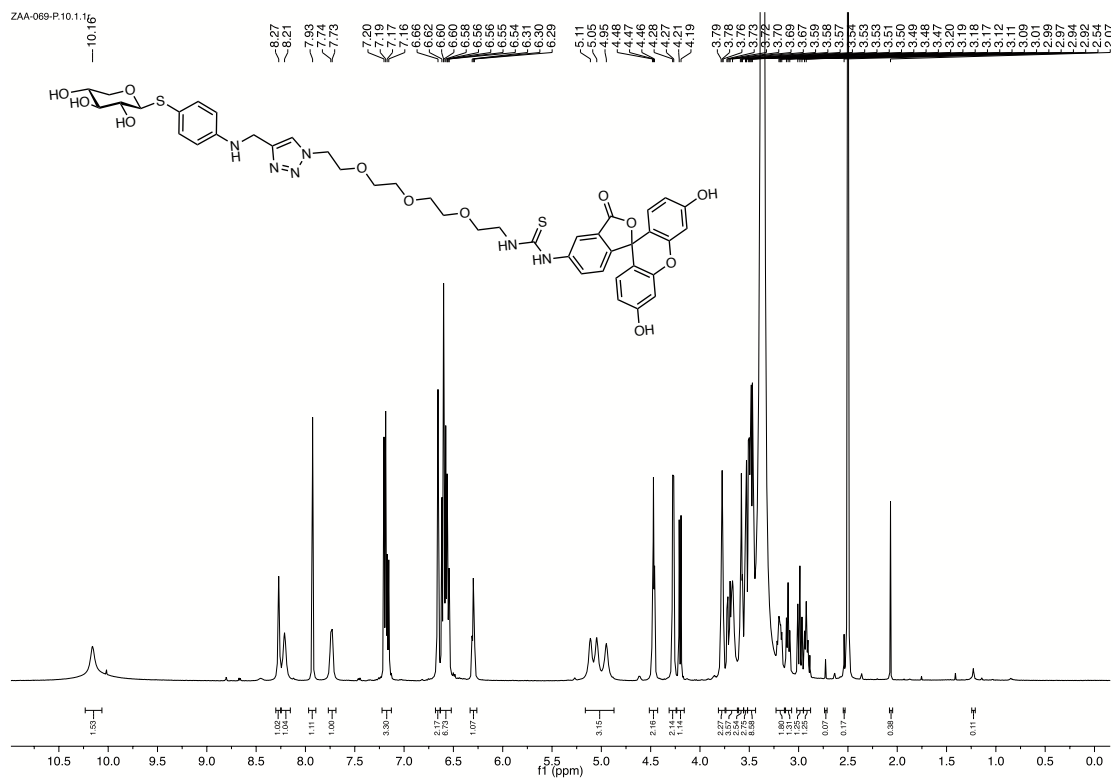
ZAA-068-P.20.1.1r



ZAA-073-P.1.20.1.1r

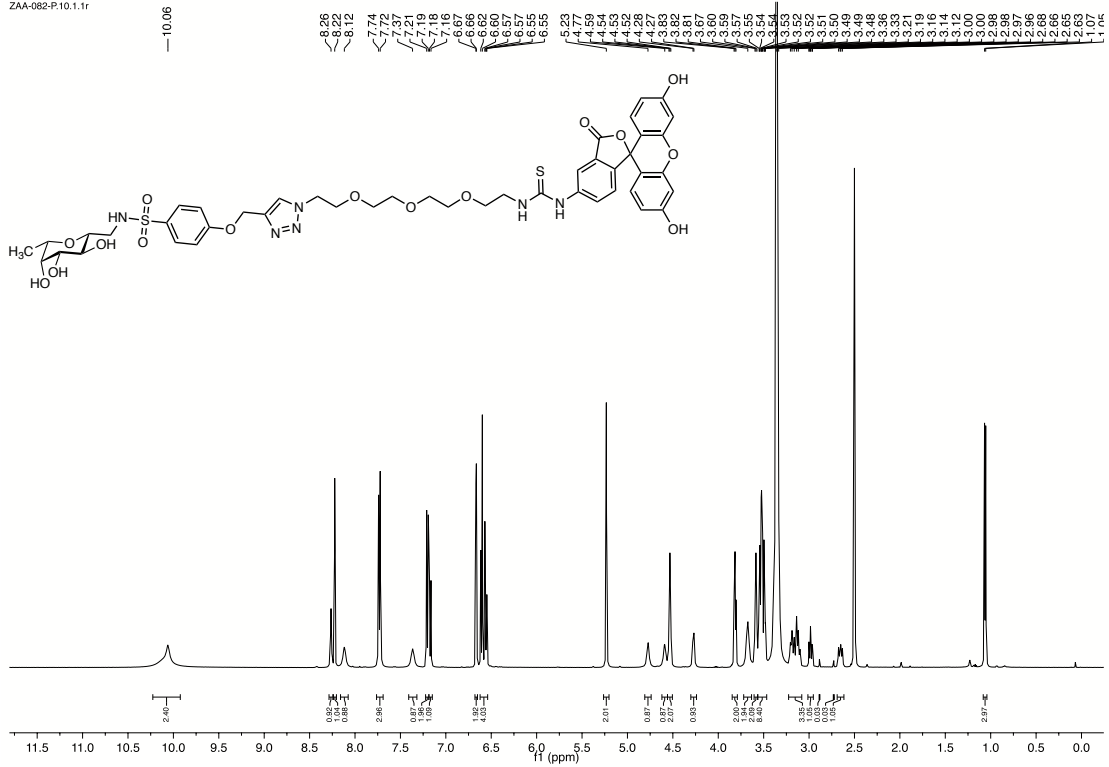


¹H and ¹³C NMR of **30p**

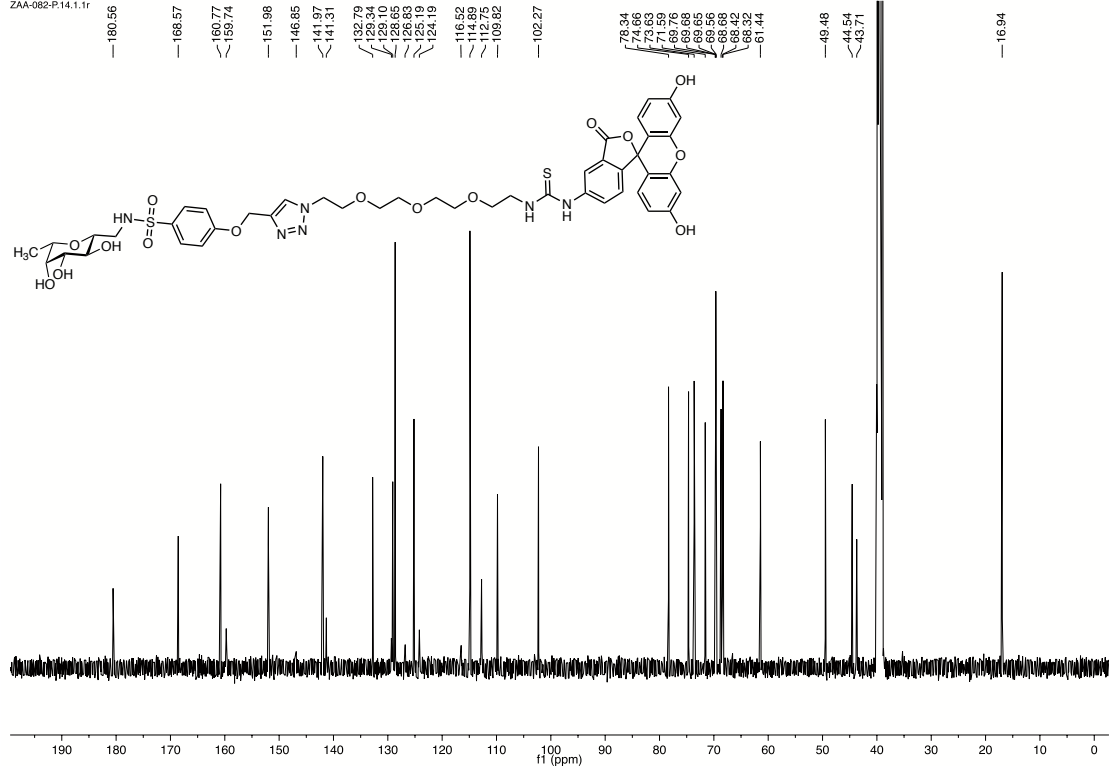


^1H and ^{13}C NMR of **32**

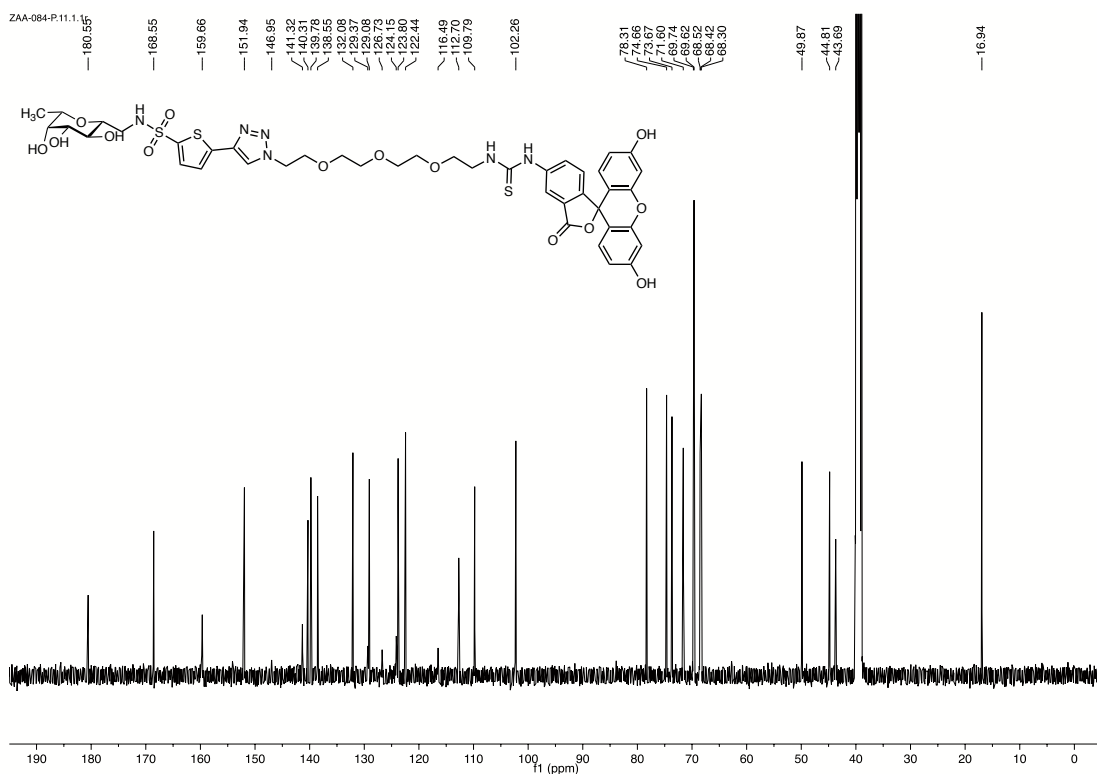
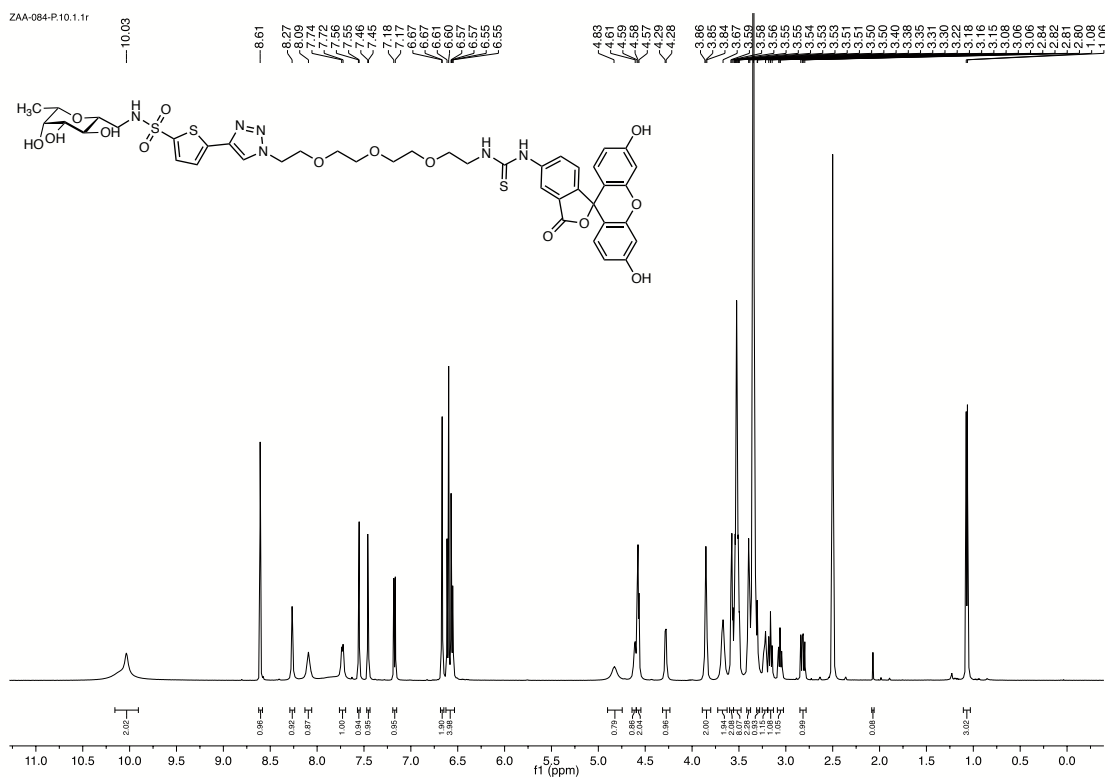
ZAA-082-P10.1.1r



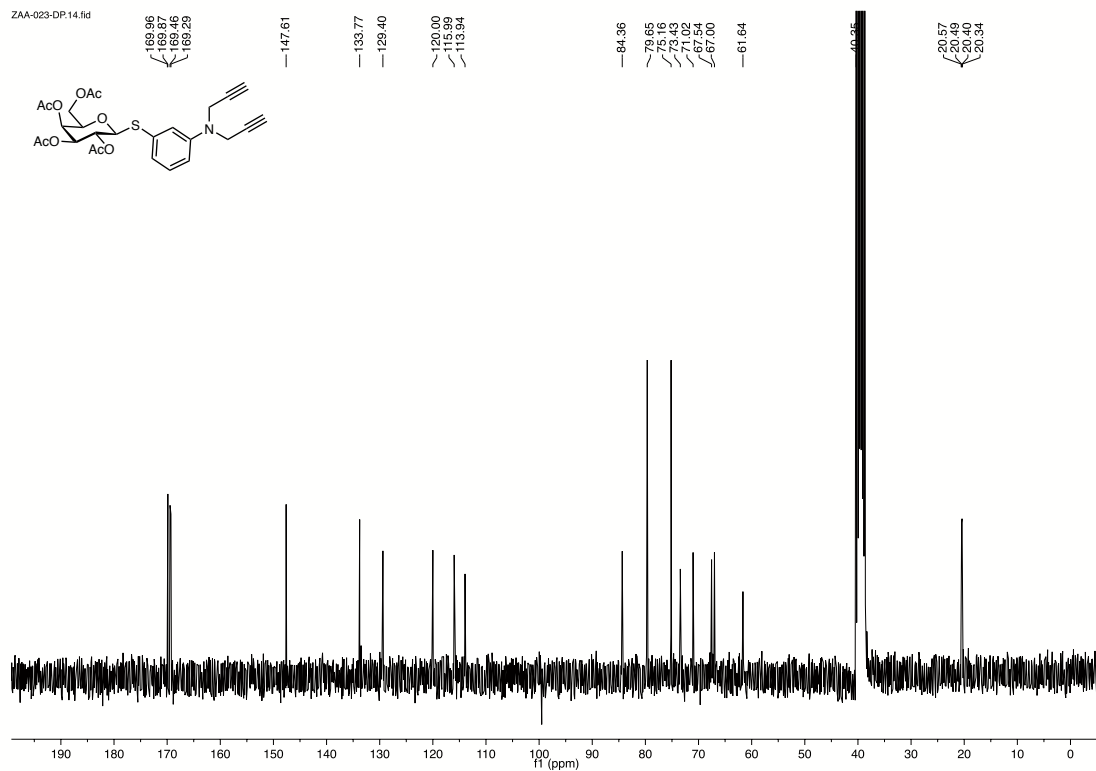
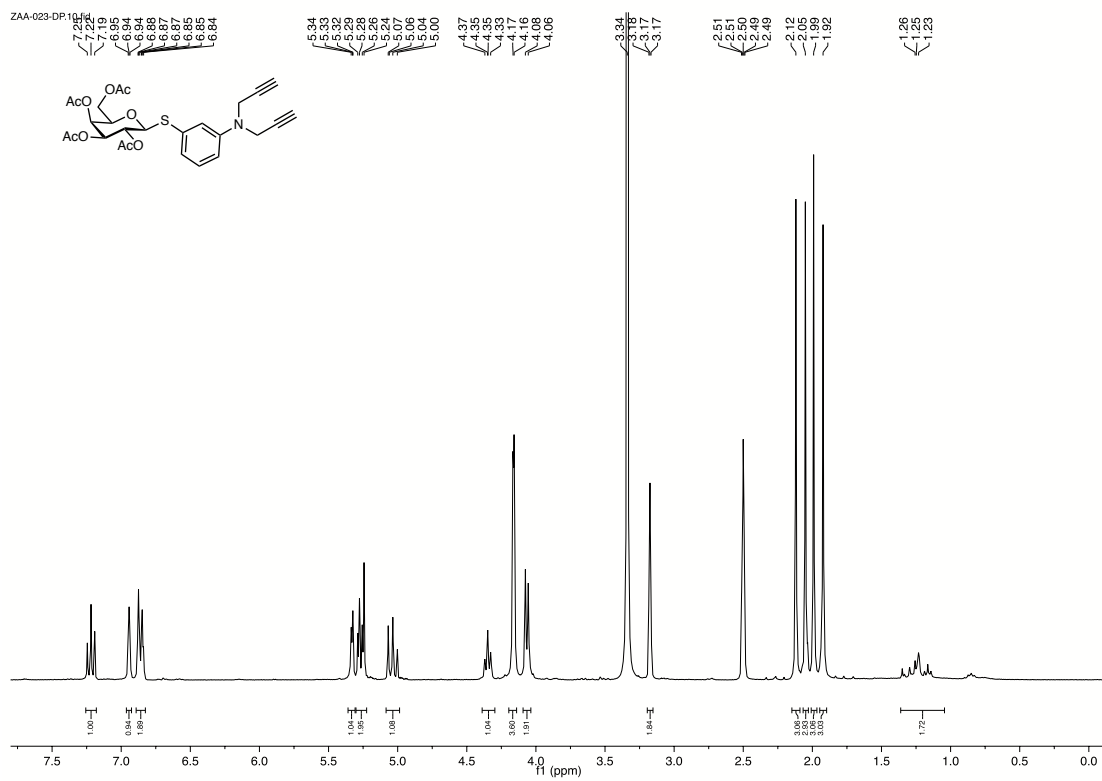
ZAA-082-P14.1.1r



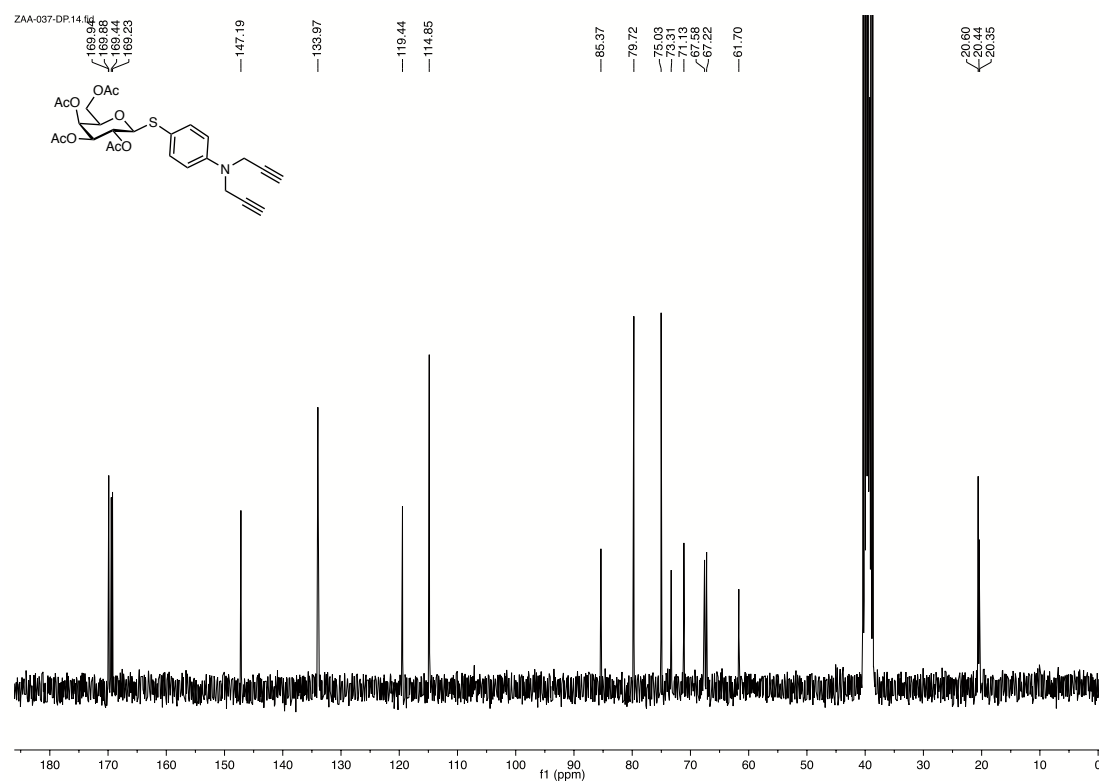
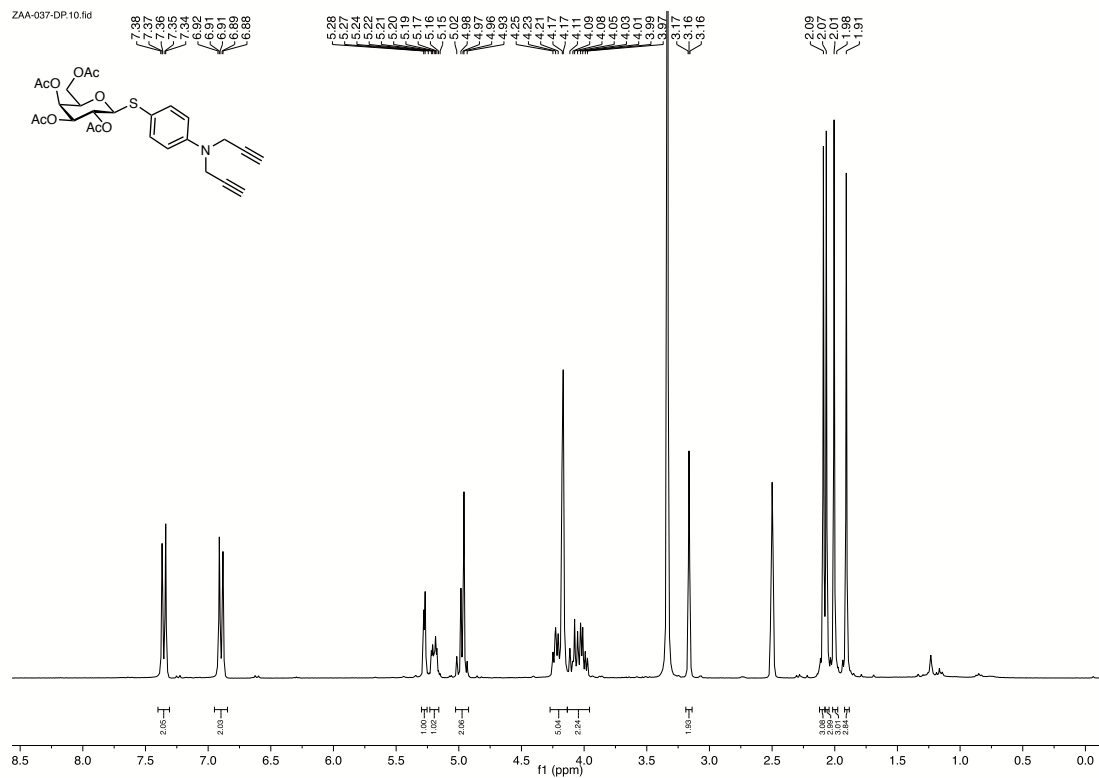
^1H and ^{13}C NMR of 34



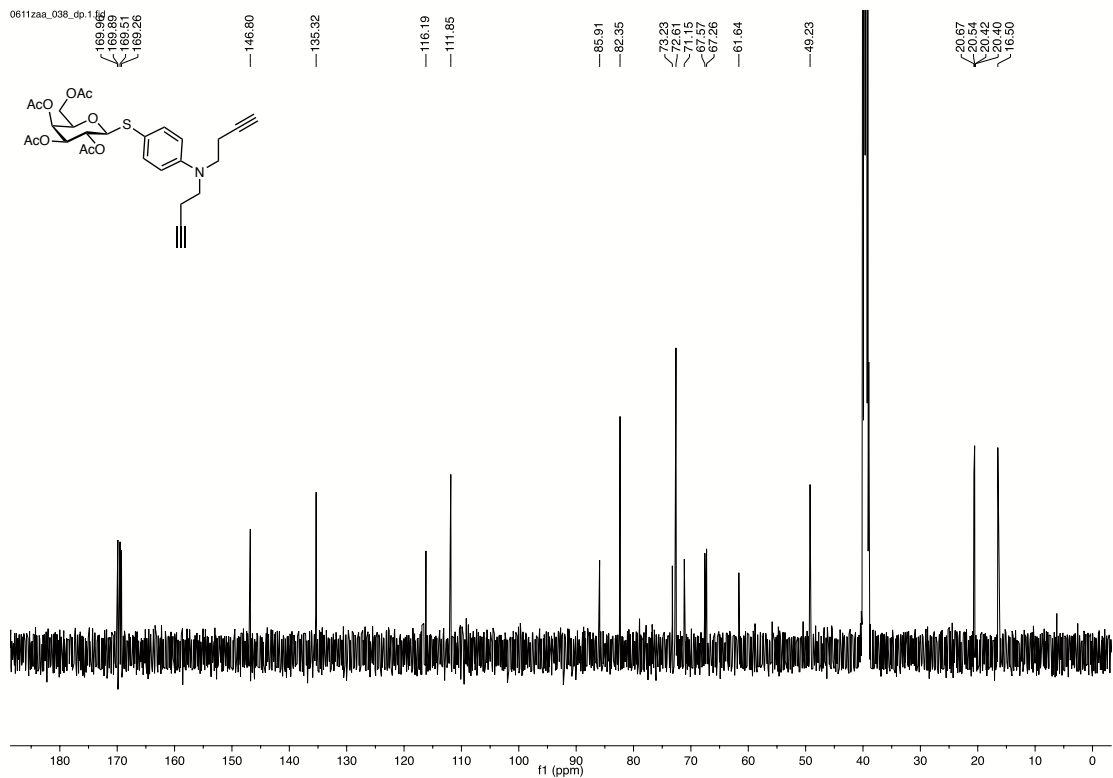
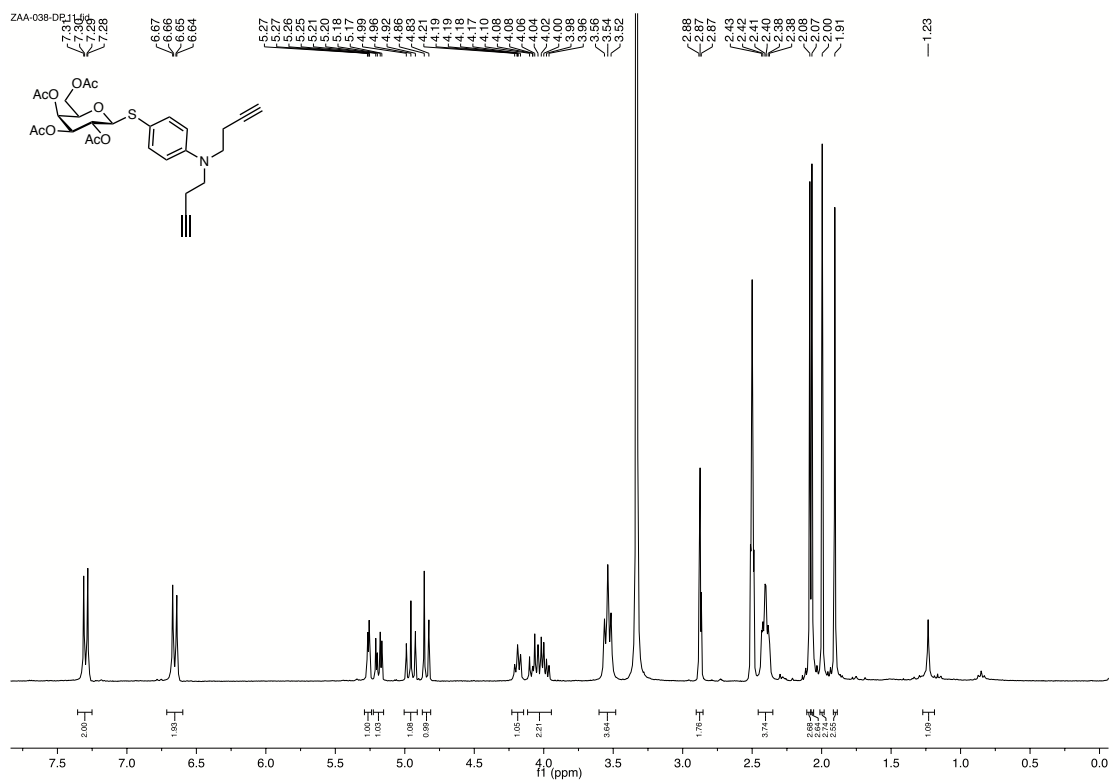
^1H and ^{13}C NMR of 35



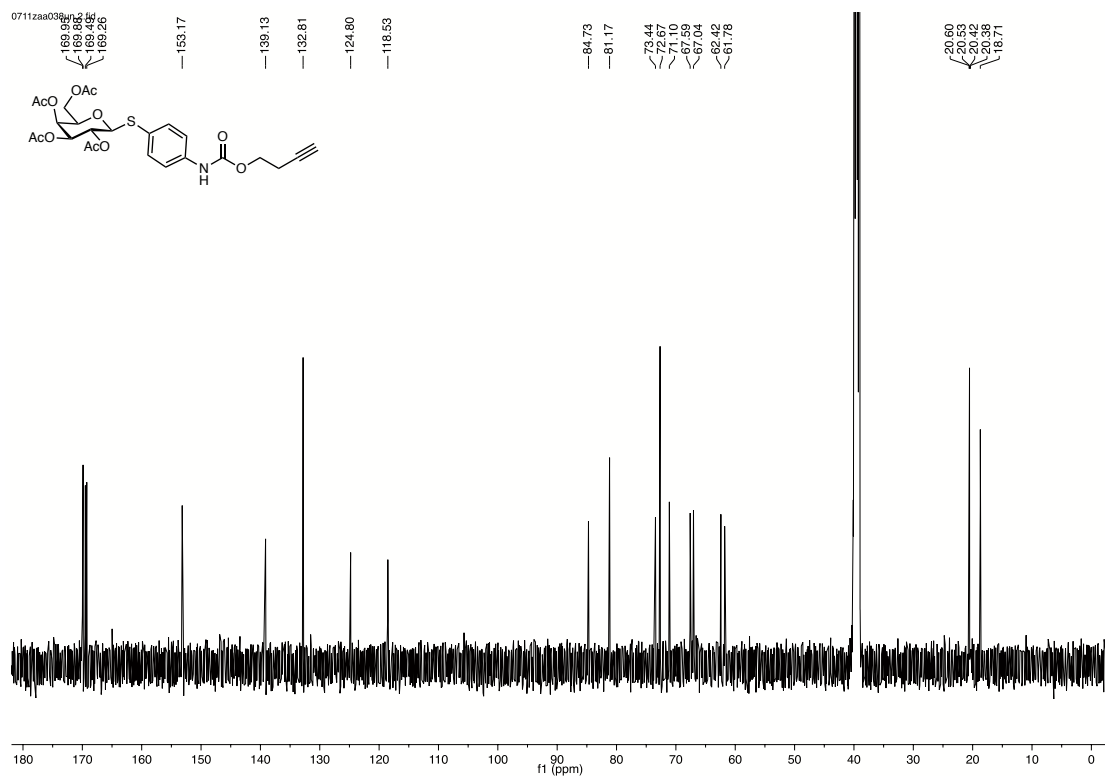
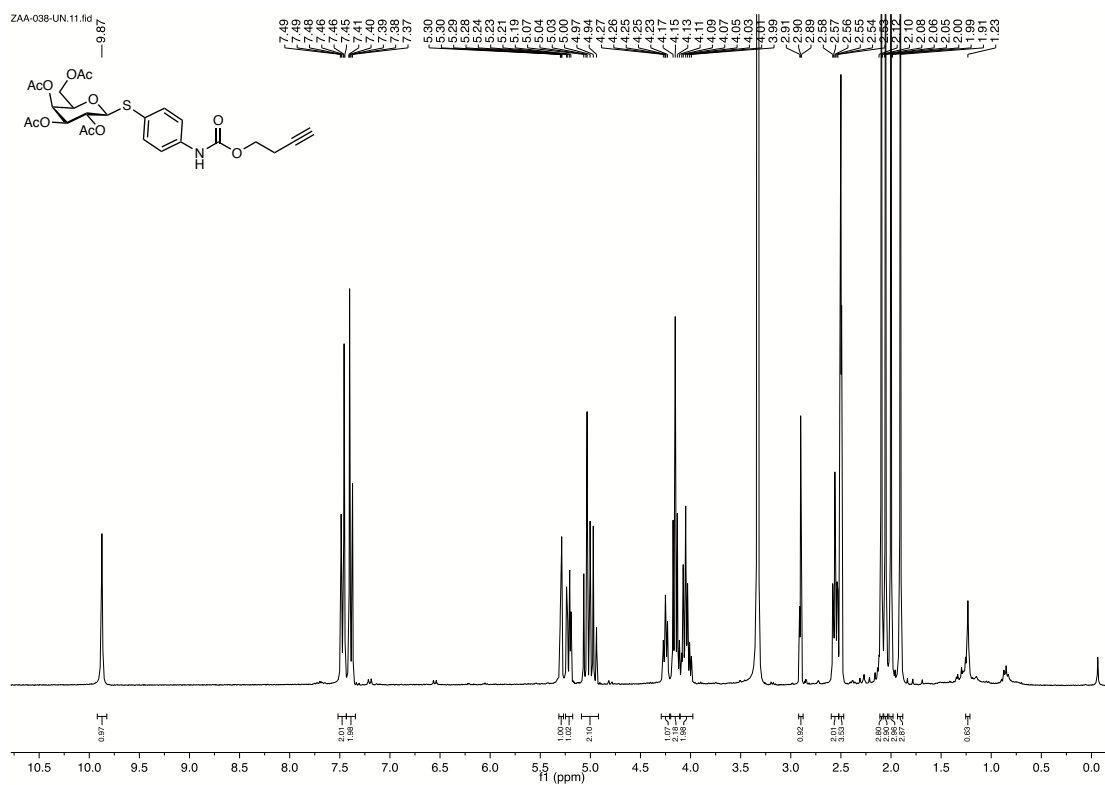
^1H and ^{13}C NMR of **39m**



^1H and ^{13}C NMR of **39p**



¹H and ¹³C NMR of **40p**



^1H and ^{13}C NMR of **41p**

6.2 Supplementary information for chapter 3.2

Supporting information

A rapid synthesis of low-nanomolar divalent LecA inhibitors in four linear steps from D-galactose pentaacetate

Eva Zahorska¹⁻³, Sakonwan Kuhaudomlarp⁴, Saverio Minervini¹, Sultaan Yousaf¹, Martin Lepsik⁴, Thorsten Kinsinger¹, Anna K. H. Hirsch^{2,3,5}, Anne Imberty⁴, Alexander Titz^{1-3*}

¹Chemical Biology of Carbohydrates (CBCH), Helmholtz Institute for Pharmaceutical Research Saarland (HIPS), Helmholtz Centre for Infection Research, D-66123 Saarbrücken, Germany

²Deutsches Zentrum für Infektionsforschung (DZIF), Standort Hannover-Braunschweig, D-38124 Braunschweig, Germany

³Department of Pharmacy, Saarland University, D-66123 Saarbrücken, Germany

⁴ Université Grenoble Alpes, CNRS, CERMAV, 38000 Grenoble, France

⁵Drug Design and Optimization (DDOP), Helmholtz Institute for Pharmaceutical Research Saarland (HIPS), Helmholtz Centre for Infection Research, D-66123 Saarbrücken, Germany

*corresponding author: alexander.titz@helmholtz-hzi.de

General experimental details

Commercial chemicals and solvents were used without further purification.

Thin layer chromatography (TLC) was performed using silica gel 60 aluminum plates containing fluorescence indicator (Merck KGaA, Darmstadt, Germany) and developed under UV light (254 nm) and using a molybdate solution (0.02 M solution of $(\text{NH}_4)_4\text{Ce}(\text{SO}_4)_4 \cdot 2\text{H}_2\text{O}$ and $(\text{NH}_4)_6\text{Mo}_7\text{O}_{24} \cdot 4\text{H}_2\text{O}$ in aqueous 10% H_2SO_4) or a potassium permanganate solution (3 g of KMnO_4 , 20 g of K_2CO_3 in 5 mL of 5% NaOH and 300 mL of water) with heating.

Medium pressure liquid chromatography (MPLC) was performed on a Teledyne Isco Combiflash Rf200 system using normal phase self-packed silica gel columns (60 Å, 400 mesh particle size, Fluka) or reversed-phase pre-packed silica gel 60 Å columns from Macherey-Nagel (C_{18} ec, endcapped). Preparative high-pressure liquid chromatography (HPLC) was performed on Waters 2545 Binary Gradient Module with a Waters 2489 UV/Vis detector using a RP-18 column (250/21 Nucleodur C18 Gravity SB, 5 µM from Macherey-Nagel, Germany).

Analytical HPLC-MS was performed on a Thermo Dionex Ultimate 3000 HPLC coupled to a Bruker amaZon SL mass spectrometer, with UV detection at 254 nm using a RP-18 column (100/2 Nucleoshell RP18plus, 2.7 µM from Macherey-Nagel, Germany) as stationary phase. High resolution mass spectrometry (HRMS) was performed on an Ultimate 3000 UPLC system coupled to a Q Exactive Focus Orbitrap system with HESI source (Thermo Fisher, Dreieich, Germany). The UPLC was operated with a C18 column (EC 150/2 Nucleodur C18 Pyramid, 3 µm from Macherey-Nagel, Germany).

^1H -NMR and ^{13}C -NMR spectra were recorded on a Bruker Avance III 500 UltraShield spectrometer at 500 MHz and 126 MHz. Chemical shifts (δ) are given in ppm and were calibrated on residual solvent peaks: chloroform- d_1 (^1H -NMR $\delta = 7.26$ ppm, ^{13}C -NMR $\delta = 77.0$ ppm), MeOH- d_4 (^1H -NMR $\delta = 3.31$ ppm, ^{13}C -NMR $\delta = 49.0$ ppm), DMSO- d_6 (^1H -NMR $\delta = 2.50$ ppm, ^{13}C -NMR $\delta = 39.51$ ppm).¹ Deuterated solvents were purchased from Eurisotop (Saarbrücken, Germany). Multiplicities are specified as s = singlet, d = doublet, t = triplet, q = quartet, m = multiplet. The spectra were assigned with the help of ^1H , ^1H -COSY; ^1H , ^{13}C -HSQC and ^1H , ^{13}C -HMBC experiments.

Compound synthesis

***m*-Methoxycarbonylphenyl 2,3,4,6-tetra-O-acetyl- β -D-galactopyranoside (3m).** β -D-galactopyranose pentaacetate² (**2**, 2.72 g, 6.97 mmol) and methyl-3-hydroxybenzoate (3.09 g, 20.4 mmol) were dissolved in dry dichloromethane (20 mL). The reaction mixture was cooled to 0 °C and BF₃·OEt₂ (2.5 mL, 20.3 mmol) was added dropwise. The mixture was allowed to warm to room temperature and stirred overnight. The reaction was poured over ice cold satd. aqueous NaHCO₃ and diluted with dichloromethane. The organic phase was separated and washed with satd. aqueous NaHCO₃ and brine, dried over anhydrous Na₂SO₄, filtered and concentrated *in vacuo*. The crude product was purified by normal phase MPLC (petrol ether/EtOAc, 5–50% EtOAc). **3m** was obtained as a white solid (2.34 g, 4.84 mmol, 69%). The compound **3m** was first reported by Xue *et al.*³

¹H NMR (500 MHz, CDCl₃) δ 7.75 (d, *J* = 7.7 Hz, 1H, ArH), 7.66 (dd, *J* = 2.3, 1.5 Hz, 1H, ArH), 7.37 (t, *J* = 8.0 Hz, 1H, ArH), 7.19 (ddd, *J* = 8.2, 2.5, 0.8 Hz, 1H, ArH), 5.51 (dd, *J* = 10.4, 7.9 Hz, 1H, H-2), 5.47 (d, *J* = 3.3 Hz, 1H, H-4), 5.12 (dd, *J* = 10.3, 3.6 Hz, 1H, H-3), 5.11 (d, *J* = 7.9 Hz, 1H, H-1), 4.24 – 4.15 (m, 2H, H-6), 4.11 (t, *J* = 6.2 Hz, 1H, H-5), 3.91 (s, 3H, OCH₃), 2.18 (s, 3H, CH₃), 2.07 (s, 3H, CH₃), 2.07 (s, 3H, CH₃), 2.01 (s, 3H, CH₃).

¹³C NMR (126 MHz, CDCl₃) δ 170.62 (1C, CH₃C=O), 170.37 (1C, CH₃C=O), 170.24 (1C, CH₃C=O), 169.53 (1C, CH₃C=O), 166.50 (1C, C=O), 156.99 (1C, ArC), 131.85 (1C, ArC), 129.74 (1C, ArCH), 124.59 (1C, ArCH), 122.00 (1C, ArCH), 117.50 (1C, ArCH), 99.49 (1C, C-1), 71.37 (1C, C-5), 70.91 (1C, C-3), 68.67 (1C, C-2), 67.03 (1C, C-4), 61.62 (1C, C-6), 52.44 (1C, OCH₃), 20.89 (1C, CH₃), 20.81 (1C, CH₃), 20.73 (2C, CH₃).

HPLC-MS: [C₂₂H₂₆O₁₂ + Na]⁺ calcd. 505.13, found 505.12.

***p*-Methoxycarbonylphenyl 2,3,4,6-tetra-O-acetyl- β -D-galactopyranoside (3p).** β -D-galactopyranose pentaacetate² (**2**, 4.18 g, 10.71 mmol) and methyl-4-hydroxybenzoate (4.8 g, 31.2 mmol) were dissolved in dry dichloromethane (20 mL). The reaction mixture was cooled to 0 °C and BF₃·OEt₂ (2.5 mL, 20.3 mmol) was added dropwise. The mixture was allowed to warm to room temperature and stirred overnight. The reaction was poured over ice cold saturated aqueous NaHCO₃ and diluted with dichloromethane. The organic phase was separated and washed with satd. aqueous NaHCO₃ and brine, dried over anhydrous Na₂SO₄, filtered and concentrated *in vacuo*. **3p** was purified by recrystallisation from ethanol (2.45 g,

5.08 mmol, 47%). The synthesis and analytical data of compound **3p** was first reported by Li *et al.*⁴

¹H NMR (500 MHz, CDCl₃) δ 8.06 – 7.95 (m, 2H, ArH), 7.08 – 6.96 (m, 2H, ArH), 5.51 (dd, *J* = 10.4, 7.9 Hz, 1H, H-2), 5.47 (d, *J* = 3.4 Hz, 1H, H-4), 5.17 – 5.07 (m, 2H, H-1, H-3), 4.25 – 4.14 (m, 2H, H-6), 4.10 (t, *J* = 6.5 Hz, 1H, H-5), 3.90 (s, 3H, CH₃), 2.19 (s, 3H, CH₃), 2.07 (d, 6H, CH₃), 2.02 (s, 3H, CH₃), 1.59 (s, 3H, CH₃).

¹³C NMR (126 MHz, CDCl₃) δ 170.50 (1C, CH₃C=O), 170.34 (1C, CH₃C=O), 170.24 (1C, CH₃C=O), 169.49 (1C, CH₃C=O), 166.60 (1C, C=O), 160.36 (1C, ArC), 131.72 (2C, ArCH), 125.19 (1C, ArC), 116.29 (2C, ArCH), 98.92 (1C, C-1), 71.40 (1C, C-5), 70.87 (1C, C-3), 68.60 (1C, C-2), 66.94 (1C, C-4), 61.54 (1C, C-6), 52.21 (1C, OCH₃), 20.86 (1C, CH₃), 20.81 (1C, CH₃), 20.79 (1C, CH₃), 20.72 (1C, CH₃).

HPLC-MS: [C₂₂H₂₆O₁₂ + Na]⁺ calcd. 505.13, found 505.12.

***m*-Methoxycarbonylphenyl β-D-galactopyranoside (4m)**. Compound **3m** (2.32 g, 4.81 mmol) was suspended in dry MeOH (40 mL) and 1 M NaOMe in MeOH (0.5 mL, 0.50 mmol) was added. The reaction mixture was stirred overnight at r.t. Amberlite IR 120/H⁺ was added to neutralize the reaction mixture to pH 7 and was then filtered. The solvent was removed *in vacuo* to give **4m** as a white solid (1.49 g, 4.75 mmol, quant.).

¹H NMR (500 MHz, DMSO-d₆) δ 7.61 – 7.57 (m, 2H, ArH), 7.45 (t, *J* = 7.9 Hz, 1H, ArH), 7.32 (ddd, *J* = 8.3, 2.5, 0.9 Hz, 1H, ArH), 5.21 (d, *J* = 5.1 Hz, 1H, OH-2), 4.89 (d, *J* = 5.7 Hz, 1H, OH-3), 4.86 (d, *J* = 7.7 Hz, 1H, H-1), 4.66 (t, *J* = 5.5 Hz, 1H, OH-6), 4.53 (d, *J* = 4.6 Hz, 1H, OH-4), 3.85 (s, 3H, OCH₃), 3.72 – 3.68 (m, 1H, H-4), 3.62 – 3.52 (m, 3H, H-2, H-5, H-6a), 3.51 – 3.46 (m, 1H, H-6b), 3.45 – 3.40 (m, 1H, H-3).

¹³C NMR (126 MHz, DMSO-d₆) δ 165.96 (1C, C=O), 157.65 (1C, ArC), 130.91 (1C, ArC), 129.95 (1C, ArCH), 122.58 (1C, ArCH), 121.32 (1C, ArCH), 116.96 (1C, ArCH), 101.36 (1C, C-1), 75.59 (1C, C-5), 73.13 (1C, C-3), 70.29 (1C, C-2), 68.07 (1C, C-4), 60.29 (1C, C-6), 52.28 (1C, OCH₃).

HPLC-MS: C₁₄H₁₇O₈⁻ [M – H]⁻ calcd. 313.09, found 313.16.

***p*-Methoxycarbonylphenyl β-D-galactopyranoside (4p)**. Compound **3p** (2.39 g, 4.95 mmol) was suspended in dry MeOH (40 mL) and 1 M NaOMe in MeOH (0.5 mL, 0.5 mmol) was added. The reaction mixture was stirred overnight at r.t. Amberlite IR 120/H⁺ was added to neutralize

the reaction mixture to pH 7 and was then filtered. The solvent was removed *in vacuo* to give **4p** as a white solid (1.55 g, 4.93 mmol, quant.).

^1H NMR (500 MHz, DMSO- d_6) δ 7.90 (d, J = 8.5 Hz, 2H, ArH), 7.12 (d, J = 8.5 Hz, 2H, ArH), 5.22 (d, J = 5.1 Hz, 1H, OH-2), 4.95 (d, J = 7.6 Hz, 1H, H-1), 4.90 (d, J = 5.6 Hz, 1H, OH-3), 4.66 (t, J = 5.5 Hz, 1H, OH-6), 4.54 (d, J = 4.6 Hz, 1H, OH-4), 3.82 (s, 3H, OCH₃), 3.71 (t, J = 4.0 Hz, 1H, H-4), 3.65 – 3.45 (m, 4H, H-2, H-5, H-6), 3.42 (dt, J = 9.1, 4.2 Hz, 1H, H-3).

^{13}C NMR (126 MHz, DMSO- d_6) δ 165.85 (1C, C=O), 161.25 (1C, ArC), 131.08 (2C, ArCH), 122.86 (1C, ArC), 116.03 (2C, ArCH), 100.41 (1C, C-1), 75.62 (1C, C-5), 73.21 (1C, C-3), 70.17 (1C, C-2), 68.07 (1C, C-4), 60.28 (1C, C-6), 51.91 (1C, OCH₃).

HPLC-MS: C₁₄H₁₇O₈⁻ [M – H]⁻ calcd. 313.09, found 313.10.

***m*-Hydrazinecarbonylphenyl β -D-galactopyranoside (1m)**. To a suspension of compound **4m** (0.87 g, 2.76 mmol) in MeOH (33 mL), NH₂NH₂·H₂O (0.86 mL, 17.73 mmol) was added. The reaction was stirred under reflux at 70 °C overnight. Solvents were removed *in vacuo* to give compound **1m** as a white solid (0.87 g, quant.).

^1H NMR (500 MHz, DMSO- d_6) δ 9.76 (s, 1H, NH), 7.47 – 7.40 (m, 2H, ArH), 7.35 (t, J = 8.1 Hz, 1H, ArH), 7.19 – 7.10 (m, 1H, ArH), 5.22 (d, J = 5.2 Hz, 1H, OH-2), 4.93 (d, J = 5.4 Hz, 1H, OH-3), 4.89 (d, J = 7.7 Hz, 1H, H-1), 4.69 (t, J = 5.4 Hz, 1H, OH-6), 4.56 (d, J = 4.6 Hz, 1H, OH-4), 4.48 (s, 2H, NH₂), 3.71 (t, J = 3.8 Hz, 1H, H-4), 3.62 – 3.43 (m, 4H, H-2, H-5, H-6), 3.43 – 3.38 (m, 1H, H-3).

^{13}C NMR (126 MHz, DMSO- d_6) δ 165.60 (1C, C=O), 157.43 (1C, ArC), 134.67 (1C, ArC), 129.44 (1C, ArCH), 120.29 (1C, ArCH), 118.91 (1C, ArCH), 114.82 (1C, ArCH), 100.92 (1C, C-1), 75.48 (1C, C-5), 73.34 (1C, C-3), 70.29 (1C, C-2), 68.02 (1C, C-4), 60.22 (1C, C-6).

HPLC-MS: [C₁₃H₁₈N₂O₇ + H]⁺ calcd. 315.12, found 315.12.

***p*-Hydrazinecarbonylphenyl β -D-galactopyranoside (1p)**. To a suspension of compound **4p** (1.70 g, 5.41 mmol) in MeOH (60 mL), NH₂NH₂·H₂O (2.52 mL, 51.95 mmol) was added. The reaction was stirred under reflux at 70 °C for 72 h. Solvents were removed *in vacuo* and the product was washed with cold MeOH. Pure compound **1p** was obtained as a white solid (1.60 g, 5.09 mmol, 94%).

^1H NMR (500 MHz, DMSO- d_6) δ 9.63 (s, 1H, NH), 7.77 (d, J = 8.4 Hz, 2H, ArH), 7.05 (d, J = 8.4 Hz, 2H, ArH), 5.19 (d, J = 5.2 Hz, 1H, OH-2), 4.93 – 4.86 (m, 2H, H-1, OH-3), 4.66 (t, J = 5.5

Hz, 1H, OH-6), 4.52 (d, $J = 4.6$ Hz, 1H, OH-4), 4.42 (s, 2H, NH₂), 3.70 (t, $J = 4.0$ Hz, 1H, H-4), 3.63 – 3.44 (m, 4H, H-2, H-5, H-6), 3.44 – 3.38 (m, 1H, H-3).

¹³C NMR (126 MHz, DMSO-d₆) δ 165.56 (1C, C=O), 159.61 (1C, ArC), 128.57 (2C, ArCH), 126.56 (1C, ArC), 115.64 (2C, ArCH), 100.56 (1C, C-1), 75.59 (1C, C-5), 73.27 (1C, C-3), 70.22 (1C, C-2), 68.15 (1C, C-4), 60.39 (1C, C-6).

HPLC-MS: [C₁₃H₁₈N₂O₇ + H]⁺ calcd. 315.12, found 315.00.

General procedure for synthesis of bis-benzaldehydes C–F

Corresponding di-halogenated hydrocarbons (1 eq.), 4-hydroxybenzaldehyde (4 eq.) and potassium carbonate (3 eq.) were dissolved in dry DMF (1.5 mL) in a microwave reaction vial. The vial was sealed and irradiated under microwave irradiation (Discover SP Sequential Microwave Synthesis System, CEM Corporation, North Carolina, USA) with maximum power 300 W at 70 °C for 3–10h. After cooling, the reaction was diluted with dichloromethane and washed with saturated aqueous NaHCO₃ and brine, dried over anhydrous Na₂SO₄, filtered and concentrated *in vacuo*. Pure products were obtained without further purification. Analytical data of compounds C–F match the literature.⁵

Bis(4-formylphenoxy) methane (C). Dichloromethane (30 μ L, 0.47 mmol), 4-hydroxybenzaldehyde (228 mg, 1.86 mmol) and potassium carbonate (138 mg, 1.42 mmol) were used following the general procedure for synthesis of bis-benzaldehydes to give compound C (99.6 mg, 0.39 mmol, 83%).

¹H NMR (500 MHz, CDCl₃) δ 9.92 (s, 2H, CHO), 7.89 – 7.85 (m, 4H, ArH), 7.25 – 7.22 (m, 4H, ArH), 5.88 (s, 2H, CH₂).

¹³C NMR (126 MHz, CDCl₃) δ 190.87 (2C, CHO), 161.40 (2C, ArC), 132.09 (4C, ArCH), 131.66 (2C, ArC), 116.49 (4C, ArCH), 89.96 (1C, CH₂).

HPLC-MS: [C₁₅H₁₂O₄ + H]⁺ calcd. 257.08, found 257.09.

1,2-Bis(4-formylphenoxy) ethane (D). 1,2-Dichloroethane (25 μ L, 0.32 mmol), 4-hydroxybenzaldehyde (165.2 mg, 1.35 mmol) and potassium carbonate (133.4 mg, 0.97 mmol) were used following the general procedure for synthesis of bis-benzaldehydes to give compound D (34.1 mg, 0.13 mmol, 40%).

^1H NMR (500 MHz, CDCl_3) δ 9.90 (s, 2H, CHO), 7.89 – 7.84 (m, 4H, ArH), 7.08 – 7.03 (m, 4H, ArH), 4.45 (s, 4H, CH_2).

^{13}C NMR (126 MHz, CDCl_3) δ 190.90 (2C, CHO), 163.53 (2C, ArC), 132.17 (4C, ArCH), 130.54 (2C, ArC), 115.01 (4C, ArCH), 66.63 (2C, CH_2).

HPLC-MS: $[\text{C}_{16}\text{H}_{14}\text{O}_4 + \text{H}]^+$ calcd. 271.10, found 271.11.

1,3-Bis(4-formylphenoxy) propane (E). 1,3-Dichloropropane (40 μL , 0.42 mmol), 4-hydroxybenzaldehyde (227.1 mg, 1.86 mmol) and potassium carbonate (192.6 mg, 1.39 mmol) were used following the general procedure for synthesis of bis-benzaldehydes to give compound **E** (102.0 mg, 0.36 mmol, 85%).

^1H NMR (500 MHz, CDCl_3) δ 9.88 (s, 2H, CHO), 7.85 – 7.81 (m, 4H, ArH), 7.04 – 6.99 (m, 4H, ArH), 4.26 (t, $J = 6.0$ Hz, 4H, $\text{CH}_2\text{CH}_2\text{CH}_2$), 2.34 (m, 2H, $\text{CH}_2\text{CH}_2\text{CH}_2$).

^{13}C NMR (126 MHz, CDCl_3) δ 190.89 (2C, CHO), 163.87 (2C, ArC), 132.14 (4C, ArCH), 130.22 (2C, ArC), 114.87 (4C, ArCH), 64.65 (2C, $\text{CH}_2\text{CH}_2\text{CH}_2$), 29.10 (1C, $\text{CH}_2\text{CH}_2\text{CH}_2$).

HPLC-MS: $[\text{C}_{17}\text{H}_{16}\text{O}_4 + \text{H}]^+$ calcd. 285.11, found 285.15.

1,4-Bis(4-formylphenoxy) butane (F). 1,4-Dibromobutane (50 μL , 0.42 mmol), 4-hydroxybenzaldehyde (211.5 mg, 1.73 mmol) and potassium carbonate (138.2 mg, 1.29 mmol) were used following the general procedure for synthesis of bis-benzaldehydes to give compound **F** (111.0 mg, 0.37 mmol, 89%).

^1H NMR (500 MHz, CDCl_3) δ 9.88 (s, 2H, CHO), 7.87 – 7.80 (m, 4H, ArH), 7.03 – 6.96 (m, 4H, ArH), 4.17 – 4.10 (m, 4H, $\text{CH}_2\text{CH}_2\text{CH}_2\text{CH}_2$), 2.06 – 2.00 (m, 4H, $\text{CH}_2\text{CH}_2\text{CH}_2\text{CH}_2$).

^{13}C NMR (126 MHz, CDCl_3) δ 190.92 (2C, CHO), 164.08 (2C, ArC), 132.15 (4C, ArCH), 130.08 (2C, ArC), 114.84 (4C, ArCH), 67.88 (2C, $\text{CH}_2\text{CH}_2\text{CH}_2\text{CH}_2$), 25.93 (2C, $\text{CH}_2\text{CH}_2\text{CH}_2\text{CH}_2$).

HPLC-MS: $[\text{C}_{18}\text{H}_{18}\text{O}_4 + \text{H}]^+$ calcd. 299.13, found 299.17.

General procedure for synthesis of acylhydrazones

Corresponding benzaldehyde **A–F** (1 eq.) and hydrazide **1m** or **1p** (3 eq.) were dissolved in 1-10 mL DMSO (unless stated otherwise) and 20-100 μ L of formic acid was added. After 4 h, the reactions were quenched to pH 8 with NH_4OH or immediately frozen with liquid nitrogen and dried *in vacuo*. The products were purified by MPLC or preparative HPLC (C18, water/acetonitrile, 15-40% acetonitrile).

Monovalent ligand A5m was synthesized following the general procedure for synthesis of acylhydrazones using benzaldehyde **A** (20 μ L, 0.15 mmol) and hydrazide **1m** (88.5 mg). Compound **A5m** (26.5 mg, 0.06 mmol, 42%) was obtained as white solid.

^1H NMR (500 MHz, DMSO-d_6) δ 11.69 (s, 1H, NH), 8.39 (s, 1H, N=CH), 7.67 (d, J = 8.7 Hz, 2H, ArH), 7.53 – 7.52 (m, 2H, ArH), 7.44 (t, J = 8.1 Hz, 1H, ArH), 7.25 (dd, J = 8.2, 1.1 Hz, 1H, ArH), 7.03 (d, J = 8.7 Hz, 2H, ArH), 5.22 (d, J = 5.1 Hz, 1H, OH-2), 4.92 – 4.90 (m, 2H, OH-3, H-1), 4.68 (t, J = 5.3 Hz, 1H, OH-6), 4.54 (d, J = 4.4 Hz, 1H, OH-4), 3.81 (s, 3H, CH_3), 3.72 (t, 1H, H-4), 3.62 – 3.54 (m, 3H, H-2, H-5, H-6a), 3.52 – 3.49 (m, 1H, H-6b), 3.45 – 3.41 (m, 1H, H-3).

^{13}C NMR (126 MHz, DMSO-d_6) δ 162.63 (1C, C=O), 160.89 (1C, ArC), 157.50 (1C, ArC), 147.79 (1C, C=N), 134.93 (1C, ArC), 129.61 (1C, ArCH), 128.74 (2C, ArCH), 126.89 (1C, ArC), 120.91 (1C, ArCH), 119.35 (1C, ArCH), 115.68 (1C, ArCH), 114.39 (2C, ArCH), 101.13 (1C, C-1), 75.60 (1C, C-5), 73.32 (1C, C-3), 70.32 (1C, C-2), 68.11 (1C, C-4), 60.35 (1C, C-6), 55.34 (1C, CH_3).

HPLC-MS: $[\text{C}_{21}\text{H}_{24}\text{N}_2\text{O}_8 + \text{H}]^+$ calcd. 433.16, found 433.10.

HRMS: $[\text{C}_{21}\text{H}_{24}\text{N}_2\text{O}_8 + \text{H}]^+$ calcd. 433.1605, found 433.1604.

Monovalent ligand A5p was synthesized following the general procedure for synthesis of acylhydrazones using benzaldehyde **A** (30 μ L, 0.24 mmol) and hydrazide **1p** (50.9 mg, 0.16 mmol). Compound **A5p** (64 mg, 0.15 mmol, 82%) was obtained as white solid.

^1H NMR (500 MHz, DMSO-d_6) δ 11.63 (s, 1H, NH), 8.38 (s, 1H, N=CH), 7.88 (d, J = 8.6 Hz, 2H, ArH), 7.67 (d, J = 8.5 Hz, 2H, ArH), 7.13 (d, J = 8.7 Hz, 2H, ArH), 7.02 (d, J = 8.6 Hz, 2H, ArH), 5.23 (d, J = 5.2 Hz, 1H, OH-2), 4.95 (d, J = 7.7 Hz, 1H, H-1), 4.91 (d, J = 5.5 Hz, 1H, OH-3), 4.68 (t, J = 5.5 Hz, 1H, OH-6), 4.55 (d, J = 4.6 Hz, 1H, OH-4), 3.81 (s, 3H, CH_3), 3.71 (t, J = 3.8 Hz, 1H, H-4), 3.65 – 3.46 (m, 4H, H-5, H-6), 3.46 – 3.40 (m, 1H, H-3).

^{13}C NMR (126 MHz, DMSO- d_6) δ 162.37 (1C, C=O), 160.78 (1C, ArC), 160.01 (1C, ArC), 147.20 (1C, N=C), 129.30 (2C, ArCH), 128.65 (2C, ArCH), 127.01 (1C, ArC), 126.66 (1C, ArC), 115.77 (2C, ArCH), 114.37 (2C, ArCH), 100.45 (1C, C-1), 75.62 (1C, C-5), 73.29 (1C, C-3), 70.22 (1C, C-2), 68.14 (1C, C-4), 60.36 (1C, C-6), 55.33 (1C, CH₃).

HPLC-MS: [C₂₁H₂₄N₂O₈ + H]⁺ calcd. 433.16, found 433.20.

HRMS: [C₂₁H₂₄N₂O₈ + H]⁺ calcd. 433.1605, found 433.1608.

Divalent ligand B5m was synthesized following the general procedure for synthesis of acylhydrazones using bisbenzaldehyde **B** (13.9 mg, 0.06 mmol) and hydrazide **1m** (62.3 mg). Compound **B5m** (11.5 mg, 0.01 mmol, 23%) was obtained as white solid.

^1H NMR (500 MHz, DMSO- d_6) δ 11.81 (s, 2H, NH), 8.45 (s, 2H, N=CH), 7.79 (d, J = 8.4 Hz, 4H, ArH), 7.54 (m, 4H, ArH), 7.45 (t, J = 8.1 Hz, 2H, ArH), 7.26 (d, J = 7.5 Hz, 2H, ArH), 7.16 (d, J = 8.4 Hz, 4H, ArH), 5.22 (d, J = 5.0 Hz, 2H, OH-2), 4.92 – 4.91 (m, 4H, H-1, OH-3), 4.69 (t, J = 5.3 Hz, 2H, OH-6), 4.55 (d, J = 4.4 Hz, 2H, OH-4), 3.72 (t, J = 3.9 Hz, 2H, H-4), 3.62 – 3.54 (m, 6H, H-2, H-5, H-6a), 3.52 – 3.48 (m, 2H, H-6b), 3.44 – 3.43 (m, 2H, H-3).

^{13}C NMR (126 MHz, DMSO- d_6) δ 162.75 (2C, C=O), 157.69 (2C, ArC), 157.52 (2C, ArC), 147.17 (2C, C=N), 134.79 (2C, ArC), 130.05 (2C, ArC), 129.64 (2C, ArCH), 129.13 (4C, ArCH), 120.96 (2C, ArCH), 119.46 (2C, ArCH), 119.17 (4C, ArCH), 115.73 (2C, ArCH), 101.15 (2C, C-1), 75.61 (2C, C-5), 73.32 (2C, C-3), 70.32 (2C, C-2), 68.10 (2C, C-4), 60.34 (2C, C-6).

HPLC-MS: [C₄₀H₄₂N₄O₁₅ + H]⁺ calcd. 819.27, found 819.34.

HRMS: [C₄₀H₄₂N₄O₁₅ + H]⁺ calcd. 819.2719, found 819.2716.

Divalent ligand B5p was synthesized following the general procedure for synthesis of acylhydrazones using bisbenzaldehyde **B** (15.6 mg, 0.07 mmol) and hydrazide **1p** (69.8 mg, 0.22 mmol). Compound **B5p** (26.9 mg, 0.03 mmol, 48%) was obtained as white solid.

^1H NMR (500 MHz, DMSO- d_6) δ 11.74 (s, 2H, NH), 8.45 (s, 2H, N=CH), 7.89 (d, J = 8.3 Hz, 4H, ArH), 7.78 (d, J = 7.9 Hz, 4H, ArH), 7.15 (d, J = 7.6 Hz, 8H, ArH), 5.23 (s, 2H, OH-2), 4.95 (d, J = 7.7 Hz, 2H, H-1), 4.91 (s, 2H, OH-3), 4.69 (s, 2H, OH-6), 4.55 (s, 2H, OH-4), 3.71 (s, 2H, H-4), 3.66 – 3.41 (m, 10H, H-2, H-3, H-5, H-6).

^{13}C NMR (126 MHz, DMSO- d_6) δ 162.52 (2C, C=O), 160.10 (2C, ArC), 157.62 (2C, ArC), 146.61 (2C, C=N), 130.16 (2C, ArC), 129.38 (4C, ArCH), 129.05 (4C, ArCH), 126.53 (2C, ArC),

119.15 (2C, ArCH), 115.82 (2C, ArCH), 100.47 (2C, C-1), 75.63 (2C, C-5), 73.30 (2C, C-3), 70.24 (2C, C-2), 68.15 (2C, C-4), 60.38 (2C, C-6).

HPLC-MS: [C₄₀H₄₂N₄O₁₅ + H]⁺ calcd. 819.27, found 819.34.

HRMS: [C₄₀H₄₂N₄O₁₅ + H]⁺ calcd. 819.2719, found 819.2724

Divalent ligand C5m was synthesized following the general procedure for synthesis of acylhydrazones using bisbenzaldehyde **C** (16.3 mg, 0.06 mmol) and hydrazide **1m** (62.1 mg, 0.20 mmol). Compound **C5m** (5.5 mg, 6.5 μmol, 10%) was obtained as white solid.

¹H NMR (500 MHz, DMSO-d₆) δ 11.76 (s, 2H, NH), 8.40 (s, 2H, N=CH), 7.71 (d, *J* = 8.6 Hz, 4H, ArH), 7.57 – 7.49 (m, 4H, ArH), 7.44 (t, *J* = 8.1 Hz, 2H, ArH), 7.28 – 7.23 (m, 2H, ArH), 7.21 (d, *J* = 8.7 Hz, 4H, ArH), 5.98 (s, 2H, CH₂), 5.25 (d, *J* = 5.1 Hz, 2H, OH-2), 4.94 (d, *J* = 5.6 Hz, 2H, OH-3), 4.91 (d, *J* = 7.7 Hz, 2H, H-1), 4.71 (t, *J* = 5.5 Hz, 2H, OH-6), 4.57 (d, *J* = 4.6 Hz, 2H, OH-4), 3.71 (t, *J* = 3.9 Hz, 2H, H-4), 3.65 – 3.46 (m, 8H, H-2, H-5, H-6), 3.46 – 3.39 (m, 2H, H-3).

¹³C NMR (126 MHz, DMSO-d₆) δ 162.73 (2C, C=O), 157.71 (2C, ArC), 157.52 (2C, ArC), 147.46 (2C, N=C), 134.87 (2C, ArC), 129.67 (2C, ArCH), 128.81 (4C, ArCH), 128.60 (2C, ArC), 120.97 (2C, ArCH), 119.42 (2C, ArCH), 116.45 (4C, ArCH), 115.70 (2C, ArCH), 101.13 (2C, C-1), 89.64 (1C, CH₂), 75.63 (2C, C-5), 73.33 (2C, C-3), 70.33 (2C, C-2), 68.12 (2C, C-4), 60.36 (2C, C-6).

HPLC-MS: [C₄₁H₄₄N₄O₁₆ + H]⁺ calcd. 849.28, found 849.35.

HRMS: [C₄₁H₄₄N₄O₁₆ + H]⁺ calcd. 849.2825, found 849.2822.

Divalent ligand C5p was synthesized following the general procedure for synthesis of acylhydrazones using bisbenzaldehyde **C** (16.6 mg, 0.06 mmol) and hydrazide **1p** (51.3 mg, 0.16 mmol). Compound **C5p** (26.8 mg, 0.03 mmol, 49%) was obtained as white solid.

¹H NMR (500 MHz, DMSO-d₆) δ 11.68 (s, 2H, NH), 8.39 (s, 2H, N=CH), 7.88 (d, *J* = 8.5 Hz, 4H, ArH), 7.71 (d, *J* = 8.3 Hz, 4H, ArH), 7.20 (d, *J* = 8.3 Hz, 4H, ArH), 7.13 (d, *J* = 8.7 Hz, 4H, ArH), 5.97 (s, 2H, CH₂), 5.24 (s, 2H, OH-2), 4.98 – 4.87 (m, 4H, H-1, OH-3), 4.70 (s, 2H, OH-6), 4.56 (s, 2H, OH-4), 3.71 (d, *J* = 3.4 Hz, 2H, H-4), 3.65 – 3.43 (m, 10H, H-2, H-3, H-5, H-6).

¹³C NMR (126 MHz, DMSO-d₆) δ 162.54 (2C, C=O), 160.09 (2C, ArC), 157.64 (2C, ArC), 146.95 (2C, N=CH), 129.38 (4C, ArCH), 128.74 (4C, ArCH), 126.62 (2C, ArC), 116.46 (4C, ArCH), 115.83 (4C, ArCH), 100.50 (2C, C-1), 89.73 (1C, CH₂), 75.65 (2C, C-5), 73.32 (2C, C-3), 70.27 (2C, C-2), 68.18 (2C, C-4), 60.41 (2C, C-6).

HPLC-MS: [C₄₁H₄₄N₄O₁₆ + H]⁺ calcd. 849.28, found 849.38.

HRMS: [C₄₁H₄₄N₄O₁₆ + H]⁺ calcd. 849.2825, found 849.2835.

Divalent ligand D5m was synthesized following the general procedure for synthesis of acyl hydrazones using bisbenzaldehyde **D** (22.3 mg, 0.08 mmol) and hydrazide **1m** (100.4 mg) in DMSO/MeCN (11 mL : 1 mL). Compound **D5m** (4.6 mg, 5.3 μmol, 6%) was obtained as white solid.

¹H NMR (500 MHz, DMSO-d₆) δ 11.71 (s, 2H, NH), 8.40 (s, 2H, N=CH), 7.69 (d, *J* = 8.6 Hz, 4H, ArH), 7.54 – 7.53 (m, 4H, ArH), 7.44 (t, *J* = 8.1 Hz, 2H, ArH), 7.25 (d, *J* = 7.1 Hz, 2H, ArH), 7.10 (d, *J* = 8.6 Hz, 4H, ArH), 5.22 (d, *J* = 4.3 Hz, 2H, OH-2), 4.90 – 4.92 (m, 4H, OH-3, H-1), 4.69 (s, 2H, OH-6), 4.55 (d, *J* = 3.8 Hz, 2H, OH-4), 4.41 (s, 4H, CH₂), 3.72 (s, 2H, H-4), 3.62 – 3.54 (m, 6H, H-2, H-5, H-6a), 3.52 – 3.48 (m, 2H, H-6b), 3.43 (d, *J* = 9.2 Hz, 2H, H-3).

¹³C NMR (126 MHz, DMSO-d₆) δ 162.65 (2C, C=O), 159.93 (2C, ArC), 157.51 (2C, ArC), 147.73 (2C, N=C), 134.92 (2C, ArC), 129.62 (2C, ArCH), 128.79 (4C, ArCH), 127.17 (2C, ArC), 120.93 (2C, ArCH), 119.37 (2C, ArCH), 115.68 (2C, ArCH), 114.95 (4C, ArCH), 101.13 (2C, C-1), 75.61 (2C, C-5), 73.32 (2C, C-3), 70.32 (2C, C-2), 68.10 (2C, C-4), 66.48 (2C, CH₂), 60.34 (2C, C-6).

HPLC-MS: [C₄₂H₄₆N₄O₁₆ + H]⁺ calcd. 863.30, found 863.37.

HRMS: [C₄₂H₄₆N₄O₁₆ + H]⁺ calcd. 863.2982, found 863.2984.

Divalent ligand D5p was synthesized following the general procedure for synthesis of acylhydrazones using bisbenzaldehyde **D** (18.9 mg, 0.06 mmol) and hydrazide **1p** (50.2 mg, 0.16 mmol) in DMSO/DMF (1 mL : 1 mL). Compound **D5p** (18.1 mg, 0.021 mmol, 33%) was obtained as white solid.

¹H NMR (500 MHz, DMSO-d₆) δ 11.65 (s, 2H, NH), 8.39 (s, 2H, N=CH), 7.92 – 7.82 (m, 4H, ArH), 7.68 (d, *J* = 8.3 Hz, 4H, ArH), 7.13 (d, *J* = 8.4 Hz, 4H, ArH), 7.09 (d, *J* = 8.3 Hz, 4H, ArH), 5.24 (s, 2H, OH-2), 4.95 (m, 4H, H-1, OH-3), 4.70 (s, 2H, OH-6), 4.57 (s, 2H, OH-4), 4.40 (s, 4H, CH₂), 3.72 (d, *J* = 3.3 Hz, 2H, H-4), 3.66 – 3.41 (m, 10H, H-2, H-3, H-5, H-6).

¹³C NMR (126 MHz, DMSO-d₆) δ 162.87 (2C, C=O), 160.47 (2C, ArC), 160.28 (2C, ArC), 147.62 (2C, N=CH), 129.76 (4C, ArCH), 129.15 (4C, ArCH), 127.74 (2C, ArC), 127.09 (2C, ArC), 116.23 (4C, ArCH), 115.39 (4C, ArCH), 100.91 (2C, C-1), 76.06 (2C, C-5), 73.74 (2C, C-3), 70.68 (2C, C-2), 68.58 (2C, C-4), 66.92 (2C, CH₂), 60.81 (2C, C-6).

HPLC-MS: [C₄₂H₄₆N₄O₁₆ + H]⁺ calcd. 863.30, found 863.40.

HRMS: [C₄₂H₄₆N₄O₁₆ + H]⁺ calcd. 863.2982, found 863.2991.

Divalent ligand E5m was synthesized following the general procedure for synthesis of acylhydrazones using bisbenzaldehyde **E** (16.5 mg, 0.06 mmol) and hydrazide **1m** (56.3 mg, 0.18 mmol). Compound **E5m** (4.9 mg, 5.8 μmol, 10%) was obtained as white solid.

¹H NMR (500 MHz, DMSO-d₆) δ 11.71 (s, 2H, NH), 8.38 (s, 2H, N=CH), 7.67 (d, *J* = 8.4 Hz, 4H, ArH), 7.53 (dt, *J* = 4.1, 1.7 Hz, 4H, ArH), 7.44 (t, *J* = 8.1 Hz, 2H, ArH), 7.25 (ddd, *J* = 8.3, 2.3, 1.1 Hz, 2H, ArH), 7.06 (d, *J* = 8.4 Hz, 4H, ArH), 5.24 (d, *J* = 5.1 Hz, 2H, OH-2), 4.98 – 4.86 (m, 4H, OH-3, H-1), 4.70 (t, *J* = 5.5 Hz, 2H, OH-6), 4.57 (d, *J* = 4.6 Hz, 2H, OH-4), 4.21 (t, *J* = 6.2 Hz, 4H, CH₂CH₂CH₂), 3.71 (t, *J* = 3.9 Hz, 2H, H-4), 3.64 – 3.45 (m, 8H, H-2, H-5, H-6), 3.45 – 3.40 (m, 2H, H-3), 2.26 – 2.17 (m, 2H, CH₂CH₂CH₂).

¹³C NMR (126 MHz, DMSO) δ 162.63 (2C, C=O), 160.12 (2C, ArC), 157.50 (2C, ArC), 147.73 (2C, N=CH), 134.94 (2C, ArC), 129.65 (2C, ArCH), 128.81 (4C, ArCH), 126.98 (2C, ArC), 120.95 (2C, ArCH), 119.37 (2C, ArCH), 115.69 (4C, ArCH), 114.91 (4C, ArCH), 101.13 (2C, C-1), 75.62 (2C, C-5), 73.32 (2C, C-3), 70.32 (2C, C-2), 68.11 (2C, C-4), 64.43 (2C, CH₂CH₂CH₂), 60.35 (2C, C-6), 28.57 (1C, CH₂CH₂CH₂).

HPLC-MS: [C₄₃H₄₈N₄O₁₆ + H]⁺ calcd. 877.31, found 877.38.

HRMS: [C₄₃H₄₈N₄O₁₆ + H]⁺ calcd. 877.3138, found 877.3136.

Divalent ligand E5p was synthesized following the general procedure for synthesis of acylhydrazones using bisbenzaldehyde **E** (18.3 mg, 0.06 mmol) and hydrazide **1p** (55.7 mg, 0.18 mmol). Compound **E5p** (17.3 mg, 0.20 mmol, 31%) was obtained as white solid.

¹H NMR (500 MHz, DMSO-d₆) δ 11.63 (s, 2H, NH), 8.38 (s, 2H, N=CH), 7.87 (d, *J* = 8.6 Hz, 4H, ArH), 7.66 (d, *J* = 8.4 Hz, 4H, ArH), 7.12 (d, *J* = 8.7 Hz, 4H, ArH), 7.05 (d, *J* = 8.5 Hz, 4H, ArH), 5.23 (s, 2H, OH-2), 4.97 – 4.88 (m, 4H, H-1, OH-3), 4.69 (s, 2H, OH-6), 4.55 (s, 2H, OH-4), 4.21 (t, *J* = 5.8 Hz, 4H, CH₂CH₂CH₂), 3.71 (s, 2H, H-4), 3.65 – 3.41 (m, 10H, H-2, H-3, H-5, H-6), 2.26 – 2.18 (m, 2H, CH₂CH₂CH₂).

¹³C NMR (126 MHz, DMSO-d₆) δ 162.41 (2C, C=O), 160.03 (4C, ArC), 147.20 (2C, N=CH), 129.32 (4C, ArCH), 128.69 (4C, ArCH), 127.10 (2C, ArC), 126.67 (2C, ArC), 115.79 (4C, ArCH),

114.89 (4C, ArCH), 100.48 (2C, C-1), 75.63 (2C, C-5), 73.30 (2C, C-3), 70.24 (2C, C-2), 68.14 (2C, C-4), 64.43 (2C, $\underline{\text{CH}_2\text{CH}_2\text{CH}_2}$), 60.37 (2C, C-6), 28.57 (1C, $\text{CH}_2\underline{\text{CH}_2\text{CH}_2}$).

HPLC-MS: $[\text{C}_{43}\text{H}_{48}\text{N}_4\text{O}_{16} + \text{H}]^+$ calcd. 877.31, found 877.40.

HRMS: $[\text{C}_{43}\text{H}_{48}\text{N}_4\text{O}_{16} + \text{H}]^+$ calcd. 877.3138, found 877.3145.

Divalent ligand F5m was synthesized following the general procedure for synthesis of acylhydrazones using bisbenzaldehyde **F** (25.6 mg, 0.09 mmol) and hydrazide **1m** (84.2 mg) in MeCN/H₂O (6 mL : 2.5 mL). Compound **F5m** (5.0 mg, 5.6 μmol , 7%) was obtained as white solid.

¹H NMR (500 MHz, DMSO-*d*₆) δ 11.69 (s, 2H, NH), 8.38 (s, 2H, N=CH), 7.66 (d, *J* = 8.7 Hz, 4H), 7.54 – 7.52 (m, 4H, ArH), 7.44 (t, *J* = 8.1 Hz, 2H, ArH), 7.24 (d, *J* = 7.2 Hz, 2H, ArH), 7.04 (d, *J* = 8.6 Hz, 4H, ArH), 5.23 (s, 2H, OH-2), 4.91 (m, 4H, H-1, OH-3), 4.70 (s, 2H, OH-6), 4.56 (s, 2H, OH-4), 4.11 (s, 4H, $\underline{\text{CH}_2\text{CH}_2\text{CH}_2\text{CH}_2}$), 3.71 (d, *J* = 2.6 Hz, 2H, H-4), 3.61 – 3.54 (m, 6H, H-2, H-5, H-6a), 3.49 (m, 2H, H-6b), 3.43 (dd, *J* = 9.5, 2.9 Hz, 2H, H-3), 1.91 (s, 4H, $\text{CH}_2\underline{\text{CH}_2\text{CH}_2\text{CH}_2}$).

¹³C NMR (126 MHz, DMSO-*d*₆) δ 162.69 (2C, C=O), 160.25 (2C, ArC), 157.49 (2C, ArC), 147.77 (2C, N=C), 135.06 (2C, ArC), 129.57 (2C, ArCH), 128.74 (4C, ArCH), 126.88 (2C, ArC), 120.93 (2C, ArCH), 119.30 (2C, ArCH), 115.68 (2C, ArCH), 114.86 (4C, ArCH), 101.14 (2C, C-1), 75.60 (2C, C-5), 73.32 (2C, C-3), 70.32 (2C, C-2), 68.09 (2C, C-4), 67.33 (2C, $\underline{\text{CH}_2\text{CH}_2\text{CH}_2\text{CH}_2}$), 60.33 (2C, C-6), 25.36 (2C, $\text{CH}_2\underline{\text{CH}_2\text{CH}_2\text{CH}_2}$).

HPLC-MS: $[\text{C}_{44}\text{H}_{50}\text{N}_4\text{O}_{16} + \text{H}]^+$ calcd. 891.33, found 891.39.

HRMS: $[\text{C}_{44}\text{H}_{50}\text{N}_4\text{O}_{16} + \text{H}]^+$ calcd. 891.3295, found 891.3298.

Divalent ligand F5p was synthesized following the general procedure for synthesis of acylhydrazones using bisbenzaldehyde **F** (18.9 mg, 0.06 mmol) and hydrazide **1p** (50.2 mg, 0.16 mmol). Compound **F5p** (11.0 mg, 0.01 mmol, 19%) was obtained as white solid.

¹H NMR (500 MHz, DMSO-*d*₆) δ 11.63 (s, 2H, NH), 8.37 (s, 2H, N=CH), 7.87 (d, *J* = 8.5 Hz, 4H, ArH), 7.66 (d, *J* = 8.3 Hz, 4H, ArH), 7.12 (d, *J* = 8.7 Hz, 4H, ArH), 7.03 (d, *J* = 8.5 Hz, 4H, ArH), 5.24 (s, 2H, OH-2), 4.93 (m, 4H, H-1, OH-3), 4.71 (s, 2H, OH-6), 4.56 (s, 2H, OH-4), 4.10 (s, 4H, $\underline{\text{CH}_2\text{CH}_2\text{CH}_2\text{CH}_2}$), 3.71 (s, 2H, H-4), 3.66 – 3.48 (m, 10H, H-2, H-3, H-5, H-6), 1.90 (s, 4H, $\text{CH}_2\underline{\text{CH}_2\text{CH}_2\text{CH}_2}$).

¹³C NMR (126 MHz, DMSO-*d*₆) δ 162.50 (2C, C=O), 160.24 (2C, ArC), 160.07 (2C, ArC), 147.34 (2C, N=CH), 129.36 (4C, ArCH), 128.74 (4C, ArCH), 126.97 (2C, ArC), 126.69 (2C, ArC),

115.85 (4C, ArCH), 114.91 (4C, ArCH), 100.51 (2C, C-1), 75.66 (2C, C-5), 73.33 (2C, C-3), 70.28 (2C, C-2), 68.19 (2C, C-4), 67.40 (2C, $\underline{\text{CH}_2\text{CH}_2\text{CH}_2\text{CH}_2}$), 60.43 (2C, C-6), 25.41 (2C, $\text{CH}_2\text{CH}_2\text{CH}_2\text{CH}_2$).

HPLC-MS: $[\text{C}_{44}\text{H}_{50}\text{N}_4\text{O}_{16} + \text{H}]^+$ calcd. 891.33, found 891.45.

HRMS: $[\text{C}_{44}\text{H}_{50}\text{N}_4\text{O}_{16} + \text{H}]^+$ calcd. 891.3295, found 891.3306.

DCC

A dynamic combinatorial library (DCL) of hydrazide **1p** with aldehydes **B–F** was formed in citrate buffer (100 mM Na-citrate, 1 mM CaCl_2 , pH 5.7) in presence of 20% of DMSO. Final concentrations in DCL were: aniline (10 mM), hydrazide **1p** (625 μM), aldehydes **B–F** (50 μM each) and LecA (62.5 μM , added at time 0 h or after 6 h) in a reaction volume of 1 mL. The DCL was left shaking at room temperature and monitored *via* HPLC-MS with a C8 column (Acquity UPLC BEH C8 column, 2.1 mm x 150 mm, 1.7 μM from Waters, Germany). Samples for HPLC-MS were prepared from 20 μL of reaction mixture mixed with 5 μL of 2 M NaOH to freeze the equilibrium and addition of 50 μL MeCN. The mixture was centrifuged at 15000 rpm in an Eppendorf tube centrifuge for 3 minutes and the supernatant was analyzed.

The formation of precipitate was observed after approx. 30 minutes in the case when LecA was added at time 0 h or immediately in the case when the LecA was added to already formed library after 6 h.

Biophysical evaluation

Expression and purification of LecA as well as competitive binding by fluorescence polarization was performed as described by Joachim *et al.*⁶ The assay was performed in TBS/ Ca^{2+} buffer (20 mM Tris, 137 mM NaCl, 2.6 mM KCl at pH 7.4 supplemented with 1 mM CaCl_2) in presence of 25% DMSO. Averages and standard deviations were calculated from at least three experiments.

Isothermal titration calorimetry was performed on an iTC200 (Malvern Panalytical) and analyzed using Microcal Origin software and MicroCal ConCat ITC software (Malvern Panalytical). LecA (100 - 200 μM) in the cell was titrated with ligand (0.85-2 mM) in TBS/ Ca^{2+} buffer at 25 °C.

Surface plasmon resonance experiments were performed on a BIACORE X100 instrument (GE Healthcare) at 25 °C. For LecA immobilization, the system was pre-equilibrated with PBS buffer (10 mM phosphate buffer pH 7.4, 2.7 mM KCl, 137 mM NaCl, 100 μ M CaCl₂, 0.05% Tween 20), followed by an activation of the CM5 chip surface by 3 injections of 1:1 N-hydroxysuccinimide (NHS)/1-ethyl-3(3-dimethylaminopropyl)carbodiimide hydrochloride (EDC) mixture on channel 1 and 2 (contact time of 540 s, flow rate 10 μ L/min) until the binding response was above 800 RU. LecA was dissolved in 10 mM sodium acetate pH 4.5 (100 μ g/mL) and injected over the activated chip surface on channel 2 (contact time of 540 s, flow rate 10 μ L/min) until the response of ~2800 RU was reached. Excess free NHS-ester groups were capped with an injection of 1 M ethanolamine (contact time 540 s, flow rate 10 μ L/min). Divalent compounds stocks solutions (50 μ M in DMSO) were prepared and then diluted with 1.05 X PBS buffer to 2.5 μ M solutions with 5% DMSO. The 2.5 μ M stocks were subsequently diluted to required concentrations in a running buffer (10 mM phosphate buffer pH 7.4, 2.7 mM KCl, 137 mM NaCl, 100 μ M CaCl₂, 0.05% Tween 20, 5% DMSO). The divalent inhibitors were subjected to single-cycle kinetics analyses (contact time of 120s and dissociation time of 120s, flow rate 30 μ L/min) consisting of injections of the analytes at 0, 10, 50, 100, and 200 nM over the immobilized-LecA. The chip surface was regenerated by 5 x injections of 5 mM galactose followed by 5 x injections of the running buffer (contact time of 120 s, flow rate 30 μ L/min). K_d determination was performed using BIACORE X100 evaluation software (version 2.0) by applying the 1:1 binding model to fit the experimental data. Affinity/Equilibrium analysis was carried out for monovalent inhibitors **A5m** and **A5p** on a CM5 chip with 3977 RU of immobilized LecA. The monovalent inhibitors stocks (5 mM in DMSO) were prepared and then diluted in 1.05 X PBS buffer to 250 μ M solutions with 5% DMSO. The 250 μ M stock was then diluted to required concentrations in a running buffer and injected over the immobilized LecA at 0, 1, 5, 10 and 20 μ M using the same SPR parameters as the divalent compound analyses, but without the regeneration step.

Expression, purification and SPR analysis of galectin-1 was performed as follows: pET3a-galectin-1 plasmid⁷ was transformed into *E. coli* BL21 (DE3) and cultured in 2 x 1 L of LB broth until OD₆₀₀ reached 0.5. The expression was then induced by addition of 1 mM isopropyl β -D-thiogalactopyranoside and further incubated at 30 °C for 3 h. Cells were harvested by

centrifugation (5000 x g, 20 min) and frozen at -20 °C. The frozen pellet was re-suspended in 30 mL of PBS buffer supplemented with 4 mM β -mercaptoethanol (β -ME) and one tablet of protease inhibitors (cOmplete™ Protease Inhibitor Cocktail, Roche) and lysed by cell disruptor (1.9 kbar). Cell lysates were centrifuged (24 000 x g, 30 min, 4 °C) to obtain supernatant, which was then filtered and loaded onto a lactosyl-sepharose 4B column⁸ pre-equilibrated with PBS buffer containing 4 mM β -mercaptoethanol (PBS/ β -ME). The column was washed with PBS/ β -ME to remove unbound protein. Bound galectin-1 was eluted with PBS/ β -ME supplemented with 50 mM lactose and collected as 2 mL fractions, which were pooled and dialyzed in 4 L of 20 mM Tris-HCl pH 7 supplemented with 1 mM dithiothreitol (DTT) for 2 days at 4 °C. The dialyzed protein was concentrated by Macrosep® Advance 3K (PALL Life Sciences) until the protein concentration reached 7.5 mg/mL. The protein was stored at 4 °C with an addition of 1 mM TCEP. Purified galectin-1 was immobilized to a CM5 chip (1500 RU) using the same methodology as described for LecA but supplementing all buffers with 1 mM DTT. Lactose solution was prepared by dissolving powder in the running buffer and further diluted to the required concentrations. The activity of immobilized galectin-1 was confirmed by injections of increasing concentration of lactose (100 – 1000 μ M, contact time = 30 s, dissociation time = 60 s, flow rate = 30 μ L/min). **A5m**, **A5p**, **C5m** and **B5p** were injected at the indicated concentrations in **Figure S3** (contact time of 120 s, dissociation time = 120 s, flow rate 30 μ L/min).

MD simulation

Ligand Building, Parametrisation and Molecular Dynamics. The four compounds were drawn in ChemDraw, ver. 18.2 and cut into fragments (Figure S4a) for simpler parametrization. Using ChemBio3D Ultra, ver. 14, they were subsequently transformed to 3D. PyMol was utilized afterwards to cap the dangling bonds and add hydrogen atoms. Parametrization of the capped fragments was done in Antechamber⁹ with GAFF force field¹⁰ and AM1-BCC charges¹¹. Thereafter the capping groups were removed, and their charge dispersed over the remaining atoms to restore neutrality.

The ligand structures were solvated in rectangular boxes of TIP3P¹² water molecules which extended to 12 Å from the solute. Na⁺/Cl⁻ counterions were added to a final concentration of

0.15 M. The systems were relaxed using the published protocols and settings^{13,14} and 1 μ s MD production run was carried out using PMEMD.CUDA software of AMBER18¹⁵ on GPUs. Analyses were performed using CPPTRAJ and graphs plotted with XMGRACE.

Protein Preparation. The structure of the LecA dimer was taken from the PDB: 5d21¹⁶. Asn/Gln/His flips and protonation of titratable protein residues was checked with the H++ program¹⁷ at pH = 7.4 (experimental condition for binding measurements) and no changes were needed. Histidine residues were monoprotonated on N δ (His58) and N ϵ (His50) based on visual inspection of their surroundings. Electronic continuum correction (ECC)¹⁸ was applied for the two calcium ions and their coordinating Asp100 side chains using charge scaling by a factor of 0.85 described previously.¹⁹

Modeling and Molecular Dynamics of Complexes. In the prepared LecA dimer, the two β -Gal phenyl residues were first extended and bonded by the tLEaP module of AMBER18. Subsequent optimization (1000 steepest descent cycles) in implicit solvent (igb=7)²⁰ of the added parts yielded the models for adding solvent and counterions to neutralize the systems. Relaxation protocols and settings were the same as above^{13,14} and the MD production runs were 300 ns long. Analyses were performed on the last 150 ns to allow for further system equilibration.

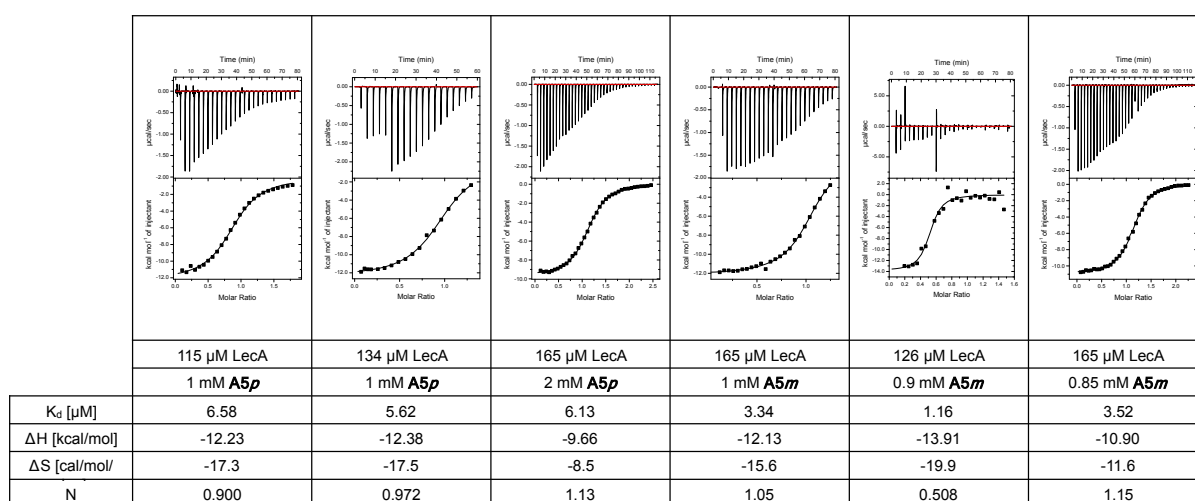


Figure S1: ITC measurements of **A5m** and **A5p** with LecA performed in TBS/ Ca^{2+} buffer at 25 $^{\circ}\text{C}$.

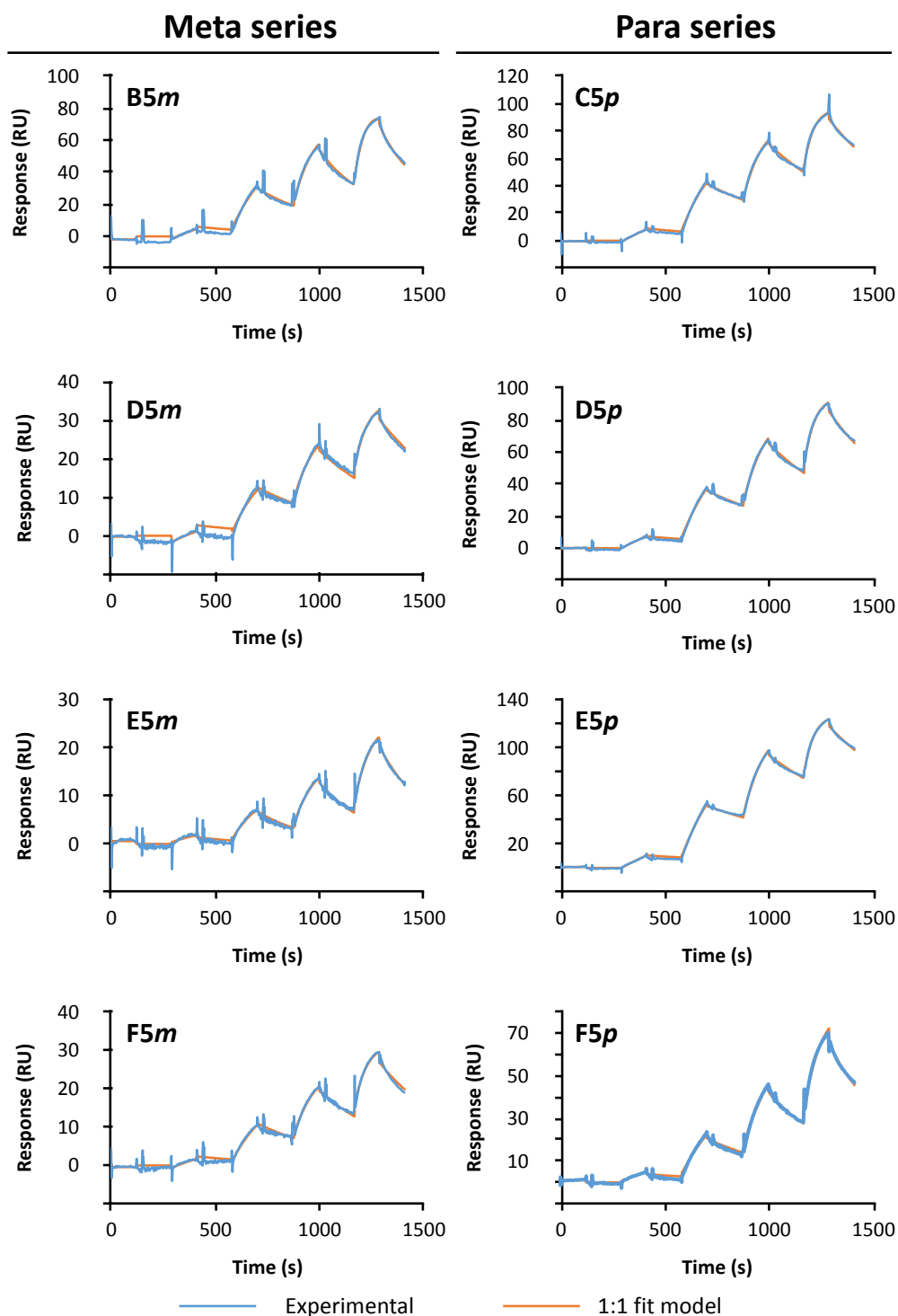


Figure S2: SPR of LecA with divalent galactosides. Sensorgrams obtained from SPR single-cycle kinetics experiments. Five different concentrations of each compound (0, 10, 50, 100, 200 nM) were sequentially injected to obtain the experimental sensorgrams (blue lines), which were then fitted by a 1:1 model (orange) on BIACORE evaluation software.

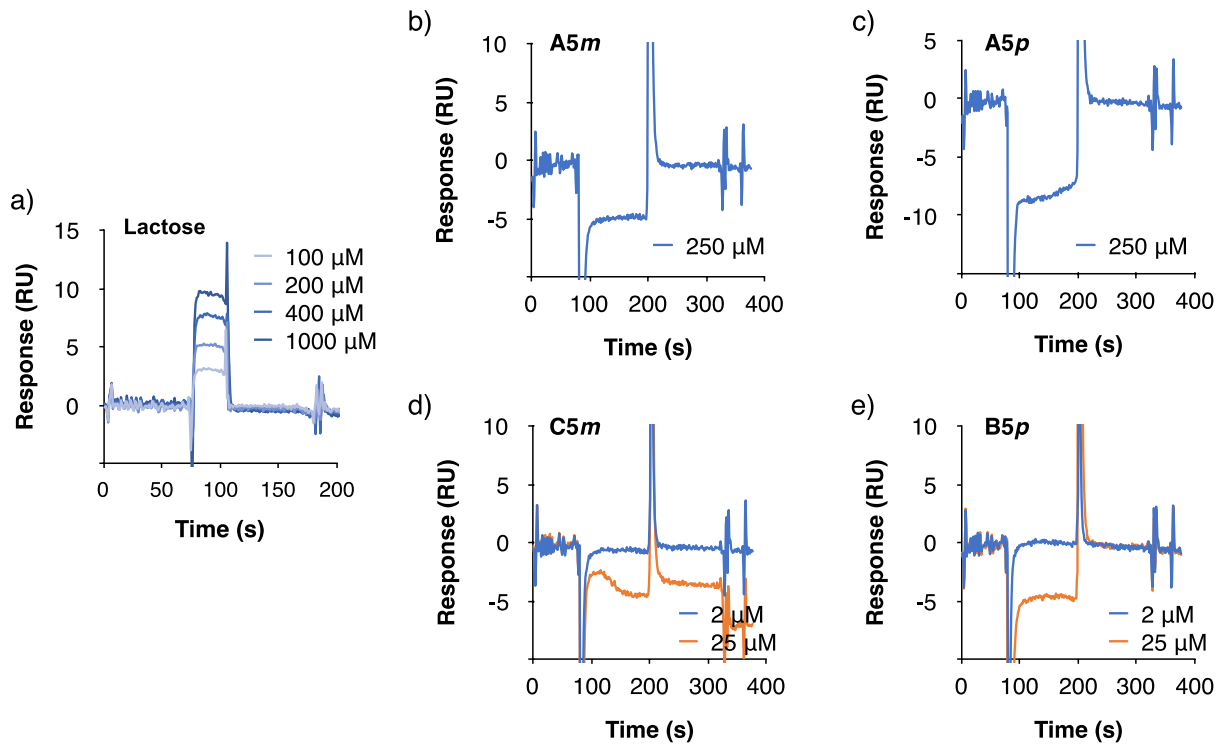


Figure S3: SPR analysis of interaction between immobilized galectin-1 and the inhibitors. The activity of immobilized galectin-1 was confirmed by injection of lactose. Spikes indicate the buffer mismatch at the beginning and the end of the contact time and the negative response in b-e is caused by the buffer mismatch due to different sample preparation and/or non-specific absorption in the reference channel.

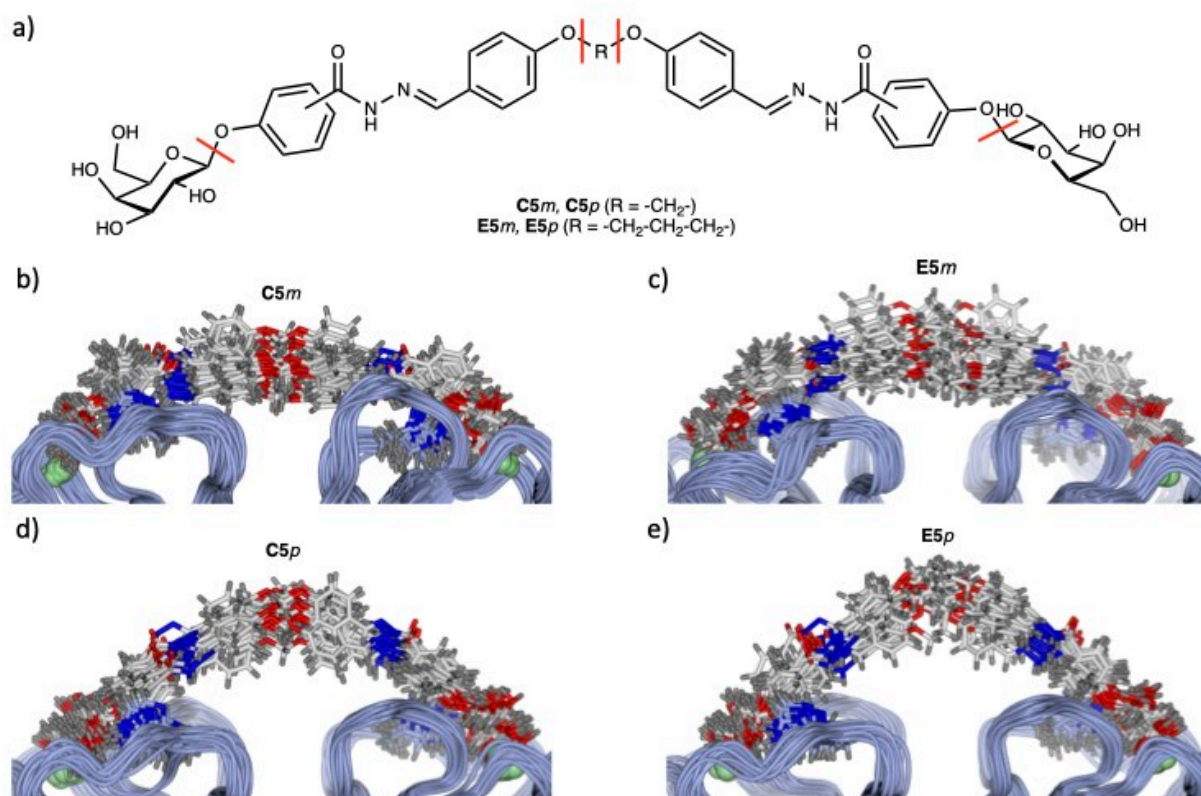
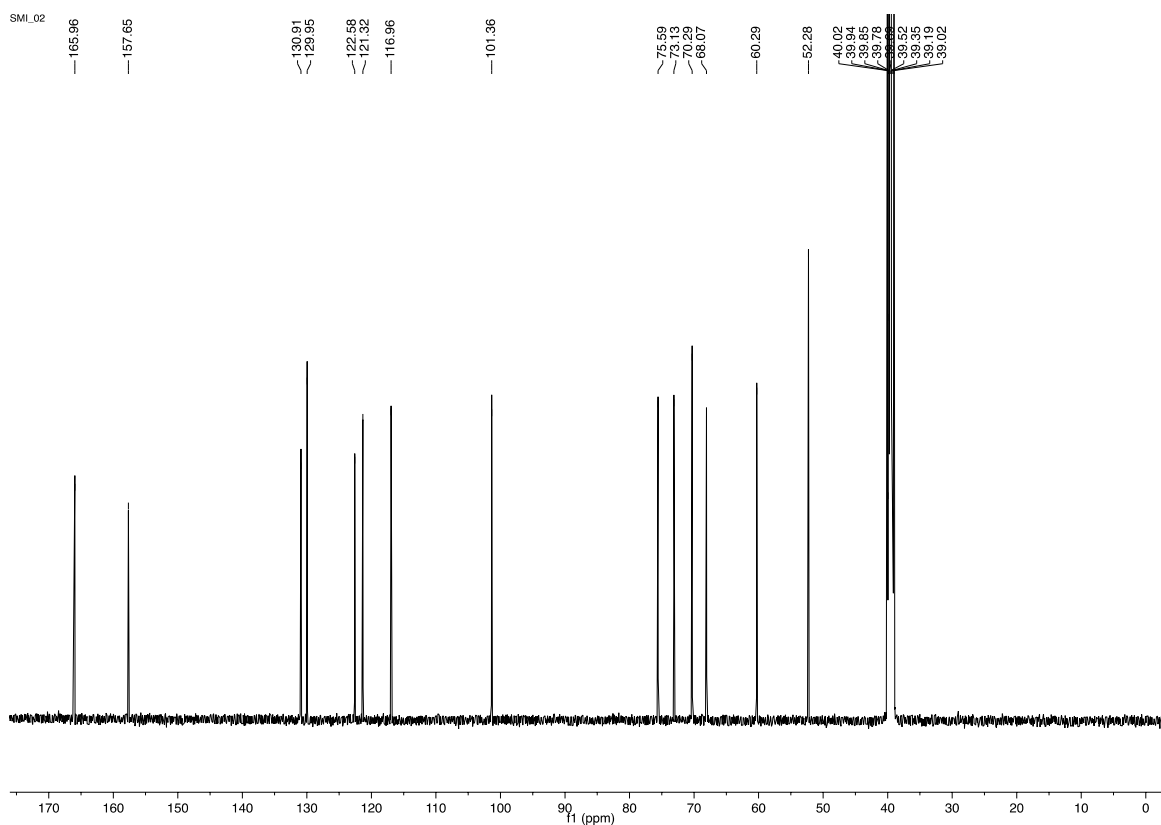
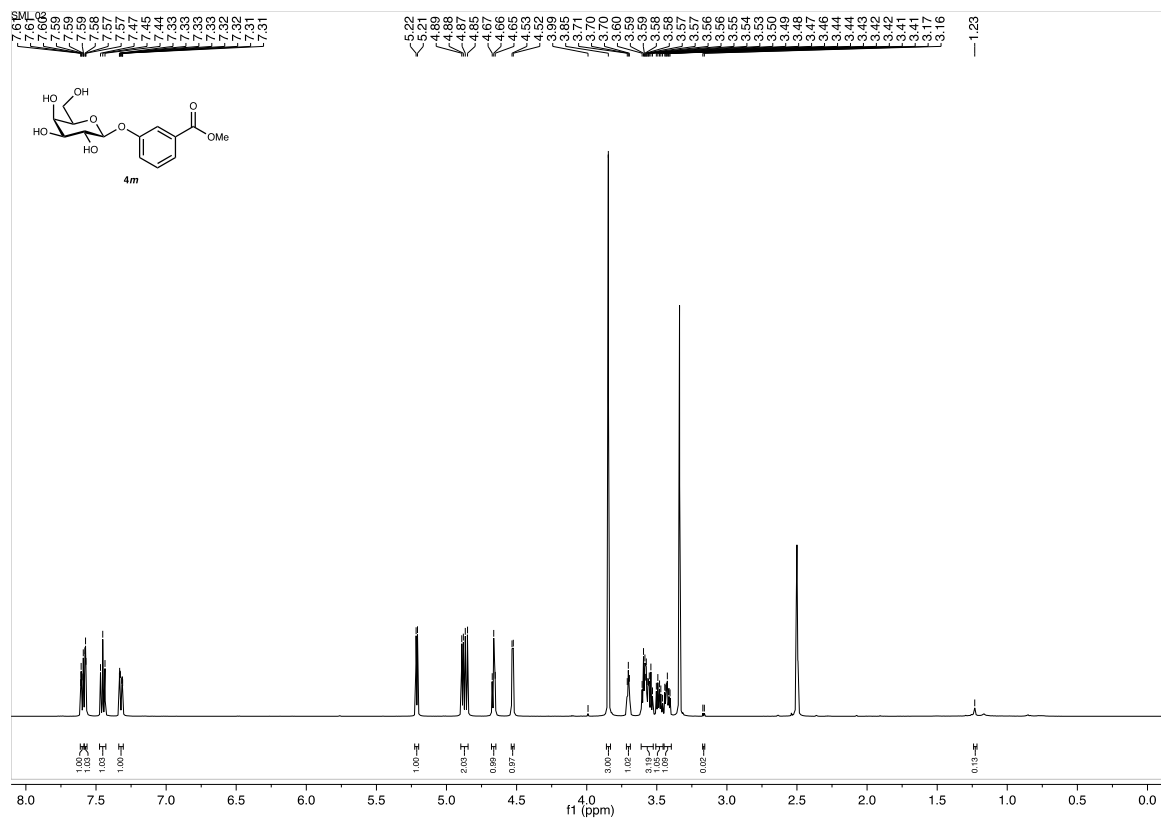
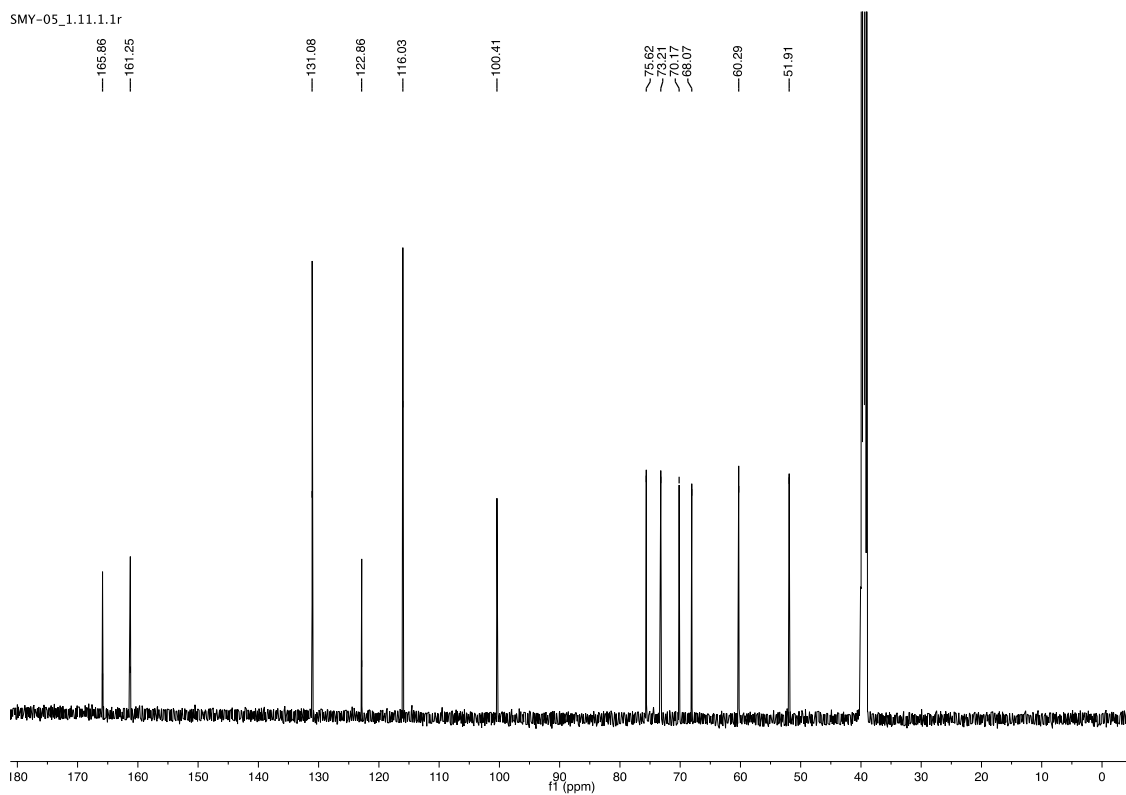
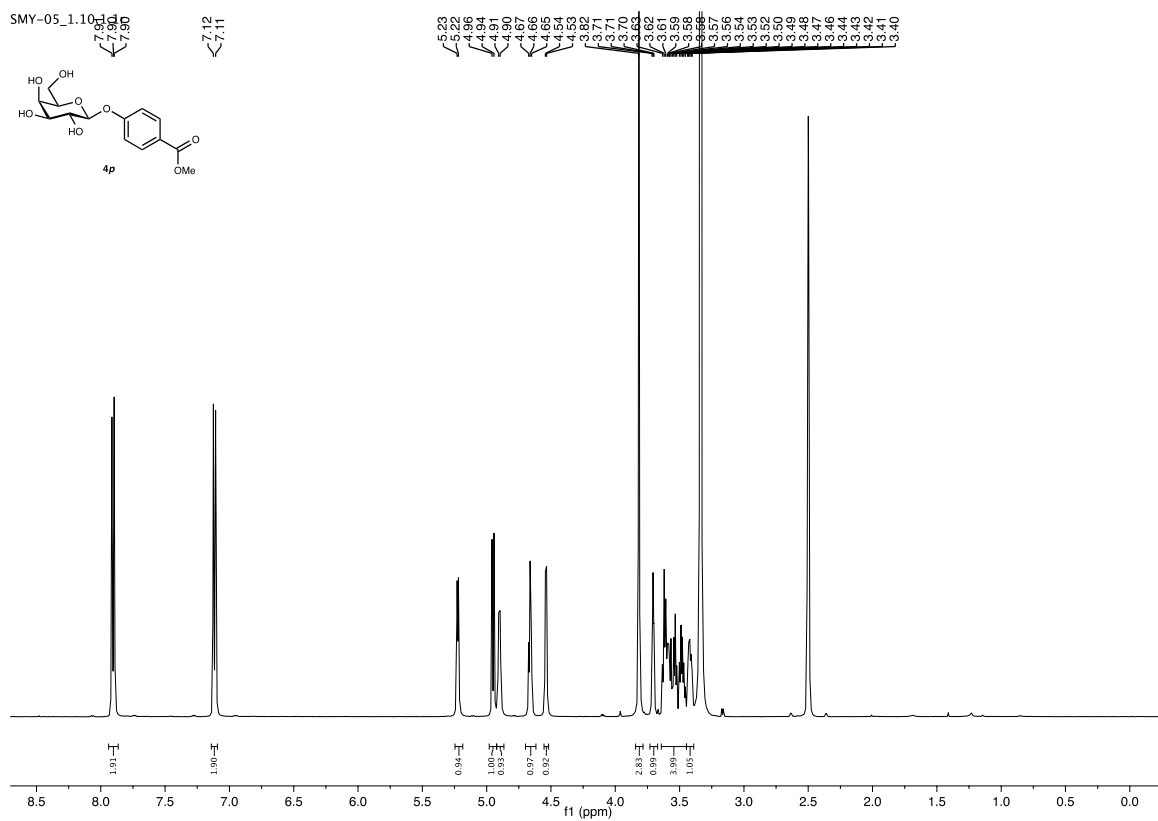


Figure S4: a) Definition of how the ligand was cut into fragments b)-e) Superpositions of 25 sampled snapshots from MD trajectories; b) **C5m**, c) **E5m**, d) **C5p**, and e) **E5p**.

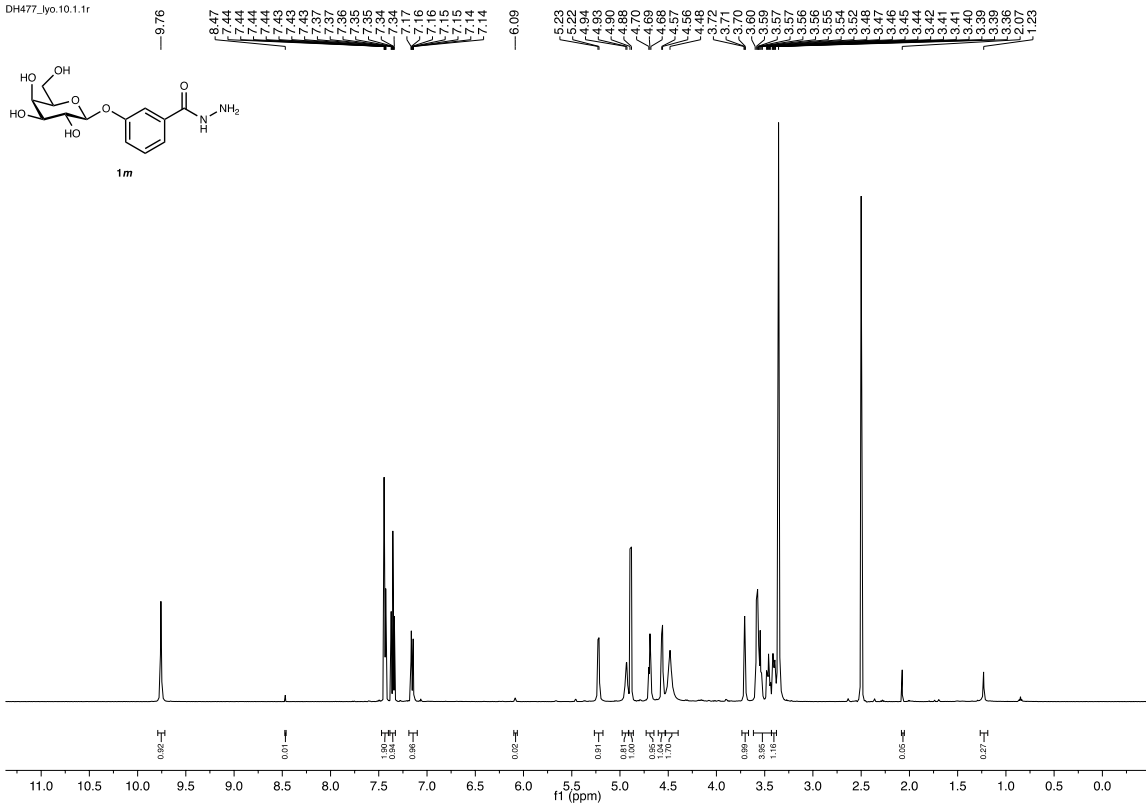


¹H and ¹³C NMR of **4m**

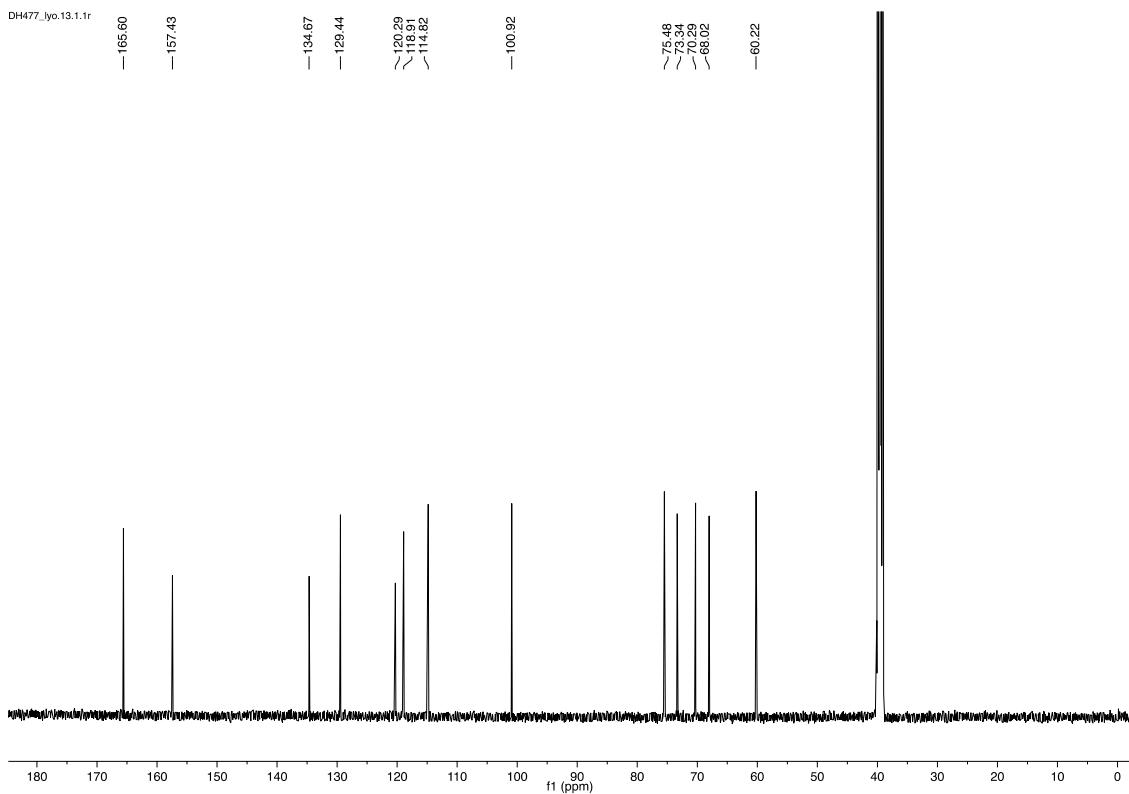


¹H and ¹³C NMR of **4p**

DH477_lyo.10.1.1r

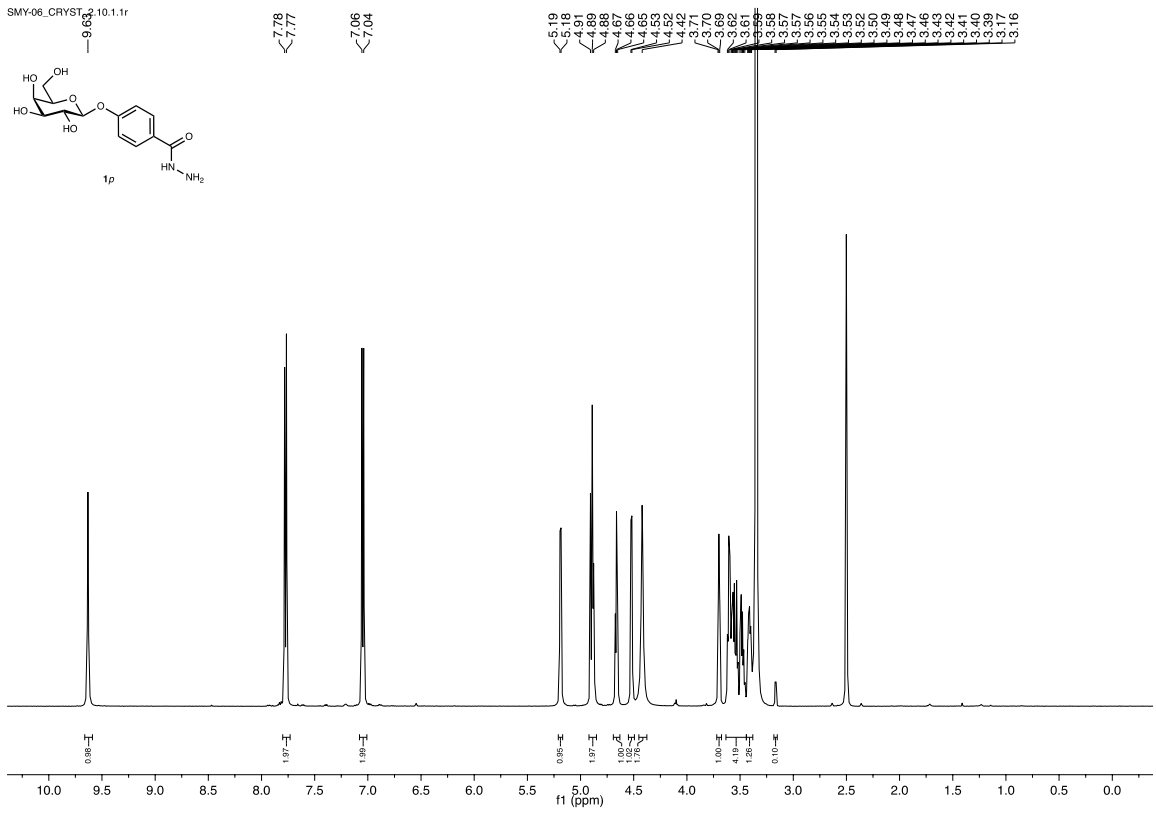
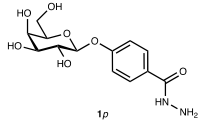


DH477_lyo.13.1.1r

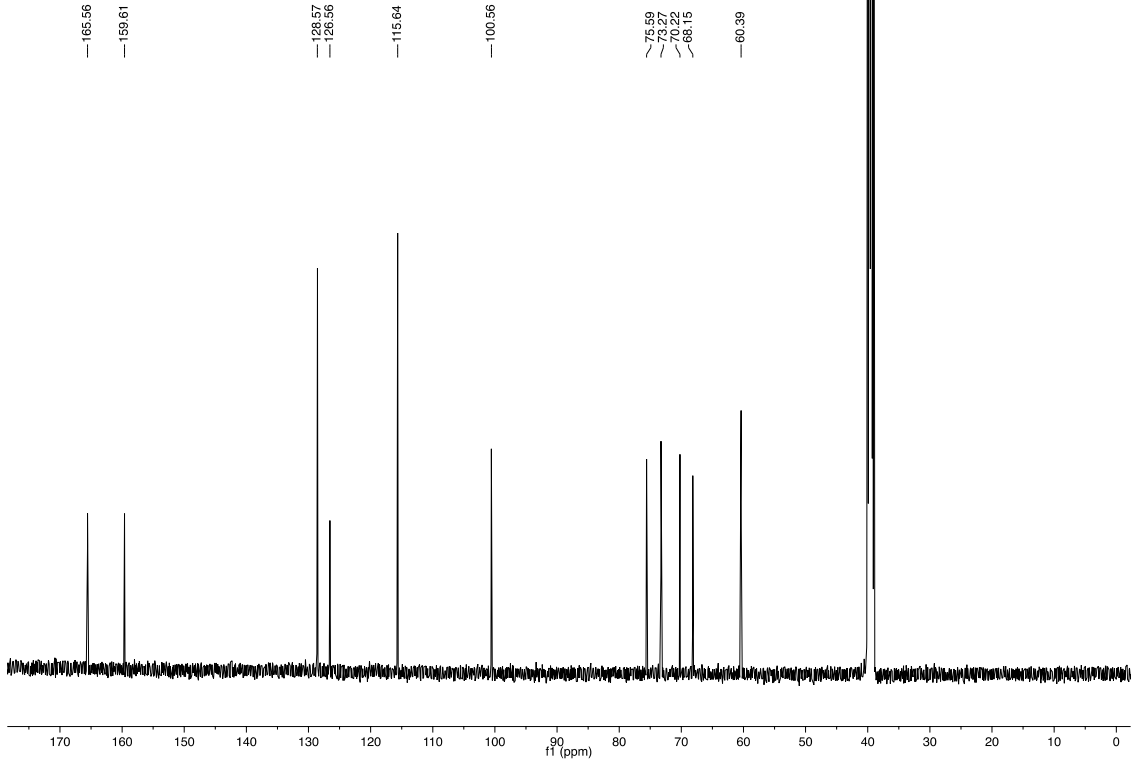


¹H and ¹³C NMR of impure **1m**

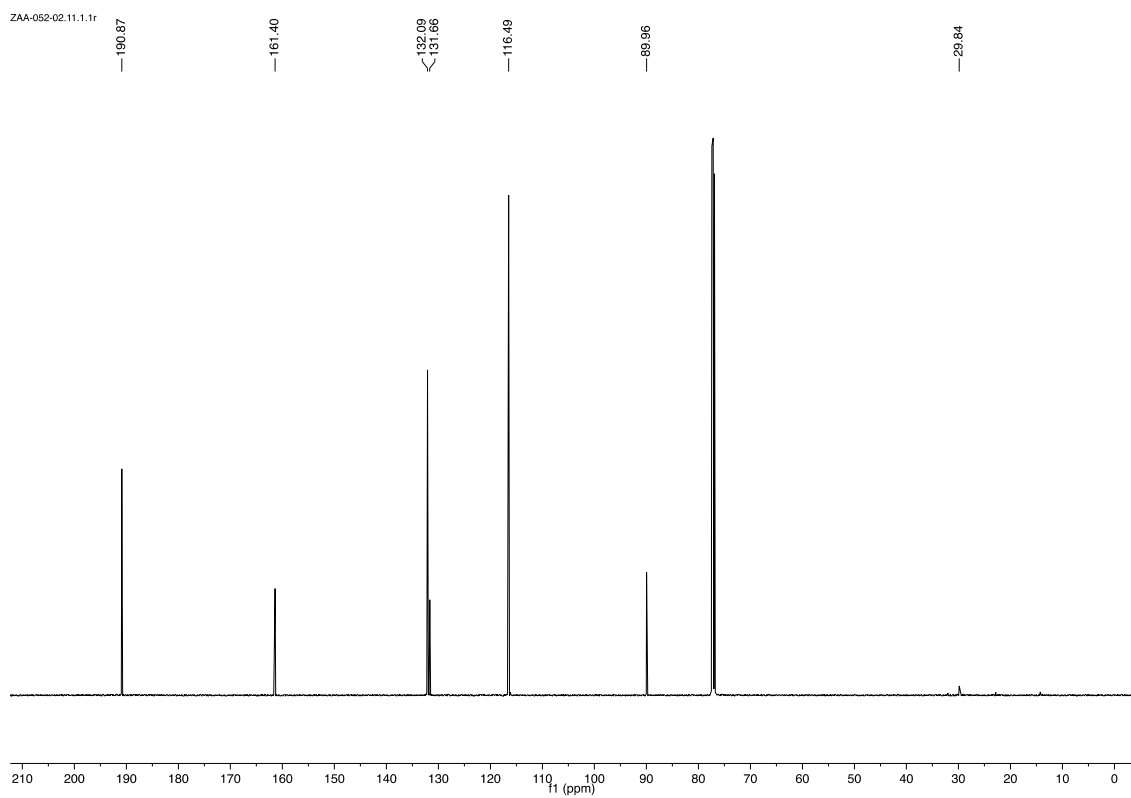
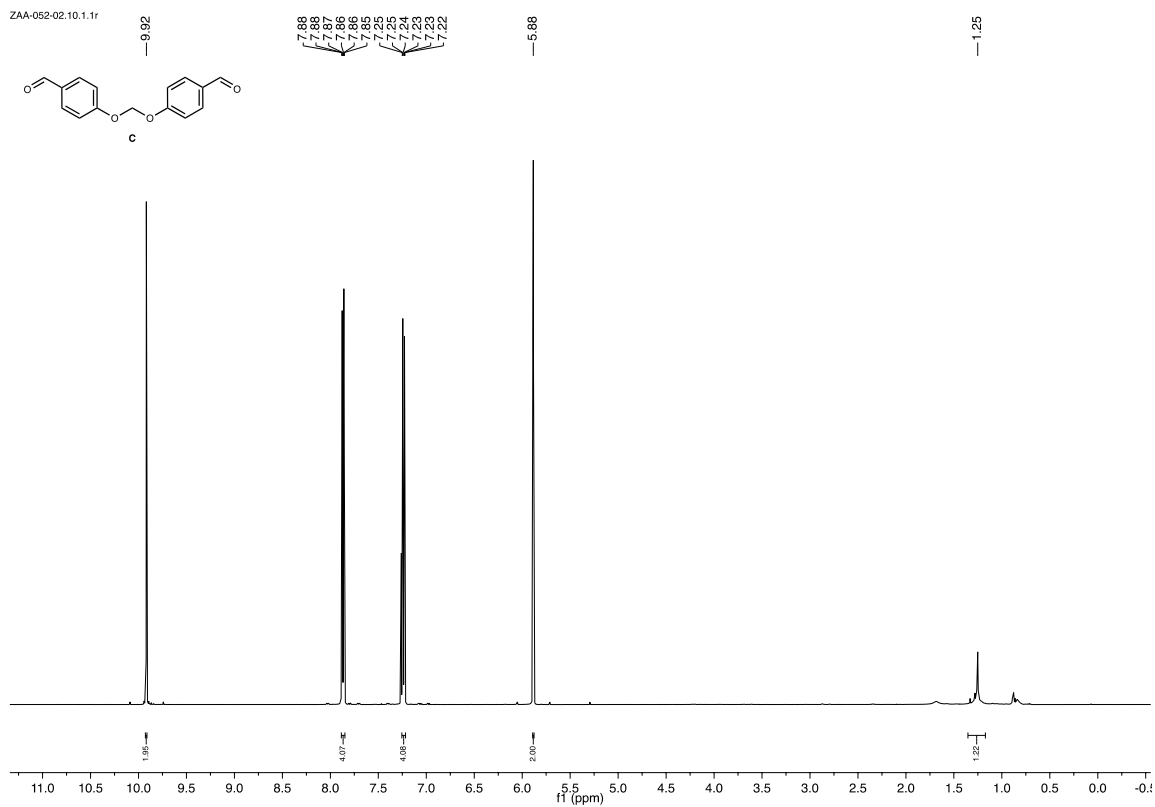
SMY-06_CRYST 10.1.1r



SMY-04_1.12.1.1r

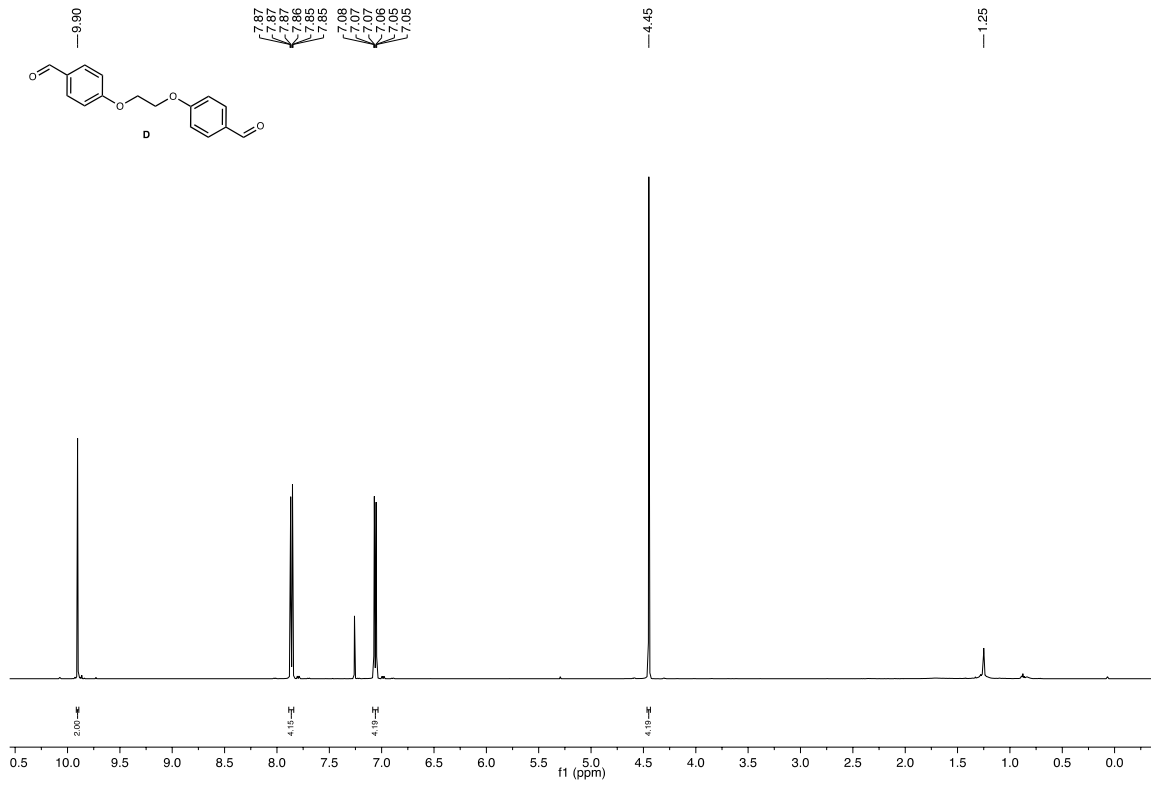


¹H and ¹³C NMR of 1p

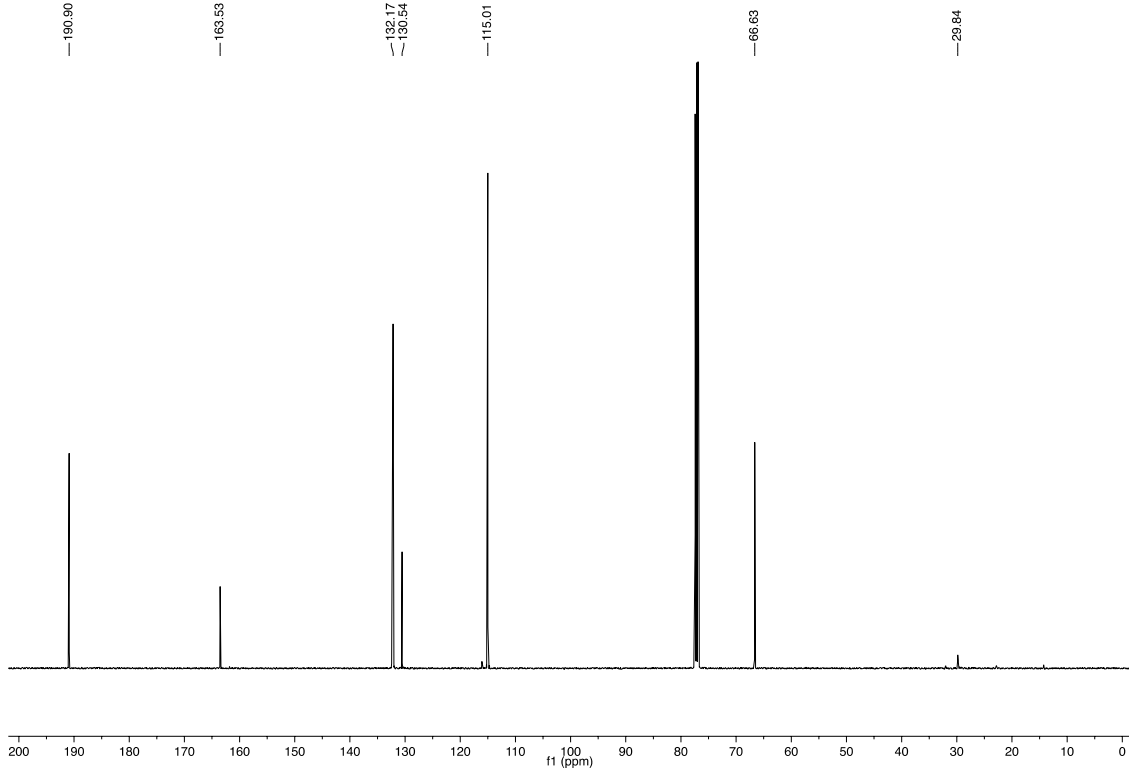


¹H and ¹³C NMR of linker C

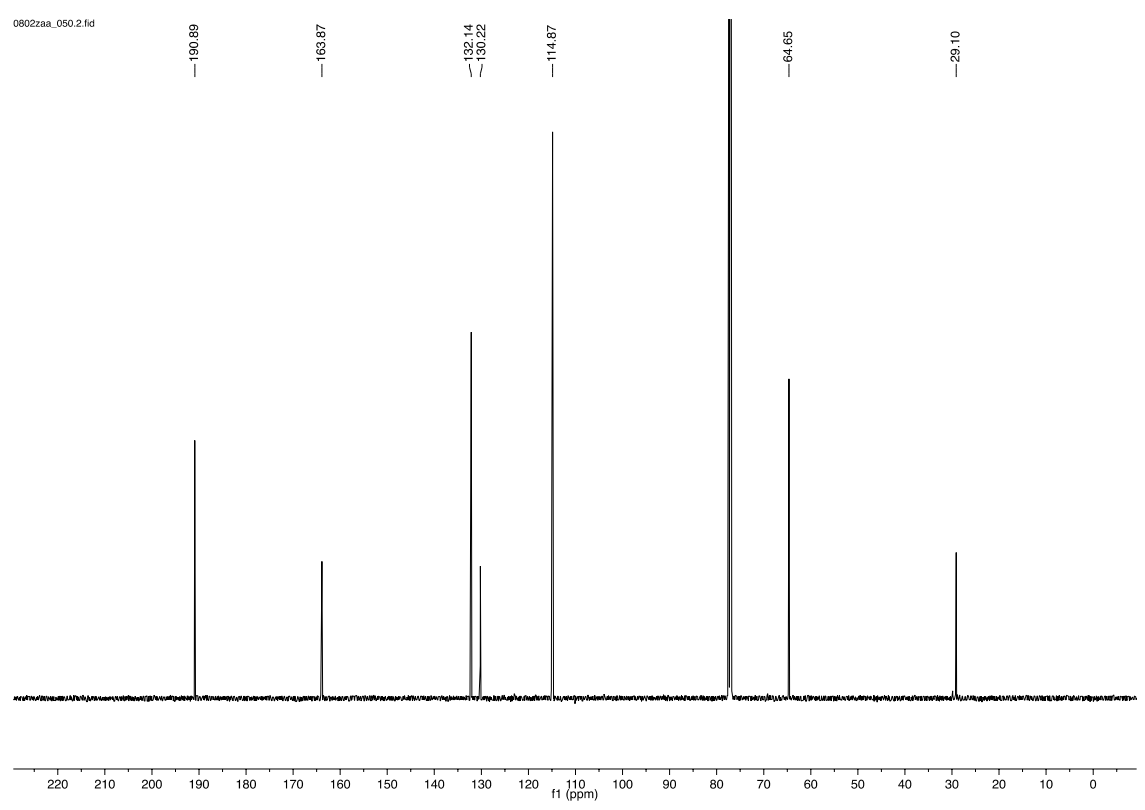
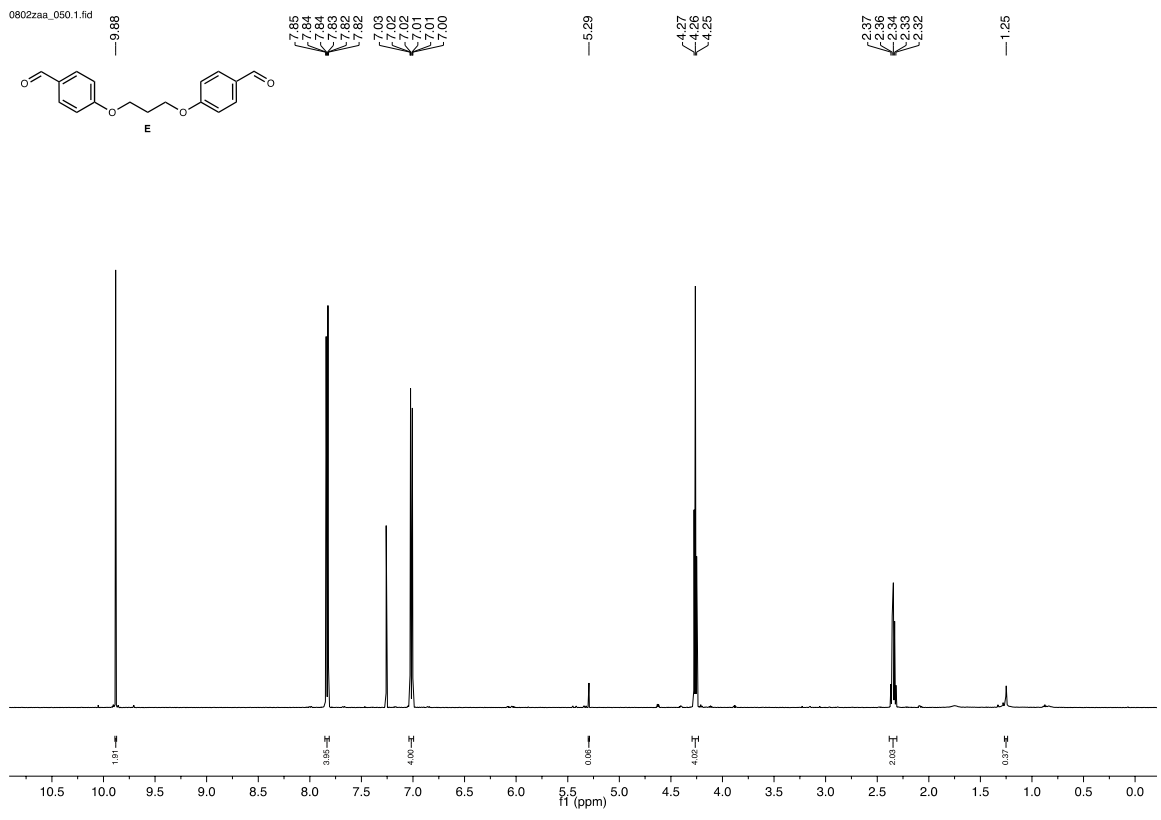
ZAA-047_049.10.1.1r



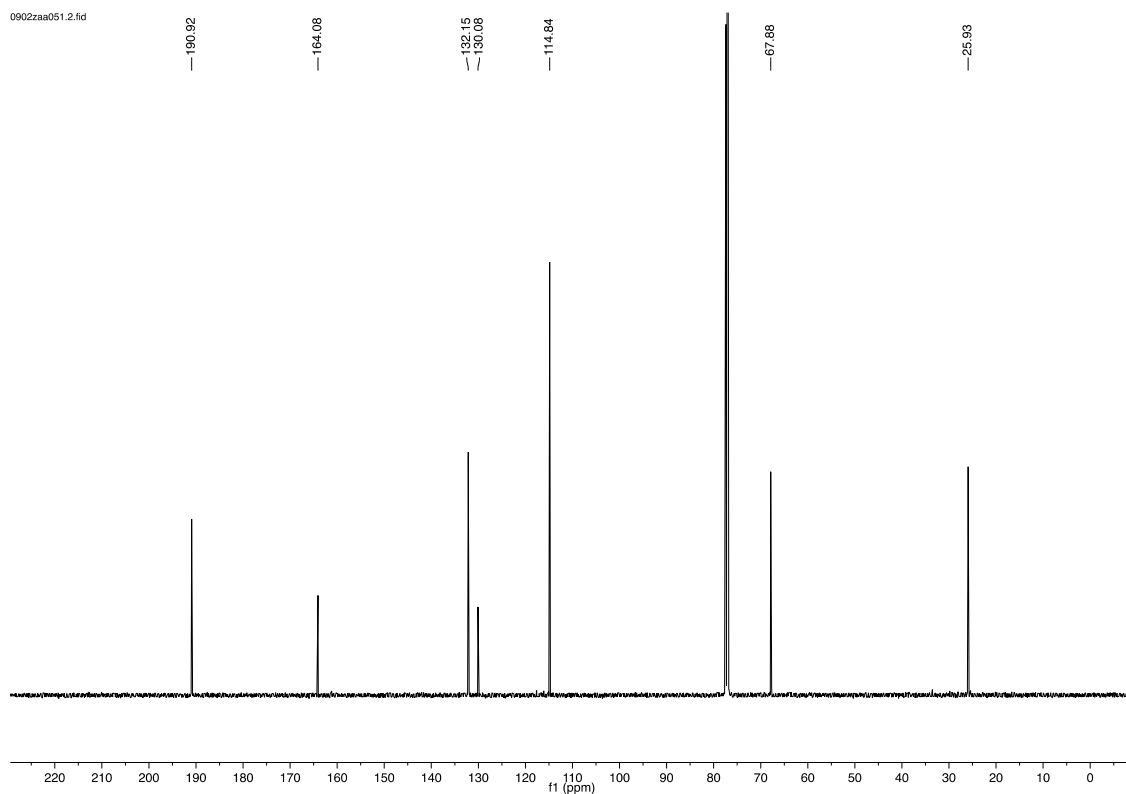
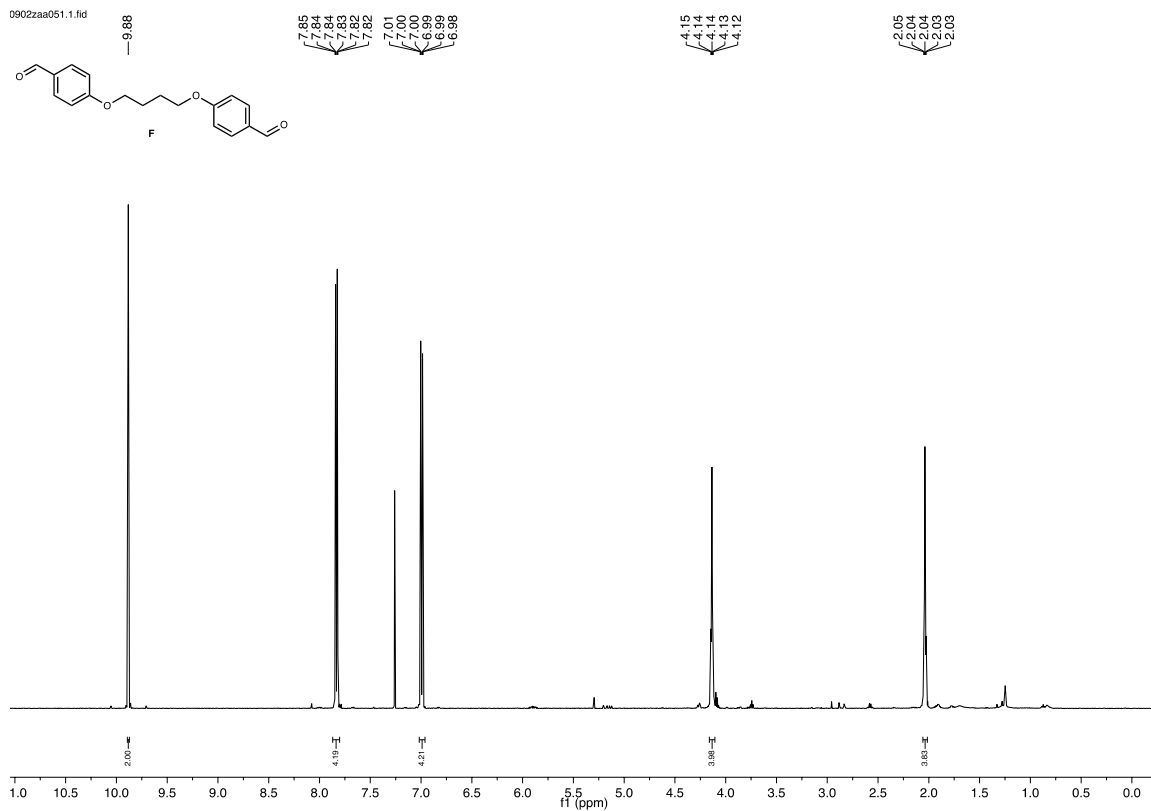
ZAA-047_049.11.1.1r



¹H and ¹³C NMR of linker D

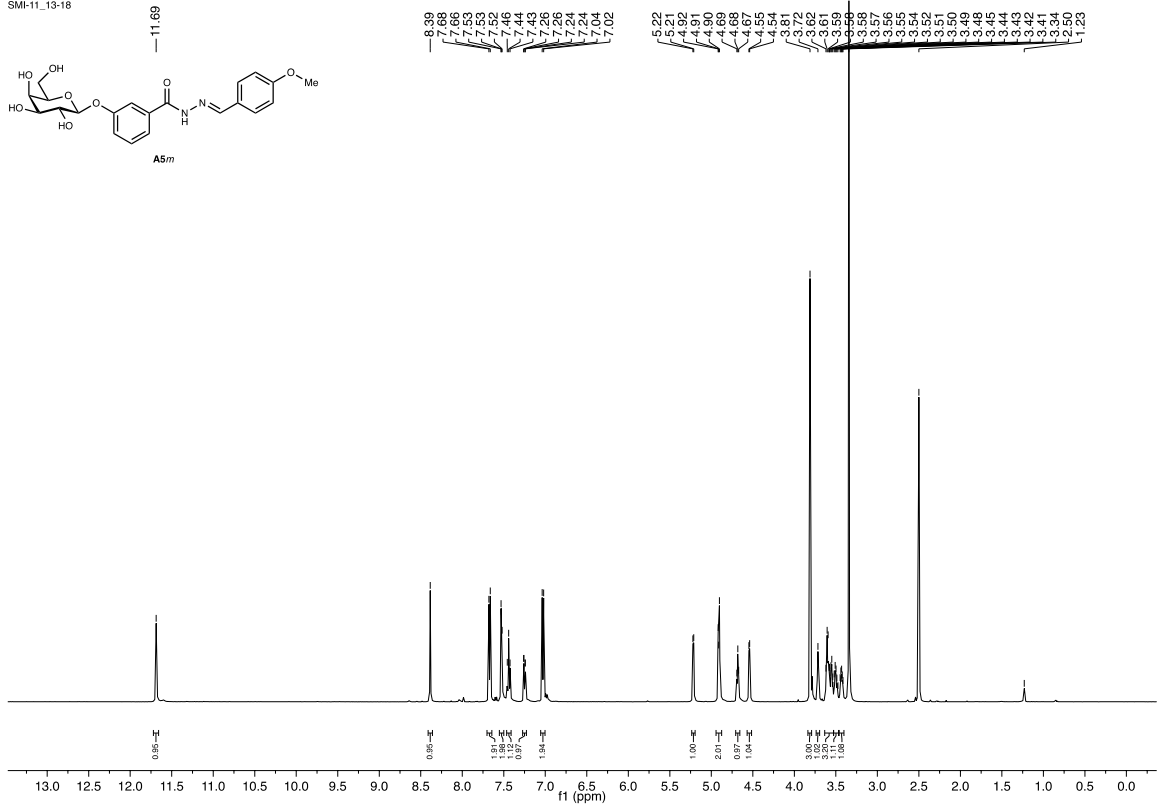
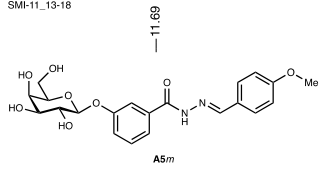


^1H and ^{13}C NMR of linker E

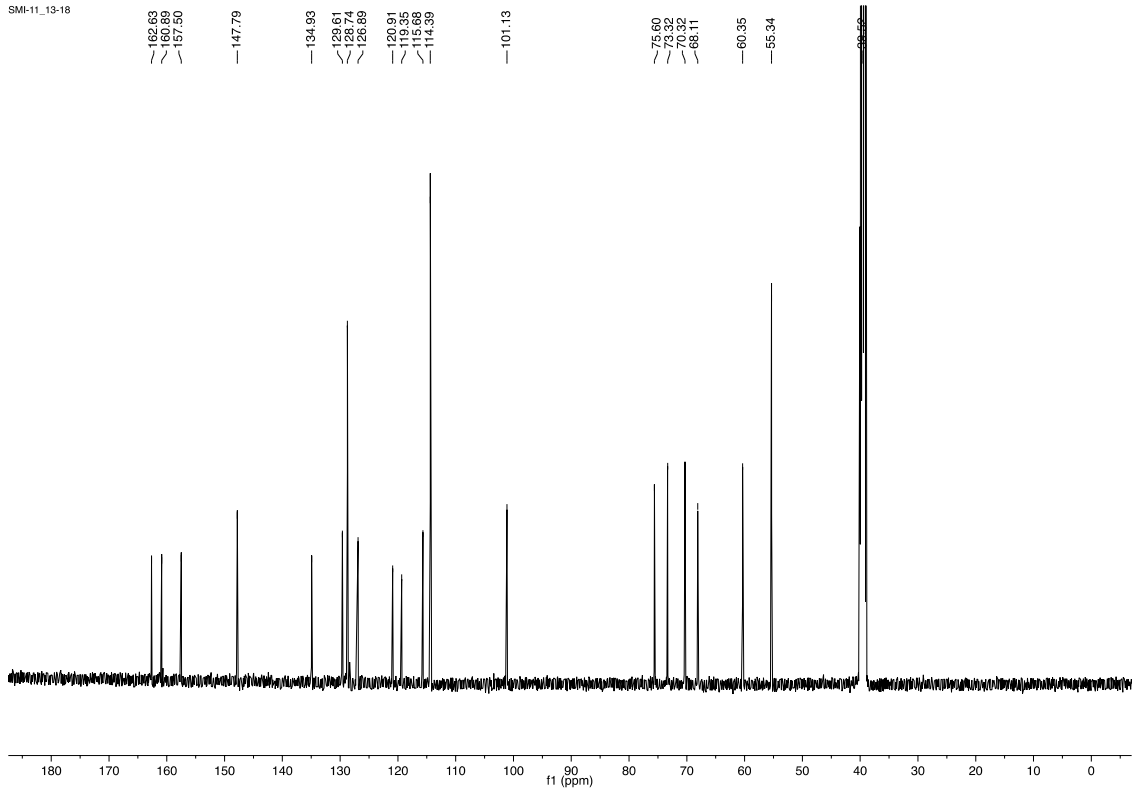


^1H and ^{13}C NMR of linker F

SMI-11_13-18

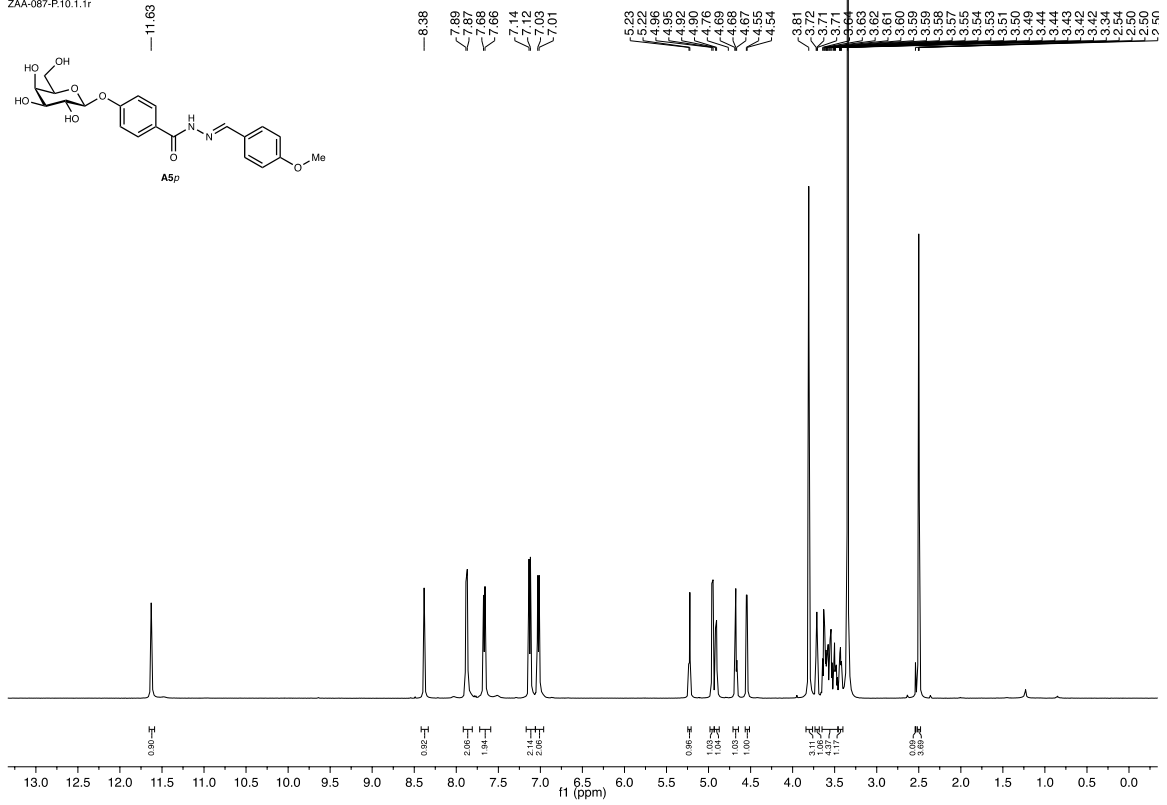
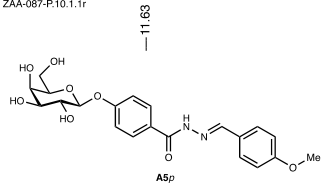


SMI-11_13-18

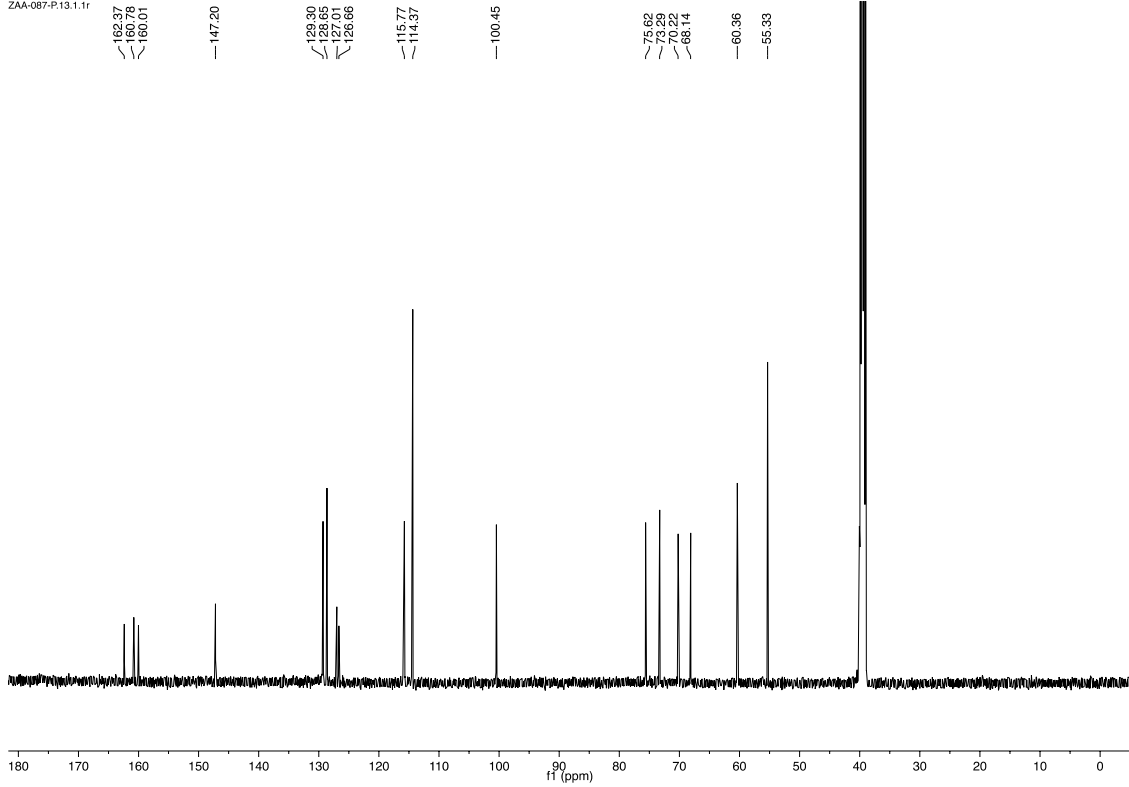


¹H and ¹³C NMR of A5m

ZAA-087-P.10.1.1r

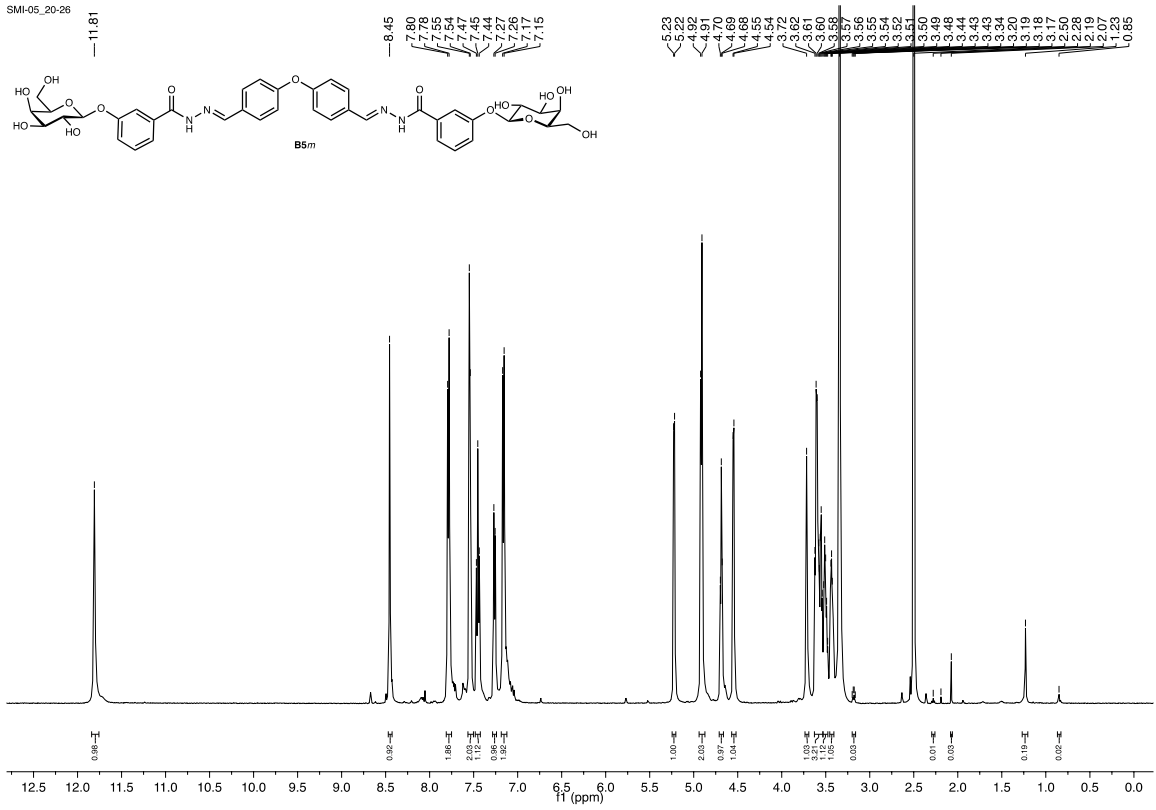


ZAA-087-P.13.1.1r

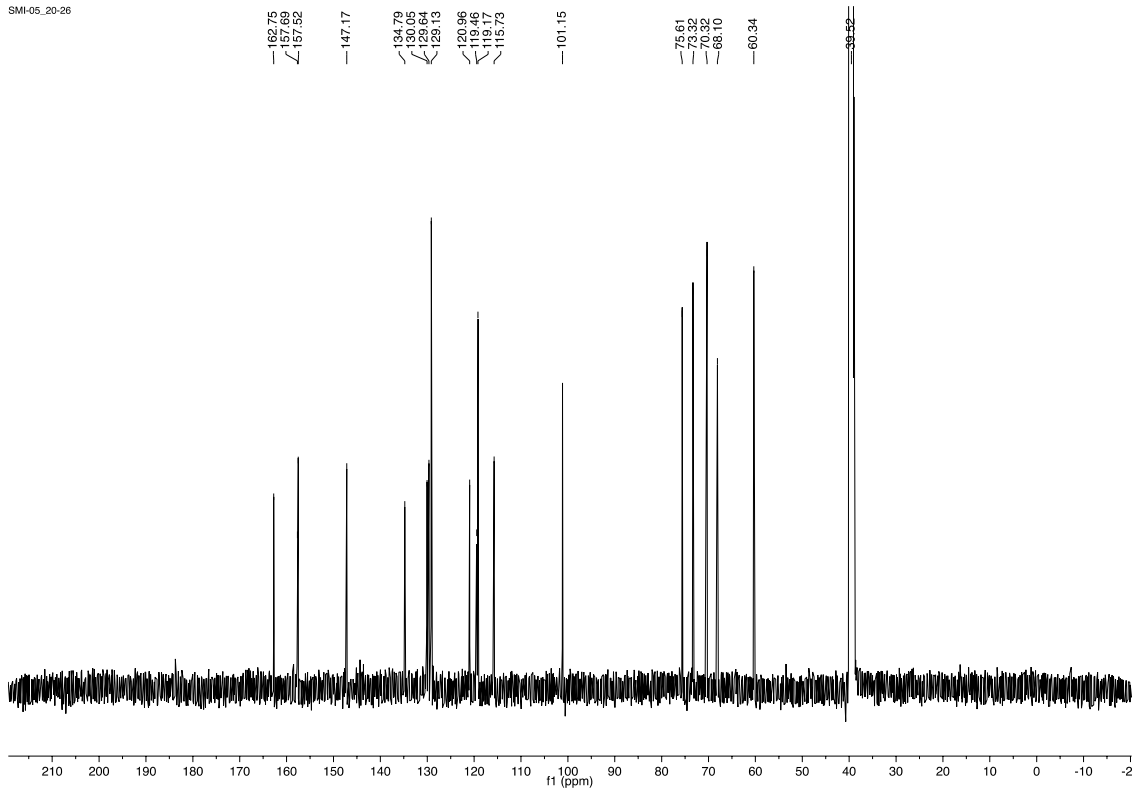


¹H and ¹³C NMR of A5p

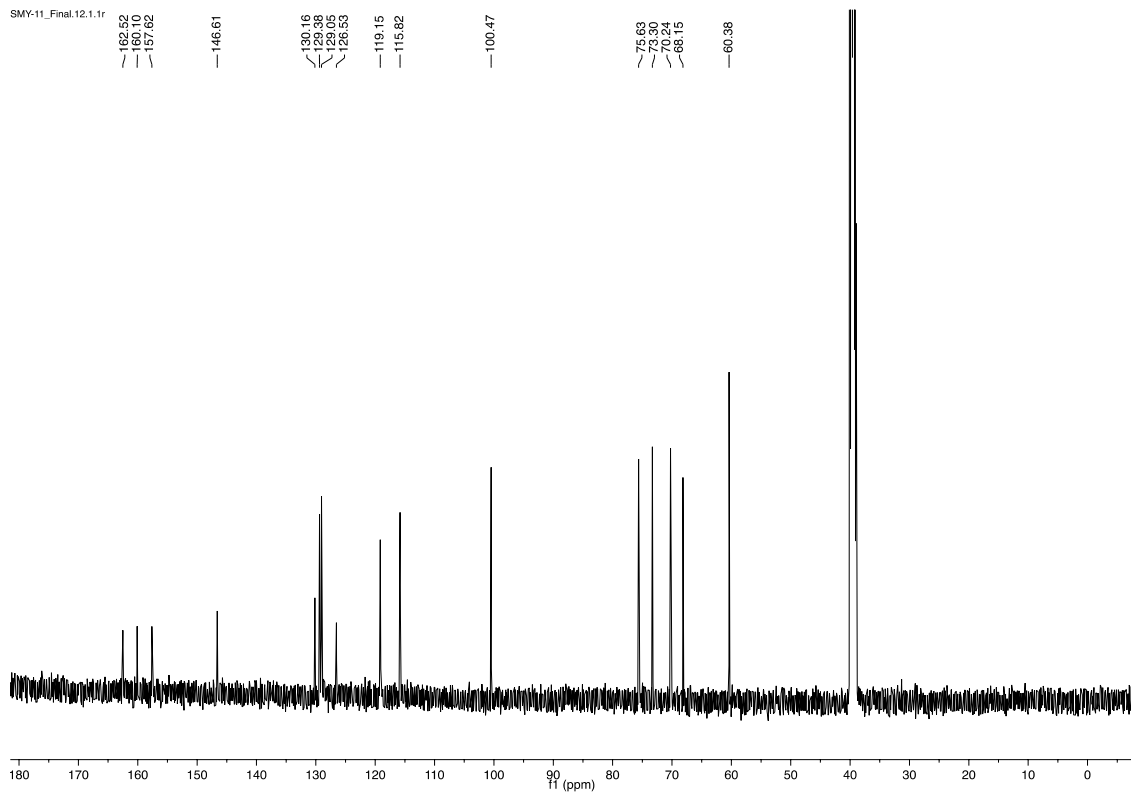
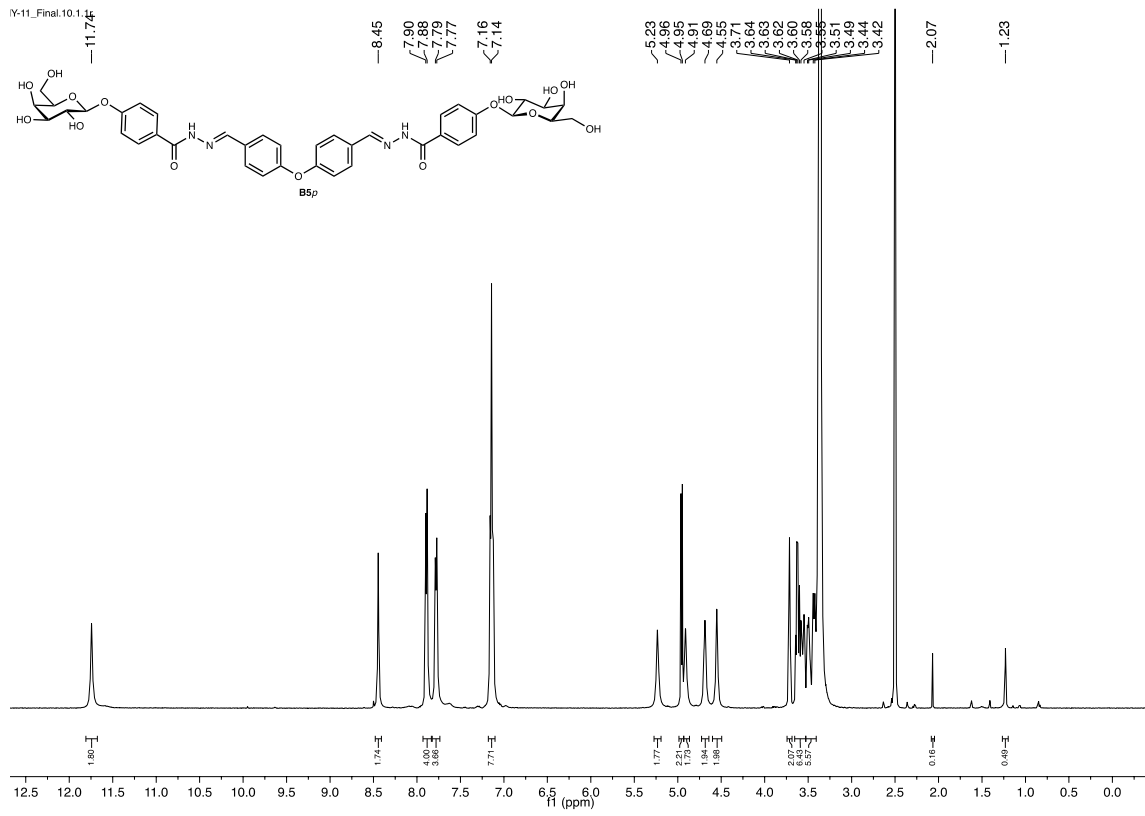
SMI-05_20-26



SMI-05_20-26

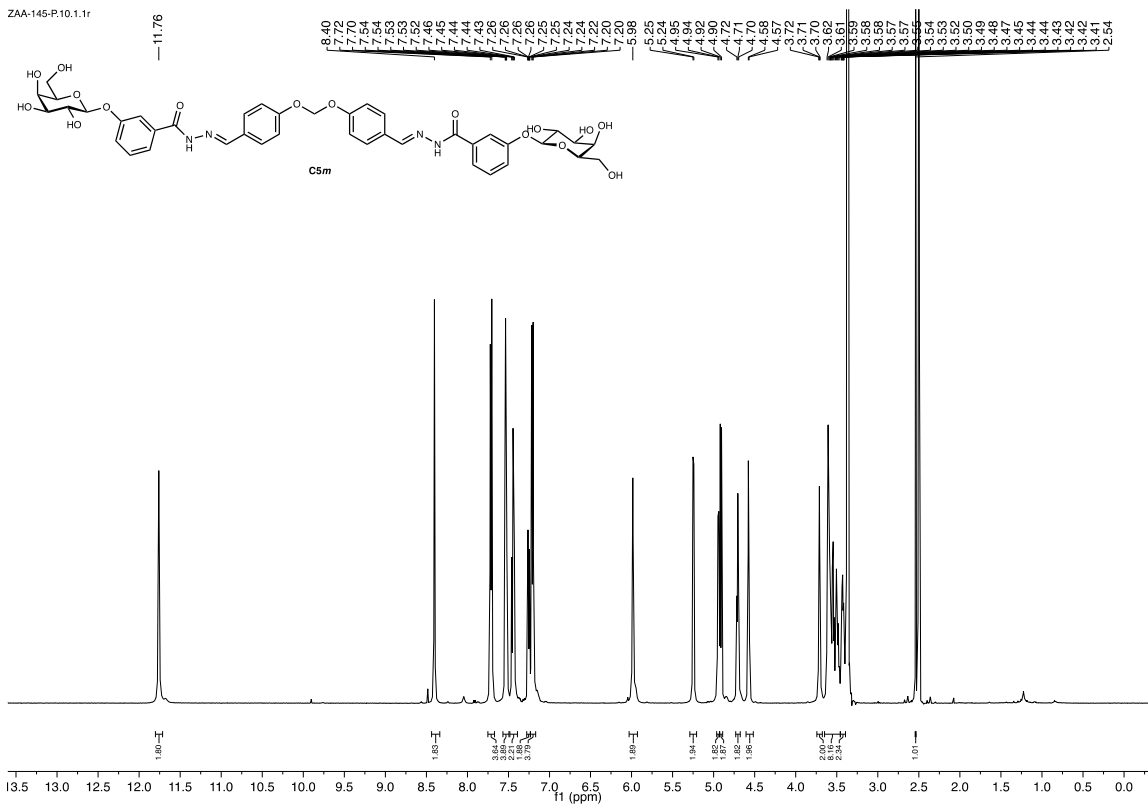


^1H and ^{13}C NMR of **B5m**

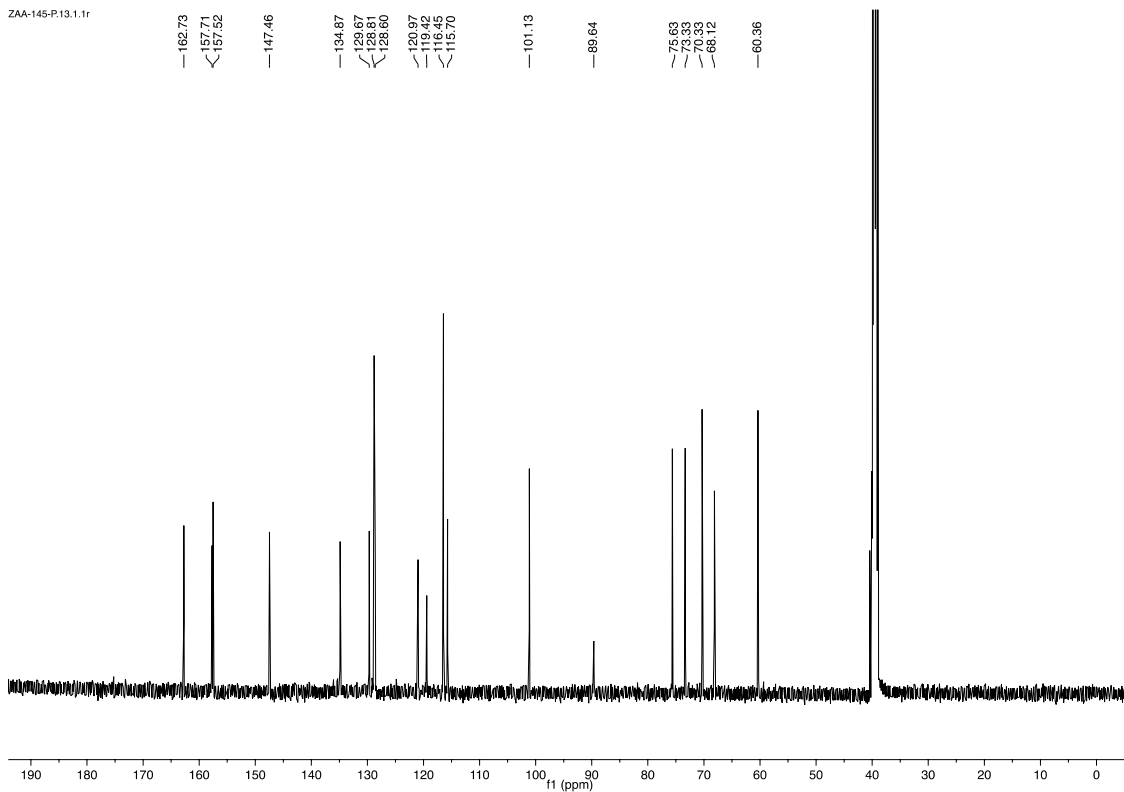


^1H and ^{13}C NMR of **B5p**

ZAA-145-P.10.1.1r

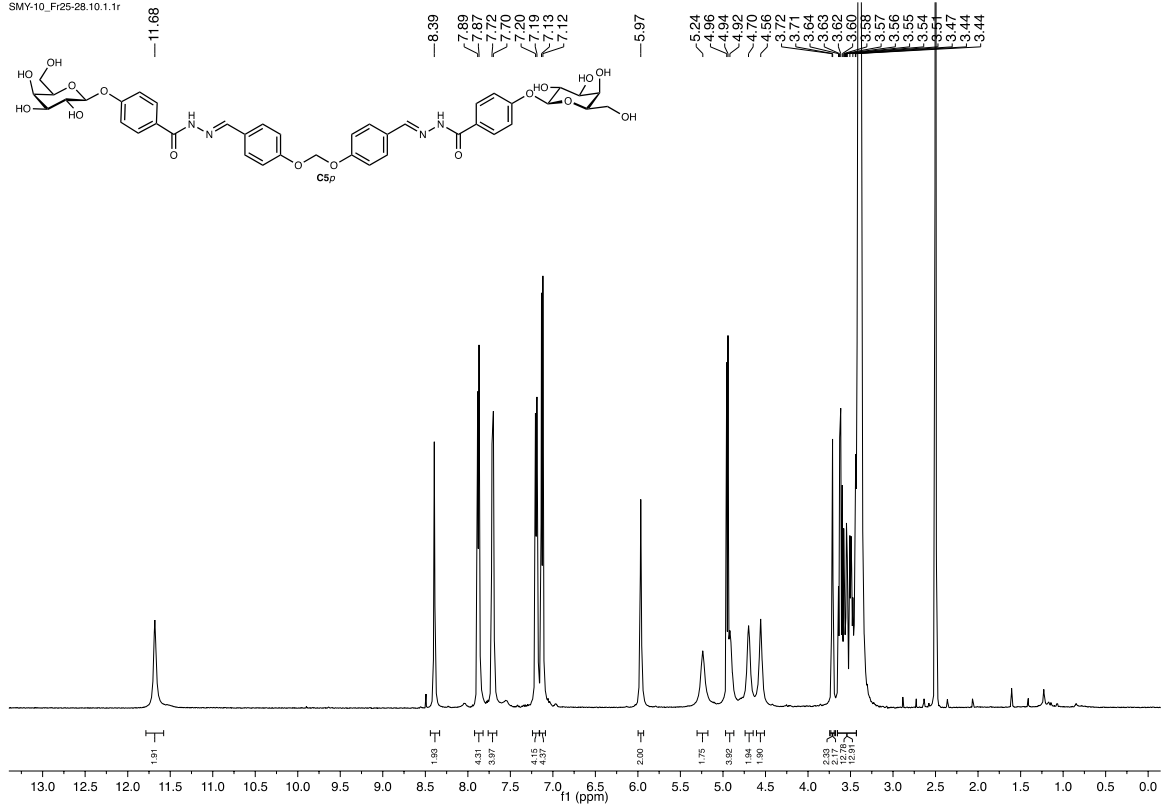


ZAA-145-P.13.1.1r

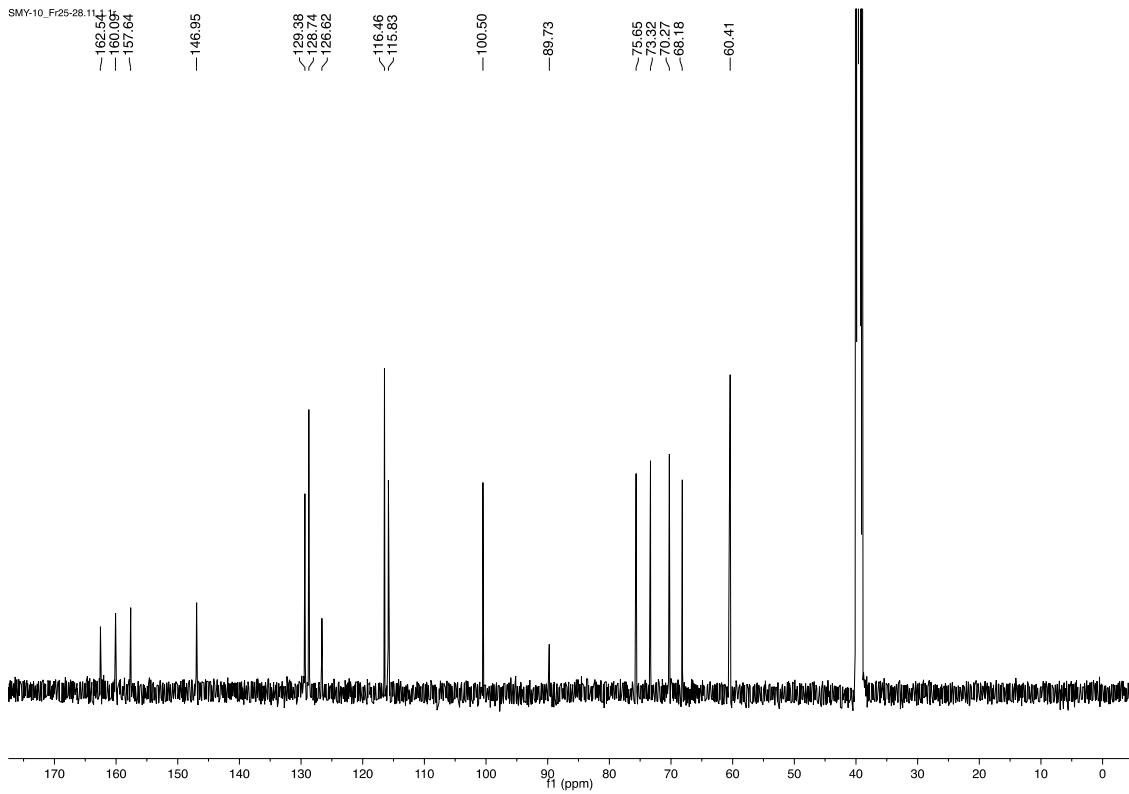


¹H and ¹³C NMR of **C5m**

SMY-10_Fr25-28.10.1.1r

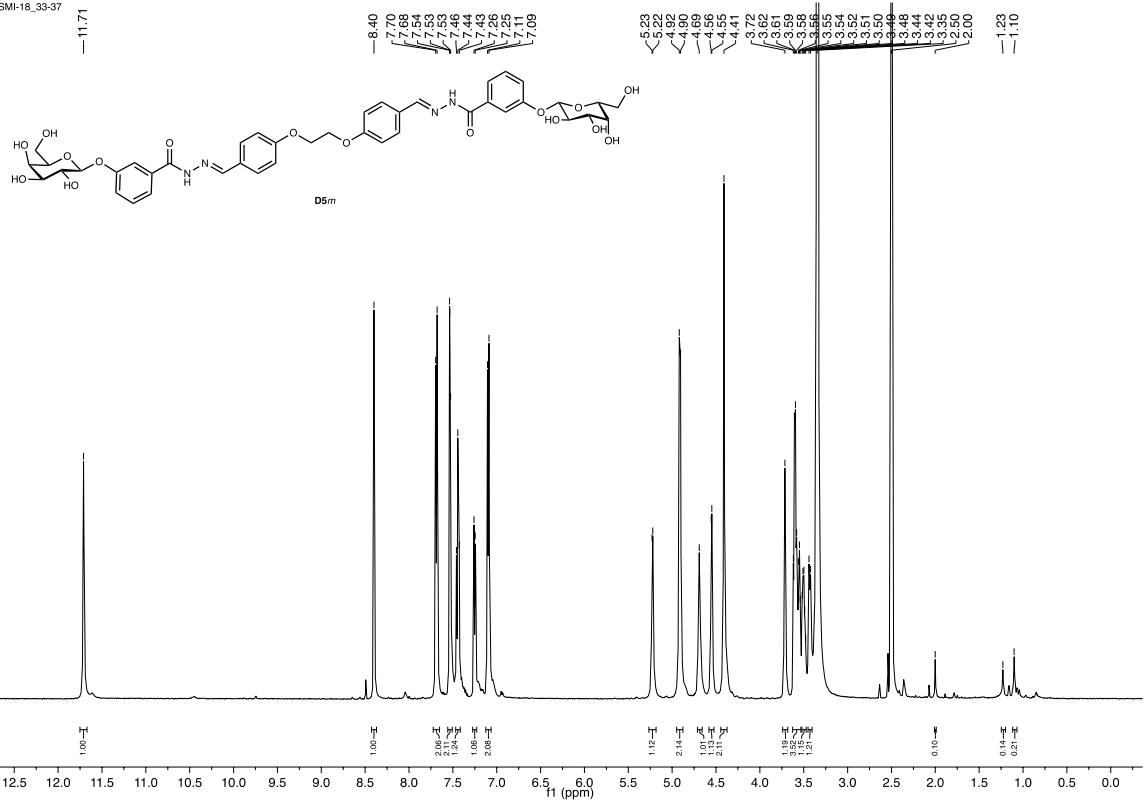


SMY-10_Fr25-28.11.1

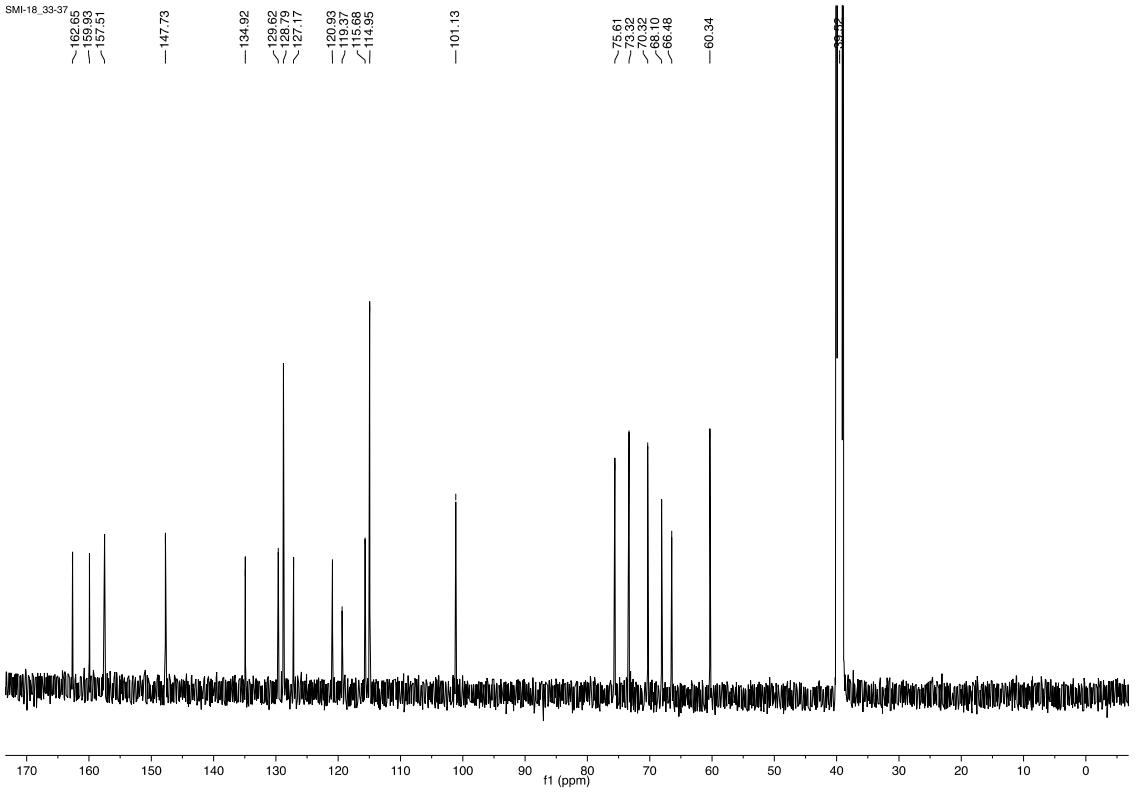


¹H and ¹³C NMR of **C5p**

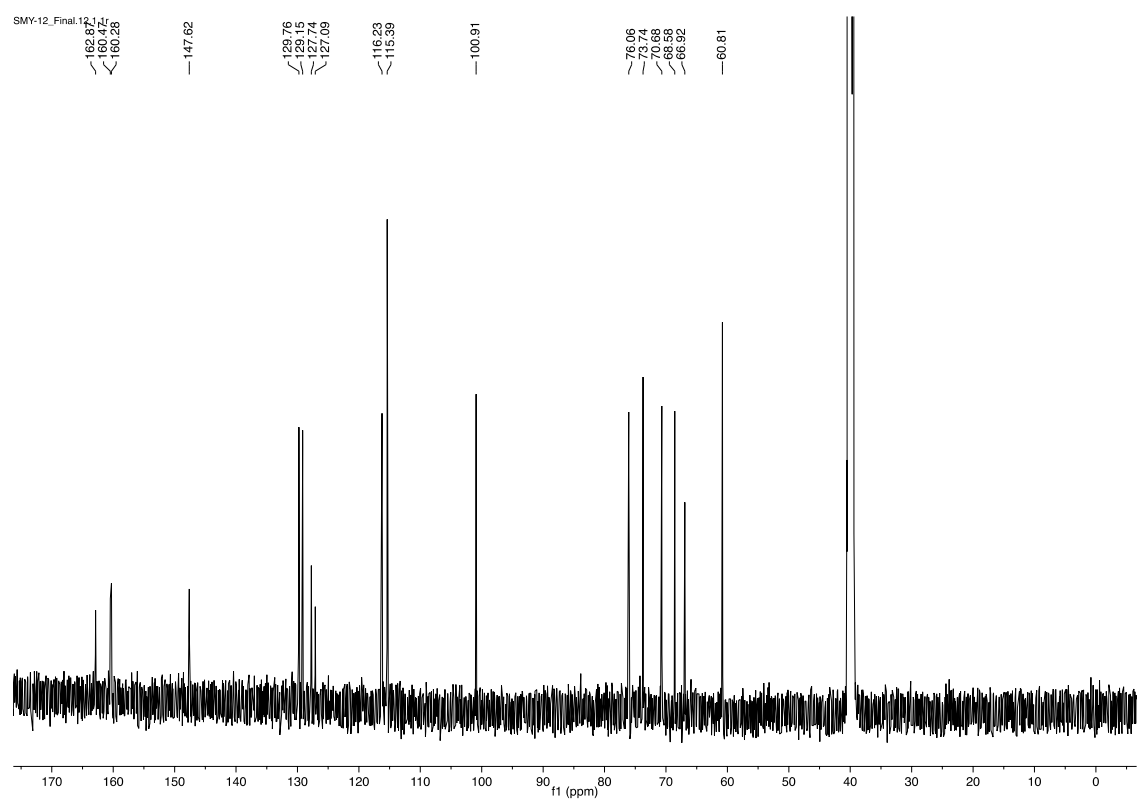
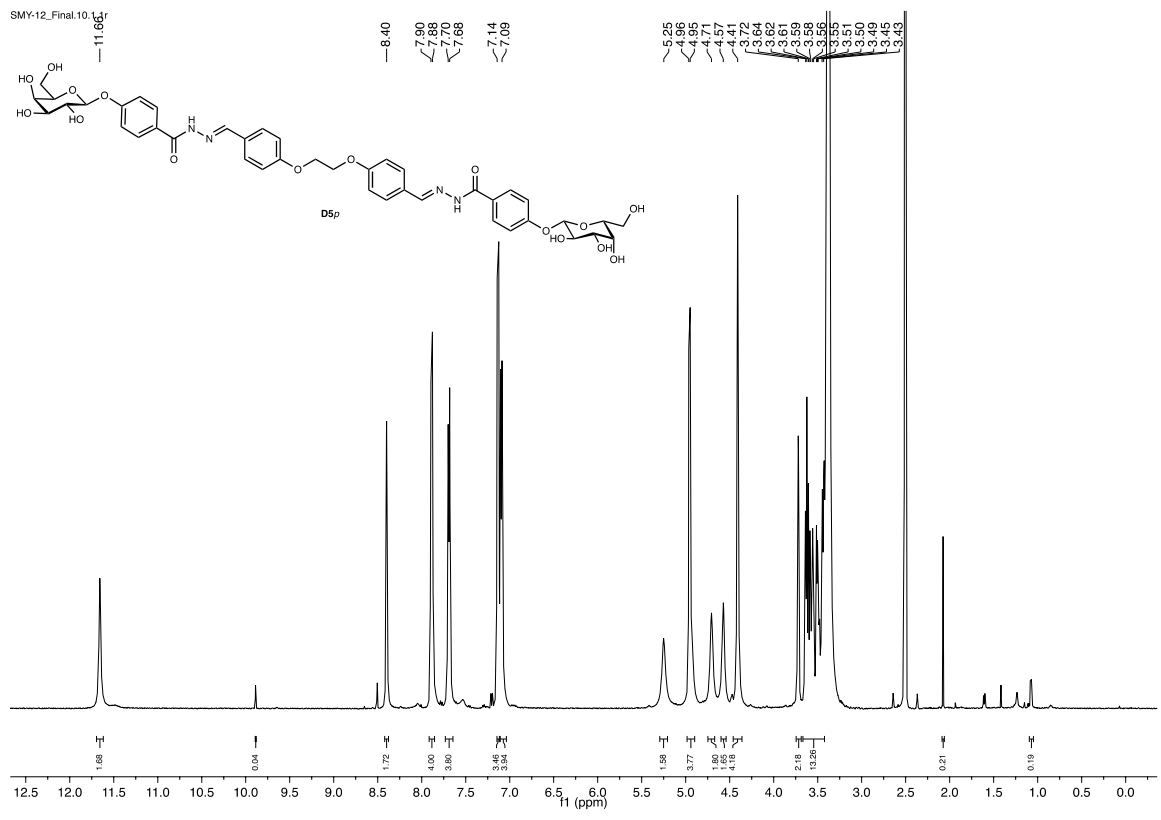
SMI-18_33-37



SMI-18_33-37

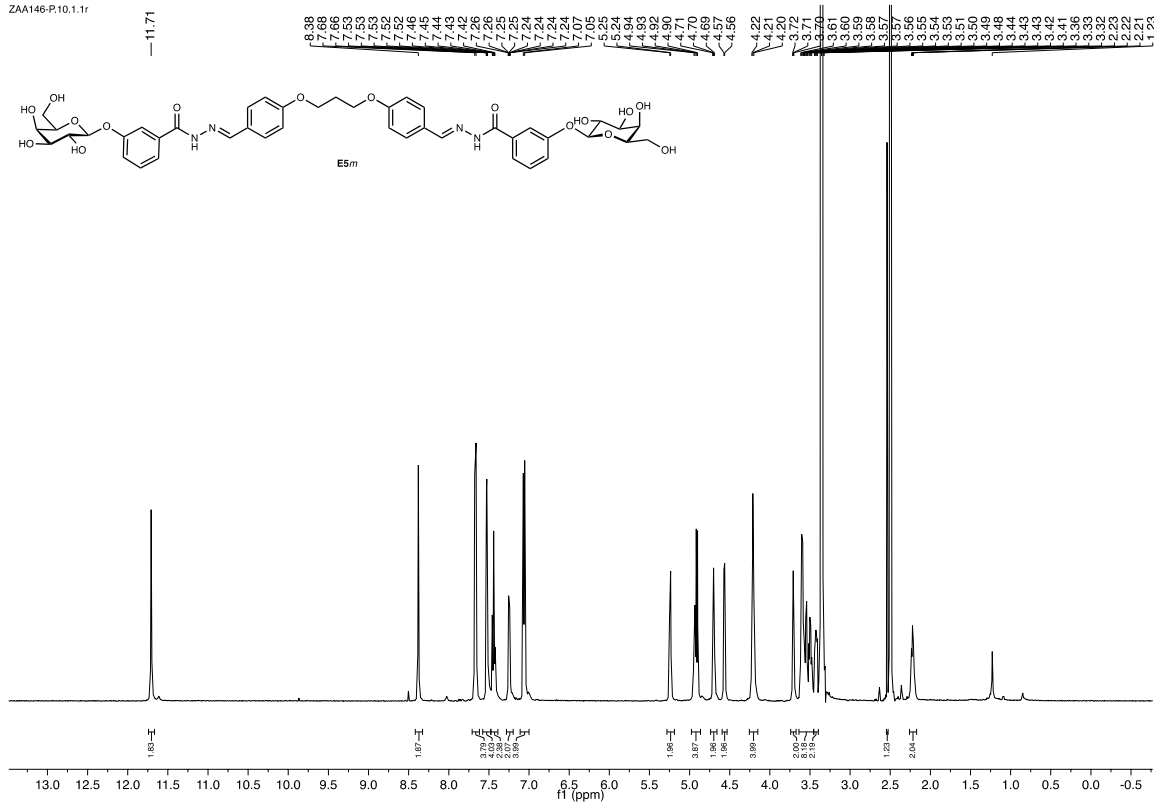


¹H and ¹³C NMR of **D5m**

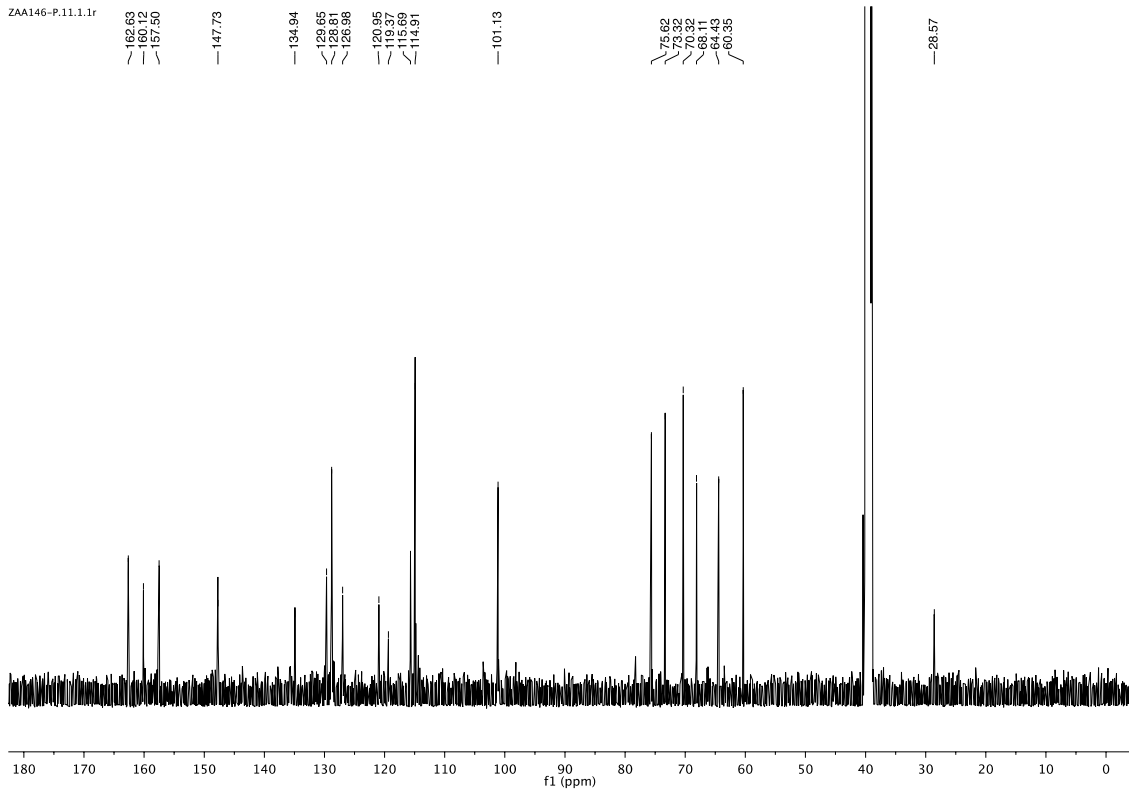


¹H and ¹³C NMR of D5p

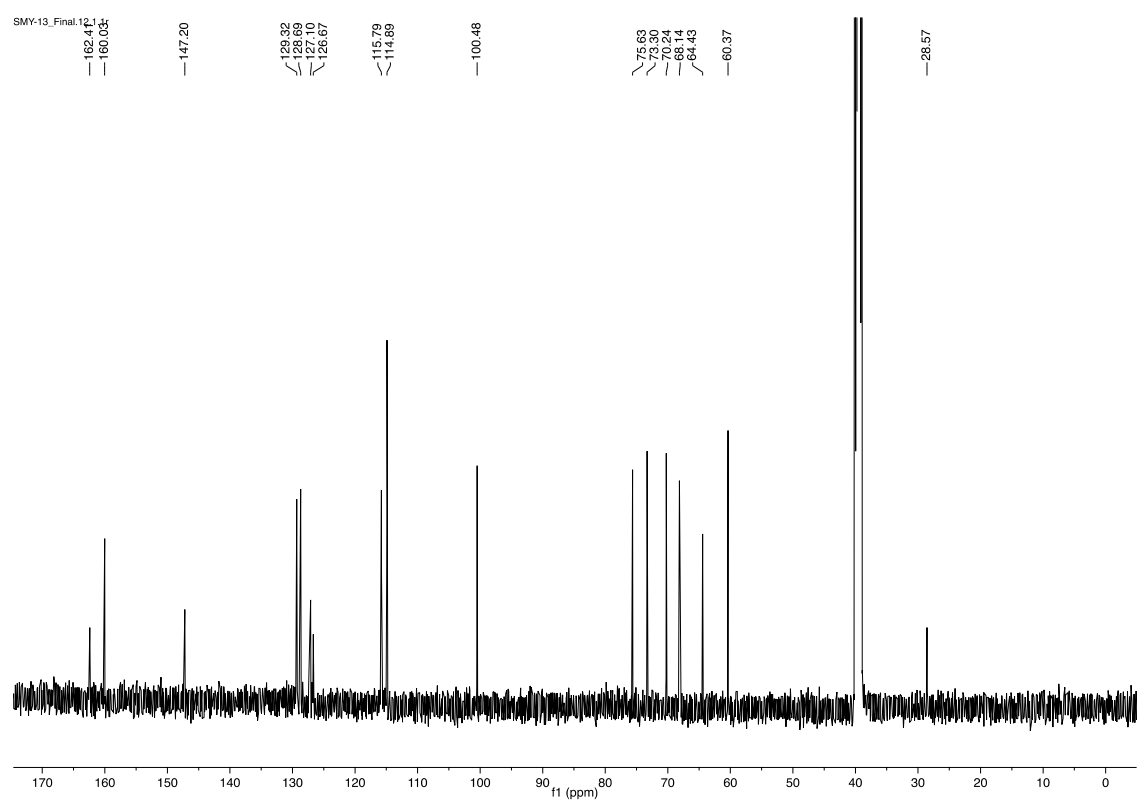
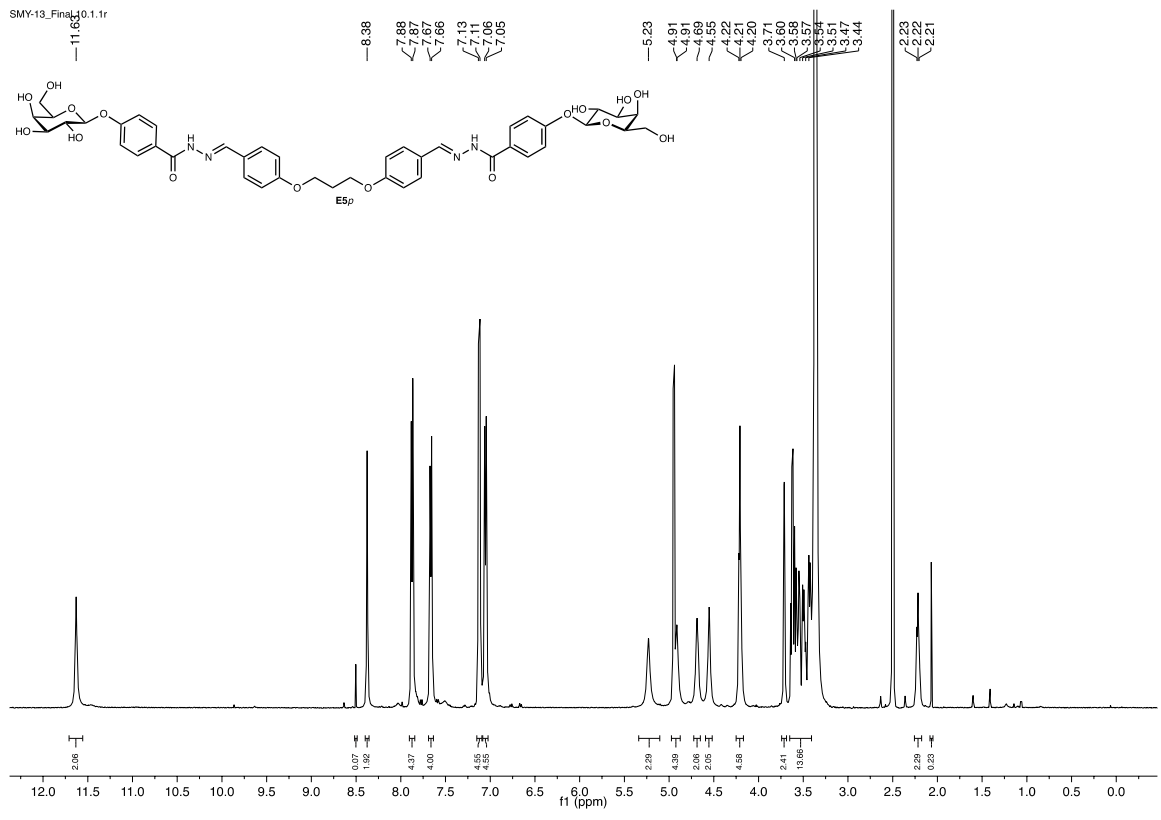
ZAA146-P.10.1.1r



ZAA146-P.11.1.1r

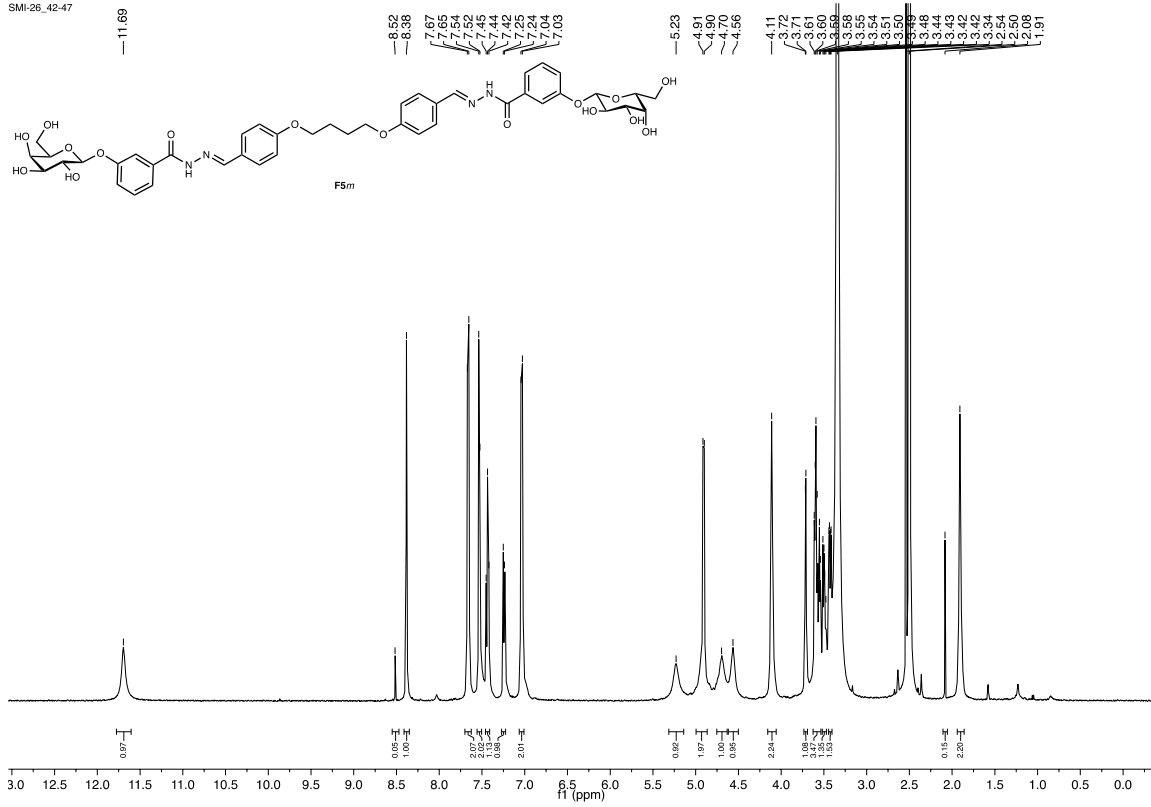


¹H and ¹³C NMR of E5m

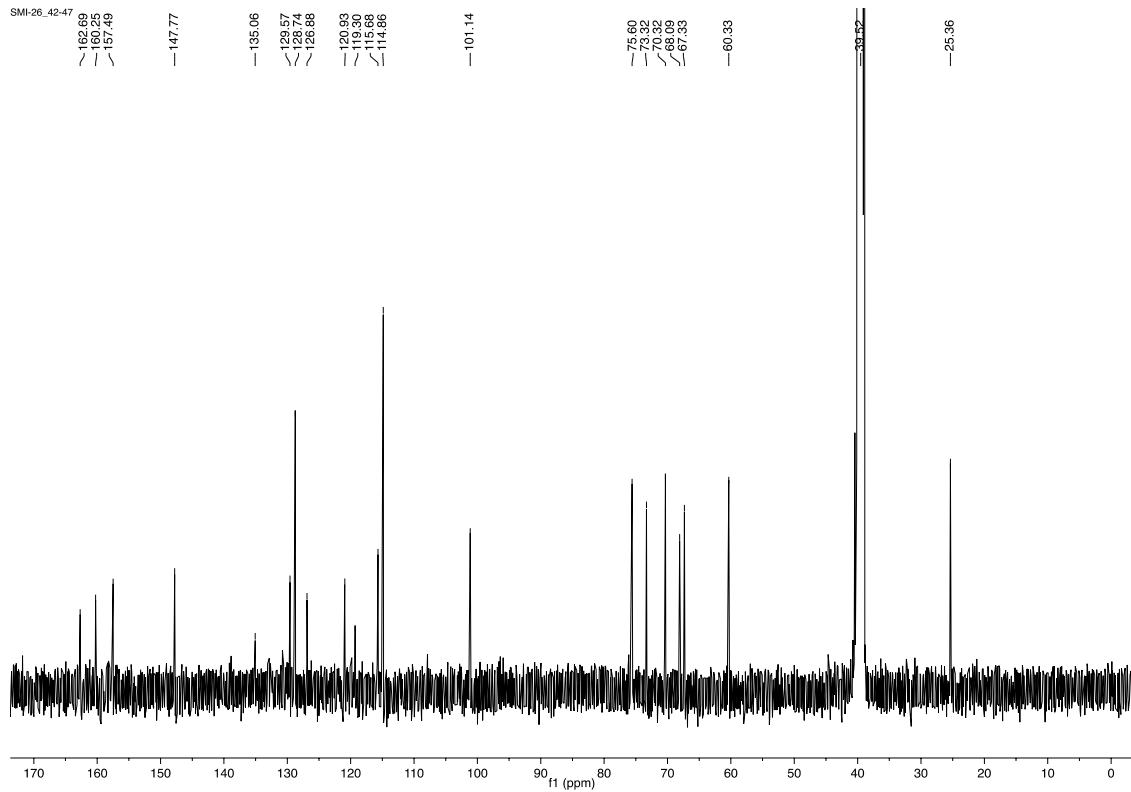


¹H and ¹³C NMR of **E5p**

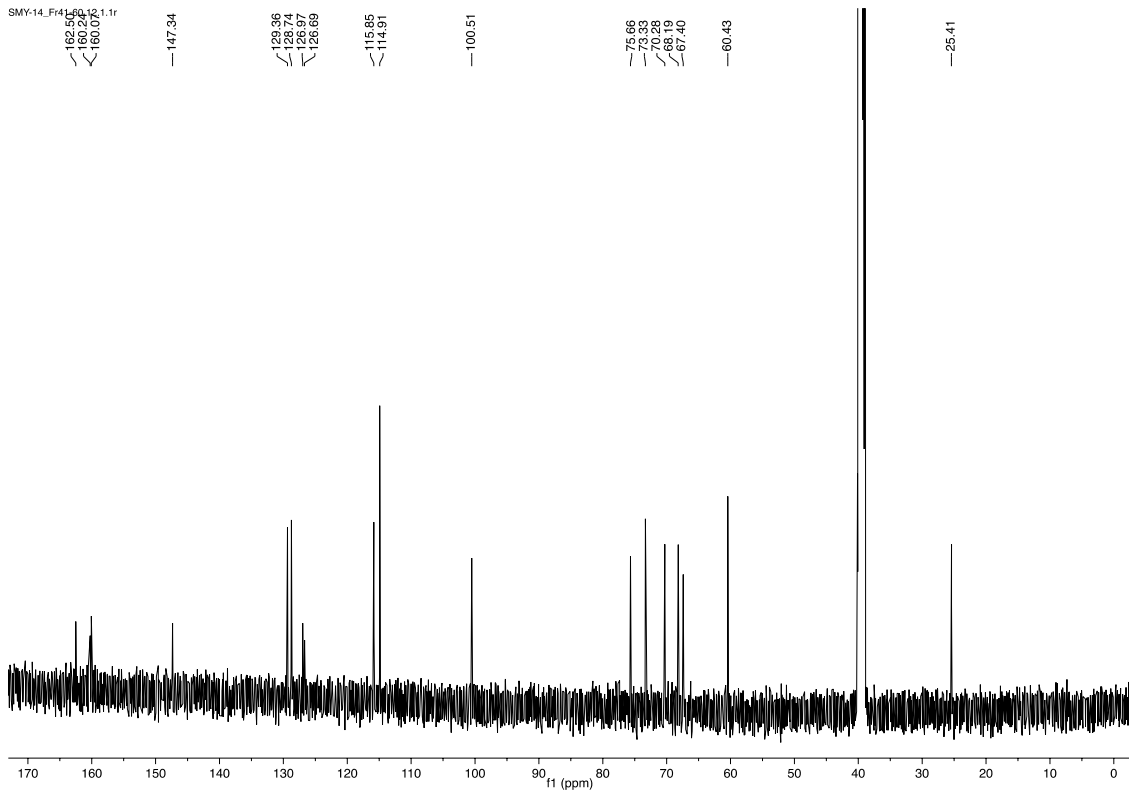
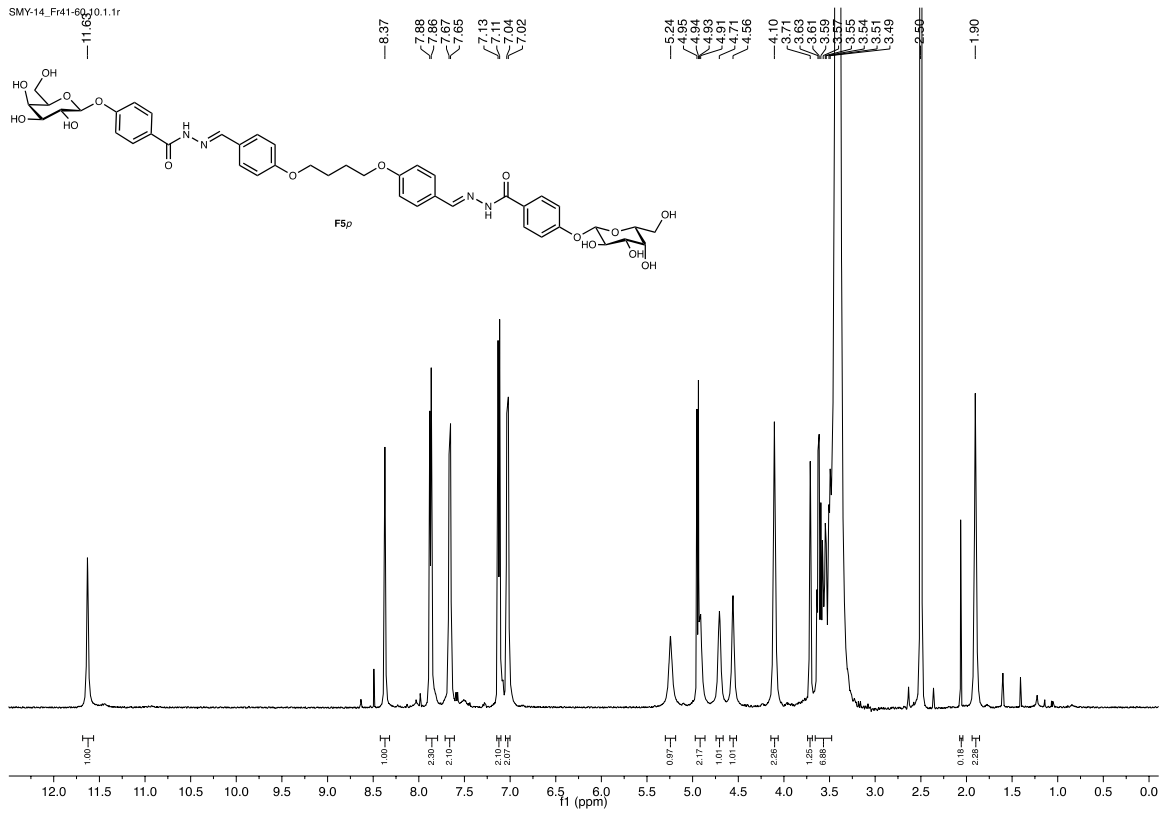
SMI-26_42-47



SMI-26_42-47



^1H and ^{13}C NMR of **F5m**



¹H and ¹³C NMR of **F5p**

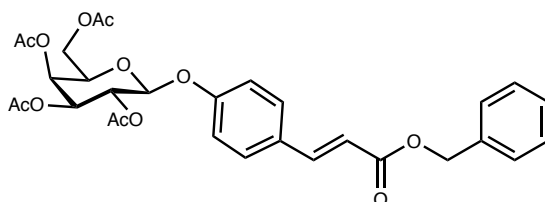
References

- 1 H. E. Gottlieb, V. Kotlyar and A. Nudelman, *J. Org. Chem.*, 1997, **62**, 7512–7515.
- 2 R. B. Cohen, K.-C. Tsou, S. H. Rutenburg and A. M. Seligman, *J. Biol. Chem.*, 1952, **195**, 239–249.
- 3 S. T. Xue, W. Y. He, L. L. Ma, H. Q. Wang, B. Wang, G. H. Zheng, X. Y. Ji, T. Zhang, Y. H. Li, J. D. Jiang and Z. R. Li, *Molecules*, 2013, **18**, 3789–3805.
- 4 Y. Li, H. Mo, G. Lian and B. Yu, *Carbohydr. Res.*, 2012, **363**, 14–22.
- 5 F. Yang, F. Xie, Y. Zhang, Y. Xia, W. Liu, F. Jiang, C. Lam, Y. Qiao, D. Xie, J. Li and L. Fu, *Bioorganic Med. Chem. Lett.*, 2017, **27**, 2166–2170.
- 6 I. Joachim, S. Rikker, D. Hauck, D. Ponader, S. Boden, R. Sommer, L. Hartmann and A. Titz, *Org. Biomol. Chem.*, 2016, **14**, 7933–7948.
- 7 S. A. Scott, K. Scott and H. Blanchard, *Acta Crystallogr. Sect. F Struct. Biol. Cryst. Commun.*, 2007, **63**, 967–971.
- 8 G. Levi and V. I. Teichberg, *J. Biol. Chem.*, 1981, **256**, 5735–5740.
- 9 J. Wang, W. Wang, P. A. Kollman and D. A. Case, *J. Mol. Graph. Model.*, 2006, **25**, 247–260.
- 10 J. Wang, R. M. Wolf, J. W. Caldwell, P. A. Kollman and D. A. Case, *J. Comput. Chem.*, 2004, **56531**, 1157–1174.
- 11 A. Jakalian, D. B. Jack and C. I. Bayly, *J. Comput. Chem.*, 2002, **23**, 1623–1641.
- 12 W. L. Jorgensen, J. Chandrasekhar, J. D. Madura, R. W. Impey and M. L. Klein, *J. Chem. Phys.*, 1983, **79**, 926–935.
- 13 L. Žáková, E. Kletvíková, V. Veverka, M. Lepšík, C. J. Watson, J. P. Turkenburg, J. Jiráček and A. M. Brzozowski, *J. Biol. Chem.*, 2013, **288**, 10230–10240.
- 14 P. Srb, M. Svoboda, L. Benda, M. Lepšík, J. Tarábek, V. Šícha, B. Grüner, K. Grantz-Šašková, J. Brynda, P. Řezáčová, J. Konvalinka and V. Veverka, *Phys. Chem. Chem. Phys.*, 2019, **21**, 5661–5673.
- 15 D. A. Case, I. Y. Ben-Shalom, S. R. Brozell, D. S. Cerutti, T. E. Cheatham, V. W. D. C. III, T. A. Darden, R. E. Duke, D. Ghoreishi, M. K. Gilson, H. Gohlke, A. W. Goetz, D. Greene, R. Harris, N. Homeyer, S. Izadi, A. Kovalenko, T. Kurtzman, T. S. Lee, S. LeGrand, P. Li, C. Lin, J. Liu, T. Luchko, R. Luo, D. J. Mermelstein, K. M. Merz, Y. Miao, G. Monard, C. Nguyen, H. Nguyen, I. Omelyan, A. Onufriev, F. Pan, R. Qi, D. R. Roe, A. Roitberg, C. Sagui, S. Schott-Verdugo, J. Shen, C. L. Simmerling, J. Smith, R. Salomon-Ferrer, J. Swails, R. C. Walker, J. Wang, H. Wei, R. M. Wolf, X. Wu, L. Xiao, York, D.M. and P. A. Kollman, *Univ. California, San Fr.*
- 16 M. Bergmann, G. Michaud, R. Visini, X. Jin, E. Gillon, A. Stocker, A. Imberty, T. Darbre and J. L. Reymond, *Org. Biomol. Chem.*, 2016, **14**, 138–148.
- 17 J. C. Gordon, J. B. Myers, T. Folta, V. Shoja, L. S. Heath and A. Onufriev, *Nucleic Acids Res.*, 2005, **33**, 368–371.
- 18 B. J. Kirby and P. Jungwirth, *J. Phys. Chem. Lett.*, 2019, **10**, 7531–7536.
- 19 I. M. Zeron, J. L. F. Abascal and C. Vega, *J. Chem. Phys.*, , DOI:10.1063/1.5121392.
- 20 J. Mongan, C. Simmerling, J. A. McCammon, D. A. Case and A. Onufriev, *J. Chem. Theory Comput.*, 2007, **3**, 156–169.

6.3 Supplementary information for chapter 3.3

Compound synthesis

4-O-(2',3',4',6'-tetra-O-acetyl-β-D-galactopyranosyl)trans-*p*-coumaric acid benzyl ester (4)



Benzyl *p*-coumarate was synthesised in analogy to Guo *et. al.*¹³² *p*-Coumaric acid (1.0 g, 6.2 mmol) was dissolved in dimethylformamide (30 mL) and Na₂CO₃ (1.5 g, 14.5 mmol) was added. Benzyl bromide (1.5 mL, 12.5 mmol) was added dropwise and stirred overnight. The reaction was concentrated *in vacuo*, diluted with water and the product was extracted into ethyl acetate, washed with half satd. brine, dried over anhydrous Na₂SO₄, filtered and concentrated *in vacuo*. The crude product was purified by normal phase MPLC (petrol ether/ethyl acetate, gradient of 10-40% ethyl acetate) to give pure benzyl *p*-coumarate (1.3 g, 5.0 mmol, 80%).

β-D-galactopyranose pentaacetate (**3**, 1.0 g, 2.6 mmol) and benzyl *p*-coumarate (1.3 g, 5.0 mmol) were dissolved in dry chloroform (20 mL) in a round bottom flask with powdered activated molecular sieve (3 Å). The reaction mixture was cooled to 0 °C and BF₃·OEt₂ (1.9 mL, 15.2 mmol) was added dropwise. The mixture was allowed to warm to room temperature and stirred overnight. The reaction was poured over ice cold satd. NaHCO₃ solution and diluted with dichloromethane. The separated organic phase was washed with satd. NaHCO₃ solution and half satd. brine, dried over anhydrous Na₂SO₄, filtered and concentrated *in vacuo*. The product **4** was purified by normal phase MPLC (petrol ether/ethyl acetate, gradient of 20-40% ethyl acetate). Compound **4** (1.1 g, 2.0 mmol, 76%) was obtained as a white solid.

¹H NMR (500 MHz, CDCl₃) δ 7.68 (d, *J* = 16.0 Hz, 1H, CH=CHCOOBn), 7.50 – 7.44 (m, 2H, ArH), 7.44 – 7.32 (m, 5H, Bn), 7.02 – 6.97 (m, 2H, ArH), 6.39 (d, *J* = 16.0 Hz, 1H, CH=CHCOOBn), 5.50 (dd, *J* = 10.5, 7.9 Hz, 1H, H-2), 5.46 (dd, *J* = 3.5, 1.1 Hz, 1H, H-4), 5.24 (s, 2H, Bn), 5.11 (dd, *J* = 10.4, 3.4 Hz, 1H, H-3), 5.08 (d, *J* = 7.9 Hz, 1H, H-1), 4.26 – 4.12 (m, 2H, H-6), 4.08 (ddd, *J* = 7.2, 6.2, 1.2 Hz, 1H, H-5), 2.19 (s, 3H, CH₃), 2.06 (s, 6H, CH₃), 2.02 (s, 3H, CH₃).

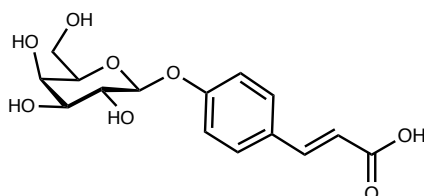
¹³C NMR (126 MHz, CDCl₃) δ 170.51 (1C, C=O), 170.37 (1C, C=O), 170.28 (1C, C=O), 169.52 (1C, C=O), 167.01 (1C, C=O), 158.43 (1C, ArC), 144.35 (1C, CH=CHCOOBn), 136.14 (1C, Bn), 129.79 (2C, ArCH), 129.63 (1C, ArC), 128.75 (2C, Bn), 128.47 (2C, Bn), 128.43 (1C, Bn), 117.12 (2C, ArCH), 116.88 (1C, CH=CHCOOBn), 99.16 (1C, C-1), 71.26 (1C, C-

5), 70.86 (1C, C-3), 68.57 (1C, C-2), 66.89 (1C, C-4), 66.51 (1C, Bn), 61.47 (1C, C-6), 20.89 (1C, CH₃), 20.83 (2C, CH₃), 20.75 (1C, CH₃).

HPLC-MS: [C₃₀H₃₂O₁₂ + NH₄]⁺ calcd. 602.22, found 602.17.

HRMS: [C₃₀H₃₂O₁₂ + NH₄]⁺ calcd. 602.2232, found 602.2234.

4-O-β-D-galactopyranosyl trans-*p*-coumaric acid (**1**)



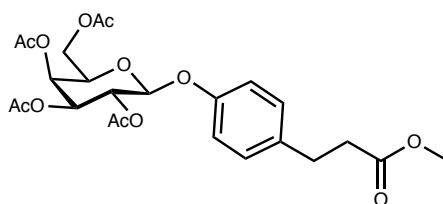
Compound **4** (1.1 g, 2.0 mmol) was suspended in methanol (48 mL). Water (32 mL) and sodium hydroxide solution (16 mL, 1 M, 16 mmol) were added. The reaction mixture was heated to 50 °C and stirred for 2 h when the reaction was neutralised with Amberlite IR 120/H⁺ and concentrated *in vacuo*. After purification by normal phase MPLC (dichloromethane/methanol with 1% formic acid, gradient of 1-20% methanol), compound **1** (554.2 mg, 1.7 mmol, 76%) was obtained as a white solid. Synthesis of compound **1** was first described by Takada *et. al.*¹³³ ¹H NMR (500 MHz, MeOH-d₄) δ 7.61 (d, *J* = 15.9 Hz, 1H, CH=CHCOOH), 7.57 – 7.51 (m, 2H, ArCH), 7.16 – 7.11 (m, 2H, ArCH), 6.37 (d, *J* = 16.0 Hz, 1H, CH=CHCOOH), 4.92 (d, *J* = 7.8 Hz, 1H, H-1), 3.93 – 3.90 (m, 1H, H-4), 3.84 – 3.69 (m, 4H, H-2, H-5, H-6), 3.59 (dd, *J* = 9.7, 3.4 Hz, 1H, H-3).

¹³C NMR (126 MHz, MeOH-d₄) δ 171.24 (1C, COOH), δ 160.82 (1C, ArC), 145.43 (1C, CH=CHCOOH), 130.63 (2C, ArCH), 130.05 (1C, ArC), 118.00 (3C, ArCH, CH=CHCOOH), 102.49 (1C, C-1), 77.07 (1C, C-5), 74.81 (1C, C-3), 72.18 (1C, C-2), 70.20 (1C, C-4), 62.40 (1C, C-6).

HPLC-MS: [C₁₅H₁₈O₈ + HCOO]⁻ calcd. 371.10, found 370.94.

HRMS: [C₁₅H₁₈O₈ + HCOO]⁻ calcd. 371.0984, found 371.0982.

Methyl 4-((2',3',4',6'-tetra-O-acetyl)-β-D-galactopyranosyl)oxy 3-phenylpropanoate (**5**)



β-D-galactopyranose pentaacetate (**3**, 1.5 g, 3.9 mmol) and methyl 3-(4-hydroxyphenyl)propanoate (1.4 g, 7.8 mmol) were dissolved in dry chloroform (20 mL) in a

round bottom flask with powdered activated molecular sieves (3 Å). The reaction mixture was cooled to 0 °C and BF₃·OEt₂ (2.4 mL, 19.5 mmol) was added dropwise, it was then allowed to warm to room temperature and stirred was continued overnight. The reaction was poured over ice cold satd. NaHCO₃ solution and diluted with dichloromethane. The organic phase was separated and washed with satd. NaHCO₃ solution and half satd. brine, dried over anhydrous Na₂SO₄, filtered and concentrated *in vacuo*. After purification by normal phase MPLC (petrol ether/ethyl acetate, gradient of 15-50% ethyl acetate), compound **5** (1.8 g, 3.4 mmol, 86%) was obtained as a white solid.

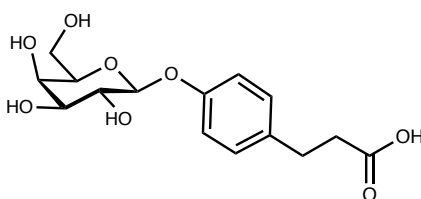
¹H NMR (500 MHz, CDCl₃) δ 7.15 – 7.08 (m, 2H, ArH), 6.95 – 6.89 (m, 2H, ArH), 5.50 – 5.43 (m, 2H, H-2, H-4), 5.09 (dd, *J* = 10.5, 3.4 Hz, 1H, H-3), 5.00 (d, *J* = 8.0 Hz, 1H, H-1), 4.26 – 4.12 (m, 2H, H-6), 4.04 (td, *J* = 6.7, 1.2 Hz, 1H, H-5), 3.66 (s, 3H, CH₂CH₂COOCH₃), 2.90 (t, *J* = 7.7 Hz, 2H, CH₂CH₂COOCH₃), 2.60 (dd, *J* = 8.2, 7.2 Hz, 2H, CH₂CH₂COOCH₃), 2.18 (s, 3H, CH₃), 2.06 (s, 3H, CH₃), 2.06 (s, 3H, CH₃), 2.01 (s, 3H, CH₃).

¹³C NMR (126 MHz, CDCl₃) δ 173.37 (1C, C=O), 170.50 (1C, C=O), 170.40 (1C, C=O), 170.29 (1C, C=O), 169.53 (1C, C=O), 155.60 (1C, ArC), 135.63 (1C, ArC), 129.50 (2C, ArCH), 117.20 (2C, ArCH), 99.97 (1C, C-1), 71.10 (1C, C-5), 70.99 (1C, C-3), 68.79 (1C, C-2), 67.01 (1C, C-4), 61.48 (1C, C-6), 51.78 (1C, CH₂CH₂COOCH₃), 35.92 (1C, CH₂CH₂COOCH₃), 30.25 (1C, CH₂CH₂COOCH₃), 20.88 (1C, CH₃), 20.81 (2C, CH₃), 20.73 (1C, CH₃).

HPLC-MS: [C₂₄H₃₀O₁₂ + NH₄]⁺ calcd. 528.21, found 528.21.

HRMS: [C₂₄H₃₀O₁₂ + NH₄]⁺ calcd. 528.2074, found 528.2080.

4-(β-D-galactopyranosyloxy)benzenepropanoic acid (**2**)



Compound **5** (179.8 mg, 0.35 mmol) was dissolved in methanol (8.5 mL). Water (5.6 mL) and sodium hydroxide solution (2.8 mL, 1 M, 2.82 mmol) were added. The reaction mixture was stirred for 1 h at r.t, then neutralised with Amberlite IR 120/H⁺ and concentrated *in vacuo*. After purification by normal phase MPLC (dichloromethane/methanol with 1% formic acid, gradient of 1-20% methanol), compound **2** (107.5 mg, 0.33 mmol, 93%) was obtained as a white solid.

¹H NMR (500 MHz, DMSO-*d*₆) δ, 7.15 – 7.09 (m, 2H, ArH), 6.95 – 6.89 (m, 2H, ArH), 4.75 (d, *J* = 7.6 Hz, 1H, H-1), 3.69 (d, *J* = 3.3 Hz, 1H, H-4), 3.57 – 3.44 (m, 4H, H-2, H-5, H-6),

3.38 (dd, $J = 9.5, 3.3$ Hz, 1H, H-3), 2.75 (t, $J = 7.6$ Hz, 2H, $\text{CH}_2\text{CH}_2\text{COOCH}_3$), 2.47 (t, $J = 7.6$ Hz, 2H, $\text{CH}_2\text{CH}_2\text{COOCH}_3$).

^{13}C NMR (126 MHz, $\text{DMSO-}d_6$) δ 174.09 (1C, C=O), 155.85 (1C, ArC), 134.16 (1C, ArC), 129.05 (2C, ArCH), 116.15 (2C, ArCH), 101.17 (1C, C-1), 75.46 (1C, C-5), 73.33 (1C, C-3), 70.30 (1C, C-2), 68.13 (1C, C-4), 60.38 (1C, C-6), 35.80 (1C, $\text{CH}_2\text{CH}_2\text{COOH}$), 29.69 (1C, $\text{CH}_2\text{CH}_2\text{COOH}$).

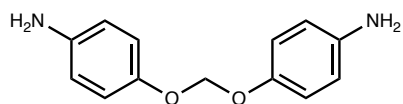
HPLC-MS: $[\text{C}_{15}\text{H}_{20}\text{O}_8 - \text{H}]^-$ calcd. 327.11, found 326.95.

HRMS: $[\text{C}_{15}\text{H}_{20}\text{O}_8 - \text{H}]^-$ calcd. 327.1085, found 327.1087.

General procedure for the synthesis of bis-anilines C–F

Corresponding di-halogenated hydrocarbons (1 eq.), 4-nitrophenol (4 eq.) and potassium carbonate (3 eq.) were dissolved in dry dimethylformamide in a microwave reaction vial. The vial was sealed and the mixture was irradiated in a Discover SP Sequential Microwave Synthesis System (CEM Corporation, North Carolina, USA) with maximum power 300 W at 70 °C for 11 h – 4 days (for **C** 10 days in oil bath, no irradiation). After cooling, the reaction was diluted with ethyl acetate and washed with satd. aqueous NaHCO_3 , dried over anhydrous Na_2SO_4 , filtered and concentrated *in vacuo*. Bis-nitro intermediates were purified by normal phase MPLC (toluene with 1% ethyl acetate and 1% triethylamine, isocratic) or in case of **E** by C18 column MPLC chromatography (water/acetonitrile with 0.1% formic acid, gradient of 40–75% acetonitrile). Pure bis-nitro intermediate was then dissolved in dichloromethane/methanol (3:1, for **C** 2:1) and Pd/C (0.01 mol%) was added. After three vacuum/ H_2 cycles the reaction was stirred under H_2 atmosphere (1 atm) overnight. The reaction was filtered over celite and concentrated *in vacuo*. Pure products were obtained without further purification. Analytical data of compounds **C–F** match the literature.^{134–136}

Bis(4-aminophenoxy) methane (C)



Dichloromethane (192 μL , 3.0 mmol), 4-nitrophenol (1.67 g, 12 mmol) and potassium carbonate (1.24 g, 9.0 mmol) in 9 mL dimethylformamide were used following the general procedure for synthesis of bis-anilines to give compound **C** (326 mg, 1.42 mmol, 47% over two steps) as a light-brown solid.

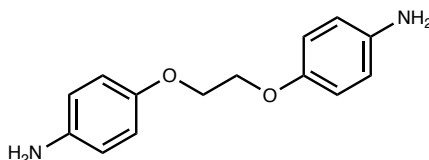
^1H NMR (500 MHz, $\text{MeOH-}d_4$) δ 6.91 – 6.84 (m, 4H, ArH), 6.74 – 6.68 (m, 4H, ArH), 5.52 (s, 2H, CH_2).

^{13}C NMR (126 MHz, MeOH- d_4) δ 151.77 (2C, ArC), 142.80 (2C, ArC), 118.98 (4C, ArCH), 118.07 (4C, ArCH), 94.31 (1C, CH₂).

HPLC-MS: [C₁₃H₁₄N₂O₂ + H]⁺ calcd. 231.11, found 231.04.

HRMS: [C₁₃H₁₄N₂O₂ + H]⁺ calcd. 231.1128, found 231.1125.

1,2-bis(4-aminophenoxy) ethane (D)



1,2-Dichloroethane (181 μL , 2.3 mmol), 4-nitrophenol (1.11 g, 8 mmol) and potassium carbonate (829 mg, 6.0 mmol) in 6 mL dimethylformamide were used following the general procedure for synthesis of bis-anilines to give compound **D** (182 mg, 0.75 mmol, 33% over two steps) as a brown-gray solid.

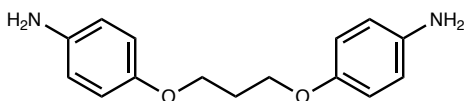
^1H NMR (500 MHz, DMSO- d_6) δ 6.81 – 6.71 (m, 4H, ArH), 6.70 – 6.54 (m, 4H, ArH), 4.12 (s, 4H, CH₂).

^{13}C NMR (126 MHz, DMSO- d_6) δ 150.95 (2C, ArC), 139.66 (2C, ArC), 116.45 (4C, ArCH), 115.44, (4C, ArCH) 66.93 (2C, CH₂).

HPLC-MS: [C₁₄H₁₆N₂O₂ + H]⁺ calcd. 245.13, found 245.05.

HRMS: [C₁₄H₁₆N₂O₂ + H]⁺ calcd. 245.1285, found 245.1281.

1,3-bis(4-aminophenoxy) propane (E)



1,3-Dichloropropane (190 μL , 2.0 mmol), 4-nitrophenol (1.11 g, 8 mmol) and potassium carbonate (829 mg, 6.0 mmol) in 6 mL dimethylformamide were used following the general procedure for synthesis of bis-anilines to give compound **E** (342 mg, 1.32 mmol, 67% over two steps) as a brown-gray solid.

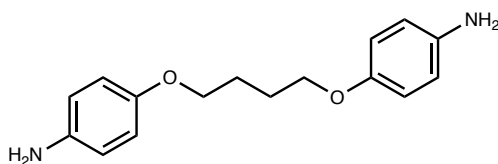
^1H NMR (500 MHz, MeOH- d_4) δ 6.80 – 6.70 (m, 8H, ArH), 4.06 (t, J = 6.2 Hz, 4H, CH₂CH₂CH₂), 2.19 – 2.09 (m, 2H, CH₂CH₂CH₂).

^{13}C NMR (126 MHz, MeOH- d_4) δ 154.21 (2C, ArC), 140.39 (2C, ArC), 118.73 (4C, ArCH), 116.67 (4C, ArCH), 66.38 (2C, CH₂CH₂CH₂), 30.67 (1C, CH₂CH₂CH₂).

HPLC-MS: [C₁₅H₁₈N₂O₂ + H]⁺ calcd. 259.14, found 259.06.

HRMS: [C₁₅H₁₈N₂O₂ + H]⁺ calcd. 259.1441, found 259.1438.

1,4-bis(4-aminophenoxy) butane (F)



1,4-Dibromobutane (236 μ L, 2.0 mmol), 4-nitrophenol (1.11 g, 8 mmol) and potassium carbonate (829 mg, 6.0 mmol) in 6 mL dimethylformamide were used following the general procedure for synthesis of bis-anilines to give compound **F** (562 mg, 2.1 mmol, quant. over two steps) as a brown-gray solid.

^1H NMR (500 MHz, MeOH- d_4) δ 6.77 (s, 8H, ArH), 4.00 – 3.92 (m, 4H, $\text{CH}_2\text{CH}_2\text{CH}_2\text{CH}_2$), 1.95 – 1.84 (m, 4H, $\text{CH}_2\text{CH}_2\text{CH}_2\text{CH}_2$).

^{13}C NMR (126 MHz, MeOH- d_4) δ 154.75 (2C, ArC), 139.21 (2C, ArC), 119.17 (4C, ArCH), 116.63 (4C, ArCH), 69.36 (2C, $\text{CH}_2\text{CH}_2\text{CH}_2\text{CH}_2$), 27.26 (2C, $\text{CH}_2\text{CH}_2\text{CH}_2\text{CH}_2$).

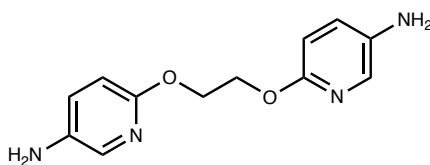
HPLC-MS: $[\text{C}_{16}\text{H}_{20}\text{N}_2\text{O}_2 + \text{H}]^+$ calcd. 273.16, found 273.07.

HRMS: $[\text{C}_{16}\text{H}_{20}\text{N}_2\text{O}_2 + \text{H}]^+$ calcd. 273.1598, found 273.1594.

General procedure for the synthesis of bis-aminopyridines H–J

Corresponding diol (1 eq.), 2-chloro-5-nitropyridine (2-3 eq.) and sodium hydride (3 eq., 60% in mineral oil) were dissolved in dry dimethylformamide and stirred at room temperature for 1 h – 2 d (for **H** 3.5 eq. of potassium carbonate was used, $T = 65\text{ }^\circ\text{C}$ for 5 d). The reaction was diluted with ice cold water and dichloromethane. Organic phase was separated and washed with half satd. brine, dried over anhydrous Na_2SO_4 , filtered and concentrated *in vacuo*. Bis-nitro intermediate was purified by normal phase MPLC (petrol ether/ethyl acetate, gradient of 5-20% ethyl acetate). Pure bis-nitro intermediate was then dissolved in dichloromethane/methanol (2:1) and Pd/C (0.02 mol%) was added. After three vacuum/ H_2 cycles the reaction was stirred under H_2 atmosphere (1 atm) for 3–4 h. The reaction was filtered over celite and concentrated *in vacuo*. Pure products were obtained without further purification.

1,2-bis((5-aminopyridin-2-yl)oxy)ethane (H)



Ethylene glycol (50 μ L, 0.89 mmol), 2-chloro-5-nitropyridine (436 mg, 2.75 mmol) and potassium carbonate (438 mg, 3.5 mmol) in 1.5 mL dimethylformamide were used following

the general procedure for synthesis of bis-aminopyridines to give compound **H** (69.0 mg, 0.28 mmol, 31% over two steps) as a light-brown solid.

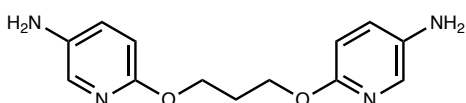
^1H NMR (500 MHz, MeOH- d_4) δ 7.61 (dd, $J = 2.9, 0.7$ Hz, 2H ArH), 7.17 (dd, $J = 8.7, 2.9$ Hz, 2H, ArH), 6.65 (dd, $J = 8.7, 0.7$ Hz, 2H, ArH), 4.44 (s, 4H, CH_2).

^{13}C NMR (126 MHz, MeOH- d_4) δ 158.46 (2C, ArC), 139.63 (2C, ArC), 133.72 (2C, ArCH), 129.40 (2C, ArCH), 111.82 (2C, ArCH), 65.88 (2C, CH_2).

HPLC-MS: $[\text{C}_{12}\text{H}_{14}\text{N}_4\text{O}_2 + \text{Na}]^+$ calcd. 269.10, found 269.05.

HRMS: $[\text{C}_{12}\text{H}_{14}\text{N}_4\text{O}_2 + \text{H}]^+$ calcd. 247.1190, found 247.1187.

1,3-bis((5-aminopyridin-2-yl)oxy)propane **I**



Propane-1,3-diol (50 μL , 0.89 mmol), 2-chloro-5-nitropyridine (279 mg, 1.76 mmol) and sodium hydride (83 mg, 2.1 mmol) in 1.5 mL dimethylformamide were used following the general procedure for synthesis of bis-aminopyridines to give compound **I** (111.4 mg, 0.43 mmol, 62% over two steps) as brown solid.

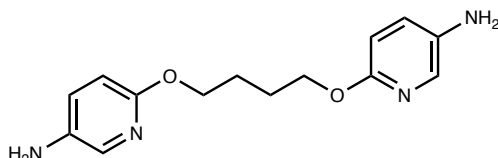
^1H NMR (500 MHz, MeOH- d_4) δ 7.60 (d, $J = 2.8$ Hz, 2H, ArH), 7.17 (dd, $J = 8.7, 2.9$ Hz, 2H, ArH), 6.64 (d, $J = 8.7$ Hz, 2H, ArH), 4.29 (t, $J = 6.3$ Hz, 4H, $\text{CH}_2\text{CH}_2\text{CH}_2$), 2.16 (p, $J = 6.3$ Hz, 2H, $\text{CH}_2\text{CH}_2\text{CH}_2$).

^{13}C NMR (126 MHz, MeOH- d_4) δ 158.76 (2C, ArC), 139.35 (2C, ArC), 133.81 (2C, ArCH), 129.48 (2C, ArCH), 111.65 (2C, ArCH), 64.18 (2C, $\text{CH}_2\text{CH}_2\text{CH}_2$), 30.21 (1C, $\text{CH}_2\text{CH}_2\text{CH}_2$).

HPLC-MS: $[\text{C}_{13}\text{H}_{16}\text{N}_4\text{O}_2 + \text{H}]^+$ calcd. 261.13, found 261.07.

HRMS: $[\text{C}_{13}\text{H}_{16}\text{N}_4\text{O}_2 + \text{H}]^+$ calcd. 261.1346, found 261.1340.

1,4-bis((5-aminopyridin-2-yl)oxy)butane **J**



Butane-1,4-diol (50 μL , 0.56 mmol), 2-chloro-5-nitropyridine (284 mg, 1.79 mmol) and sodium hydride (72 mg, 1.9 mmol) in 1.5 mL dimethylformamide were used following the general procedure for synthesis of bis-aminopyridines to give the bis-nitro intermediate (143 mg, 0.43 mmol, 76%). The bis-nitro intermediate (125 mg, 0.38 mmol) was reduced to give pure compound **J** (104 mg, 0.38 mmol, quant.) as a brown solid.

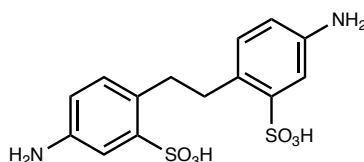
^1H NMR (500 MHz, MeOH- d_4) δ 7.60 (d, J = 2.9 Hz, 2H, ArH), 7.17 (dd, J = 8.7, 2.9 Hz, 2H, ArH), 6.62 (d, J = 8.7 Hz, 2H, ArH), 4.22 – 4.16 (m, 4H, $\text{CH}_2\text{CH}_2\text{CH}_2\text{CH}_2$), 1.93 – 1.85 (m, 4H, $\text{CH}_2\text{CH}_2\text{CH}_2\text{CH}_2$).

^{13}C NMR (126 MHz, MeOH- d_4) δ 158.86 (2C, ArC), 139.36 (2C, ArC), 133.78 (2C, ArCH), 129.47 (2C, ArCH), 111.62 (2C, ArCH), 67.09 (2C, $\text{CH}_2\text{CH}_2\text{CH}_2\text{CH}_2$), 27.05 (2C, $\text{CH}_2\text{CH}_2\text{CH}_2\text{CH}_2$).

HPLC-MS: $[\text{C}_{14}\text{H}_{18}\text{N}_4\text{O}_2 + \text{H}]^+$ calcd. 275.15, found 275.10.

HRMS: $[\text{C}_{14}\text{H}_{18}\text{N}_4\text{O}_2 + \text{H}]^+$ calcd. 275.1503, found 275.1497.

6,6'-(ethane-1,2-diyl)bis(3-aminobenzenesulfonic acid) (**L**)



Compound **L** was synthesized according to Bazanova *et al.*¹³⁷ 4,4'-Diaminostilbene-2,2'-disulfonic acid (**13**, 235.5 mg, 0.64 mmol) was completely dissolved in water (10 mL) after addition of 1 drop of satd. NaOH aqueous solution, and then Raney Ni was added. After three vacuum/ H_2 cycles the reaction was stirred under H_2 atmosphere (1 atm) for 4 days. The reaction was filtered over celite and lyophilized. Because conversion was incomplete, the reaction crude was re-dissolved in water (5 mL) and 1 drop of satd. NaOH aqueous solution. Raney Ni was added and after three vacuum/ H_2 cycles the reaction was stirred under H_2 atmosphere (1 atm) for 2 additional days. The reaction was filtered over celite and lyophilized. Reaction crude was re-dissolved in water (10 mL) and pure product **L** (150.6 mg, 0.40 mmol, 64%) was precipitated after acidification with HCl (2 M) as a white solid.

^1H NMR (500 MHz, D_2O) δ 7.28 (dd, J = 2.4, 0.9 Hz, 2H, ArH), 7.13 (d, J = 8.0 Hz, 2H, ArH), 6.85 (ddd, J = 8.1, 2.5, 0.9 Hz, 2H, ArH), 3.15 (s, 4H, CH_2).

^{13}C NMR (126 MHz, D_2O) δ 144.12 (2C, ArC), 141.07 (2C, ArC), 132.63 (2C, ArCH), 130.22 (2C, ArC), 119.20 (2C, ArCH), 114.50 (2C, ArCH), 33.46 (2C, CH_2).

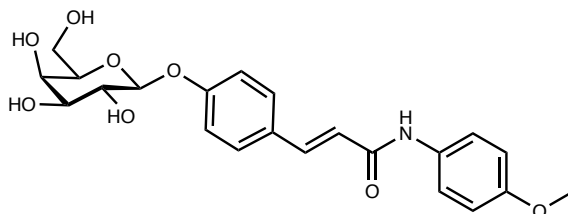
HPLC-MS: $[\text{C}_{14}\text{H}_{16}\text{N}_2\text{O}_6\text{S}_2 - \text{H}]^-$ calcd. 371.0377, found 370.93.

General procedure for synthesis of amides

Corresponding anilines **A–F** or aminopyridines **G–J** (1 eq.) and carboxylate-bearing galactosides **1** or **2** (2.5 eq.) were dissolved in dry dimethylformamide. HBTU (2.5 eq.) and DIPEA (5 eq.) were added. Reactions were stirred at r.t. until completion, then diluted with

water and lyophilized. The products were purified by MPLC or preparative HPLC (C18, water/acetonitrile with 0.1% formic acid).

Monovalent ligand A1



4-methoxyaniline (**A**, 20.8 mg, 169 μmol), coumarate **1** (33.9 mg, 104 μmol) and HBTU (51.4 mg, 136 μmol) were dissolved in dimethylformamide (1 mL) and DIPEA (30 μL , 172 μmol) was added. The reaction was stirred at r.t. for 1 h, then diluted with water and lyophilized. The product was purified by preparative reverse-phase HPLC (water/acetonitrile with 0.1% formic acid, gradient of 15-40% acetonitrile) and compound **A14** (15.9 mg, 37 μmol , 35%) was obtained as a white solid.

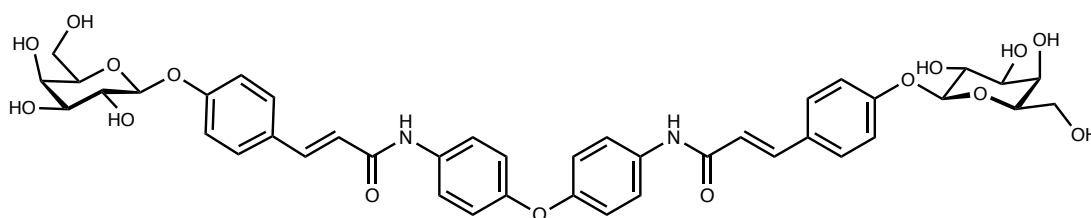
^1H NMR (500 MHz, $\text{DMSO-}d_6$) δ 10.00 (s, 1H, NH), 7.63 – 7.58 (m, 2H, ArH), 7.58 – 7.53 (m, 2H, ArH), 7.51 (d, $J = 15.7$ Hz, 1H, $\text{CH}=\text{CHCONH}$), 7.11 – 7.05 (m, 2H, ArH), 6.94 – 6.86 (m, 2H, ArH), 6.66 (d, $J = 15.7$ Hz, 1H, $\text{CH}=\text{CHCONH}$), 4.89 (d, $J = 7.7$ Hz, 1H, H-1), 3.73 (s, 3H, OCH_3), 3.71 (d, $J = 3.0$ Hz, 1H, H-4), 3.63 – 3.47 (m, 4H, H-2, H-5, H-6), 3.44 – 3.40 (m, 1H, H-3).

^{13}C NMR (126 MHz, $\text{DMSO-}d_6$) δ 163.37 (1C, C=O), 158.65 (1C, ArC), 155.23 (1C, ArC), 139.31 (1C, $\text{CH}=\text{CHCONH}$), 132.58 (1C, ArC), 129.11 (2C, ArCH), 128.43 (1C, ArC), 120.65 (2C, ArCH), 120.34 (1C, $\text{CH}=\text{CHCONH}$), 116.61 (2C, ArCH), 113.95 (2C, ArCH), 100.69 (1C, C-1), 75.59 (1C, C-5), 73.28 (1C, C-3), 70.23 (1C, C-2), 68.13 (1C, C-4), 60.37 (1C, C-6), 55.19 (1C, OCH_3).

HPLC-MS: $[\text{C}_{22}\text{H}_{25}\text{NO}_8 + \text{H}]^+$ calcd. 432.17, found 432.13.

HRMS: $[\text{C}_{22}\text{H}_{25}\text{NO}_8 + \text{H}]^+$ calcd. 432.1653, found 432.1652.

Divalent Ligand B1



4,4'-Oxydianiline **B** (10.1 mg, 50.4 μmol), compound **1** (38.2 mg, 117 μmol) and HBTU (53.1 mg, 140 μmol) were dissolved in dimethylformamide (1 mL) and DIPEA (50 μL , 287 μmol)

was added. The reaction was stirred at r.t. overnight, then dried *in vacuo*. The product was purified by preparative reverse-phase HPLC (water/acetonitrile with 0.1% formic acid, gradient of 20-35% acetonitrile) and compound **B14** (28.3 mg, 34.6 μmol , 69%) was obtained as pale-yellow solid.

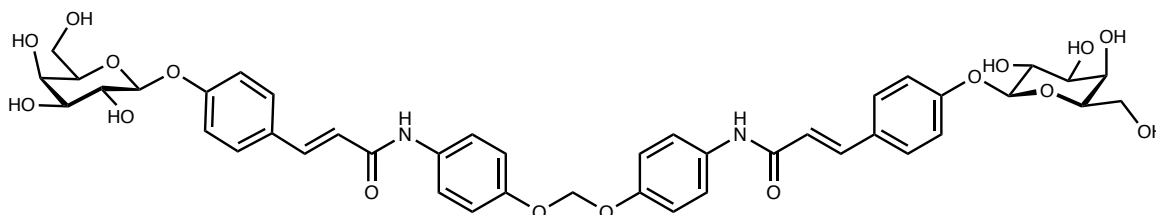
^1H NMR (500 MHz, $\text{DMSO-}d_6$) δ 10.18 (s, 2H, NH), 7.73 – 7.67 (m, 4H, ArH), 7.60 – 7.50 (m, 6H, ArH, $\text{CH}=\text{CHCONH}$), 7.11 – 7.04 (m, 4H, ArH), 7.02 – 6.95 (m, 4H, ArH), 6.68 (d, $J = 15.7$ Hz, 2H, $\text{CH}=\text{CHCONH}$), 4.90 (d, $J = 7.7$ Hz, 2H, H-1), 3.81 – 3.35 (m, 12H, H-2, H-3, H-4, H-5, H-6).

^{13}C NMR (126 MHz, $\text{DMSO-}d_6$) δ 163.64 (2C, C=O), 158.75 (2C, ArC), 152.55 (2C, ArC), 139.74 (2C, $\text{CH}=\text{CHCONH}$), 135.00 (2C, ArC), 129.24 (4C, ArCH), 128.36 (2C, ArC), 120.82 (4C, ArCH), 120.15 (2C, $\text{CH}=\text{CHCONH}$), 118.85 (4C, ArCH), 116.63 (4C, ArCH), 100.66 (2C, C-1), 75.62 (2C, C-5), 73.29 (2C, C-3), 70.24 (2C, C-2), 68.15 (2C, C-4), 60.38 (2C, C-6).

HPLC-MS: $[\text{C}_{42}\text{H}_{44}\text{N}_2\text{O}_{15} + \text{H}]^+$ calcd. 817.28, found 817.33.

HRMS: $[\text{C}_{42}\text{H}_{44}\text{N}_2\text{O}_{15} + \text{H}]^+$ calcd. 817.2814, found 817.2805.

Divalent Ligand C1



Bis(4-aminophenoxy)methane **C** (7.9 mg, 34 μmol), compound **1** (25.3 mg, 76 μmol) and HBTU (32.7 mg, 86 μmol) were dissolved in dimethylformamide (3 mL) and DIPEA (9 μL , 52 μmol) was added. The reaction was stirred at r.t. for 2 days, then dried *in vacuo*. The product was purified by preparative reverse-phase HPLC (water/acetonitrile with 0.1% formic acid, gradient of 25-45% acetonitrile) and compound **C1** (6.9 mg, 8.1 μmol , 24%) was obtained as a white solid.

^1H NMR (500 MHz, $\text{DMSO-}d_6$) δ 10.07 (s, 2H, NH), 7.67 – 7.60 (m, 4H, ArH), 7.59 – 7.54 (m, 4H, ArH), 7.52 (d, $J = 15.6$ Hz, 2H, $\text{CH}=\text{CHCONH}$), 7.12 – 7.02 (m, 8H, ArH), 6.67 (d, $J = 15.6$ Hz, 2H, $\text{CH}=\text{CHCONH}$), 5.77 (s, 2H, CH_2), 5.19 (d, $J = 5.2$ Hz, 2H, OH-2), 4.92 – 4.84 (m, 4H, H-1, OH-3), 4.66 (t, $J = 5.5$ Hz, 2H, OH-6), 4.52 (d, $J = 4.6$ Hz, 2H, OH-4), 3.71 (t, $J = 4.1$ Hz, 2H, H-4), 3.64 – 3.45 (m, 8H, H-2, H-5, H-6), 3.42 (ddd, $J = 9.3, 5.3, 3.2$ Hz, 2H, H-3).

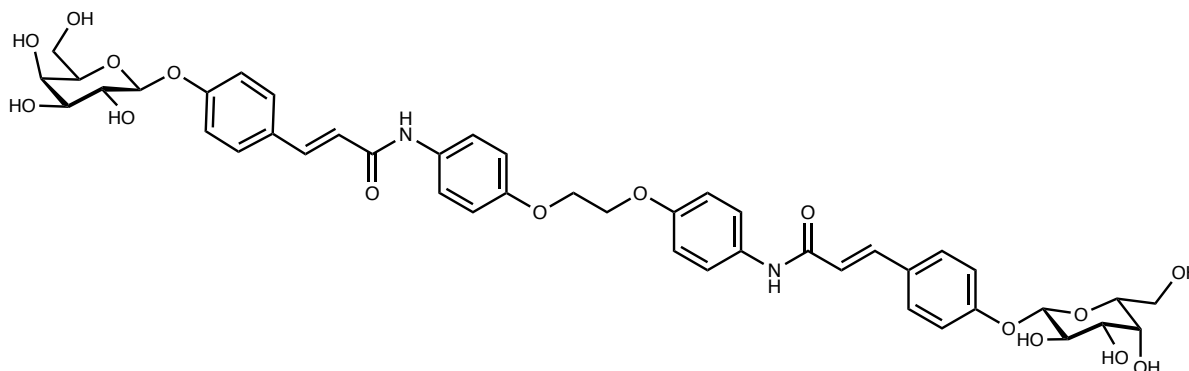
^{13}C NMR (126 MHz, $\text{DMSO-}d_6$) δ 163.49 (2C, C=O), 158.68 (2C, ArC), 152.19 (2C, ArC), 139.52 (2C, $\text{CH}=\text{CHCONH}$), 134.09 (2C, ArC), 129.14 (4C, ArCH), 128.38 (2C, ArC), 120.59

(4C, ArCH), 120.23 (2C, CH=CHCONH), 116.60 (4C, ArCH), 116.59 (4C, ArCH), 100.68 (2C, C-1), 90.81 (1C, CH₂), 75.58 (2C, C-5), 73.27 (2C, C-3), 70.22 (2C, C-2), 68.12 (2C, C-4), 60.36 (2C, C-6).

HPLC-MS: [C₄₃H₄₆N₂O₁₆ + H]⁺ calcd. 847.29, found 847.33

HRMS: [C₄₃H₄₆N₂O₁₆ + H]⁺ calcd. 847.2920, found 847.2924.

Divalent Ligand D1



Bis(4-aminophenoxy)ethane **D** (7.3 mg, 0.03 mmol), compound **1** (21.6 mg, 66 μmol) and HBTU (25.2 mg, 66 μmol) were dissolved in dimethylformamide (4 mL) and DIPEA (7 μL, 40 μmol) was added. The reaction was stirred at r.t. for 2 days, then dried *in vacuo*. The product was purified by preparative reverse-phase HPLC (water/acetonitrile supplemented with 0.1% formic acid, gradient of 25-45% acetonitrile) and compound **D1** (4.5 mg, 5.2 μmol, 17%) was obtained as a white solid.

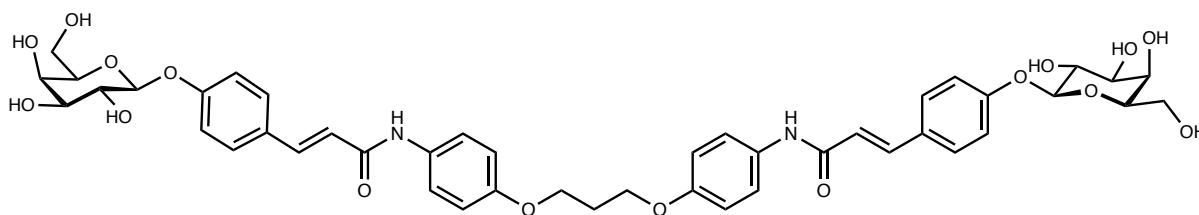
¹H NMR (500 MHz, DMSO-*d*₆) δ 10.04 (s, 2H, NH), 7.65 – 7.60 (m, 4H, ArH), 7.58 – 7.54 (m, 4H, ArH), 7.52 (d, *J* = 15.5 Hz, 2H, CH=CHCONH), 7.08 (d, *J* = 8.7 Hz, 4H, ArH), 7.01 – 6.91 (m, 4H, ArH), 6.67 (d, *J* = 15.7 Hz, 2H, CH=CHCONH), 4.89 (d, *J* = 7.7 Hz, 2H, H-1), 4.28 (s, 4H, CH₂), 3.70 (d, *J* = 3.3 Hz, 2H, H-4), 3.63 – 3.46 (m, 8H, H-2, H-5, H-6), 3.42 (dd, *J* = 9.5, 3.3 Hz, 4H, H-3).

¹³C NMR (126 MHz, DMSO-*d*₆) δ 163.41 (2C, C=O), 158.67 (2C, ArC), 154.29 (2C, ArC), 139.39 (2C, CH=CHCONH), 132.85 (2C, ArC), 129.16 (4C, ArCH), 128.43 (2C, ArC), 120.64 (4C, ArCH), 120.32 (2C, CH=CHCONH), 116.61 (4C, ArCH), 114.65 (4C, ArCH), 100.67 (2C, C-1), 75.60 (2C, C-5), 73.28 (2C, C-3), 70.23 (2C, C-2), 68.14 (2C, C-4), 66.51 (2C, CH₂), 60.37 (2C, C-6).

HPLC-MS: [C₄₄H₄₈N₂O₁₆ + H]⁺ calcd. 861.31, found 861.36.

HRMS: [C₄₄H₄₈N₂O₁₆ + H]⁺ calcd. 861.3077, found 861.3083.

Divalent Ligand E1



Bis(4-aminophenoxy)propane **E** (11.2 mg, 43.3 μmol), compound **1** (30.8 mg, 94.4 μmol) and HBTU (38.1 mg, 100 μmol) were dissolved in dimethylformamide (1 mL) and DIPEA (20 μL , 115 μmol) was added. The reaction was stirred at r.t. overnight, then dried *in vacuo*. The product was purified by preparative reverse-phase HPLC (water/acetonitrile with 0.1% formic acid, gradient of 20-50% acetonitrile) and compound **E1** (25.9 mg, 29.6 μmol , 68%) was obtained as a pale-yellow solid.

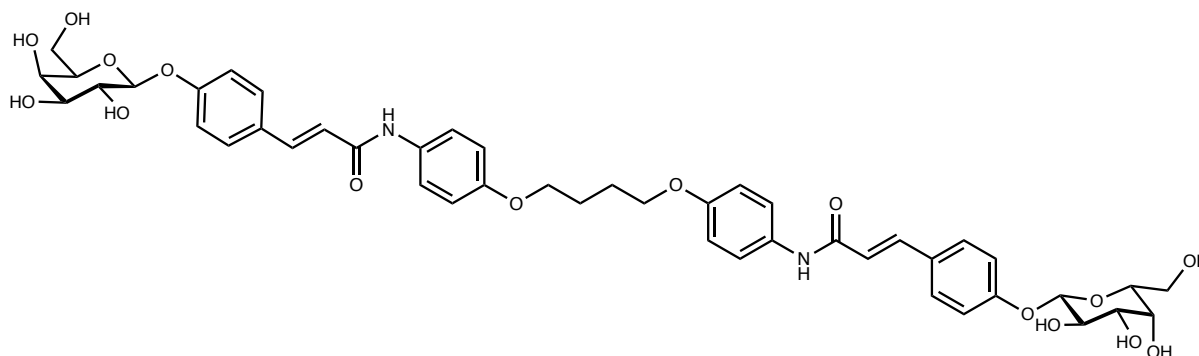
^1H NMR (500 MHz, $\text{DMSO-}d_6$) δ 10.02 (s, 2H, NH), 7.63 – 7.58 (m, 4H, ArH), 7.58 – 7.53 (m, 4H, ArH), 7.51 (d, $J = 15.6$ Hz, 2H, $\text{CH}=\text{CHCONH}$), 7.10 – 7.05 (m, 4H, ArH), 6.96 – 6.91 (m, 4H, ArH), 6.66 (d, $J = 15.7$ Hz, 2H, $\text{CH}=\text{CHCONH}$), 5.21 (s, 2H, OH-2), 4.89 (d, $J = 7.7$ Hz, 4H, H-1, OH-3), 4.68 (s, 2H, OH-6), 4.55 (s, 2H, OH-4), 4.10 (t, $J = 6.2$ Hz, 4H, $\text{CH}_2\text{CH}_2\text{CH}_2$), 3.70 (d, $J = 3.2$ Hz, 2H, H-4), 3.63 – 3.46 (m, 8H, H-2, H-5, H-6), 3.41 (dd, $J = 9.5, 3.3$ Hz, 2H, H-3), 2.20 – 2.11 (m, 2H, $\text{CH}_2\text{CH}_2\text{CH}_2$).

^{13}C NMR (126 MHz, $\text{DMSO-}d_6$) δ 163.39 (2C, C=O), 158.67 (2C, ArC), 154.47 (2C, ArC), 139.36 (2C, $\text{CH}=\text{CHCONH}$), 132.70 (2C, ArC), 129.16 (4C, ArCH), 128.43 (2C, ArC), 120.63 (4C, ArCH), 120.34 (2C, $\text{CH}=\text{CHCONH}$), 116.61 (4C, ArCH), 114.60 (4C, ArCH), 100.67 (2C, C-1), 75.61 (2C, C-5), 73.28 (2C, C-3), 70.23 (2C, C-2), 68.15 (2C, C-4), 64.37 (2C, $\text{CH}_2\text{CH}_2\text{CH}_2$), 60.38 (2C, C-6), 28.77 (1C, $\text{CH}_2\text{CH}_2\text{CH}_2$).

HPLC-MS: $[\text{C}_{45}\text{H}_{50}\text{N}_2\text{O}_{16} + \text{H}]^+$ calcd. 875.32, found 875.40.

HRMS: $[\text{C}_{45}\text{H}_{50}\text{N}_2\text{O}_{16} + \text{H}]^+$ calcd. 875.3233, found 875.3223.

Divalent Ligand F1



Bis(4-aminophenoxy)butane **F** (11.7 mg, 43.0 μmol), compound **1** (33.3 mg, 102 μmol) and HBTU (37.1 mg, 97.8 μmol) were dissolved in dimethylformamide (1 mL) and DIPEA (20 μL , 115 μmol) was added. The reaction was stirred at r.t. overnight, then dried *in vacuo*. The product was purified by preparative reverse-phase HPLC (water/acetonitrile with 0.1% formic acid, gradient of 25-45% acetonitrile) and compound **F1** (22.8 mg, 25.6 μmol , 60%) was obtained as a pale-yellow solid.

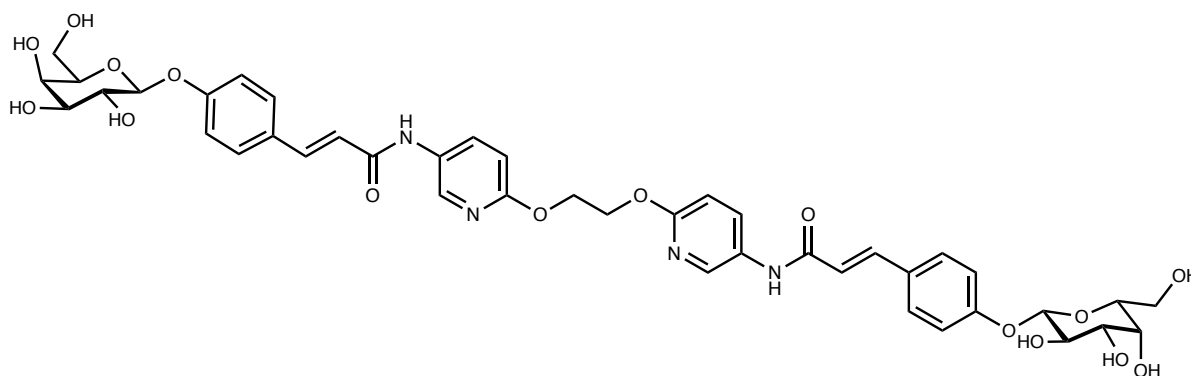
^1H NMR (500 MHz, $\text{DMSO-}d_6$) δ 10.00 (s, 2H, NH), 7.62 – 7.58 (m, 4H, ArH), 7.58 – 7.54 (m, 4H, ArH), 7.51 (d, $J = 15.6$ Hz, 2H, $\text{CH}=\text{CHCONH}$), 7.08 (d, $J = 8.7$ Hz, 4H, ArH), 6.94 – 6.89 (m, 4H, ArH), 6.67 (d, $J = 15.7$ Hz, 2H, $\text{CH}=\text{CHCONH}$), 5.19 (d, $J = 5.2$ Hz, 2H, OH-2), 4.93 – 4.84 (m, 4H, H-1, OH-3), 4.67 (t, $J = 5.5$ Hz, 2H, OH-6), 4.52 (d, $J = 4.6$ Hz, 2H, OH-4), 4.00 (d, $J = 5.7$ Hz, 4H, $\text{CH}_2\text{CH}_2\text{CH}_2\text{CH}_2$), 3.71 (t, $J = 4.2$ Hz, 2H, H-4), 3.63 – 3.46 (m, 8H, H-2, H-5, H-6), 3.45 – 3.39 (m, 2H, H-3), 1.90 – 1.80 (m, 4H, $\text{CH}_2\text{CH}_2\text{CH}_2\text{CH}_2$).

^{13}C NMR (126 MHz, $\text{DMSO-}d_6$) δ 163.36 (2C, C=O), 158.65 (2C, ArC), 154.61 (2C, ArC), 139.31 (2C, $\text{CH}=\text{CHCONH}$), 132.55 (2C, ArC), 129.11 (4C, ArCH), 128.44 (2C, ArC), 120.64 (2C, ArC), 120.36 (2C, $\text{CH}=\text{CHCONH}$), 116.61 (4C, ArCH), 114.57 (4C, ArCH), 100.69 (2C, C-1), 75.59 (2C, C-5), 73.28 (2C, C-3), 70.23 (2C, C-2), 68.14 (2C, C-4), 67.29 (2C, $\text{CH}_2\text{CH}_2\text{CH}_2\text{CH}_2$), 60.37 (2C, C-6), 25.50 (2C, $\text{CH}_2\text{CH}_2\text{CH}_2\text{CH}_2$).

HPLC-MS: $[\text{C}_{46}\text{H}_{52}\text{N}_2\text{O}_{16} + \text{H}]^+$ calcd. 889.34, found 889.42.

HRMS: $[\text{C}_{46}\text{H}_{52}\text{N}_2\text{O}_{16} + \text{H}]^+$ calcd. 889.3423, found 889.3383.

Divalent Ligand H1



1,2-bis((5-aminopyridin-2-yl)oxy)ethane **H** (14.8 mg, 60.1 μmol), compound **1** (51.7 mg, 158 μmol) and HBTU (60.1 mg, 158 μmol) were dissolved in dimethylformamide (1.5 mL) and DIPEA (55 μL , 316 μmol) was added. The reaction was stirred at r.t. overnight, then lyophilized. The product was purified by preparative reverse-phase HPLC (water/acetonitrile supplemented with 0.1% formic acid, gradient of 15-40% acetonitrile) and compound **H1** (37.9 mg, 43.9 μmol , 73%) was obtained as a pale-yellow solid.

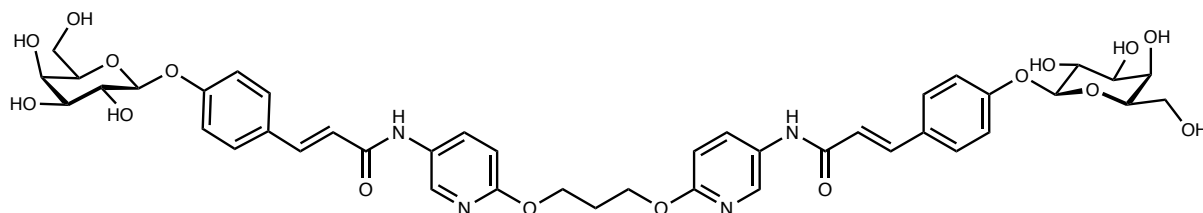
^1H NMR (500 MHz, $\text{DMSO-}d_6$) δ 10.19 (s, 2H, NH), 8.46 (d, $J = 2.9$ Hz, 2H, ArH), 8.02 (dd, $J = 8.9, 2.7$ Hz, 2H, ArH), 7.60 – 7.52 (m, 6H, ArH, $\text{CH}=\text{CHCONH}$), 7.11 – 7.05 (m, 4H, ArH), 6.87 (d, $J = 8.9$ Hz, 2H, ArH), 6.66 (d, $J = 15.7$ Hz, 2H, $\text{CH}=\text{CHCONH}$), 4.90 (d, $J = 7.7$ Hz, 2H, H-1), 4.56 (s, 4H, CH_2), 3.71 (d, $J = 3.8$ Hz, 2H, H-4), 3.63 – 3.46 (m, 8H, H-2, H-5, H-6), 3.42 (dd, $J = 9.5, 3.3$ Hz, 2H, H-3).

^{13}C NMR (126 MHz, $\text{DMSO-}d_6$) δ 163.85 (2C, C=O), 158.99 (2C, ArC), 158.78 (2C, ArC), 140.02 (2C, $\text{CH}=\text{CHCONH}$), 137.36 (2C, ArCH), 131.42 (2C, ArCH), 130.53 (2C, ArC), 129.25 (4C, ArCH), 128.25 (2C, ArC), 119.61 (2C, $\text{CH}=\text{CHCONH}$), 116.62 (4C, ArCH), 110.48 (2C, ArCH), 100.67 (2C, C-1), 75.59 (2C, C-5), 73.27 (2C, C-3), 70.22 (2C, C-2), 68.13 (2C, C-4), 64.11 (2C, CH_2), 60.36 (2C, C-6).

HPLC-MS: $[\text{C}_{42}\text{H}_{46}\text{N}_4\text{O}_{16} + \text{H}]^+$ calcd. 863.30, found 863.34.

HRMS: $[\text{C}_{42}\text{H}_{46}\text{N}_4\text{O}_{16} + \text{H}]^+$ calcd. 863.2982, found 863.2977.

Divalent Ligand II



1,3-bis((5-aminopyridin-2-yl)oxy)propane **I** (14.8 mg, 56.9 μmol), compound **1** (40.4 mg, 124 μmol) and HBTU (51.4 mg, 136 μmol) were dissolved in dimethylformamide (1.5 mL) and DIPEA (50 μL , 287 μmol) was added. The reaction was stirred at r.t. overnight, then lyophilized. The product was purified by preparative reverse-phase HPLC (water/acetonitrile supplemented with 0.1% formic acid, gradient of 15-40% acetonitrile) and compound **II** (22.7 mg, 25.9 μmol , 46%) was obtained as a white solid.

^1H NMR (500 MHz, $\text{DMSO-}d_6$) δ 10.18 (s, 2H, NH), 8.44 (d, $J = 2.6$ Hz, 2H, ArH), 8.00 (dd, $J = 8.9, 2.7$ Hz, 2H, ArH), 7.61 – 7.50 (m, 6H, ArH, $\text{CH}=\text{CHCONH}$), 7.08 (d, $J = 8.5$ Hz, 4H, ArH), 6.83 (d, $J = 8.8$ Hz, 2H, ArH), 6.66 (d, $J = 15.7$ Hz, 2H, $\text{CH}=\text{CHCONH}$), 5.20 (s, 2H, OH-2), 4.95 – 4.82 (m, 4H, H-1, OH-3), 4.67 (s, 2H, OH-6), 4.53 (s, 2H, OH-4), 4.37 (t, $J = 6.4$ Hz, 4H, $\text{CH}_2\text{CH}_2\text{CH}_2$), 3.71 (d, $J = 3.0$ Hz, 2H, H-4), 3.64 – 3.45 (m, 8H, H-2, H-5, H-6), 3.45 – 3.39 (m, 2H, H-3), 2.16 (p, $J = 6.4$ Hz, 2H, $\text{CH}_2\text{CH}_2\text{CH}_2$).

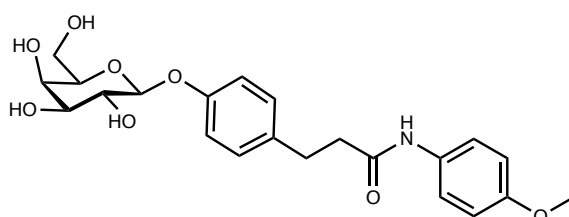
^{13}C NMR (126 MHz, $\text{DMSO-}d_6$) δ 163.82 (2C, C=O), 159.26 (2C, ArC), 158.77 (2C, ArC), 139.97 (2C, $\text{CH}=\text{CHCONH}$), 137.51 (2C, ArCH), 131.32 (2C, ArCH), 130.35 (2C, ArC), 129.24 (4C, ArCH), 128.26 (2C, ArC), 119.65 (2C, $\text{CH}=\text{CHCONH}$), 116.62 (2C, ArCH),

110.35 (2C, ArCH), 100.67 (2C, C-1), 75.60 (2C, C-5), 73.27 (2C, C-3), 70.22 (2C, C-2), 68.13 (2C, C-4), 62.54 (2C, $\underline{\text{C}}\text{H}_2\text{CH}_2\underline{\text{C}}\text{H}_2$), 60.36 (2C, C-6), 28.38 (1C, $\text{CH}_2\underline{\text{C}}\text{H}_2\text{CH}_2$).

HPLC-MS: $[\text{C}_{43}\text{H}_{48}\text{N}_4\text{O}_{16} + \text{H}]^+$ calcd. 877.31, found 877.32.

HRMS: $[\text{C}_{43}\text{H}_{48}\text{N}_4\text{O}_{16} + \text{H}]^+$ calcd. 877.3138, found 877.3138.

Monovalent ligand A2



4-methoxyaniline **A** (12.1 mg, 98.1 μmol), compound **2** (36.4 mg, 111 μmol) and HBTU (47.1 mg, 124 μmol) were dissolved in dimethylformamide (1.5 mL) and DIPEA (20 μL , 115 μmol) was added. The reaction was stirred at r.t. for 3 h, then dried *in vacuo*. The product was purified by preparative reverse-phase HPLC (water/acetonitrile supplemented with 0.1% formic acid, gradient of 15-40% acetonitrile) and compound **A2** (36.7 mg, 84.7 μmol , 86%) was obtained as a white solid.

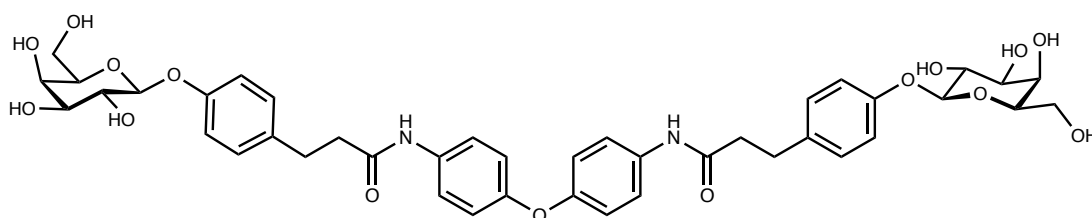
^1H NMR (500 MHz, $\text{DMSO-}d_6$) δ 9.73 (s, 1H, NH), 7.50 – 7.44 (m, 2H, ArH), 7.18 – 7.11 (m, 2H, ArH), 6.96 – 6.91 (m, 2H, ArH), 6.88 – 6.82 (m, 2H, ArH), 4.75 (d, $J = 7.7$ Hz, 1H, H-1), 3.71 (s, 3H, CH_3), 3.68 (d, $J = 3.3$ Hz, 1H, H-4), 3.57 – 3.43 (m, 4H, H-2, H-5, H-6), 3.38 (dd, $J = 9.5, 3.3$ Hz, 2H, H-3), 2.83 (t, $J = 7.7$ Hz, 2H, $\underline{\text{C}}\text{H}_2\text{CH}_2\text{CONH}$), 2.54 (dd, $J = 8.6, 6.8$ Hz, 2H, $\text{CH}_2\underline{\text{C}}\text{H}_2\text{CONH}$).

^{13}C NMR (126 MHz, $\text{DMSO-}d_6$) δ 169.91 (1C, C=O), 155.84 (1C, ArC), 155.04 (1C, ArC), 134.39 (1C, ArC), 132.42 (1C, ArC), 129.05 (2C, ArCH), 120.62 (2C, ArCH), 116.18 (2C, ArCH), 113.80 (2C, ArCH), 101.14 (1C, C-1), 75.44 (1C, C-5), 73.31 (1C, C-3), 70.30 (1C, C-2), 68.15 (1C, C-4), 60.40 (1C, C-6), 55.14 (1C, CH_3), 38.14 (1C, $\text{CH}_2\underline{\text{C}}\text{H}_2\text{CONH}$), 30.15 (1C, $\underline{\text{C}}\text{H}_2\text{CH}_2\text{CONH}$).

HPLC-MS: $[\text{C}_{22}\text{H}_{27}\text{NO}_8 + \text{H}]^+$ calcd. 434.18, found 434.08.

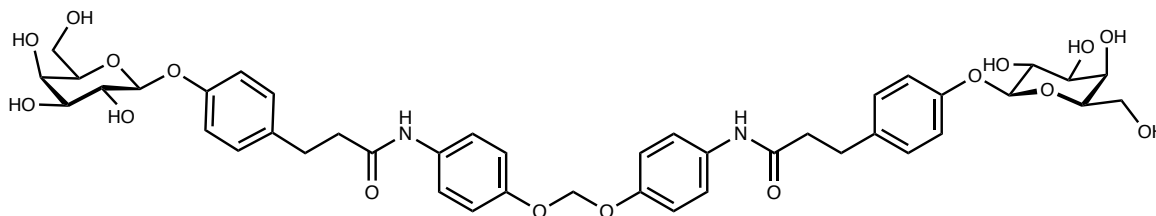
HRMS: $[\text{C}_{22}\text{H}_{27}\text{NO}_8 + \text{H}]^+$ calcd. 434.1809, found 434.1809.

Divalent ligand B2



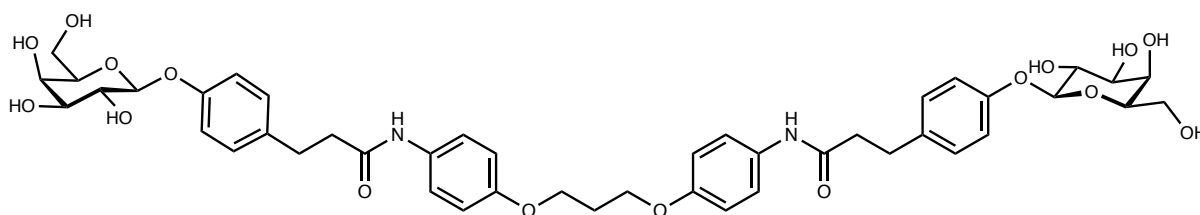
4,4'-Oxydianiline **B** (10.2 mg, 50.9 μmol), compound **2** (40.1 mg, 122 μmol) and HBTU (50.9 mg, 134 μmol) were dissolved in dimethylformamide (1 mL) and DIPEA (25 μL , 144 μmol) was added. The reaction was stirred at r.t. for 3 h, then dried *in vacuo*. The product was purified by preparative reverse-phase HPLC (water/acetonitrile with 0.1% formic acid, gradient of 15-40% acetonitrile) and compound **B2** (10.2 mg, 12.4 μmol , 24%) was obtained as a white solid. ^1H NMR (500 MHz, $\text{DMSO-}d_6$) δ 9.91 (s, 2H, NH), 7.58 – 7.52 (m, 4H, ArH), 7.17 – 7.12 (m, 4H, ArH), 6.96 – 6.88 (m, 8H, ArH), 4.76 (d, $J = 7.7$ Hz, 2H, H-1), 3.68 (d, $J = 3.3$ Hz, 2H, H-4), 3.56 – 3.44 (m, 8H, H-2, H-5, H-6), 3.38 (dd, $J = 9.5, 3.3$ Hz, 2H, H-3), 2.84 (t, $J = 7.6$ Hz, 4H, $\text{CH}_2\text{CH}_2\text{CONH}$), 2.56 (t, $J = 7.7$ Hz, 4H, $\text{CH}_2\text{CH}_2\text{CONH}$). ^{13}C NMR (126 MHz, $\text{DMSO-}d_6$) δ 170.23 (2C, C=O), 155.88 (2C, ArC), 152.38 (2C, ArC), 134.80 (2C, ArC), 134.34 (2C, ArC), 129.11 (4C, ArCH), 120.71 (4C, ArCH), 118.70 (4C, ArCH), 116.19 (4C, ArCH), 101.11 (2C, C-1), 75.47 (2C, C-5), 73.32 (2C, C-3), 70.31 (2C, C-2), 68.18 (2C, C-4), 60.42 (2C, C-6), 38.21 (2C, $\text{CH}_2\text{CH}_2\text{CONH}$), 30.12 (2C, $\text{CH}_2\text{CH}_2\text{CONH}$). HPLC-MS: $[\text{C}_{42}\text{H}_{48}\text{N}_2\text{O}_{15} + \text{H}]^+$ calcd. 821.31, found 821.30. HRMS: $[\text{C}_{42}\text{H}_{48}\text{N}_2\text{O}_{15} - \text{H}]^-$ calcd. 819.2982, found 819.2981.

Divalent ligand C2



Bis(4-aminophenoxy)methane **C** (11.6 mg, 50.4 μmol), compound **2** (41.5 mg, 126 μmol) and HBTU (48.7 mg, 128 μmol) were dissolved in dimethylformamide (1 mL) and DIPEA (25 μL , 144 μmol) was added. The reaction was stirred at r.t. for 3 h, then dried *in vacuo*. The product was purified by preparative reverse-phase HPLC (water/acetonitrile with 0.1% formic acid, 15-40% acetonitrile) and compound **C2** (39.3 mg, 46.2 μmol , 92%) was obtained as a white solid. ^1H NMR (500 MHz, $\text{DMSO-}d_6$) δ 9.83 (s, 2H, NH), 7.54 – 7.47 (m, 4H, ArH), 7.17 – 7.11 (m, 4H, ArH), 7.04 – 6.96 (m, 4H, ArH), 6.96 – 6.89 (m, 4H, ArH), 5.72 (s, 2H, OCH_2O), 4.76 (d, $J = 7.7$ Hz, 2H, H-1), 3.68 (d, $J = 3.3$ Hz, 2H, H-4), 3.57 – 3.43 (m, 8H, H-2, H-5, H-6), 3.38 (dd, $J = 9.5, 3.3$ Hz, 2H, H-3), 2.83 (t, $J = 7.7$ Hz, 4H, $\text{CH}_2\text{CH}_2\text{CONH}$), 2.58 – 2.52 (m, 4H, $\text{CH}_2\text{CH}_2\text{CONH}$). ^{13}C NMR (126 MHz, $\text{DMSO-}d_6$) δ 170.11 (2C, C=O), 155.87 (2C, ArC), 152.03 (2C, ArC), 134.38 (2C, ArC), 133.97 (2C, ArC), 129.10 (4C, ArCH), 120.53 (4C, ArCH), 116.48 (4C, ArCH), 116.19 (4C, ArCH), 101.12 (2C, C-1), 90.78 (1C, OCH_2O), 75.47 (2C, C-5), 73.32 (2C,

Divalent ligand E2



1,3-bis(4-aminophenoxy)propane **E** (11.7 mg, 45.3 μmol), compound **2** (34.3 mg, 104 μmol) and HBTU (46.1 mg, 122 μmol) were dissolved in dimethylformamide (1 mL) and DIPEA (40 μL , 227 μmol) was added. The reaction was stirred at r.t. for 24 h, then dried *in vacuo*. The product was purified by preparative reverse-phase HPLC (water/acetonitrile with 0.1% formic acid, gradient of 20-45% acetonitrile) and compound **E2** (16.6 mg, 18.9 μmol , 42%) was obtained as a white solid.

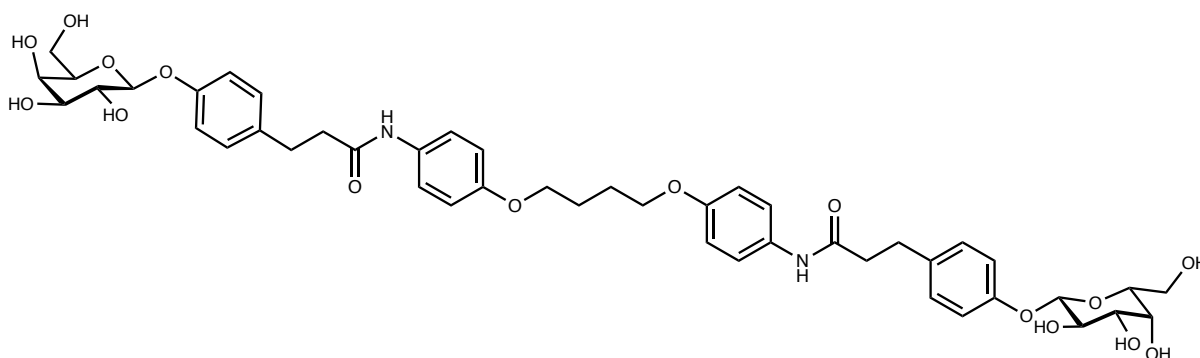
^1H NMR (500 MHz, $\text{DMSO-}d_6$) δ 9.74 (s, 2H, NH), 7.49 – 7.44 (m, 4H, ArH), 7.17 – 7.12 (m, 4H, ArH), 6.96 – 6.91 (m, 4H, ArH), 6.90 – 6.85 (m, 4H, ArH), 5.11 (d, $J = 5.1$ Hz, 2H, OH-2), 4.83 (d, $J = 5.6$ Hz, 2H, OH-3), 4.75 (d, $J = 7.7$ Hz, 2H, H-1), 4.63 (t, $J = 5.3$ Hz, 2H, OH-6), 4.47 (d, $J = 4.6$ Hz, 2H, OH-4), 4.07 (t, $J = 6.3$ Hz, 4H, $\text{CH}_2\text{CH}_2\text{CH}_2$), 3.68 (t, $J = 4.1$ Hz, 2H, H-4), 3.57 – 3.43 (m, 8H, H-2, H-5, H-6), 3.41 – 3.36 (m, 2H, H-3), 2.83 (t, $J = 7.7$ Hz, 4H, $\text{CH}_2\text{CH}_2\text{CONH}$), 2.56 – 2.51 (m, 4H, $\text{CH}_2\text{CH}_2\text{CONH}$), 2.16 – 2.08 (m, 2H, $\text{CH}_2\text{CH}_2\text{CH}_2$).

^{13}C NMR (126 MHz, $\text{DMSO-}d_6$) δ 169.91 (2C, C=O), 155.83 (2C, ArC), 154.25 (2C, ArC), 134.39 (2C, ArC), 132.52 (2C, ArC), 129.05 (4C, ArCH), 120.59 (4C, ArCH), 116.18 (4C, ArCH), 114.45 (4C, ArCH), 101.14 (2C, C-1), 75.44 (2C, C-5), 73.31 (2C, C-3), 70.29 (2C, C-2), 68.15 (2C, C-4), 64.34 (2C, $\text{CH}_2\text{CH}_2\text{CH}_2$), 60.39 (2C, C-6), 38.15 (2C, $\text{CH}_2\text{CH}_2\text{CONH}$), 30.14 (2C, $\text{CH}_2\text{CH}_2\text{CONH}$), 28.74 (1C, $\text{CH}_2\text{CH}_2\text{CH}_2$).

HPLC-MS: $[\text{C}_{45}\text{H}_{54}\text{N}_2\text{O}_{16} + \text{H}]^+$ calcd. 879.35, found 879.39.

HRMS: $[\text{C}_{45}\text{H}_{54}\text{N}_2\text{O}_{16} + \text{H}]^+$ calcd. 879.3546, found 879.3538.

Divalent ligand F2



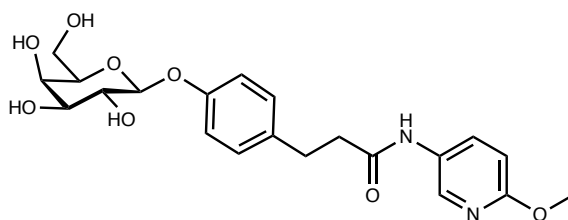
1,4-bis(4-aminophenoxy)butane **F** (36.5 mg, 134 μmol), compound **2** (104 mg, 317 μmol) and HBTU (142 mg, 375 μmol) were dissolved in dimethylformamide (3 mL) and DIPEA (60 μL , 344 μmol) was added. The reaction was stirred at r.t. for 2 h, then dried *in vacuo*. The product was purified by reverse-phase MPLC (water/acetonitrile with 0.1% formic acid, gradient of 20-35% acetonitrile) and compound **F2** (13.7 mg, 15.3 μmol , 11%) was obtained as a white solid. ^1H NMR (500 MHz, $\text{DMSO-}d_6$) δ 9.77 (s, 2H, NH), 7.49 – 7.43 (m, 4H, ArH), 7.18 – 7.11 (m, 4H, ArH), 6.95 – 6.89 (m, 4H, ArH), 6.89 – 6.82 (m, 4H, ArH), 5.16 (d, J = 5.2 Hz, 2H, OH-2), 4.91 (d, J = 5.5 Hz, 2H, OH-3), 4.76 (d, J = 7.7 Hz, 2H, H-1), 4.68 (t, J = 5.3 Hz, 2H, OH-6), 4.54 (d, J = 4.6 Hz, 2H, OH-4), 3.97 (d, J = 5.4 Hz, 4H, $\text{CH}_2\text{CH}_2\text{CH}_2\text{CH}_2$), 3.68 (t, J = 4.0 Hz, 2H, H-4), 3.57 – 3.42 (m, 8H, H-2, H-5, H-6), 3.41 – 3.37 (m, 2H, H-3), 2.83 (t, J = 7.7 Hz, 4H, $\text{CH}_2\text{CH}_2\text{CONH}$), 2.56 – 2.51 (m, 4H, $\text{CH}_2\text{CH}_2\text{CONH}$), 1.88 – 1.78 (m, 4H, $\text{CH}_2\text{CH}_2\text{CH}_2\text{CH}_2$).

^{13}C NMR (126 MHz, $\text{DMSO-}d_6$) δ 169.93 (2C, C=O), 155.86 (2C, ArC), 154.41 (2C, ArC), 134.40 (2C, ArC), 132.43 (2C, ArC), 129.10 (4C, ArCH), 120.60 (4C, ArCH), 116.18 (4C, ArCH), 114.43 (4C, ArCH), 101.12 (2C, C-1), 75.47 (2C, C-5), 73.33 (2C, C-3), 70.31 (2C, C-2), 68.15 (2C, C-4), 67.24 (2C, $\text{CH}_2\text{CH}_2\text{CH}_2\text{CH}_2$), 60.40 (2C, C-6), 38.20 (2C, $\text{CH}_2\text{CH}_2\text{CONH}$), 30.19 (2C, $\text{CH}_2\text{CH}_2\text{CONH}$), 25.52 (2C, $\text{CH}_2\text{CH}_2\text{CH}_2\text{CH}_2$).

HPLC-MS: $[\text{C}_{46}\text{H}_{56}\text{N}_2\text{O}_{16} + \text{H}]^+$ calcd. 893.37, found 893.43.

HRMS: $[\text{C}_{46}\text{H}_{56}\text{N}_2\text{O}_{16} + \text{H}]^+$ calcd. 893.3736, found 893.3691.

Monovalent Ligand **G2**



5-amino-2-methoxypyridine **G** (7.4 mg, 59.6 μmol), compound **2** (15.0 mg, 45.7 μmol) and HBTU (23.0 mg, 60.6 μmol) were dissolved in dimethylformamide (1.5 mL) and DIPEA (20 μL , 118 μmol) was added. The reaction was stirred at r.t. overnight, then lyophilized. The product was purified by preparative reverse-phase HPLC (water/acetonitrile supplemented with 0.1% formic acid, gradient of 15-30% acetonitrile) and compound **G2** (15.0 mg, 34.5 μmol , 76%) was obtained as a white solid.

^1H NMR (500 MHz, $\text{DMSO-}d_6$) δ 9.94 (s, 1H, NH), 8.31 (dd, J = 2.7, 0.6 Hz, 1H, ArH), 7.87 (dd, J = 8.9, 2.7 Hz, 1H, ArH), 7.17 – 7.12 (m, 2H, ArH), 6.96 – 6.91 (m, 2H, ArH), 6.78 (d, J = 8.8 Hz, 1H, ArH), 5.15 (d, J = 5.2 Hz, 1H, OH-2), 4.88 (d, J = 5.6 Hz, 1H, OH-3), 4.76 (d, J

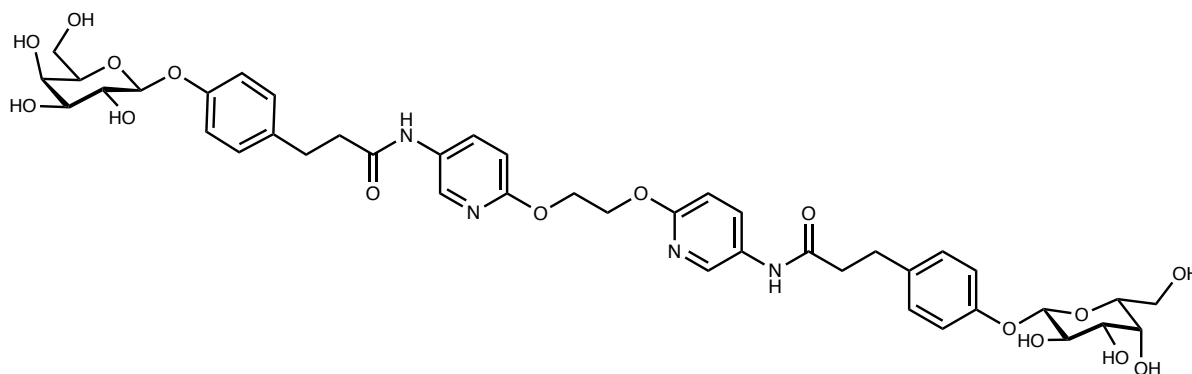
= 7.7 Hz, 1H, H-1), 4.65 (t, J = 5.3 Hz, 1H, OH-6), 4.51 (d, J = 4.6 Hz, 1H, OH-4), 3.80 (s, 3H, CH₃), 3.68 (t, J = 4.1 Hz, 1H, H-4), 3.57 – 3.43 (m, 4H, H-2, H-5, H-6), 3.41 – 3.37 (m, 1H, H-3), 2.84 (t, J = 7.7 Hz, 2H, CH₂CH₂CONH), 2.60 – 2.53 (m, 2H, CH₂CH₂CONH).

¹³C NMR (126 MHz, DMSO-*d*₆) δ 170.49 (1C, C=O), 159.50 (1C, ArC), 155.89 (1C, ArC), 137.47 (1C, ArCH), 134.26 (1C, ArC), 131.42 (1C, ArCH), 130.17 (1C, ArC), 129.12 (2C, ArCH), 116.20 (2C, ArCH), 110.13 (1C, ArCH), 101.10 (1C, C-1), 75.47 (1C, C-5), 73.33 (1C, C-3), 70.31 (1C, C-2), 68.17 (1C, C-4), 60.41 (1C, C-6), 53.17 (1C, CH₃), 38.01 (1C, CH₂CH₂CONH), 30.07 (1C, CH₂CH₂CONH).

HPLC-MS: [C₂₁H₂₆N₂O₈ + H]⁺ calcd. 435.18, found 435.17.

HRMS: [C₂₁H₂₆N₂O₈ + H]⁺ calcd. 435.1762, found 435.1756.

Divalent Ligand H2



1,2-bis((5-aminopyridin-2-yl)oxy)ethane **H** (12.1 mg, 49.1 μ mol), compound **2** (46.4 mg, 141 μ mol) and HBTU (60.2 mg, 159 μ mol) were dissolved in dimethylformamide (1.5 mL) and DIPEA (50 μ L, 287 μ mol) was added. The reaction was stirred at r.t. overnight, then lyophilized. The product was purified by preparative reverse-phase HPLC (water/acetonitrile supplemented with 0.1% formic acid, gradient of 15-30% acetonitrile) and compound **H2** (19.6 mg, 22.6 μ mol, 46%) was obtained as a pale-yellow solid.

¹H NMR (500 MHz, DMSO-*d*₆) δ 9.93 (s, 2H, NH), 8.32 (d, J = 2.6 Hz, 2H, ArH), 7.88 (dd, J = 8.9, 2.7 Hz, 2H, ArH), 7.18 – 7.12 (m, 4H, ArH), 6.97 – 6.91 (m, 4H, ArH), 6.81 (d, J = 8.9 Hz, 2H, ArH), 4.76 (d, J = 7.7 Hz, 2H, H-1), 4.51 (s, 4H, CH₂), 3.68 (d, J = 3.3 Hz, 2H, H-4), 3.57 – 3.44 (m, 8H, H-2, H-5, H-6), 3.38 (dd, J = 9.5, 3.3 Hz, 2H, H-3), 2.85 (t, J = 7.7 Hz, 4H, CH₂CH₂CONH), 2.57 (t, J = 7.7 Hz, 4H, CH₂CH₂CONH).

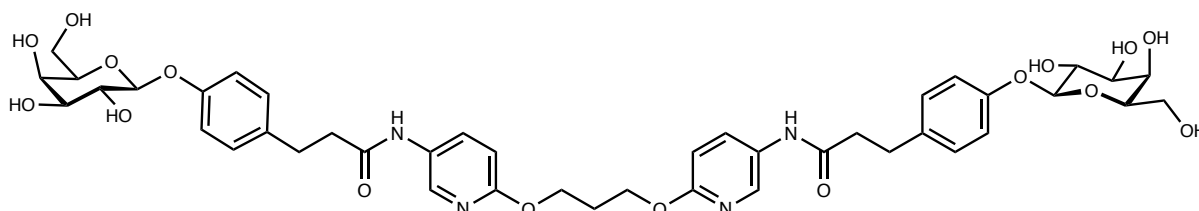
¹³C NMR (126 MHz, DMSO-*d*₆) δ 170.47 (2C, C=O), 158.88 (2C, ArC), 155.86 (2C, ArC), 137.33 (2C, ArCH), 134.24 (2C, ArC), 131.48 (2C, ArCH), 130.30 (2C, ArC), 129.06 (4C, ArCH), 116.20 (4C, ArCH), 110.35 (2C, ArCH), 101.12 (2C, C-1), 75.45 (2C, C-5), 73.31 (2C,

C-3), 70.30 (2C, C-2), 68.16 (2C, C-4), 64.05 (2C, CH₂), 60.40 (2C, C-6), 37.98 (2C, CH₂CH₂CONH), 30.03 (2C, CH₂CH₂CONH).

HPLC-MS: [C₄₂H₅₀N₄O₁₆ + H]⁺ calcd. 867.33, found 867.35.

HRMS: [C₄₂H₅₀N₄O₁₆ + H]⁺ calcd. 867.3295, found 867.3296.

Divalent Ligand **12**



1,3-bis((5-aminopyridin-2-yl)oxy)propane **1** (14.7 mg, 56.5 μmol), compound **2** (40.7 mg, 124 μmol) and HBTU (49.8 mg, 131 μmol) were dissolved in dimethylformamide (1.5 mL) and DIPEA (50 μL, 287 μmol) was added. The reaction was stirred at r.t. overnight, then lyophilized. The product was purified by preparative reverse-phase HPLC (water/acetonitrile supplemented with 0.1% formic acid, gradient of 15-40% acetonitrile) and compound **12** (20.2 mg, 22.9 μmol, 41%) was obtained as a white solid.

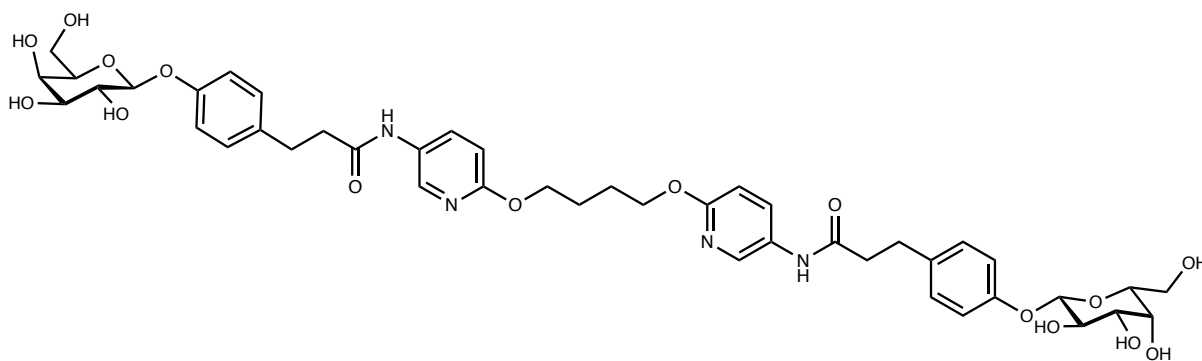
¹H NMR (500 MHz, DMSO-*d*₆) δ 9.91 (s, 2H, NH), 8.30 (d, *J* = 2.7 Hz, 2H, ArH), 7.86 (dd, *J* = 8.9, 2.7 Hz, 2H, ArH), 7.15 (d, *J* = 8.3 Hz, 4H, ArH), 6.99 – 6.89 (m, 4H, ArH), 6.78 (d, *J* = 8.9 Hz, 2H, ArH), 5.12 (d, *J* = 5.2 Hz, 2H, OH-2), 4.84 (d, *J* = 5.6 Hz, 2H, OH-3), 4.76 (d, *J* = 7.7 Hz, 2H, H-1), 4.63 (t, *J* = 5.2 Hz, 2H, OH-6), 4.48 (d, *J* = 4.6 Hz, 2H, OH-4), 4.33 (t, *J* = 6.3 Hz, 4H, CH₂CH₂CH₂), 3.68 (t, *J* = 4.0 Hz, 2H, H-4), 3.60 – 3.43 (m, 8H, H-2, H-5, H-6), 3.41 – 3.37 (m, 2H, H-3), 2.84 (t, *J* = 7.6 Hz, 4H, CH₂CH₂CONH), 2.57 (t, *J* = 7.7 Hz, 4H, CH₂CH₂CONH), 2.12 (p, *J* = 6.3 Hz, 2H, CH₂CH₂CH₂).

¹³C NMR (126 MHz, DMSO-*d*₆) δ 170.45 (2C, C=O), 159.14 (2C, ArC), 155.87 (2C, ArC), 137.48 (2C, ArCH), 134.25 (2C, ArC), 131.40 (2C, ArCH), 130.12 (2C, ArC), 129.07 (4C, ArCH), 116.20 (4C, ArCH), 110.23 (2C, ArCH), 101.13 (2C, C-1), 75.45 (2C, C-5), 73.32 (2C, C-3), 70.30 (2C, C-2), 68.15 (2C, C-4), 62.49 (2C, CH₂CH₂CH₂), 60.40 (2C, C-6), 37.97 (2C, CH₂CH₂CONH), 30.05 (2C, CH₂CH₂CONH), 28.35 (1C, CH₂CH₂CH₂).

HPLC-MS: [C₄₃H₅₂N₄O₁₆ + H]⁺ calcd. 881.35, found 881.33.

HRMS: [C₄₃H₅₂N₄O₁₆ + H]⁺ calcd. 881.3451, found 881.3446.

Divalent Ligand J2



1,4-bis((5-aminopyridin-2-yl)oxy)butane **J** (10.5 mg, 38.3 μmol), compound **2** (46.5 mg, 142 μmol) and HBTU (45.5 mg, 120 μmol) were dissolved in dimethylformamide (1.5 mL) and DIPEA (40 μL , 230 μmol) was added. The reaction was stirred at r.t. overnight, then lyophilized. The product was purified by preparative reverse-phase HPLC (water/acetonitrile supplemented with 0.1% formic acid, gradient of 15–45% acetonitrile) and compound **J2** (16.2 mg, 18.1 μmol , 47%) was obtained as a white solid.

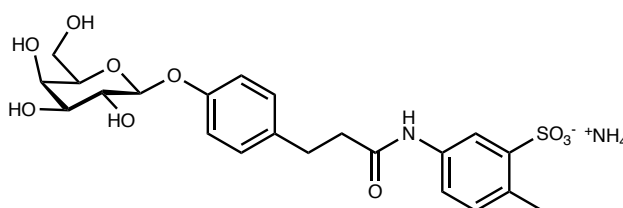
^1H NMR (500 MHz, $\text{DMSO-}d_6$) δ 9.90 (s, 2H, NH), 8.29 (d, $J = 2.7$ Hz, 2H, ArH), 7.86 (dd, $J = 8.9, 2.7$ Hz, 2H, ArH), 7.17 – 7.12 (m, 4H, ArH), 6.96 – 6.91 (m, 4H, ArH), 6.76 (d, $J = 8.8$ Hz, 2H, ArH), 5.11 (d, $J = 5.1$ Hz, 2H, OH-2), 4.83 (d, $J = 5.6$ Hz, 2H, OH-3), 4.76 (d, $J = 7.7$ Hz, 2H, H-1), 4.63 (t, $J = 5.3$ Hz, 2H, OH-6), 4.47 (d, $J = 4.6$ Hz, 2H, OH-4), 4.24 (q, $J = 4.4, 3.0$ Hz, 4H, $\text{CH}_2\text{CH}_2\text{CH}_2\text{CH}_2$), 3.68 (t, $J = 4.1$ Hz, 2H, H-4), 3.57 – 3.43 (m, 8H, H-2, H-5, H-6), 3.42 – 3.36 (m, 2H, H-3), 2.84 (t, $J = 7.7$ Hz, 4H, $\text{CH}_2\text{CH}_2\text{CONH}$), 2.60 – 2.54 (m, 4H, $\text{CH}_2\text{CH}_2\text{CONH}$), 1.84 – 1.77 (m, 4H, $\text{CH}_2\text{CH}_2\text{CH}_2\text{CH}_2$).

^{13}C NMR (126 MHz, $\text{DMSO-}d_6$) δ 170.43 (2C, C=O), 159.28 (2C, ArC), 155.86 (2C, ArC), 137.51 (2C, ArCH), 134.25 (2C, ArC), 131.39 (2C, ArCH), 130.01 (2C, ArC), 129.06 (4C, ArCH), 116.19 (4C, ArCH), 110.17 (2C, ArCH), 101.12 (2C, C-1), 75.45 (2C, C-5), 73.32 (2C, C-3), 70.30 (2C, C-2), 68.15 (2C, C-4), 65.14 (2C, $\text{CH}_2\text{CH}_2\text{CH}_2\text{CH}_2$), 60.40 (2C, C-6), 37.97 (2C, $\text{CH}_2\text{CH}_2\text{CONH}$), 30.04 (2C, $\text{CH}_2\text{CH}_2\text{CONH}$), 25.38 (2C, $\text{CH}_2\text{CH}_2\text{CH}_2\text{CH}_2$).

HPLC-MS: $[\text{C}_{44}\text{H}_{54}\text{N}_4\text{O}_{16} + \text{H}]^+$ calcd. 895.36, found 895.36.

HRMS: $[\text{C}_{44}\text{H}_{54}\text{N}_4\text{O}_{16} + \text{H}]^+$ calcd. 895.3608, found 895.3601.

Monovalent ligand K2



5-Amino-2-methylbenzenesulfonic acid **K** (11.0 mg, 58.8 μmol), galactoside **2** (15.0 mg, 45.7 μmol) and PyBOP (31.0 mg, 59.6 μmol) were dissolved in dimethylformamide (1.5 mL) and N-methylmorpholine (20 μL , 178 μmol) was added. The reaction was stirred at r.t. overnight, then lyophilized. The product was purified by preparative reverse-phase HPLC (5 mM ammonium bicarbonate at pH 7/acetonitrile, gradient of 5-20% acetonitrile) and compound **K2** (16.0 mg, 32.2 μmol , 70%) was obtained as a white solid.

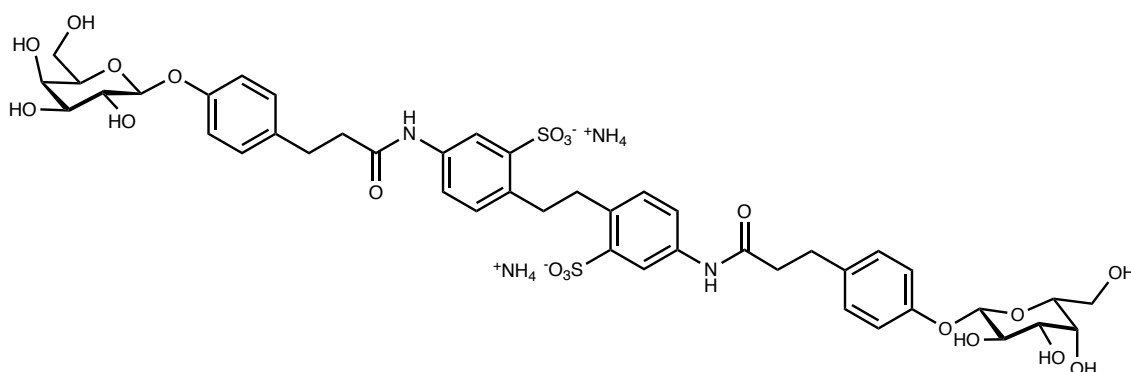
^1H NMR (500 MHz, $\text{DMSO-}d_6$) δ 9.88 (s, 1H, NH), 7.78 (d, $J = 2.4$ Hz, 1H, ArH), 7.63 (dd, $J = 8.2, 2.4$ Hz, 1H, ArH), 7.14 (d, $J = 8.6$ Hz, 2H, ArH), 7.09 (s, 3H, ammonia), 7.02 (d, $J = 8.2$ Hz, 1H, ArH), 6.95 – 6.91 (m, 2H, ArH), 5.13 (d, $J = 5.2$ Hz, 1H, OH-2), 4.86 (d, $J = 5.6$ Hz, 1H, OH-3), 4.76 (d, $J = 7.7$ Hz, 1H, H-1), 4.66 (t, $J = 5.2$ Hz, 1H, OH-6), 4.49 (d, $J = 4.7$ Hz, 1H, OH-4), 3.67 (t, $J = 4.0$ Hz, 1H, H-4), 3.57 – 3.43 (m, 4H, H-2, H-5, H-6), 3.40 – 3.37 (m, 1H, H-3), 2.83 (t, $J = 7.7$ Hz, 2H, $\text{CH}_2\text{CH}_2\text{CONH}$), 2.58 – 2.52 (m, 2H, $\text{CH}_2\text{CH}_2\text{CONH}$), 2.43 (s, 3H, CH_3).

^{13}C NMR (126 MHz, DMSO) δ 170.28 (1C, C=O), 155.87 (1C, ArC), 146.50 (1C, ArC), 136.15 (1C, ArC), 134.41 (1C, ArC), 130.78 (1C, ArCH), 129.90 (1C, ArC), 129.10 (2C, ArCH), 119.11 (1C, ArCH), 117.80 (1C, ArCH), 116.21 (2C, ArCH), 101.15 (1C, C-1), 75.45 (1C, C-5), 73.31 (1C, C-3), 70.33 (1C, C-2), 68.19 (1C, C-4), 60.40 (1C, C-6), 38.29 (1C, $\text{CH}_2\text{CH}_2\text{CONH}$), 30.20 (1C, $\text{CH}_2\text{CH}_2\text{CONH}$), 19.53 (1C, CH_3).

HPLC-MS: $[\text{C}_{22}\text{H}_{30}\text{N}_2\text{O}_{10}\text{S} - \text{H}]^-$ calcd. 496.13, found 496.12.

HRMS: $[\text{C}_{22}\text{H}_{30}\text{N}_2\text{O}_{10}\text{S} - \text{H}]^-$ calcd. 496.1283, found 496.1289.

Divalent ligand L2



Sulfonated linker **L** (21.6 mg, 58.0 μmol), galactoside **2** (59.0 mg, 198 μmol) and PyBOP (74.3 mg, 143 μmol) were suspended in dimethylformamide (1.5 mL) and N-methylmorpholine (50 μL , 455 μmol) was added. The reaction was stirred at r.t. overnight, then lyophilized. The product was purified by preparative reverse-phase HPLC (5 mM ammonium bicarbonate at pH

7/acetonitrile, gradient of 5-20% acetonitrile) and compound **L2** (30.4 mg, 29.6 μmol , 51%) was obtained as a white solid.

^1H NMR (500 MHz, $\text{DMSO-}d_6$) δ 9.88 (s, 2H, NH), 7.85 (d, $J = 2.3$ Hz, 2H, ArH), 7.59 (dd, $J = 8.2, 2.3$ Hz, 2H, ArH), 7.19 (d, $J = 8.3$ Hz, 2H, ArH), 7.17 – 7.13 (m, 4H, ArH), 6.98 – 6.89 (m, 4H, ArH), 4.77 (d, $J = 7.7$ Hz, 2H, H-1), 3.67 (d, $J = 3.3$ Hz, 2H, H-4), 3.57 – 3.44 (m, 8H, H-2, H-5, H-6), 3.38 (dd, $J = 9.8, 3.6$ Hz, 2H, H-3), 3.18 (s, 4H, $\text{ArCH}_2\text{CH}_2\text{Ar}$), 2.84 (t, $J = 7.7$ Hz, 4H, $\text{CH}_2\text{CH}_2\text{CONH}$), 2.55 (t, $J = 7.6$ Hz, 4H, $\text{CH}_2\text{CH}_2\text{CONH}$).

^{13}C NMR (126 MHz, $\text{DMSO-}d_6$) δ 170.26 (2C, C=O), 155.88 (2C, ArC), 146.15 (2C, ArC), 135.89 (2C, ArC), 135.24 (2C, ArC), 134.48 (2C, ArC), 130.49 (2C, ArCH), 129.13 (4C, ArCH), 119.37 (2C, ArCH), 117.98 (2C, ArCH), 116.24 (4C, ArCH), 101.17 (2C, C-1), 75.46 (2C, C-5), 73.32 (2C, C-3), 70.36 (2C, C-2), 68.21 (2C, C-4), 60.41 (2C, C-6), 38.34 (2C, $\text{CH}_2\text{CH}_2\text{CONH}$), 33.77 (2C, $\text{ArCH}_2\text{CH}_2\text{Ar}$), 30.24 (2C, $\text{CH}_2\text{CH}_2\text{CONH}$).

HPLC-MS: $[\text{C}_{44}\text{H}_{52}\text{N}_2\text{O}_{20}\text{S}_2 - 2\text{H}]^{2-}$ calcd. 495.12, found 495.11.

HRMS: $[\text{C}_{44}\text{H}_{52}\text{N}_2\text{O}_{20}\text{S}_2 - \text{H}]^-$ calcd. 991.2482, found 991.2531.

Synthesis of compound **14** was described by Zahorska *et. al.*.¹¹¹

Biophysical evaluation

Expression and purification of LecA as well as competitive binding by fluorescence polarization was performed as described by Joachim *et al.*⁶¹ The assay was performed in TBS/Ca²⁺ buffer (20 mM Tris, 137 mM NaCl, 2.6 mM KCl at pH 7.4 supplemented with 1 mM CaCl₂) in presence of 25% DMSO. Averages and standard deviations were calculated from at least three independent experiments.

Isothermal titration calorimetry was performed on an iTC200 (Malvern Panalytical) and the data were analyzed using Microcal Origin software (Malvern Panalytical). LecA (50 - 180 μ M) in the cell was titrated with ligand (0.25 -1.5 mM) in TBS/Ca²⁺ buffer at 25 °C. Steep titration slopes achieved with the divalent ligands were the result of high amount of protein present and the high binding affinity of the ligand (high 'value of c').¹³⁸ However, LecA protein concentration lower than 50 μ M resulted in insufficient signal as a consequence of the low heat released upon binding.

Surface plasmon resonance experiments were performed on a BIACORE X100 instrument (GE Healthcare) at 25 °C as described by Zahorska *et. al.*¹¹¹ Averages and standard deviations were calculated from three independent experiments.

Kinetic solubility was determined on the analytical HPLC-MS using Compass QuantAnalysis quantification software (Bruker). Samples were prepared from DMSO stock solutions by dilution with TBS/Ca²⁺ buffer to 100 μ M with 1% DMSO present. Samples were incubated on a shaker for 1 h at r.t., centrifuged (15000 rpm, 10 min) and supernatants were analyzed by HPLC-MS and fitted to the individual calibration curves.

ADME assays

Every experiment was repeated independently at least three times.

Plasma stability assay

Each compound dissolved in DMSO was added to mouse plasma (pH 7.4, 37°C) or to human plasma (pH 7.4, 37°C) to yield a final concentration of 1 μ M. In addition, procaine and procainamide (dissolved in DMSO) were added to mouse plasma or to human plasma (pH 7.4, 37°C) to yield a final concentration of 1 μ M. Procaine served as positive control as it is unstable in mouse plasma. Procainamide served as negative control as it is stable in mouse plasma. The samples were incubated for 0 min, 15 min, 30 min, 60 min, 90 min, 120 min and 240 min at 37°C. At each time point, 10 μ l of the respective sample was extracted with 90 μ l acetonitrile and 1 μ l of caffeine as internal standard for 5 min at 2000 rpm on a MixMate® vortex mixer (Eppendorf). Acetonitrile and caffeine were dispensed using a Mantis Formulatrix®. Then

samples were centrifuged for 20 min at 2.270 x g at 4°C and the supernatants were transferred to 96well Greiner V-bottom plates. Peak areas of each compound and of the internal standard were analyzed using the MultiQuant 3.0 software (AB Sciex). Peak areas of the respective compound were normalized to the internal standard peak area and to the respective peak areas at time point 0 min: (C/D)/(A/B) with A: peak area of the compound at time point 0 min, B: peak area of the internal standard at time point 0 min, C: peak area of the compound at the respective time point, D: peak area of the internal standard at the respective time point.

In vitro metabolic stability assay

S9 liver microsomes (mouse and human, Thermo Fisher) were thawed slowly on ice. 20 mg/ml of microsomes, 2 µl of a 100 µM solution of every compound and 183 µl of 100 mM phosphate buffer were incubated 5 min at 37°C in a water bath. Reactions were initiated using 10 µl of 20 mM NADPH (Roth). Samples were incubated in three replicates at 37°C under gentle agitation at 150 rpm. At 0, 5, 15, 30, and 60 min, reactions were terminated by the addition of 180 µl acetonitrile using a Mantis Formulatrix® dispenser. Samples were vortexed for 5 min using an Eppendorf MixMate® vortex mixer and centrifuged at 2.270 x g for 20 min at 4°C. The supernatants were transferred to 96-well Greiner V-bottom plates, sealed and analyzed according to the section HPLC-MS analysis. Peak areas of the respective time point of the compounds were normalized to the peak area at time point 0 min. Then half-life was calculated using linear regression (Microsoft Excel®). Cl_{int} [µl/min/mg protein] was calculated using the following formula:

$$Cl_{int} = 0.693 / (0.005 \times t_{1/2})$$

Assessment of plasma protein binding

Plasma protein binding was assessed using the rapid equilibrium device (RED) system from ThermoFisher. Compounds were dissolved in DMSO. Naproxene served as control as it shows high plasma protein binding. Compounds were diluted in murine plasma (from CD-1 mice, pooled) or in human plasma (human donors, both genders, pooled) to a final concentration of 1 µM. Dialysis buffer and plasma samples were added to the respective chambers according to the manufacturer's protocol. The RED plate was sealed with a tape and incubated at 37°C for 2 hours at 800 rpm on an Eppendorf MixMate® vortex-mixer. Then samples were withdrawn from the respective chambers. To 25 µl of each dialysis sample, 25 µl of plasma and to 25 µl of plasma sample, 25 µl of dialysis buffer was added. Then 150 µl ice-cold extraction solvent (ACN/H₂O (90:10) containing 12.5 ng/ml caffeine as internal standard) was added. Samples were incubated for 30 min on ice. Then samples were centrifuged at 4°C at 2270 x g for 10 min.

Supernatants were transferred to Greiner V-bottom 96-well plates and sealed with a tape. The percentage of bound compound was calculated as follows:

$$(1) \% \text{ free} = (\text{concentration buffer chamber} / \text{concentration plasma chamber}) * 100$$

$$\% \text{ bound} = 100 \% - \% \text{ free}$$

HPLC-MS analysis

Samples were analyzed using an Agilent 1290 Infinity II HPLC system coupled to an AB Sciex QTrap 6500plus mass spectrometer. LC conditions were as follows: column: Agilent Zorbax Eclipse Plus C18, 50x2.1 mm, 1.8 μm ; temperature: 30°C; injection volume: 5 μl per sample; flow rate: 700 $\mu\text{l}/\text{min}$. Samples were run under acidic and buffered conditions. Solvents for acidic conditions: A1: water + 0.1 % formic acid; solvent B1: 95 % acetonitrile/5 % H_2O + 0.1 % formic acid; solvents for buffered conditions: A2: 95 % water + 5 % acetonitrile + 5 mM ammonium acetate + 40 μL acetic acid; B2: 95 % acetonitrile + 5 % water + 5 mM ammonium acetate + 40 μL acetic acid. The same gradient was applied for acidic and buffered conditions: 99 % A at 0 min, 99 % A until 1 min, 99 % - 0% A from 1 min to 4.0 min, 0 % A until 5.0 min. Mass transitions for controls and compounds are depicted in the following table.

	Q1 mass	Q3 mass	DP [volts]	CE [volts]	CXP [volts]
Caffeine	195.024	138.0	130.0	25.0	14.0
Caffeine	195.024	110.0	130.0	31.0	18.0
14	861.223	699.1	-125.0	-24.0	-39.0
14	861.223	417.0	-125.0	-54.0	-19.0
H2	865.252	541.1	-145.0	-48.0	-25.0
H2	865.252	703.2	-145.0	-30.0	-35.0
D2	863.289	539.0	-145.0	-50.0	-23.0
D2	863.289	701.1	-145.0	-30.0	-35.0
D1	859.229	697.1	-115.0	-24.0	-37.0
D1	859.220	415.0	-115.0	-54.0	-19.0
H1	861.239	699.1	-160.0	-26.0	-35.0
H1	861.239	537.1	-160.0	-40.0	-27.0
L2	511.394	255.1	-35.0	-14.0	-23.0
L2	511.304	283.1	-35.0	-20.0	-17.0
L2	495.068	333.0	-55.0	-40.0	-35.0
L2	495.068	413.9	-55.0	-30.0	-17.0

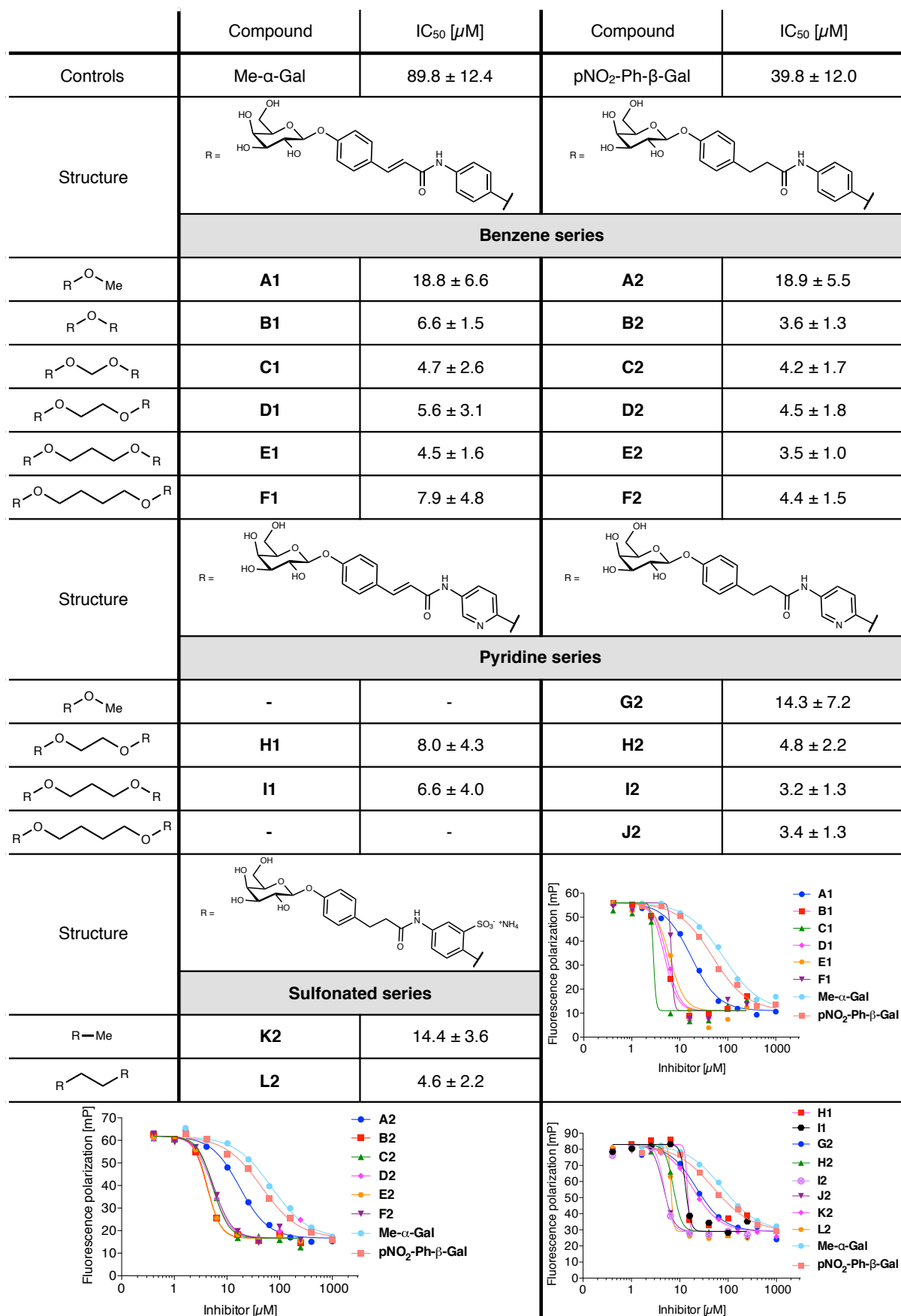


Figure S1: Evaluation of amide divalent LecA ligands in a competitive binding assay based on fluorescence polarization. Divalent ligands showed steep titration slopes indicating the lower assay limit was reached. One

representative experiment is shown for each series. Averages and standard deviations from at least three independent titrations of triplicates each.

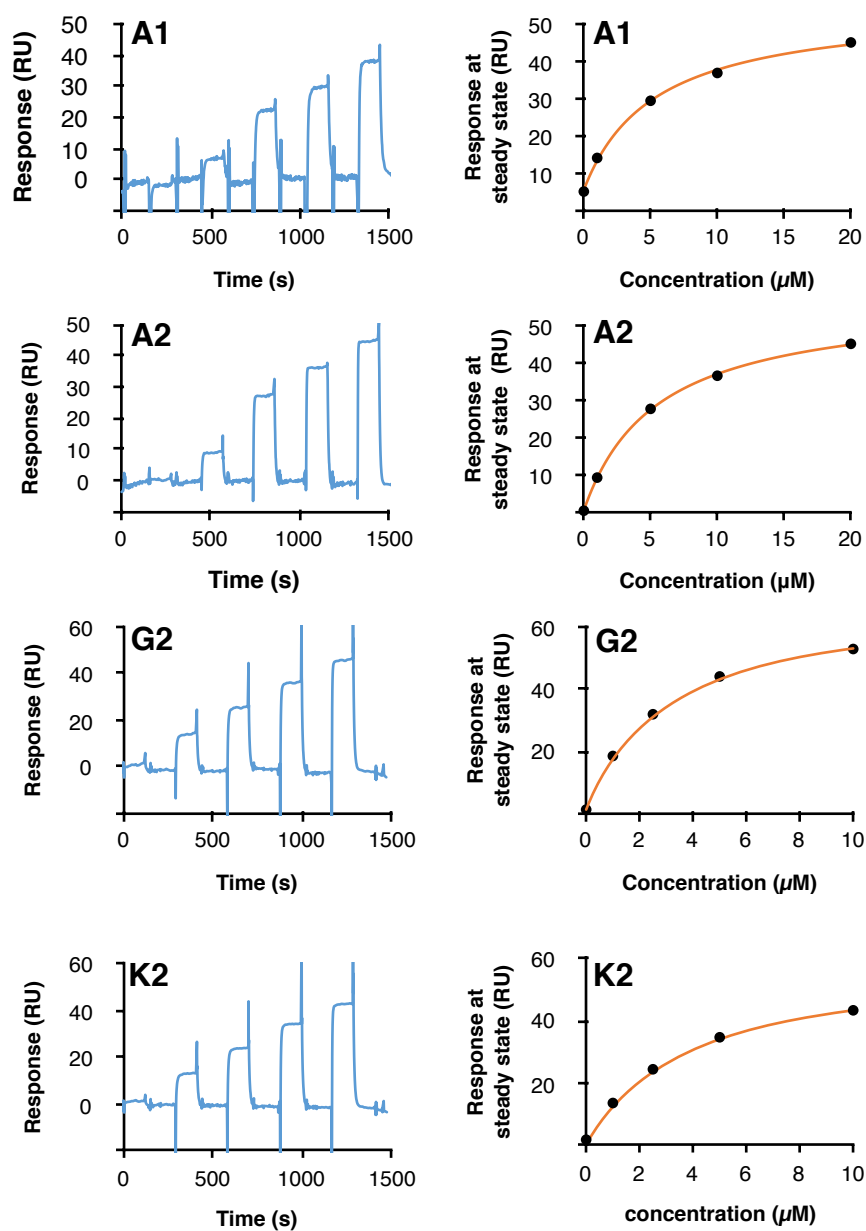


Figure S2: SPR sensograms (left panel) and analyses (right panel) of the monovalent LecA ligands.

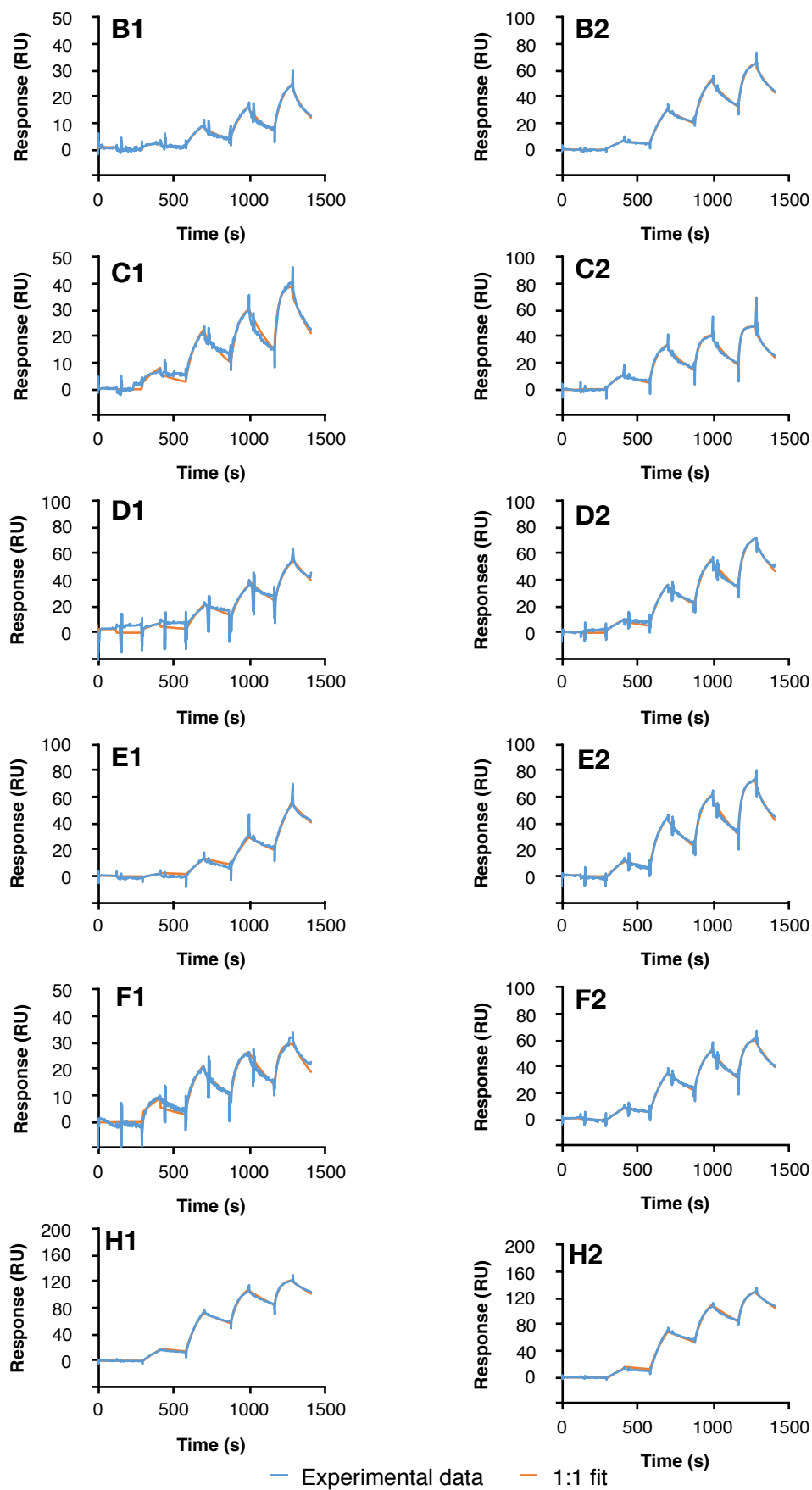


Figure S3: SPR of divalent LecA ligands. Sensorgrams obtained from SPR single-cycle kinetics experiments. Five different concentrations of each compound (0, 10, 50, 100, 200 nM) were sequentially injected to obtain the

experimental sensorgrams (blue lines), which were then fitted by a 1:1 model (orange) on BIACORE evaluation software.

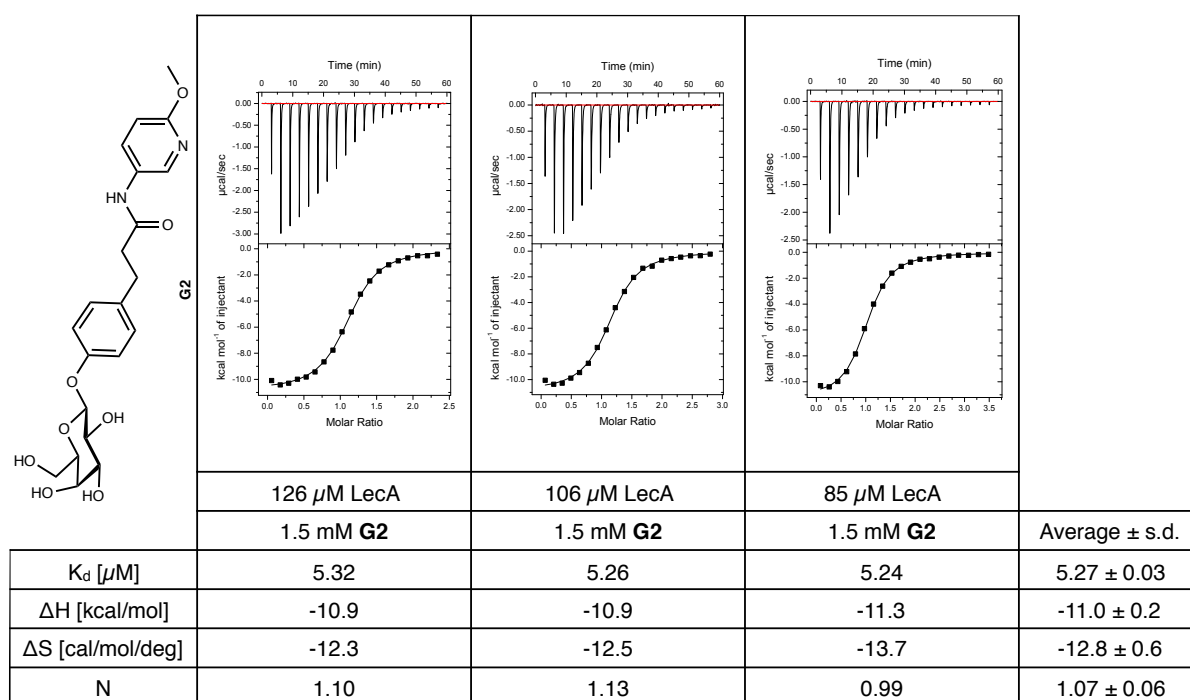


Figure S4: ITC measurements of monovalent ligand **G2** with LecA performed in TBS/ Ca^{2+} buffer at 25 °C.

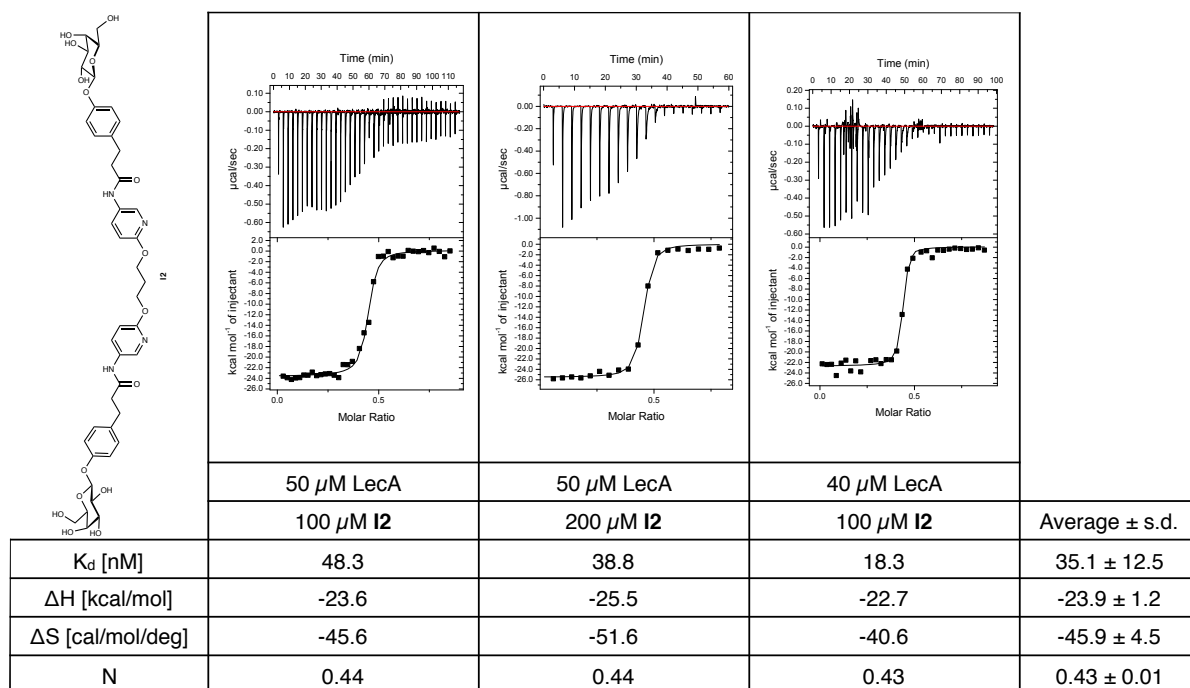


Figure S5: ITC measurements of divalent ligand **I2** with LecA performed in TBS/ Ca^{2+} buffer with 5% DMSO at 25 °C.

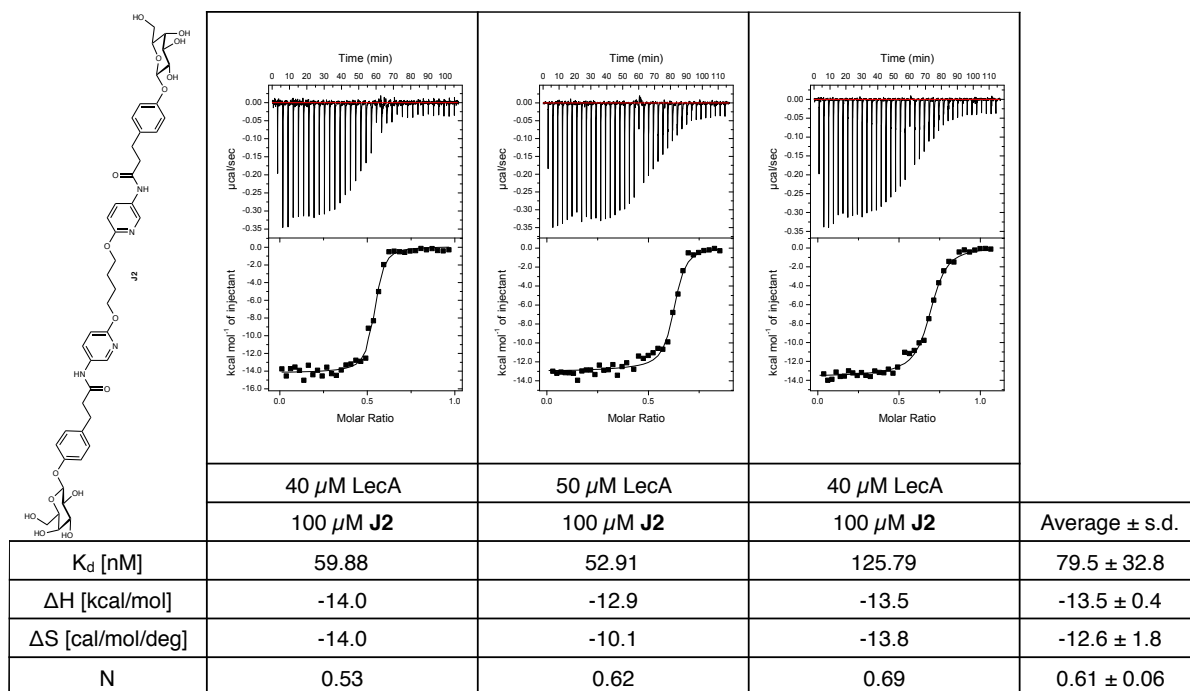


Figure S6: ITC measurements of divalent ligand **J2** with LecA performed in TBS/ Ca^{2+} buffer with 5% DMSO at 25 °C.

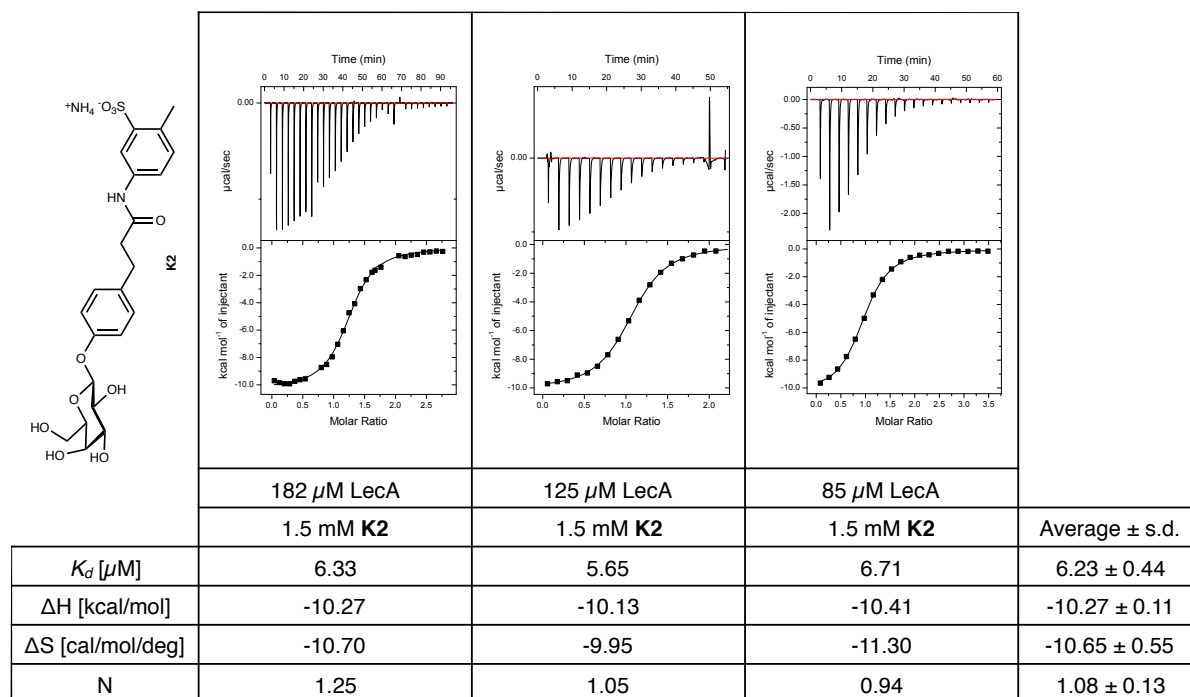


Figure S7: ITC measurements of monovalent ligand **K2** with LecA performed in TBS/ Ca^{2+} buffer at 25 °C.

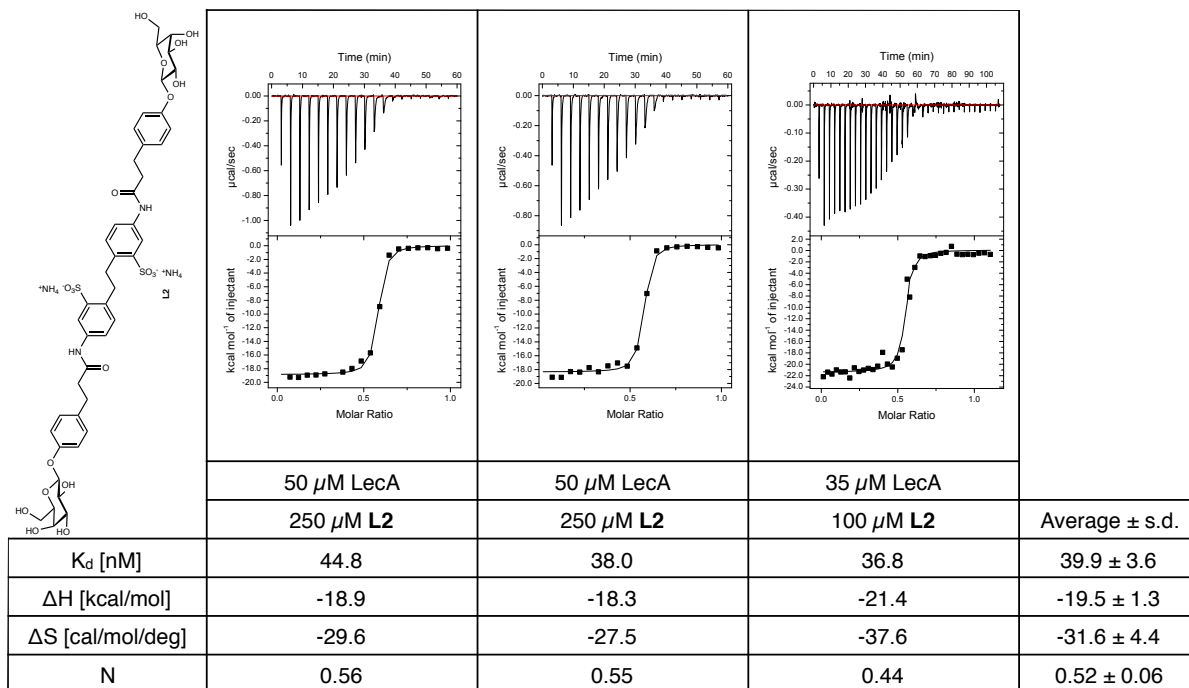
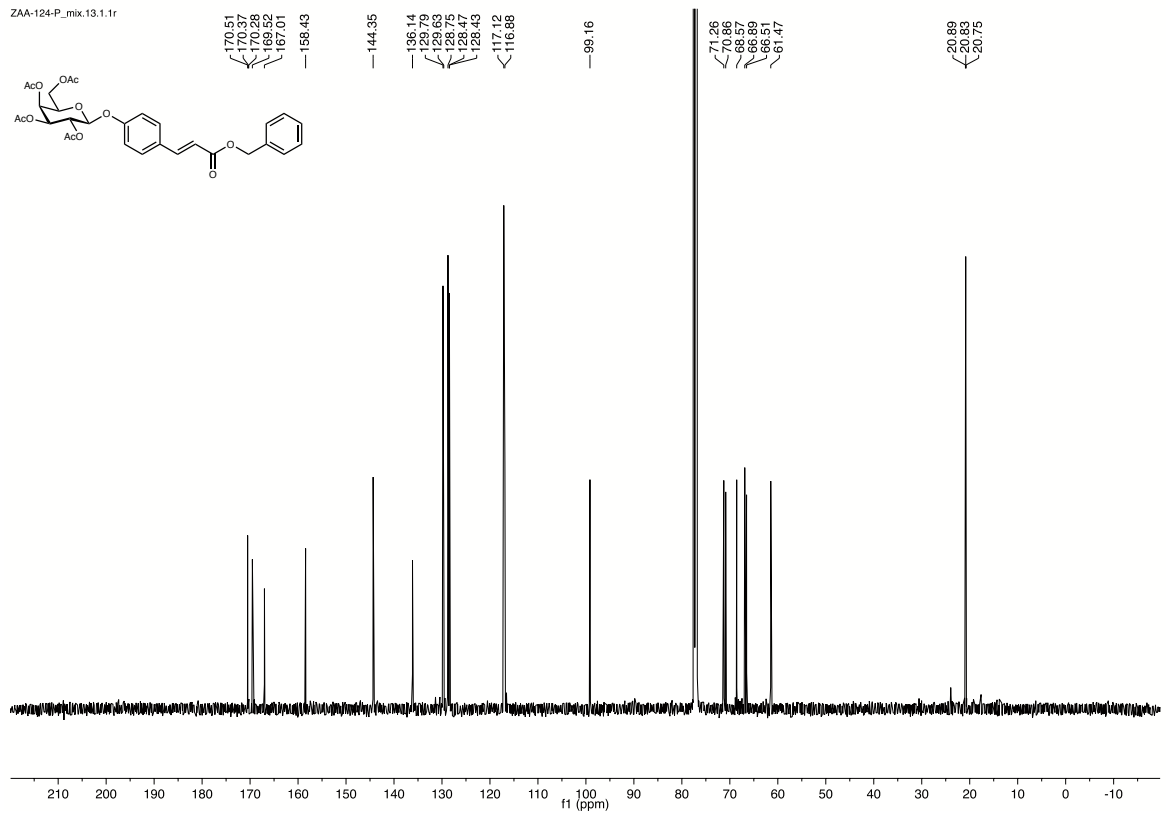
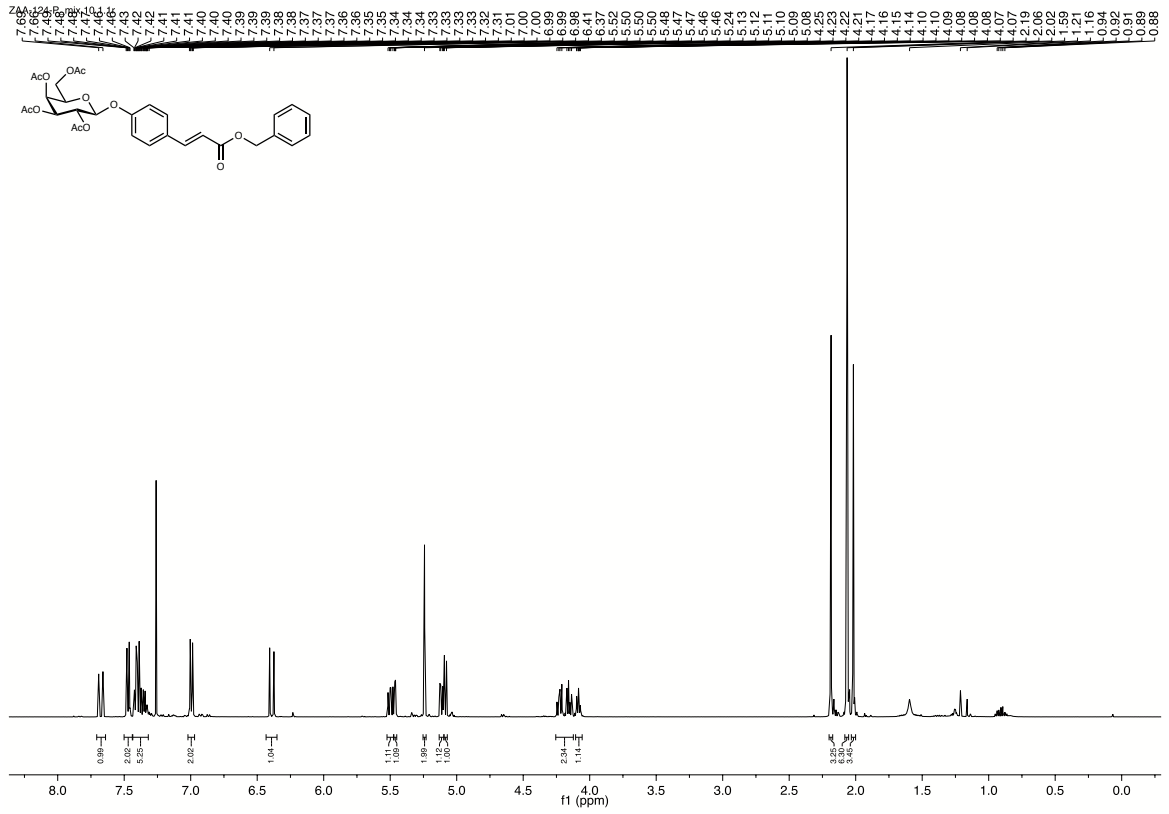
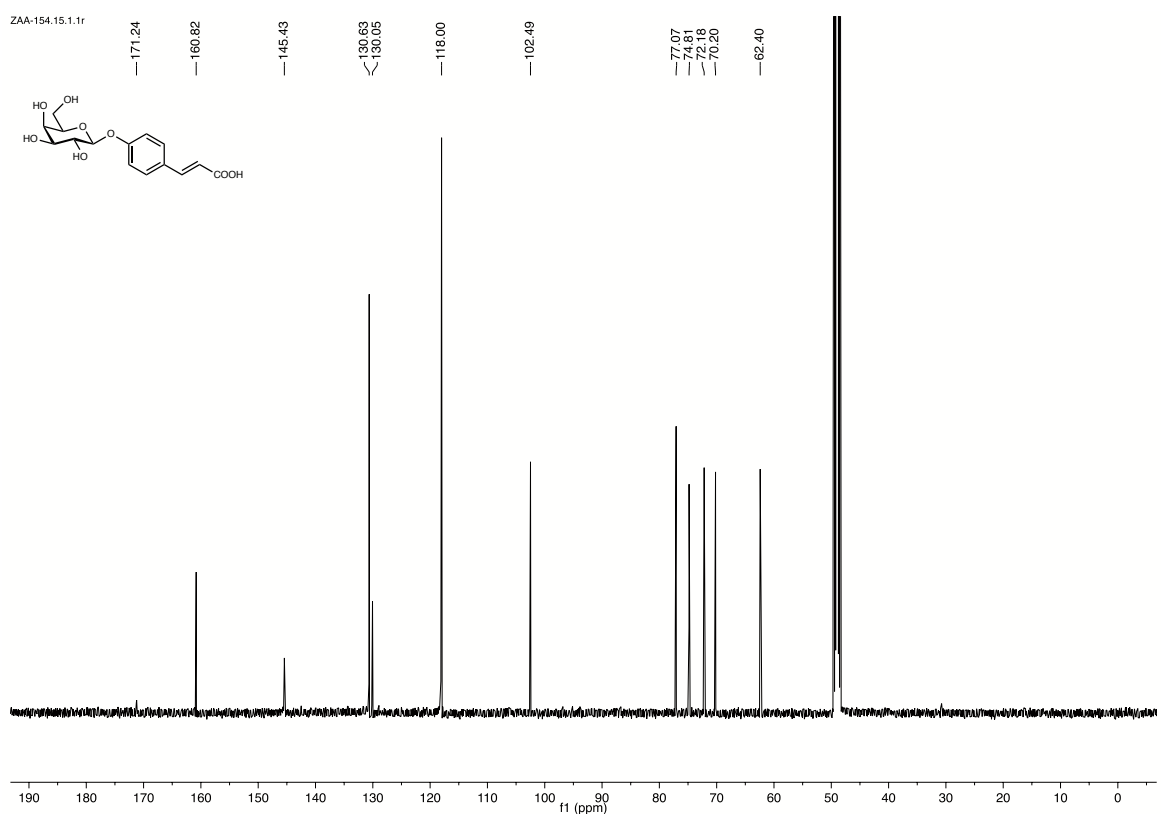
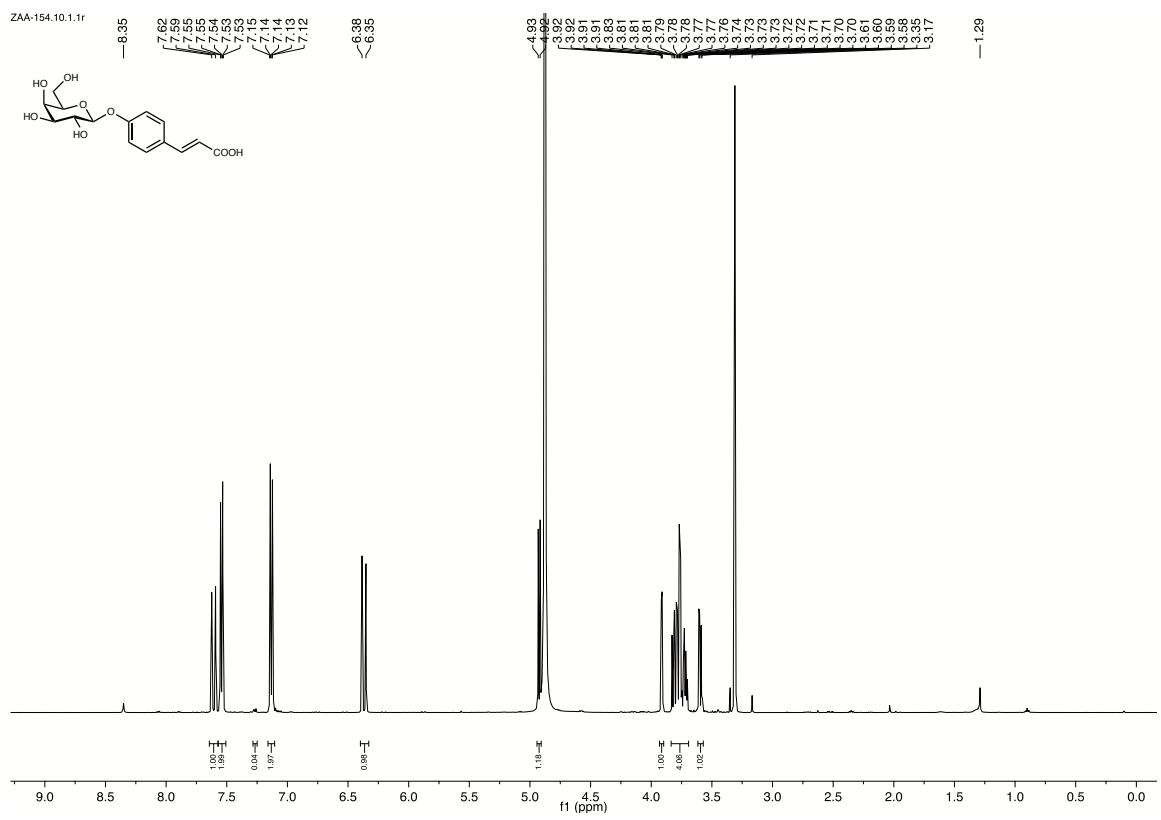


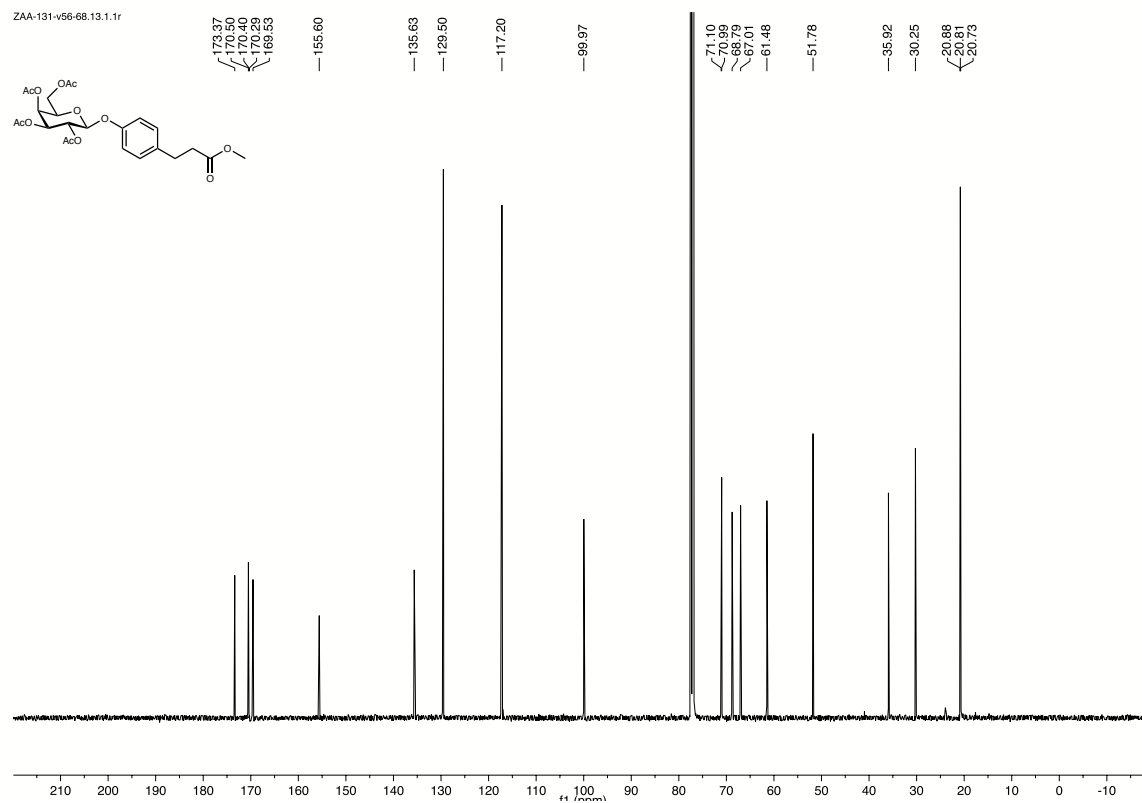
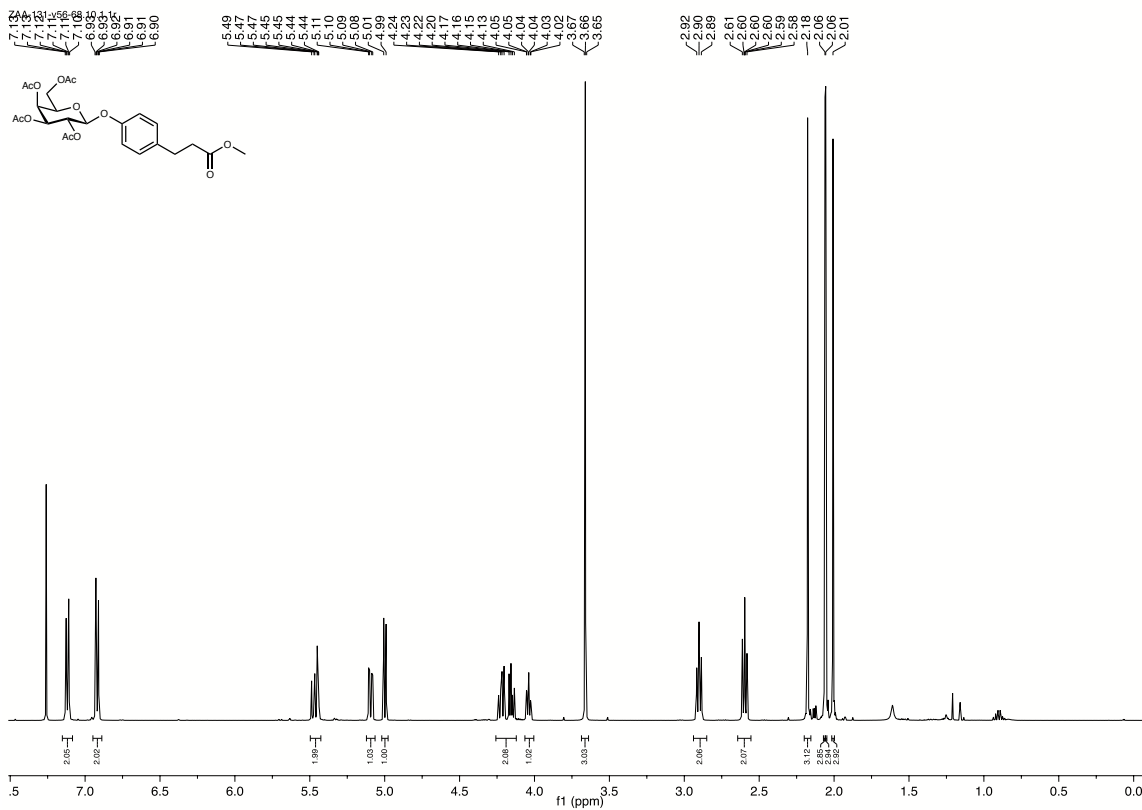
Figure S8: ITC measurements of L2 with LecA performed in TBS/Ca²⁺ buffer at 25 °C.



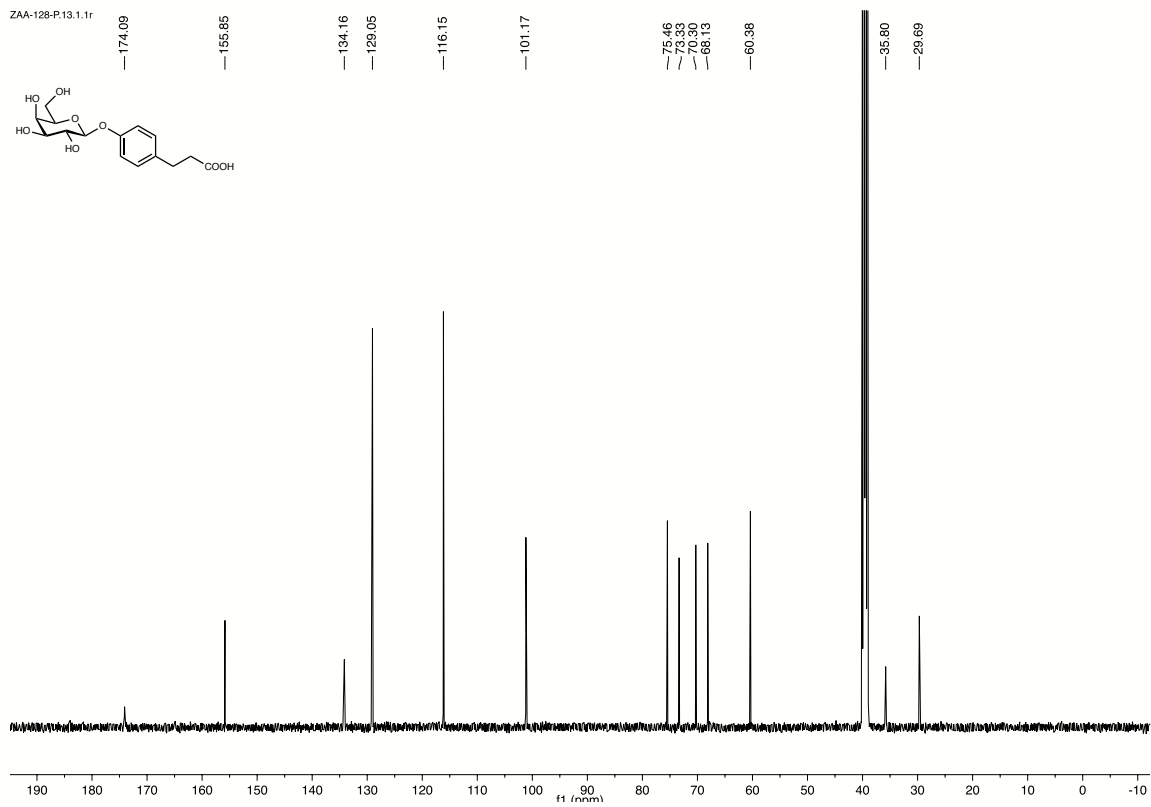
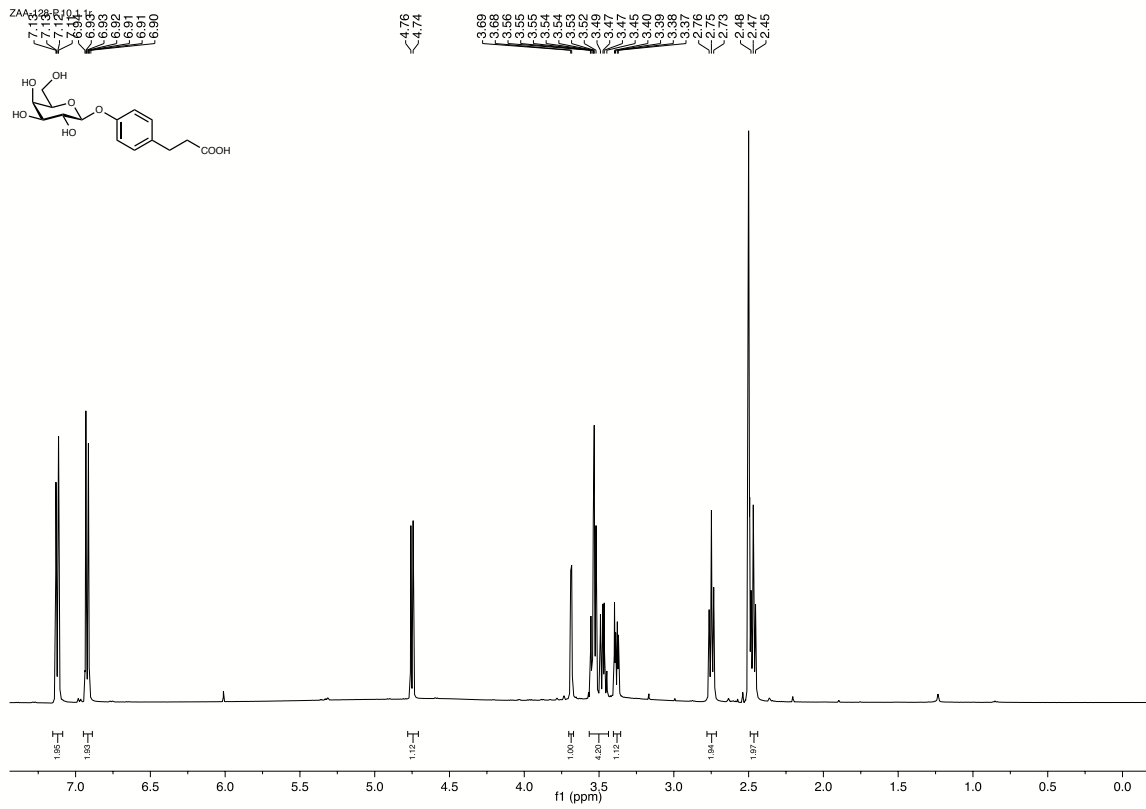
^1H and ^{13}C NMR of 4



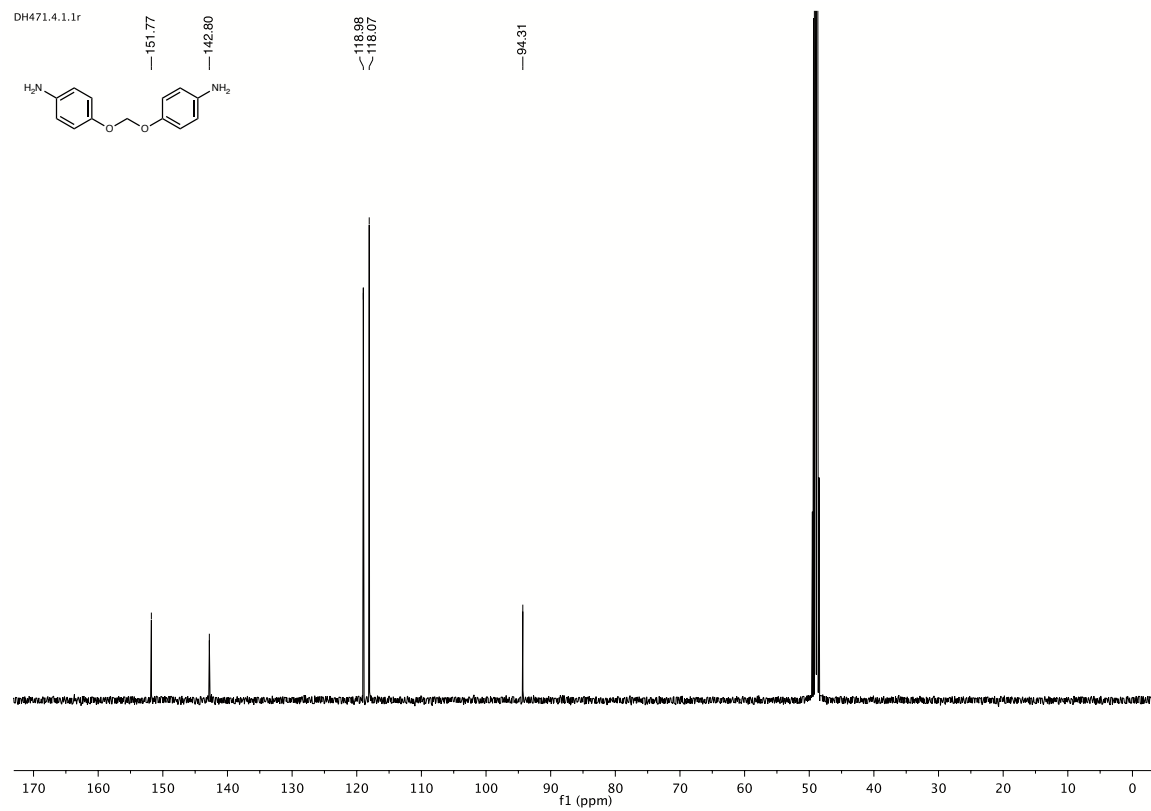
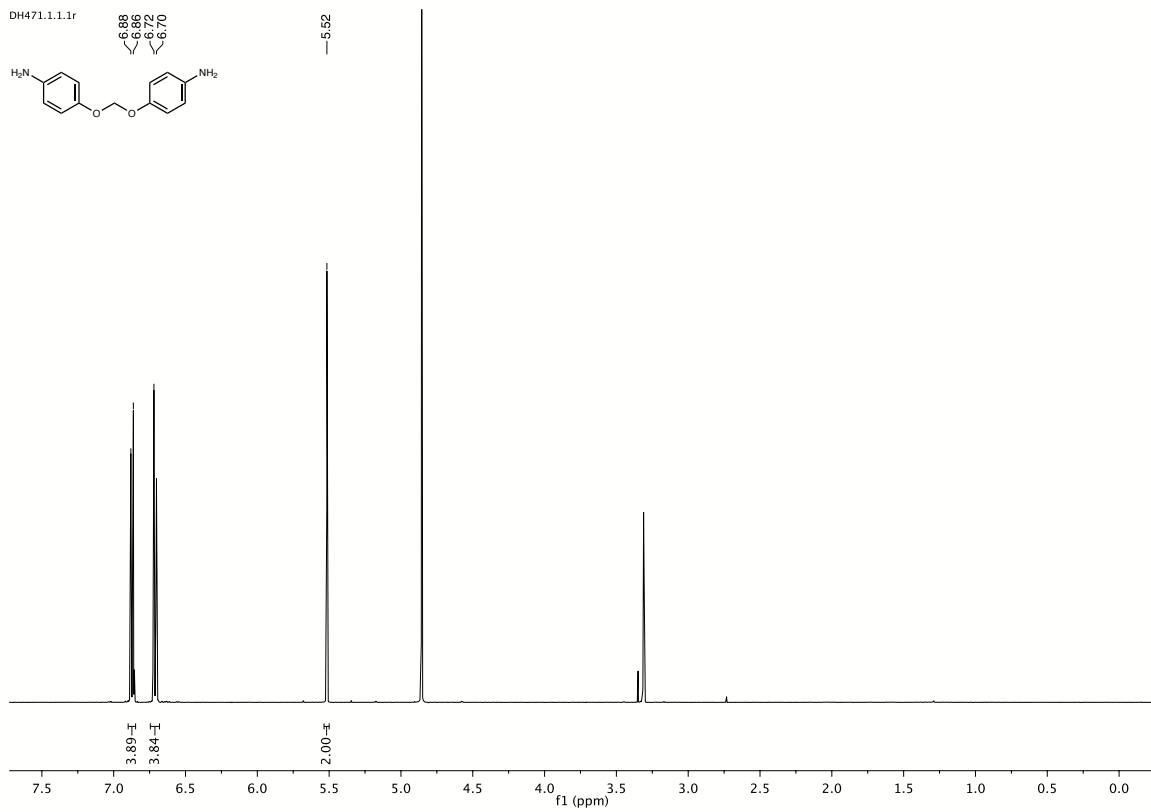
^1H and ^{13}C NMR of **1**



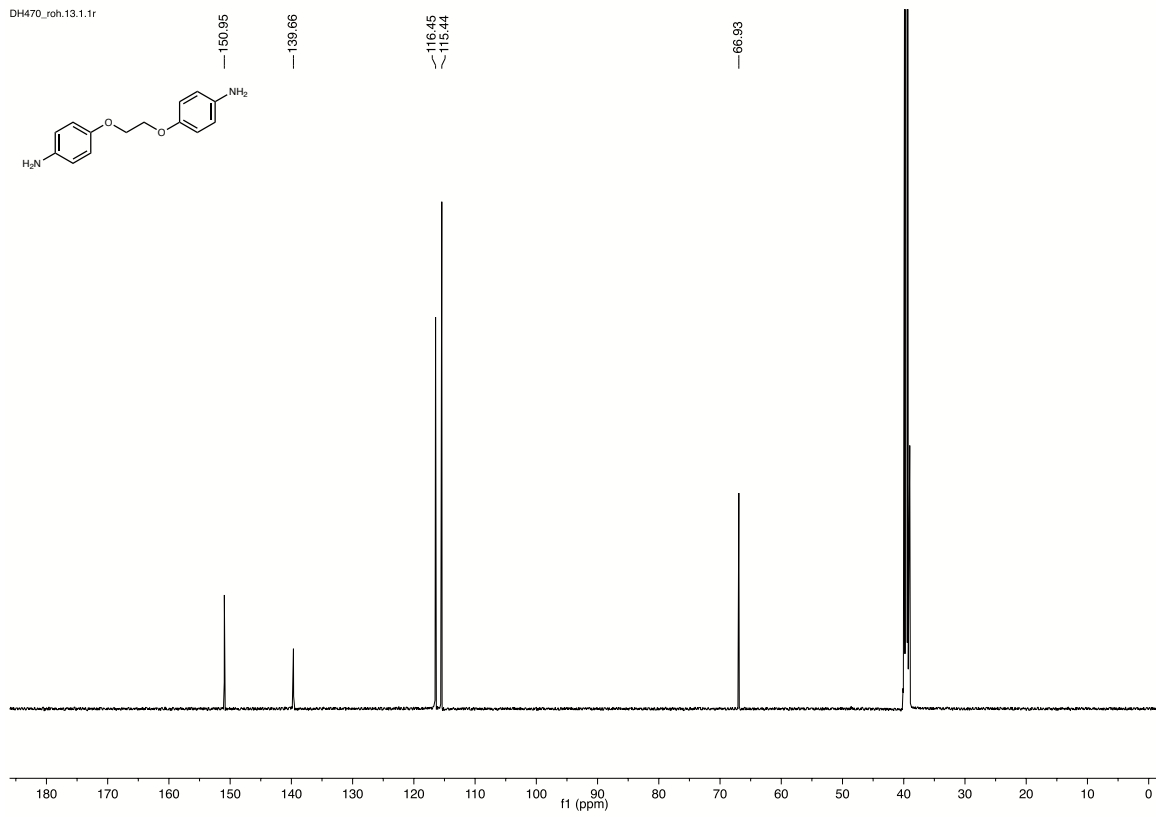
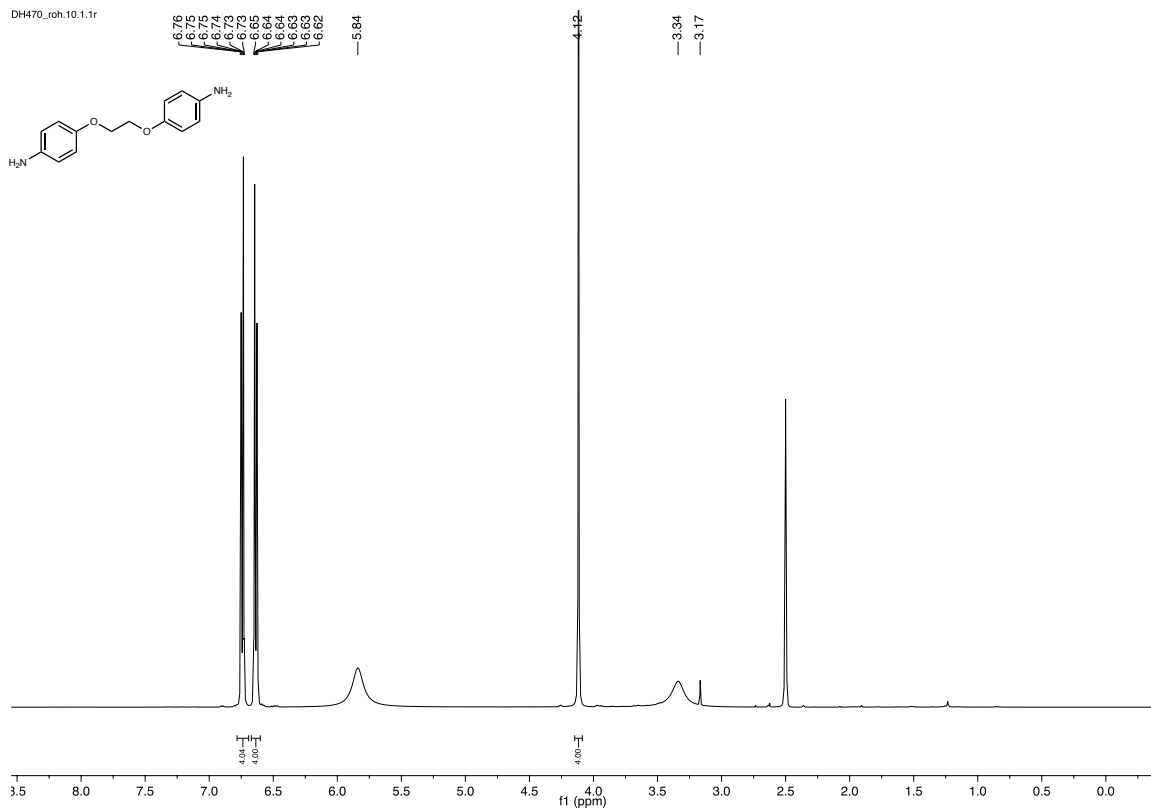
¹H and ¹³C NMR of **5**



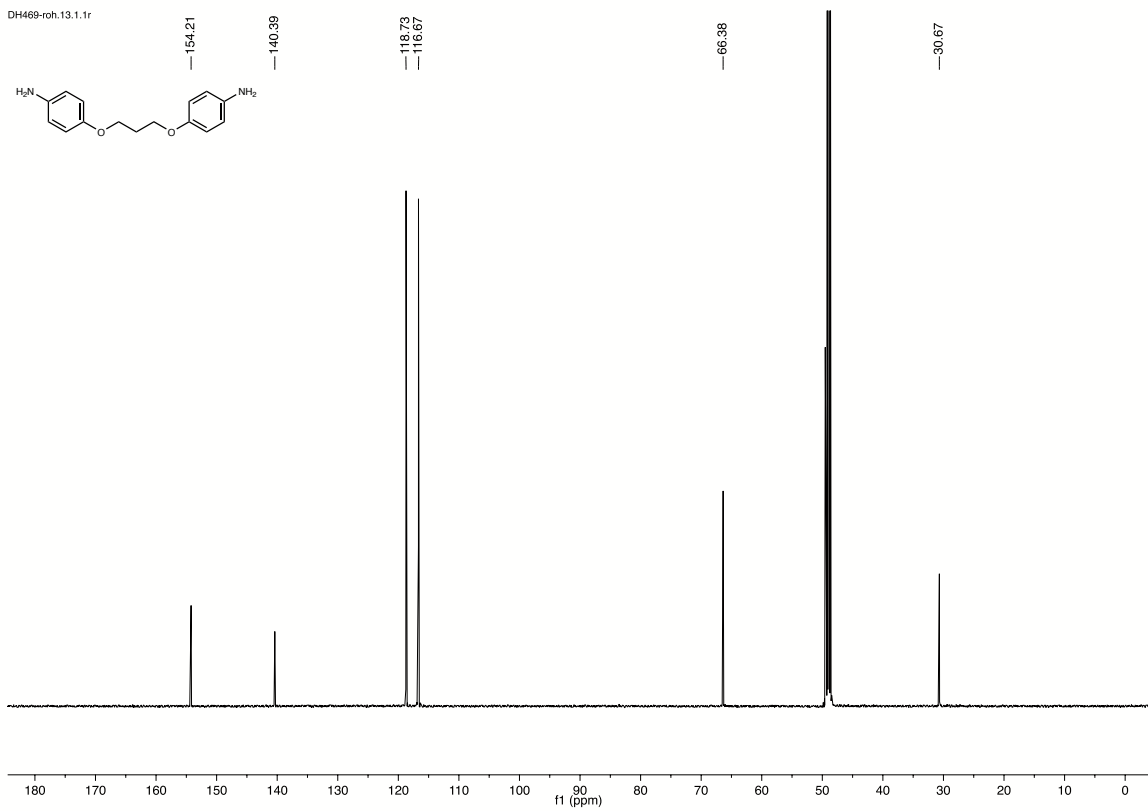
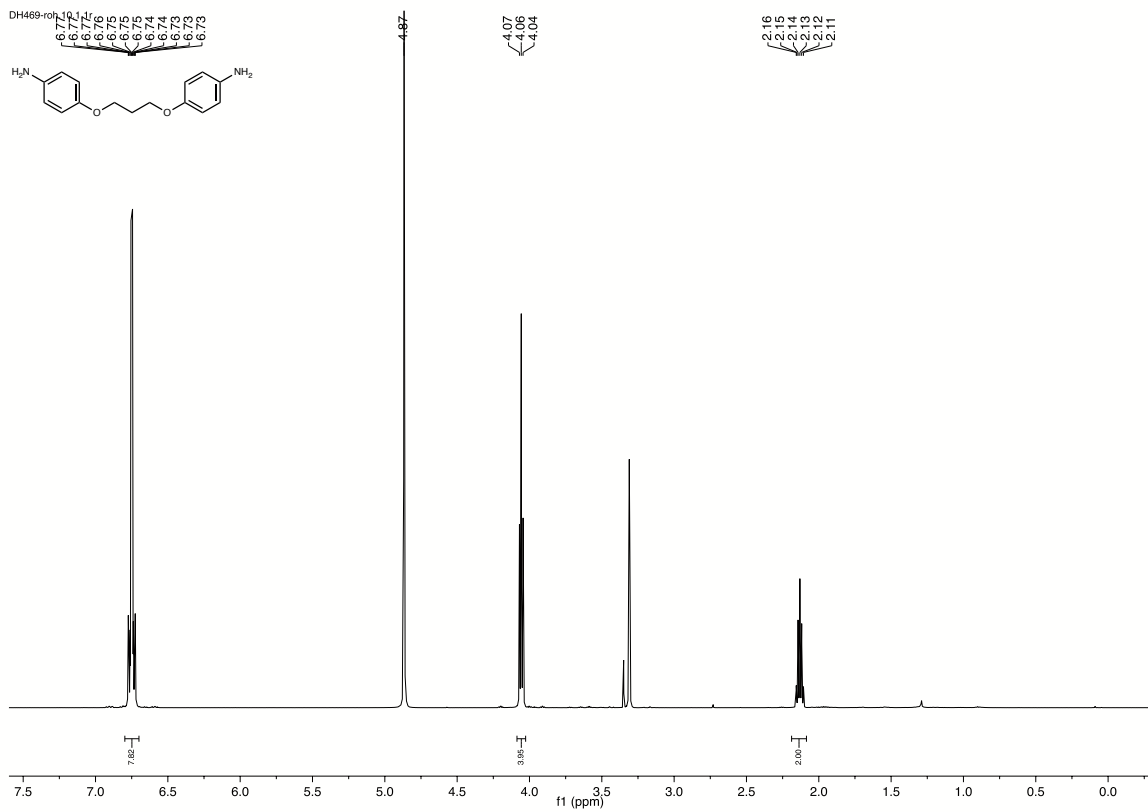
^1H and ^{13}C NMR of **2**



^1H and ^{13}C NMR of **C**

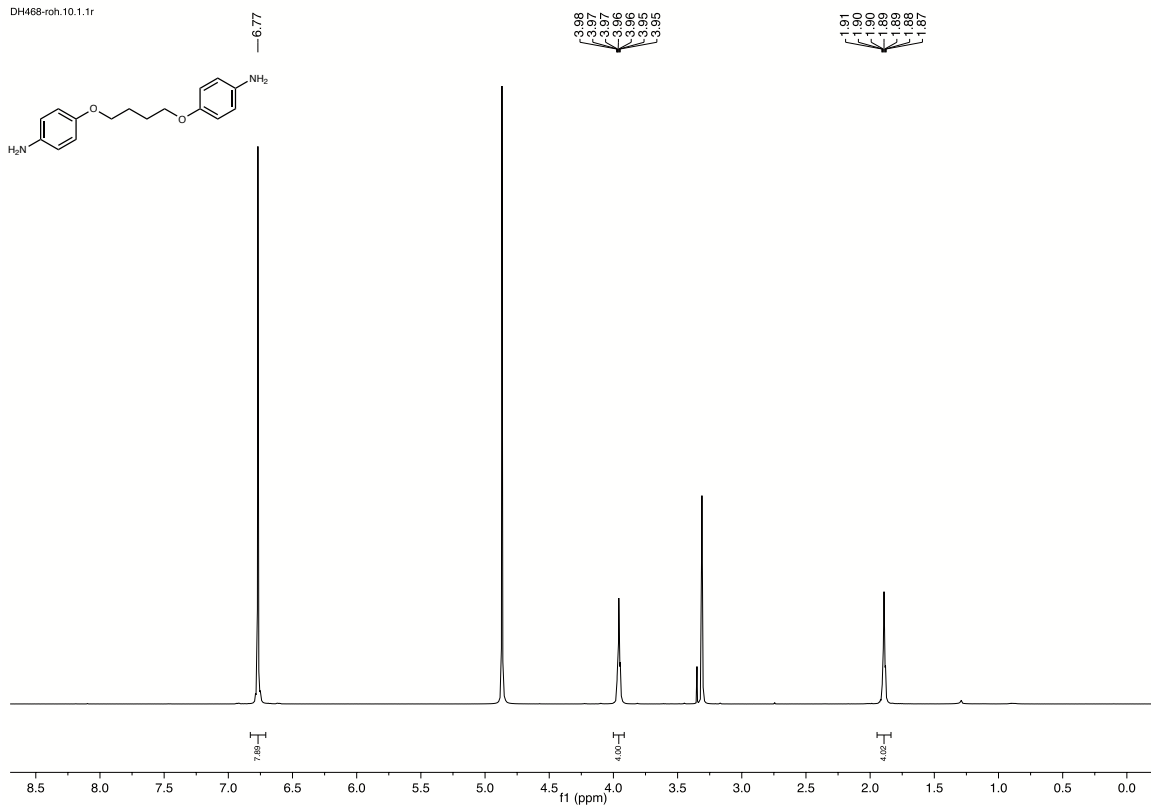


^1H and ^{13}C NMR of **D**

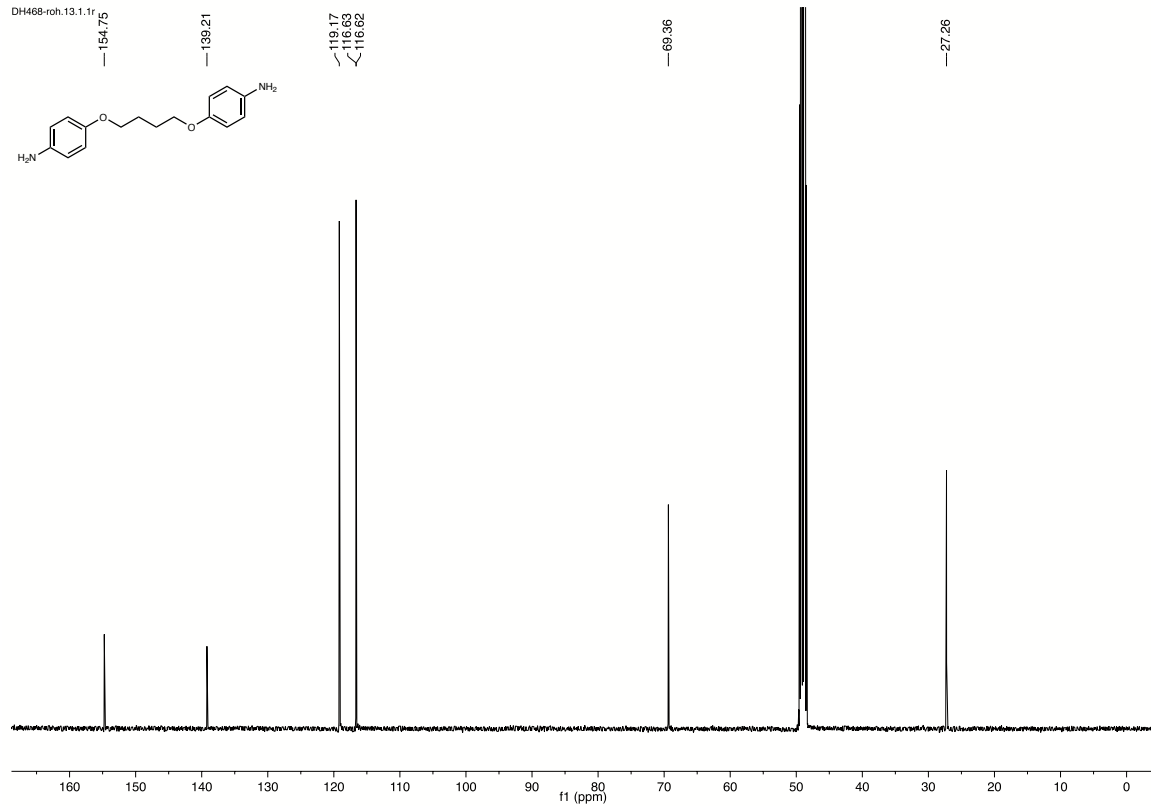


^1H and ^{13}C NMR of **E**

DH468-roh.10.1.1r

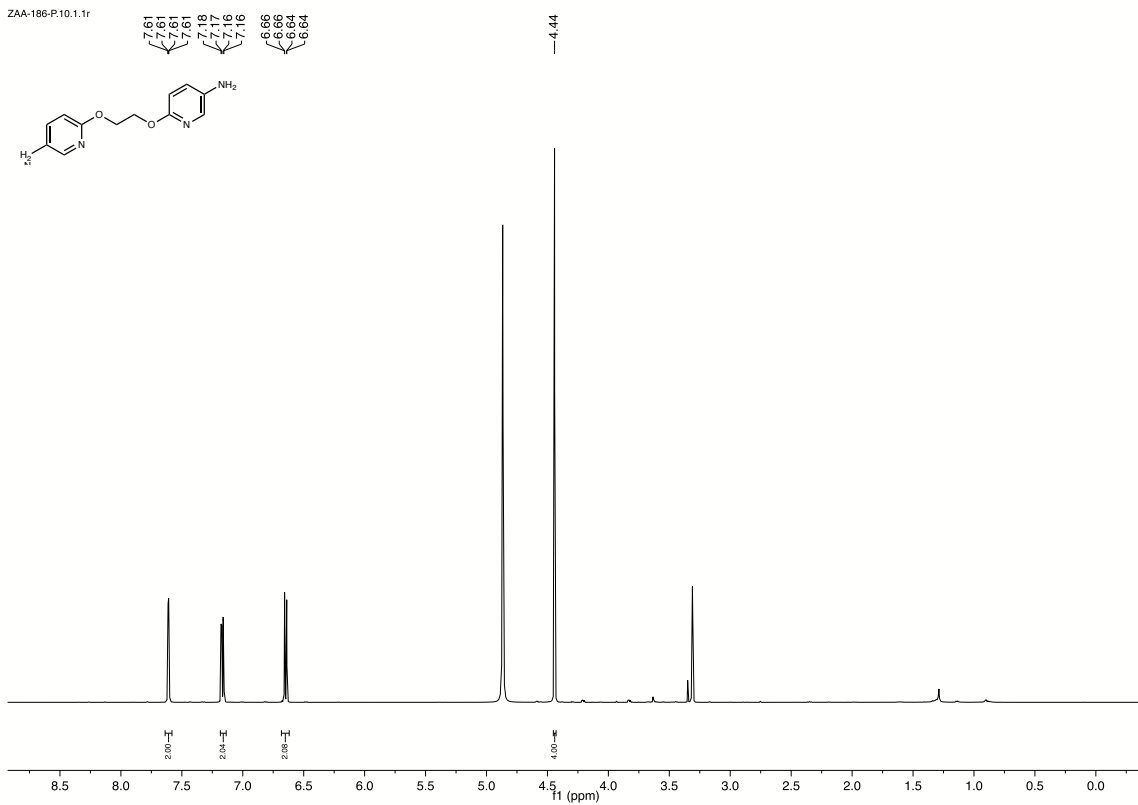


DH468-roh.13.1.1r

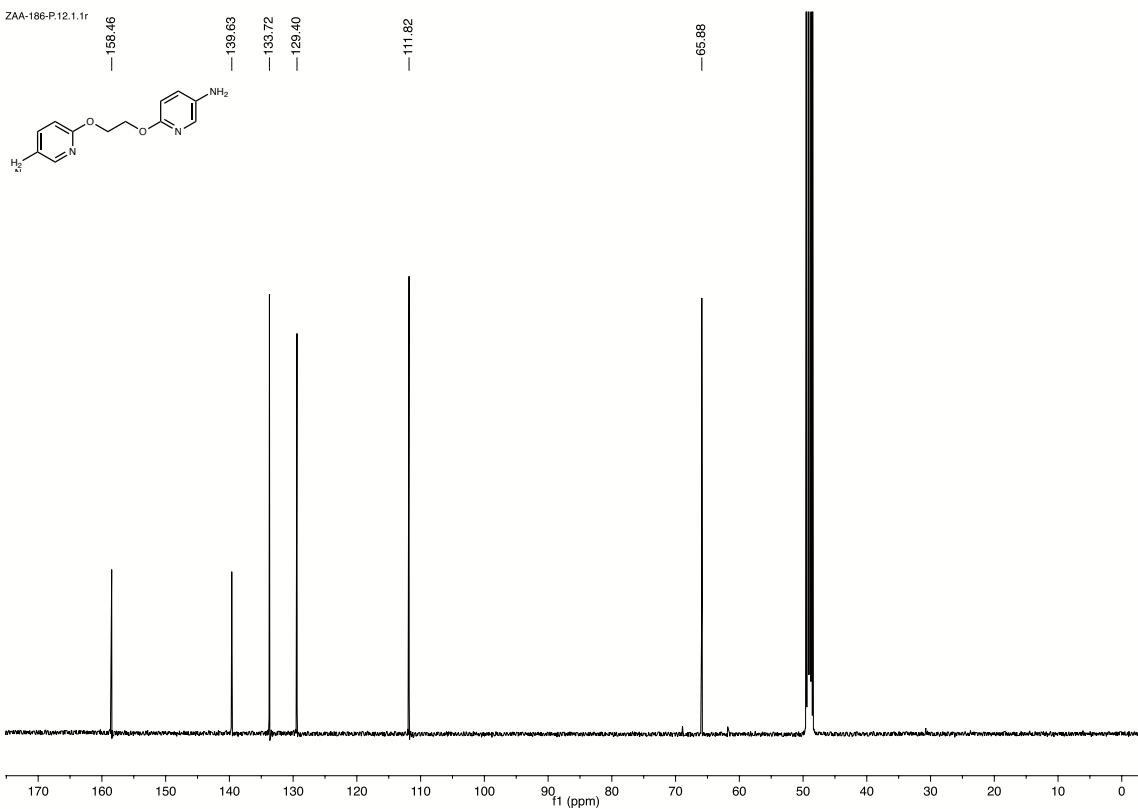


¹H and ¹³C NMR of F

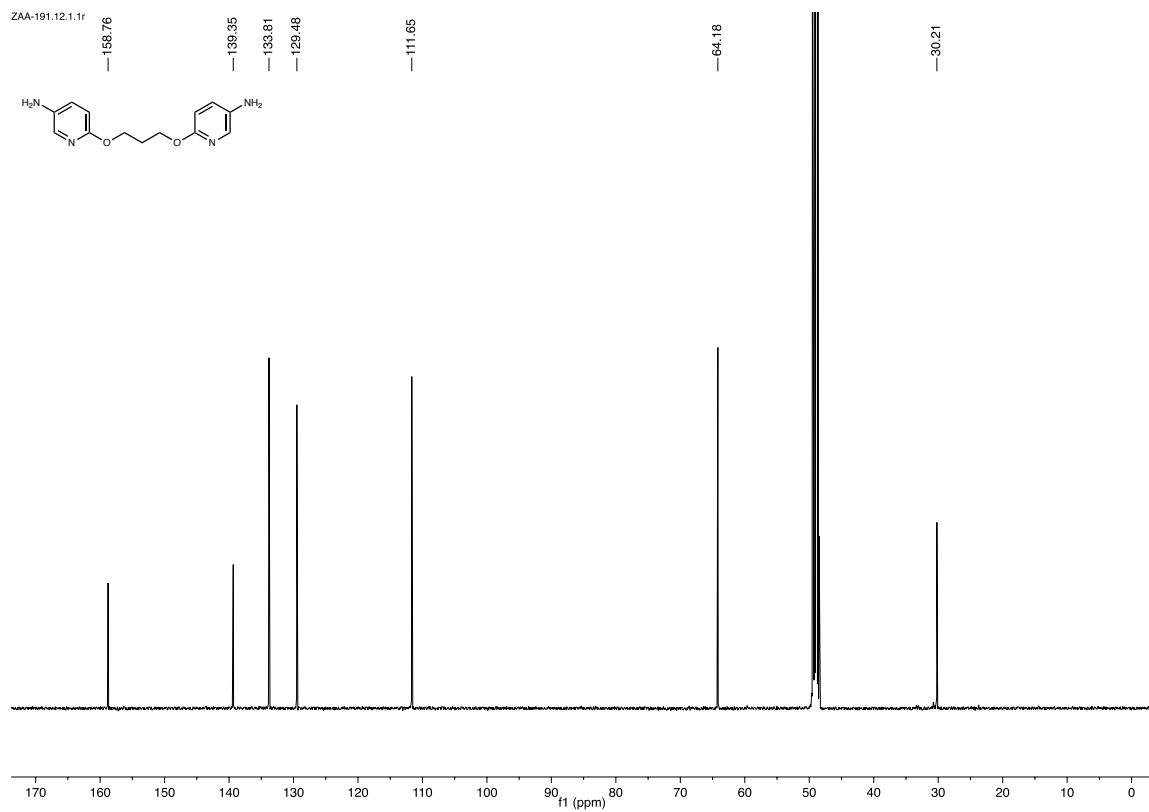
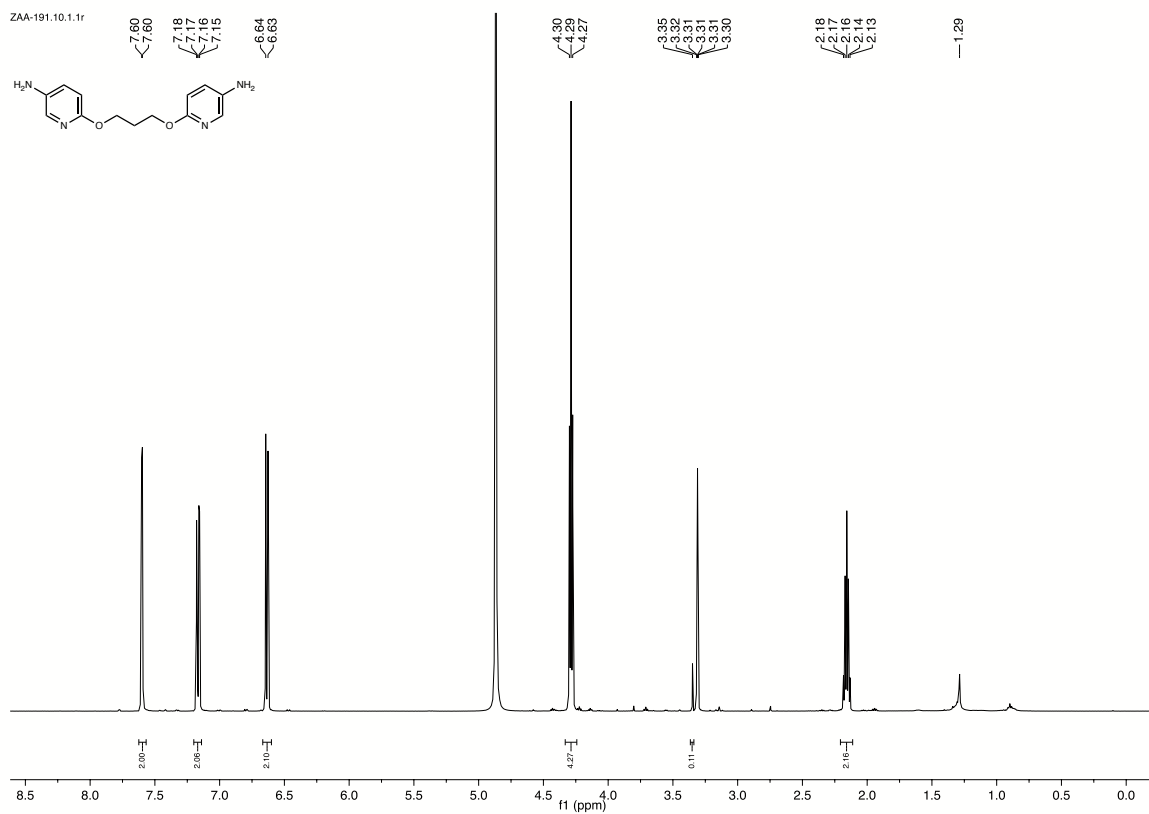
ZAA-186-P.10.1.1r



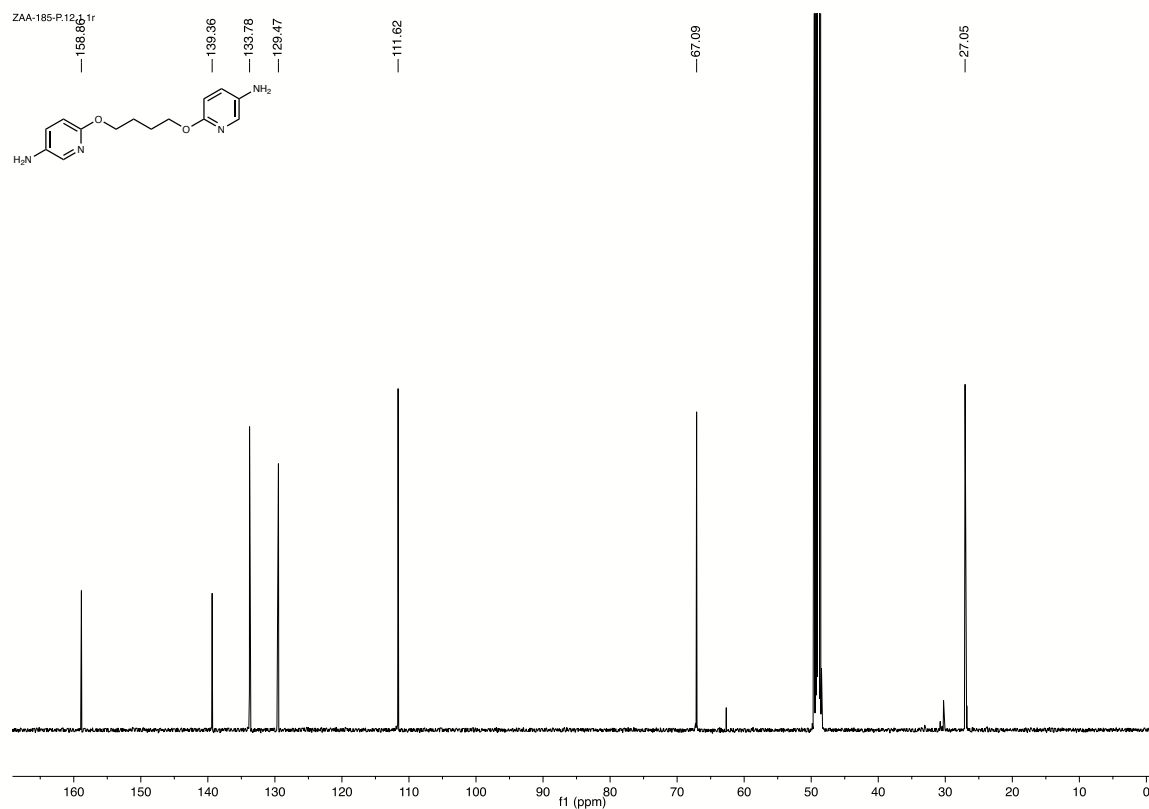
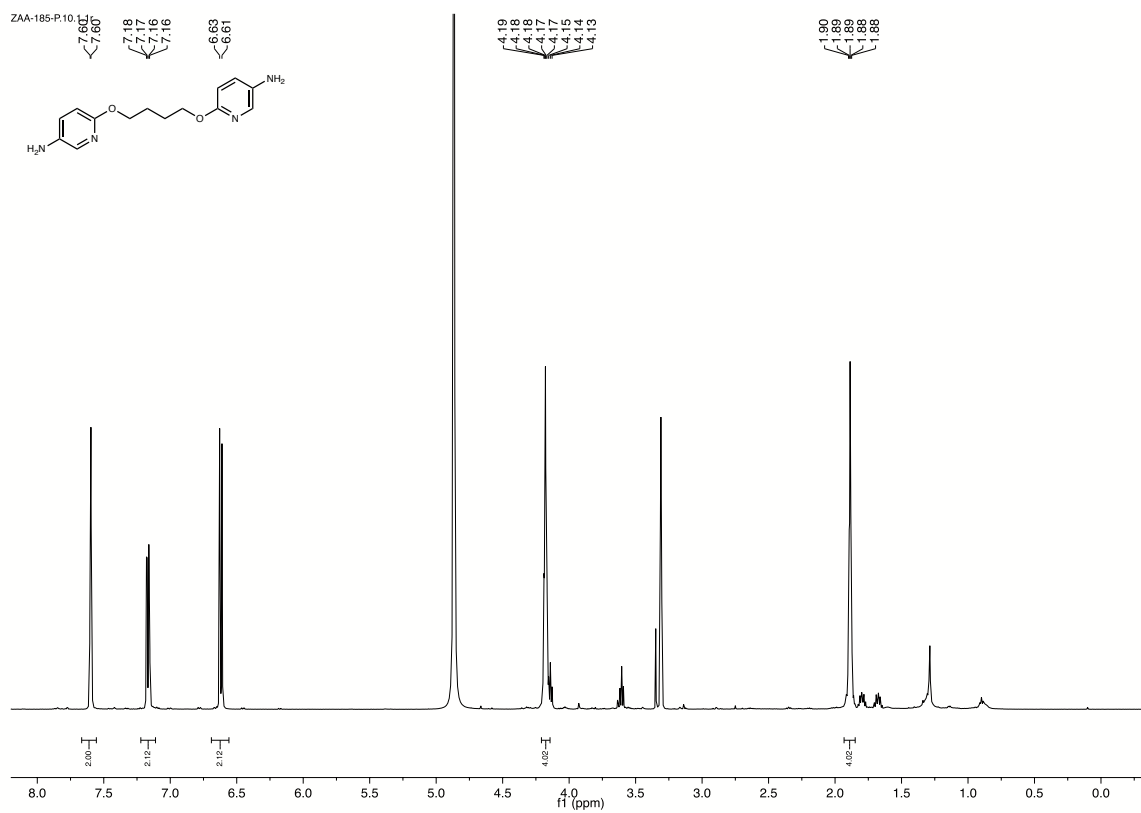
ZAA-186-P.12.1.1r



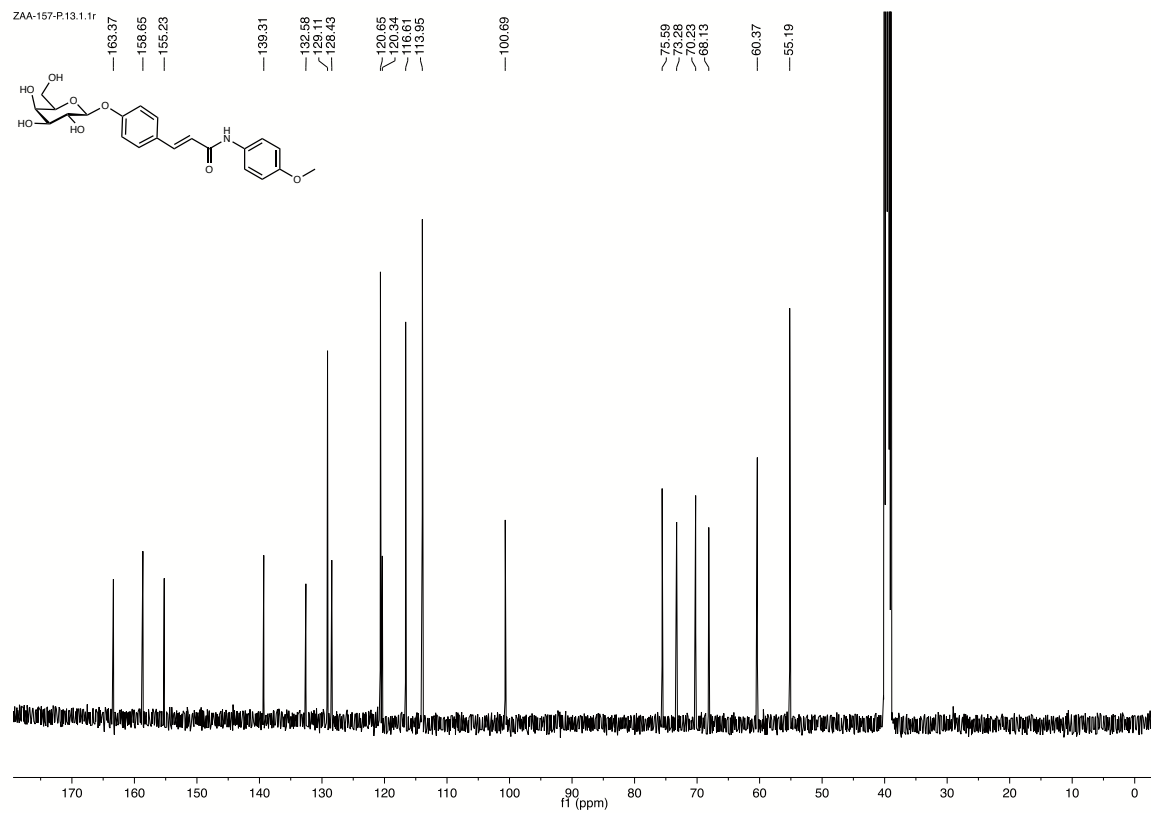
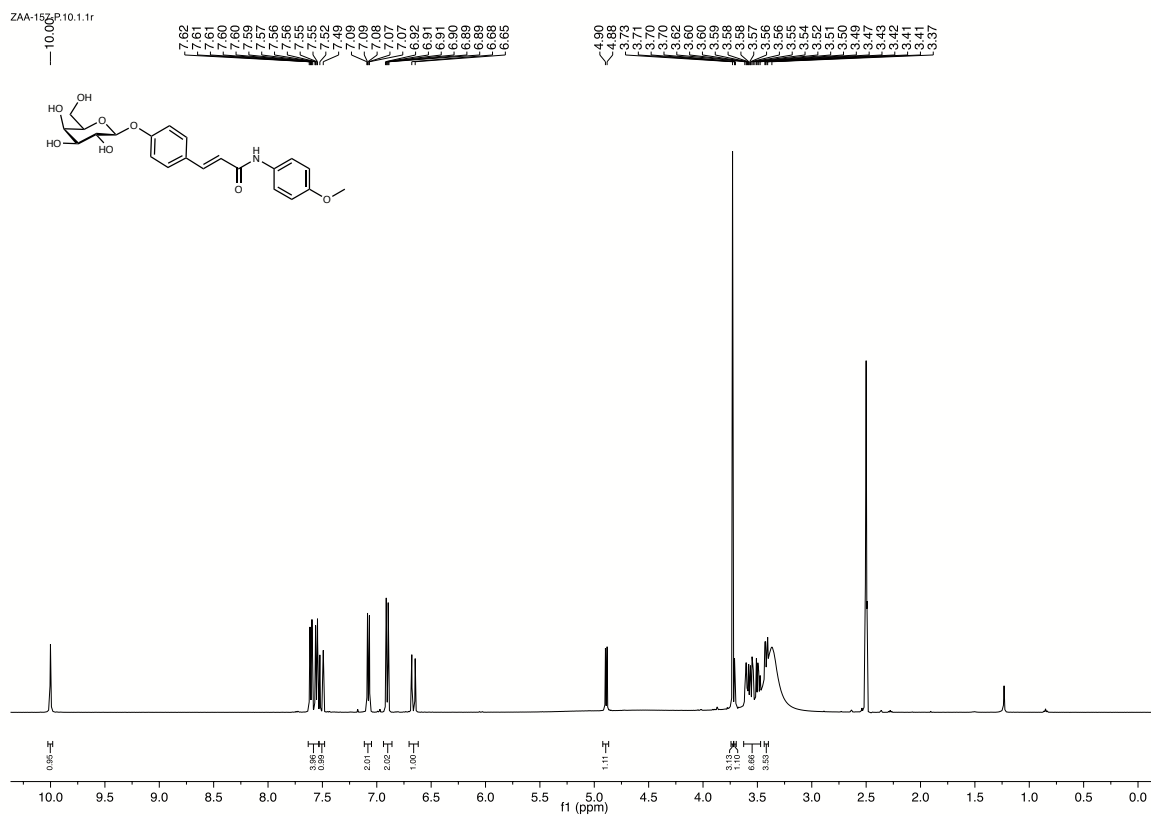
¹H and ¹³C NMR of **H**



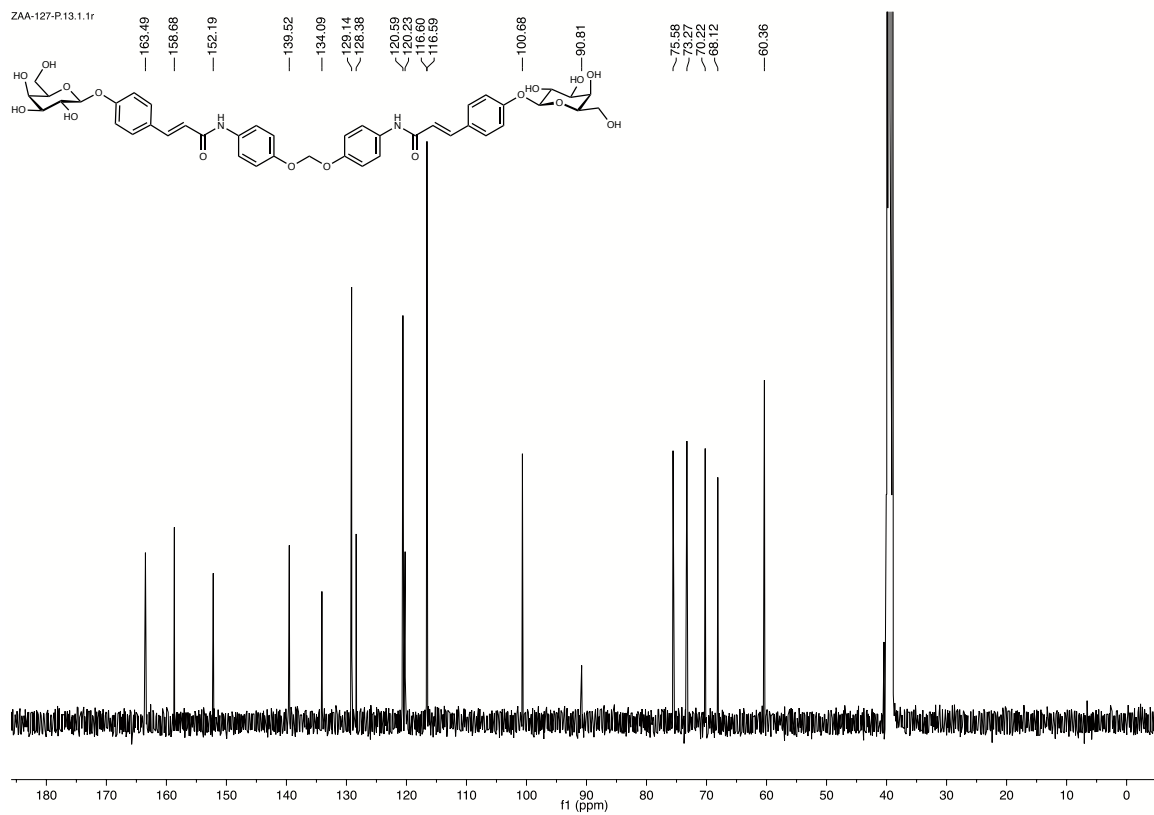
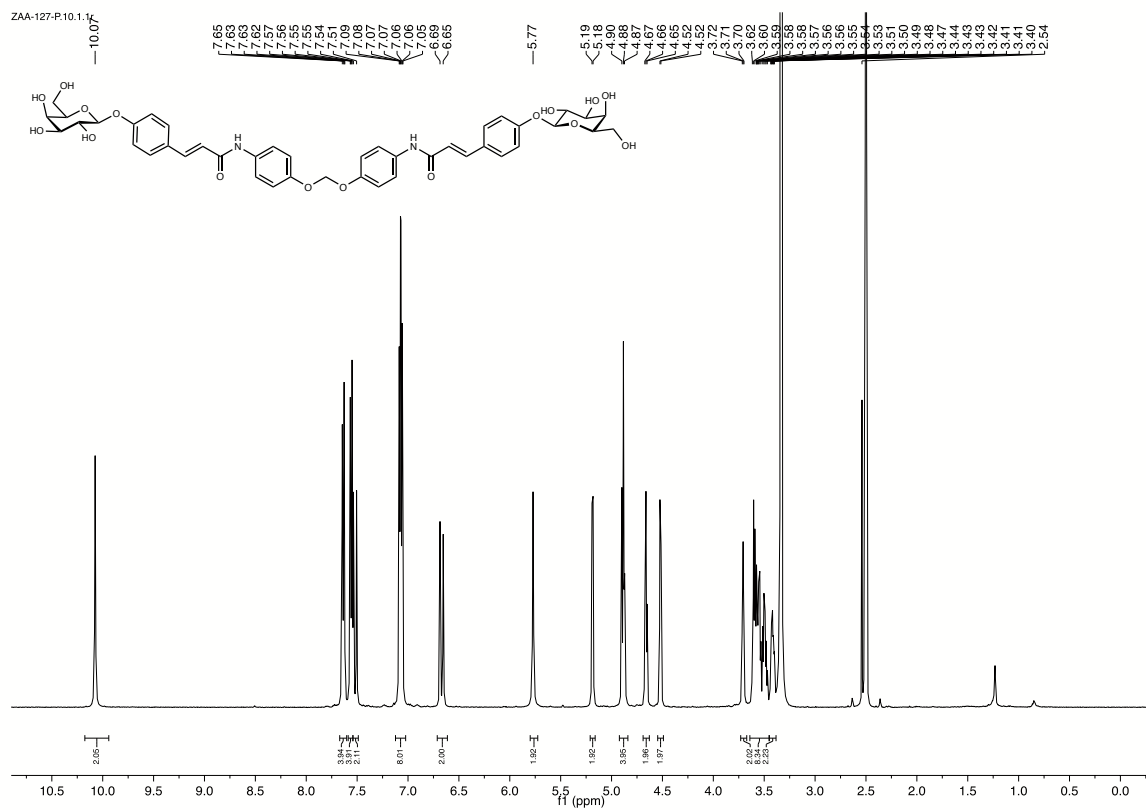
^1H and ^{13}C NMR of **I**



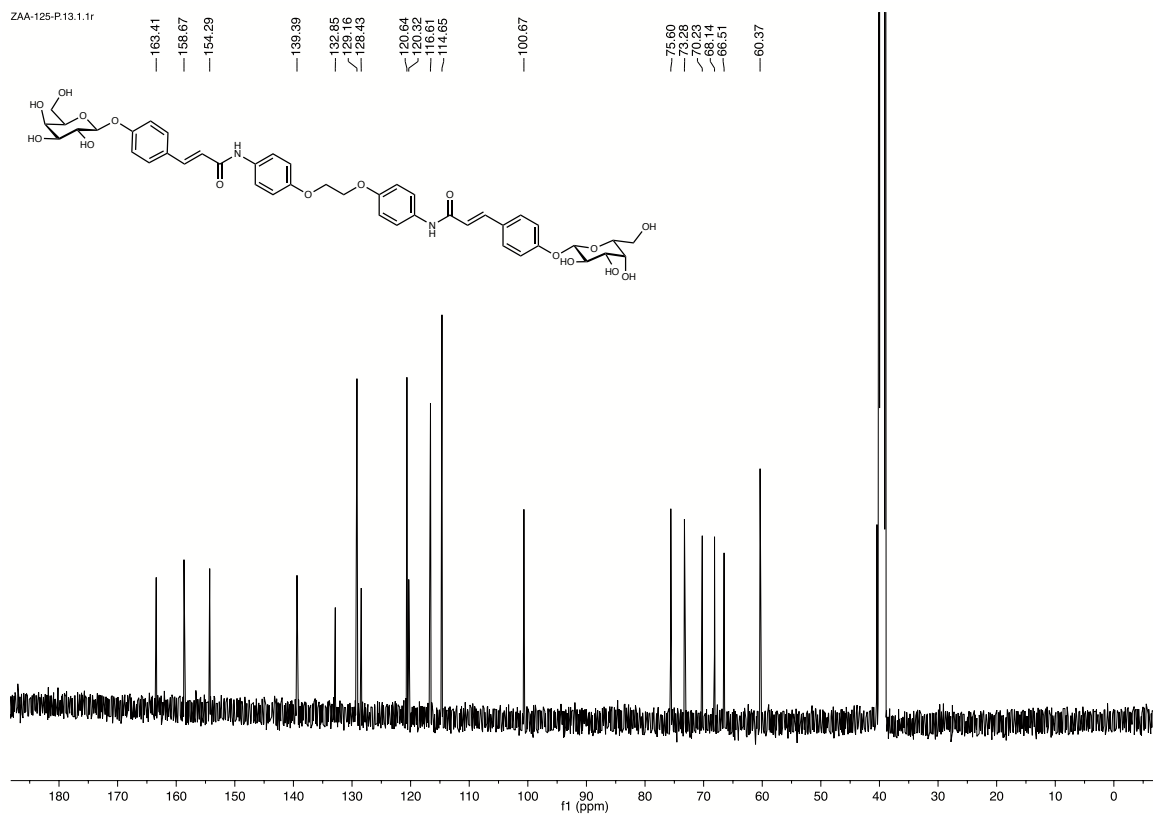
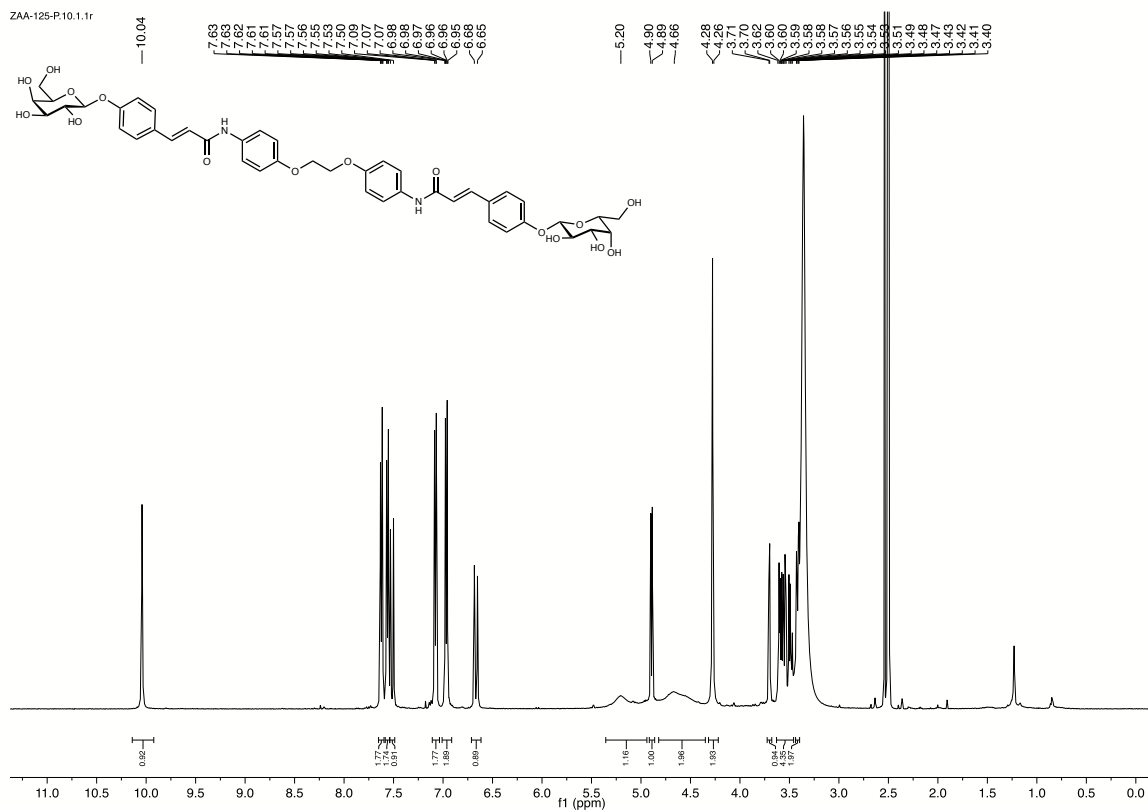
^1H and ^{13}C NMR of J



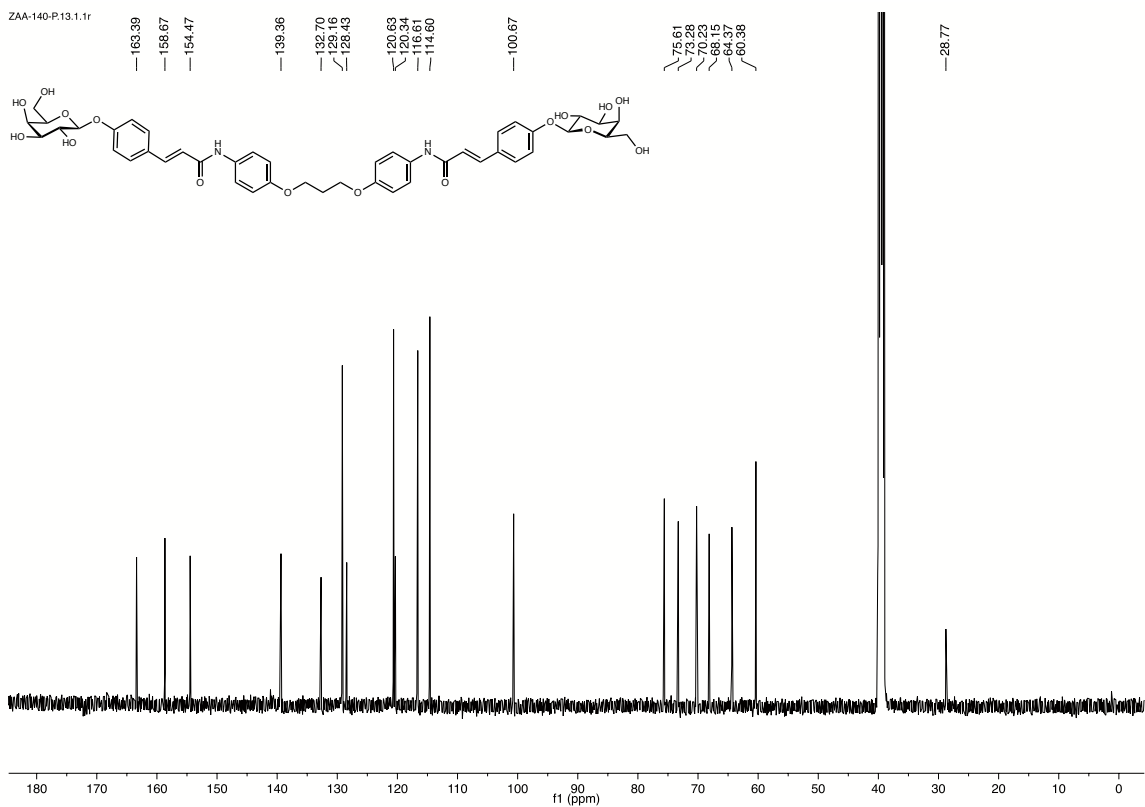
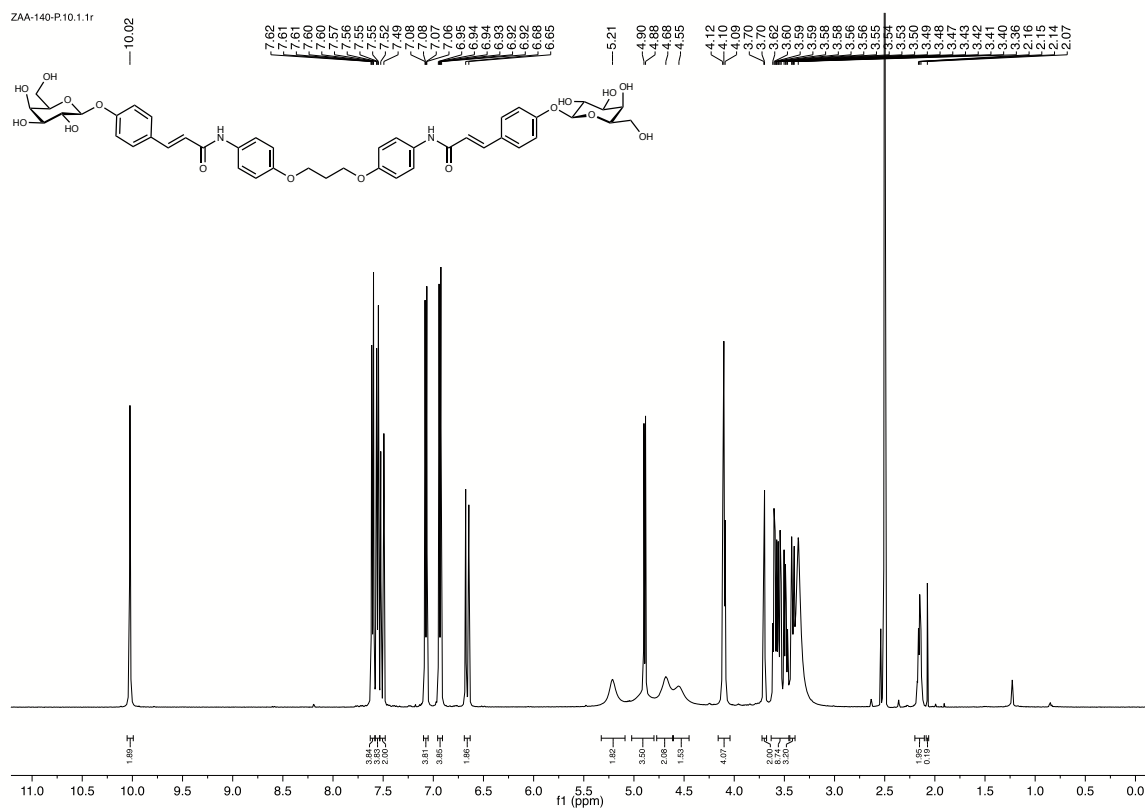
¹H and ¹³C NMR of A1



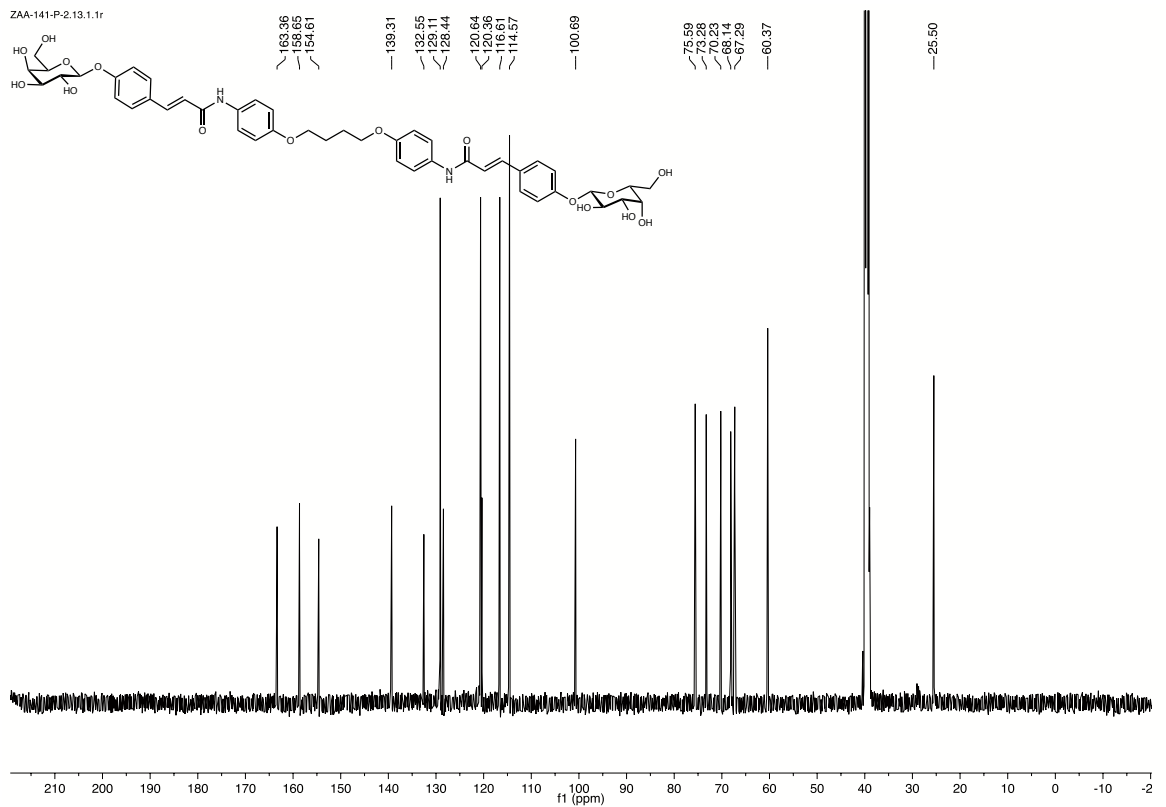
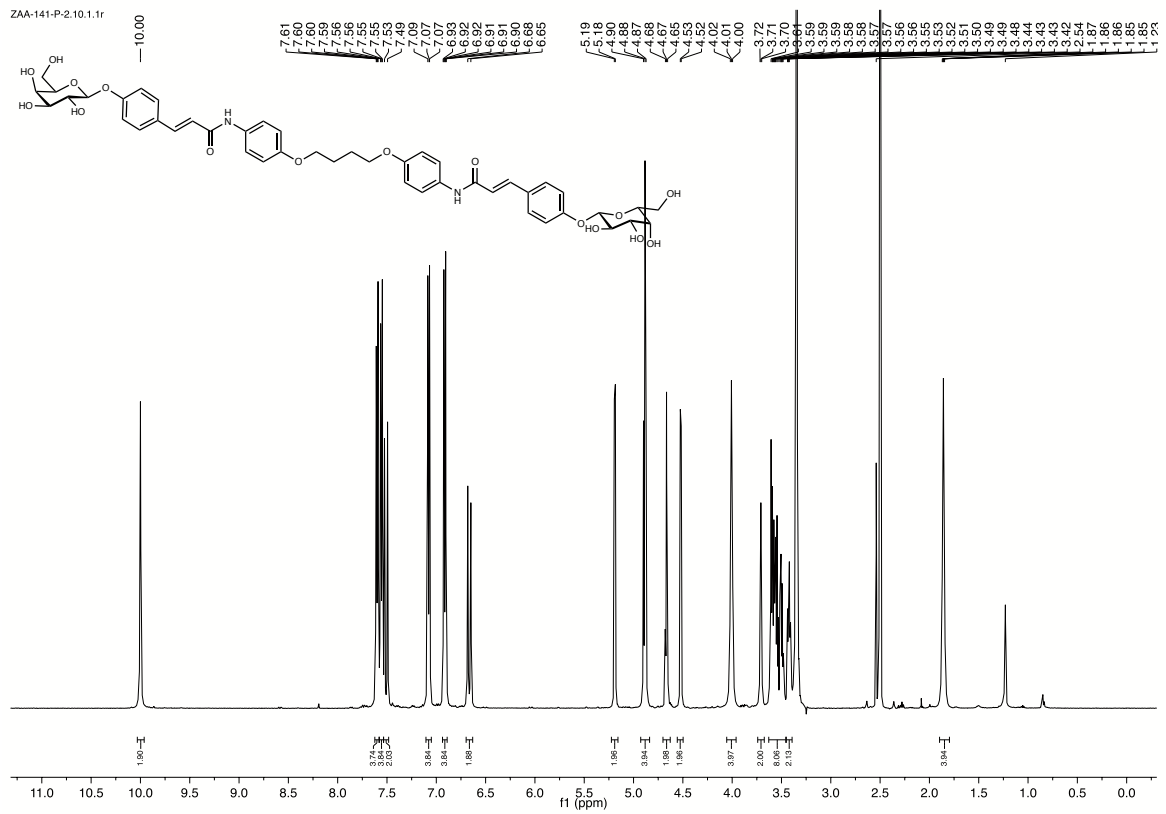
^1H and ^{13}C NMR of C1



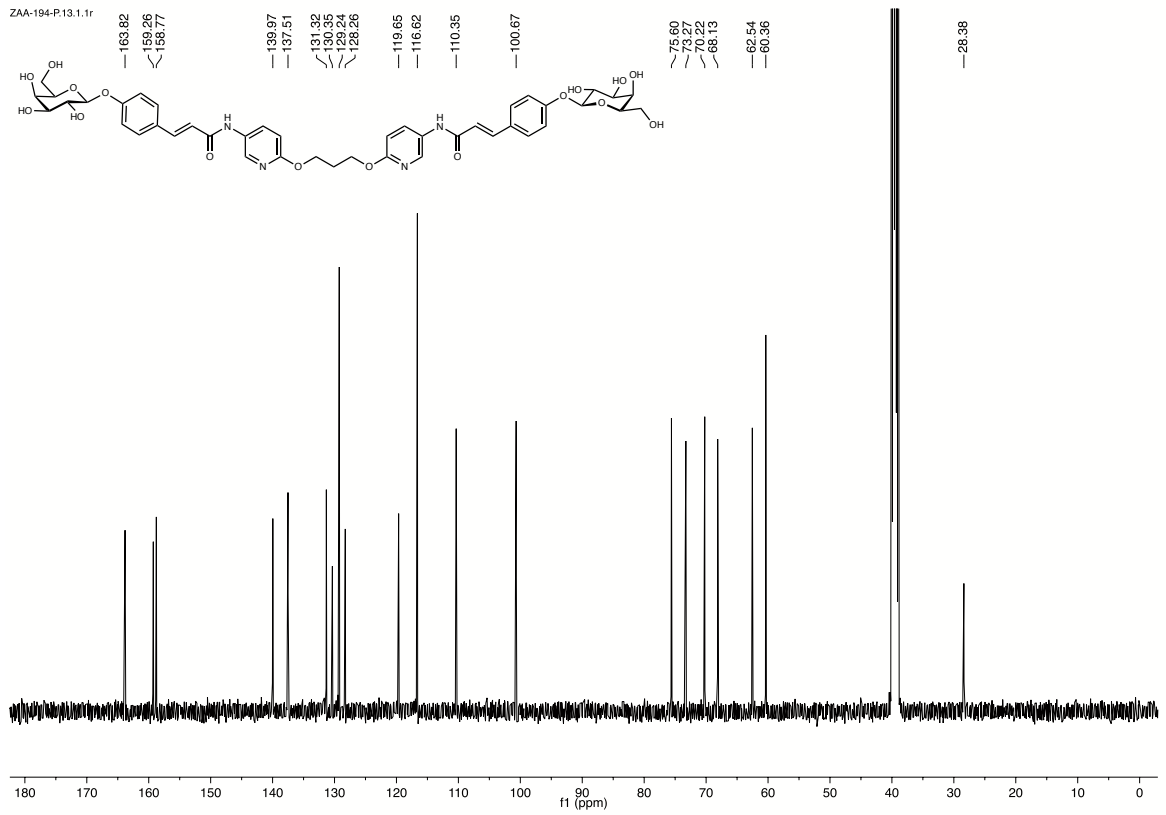
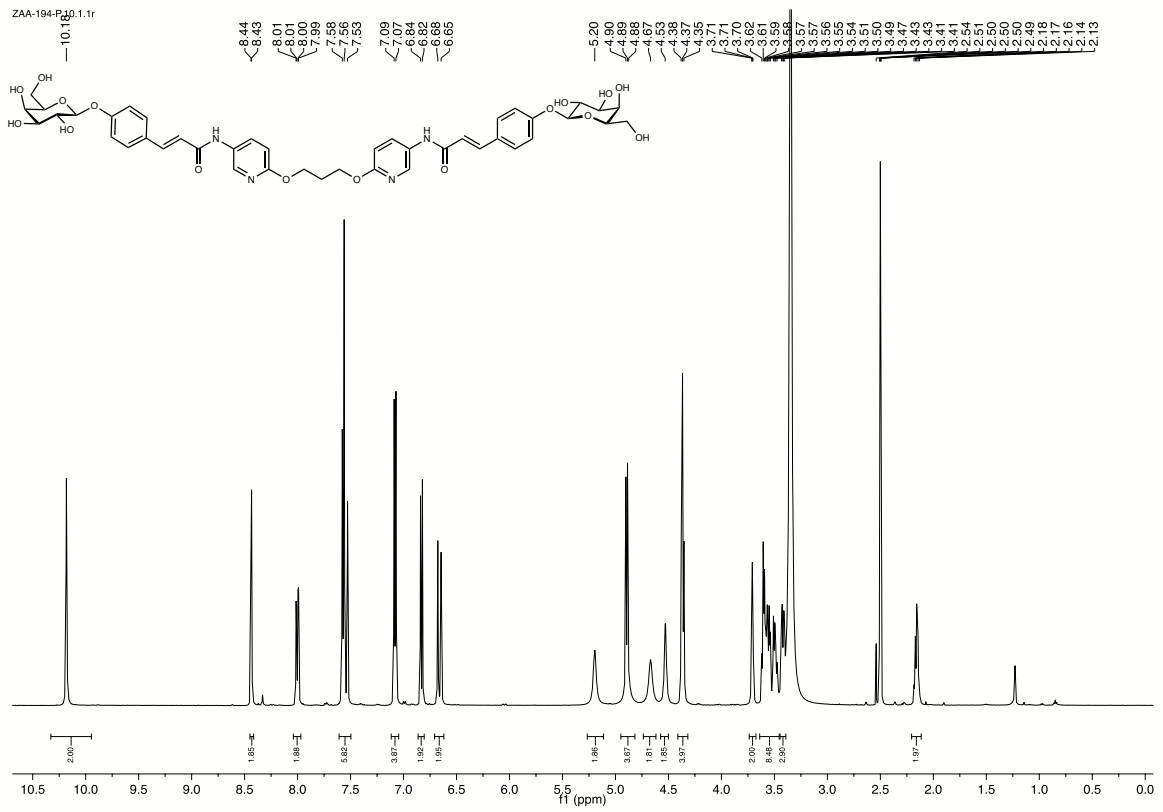
^1H and ^{13}C NMR of **D1**



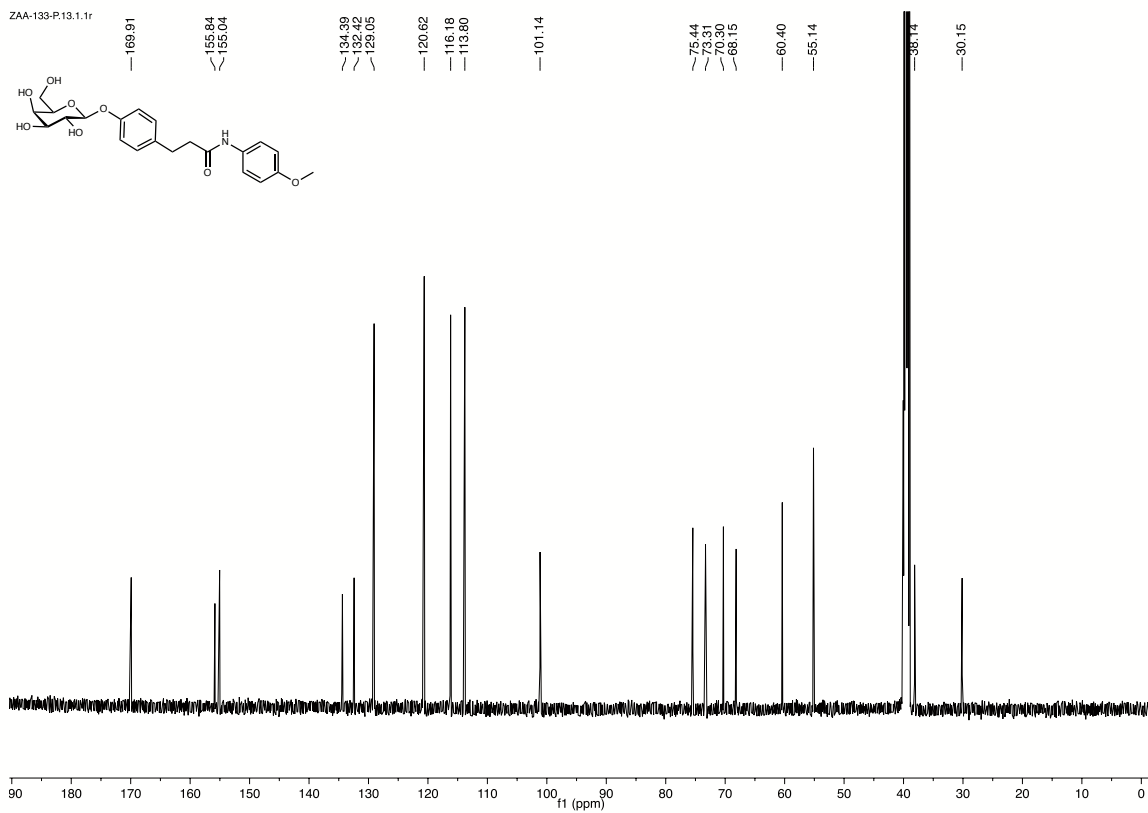
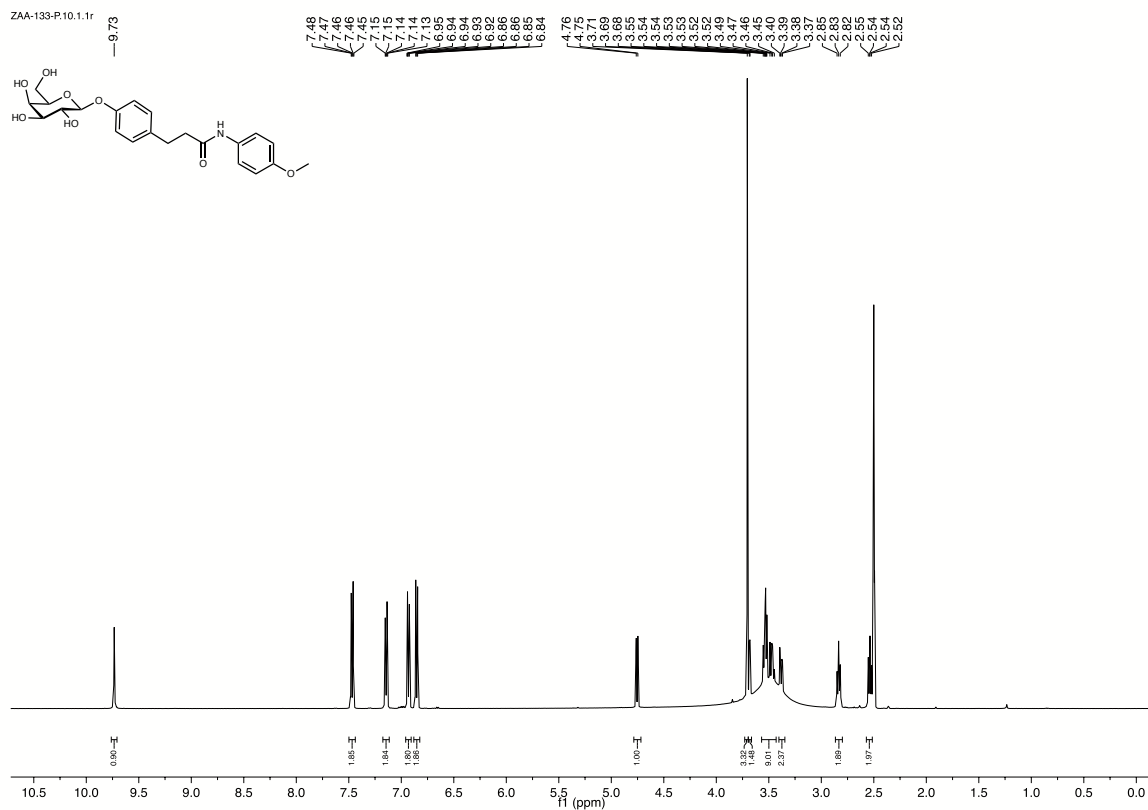
¹H and ¹³C NMR of E1



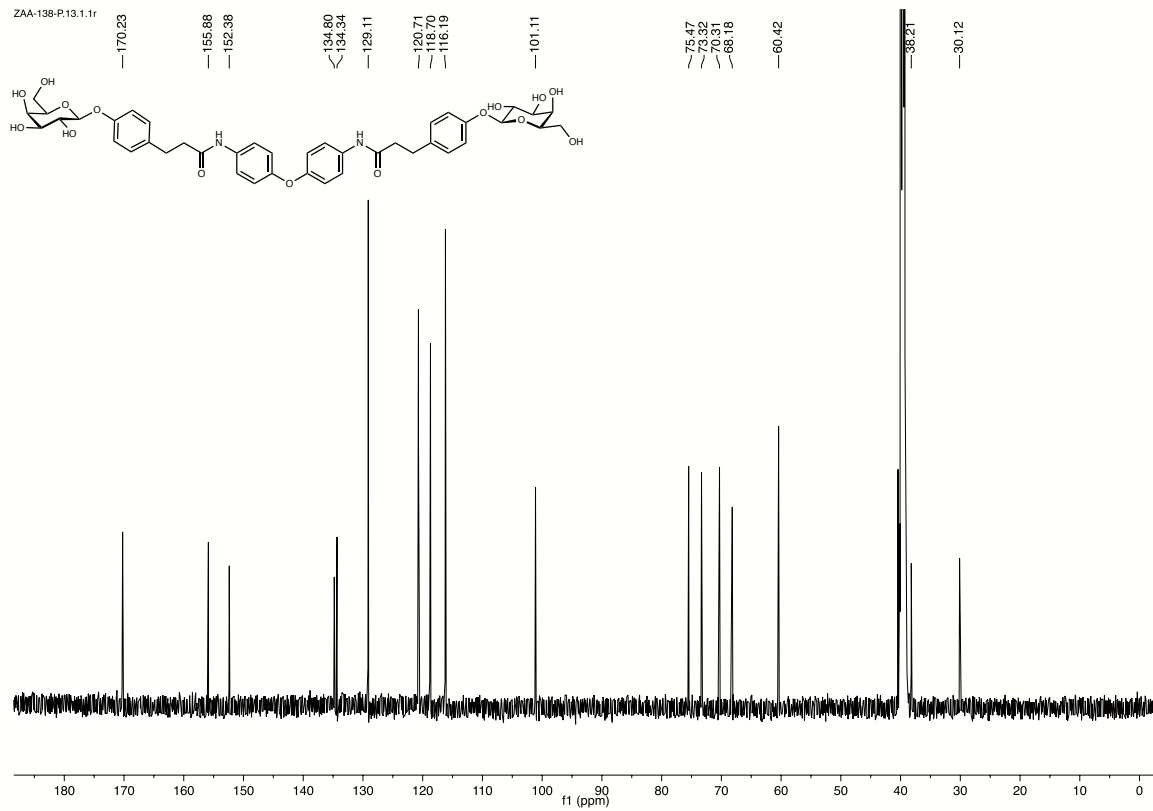
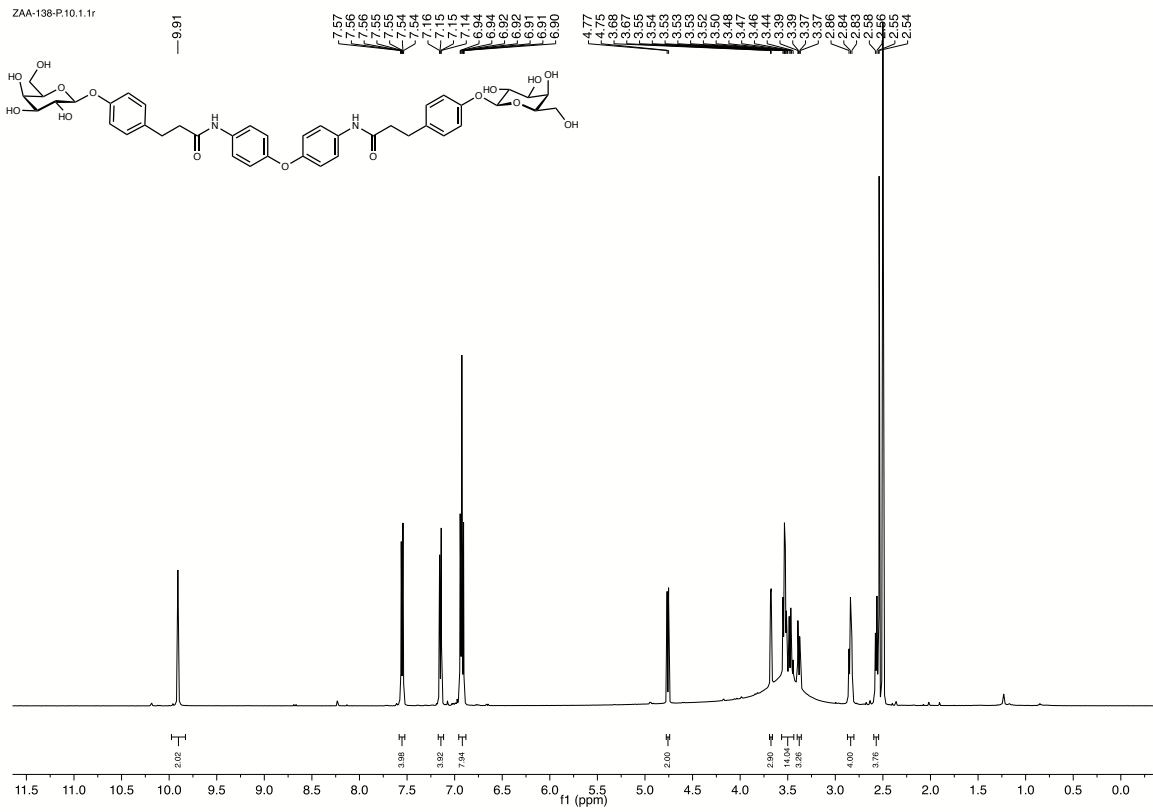
^1H and ^{13}C NMR of F1



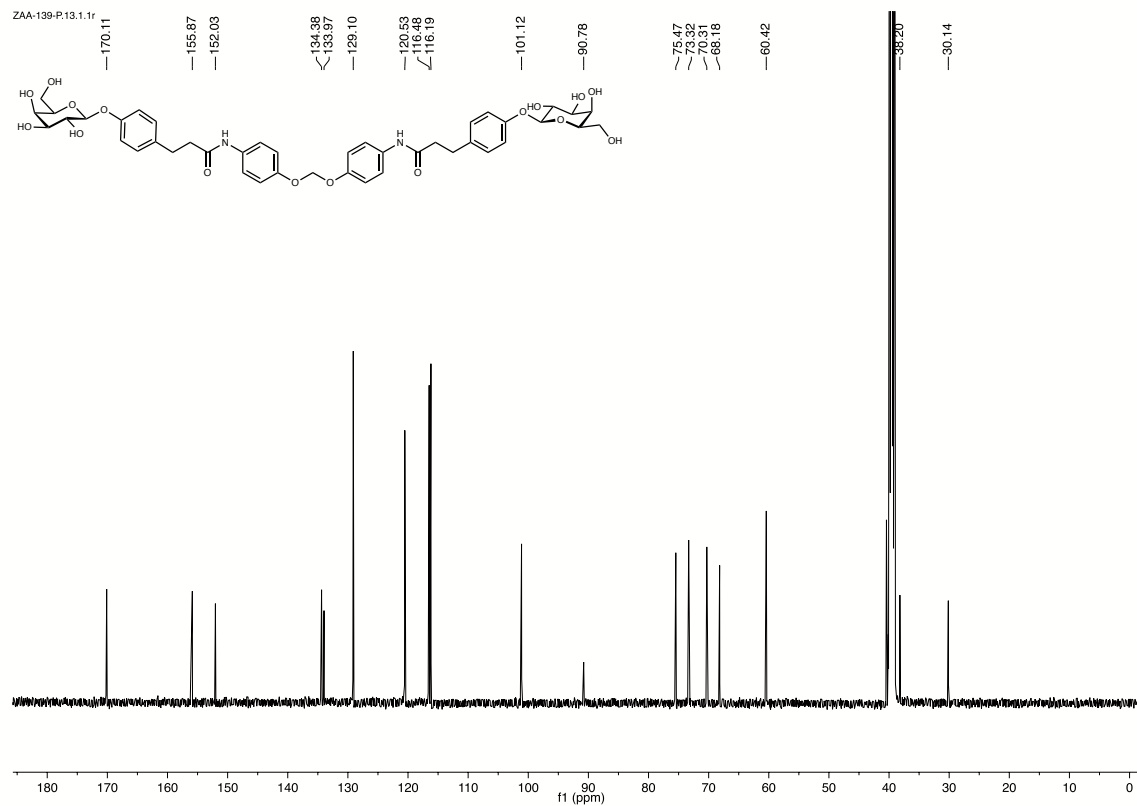
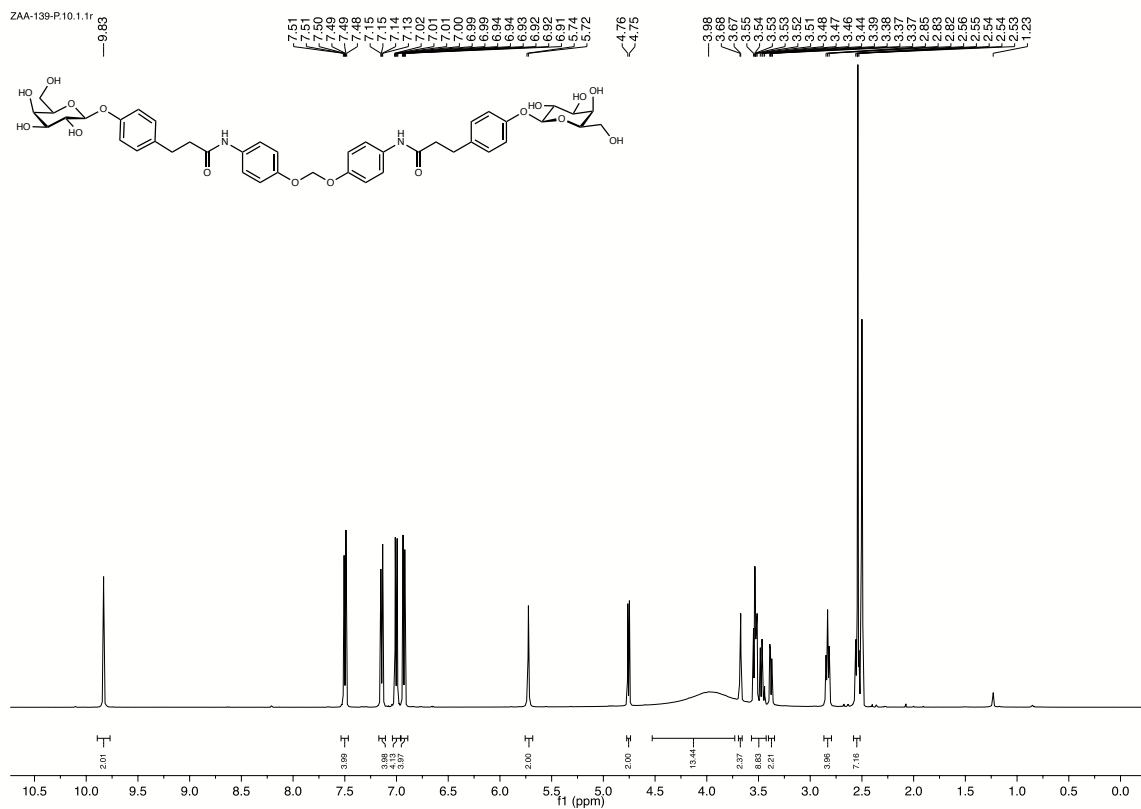
^1H and ^{13}C NMR of **11**



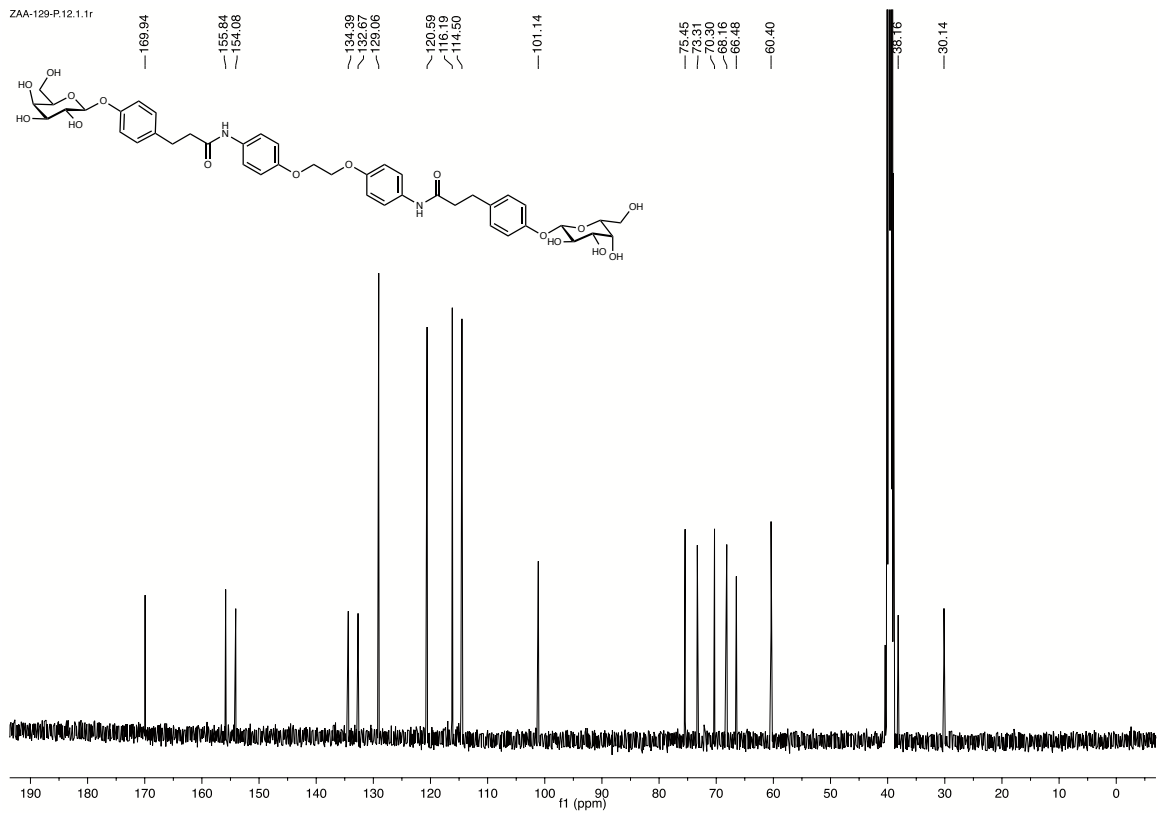
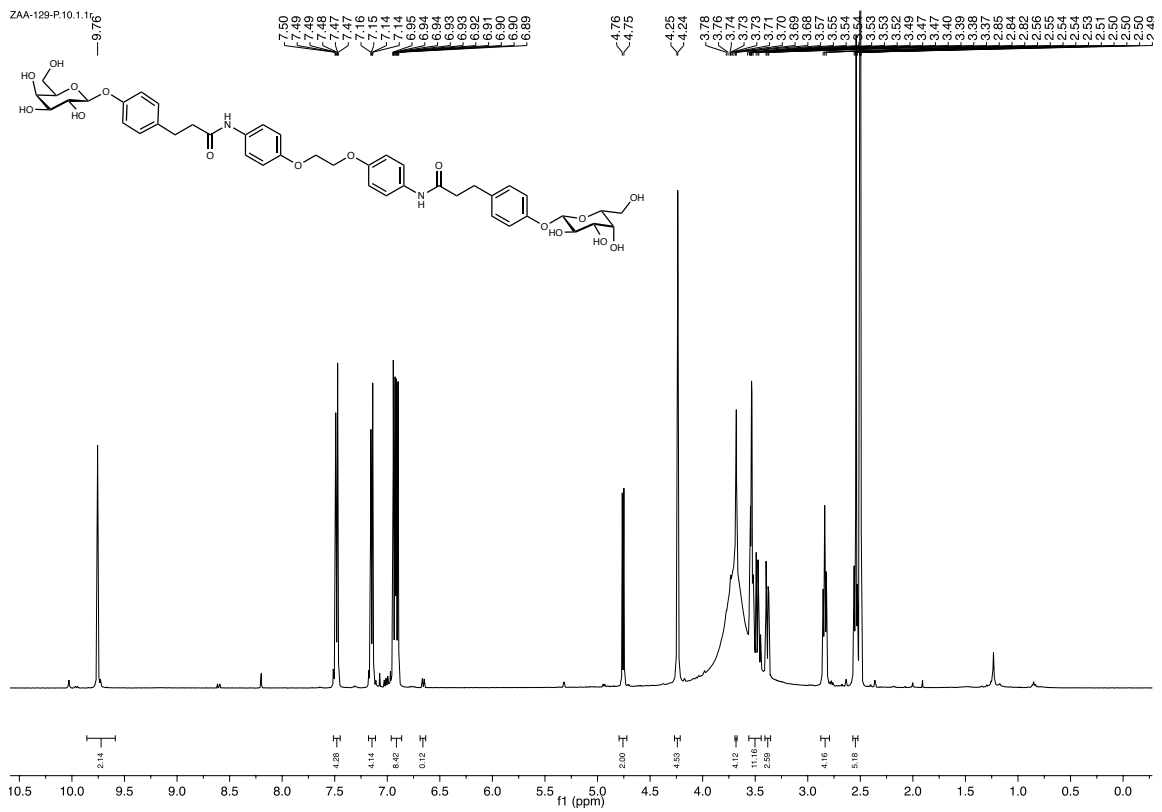
^1H and ^{13}C NMR of A2



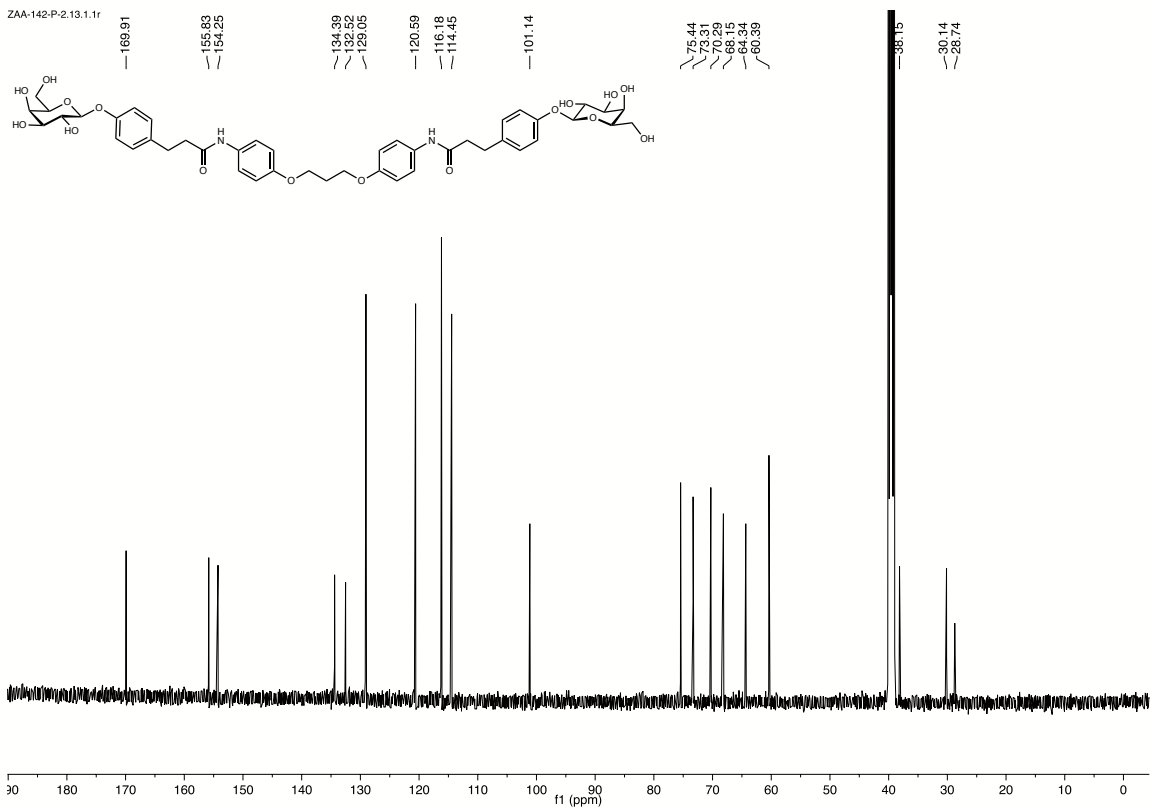
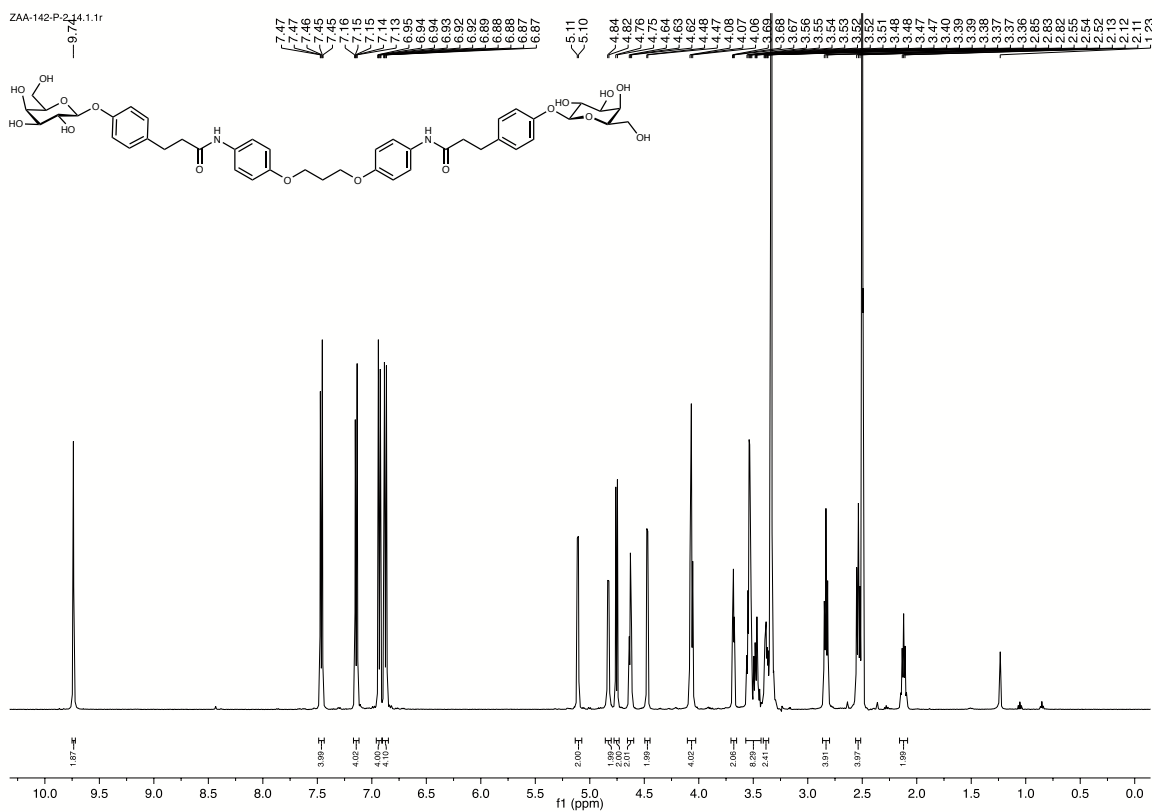
^1H and ^{13}C NMR of **B2**



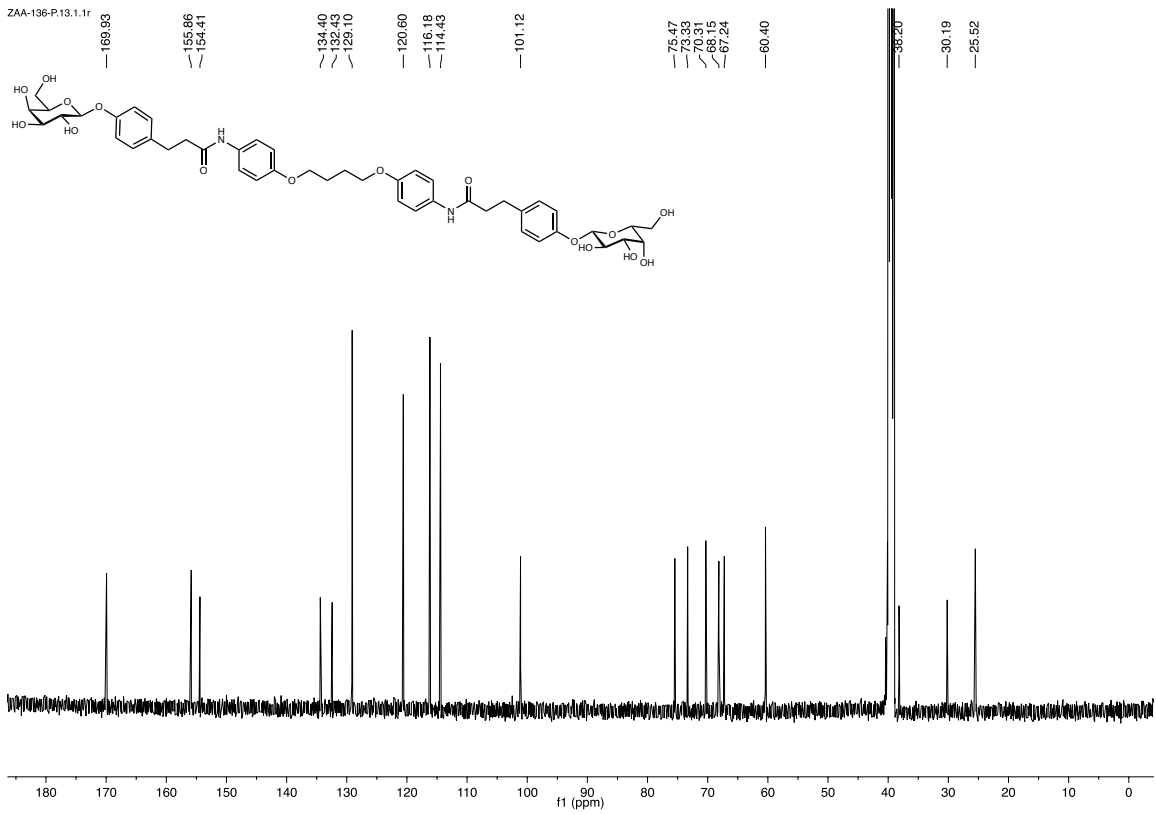
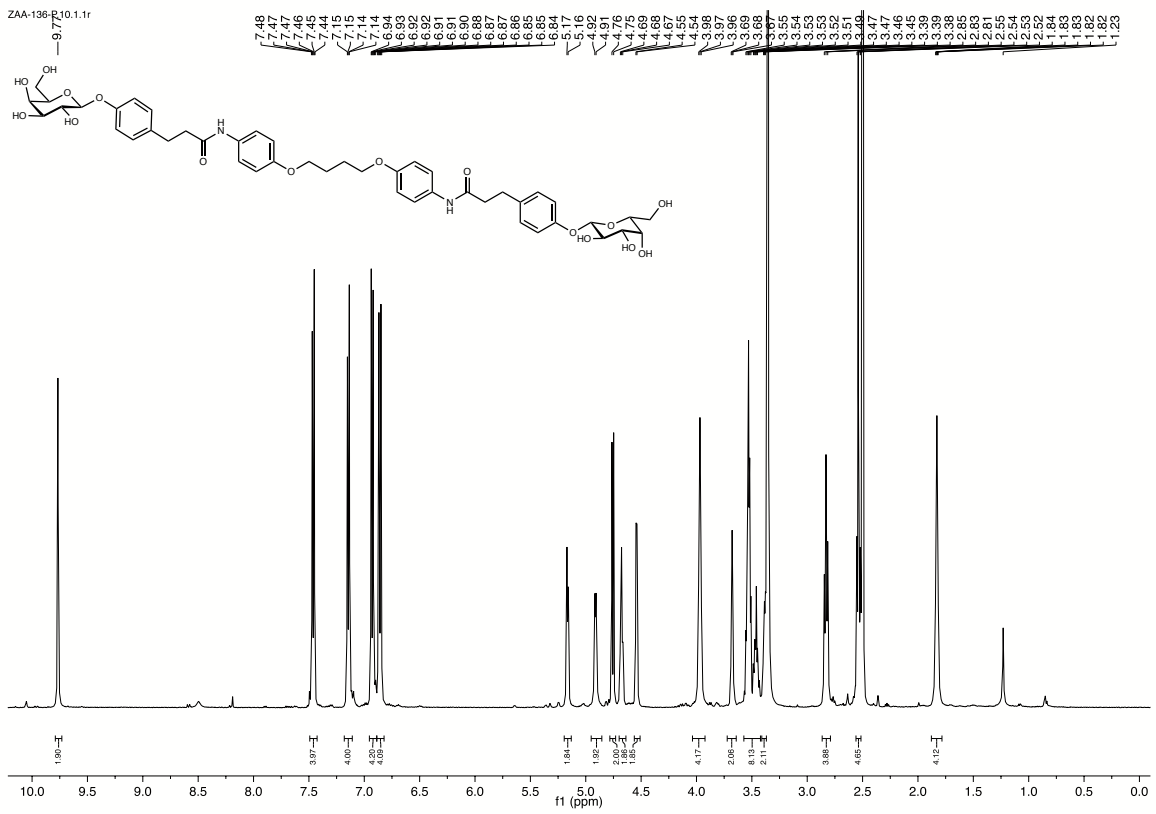
^1H and ^{13}C NMR of C2



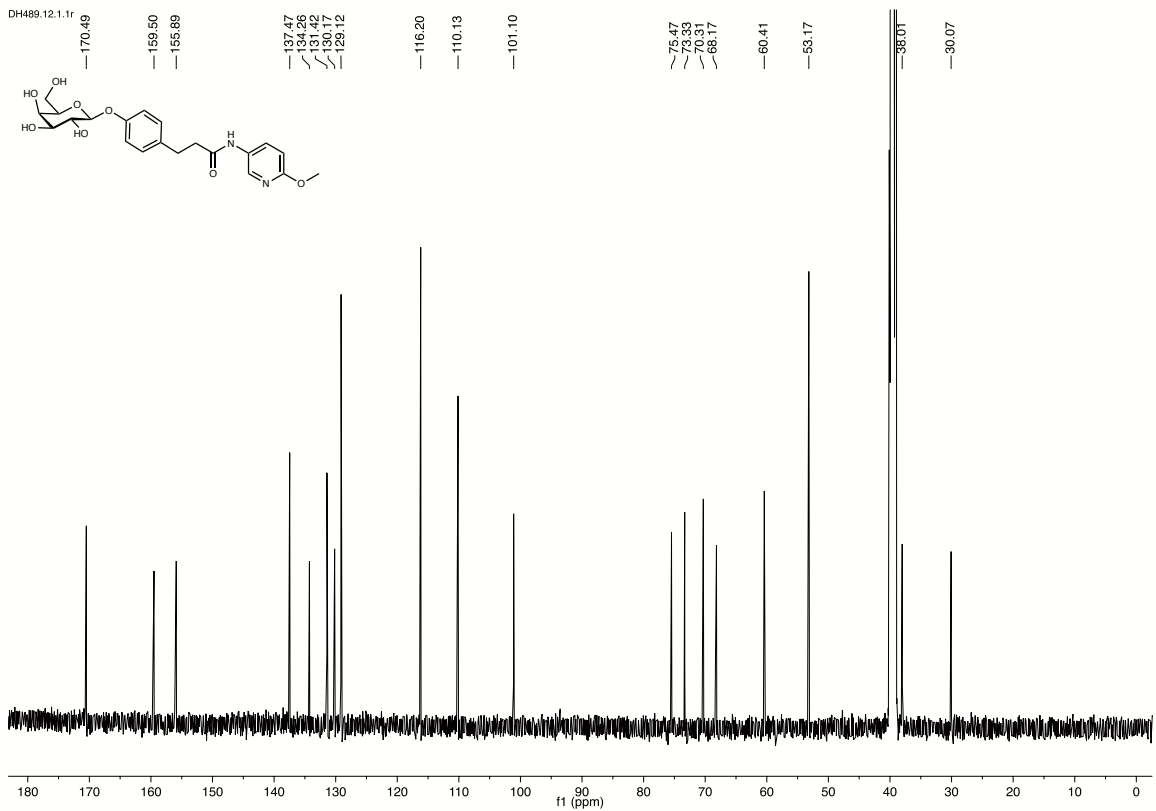
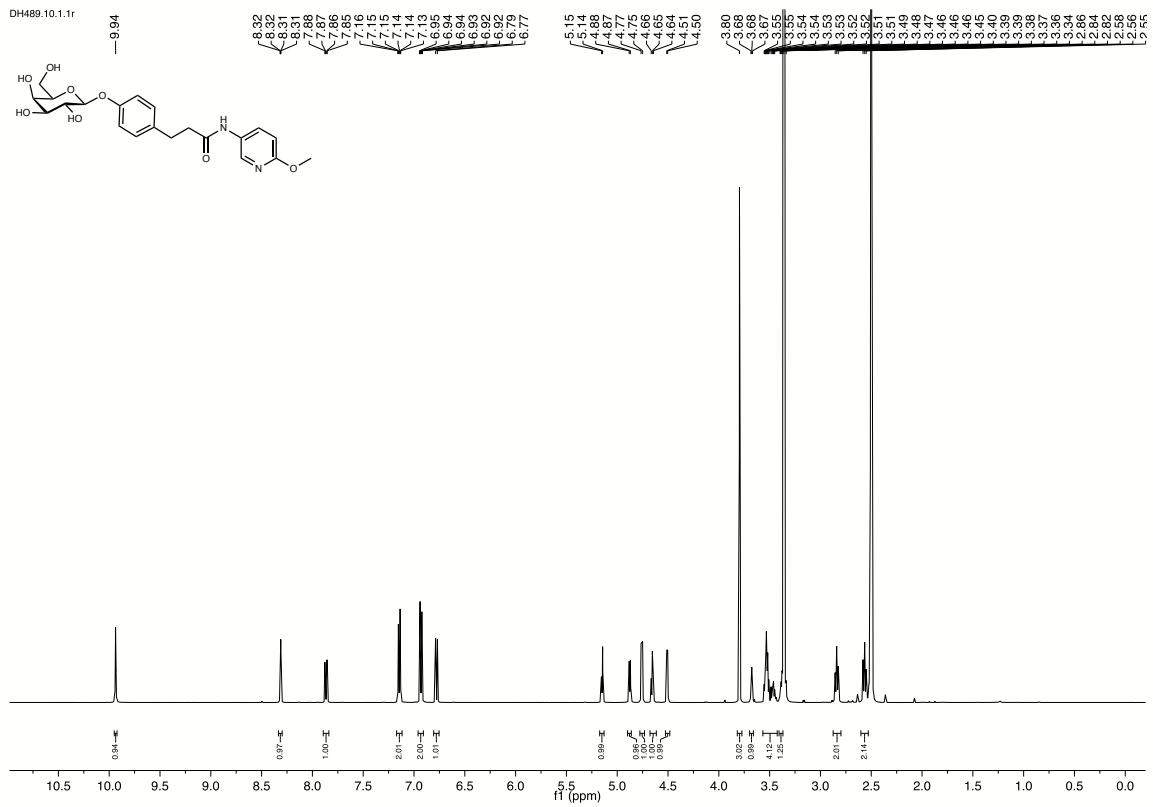
^1H and ^{13}C NMR of **D2**



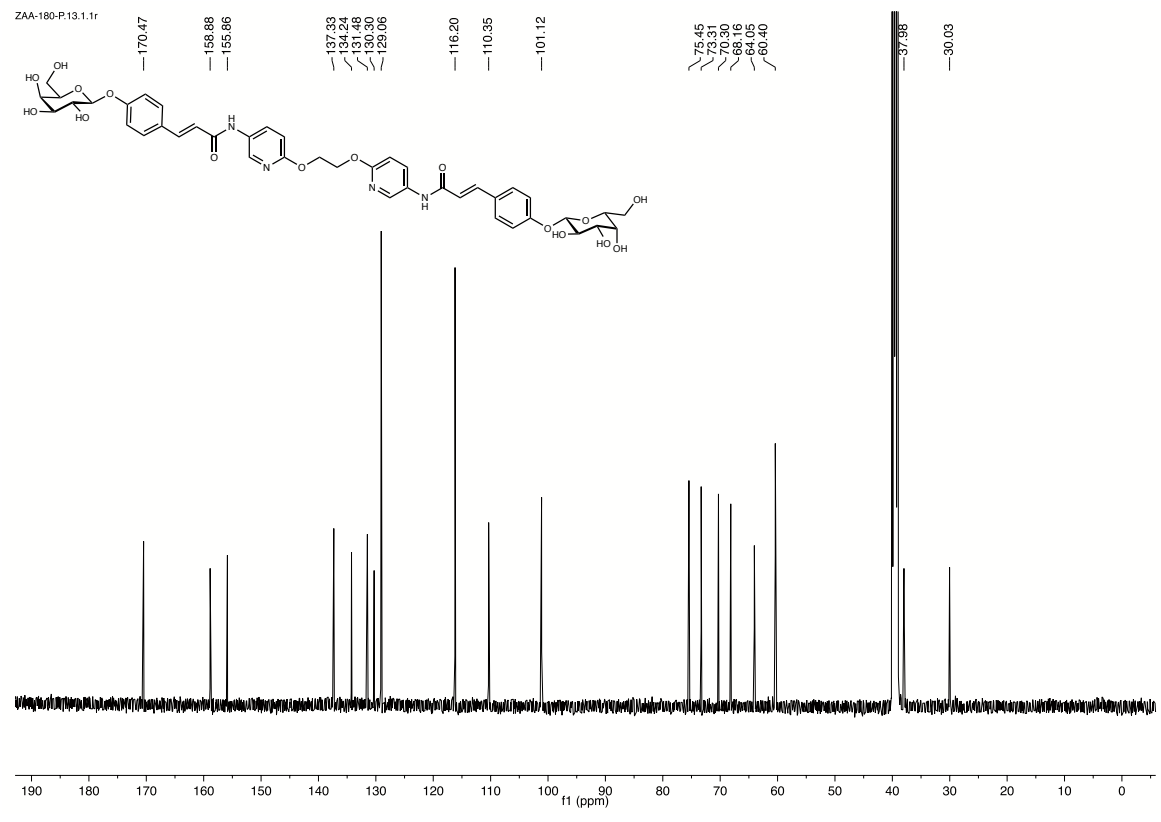
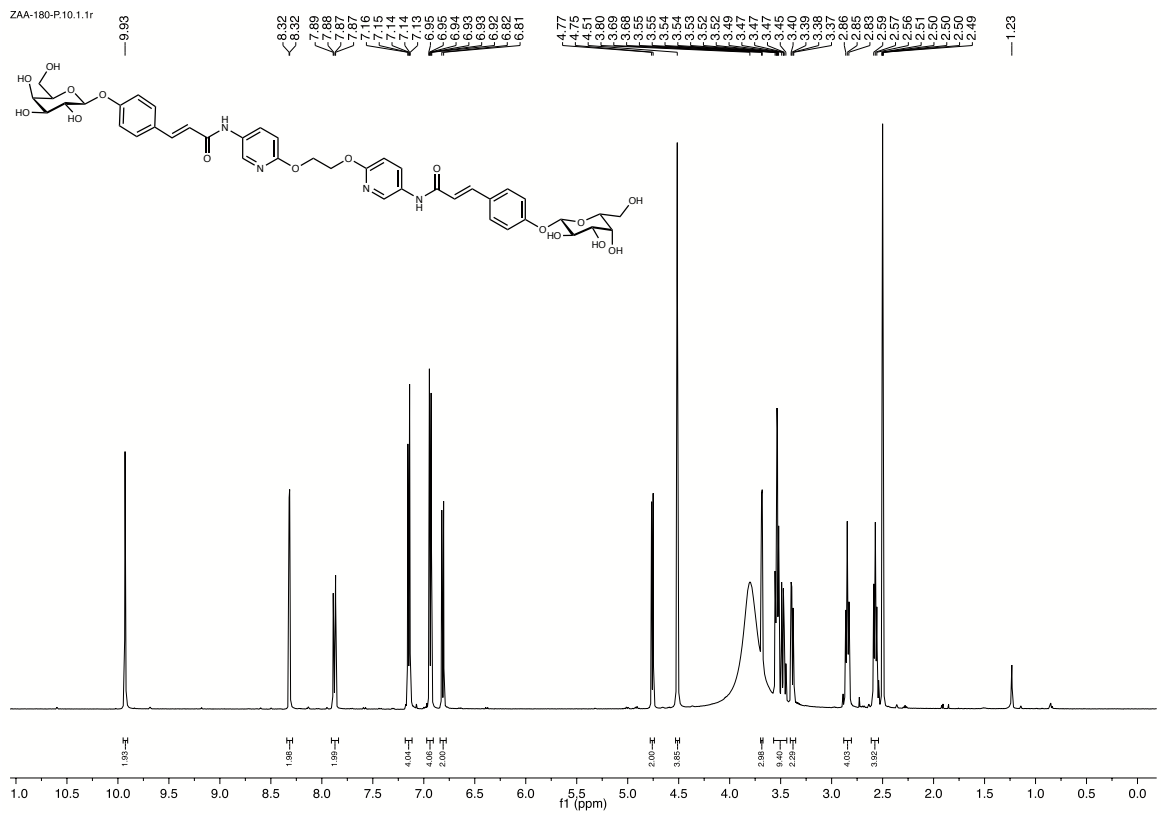
^1H and ^{13}C NMR of **E2**



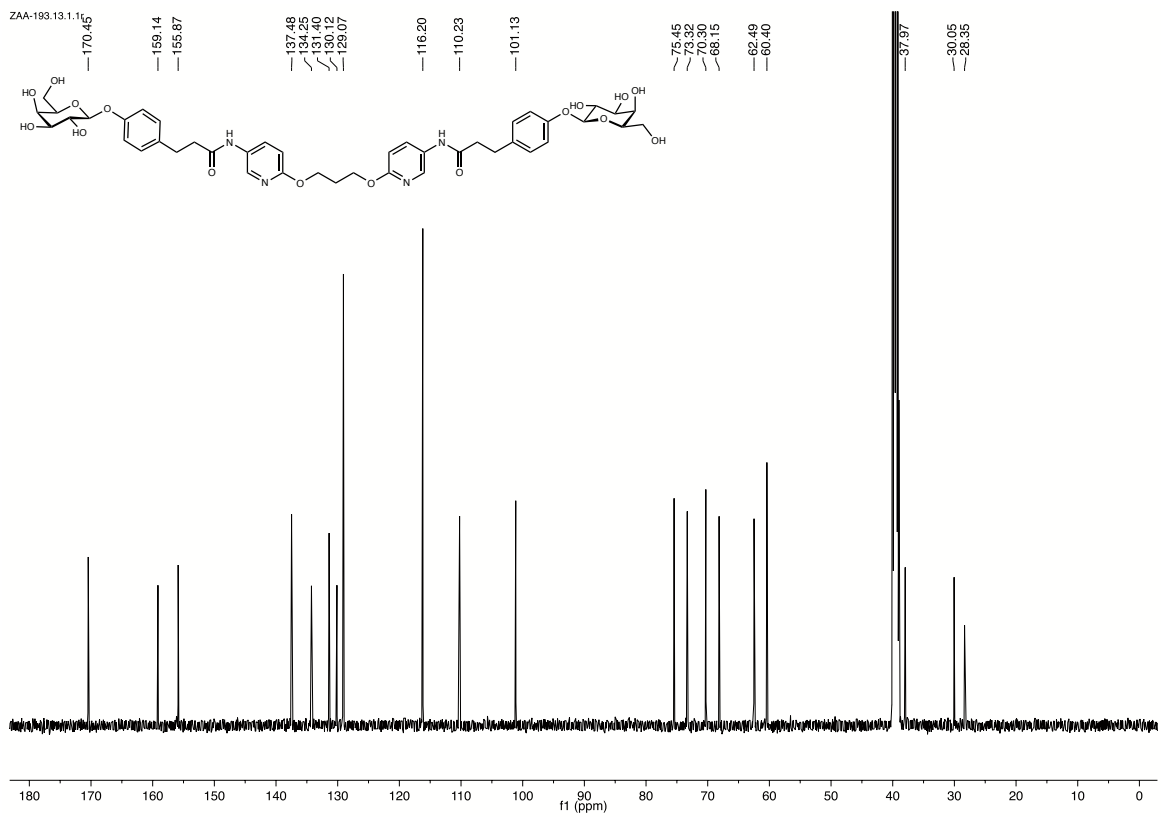
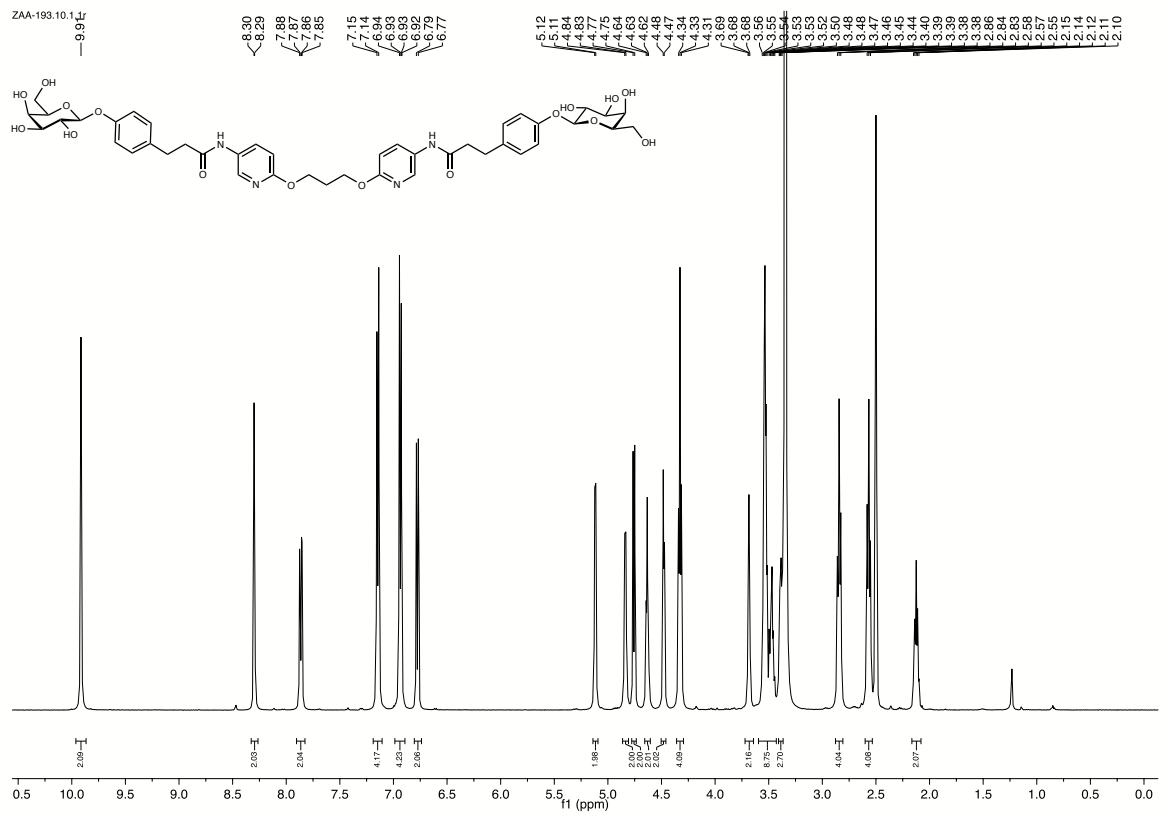
^1H and ^{13}C NMR of F2



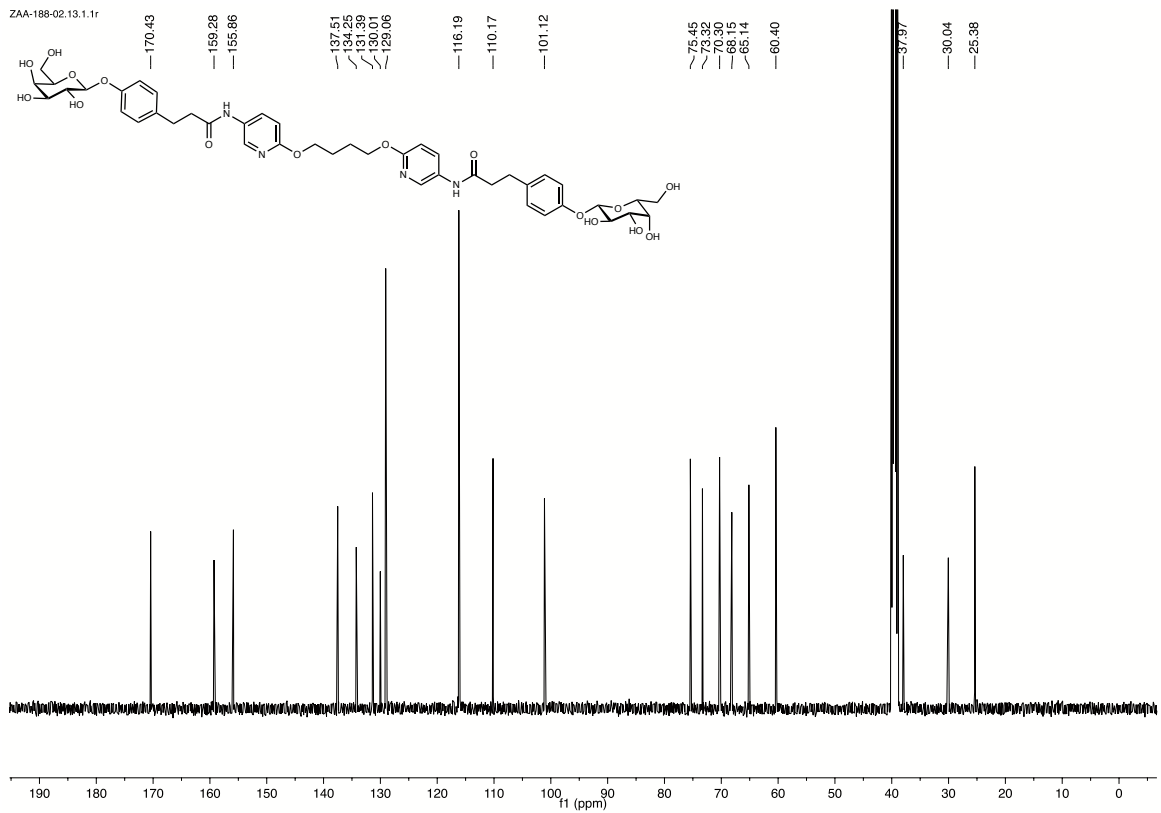
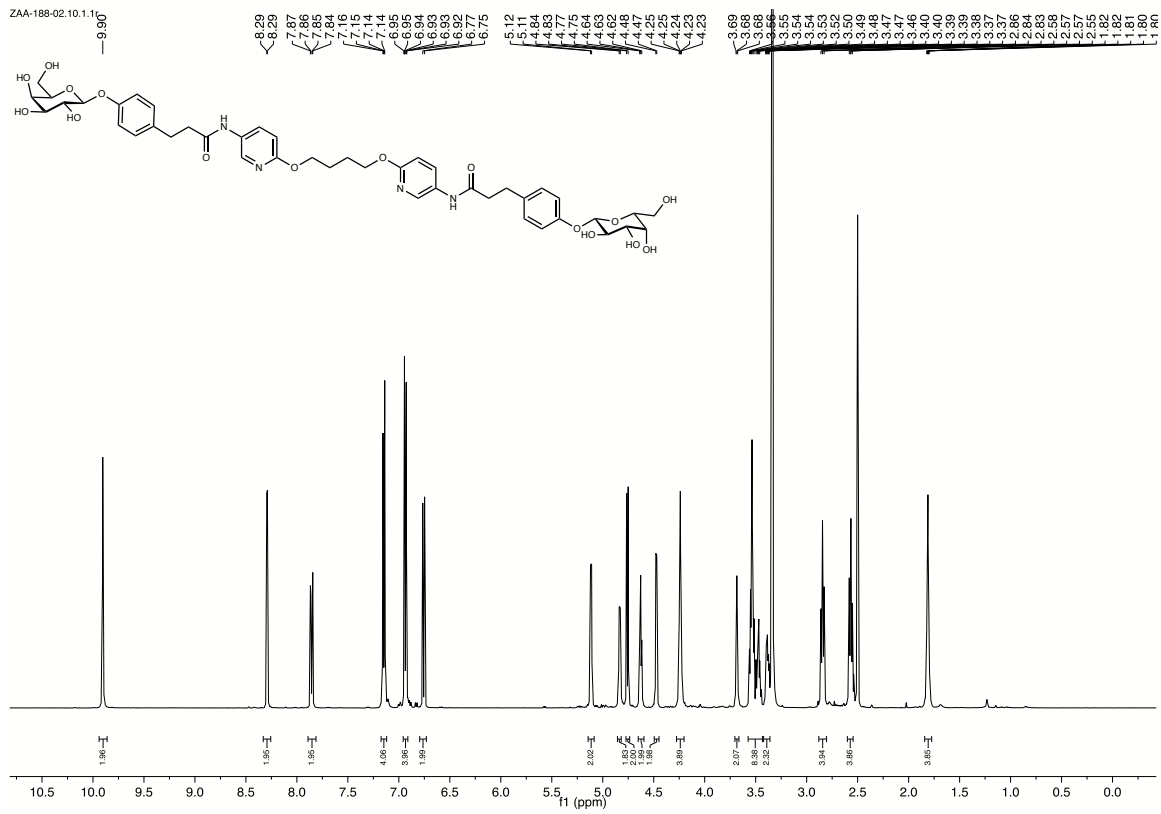
^1H and ^{13}C NMR of **G2**



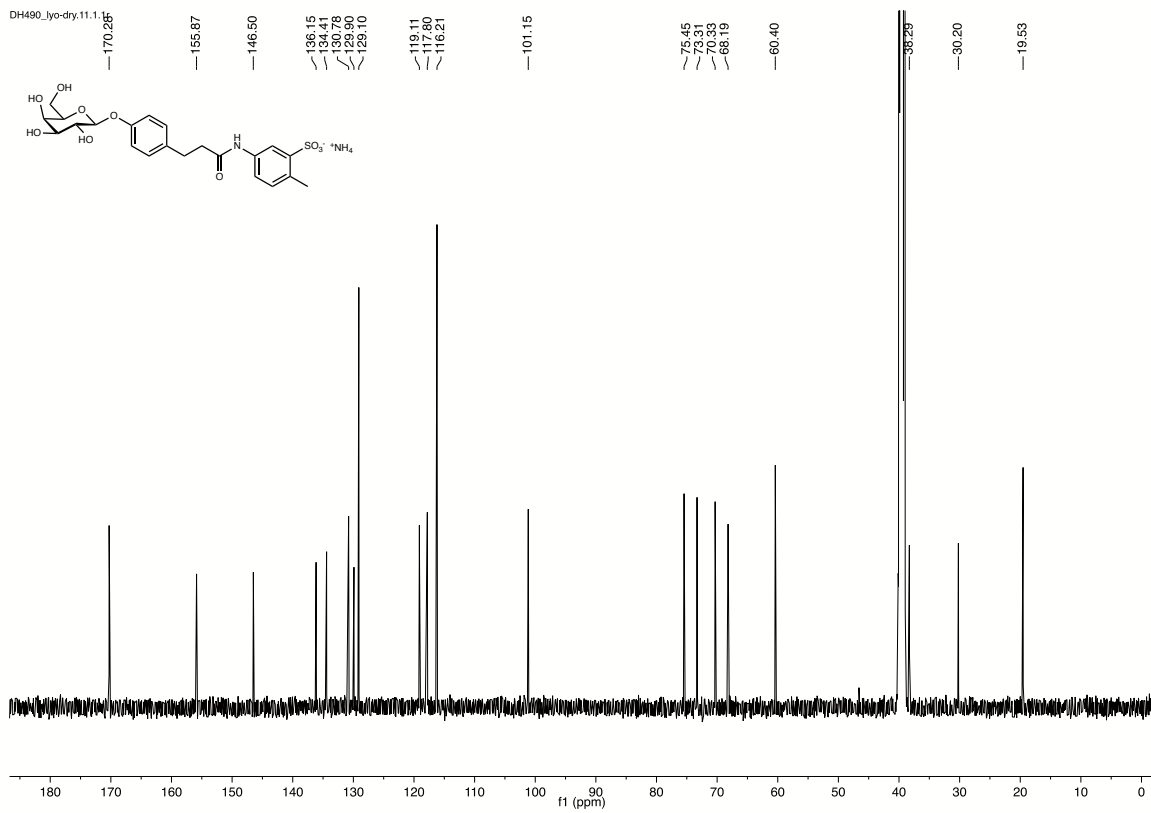
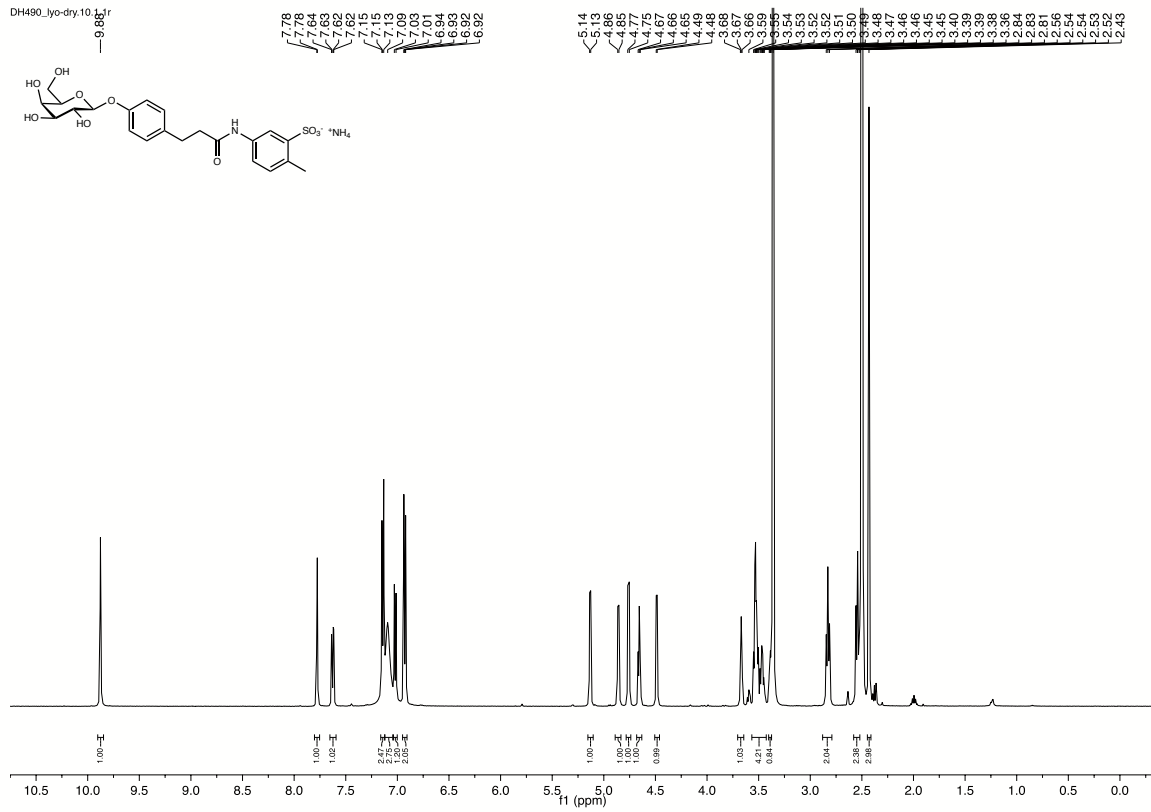
^1H and ^{13}C NMR of **H2**



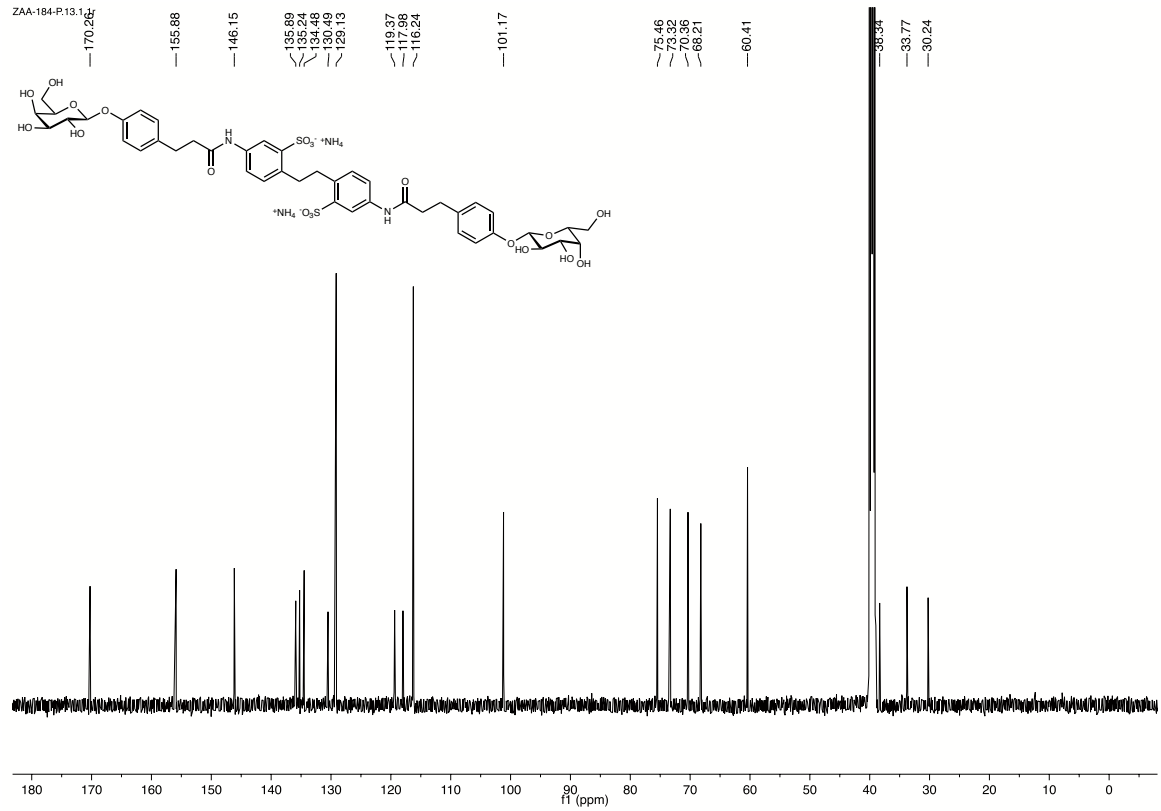
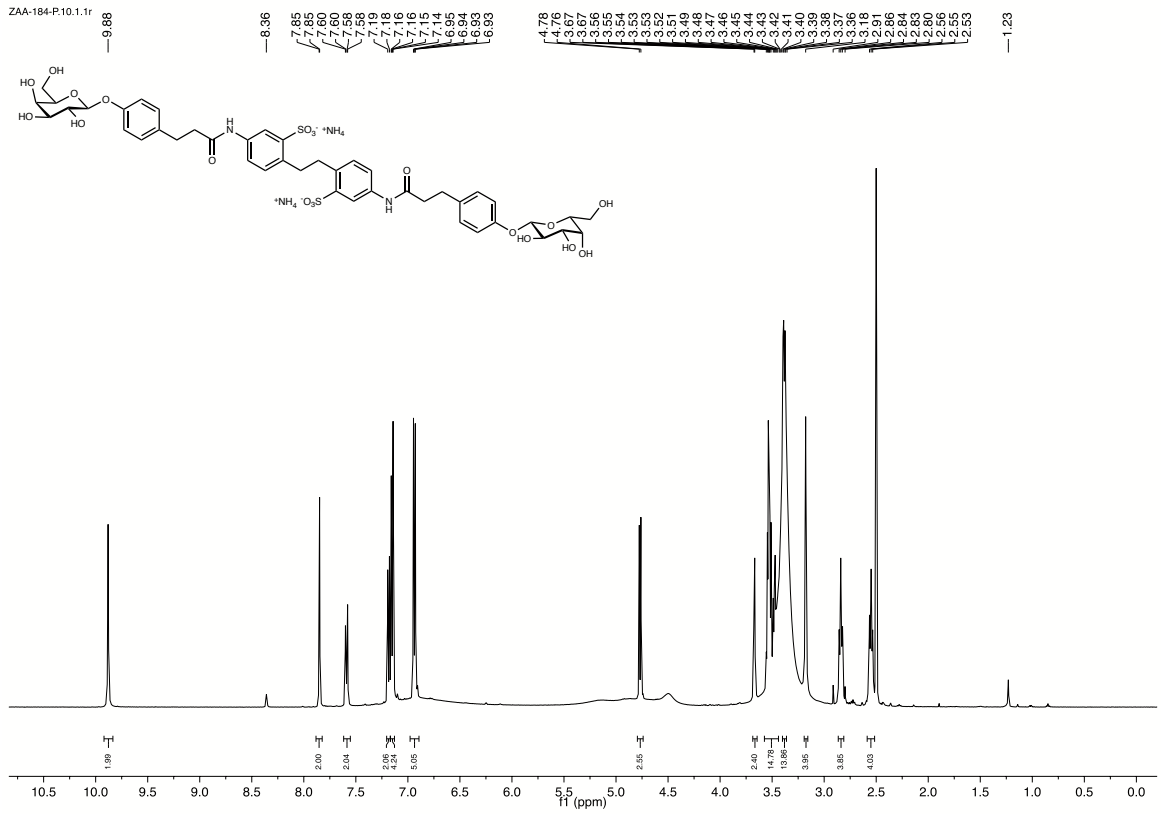
^1H and ^{13}C NMR of **12**



^1H and ^{13}C NMR of **J2**



^1H and ^{13}C NMR of **K2**

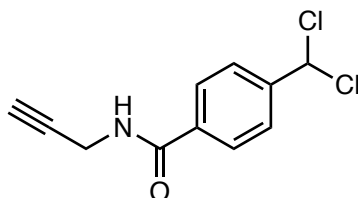


¹H and ¹³C NMR of L2

6.4 Supplementary information for chapter 3.4

Compounds synthesis

4-(Dichloromethyl)-N-(prop-2-yn-1-yl)benzamide (3)



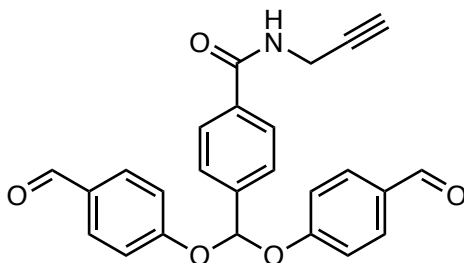
4-Formylbenzoic acid (**2**, 283.0 mg, 1.89 mmol) was dissolved in thionyl chloride (6 mL, 82.21 mmol). The reaction was stirred at 80 °C for 20 h. The solvent was removed *in vacuo*. Crude 4-(dichloromethyl)benzoyl chloride intermediate (98.0 mg) was dissolved in dichloromethane (2 mL). The reaction was cooled to 0 °C and triethyl amine (183 μL, 1.32 mmol) and propargyl amine (56 μL, 0.88 mmol) were added dropwise. The mixture was allowed to warm to room temperature and stirred for 3 h. The reaction was poured over water and extracted with dichloromethane. Combined organic phases were washed with satd. NaHCO₃ and brine, dried over anhydrous Na₂SO₄, filtered and concentrated *in vacuo*. The product was purified by normal phase MPLC (petrol ether/ethyl acetate, 5–60% ethyl acetate). Compound **10** was obtained as a white solid (17.2 mg, 0.07 mmol, 16% over two steps).

¹H NMR (500 MHz, CDCl₃) δ 7.82 (d, *J* = 8.1 Hz, 2H, ArH), 7.65 (d, *J* = 8.1 Hz, 2H, ArH), 6.73 (s, 1H, CHCl₂), 6.33 (s, 1H, NH), 4.27 (dd, *J* = 5.0, 2.3, 2H, CH₂), 2.30 (s, 1H, C≡CH).

¹³C NMR (126 MHz, CDCl₃) δ 166.21 (C=O), 143.69 (ArC), 135.22 (ArC), 127.74 (2C, ArCH), 126.69 (2C, ArCH), 79.30 (C≡CH), 72.31 (C≡CH), 70.89 (CHCl₂), 30.04 (CH₂).

HPLC-MS: [C₁₁H₉Cl₂NO + H]⁺ calcd. 242.01, found 241.89.

4-(Bis(4-formylphenoxy)methyl)-N-(prop-2-yn-1-yl)benzamide (4)



Compound **3** (35.9 mg, 0.15 mmol), 4-hydroxybenzaldehyde (106 mg, 1.59 mmol) and potassium carbonate (91.5 mg, 0.66 mmol) were dissolved in dry dimethylformamide (5 mL), heated to 80 °C and stirred for 44 h. After cooling down to room temperature, the 4-hydroxybenzaldehyde (72.5 mg, 0.65 mmol) and potassium carbonate (92.1 mg, 0.67 mmol) were added. The reaction was heated to 80 °C and stirred for additional 24 h. After cooling

down to room temperature, the reaction was diluted with ethyl acetate and washed with water, satd. NaHCO₃ and brine, dried over anhydrous Na₂SO₄, filtered and concentrated *in vacuo*. The product was purified by normal phase MPLC (petrol ether/ethyl acetate, 10–70% ethyl acetate). **4** was obtained as a white solid (41.2 mg, 0.10 mmol, 67%).

¹H NMR (500 MHz, CDCl₃) δ 9.89 (s, 2H, CHO), 7.86 (d, *J* = 7.8 Hz, 2H, ArH), 7.81 (d, *J* = 8.4 Hz, 4H, ArH), 7.70 (d, *J* = 8.0 Hz, 2H, ArH), 7.13 (d, *J* = 8.3 Hz, 4H, ArH), 6.93 (s, 1H, CH), 6.41 (s, 1H, NH), 4.25 (dd, *J* = 4.6, 2.1 Hz, 2H, CH₂), 2.28 (s, 1H, C≡CH).

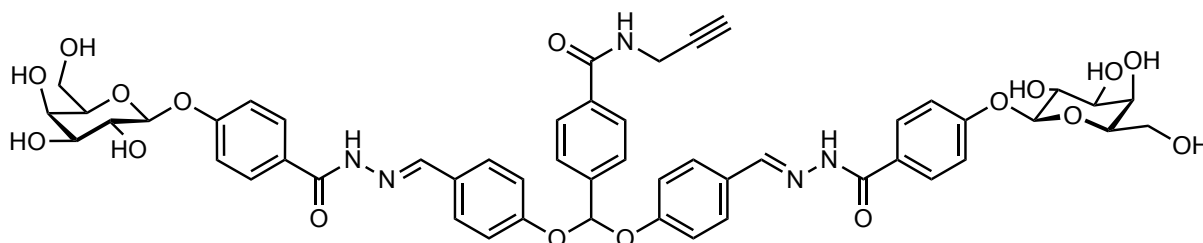
¹³C NMR (126 MHz, CDCl₃) δ 190.87 (O=CH), 166.51 (C=O), 160.20 (ArC), 139.22 (ArC), 135.24 (ArC), 132.05 (4C, ArCH), 131.74 (ArC), 127.85 (2C, ArCH), 127.16 (2C, ArCH), 117.58 (4C, ArCH), 98.92 (CH), 79.26 (C≡CH), 72.29 (C≡CH), 30.04 (CH₂).

HPLC-MS: [C₂₅H₁₉NO₅ + H]⁺ calcd. 414.13, found 414.10.

HRMS: [C₂₅H₁₉NO₅ + H]⁺ calcd. 414.1336, found 414.1333.

Synthesis of galactoside **5** is described in Chapter 6.2 under compound number **1p** and synthesis of azide modified fluorescein **6** is described in Chapter 6.1 under compound number **28**.

Divalent ligand **7**



Compound **4** (15.1 mg, 36.5 μmol) and hydrazide **5** (51.6 mg, 164 μmol) were dissolved in 1.5 mL dimethyl sulfoxide and 20 μL of formic acid was added. After 2.5 h, the reaction was lyophilized. The compound **7** was purified by preparative HPLC (water/acetonitrile, gradient of 15–40% acetonitrile). Compound **7** (32.3 mg, 32.1 μmol, 83%) was obtained as a white solid.

¹H NMR (500 MHz, DMSO-*d*₆) δ 11.70 (s, 2H, N-NH), 9.03 (t, *J* = 5.6 Hz, 1H, CONH), 8.38 (s, 2H, N=CH), 7.94 (d, *J* = 8.1 Hz, 2H, ArH), 7.88 (d, *J* = 8.4 Hz, 4H, ArH), 7.80 (d, *J* = 8.0 Hz, 2H, ArH), 7.68 (d, *J* = 8.3 Hz, 4H, ArH), 7.37 (s, 1H, CH), 7.23 – 7.03 (m, 8H, ArH), 5.25 (s, 2H, OH-2), 5.03 – 4.85 (m, 4H, H-1, OH-3), 4.70 (s, 2H, OH-6), 4.57 (s, 2H, OH-4), 4.06 (dd, *J* = 5.6, 2.6 Hz, 2H, CH₂), 3.72 (d, *J* = 3.3 Hz, 2H, H-4), 3.67 – 3.47 (m, 8H, H-2, H-5, H-6), 3.47 – 3.41 (m, 2H, H-3), 3.14 (t, *J* = 2.5 Hz, 1H, C≡CH).

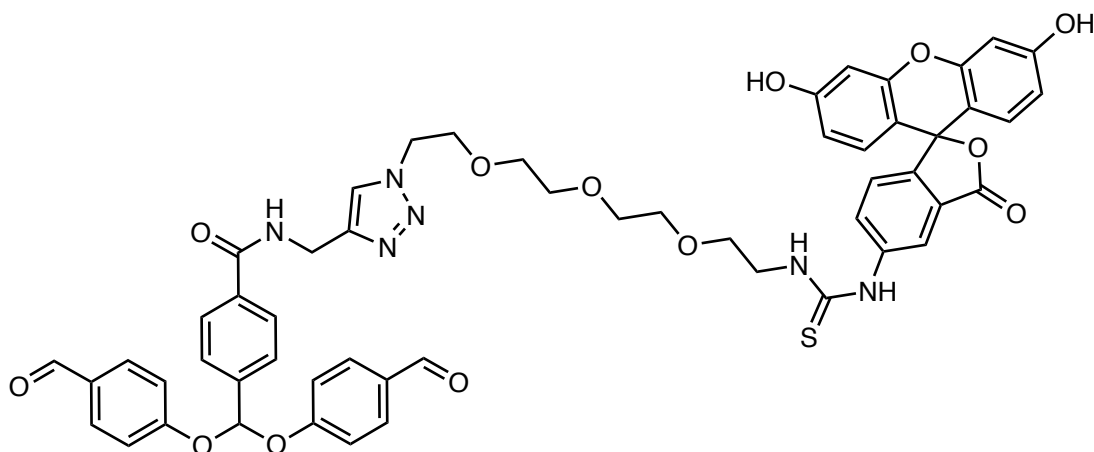
¹³C NMR (126 MHz, DMSO-*d*₆) δ 165.59 (1C, C=O), 162.48 (2C, C=O), 160.09 (2C, ArC), 156.85 (2C, ArC), 146.82 (2C, N=CH), 139.73 (1C, ArC), 134.93 (1C, ArC), 129.40 (4C, ArCH), 128.92 (2C, ArC), 128.71 (4C, ArCH), 127.75 (2C, ArCH), 127.01 (2C, ArCH), 126.56

(2C, ArC), 117.26 (4C, ArCH), 115.81 (4C, ArCH), 100.45 (2C, C-1), 98.09 (1C, CH), 81.27 (1C, $\underline{C}\equiv\text{CH}$), 75.65 (2C, C-5), 73.32 (2C, C-3), 73.06 (1C, $\underline{C}\equiv\text{CH}$), 70.25 (2C, C-2), 68.18 (2C, C-4), 60.40 (2C, C-6), 28.61 (1C, CH_2).

HPLC-MS: $[\text{C}_{51}\text{H}_{51}\text{N}_5\text{O}_{17} + \text{H}]^+$ calcd. 1006.34, found 1006.44.

HRMS: $[\text{C}_{51}\text{H}_{51}\text{N}_5\text{O}_{17} + \text{H}]^+$ calcd. 1006.3353, found 1006.3359.

Bis-benzaldehyde fluorescent linker 8



Azide modified fluorescein (**6**, 16.9 mg, 27.8 μmol) and bis-benzaldehyde **4** (10.3 mg, 24.9 μmol) were dissolved in dimethylformamide (1.5 mL). CuSO_4 solution (75 μL , 100 mM in water, 7.5 μmol) and sodium ascorbate solution (75 μL , 100 mM in water, 7.5 μmol) were added. The reaction was stirred at r.t. for 2 days and then dried *in vacuo*. The product **8** was purified by preparative HPLC (water/acetonitrile with 0.1% formic acid, gradient of 30–60% acetonitrile). Compound **8** was obtained as a yellow solid (16.7 mg, 16.4 μmol , 66%).

^1H NMR (500 MHz, DMSO-d_6) δ 10.14 (s, 2H, OH-fluorescein), 10.05 (s, 1H, NH-thiourea), 9.87 (s, 2H, CHO), 9.11 (t, $J = 5.7$ Hz, 1H, NH-thiourea), 8.27 (s, 1H, ArH-fluorescein), 8.10 (s, 1H, CONH), 7.98 – 7.91 (m, 3H, ArH, CH-triazole), 7.87 (d, $J = 8.7$ Hz, 4H, ArH), 7.79 (d, $J = 8.3$ Hz, 2H, ArH), 7.73 (d, $J = 7.8$ Hz, 1H, ArH-fluorescein), 7.57 (s, 1H, CH), 7.25 (d, $J = 8.7$ Hz, 4H, ArH), 7.17 (d, $J = 8.3$ Hz, 1H, ArH-fluorescein), 6.67 (d, $J = 2.2$ Hz, 2H, ArH-fluorescein), 6.62 – 6.53 (m, 4H, ArH-fluorescein), 4.53 – 4.44 (m, 4H, CH_2), 3.78 (t, $J = 5.2$ Hz, 2H, CH_2), 3.67 (s, 2H, CH_2), 3.57 (t, $J = 5.4$ Hz, 2H, CH_2), 3.54 – 3.44 (m, 8H, CH_2).

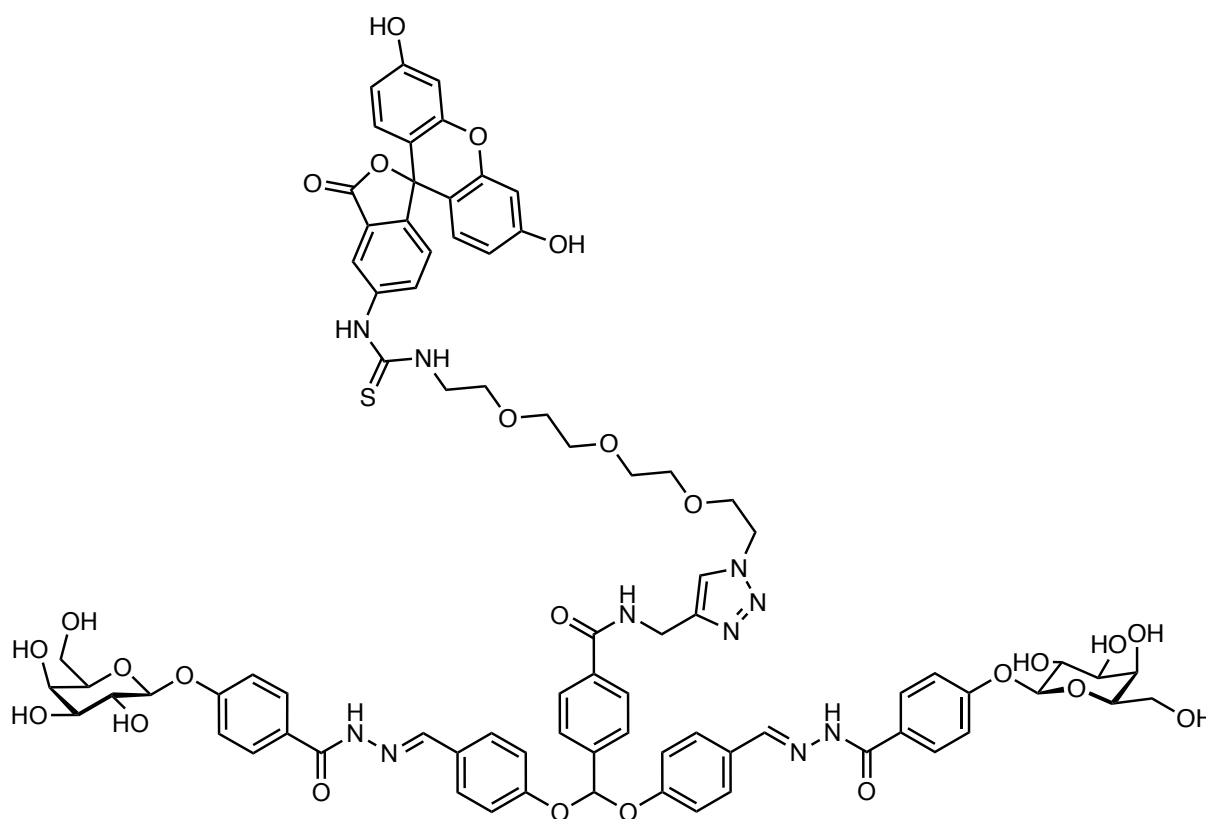
^{13}C NMR (126 MHz, DMSO-d_6) δ 191.50 (2C, $\text{O}=\text{CH}$), 180.53 (1C, $\text{C}=\text{S}$), 168.55 (1C, $\text{C}=\text{O}$, fluorescein), 165.60 (1C, $\text{C}=\text{O}$), 159.96 (2C, ArC), 159.51 (2C, ArC-fluorescein), 151.90 (2C, ArC-fluorescein), 147.16 (2C, ArC-fluorescein), 144.86 (1C, $\underline{C}\equiv\text{CH}$ -triazole), 141.33 (1C, ArC-fluorescein), 138.66 (1C, ArC), 135.48 (1C, ArC), 131.81 (4C, ArCH), 131.10 (2C, ArC) 129.44 (1C, ArC-fluorescein), 129.08 (4C, ArCH-fluorescein), 127.81 (2C, ArCH), 126.91 (2C, ArCH), 126.58 (1C, ArC-fluorescein), 124.11 (1C, ArCH-fluorescein), 123.33 (1C,

C=CH-triazole), 117.01 (4C, ArCH), 116.37 (1C, ArCH-fluorescein), 112.61 (1C, ArCH-fluorescein), 109.72 (2C, ArC-fluorescein), 102.25 (2C, ArCH-fluorescein), 97.59 (1C, CH), 69.73 (1C, CH₂), 69.64 (2C, CH₂), 69.54 (1C, CH₂), 68.75 (1C, CH₂), 68.41 (1C, CH₂), 49.29 (1C, CH₂), 43.71 (1C, CH₂), 34.90 (1C, CH₂).

HPLC-MS: [C₅₄H₄₈N₆O₁₃S + 2H]²⁺ calcd. 511.16, found 511.15.

HRMS: [C₅₄H₄₈N₆O₁₃S + 2H]²⁺ calcd. 511.1573, found 511.1572.

Divalent fluorescent ligand **9**



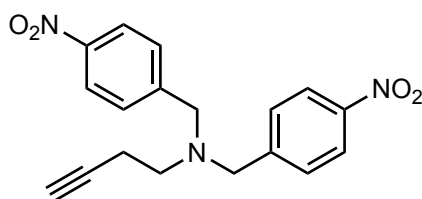
Compound **8** (4.4 mg, 4.3 μmol) and hydrazide **5** (5.8 mg, 18.5 μmol) were dissolved in 450 μL dimethyl sulfoxide and 40 μL of formic acid was added. After 7.5 h, the reaction was diluted with water and lyophilized. Purification by preparative HPLC (water/acetonitrile with 0.1% formic acid, gradient of 15–40% acetonitrile) gave product **9** (2.9 mg, 1.5 μmol, 35%, ≈90% purity) as a yellow powder.

HPLC-MS: [C₈₀H₈₀N₁₀O₂₅S + 2H]²⁺ calcd. 807.26, found 807.78.

HRMS: [C₈₀H₈₀N₁₀O₂₅S + 2H]²⁺ calcd. 807.2581, found 807.2589.

Monohydrolyzed product (impurity) HPLC-MS: [C₆₇H₆₄N₈O₁₉S + 2H]²⁺ calcd. 659.21, found 659.30.

N,N-Bis(4-nitrobenzyl)but-3-yn-1-amine (**11**)



But-3-yn-1-amine hydrochloride (**10**, 55.2 mg, 0.55 mmol), 4-nitrobenzyl bromide (327 mg, 1.52 mmol) and potassium carbonate (264 mg, 1.91 mmol) were suspended in dimethylformamide (4 mL) and stirred at r.t. overnight. The reaction was diluted with dichloromethane and water, organic phase was washed with satd. aqueous NaHCO₃ and half satd. brine, dried over anhydrous Na₂SO₄, filtered and concentrated *in vacuo*. Purification by normal phase MPLC (petrol ether/ethyl acetate, 5–35% ethyl acetate) gave **11** (134 mg, 0.39 mmol, 75%) as a pale-yellow solid.

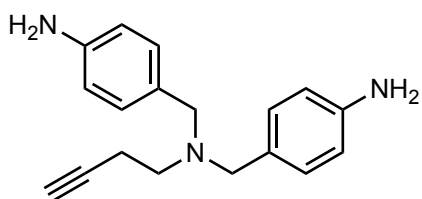
¹H NMR (500 MHz, Acetone-d₆) δ 8.24 – 8.16 (m, 4H, ArCH), 7.76 (d, *J* = 8.7 Hz, 4H, ArCH), 3.85 (s, 4H, Ar-CH₂), 2.73 (td, *J* = 7.2, 1.4 Hz, 2H, CH₂CH₂N), 2.52 – 2.45 (m, 2H, CH₂CH₂N), 2.43 (t, *J* = 2.7 Hz, 1H, C≡CH).

¹³C NMR (126 MHz, Acetone-d₆) δ 148.49 (2C, ArC), 148.07 (2C, ArC), 130.45 (4C, ArCH), 124.19 (4C, ArCH), 83.26 (1C, C≡CH), 71.06 (1C, C≡CH), 58.04 (2C, Ar-CH₂), 53.19 (1C, CH₂CH₂N), 17.40 (1C, CH₂CH₂N).

HPLC-MS: [C₁₈H₁₇N₃O₄ + H]⁺ calcd. 340.13, found 340.15.

HRMS: [C₁₈H₁₇N₃O₄ + H]⁺ calcd. 340.1292, found 340.1289.

N,N-Bis(4-aminobenzyl)but-3-yn-1-amine (**12**)



Compound **11** (21.8 mg, 64.2 μmol), iron powder (17.7 mg, 317 μmol) and CaCl₂ (22.4 mg, 202 μmol) were suspended in ethanol/water mixture (1 mL, 8:2) under argon atmosphere. The reaction was stirred at r.t. for 1 day, heated to 40 °C for 2 days and then stirred at r.t. for 1 week. The iron was filtered off and the reaction was dried *in vacuo*. Purification by normal phase MPLC (petrol ether/ethyl acetate with 2% NH₃OH, 10–50% ethyl acetate) gave product **12** (12.5 mg, 44.7 μmol, 70%, impure) as a yellow powder.

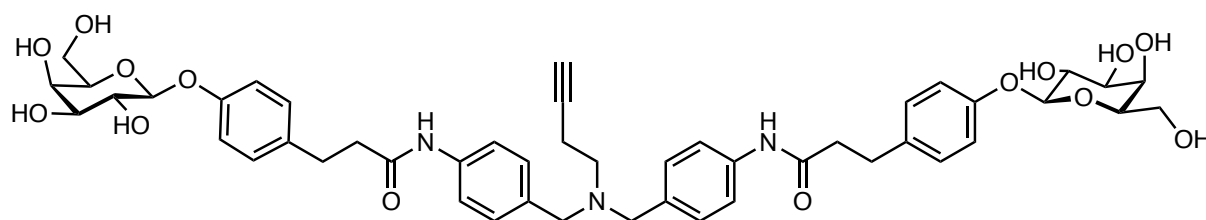
^1H NMR (500 MHz, MeOH- d_4) δ 7.08 (d, J = 8.0 Hz, 4H, ArH), 6.70 (d, J = 7.9 Hz, 4H, ArH), 3.47 (s, 4H, Ar- CH_2N), 2.60 (t, J = 7.6 Hz, 2H, $\text{CH}\equiv\text{CCH}_2\text{CH}_2\text{N}$), 2.33 – 2.27 (m, 2H, $\text{CH}\equiv\text{CCH}_2\text{CH}_2\text{N}$), 2.19 (t, J = 2.7 Hz, 1H, $\text{CH}\equiv\text{C}$).

^{13}C NMR (126 MHz, MeOH- d_4) δ 147.61 (2C, ArC), 131.12 (2C, ArCH), 129.44 (2C, ArC), 116.56 (2C, ArCH), 83.46 (1C, $\text{CH}\equiv\text{C}$), 70.27 (1C, $\text{CH}\equiv\text{C}$), 58.38 (2C, Ar- CH_2N), 52.61 (1C, $\text{CH}\equiv\text{CCH}_2\text{CH}_2\text{N}$), 17.13 (1C, $\text{CH}\equiv\text{CCH}_2\text{CH}_2\text{N}$).

HPLC-MS: $[\text{C}_{18}\text{H}_{21}\text{N}_3 + \text{H}]^+$ calcd. 280.18, found 280.13.

HRMS: $[\text{C}_{18}\text{H}_{21}\text{N}_3 + \text{H}]^+$ calcd. 280.1809, found 280.1804.

Divalent ligand 14



Bis-aniline linker **12** (26.7 mg, 95.6 μmol), galactoside **13** (71.7 mg, 218 μmol , in two portions over 2 days), HBTU (89.9 mg, 237 μmol , in two portions over 2 days) were dissolved in dimethylformamide (2 mL) and DIPEA (70 μL , 402 μmol) was added. Reaction was stirred at r.t. for 2 days, then dried *in vacuo*. Purification by preparative reverse-phase HPLC (water/acetonitrile supplemented with 0.1% formic acid, gradient of 10–40% acetonitrile) gave **14** (14.6 mg, 16.2 μmol , 17%) as a white solid.

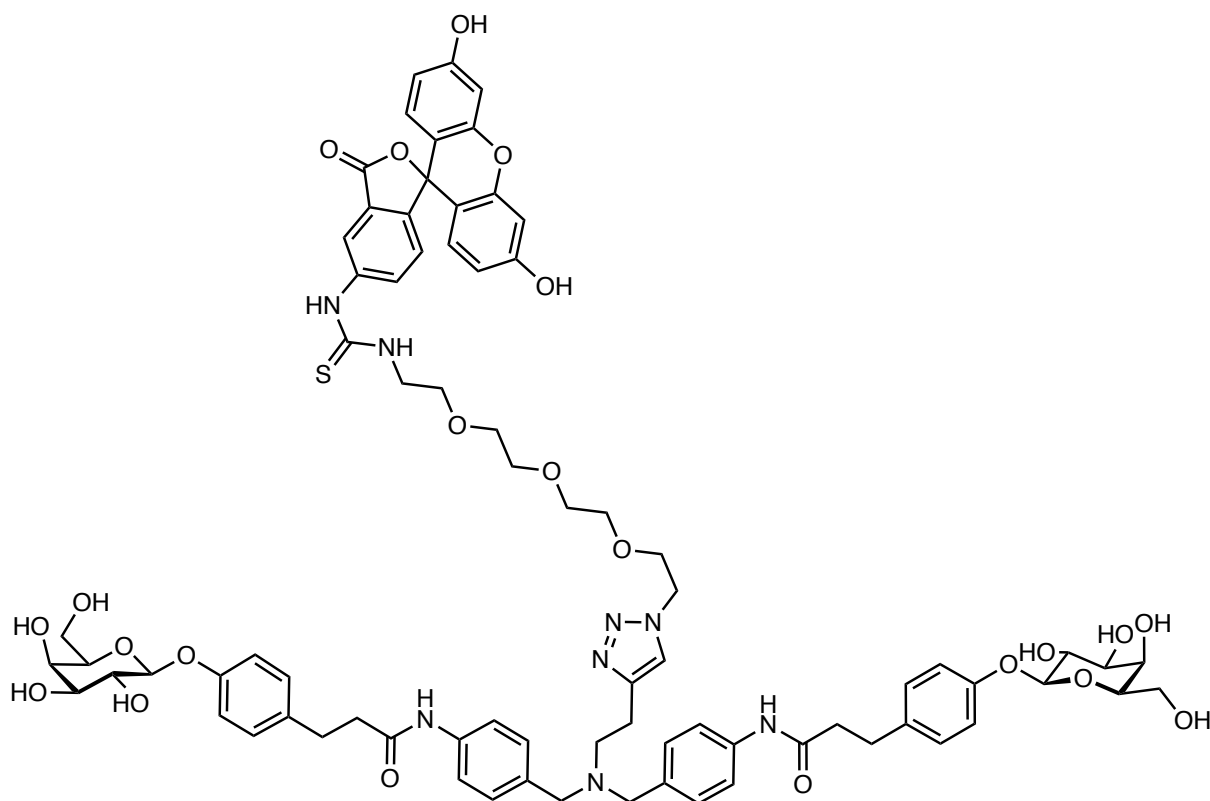
^1H NMR (500 MHz, DMSO) δ 9.90 (s, 2H, NH), 7.52 (d, J = 8.5 Hz, 4H, ArH), 7.26 (d, J = 8.4 Hz, 4H, ArH), 7.18 – 7.12 (m, 4H, ArH), 6.97 – 6.90 (m, 4H, ArH), 5.15 (s, 2H, OH-2), 4.87 (s, 2H, OH-3), 4.76 (d, J = 7.7 Hz, 2H, H-1), 4.66 (s, 2H, OH-6), 4.50 (s, 2H, OH-4), 3.67 (s, 2H, H-4), 3.58 – 3.41 (m, 14H, H-2, H-3, H-5, H-6, Ar- CH_2N), 2.84 (t, J = 7.7 Hz, 4H $\text{CH}_2\text{CH}_2\text{CONH}$), 2.77 (t, J = 2.6 Hz, 1H, $\text{CH}\equiv\text{C}$), 2.57 (t, J = 7.7 Hz, 4H, $\text{CH}_2\text{CH}_2\text{CONH}$), 2.53 – 2.51 (m, 2H, $\text{CH}\equiv\text{CCH}_2\text{CH}_2\text{N}$), 2.35 – 2.29 (m, J = 7.5, 2.7 Hz, 2H, $\text{CH}\equiv\text{CCH}_2\text{CH}_2\text{N}$).

^{13}C NMR (126 MHz, DMSO) δ 170.39 (2C, C=O), 155.88 (2C, ArC), 138.07 (2C, ArC), 134.38 (2C, ArC), 133.75 (2C, ArC), 129.12 (4C, ArCH), 128.92 (4C, ArCH), 118.95 (4C, ArCH), 116.21 (4C, ArCH), 101.12 (2C, C-1), 83.26 (1C, $\text{CH}\equiv\text{C}$), 75.48 (2C, C-5), 73.33 (2C, C-3), 71.99 (1C, $\text{CH}\equiv\text{C}$), 70.32 (2C, C-2), 68.19 (2C, C-4), 60.42 (2C, C-6), 56.51 (2C, Ar- CH_2N), 51.10 (1C, $\text{CH}\equiv\text{CCH}_2\text{CH}_2\text{N}$), 38.29 (2C, $\text{CH}_2\text{CH}_2\text{CONH}$), 30.12 (2C, $\text{CH}_2\text{CH}_2\text{CONH}$), 15.95 (1C, $\text{CH}\equiv\text{CCH}_2\text{CH}_2\text{N}$).

HPLC-MS: $[\text{C}_{48}\text{H}_{57}\text{N}_3\text{O}_{14} + \text{H}]^+$ calcd. 900.39, found 900.34.

HRMS: $[\text{C}_{48}\text{H}_{57}\text{N}_3\text{O}_{14} + \text{H}]^+$ calcd. 900.3914, found 900.3911.

Divalent fluorescent ligand **15**



Azide modified fluorescein (**6**, 4.6 mg, 7.6 μmol) and divalent ligand **14** (4.44 mg, 4.9 μmol) were dissolved in dimethylformamide (500 μL). CuSO_4 solution (30 μL , 100 mM in water, 3 μmol) and sodium ascorbate solution (100 μL , 100 mM in water, 10 μmol) were added. The reaction was stirred at r.t. for 5 days then warmed up to 35 $^\circ\text{C}$ for one day. After lyophilization, the product was purified by preparative HPLC (water/acetonitrile with 1% formic acid, 20–40% acetonitrile). The product **15** was obtained as a yellow solid (4 mg, 2.7 μmol , 54%).

^1H NMR (500 MHz, DMSO) δ 10.21 (s, 2H, NH-thiourea), 9.86 (s, 2H, NHC=O), 8.37 – 8.21 (m, 2H, ArH-fluorescein, NH-thiourea), 7.75 (d, $J = 8.3$ Hz, 1H, ArH-fluorescein), 7.70 (s, 1H, CH-triazole), 7.51 (d, $J = 8.3$ Hz, 4H, ArH), 7.21 (d, $J = 8.2$ Hz, 4H, ArH), 7.17 (s, 1H, ArH-fluorescein), 7.14 (d, $J = 8.8$ Hz, 4H, ArH), 6.96 – 6.90 (m, 4H, ArH), 6.67 (d, $J = 2.3$ Hz, 2H, ArH-fluorescein), 6.62 – 6.53 (m, 4H, ArH-fluorescein), 5.11 (s, 2H, OH-2), 4.83 (s, 2H, OH-3), 4.75 (d, $J = 7.6$ Hz, 2H, H-1), 4.63 (s, 2H, OH-6), 4.52 – 4.45 (m, 2H, OH-4), 4.43 (t, $J = 5.3$ Hz, 2H, $\text{CH}_2\text{-PEG}$), 3.76 (t, $J = 5.3$ Hz, 2H, $\text{CH}_2\text{-PEG}$), 3.72 – 3.64 (s, 4H, H-4, $\text{CH}_2\text{-PEG}$), 3.61 – 3.38 (m, 31H, H-2, H-3, H-5, H-6, $\text{Ar-CH}_2\text{N}$, $\text{CH}_2\text{-PEG}$), 2.88 – 2.74 (m, 6H, $\text{CH}_2\text{CH}_2\text{CONH}$, triazole- $\text{CH}_2\text{CH}_2\text{N}$), 2.62 – 2.53 (m, 6H, $\text{CH}_2\text{CH}_2\text{CONH}$, triazole- $\text{CH}_2\text{CH}_2\text{N}$).

^{13}C NMR (126 MHz, DMSO) δ 180.56(1C, C=S), 170.30 (2C, NHC=O), 168.55 (1C, C=O), 159.57 (2C, ArC-fluorescein), 155.84 (2C, ArC), 151.91 (2C, ArC-fluorescein), 144.97 (1C, $\text{C}=\text{CH}$ -triazole), 141.43 (1C, ArC-fluorescein), 137.96 (2C, ArC), 134.35 (2C, ArC), 133.81

(2C, ArC), 129.04 (6C, ArCH, ArCH-fluorescein), 128.85 (4C, ArCH), 124.06 (1C, ArCH-fluorescein), 122.38 (1C, C=CH-triazole), 118.87 (4C, ArCH), 116.19 (5C, ArCH, ArC-fluorescein), 112.64 (1C, ArCH-fluorescein), 109.74 (1C, ArC-fluorescein), 102.24 (2C, ArCH-fluorescein), 101.13 (2C, C-1), 75.44 (2C, C-5), 73.31 (2C, C-3), 70.30 (2C, C-2), 69.72 (1C, CH₂-PEG), 69.64 (2C, CH₂-PEG), 69.55 (1C, CH₂-PEG), 68.81 (1C, CH₂-PEG), 68.41 (1C, CH₂-PEG), 68.15 (2C, C-4), 60.39 (2C, C-6), 56.74 (2C, Ar-CH₂N), 52.40 (1C, triazole-CH₂CH₂N), 49.16 (1C, CH₂-PEG), 43.67 (1C, CH₂-PEG), 38.24 (2C, CH₂CH₂CONH), 30.08 (2C, CH₂CH₂CONH), 22.87 (1C, triazole-CH₂CH₂N).

HPLC-MS: [C₇₇H₈₆N₈O₂₂S + 2H]²⁺ calcd. 754.29, found 754.72.

HRMS: [C₇₇H₈₆N₈O₂₂S + 2H]²⁺ calcd. 754.2862, found 754.2836.

Synthesis of galactoside **13** is described in Chapter 6.3 under compound number **2**.

Biophysical evaluation

Expression and purification of LecA as well as fluorescence polarization assay were performed as described by Joachim *et al.*⁶¹ The competitive binding assay was performed in TBS/Ca²⁺ buffer (20 mM Tris, 137 mM NaCl, 2.6 mM KCl at pH 7.4 supplemented with 1 mM CaCl₂) in presence of 25% DMSO. Direct binding affinity determination to LecA was performed with direct titration of the fluorescent ligands with the protein in TBS/Ca²⁺ buffer (DMSO << 1%). Fluorescence was measured on a PheraStar FS microplate reader (BMG Labtech, GmbH, Germany) after 1 h and 24 h – no significant deviation based on incubation time were observed. Averages and standard deviations were calculated from at least two independent experiments.

Surface plasmon resonance experiments were performed on a BIACORE X100 instrument (GE Healthcare) at 25 °C as described in Chapter 6.2. Averages and standard deviations were calculated from at least three independent experiments.

Generic Display Report (all)

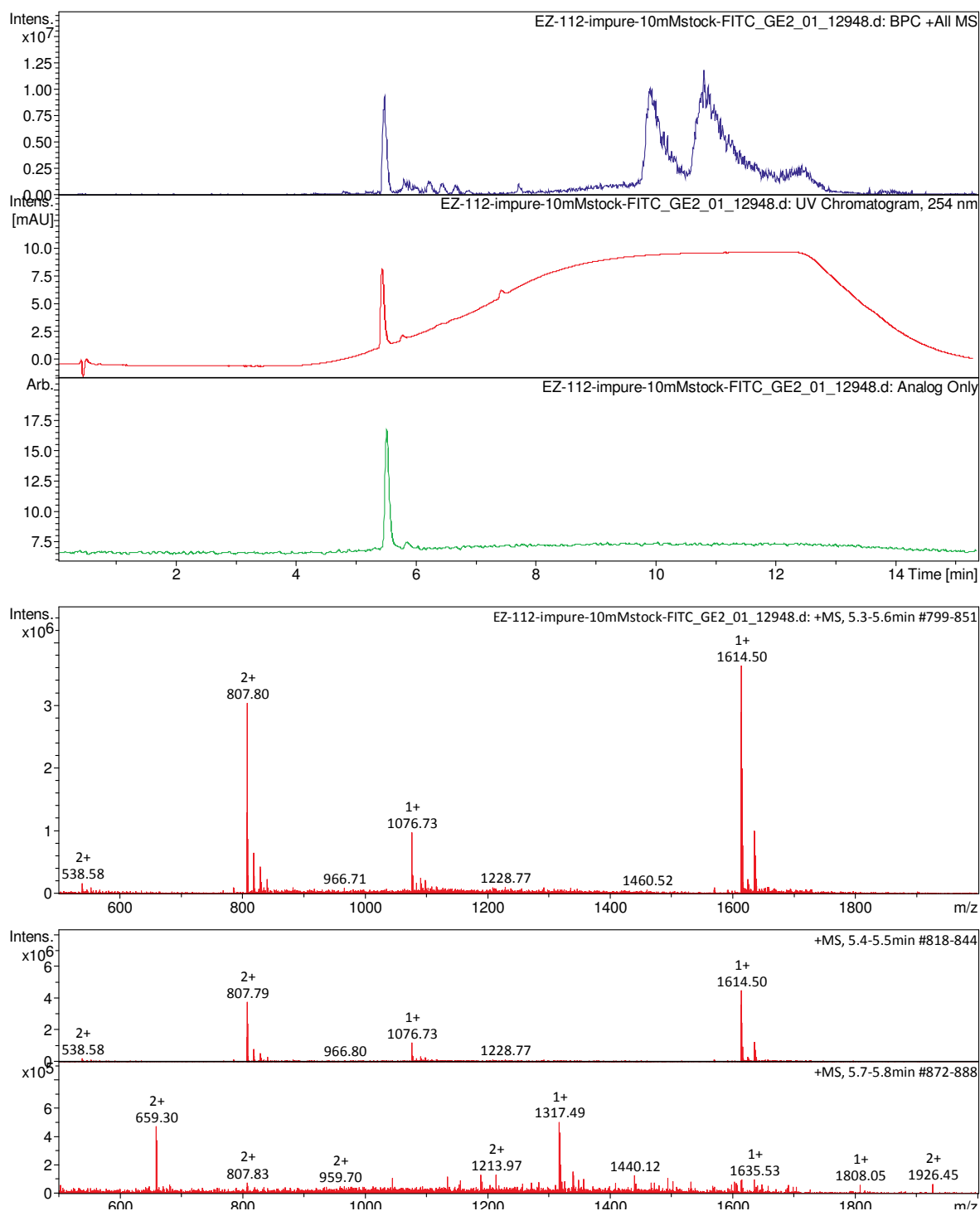


Figure S1: HPLC-MS chromatogram of the divalent fluorescent ligand **9** from its DMSO stock. The analogue window (in green) display fluorescent detector signal set for fluorescein. The m/z of the major peak with retention time 5.5 min corresponds to compound **9** (m/z 807.8²⁺) while the minor peak with retention time 5.8 min corresponds to monohydrolyzed side product (m/z 659.3²⁺).

Generic Display Report (all)

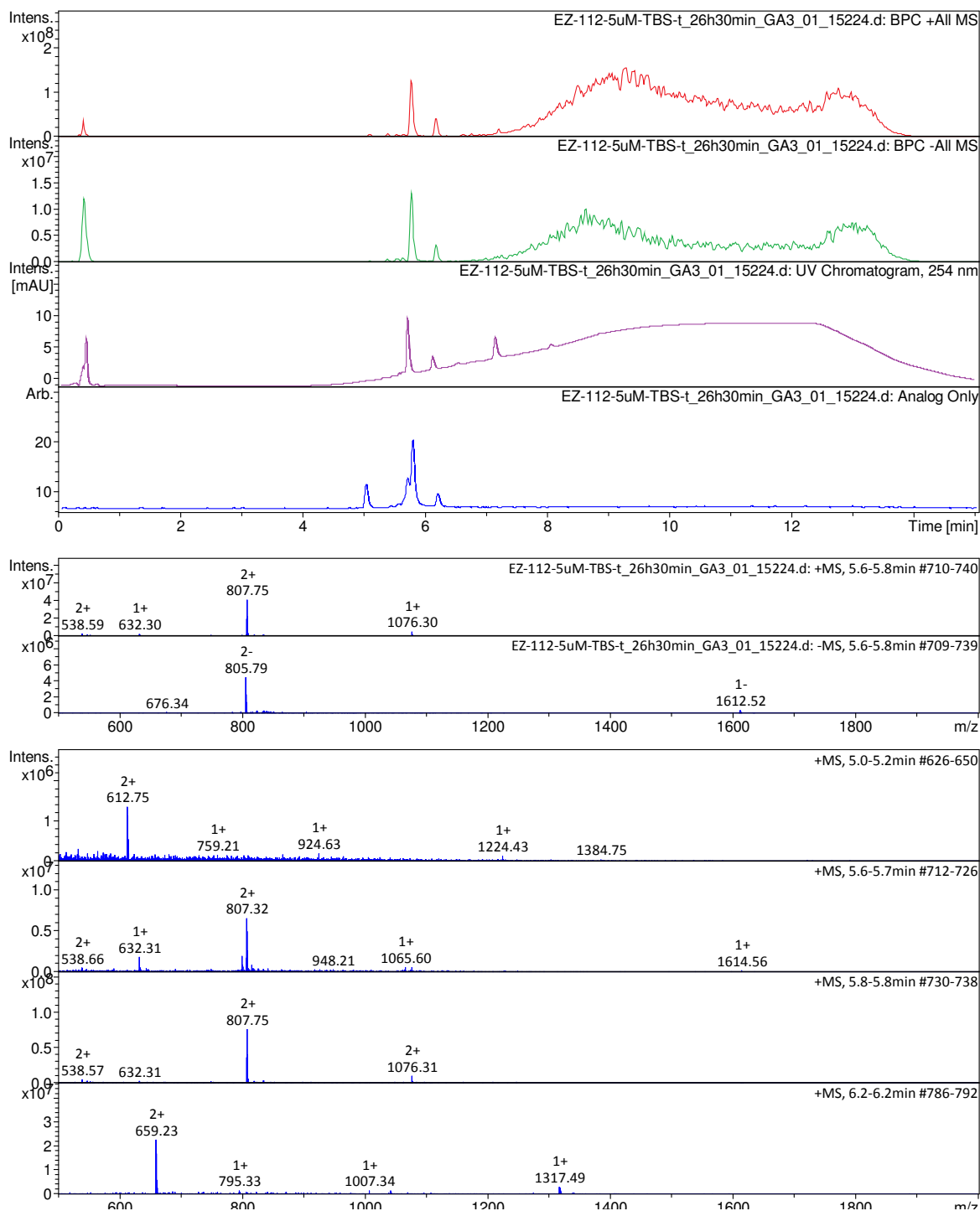


Figure S2: HPLC-MS chromatogram of the divalent fluorescent ligand **9** in TBS/Ca²⁺ buffer after 26 h. The analogue window (in blue) display fluorescent detector signal set for fluorescein. New fluorescent peak of unknown identity was observed with retention time 5.1 min. The major peak, split by a shoulder, with retention time 5.5 min corresponds to compound **9** (m/z 807.8²⁺).

Generic Display Report (all)

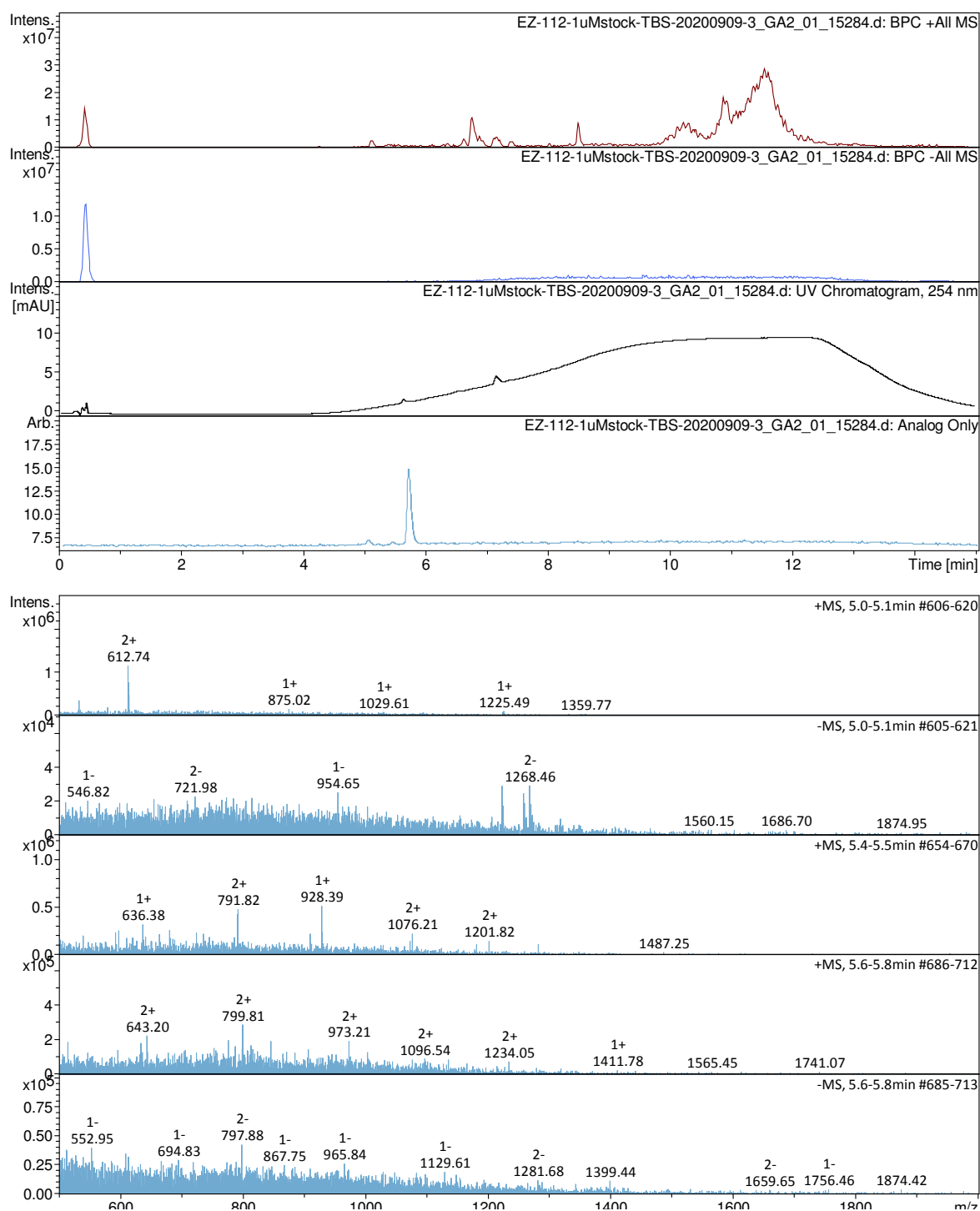


Figure S3: HPLC-MS chromatogram of divalent fluorescent ligand **9** stock in TBS/Ca²⁺ buffer used for fluorescence polarization assay. The analogue window (in light blue) display fluorescent detector signal set for fluorescein. The fluorescent peak no longer corresponded to ligand **9** (m/z 807.8²⁺).

Generic Display Report (all)

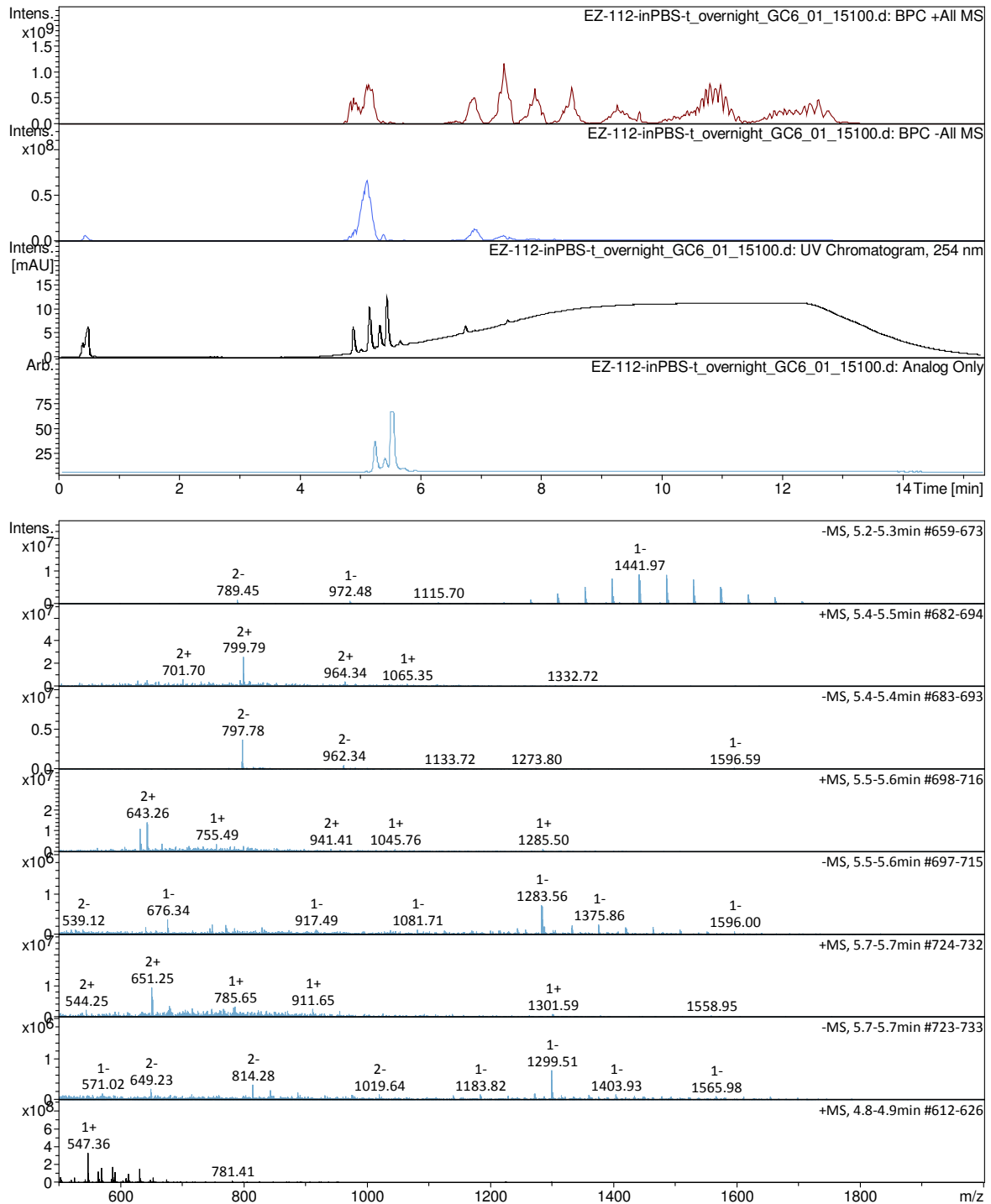


Figure S4: HPLC-MS chromatogram of divalent fluorescent ligand **9** in PBS buffer (10 mM phosphate buffer pH 7.4, 2.7 mM KCl, 137 mM NaCl, 100 μ M CaCl₂, 0.05% Tween 20) after overnight incubation (\approx 16 h). The analogue window (in light blue) display fluorescent detector signal set for fluorescein. The fluorescent peaks no longer corresponded to ligand **9** (m/z 807.8²⁺).

Generic Display Report

Analysis Info

Analysis Name C:\Users\eza17\Documents\LCMS\EZ-SMY10-inTBS-24h_GA6_01_18147.d
Method 18147.m
Sample Name EZ-SMY10-inTBS-24h
Comment

Acquisition Date 06.05.2021 07:58:59

Operator cbch
Instrument amaZon SL

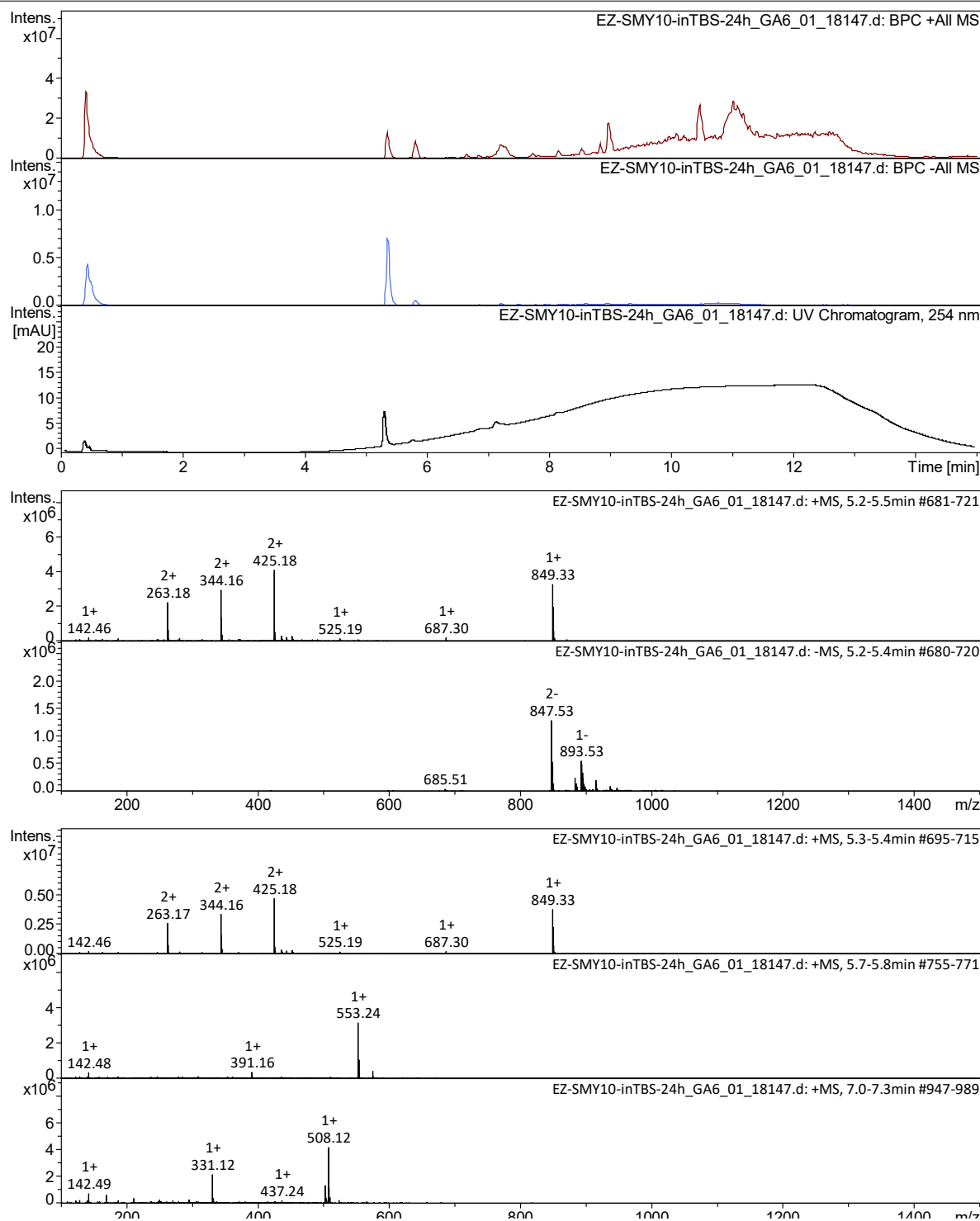


Figure S5: HPLC-MS chromatogram of the parent acylhydrazone ligand **1** (m/z 849.28¹⁺) in TBS/Ca²⁺ buffer after 24 h.

Generic Display Report

Analysis Info

Analysis Name C:\Users\leza17\Documents\LCMS\EZ-116-inTBS-36h_GA5_01_18153.d
Method 18153.m
Sample Name EZ-116-inTBS-36h
Comment

Acquisition Date 06.05.2021 22:55:45

Operator cbch

Instrument amaZon SL

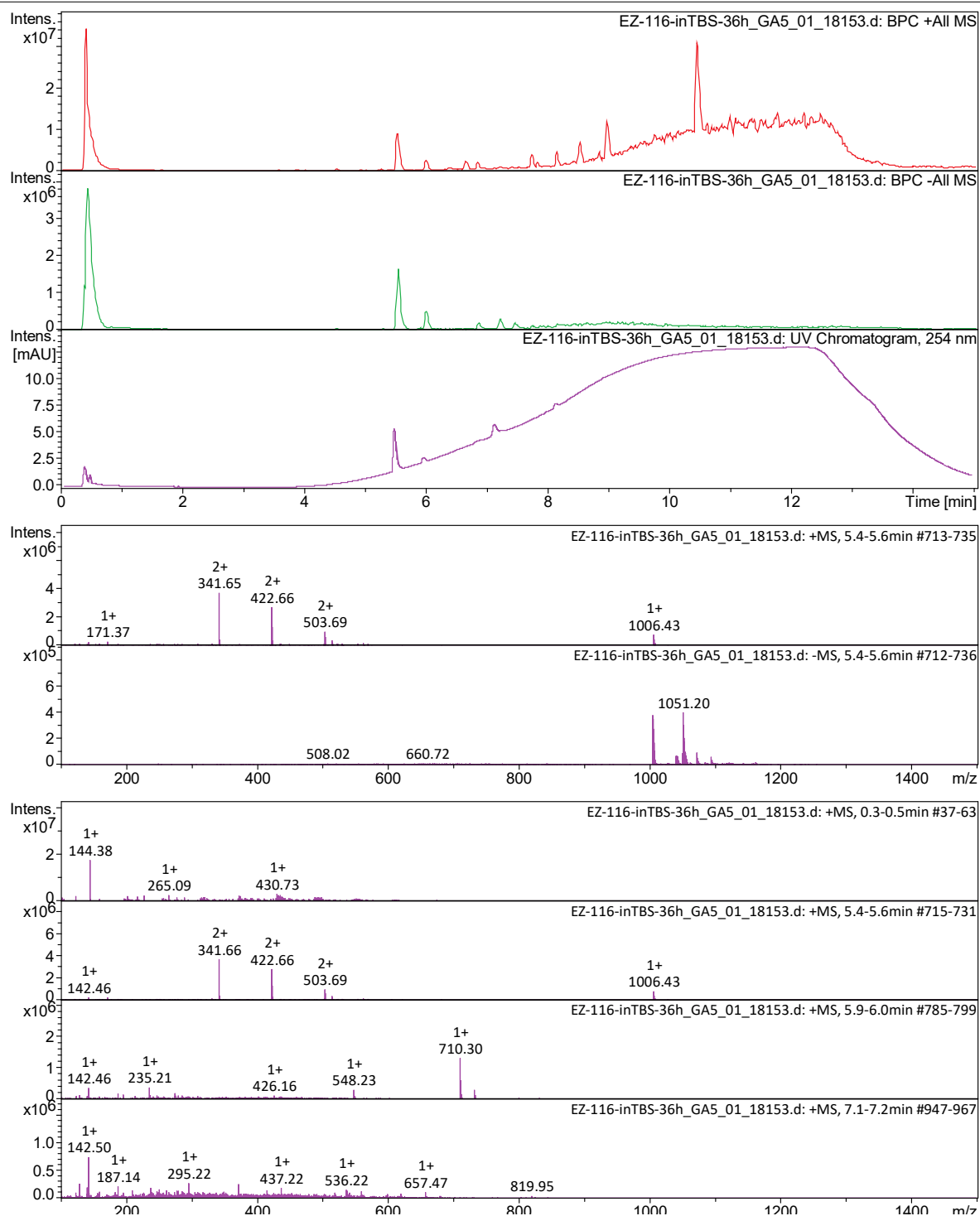


Figure S6: HPLC-MS chromatogram of the branched divalent acylhydrazone ligand **7** (m/z 1006.34¹⁺) in TBS/Ca²⁺ buffer after 36 h.

Generic Display Report (all)

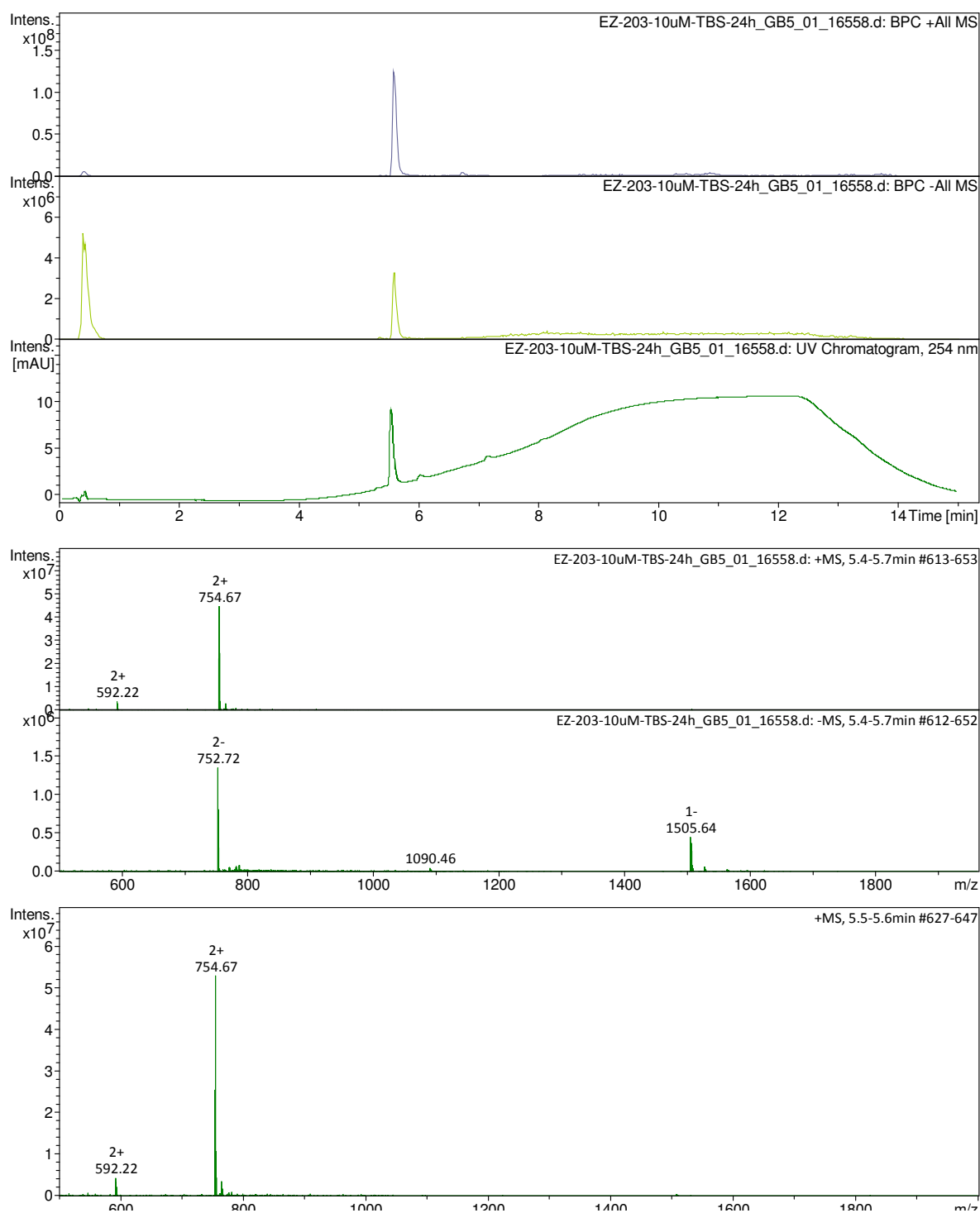
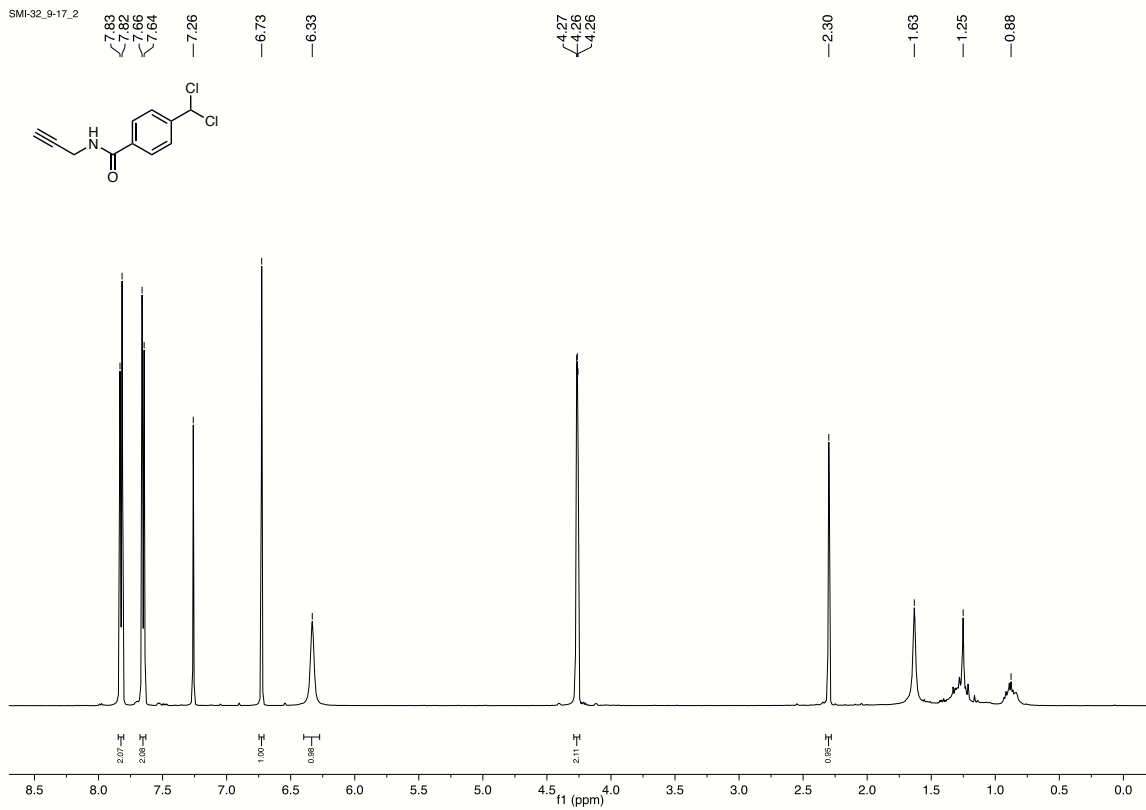
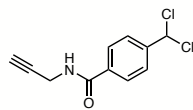
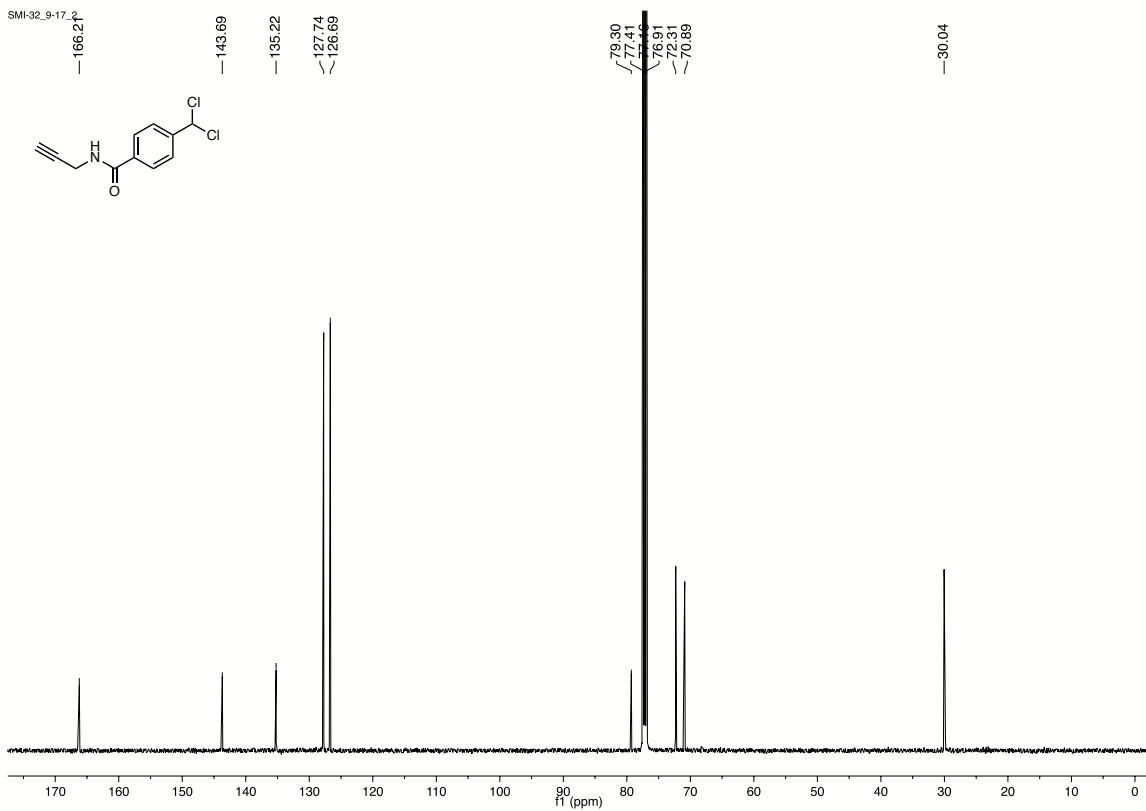
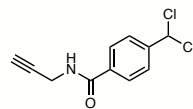


Figure S7: HPLC-MS chromatogram of divalent fluorescent ligand **15** (m/z 754.67²⁺) in TBS/Ca²⁺ buffer after 24 h that was used for fluorescence polarization assay.

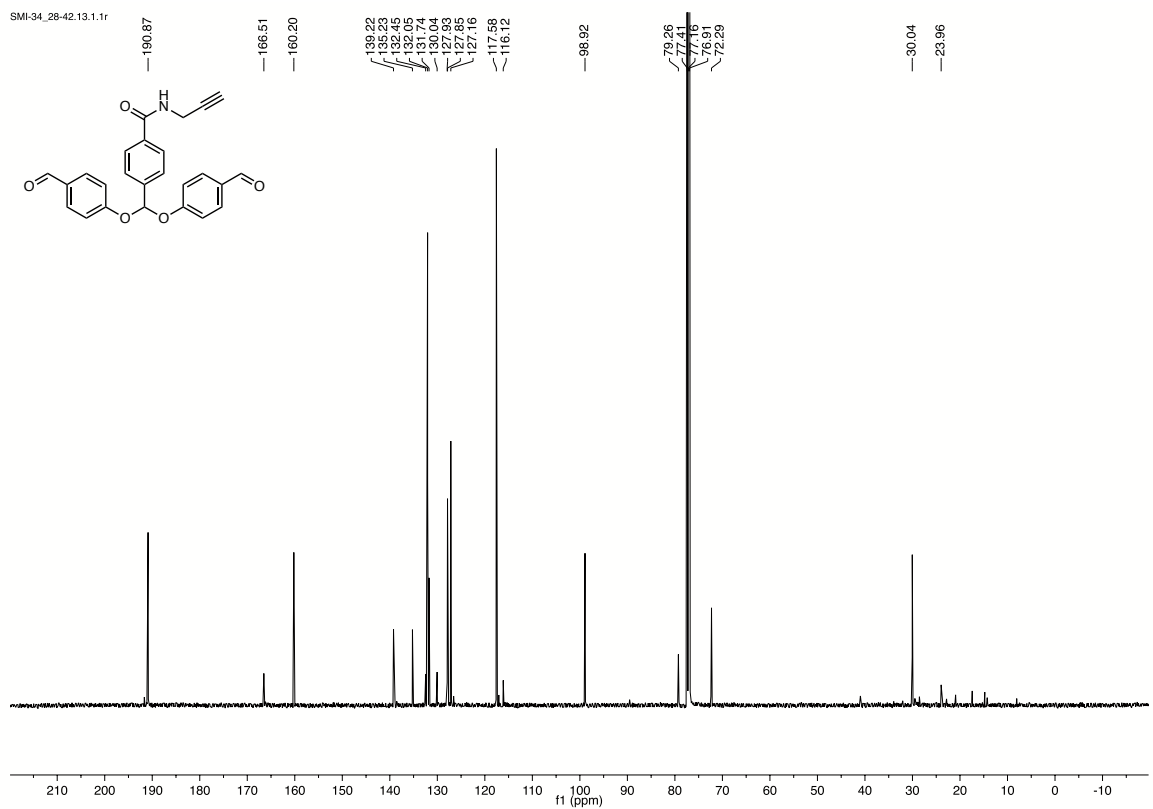
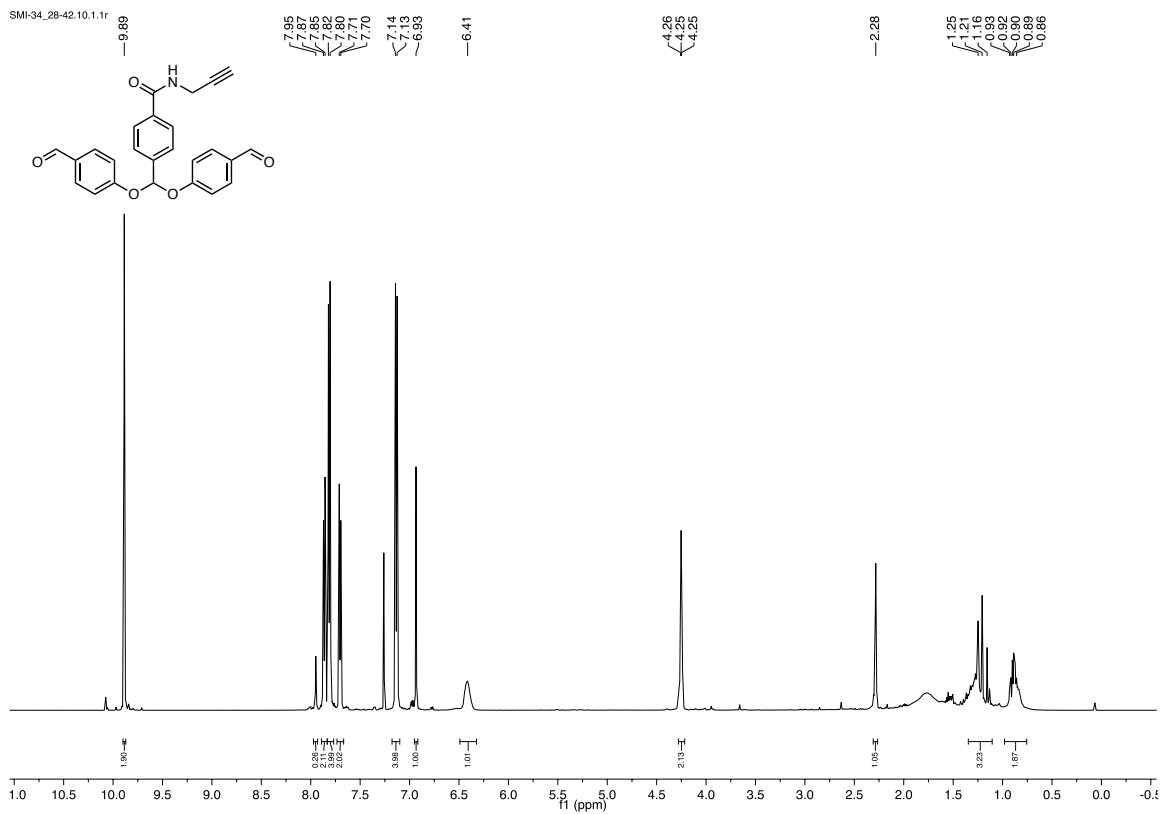
SMI-32_9-17_2



SMI-32_9-17_2

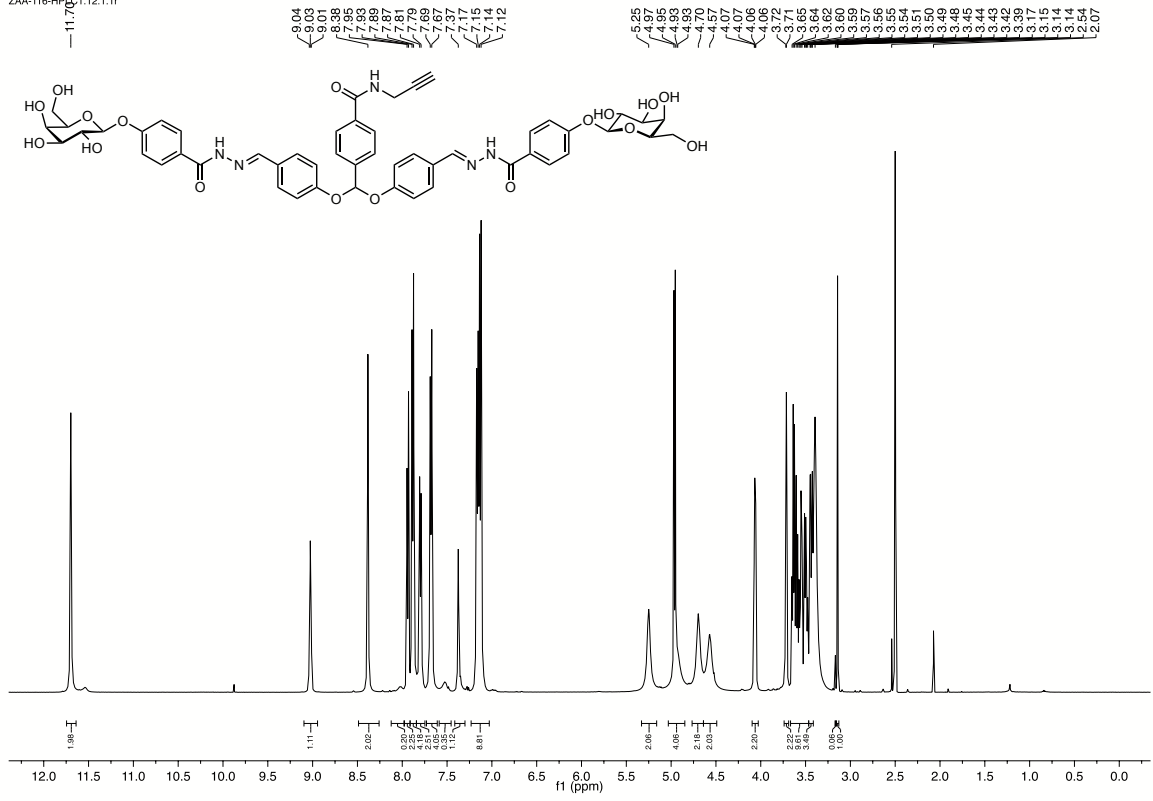


¹H and ¹³C NMR of 3

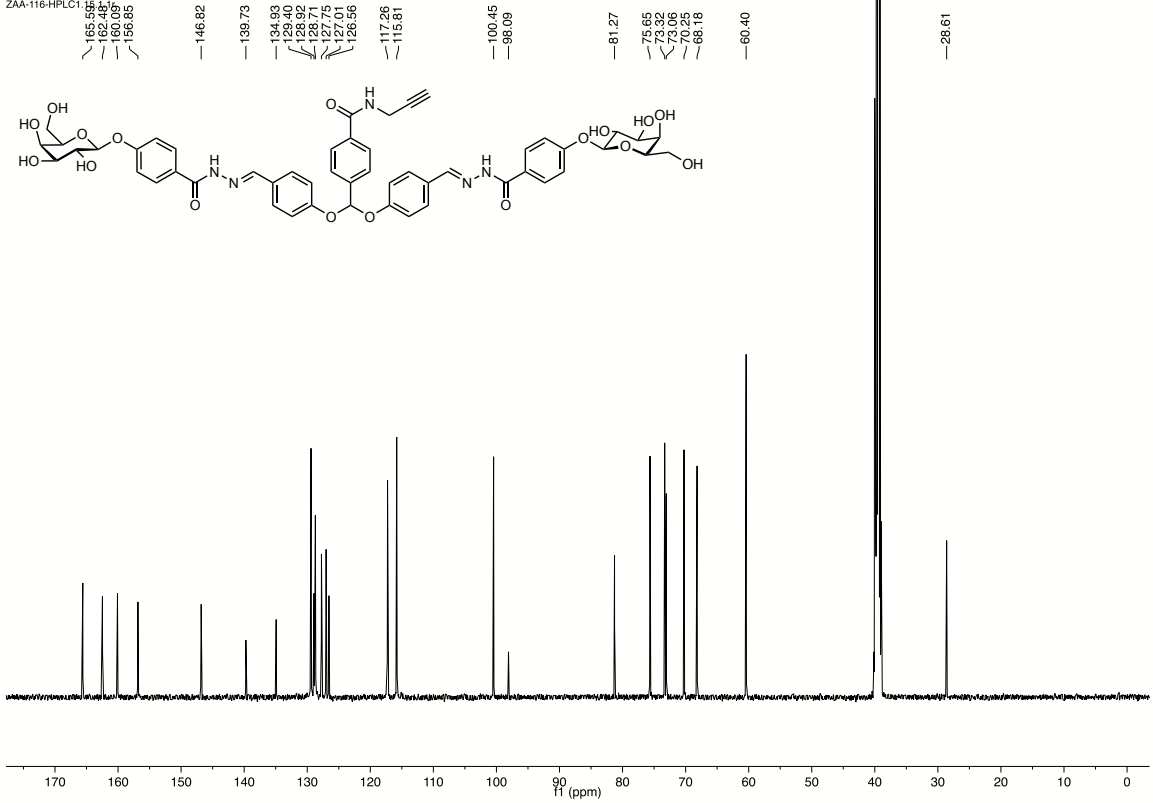


^1H and ^{13}C NMR of 4

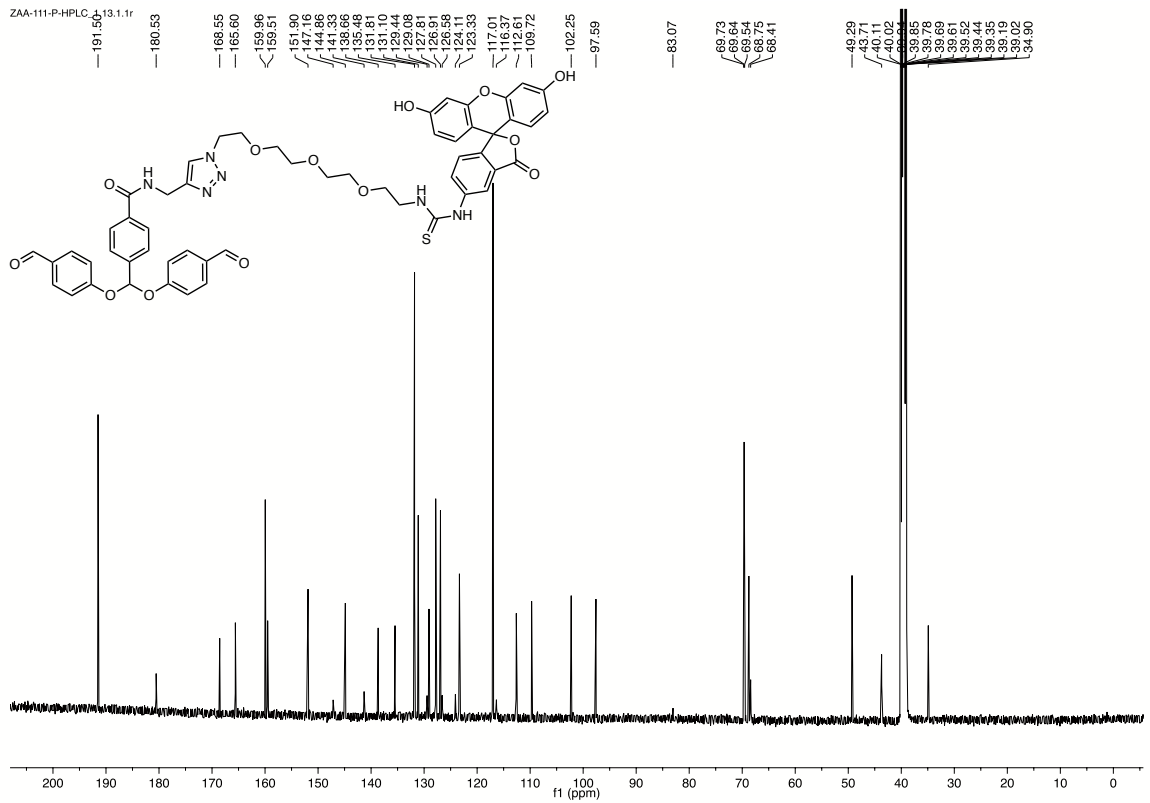
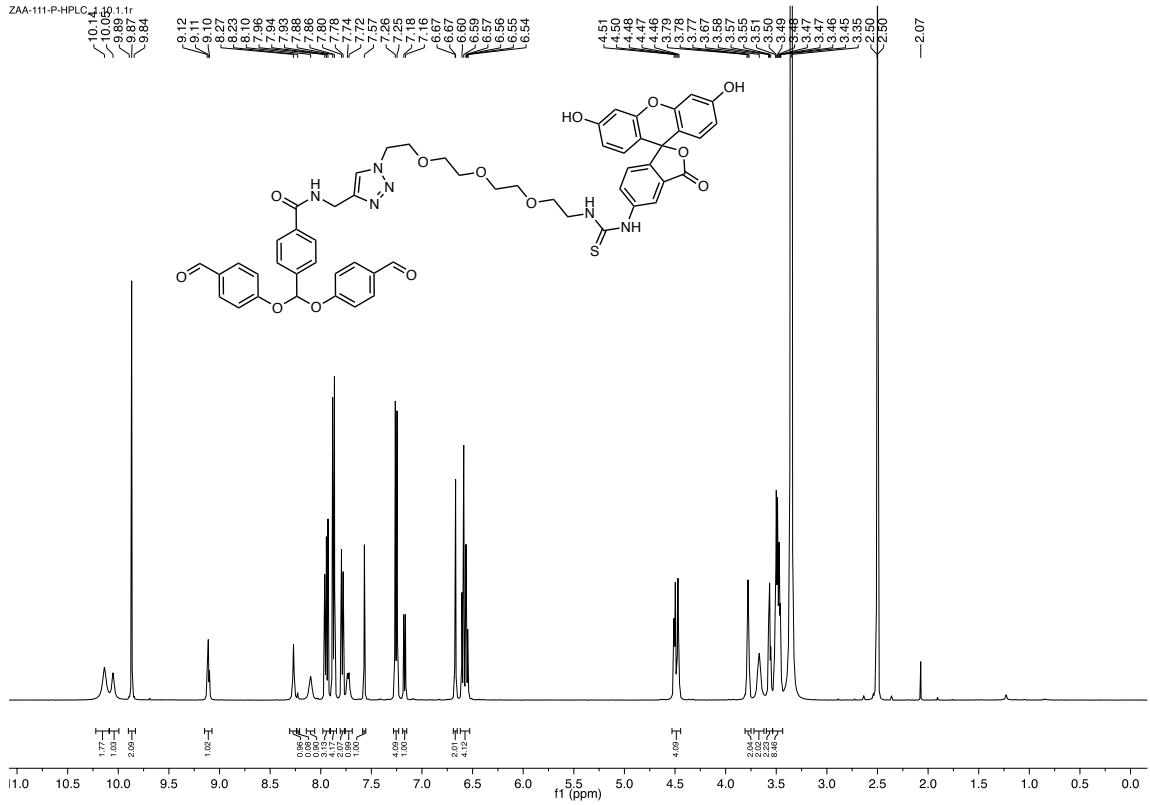
ZAA-116-HPLC1.12.1.1f



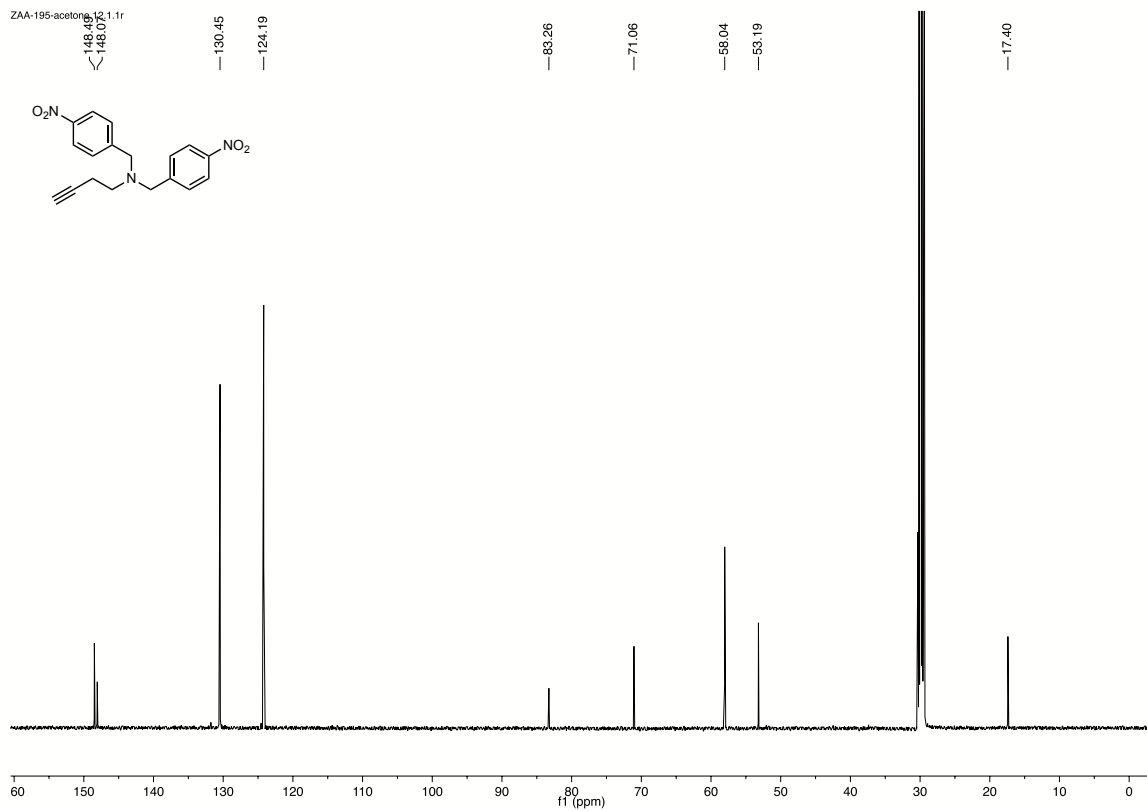
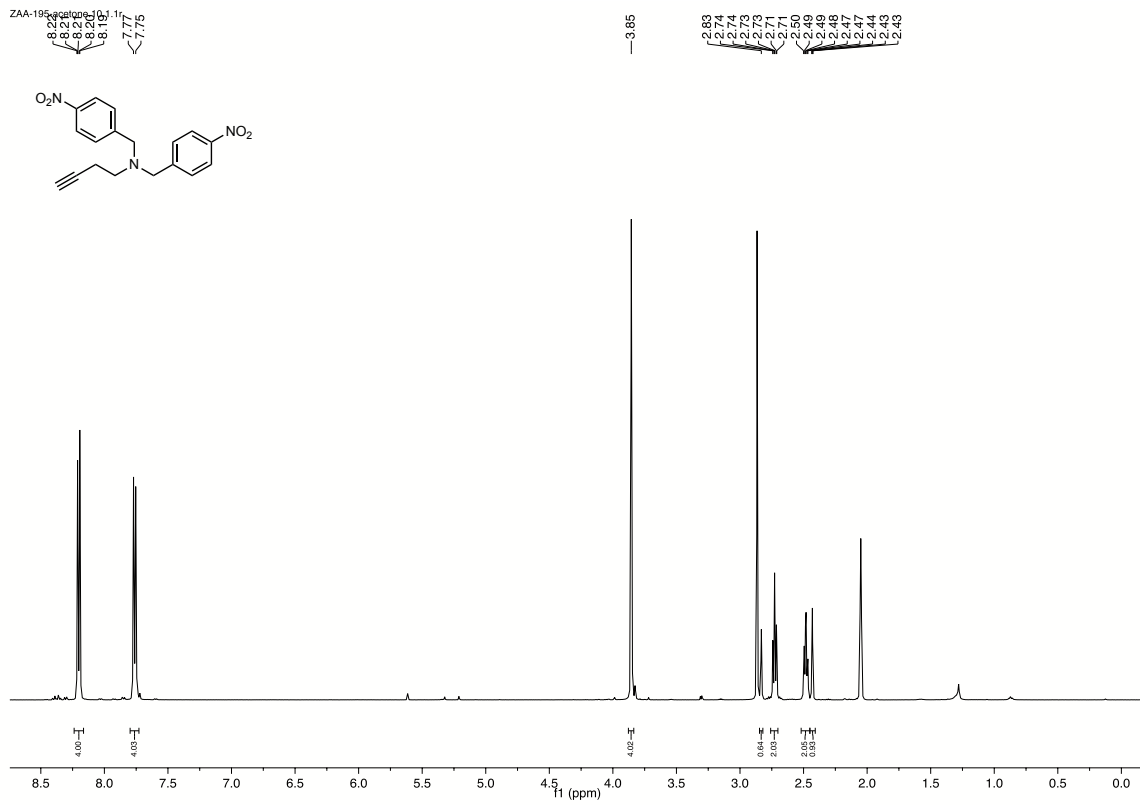
ZAA-116-HPLC1.12.1.1f



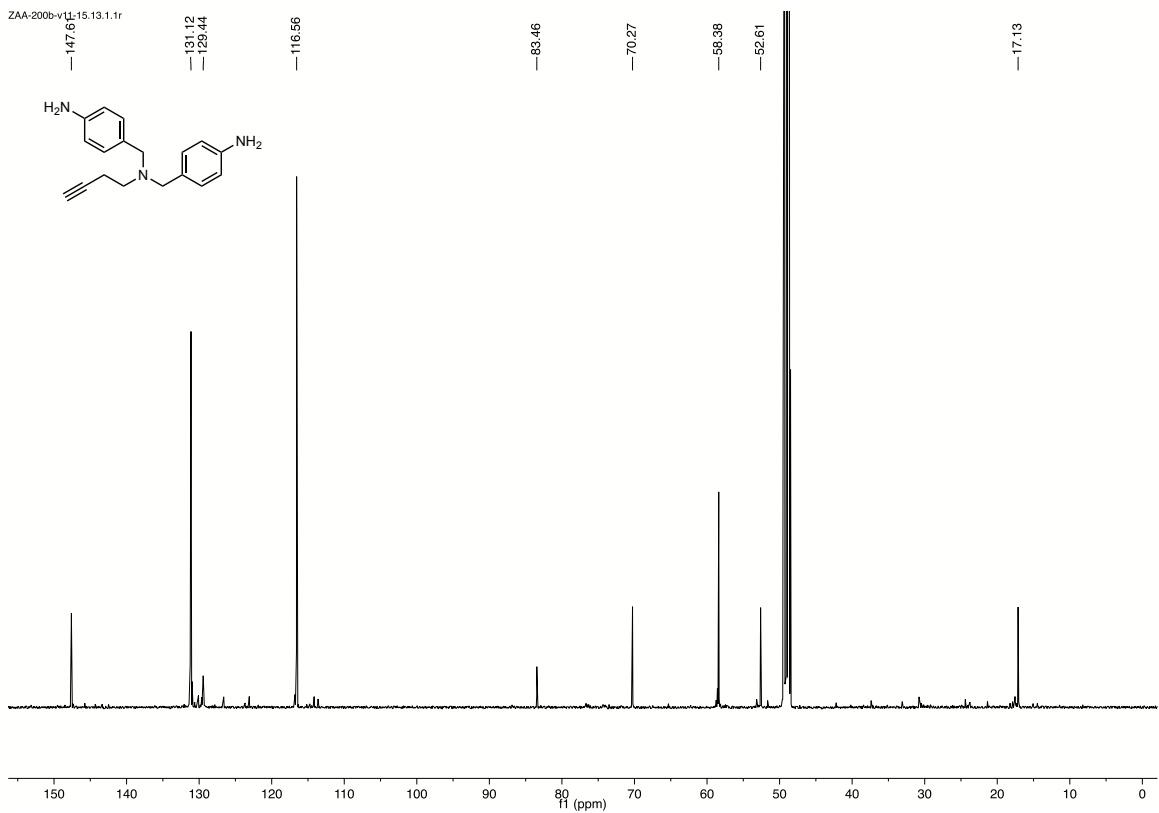
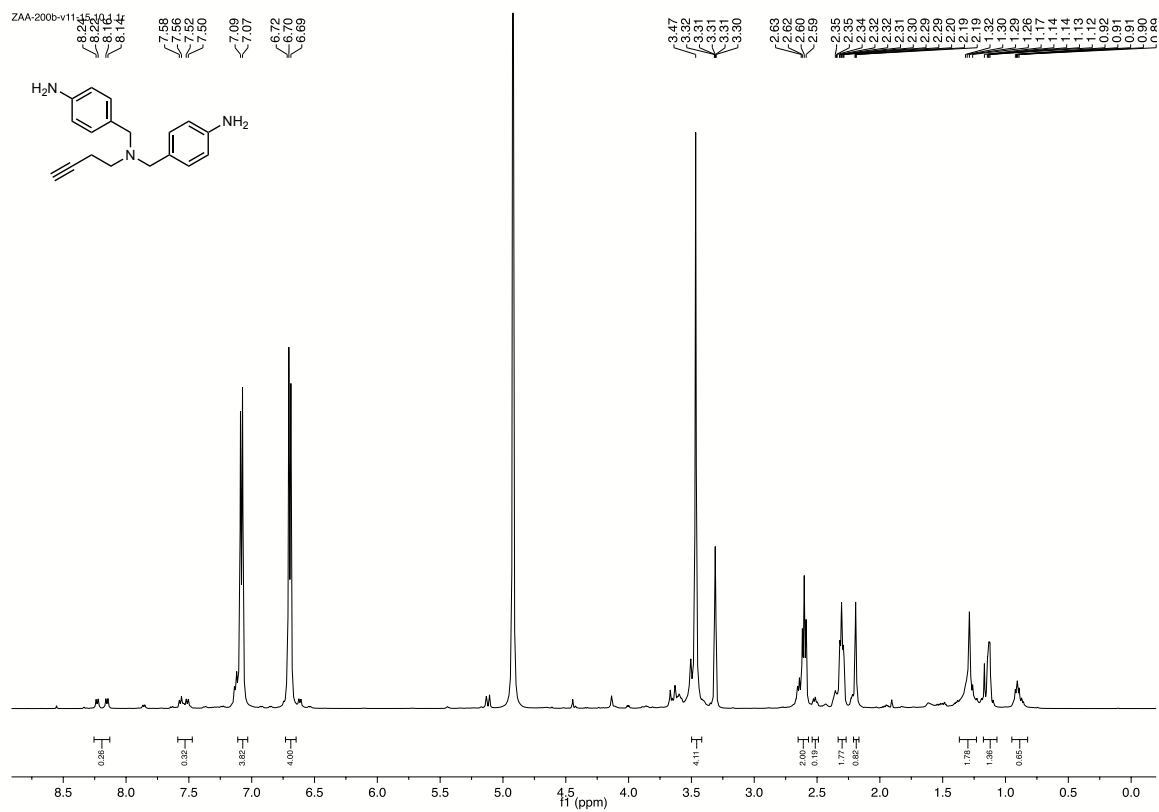
¹H and ¹³C NMR of 7



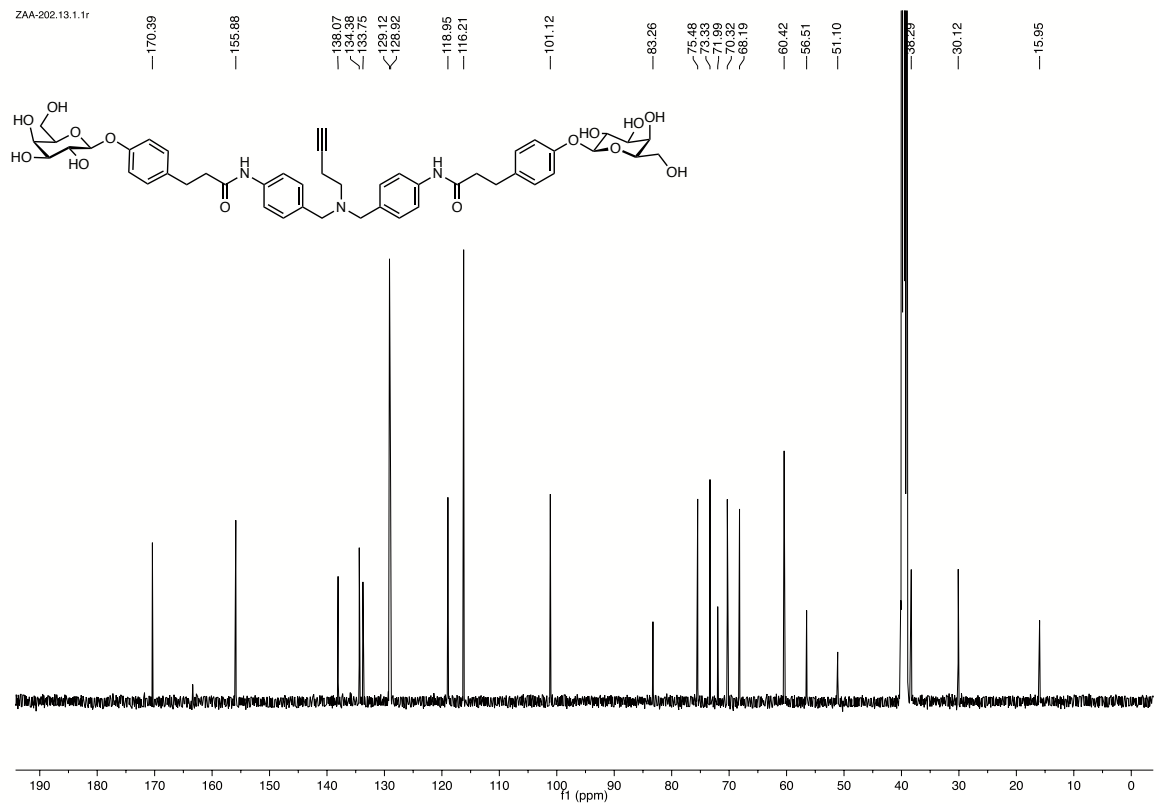
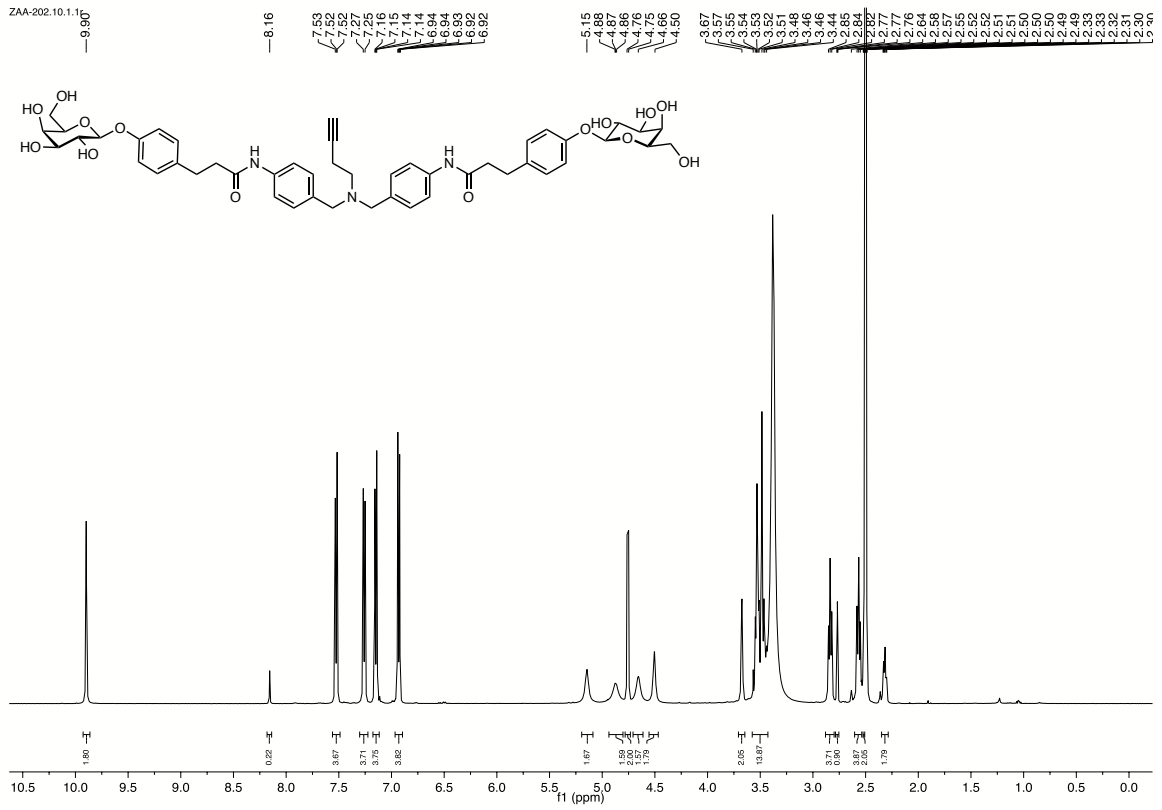
^1H and ^{13}C NMR of **8**



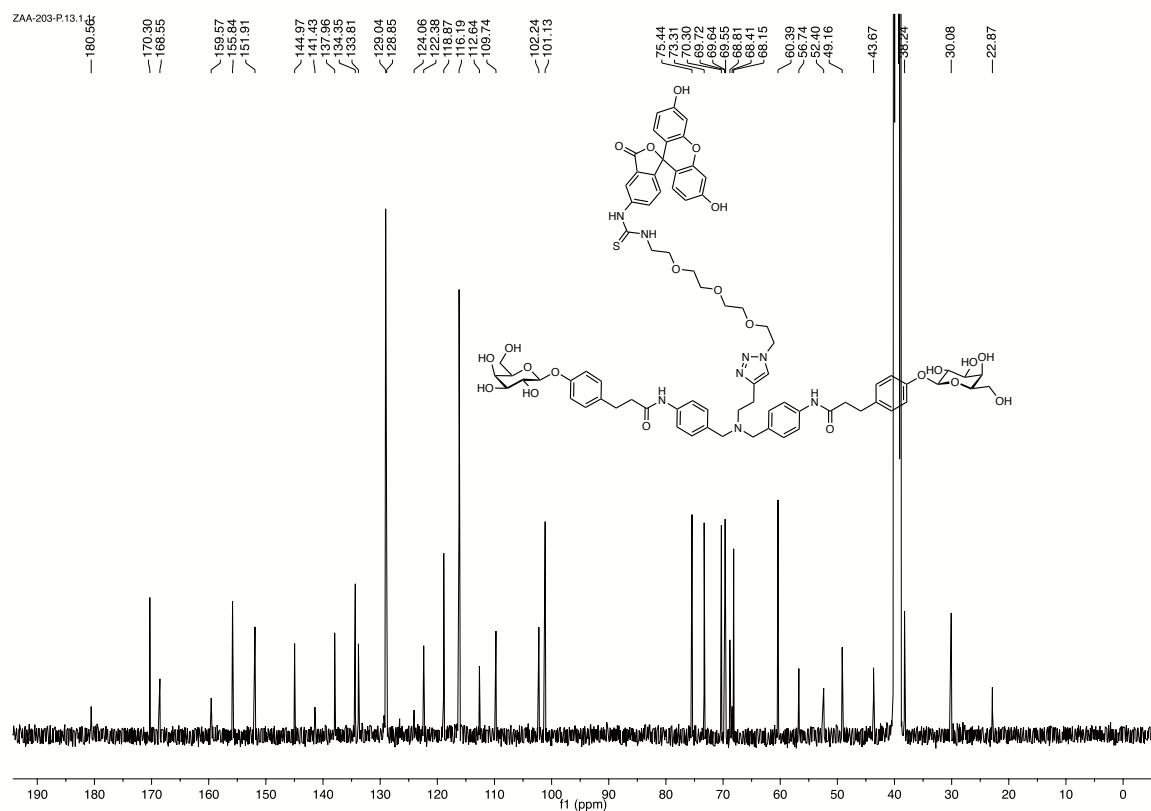
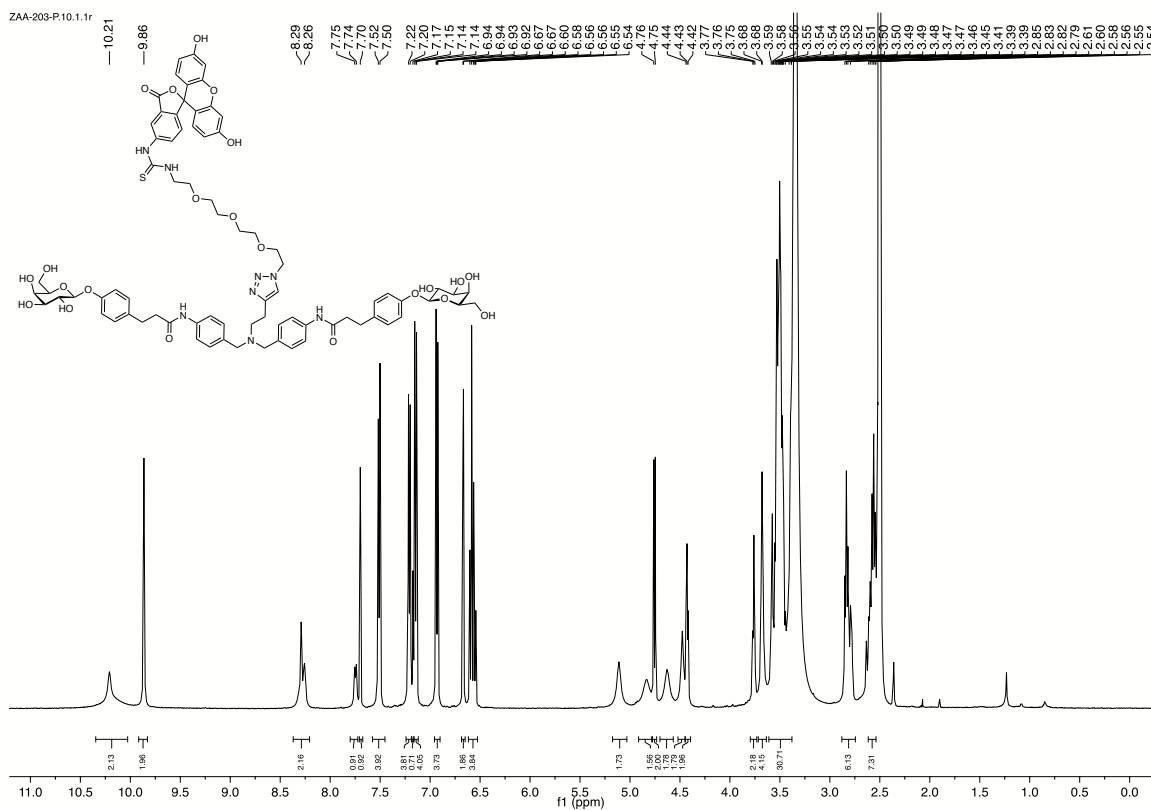
^1H and ^{13}C NMR of **11**



^1H and ^{13}C NMR of 12



^1H and ^{13}C NMR of 14



^1H and ^{13}C NMR of 15

6.5 Directing Drugs to Bugs: Antibiotic-Carbohydrate Conjugates

Targeting Biofilm-Associated Lectins of *Pseudomonas aeruginosa*

Authors: Joscha Meiers, Eva Zahorska, Teresa Röhrig, Dirk Hauck, Stefanie Wagner, and Alexander Titz

Published in: *Journal of Medicinal Chemistry*, 2020, **63**, 11707–11724.

DOI: 10.1021/acs.jmedchem.0c00856

Directing Drugs to Bugs: Antibiotic-Carbohydrate Conjugates Targeting Biofilm-Associated Lectins of *Pseudomonas aeruginosa*

Joscha Meiers, Eva Zahorska, Teresa Röhrig, Dirk Hauck, Stefanie Wagner, and Alexander Titz*

Cite This: *J. Med. Chem.* 2020, 63, 11707–11724

Read Online

ACCESS |



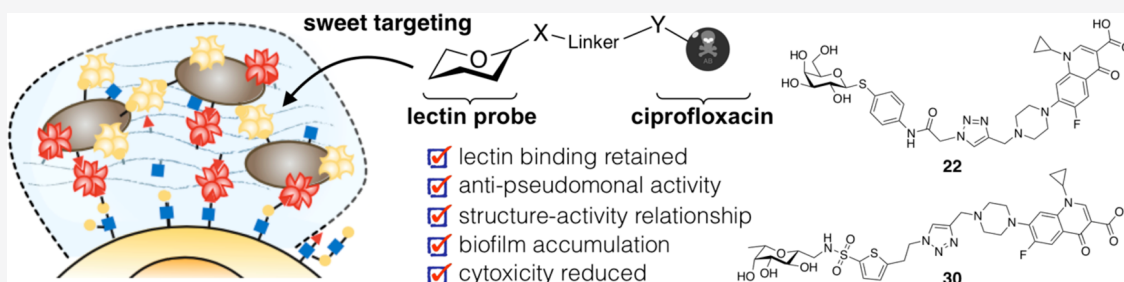
Metrics & More



Article Recommendations



Supporting Information



ABSTRACT: Chronic infections by *Pseudomonas aeruginosa* are characterized by biofilm formation, which effectively enhances resistance toward antibiotics. Biofilm-specific antibiotic delivery could locally increase drug concentration to break antimicrobial resistance and reduce the drug's peripheral side effects. Two extracellular *P. aeruginosa* lectins, LecA and LecB, are essential structural components for biofilm formation and thus render a possible anchor for biofilm-targeted drug delivery. The standard-of-care drug ciprofloxacin suffers from severe systemic side effects and was therefore chosen for this approach. We synthesized several ciprofloxacin-carbohydrate conjugates and established a structure–activity relationship. Conjugation of ciprofloxacin to lectin probes enabled biofilm accumulation *in vitro*, reduced the antibiotic's cytotoxicity, but also reduced its antibiotic activity against planktonic cells due to a reduced cell permeability and on target activity. This work defines the starting point for new biofilm/lectin-targeted drugs to modulate antibiotic properties and ultimately break antimicrobial resistance.

INTRODUCTION

The Gram-negative, opportunistic pathogen *Pseudomonas aeruginosa* has become a serious threat^{1–3} for immunocompromised patients (e.g., geriatrics, untreated HIV patients,^{4,5} and cancer patients⁶) and people suffering from cystic fibrosis (CF). Severe infections with *P. aeruginosa* can lead to recurrent pneumonia, lung damage, and sepsis.⁷ Its intrinsic antimicrobial resistance and its ability to acquire further resistances, which often lead to multidrug-/extensively drug-resistant (MDR/XDR) strains, are major obstacles for therapeutic treatment.⁸ As a consequence, the WHO stated *P. aeruginosa* in 2017 to be a critical priority 1 pathogen, which increases research and therapeutic focus on this particular Gram-negative pathogen.⁹ The ability to colonize almost any part of the human body can lead to various infected tissues, e.g., chronic wound infections, catheter-associated urinary tract infections or pneumonia, and further challenges clinicians to find an appropriate antibiotic therapy. Additionally, pharmacokinetic properties such as tissue distribution, oral bioavailability, and others vary from antibiotic to antibiotic. Thus, not every drug can reach the specific site of infection. Further, high drug levels at sensitive tissues can lead to hazardous side effects, e.g., ototoxicity of many aminoglycosides or tendon rupture and neuropathy after extensive use of fluoroquinolones.

The ability to form biofilms is a hallmark of chronic *P. aeruginosa* infections. During this stage of living, the cells cluster together in a biofilm matrix and produce a highly impenetrable barrier against host immune defense or antibiotics.^{10,11} These biofilm cells can show an up to 1000-fold increase in resistance against antibiotic drugs.¹² Despite the highly complex composition of the *P. aeruginosa* biofilm, the two quorum-sensing¹³ regulated extracellular virulence factors LecA¹⁴ and LecB¹⁵ (formerly called PA-IL and PA-IIL^{16–18}) stand out. It is assumed that these Ca²⁺-dependent tetravalent proteins crosslink bacteria with the biofilm matrix as well as host tissue via glycan binding (Figure 1). It was shown that these carbohydrate-binding proteins (i.e., lectins), amongst other biological roles, are crucial for biofilm formation and its structural integrity by *P. aeruginosa*.^{14,15} In the case of the D-mannose(D-Man)- and L-fucose(L-Fuc)-binding LecB, da Silva et al. recently showed that it organizes the localization of the

Received: May 20, 2020

Published: September 14, 2020



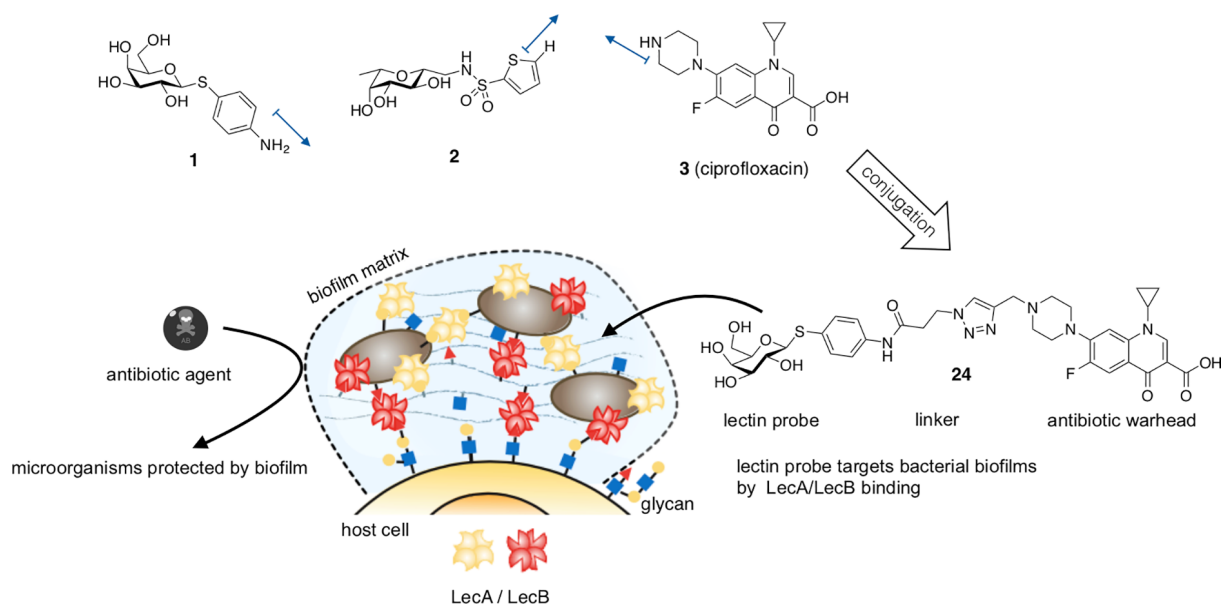


Figure 1. The lectin inhibitors **1** and **2** are conjugated to the antibiotic ciprofloxacin (**3**) resulting in pathogen-specific, lectin-targeted antibiotics. These compounds target the biofilm-associated lectins LecA and LecB and therefore increase local antibiotic concentration at the site of infection, resulting in fewer side effects caused by unspecific distribution and tissue accumulation. Blue arrows display growth vectors used in this work.

exopolysaccharide Psl in the biofilm matrix.¹⁹ Further, both lectins also play roles in the direct infection process: LecB conveys virulence through carbohydrate-dependent inhibition of human ciliary beating,²⁰ interference with repair of wounded tissues,^{21,22} and activation of B-cells.²³ Next to its biofilm-related roles, it was shown that the D-galactose-binding LecA triggers host cell signaling pathways²⁴ and mediates membrane invaginations after binding to its cellular receptor, the glycosphingolipid Gb3.²⁵ *In vivo*, both proteins are involved in the *P. aeruginosa* infection process and host colonization in a murine infection model.^{26,27} Interestingly, a study of *P. aeruginosa* infected CF patients and a case report on a pulmonary infected infant reported that the bacterial load in infected airways can be reduced by intrapulmonary application of fucose and galactose.^{28–30} Although *P. aeruginosa* is genetically highly diverse and adaptable,^{31,32} the protein sequence of LecA is highly conserved amongst clinical isolates. On the other hand, LecB does vary and can be clustered in either PAO1-like or PA14-like structures.³³ However, both LecB variants bind to same glycosides, making the design of LecB-inhibitors against a wide range of clinical *P. aeruginosa* strain isolates possible.^{33,34}

Lectin-carbohydrate interactions are usually characterized by weak binding affinity, which Nature circumvents by multivalent presentation of ligand or receptor.³⁵ Due to the high therapeutic interest, many compounds have been designed to inhibit LecA or LecB,^{36–38} most of them showing high affinity on the target in a multivalent fashion.^{39,40} Interestingly, LecB-directed multivalent molecules with nanomolar on-target activity required millimolar concentrations to inhibit biofilm formation of *P. aeruginosa*.²⁶ One possible explanation is the creation of additional crosslinks due to the protein's and ligand's multivalent structure, resulting in an undesired stabilization of the biofilm at therapeutic concentrations of the multivalent ligand.

We have previously identified monovalent LecB inhibitors, sulfonamide-capped mannosides, and C-glycosides combining pharmacophores of its natural ligands, fucose and man-

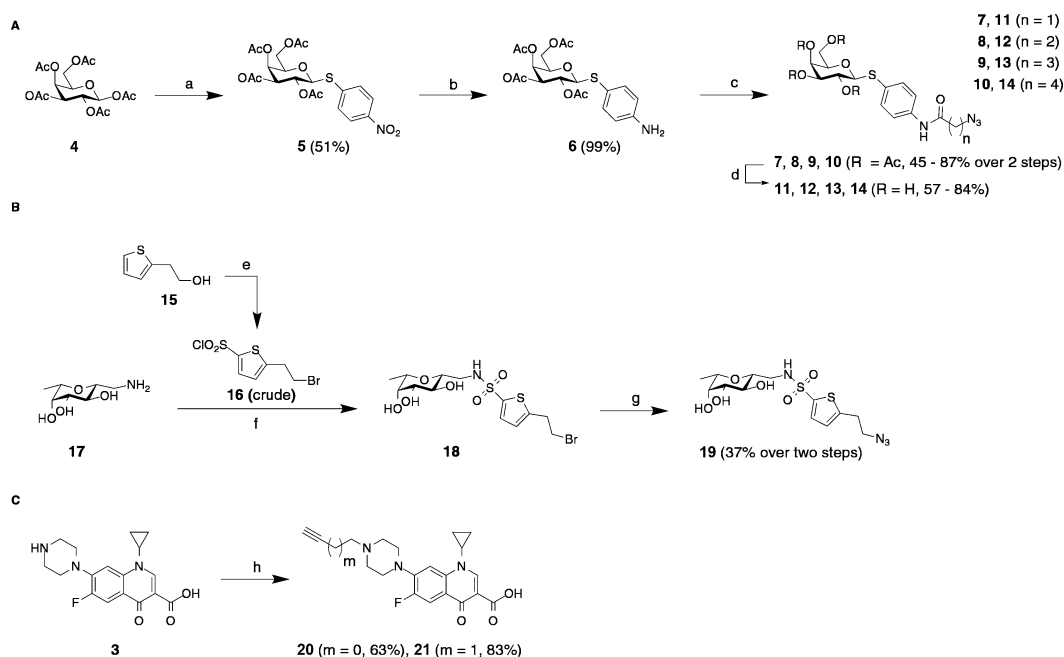
nose.^{41–43} Recently, we reported the first drug-like, oral bioavailable LecB inhibitor **1** and established its SAR.^{44,45} Glycomimetic **1** showed excellent binding affinity against LecB and inhibited biofilm formation *in vitro* at micromolar concentrations. In mice, high plasma and urine concentrations were obtained after oral application.

Whilst LecB can be inhibited with high affinity ligands, LecA only shows moderate binding affinity against monovalent galactose-based compounds.^{36–38,46} Instead of a multivalent ligand presentation, we circumvented the rapid dissociation of the ligand–receptor complex by introduction of an electrophilic warhead in the first covalent lectin inhibitor. After conjugation of this galactose-based epoxide to a fluorescent dye, we used the resulting LecA-targeted dye to stain *P. aeruginosa* biofilms *in vitro*, proposing its potential use as biofilm-recognizing diagnostic tools.⁴⁷

Fluoroquinolone antibiotics are frequently used to treat a plethora of bacterial infections. The most common representative of this class is the drug ciprofloxacin, which is amongst other indications being used in cystic fibrosis-associated bronchopulmonary *P. aeruginosa* infections. Although fluoroquinolones were originally described to be pharmacologically safe, clinical phase IV studies revealed partially irreversible side effects like tendon ruptures or neuropathy, resulting from high tissue penetration and off-target effects. As a consequence, the fluoroquinolones have been categorized by drug agencies as high risk drugs and the U.S. Food and Drug Administration (FDA) issued a “black box” warning label,⁴⁸ and the German Federal Institute for Drugs and Medical devices (BfArM) informed medical professionals about prescription restrictions in 2019.

Paul Ehrlich coined the concept of a “magic bullet”, describing molecules that would specifically target only pathogenic bacteria or tumor cells.⁴⁹ One hundred fifty years later, this approach is on the way to become common therapeutic practice: Antibody-drug conjugates like trastuzumab-emtansine⁵⁰ led to a great success in cancer therapy and are also being studied in antimicrobial research.⁵¹ Further,

Scheme 1. Chemical Synthesis of the (A) LecA-Targeting (11–14) and (B) LecB-Targeting (19) Probes and (C) Alkyne Ciprofloxacin Derivatives 20 and 21^a



^aReagents and conditions: (a) *p*-nitrothiophenol, BF₃·Et₂O, CH₂Cl₂, 0 °C to r.t., 16 h; (b) H₂, Pd/C, CH₂Cl₂, r.t., 24 h; (c) (i) Br(CH₂)_nCOHal, Et₃N, or K₂CO₃, DMF, 0 °C to r.t., 1–4 h, (ii) NaN₃, DMF, r.t., 4 h; (d) cat. NaOMe, MeOH, r.t., 1 h; (e) (i) PBr₃, CH₂Cl₂, 0 °C to r.t., 1 h, (ii) HSO₃Cl, CH₂Cl₂, 0 °C to r.t., 3 h; (f) crude **16**, K₂CO₃, DMF, r.t., 5 h; (g) NaN₃, DMF, r.t., 5 h; (h) propargylbromide or 4-bromo-but-1-yne, Et₃N, DMF, 70 °C, 1–4 d.

many antibiotic conjugates have been described so far, mainly targeting bacterial uptake mechanisms or non-targeted dual acting antibiotics (reviewed in refs 52, 53). Interestingly, carbohydrate conjugates of ciprofloxacin were described to increase bacterial cell uptake via sugar transporters.^{54,55} Inspired by the successful detection of *P. aeruginosa* biofilms with LecA-directed dyes, we aimed to conjugate glycomimetics to ciprofloxacin in order to target the extracellular *P. aeruginosa*-specific, biofilm-related virulence factors LecA and LecB. By exploiting lectin accumulation in the *P. aeruginosa* biofilm, the targeted conjugates shall deliver their antibiotic cargo specifically to the site of infection. Thus, an enhanced local drug concentration could overcome antimicrobial resistance and lower nonspecific drug distribution, potentially reducing systemic side effects (Figure 1). Here, we report the synthesis of the first lectin-targeted antibiotic conjugates and their microbiological and biochemical evaluation. We describe an antimicrobial structure–activity relationship of these lectin binding conjugates and show their biofilm accumulation *in vitro*.

RESULTS AND DISCUSSION

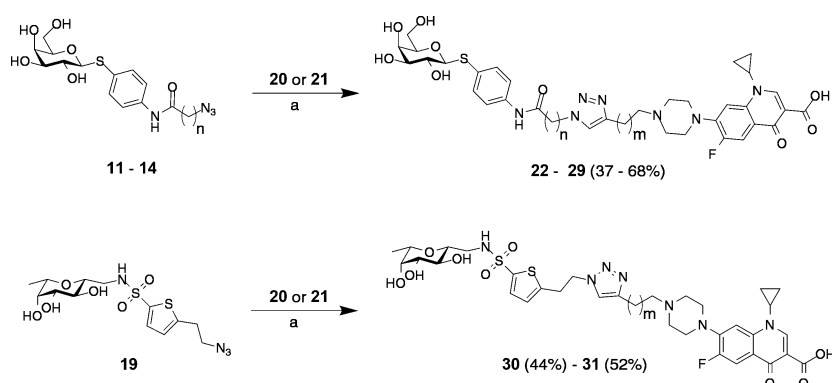
Design. The design of the lectin-targeted conjugates followed the established structure–activity relationships (SAR) of their individual components, i.e., targeting moiety and ciprofloxacin cargo.

The targeted lectins LecA and LecB both show shallow carbohydrate binding sites on their protein surfaces. As a consequence, linking a cargo to specific sites at the published probes without losing lectin inhibition activity was plausible. The SAR of D-galactose-based LecA inhibitors revealed β-linked aromatic aglycons to be vital for potent LecA inhibition. Further substitutions at the aromatic aglycon only result in

minor changes in binding affinity.^{56–58} In the complex with LecA, the ligand's surface-exposed phenyl aglycon reveals a potential growth vector for the conjugation of cargo to the para-position.⁵⁹ As this linking strategy was used to stain *P. aeruginosa* biofilms *in vitro*,⁴⁷ we decided to similarly link an antibiotic cargo, using **1** as a LecA targeting probe. To increase the metabolic stability, the O-glycosidic structure was replaced with a thioglycoside. The potent LecB inhibitor **2** displays a C-glycosidic hybrid structure, merging target interactions of D-mannose and L-fucose. The attachment of an aromatic sulfonamide addressed an additional subpocket on LecB.^{41–44} Analysis of the co-crystal structure of LecB in complex with **2** and extensive SAR studies⁴⁵ revealed a potential growth vector on position 5 of the thiophene ring for subsequent conjugation to the antibiotic cargo.

Fluoroquinolones represent a highly active class of antibiotics, deriving from their predecessor nalidixic acid. The SAR of the fluoroquinolones^{60–63} is well described and exploited in several antimicrobial conjugates. Its main pharmacophore, 6-fluoro-quinolone-3-carboxylic acid, is essential for inhibition of its intracellular target, bacterial gyrase. Substitutions at position 7 mainly modify and fine-tune pharmacokinetic properties and strain specificity. In the case of ciprofloxacin, the presence of a piperazine increases anti-pseudomodal activity.⁶⁴ We chose to derivatize the synthetically accessible secondary amine of the piperazine ring to a tertiary amine as this would result only in a smaller change of its physicochemical properties that influence porin-mediated bacterial cell uptake, as compared to, e.g., amide formation. Furthermore, analysis of the co-crystal structure⁶⁵ of ciprofloxacin with the GyrA/GyrB heterodimer showed a possible growth vector at this position (Figure 1).

Copper-catalyzed Huisgen-type [3+2] cycloaddition of terminal alkynes and terminal azides was chosen as a

Scheme 2. Assembly of the Lectin-Targeted Ciprofloxacin Conjugates^a

^aReagents and conditions: (a) cat. CuSO₄, cat. sodium ascorbate, DMF/H₂O, r.t. 16 h, r.t. (for 11–14) or 40 °C (for 19).

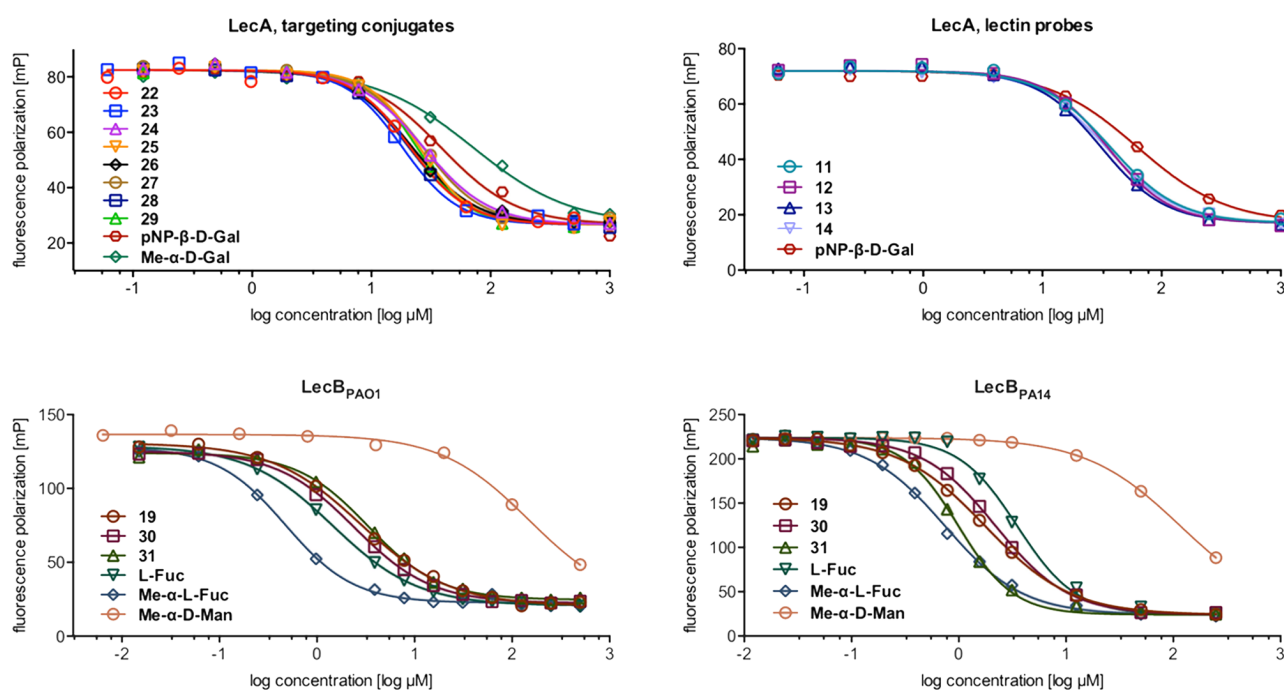


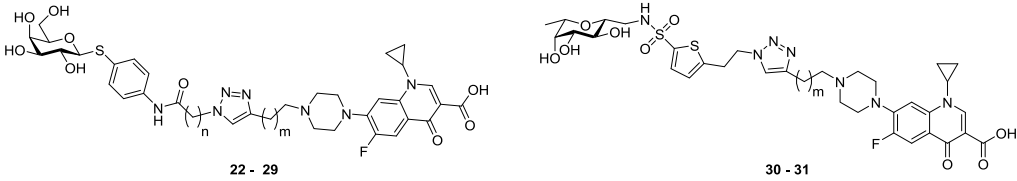
Figure 2. Competitive binding assay of lectin-targeted ciprofloxacin conjugates 22–31, lectin probes 11–14 and 19, and control compounds with LecA, LecB_{PAO1}, and LecB_{PA14}. One representative titration of triplicates on one plate is shown for each compound (IC₅₀ in Table 1 and K_i in Table S1).

convenient and modular way of linking both moieties. Further, we decided to analyze the impact of the linker length and flexibility on antibiotic activity by stepwise introduction of methylene spacers.

Synthesis. The LecA-targeting precursor **6** (Scheme 1) was synthesized in analogy to Casoni et al.⁶⁶ Glycosylation of the acceptor *para*-nitrothiophenol with galactose pentaacetate (**4**) using BF₃·Et₂O as a Lewis acid resulted in thioglycoside **5** in 51% yield. Palladium-catalyzed hydrogenation gave the corresponding aniline **6** quantitatively. Compound **6** was then treated with various ω -bromo acylhalides followed by a nucleophilic substitution with sodium azide to the corresponding azides **7**–**10** in one pot. The usage of triethylamine during the amide coupling led to β -elimination in the case of the propionic acid derivative **7** or γ -lactam formation in the case of bromide **13**, which could be circumvented by using potassium carbonate as a base. Deprotection of acetates **7**–**10** under Zemplén conditions resulted in the LecA-probes **11**–**14**.

Based on the results from the antimicrobial susceptibility testing (*vide infra*), we synthesized only one LecB probe (Scheme 1). β -C-glycoside **17** was synthesized as reported.⁴² Thiophene building block **16** was synthesized from **15** in two steps: The primary alcohol **15** was transformed to the corresponding bromide with phosphorous tribromide followed by chlorosulfonation of the thiophene in position 5 with chlorosulfonic acid. Crude sulfonylchloride **16** was reacted with amine **17** to yield sulfonamide **18**. This intermediate was stirred with sodium azide to give compound **19** in an overall yield of 37% over two steps based on the amine starting material **17**.

Alkylation of ciprofloxacin with propargyl bromide or 4-bromobut-1-yne in DMF at elevated temperatures yielded the corresponding terminal alkynes **20** and **21**. Finally, copper-catalyzed 1,3-dipolar cycloaddition of alkynes **20** and **21** with azides **11**–**14** and **19** resulted in the lectin-targeted ciprofloxacin conjugates **22**–**31** (Scheme 2).

Table 1. Competitive Binding Assay of Lectin-Targeted Ciprofloxacin Conjugates and Control Compounds with LecA, LecB_{PAO1}, and LecB_{PA14}^a


LecA			
compound	n	m	IC ₅₀ ± s.d. [μM]
11	1		31.7 ± 11
12	2		30.9 ± 8.7
13	3		31.1 ± 8.3
14	4		29.9 ± 9.5
22	1	0	30.4 ± 8.0
23	1	1	21.6 ± 5.5
24	2	0	32.2 ± 3.3
25	2	1	28.0 ± 1.8
26	3	0	27.3 ± 4.0
27	3	1	29.3 ± 3.7
28	4	0	28.3 ± 8.1
29	4	1	26.2 ± 2.4
Me-α-D-Gal		controls	71.7 ± 16
pNP-β-D-Gal			52.7 ± 13
LecB _{PAO1}			
compound	m	IC ₅₀ ± s.d. [μM]	LecB _{PA14}
19	LecB-probe	3.91 ± 1.6	IC ₅₀ ± s.d. [μM]
30	0	2.37 ± 1.2	1.87 ± 0.21
31	1	2.53 ± 0.87	2.24 ± 0.23
Me-α-D-Man		166 ± 22	1.00 ± 0.06
L-Fuc	controls	2.63 ± 1.7	101 ± 10
Me-α-L-Fuc		0.534 ± 0.07	2.46 ± 0.33
			0.79 ± 0.11

^aMeans and standard deviations were determined from a minimum of three independent experiments. K_i calculated from IC₅₀ is shown in Table S1.

Biophysical and Microbiological Evaluation. Competitive Lectin Binding Assay Based on Fluorescence Polarization. To analyze lectin binding of the targeted antibiotics, we quantified their binding affinity to LecA or LecB in the previously reported competitive binding assays.^{33,41,58}

The binding affinity of the LecA-targeting conjugates 22–29 did not significantly differ from their corresponding lectin probes 11–14 (Figure 2 and Table 1), reaching IC₅₀ values from 26 to 30 μM. Thus, they show an up to 2-fold increased inhibitory activity against LecA compared to *p*-nitrophenyl β-D-galactoside (pNP-β-D-Gal, IC₅₀ = 52.7 ± 13 μM) and an up to 3-fold increase compared to methyl α-D-galactoside (Me-α-D-Gal, IC₅₀ = 71.7 ± 16 μM), which served as reference compounds in this study.

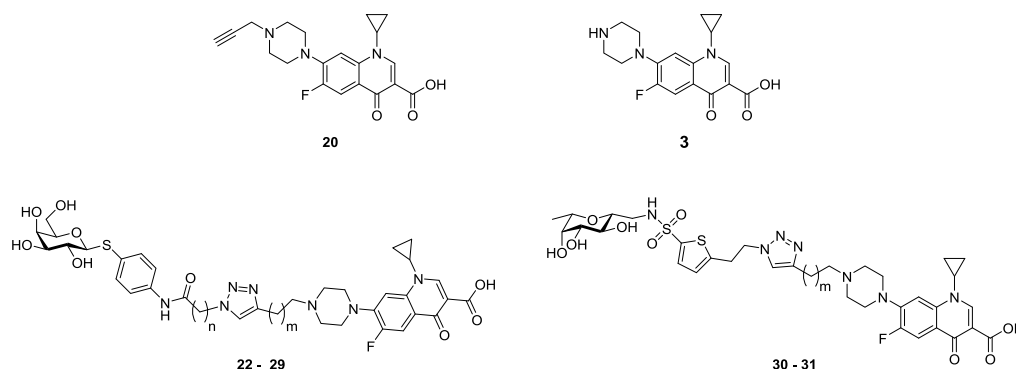
Competitive binding assays against LecB_{PAO1} (Figure 2 and Table 1) revealed IC₅₀ values in the one digit micromolar range for LecB probe 19 (IC₅₀ = 3.91 ± 1.6 μM) and its corresponding conjugates 30 and 31 (IC₅₀ = 2.37 ± 1.2 and 2.53 ± 0.87 μM, respectively), which is in the range of L-fucose (IC₅₀ = 2.63 ± 1.7 μM). The two glycosides, methyl α-D-mannoside (Me-α-D-Man) and methyl α-L-fucoside (Me-α-L-Fuc), which resemble terminal glycan structures recognized by LecB showed IC₅₀ values of 166 ± 22 and 0.534 ± 0.07 μM, respectively. The inhibition assay on LecB_{PA14} showed similar trends (Table 1). As observed previously,³³ LecB_{PA14} binds its ligands with higher affinity (e.g., IC₅₀ of 1.00 μM vs 2.53 μM for compound 31). Since *P. aeruginosa* PA14 and PAO1 are

representative for many clinical isolates, a broad range of *P. aeruginosa* strains can be targeted by these conjugates.

Comparing the conjugates with the unlinked lectin probes showed in all cases a comparable binding affinity. Further, all compounds showed better binding than Me-α-D-Gal (LecA) or Me-α-D-Man (LecB). Due to the highly optimized structure of the fucose-mannose pharmacophore, the LecB targeting compounds were comparably active on LecB as L-fucose. In conclusion, the topology of the carbohydrate binding sites in both proteins allowed the conjugation with an antibiotic cargo without influencing lectin binding.

Antibiotic Susceptibility Assay. The antibiotic activity of lectin-targeted ciprofloxacin conjugates 22–31 was tested against a panel of Gram-positive and Gram-negative bacteria (Table 2). The model organisms *E. coli* MG1655 (a common lab strain), *E. coli* DSM 1116 (an antibiotic susceptibility reference strain recommended by the DSMZ), and the Gram-positive *Staphylococcus carnosus* DSM 20501 were tested first to assess Gram-negative specific antibiotic activity and strain specificity. Afterward, the antibiotic activity against the two *P. aeruginosa* strains PA14 and PAO1 was studied. These two important reference strains represent a broad range of clinical isolates and are well studied in the literature.³³ To determine the effect of the lectins' presence on antibiotic activity, we used the lectin-deficient knockout mutants of *P. aeruginosa* PA14, i.e., PA14 Δ*lecA* and PA14 Δ*lecB*. Ciprofloxacin (3) and the synthetic intermediate 20 were used as reference compounds

Table 2. Antibacterial Activity of Lectin Targeted Conjugates **22–31**, **20**, and Ciprofloxacin (**3**) against a Panel of Bacterial Organisms. LecA-targeting galactosides were generally more active than the LecB-targeting conjugates. A shorter linker length on the side of the antibiotic led to increased antimicrobial activity^a



compound	target: LecA								target: LecB		references	
	22	23	24	25	26	27	28	29	30	31	20	3
molecular mass [g/mol]	739.8	753.8	753.8	767.8	767.8	781.9	781.9	795.9	761.8	775.9	369.4	331.3
linker length n/m	1/0	1/1	2/0	2/1	3/0	3/1	4/0	4/1	-/0	-/1	0	
test organism	MIC [$\mu\text{g}/\text{mL}$]											
<i>E. coli</i> K12 MG1655	2	8–16	2	16	1–2	16	2–4	16	8–16	16	n.d.	<0.125
<i>E. coli</i> DSM 1116	2–4	16	2–4	32	2–32	4–32	4–32	4–32	16–32	32	n.d.	<0.125
<i>S. carnosus</i> DSM 20501	32	64	32	>64	16	64	8	≥ 64	>64	>64	n.d.	<0.125
<i>P. aeruginosa</i> PA14 wt	16	≥ 64	8–16	>64	8–16	>64	32	>64	64	>64	2–4	0.025–0.1
<i>P. aeruginosa</i> PA14 wt + 1 $\mu\text{g}/\text{mL}$ PMBN	4–16	16–64	8–16	32–64	4	32–64	2–8	32–64	64	64	0.025–0.5	0.025
<i>P. aeruginosa</i> PA14 ΔlecA	16–32	≥ 64	8–16	>64	8–16	>64	32	>64	≥ 64	>64	4–8	0.05–0.08
<i>P. aeruginosa</i> PA14 ΔlecB	16–32	≥ 64	8–32	>64	8–16	>64	32–64	>64	64	>64	4	0.05–0.08
<i>P. aeruginosa</i> PAO1 wt	16–32	>64	16	>64	16–32	>64	32–64	>64	≥ 64	>64	4–8	0.025–0.08
<i>P. aeruginosa</i> PAO1 wt + 1 $\mu\text{g}/\text{mL}$ PMBN	4–8	32–64	4–8	32–64	4–8	32–64	8–16	32–64	32–64	≥ 64	1–2	0.025–0.05

^aData is presented as minimal inhibitory concentration (MIC) range from at least three independent experiments. Molar MIC is given in Table S2. n.d. = not determined.

to study the effect of piperazine *N*-alkylation on antibiotic activity.

Ciprofloxacin is known to be particularly active against Gram-negative compared to Gram-positive organisms. Both *E. coli* strains showed higher susceptibility against the ciprofloxacin conjugates than the Gram-positive organism *S. carnosus*. Comparing both *E. coli* strains, the antibiotic susceptibility reference strain (DSM 1116) showed similar or slightly higher MIC values (Table 2).

Compared to *E. coli*, *P. aeruginosa* PA14 and PAO1 both showed lower susceptibility against all compounds tested, which was expected due to the well-known increased intrinsic antimicrobial resistance of *P. aeruginosa*. It was also observed that the clinical isolate PAO1 was similarly or slightly less susceptible than the clinical isolate PA14. Importantly, some of the lectin-targeted conjugates reached antibiotic activity down to 8 $\mu\text{g}/\text{mL}$ against planktonic *P. aeruginosa* (Table 2).

Comparing the MIC values amongst the different conjugates and the reference compounds **20** and ciprofloxacin (**3**), we observed a structure–activity relationship: Conjugates containing galactosides as lectin-targeting probes showed higher antimicrobial activity than LecB-targeting compounds, which are based on a C-glycosidic hybrid structure. It has been previously postulated that galactosides are recognized by the bacterial sugar uptake machinery,^{54,55} which would result in an active transportation over the Gram-negative cell wall. A comparative study by O’Shea and Moser⁶⁸ on commonly used

antibiotics showed that especially *P. aeruginosa* active compounds have clogD values of <0. LogD calculation (data not shown) of all conjugates **22–31** and **20** revealed positive values, which could explain the reduction in antimicrobial activity with respect to ciprofloxacin (**3**) showing a clogD of <0.

Further, a decreased linker length between triazole and ciprofloxacin (entitled m in the structure drawings) amplified the antibiotic activity in all cases, independent of the carbohydrate probe or microorganism tested. This effect becomes most evident in case of *E. coli* K12 MG1655, where an up to 8-fold increase in MIC could be observed (e.g., **24** vs **25**, Table 2). We assume that changing the distance between the tertiary amine and the electron-withdrawing triazole affects the amine’s basicity, which is believed to play a role in porin diffusion.⁶⁷ The parent drug ciprofloxacin reached MIC values of 0.025–0.1 $\mu\text{g}/\text{mL}$ against *P. aeruginosa*, while the propargylated derivative **20** showed MIC values of 2–4 $\mu\text{g}/\text{mL}$ against *P. aeruginosa* PA14 and 4–8 $\mu\text{g}/\text{mL}$ against *P. aeruginosa* PAO1, thereby reaching the concentration range of the most potent conjugates. As alkylation of ciprofloxacin alone already led to a significant decrease in activity, conjugation at the secondary amine in the piperazine ring is most likely responsible for the decreased antibiotic activity.^{60–62}

Regarding total linker size, increasing length resulted in higher MIC values (e.g., **22** vs **29**), which can be explained by a size exclusion effect of outer membrane porins. It is believed

that these barrel-formed, hydrophilic channels play crucial roles for membrane permeation of hydrophilic compounds and are limited to a certain molecular weight or three-dimensional molecular structure.^{67,68} Further, the introduction of additional methylene groups results in an increased number of rotatable bonds and increased lipophilicity, which is also described to reduce bacterial cell uptake.^{67,68} We compared retention times from reversed-phase HPLC analyses as a surrogate parameter for lipophilicity (Table S4 and Figure S4). Two trends were observed that correlated with the antimicrobial activity assays: (i) In general, all galactose-based conjugates showed lower retention times than the C-glycosides indicative for higher polarity, and (ii) the stepwise introduction of methylene groups in both linkers led to a stepwise increase in retention times indicating higher lipophilicity, which correlated with the reduced antimicrobial activity. Only the shortest galactose-based conjugates **22** and **23** ($n = 1$, $m = 0$ or 1 , respectively) showed retention times slightly higher than expected in their series, which may be a result of an intramolecular hydrogen bonding between the amide NH and the central nitrogen atom of the triazole for $n = 1$ altering their conformation and thus their physicochemical properties. We observed that the most anti-*Pseudomonas* active compound **24** showed the lowest retention time amongst the conjugates. Thus, we conclude that the conjugates' lipophilicity is an important parameter for antimicrobial activity. Ciprofloxacin (**3**) was eluted much earlier than all conjugates, reflecting its higher hydrophilicity.

Polymyxin B nonapeptide (PMBN) is a membrane-active antimicrobial compound that is used at sub-MIC concentrations to increase outer membrane permeability. Without being lethal to the microbe, this can provide information on bacterial cellular uptake of antimicrobial drugs. In our studies, all conjugates, except **24** and **30**, benefit from the presence of the permeabilizer at least twofold (e.g., **26**, Table 2). Interestingly, the MIC of reference compound **20** was increased most and reached high antimicrobial activity approximating ciprofloxacin. Thus, the drop in antibiotic activity for the conjugates can partially be explained by decreased cell wall permeability, as a consequence of derivatization of the secondary amine. As expected, unmodified ciprofloxacin benefitted only marginally by the addition of PMBN.

Gyrase-Dependent DNA Supercoiling Inhibition Assay. The antimicrobial susceptibility assays revealed a decrease in antibiotic activity after conjugation (Table 2). We showed that this decrease is most likely caused by a reduced bacterial cellular uptake as shown by the co-incubation experiments with membrane permeabilizer. However, the addition of PMBN did not result in MIC values comparable to ciprofloxacin, suggesting that further features are affected by conjugation of ciprofloxacin to the lectin probes. Thus, we investigated the compounds' ability to inhibit bacterial gyrase, the target of ciprofloxacin.

We compared the gyrase inhibition activity of three conjugates (**22**, **23**, and **30**), while the propargylated ciprofloxacin derivative **20** and unmodified ciprofloxacin (**3**) were used as controls (Figure 3). Gyrase-inhibition leads to a reduction of supercoiled DNA, which can be visualized by gel electrophoresis. Ciprofloxacin was the most active compound, reaching full inhibition of plasmid supercoiling in the nanomolar range. Compound **20** ($IC_{50} = 0.7 \pm 0.1 \mu M$) was less active than ciprofloxacin; however, it still showed an IC_{50} in the nanomolar range, suggesting that modification in this

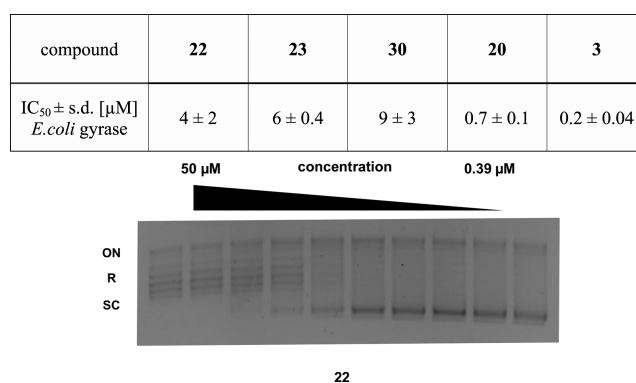


Figure 3. Effect of **20**, **22**, **23**, **30**, and ciprofloxacin (**3**) on gyrase-catalyzed DNA supercoiling. Propargylation (**20**) decreased the inhibitory concentration only by a factor of 3.5 compared to **3**. Gyrase inhibition as a putative mode of action was confirmed as all conjugates inhibit gyrase-catalyzed DNA supercoiling. Mean and standard deviations were determined from three independent experiments. A representative titration of *E. coli* gyrase with **22** in a supercoiling inhibition assay is shown. Controls: plasmid without gyrase and inhibitor (leftmost band) and plasmid with gyrase and without inhibitor (rightmost band). ON, open circular/nicked plasmid; R, relaxed topoisomers; SC, supercoiled topoisomers of *E. coli* DNA.

region of the molecule as concluded from the crystal structure analysis is indeed possible. The lectin-targeting conjugates were also potent inhibitors of gyrase supercoiling activity in the single digit micromolar range, although they were not as potent as reference compounds **20** and **3**. This decrease in activity explains why the compounds did not reach the antibiotic activity of *N*-propargyl ciprofloxacin (**20**) after membrane permeabilization with PMBN.

***P. aeruginosa* Biofilm Accumulation Assay.** Since the carbohydrate-ciprofloxacin conjugates **22–31** bind their respective lectins in a competitive binding assay, we investigated the ability of two representative lectin-targeting conjugates to accumulate in *P. aeruginosa* biofilms *in vitro* (Figure 4).

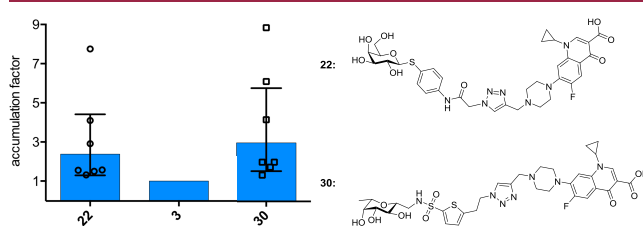


Figure 4. Accumulation of **22** (targeting LecA) and **30** (targeting LecB) in *P. aeruginosa* PAO1 biofilm relative to ciprofloxacin (**3**). Each data point reflects the relative accumulation compared to ciprofloxacin of a single independent assay with at least three technical replicates. Bars show geometric mean and 95% confidence interval (see the Supporting Information for more detailed information, Figure S2).

For this purpose, biofilms were grown on peg lids in a 96-well format that allows incubation and washing steps in a batch format. After 24 h of bacterial growth, *P. aeruginosa* PAO1 formed a visible biofilm on the pegs, which was used for compound accumulation assays. After one washing step to remove planktonic bacteria, the biofilm was immersed for 10 min into solutions containing two lectin-targeting conjugates (**22** and **30**) or ciprofloxacin (**3**) at $100 \mu M$. After a

Table 3. Early ADMET Data on Two Representative Lectin-Targeted Conjugates (22 and 30) and Ciprofloxacin (3): All Compounds Were Metabolically Stable in Human Plasma and Microsomal Fractions. Cytotoxicity was reduced compared to ciprofloxacin^a

compound	metabolic stability			plasma protein binding [%]	cytotoxicity @ 100 μ M [% inhibition]	
	$t_{1/2}$ [min]	CL _{MIC} [μ L/min/mg protein]			human plasma	HEK293
	human plasma	MLM	HLM			
22	>150	10	10	69 \pm 7	8 \pm 4	5 \pm 22
30	>150	10	15	75 \pm 10	11 \pm 12	−9 \pm 15
3	>150	n.d.	n.d.	33 \pm 2	48 \pm 5	18 \pm 11

^aData is presented as mean and standard deviation from at least two independent experiments (exception: one experiment for CL_{MIC} data). MLM, mouse liver microsomes; HLM, human liver microsomes; n.d., not determined.

subsequent washing step to remove an unspecifically bound compound, the biofilm was disrupted and the amount of bound compound was quantified by LC-MS/MS.

Although the assay showed variation in absolute compound binding between biological replicates (Figure S2), we observed an obvious trend: the lectin targeted conjugates reached higher concentrations in the bacterial biofilm than the unmodified ciprofloxacin, independent of their lectin targeting moiety (Figure 4). These results are fundamental for the future development of further biofilm targeting antibiotic conjugates.

In Vitro Early ADMET. Metabolic stability of two representative conjugates (22 and 30) and ciprofloxacin (3) as the parent molecule was studied *in vitro* against human plasma, human liver microsomes, and mouse liver microsomes (Table 3). The data reveals high metabolic stability in all matrices tested: half-life in human plasma was above 150 min for all compounds and microsomal clearance by mouse and human liver microsomes was very low on the lectin-targeting compounds. Both conjugates showed clearance of 10 μ L/min/mg protein by human liver microsomes, reaching the assay's lower limit. Against mouse liver microsomes, compound 22 also reached the assay limit of 10 μ L/min/mg protein, whereas 30 was slightly less stable (CL_{MIC} = 15 μ L/min/mg protein) but still classified in the most stable category of this assay (\leq 15 μ L/min/mg protein). Thus, the compounds are considered metabolically stable, fitting the molecular design approach as S-/C-glycosides. Both conjugates showed higher plasma protein binding than ciprofloxacin (69 \pm 7% for 22, 75 \pm 10% for 30 vs 33 \pm 2% for 3).

Acute cytotoxicity was tested against a human embryonic kidney cell line (HEK 293) and adenocarcinoma human alveolar basal epithelial cells (A549). Compounds 22 and 30 showed no cytotoxicity at 100 μ M after 48 h incubation, whereas ciprofloxacin showed detectable cytotoxicity (48 \pm 5% inhibition) against HEK 293 cells (Table 3). Furthermore, penetration over cultured human airway epithelial cells (Calu-3 HTB-55) was assessed *in vitro* via a Transwell system to analyze the compounds ability to permeate over mammalian cell membranes. No detectable permeation (apical to basal) was observed for compounds 22 and 30 after 4 h, while 10% ciprofloxacin was permeated after 4 h (data not shown). The low acute toxicity against human alveolar basal epithelial cells and the low lung cell permeation suggest the possibility of pulmonary application routes for patients suffering from cystic fibrosis.

CONCLUSIONS AND OUTLOOK

Biofilms present a hallmark in chronic *P. aeruginosa* infections. The ability to protect against the host immune system and

antibiotic treatment renders this chemo-mechanic barrier as a strong virulence factor. Notably, it is not advisable to solely focus MIC optimization on planktonic cells during the development of new antibiotics but rather to find new therapeutic strategies. As an example, Müssen et al. showed that biofilm susceptibility of clinical *P. aeruginosa* isolates cannot be deduced from commonly studied phenotypes like MIC or minimal bactericidal concentration values.⁶⁹ Delivering antibiotics specifically to the site of infection could decrease potential side effects and enhance efficacy. In this work, we developed and characterized the first *P. aeruginosa* lectin-targeted antibiotic conjugates. Based on our previous work, we conjugated ciprofloxacin to LecA and LecB probes and varied the linker length.

The antibiotic conjugates showed effective lectin binding against LecA and both LecB variants from *P. aeruginosa* PAO1 and PA14, which represent a broad range of clinical isolates of *P. aeruginosa*. A structure–activity relationship regarding the antimicrobial activity of the synthesized conjugates could be established. In general, a shorter spacer between triazole and antibiotic as well as a D-galactose-based lectin probe was preferred. The observed reduction in antibiotic activity could be rationalized due to a higher molecular weight, decreasing the ability to penetrate the Gram-negative cell wall. Comparison with N-propargylated ciprofloxacin showed, that alkylation of the secondary amine of the piperazine ring already resulted in a decreased antibiotic activity. Further, we proved the inhibition of gyrase-catalyzed DNA supercoiling as the conjugates' antimicrobial mode of action.

In the first *P. aeruginosa* biofilm accumulation assay, we observed an enrichment of lectin-targeting conjugates compared to ciprofloxacin, which could compensate for the decrease in antimicrobial activity. Since cytotoxicity of both conjugates was decreased compared to ciprofloxacin especially against kidney cells, and the biofilm accumulation was achieved, a reduction of the severe systemic side effects of ciprofloxacin is possible. Further, *in vitro* metabolism assays showed good metabolic stability supporting the conjugates' design as S- or C-glycosides.

This work reports the first *P. aeruginosa* biofilm-targeted antibiotics and analyzes their properties on lectin binding, antimicrobial activity, target inhibition, and biofilm enrichment. *In vitro* studies revealed a reduced cytotoxicity of the conjugates compared to the parent drug ciprofloxacin. Future work will address the improvement of antimicrobial activity of the antibiotic conjugates. Our modular synthesis allows the conjugation of lectin probes to other antibiotics, leading to future generations of biofilm targeting antibiotics.

EXPERIMENTAL SECTION

Chemical Synthesis. Thin layer chromatography (TLC) was performed on Silica Gel 60 coated aluminum sheets containing a fluorescence indicator (Merck KGaA, Darmstadt, Germany) and developed under UV light (254 nm) and aqueous KMnO₄ solution or a molybdate solution (a 0.02 M solution of ammonium cerium sulfate dihydrate and ammonium molybdate tetrahydrate in aqueous 10% H₂SO₄). Self-packed Silica Gel 60 columns (60 Å, 400 mesh particle size, Fluka, for normal-phase liquid chromatography) or Chromabond Flash RS15 C₁₈ ec columns (Macherey-Nagel, Düren, Germany, for reversed-phase liquid chromatography), and a Teledyne Isco Combiflash Rf200 system were used for preparative medium pressure liquid chromatography (MPLC). Nuclear magnetic resonance (NMR) spectroscopy was performed on a Bruker Avance III 500 UltraShield spectrometer at 500 MHz (¹H) or 126 MHz (¹³C). Chemical shifts are given in parts per million (ppm) and were calibrated on residual solvent peaks as an internal standard. Multiplicities were specified as s (singlet), d (doublet), t (triplet), q (quartet), or m (multiplet). The signals were assigned with the help of ¹H,¹H COSY, and DEPT-135-edited ¹H,¹³C HSQC experiments. Assignment numbering of the C-glycoside atoms and groups corresponds to the numbering in fucose. Assignment numbering of the galactoside atoms and groups corresponds to the numbering in galactose. Assignment numbering of the ciprofloxacin atoms and groups corresponds to the numbering in ciprofloxacin (cipro).⁷⁰ Commercial chemicals and solvents were used without further purification. Deuterated solvents were purchased from Eurisotop (Saarbrücken, Germany). Ciprofloxacin and polymyxin B nonapeptide-HCl (PMBN) was purchased from Sigma-Aldrich (purity ≥98%, HPLC, Merck KGaA, Darmstadt, Germany), and ciprofloxacin-HCl was purchased from Cayman Chemical (Ann Arbor, Michigan, USA). If not stated otherwise, the purity of the final compounds was further analyzed by HPLC-UV, and all UV active compounds had a purity of at least 95%. Chromatographic separation was performed on a Dionex Ultimate 3000 HPLC (Thermo Scientific, Germany) with UV detection at 254 nm using a RP-18 column (100/2 Nucleoshell RP18plus, 2.7 μm, from Macherey-Nagel, Germany) as a stationary phase. LCMS-grade distilled MeCN and double distilled H₂O were used as mobile phases containing formic acid (0.1% v/v). In a gradient run, an initial concentration of 5% MeCN in H₂O was increased to 95% during 7 min at a flow rate 600 μL/min. The injection volume was 4 μL of 1 mM compound in H₂O/DMSO = 100:1. UPLC-HRMS for key compounds were obtained using a RP-18 column (EC 150/2 Nucleodur C18 Pyramid, 3 μm, from Macherey-Nagel, Germany) and a Q Exactive Focus Orbitrap spectrometer (Thermo Scientific, Germany). The data was analyzed using Xcalibur data acquisition and interpretation software (Thermo Scientific, Germany).

General procedure (i) for amide couplings of **6**: Aniline **6** and K₂CO₃ (2 eq.) were dispersed in dry DCM (0.1 M) and cooled (0 °C). The corresponding (*ω*-bromo)acylhalide was added dropwise under vigorous stirring. After stirring for 15 min, the reaction was allowed to warm to r.t. and stirred for 1–4 h until full conversion as monitored by TLC (PE:EtOAc) or HPLC-MS. The reaction was quenched with ice-cold water. The organic phase was washed with brine, and combined organic layers were dried over anhydrous Na₂SO₄. After filtration, the solvent was evaporated *in vacuo*.

General procedure (ii) for S_N2 reactions with NaN₃ toward **7–10**: The crude starting material was dissolved in dry DMF (0.1 M). A 5 eq. solution of NaN₃ was added, and the reaction was stirred at r.t. until completion (monitored by HPLC-MS). Then, the reaction was diluted with an excess of water and extracted with EtOAc (3x). The combined organic layers were washed with half satd. brine and dried over anhydrous Na₂SO₄. After filtration, the solvent was evaporated *in vacuo* and the products were purified by MPLC (PE:EtOAc, 30–80%).

General procedure (iii) for the Zemplén deprotection of **7–10**: The starting material was suspended in dry MeOH (0.1 M) and a freshly prepared solution of NaOMe in MeOH (1 M) was added

dropwise to 10 mol %. The reaction was stirred for 1–2 h until the disappearance of the starting material, monitored by TLC (PE:EtOAc, 4:6). Then, the reaction was diluted with MeOH and neutralized with Amberlite IR-120 H⁺ exchange resin. The resin was filtered off, and the solvent was evaporated *in vacuo*. Purification was performed by reversed-phase MPLC (MeCN:H₂O, 10–20%, 0.1% formic acid). The solvent was removed by lyophilization.

General procedure (iv) for the copper-catalyzed click reaction toward conjugates **22–31**: Alkyne (1.1 eq.) and azide (1 eq.) were dissolved in 1 mL of dry DMF (purged with argon). CuSO₄·7H₂O (10 mol %) and sodium ascorbate (20 mol %) were added as aqueous solutions from freshly prepared stock solutions (100 mM). The mixture was stirred at r.t. or 40 °C for 16–24 h. Reaction progress was monitored by HPLC-MS. After full conversion, the solvents were evaporated *in vacuo* followed by purification via RP-MPLC (MeCN:H₂O, 10–20%, 0.1% formic acid). The solvent was removed by lyophilization.

p-Nitrophenyl 2,3,4,6-Tetra-O-acetyl-β-D-thiogalactopyranoside (5). Galactose pentaacetate (**4**, 2.0 g, 5.1 mmol, 1 eq.) and *p*-nitrothiophenol (2.4 g, 15.3 mmol, 3 eq.) were dissolved in 20 mL dry CH₂Cl₂ in a heat-dried flask under a N₂ atmosphere. The mixture was cooled (0 °C), and BF₃·Et₂O (3.2 mL, 25.5 mmol, 5 eq.) was added dropwise under vigorous stirring. Afterward, the reaction was allowed to warm to r.t. and stirred overnight (17 h). Reaction progress was monitored by TLC (Tol:EtOAc, 9:1). After consumption of the starting material, the reaction was poured on ice water. The organic phase was isolated and washed with aq. satd. NaHCO₃. The combined organic layers were washed with half satd. brine and dried over anhydrous Na₂SO₄. After filtration, the solvent was removed *in vacuo*. Purification by MPLC (SiO₂, EtOAc in toluene, 5–20%) gave the product as a pale yellow amorphous solid (1.3 g, 51%). ¹H NMR (500 MHz, CHCl₃-*d*) δ 8.16 (d, *J* = 8.8 Hz, 2H, Ar-H), 7.61 (d, *J* = 8.8 Hz, 2H, Ar-H), 5.47 (d, *J* = 3.2 Hz, 1H, glyco-H-4), 5.29 (t, *J* = 10.0 Hz, 1H, glyco-H-2), 5.10 (dd, *J* = 9.9, 3.3 Hz, 1H, glyco-H-3), 4.86 (d, *J* = 10.0 Hz, 1H, glyco-H-1), 4.21 (dd, *J* = 11.5, 7.2 Hz, 1H, glyco-H-6), 4.14 (dd, *J* = 11.5, 5.8 Hz, 1H, glyco-H-6'), 4.04 (t, *J* = 6.5 Hz, 1H, glyco-H-5), 2.35 (s, 3H, Ac-CH₃), 2.16 (s, 3H, Ac-CH₃), 2.09 (s, 3H, Ac-CH₃), 2.08 (s, 3H, Ac-CH₃), 1.99 (s, 3H, Ac-CH₃); ¹³C NMR (126 MHz, CHCl₃-*d*) δ 170.44 (C=O), 170.15 (C=O), 170.08 (C=O), 169.50 (C=O), 146.96 (Ar-C), 142.52 (Ar-C), 130.52 (Ar-C), 123.97 (Ar-C), 84.97 (glyco-C-1), 74.97 (glyco-C-5), 71.85 (glyco-C-3), 67.20 (glyco-C-4), 66.84 (glyco-C-2), 61.81 (glyco-C-6), 20.88 (Ac-CH₃), 20.84 (Ac-CH₃), 20.79 (Ac-CH₃), 20.68 (Ac-CH₃). LR-MS: *m/z* = 503.16, [M + Na]⁺. Spectroscopic data is in accordance with the literature.⁷¹

p-Aminophenyl 2,3,4,6-Tetra-O-acetyl-β-D-thiogalactopyranoside (6). Compound **6** was synthesized according to Casoni et al.⁶⁶ *p*-nitrophenyl 2,3,4,6-tetra-O-acetyl-β-D-galactothiopyranoside (**5**, 1.0 g, 2.06 mmol, 1 eq.) was dissolved in 70 mL of dry DCM and Pd/C (50 mg, 5 wt %) was added. The reaction vessel was flushed several times with hydrogen and subsequently stirred under a hydrogen atmosphere (1 bar) for 48 h. The reaction was followed by TLC (PE:EtOAc, 1:1). After completion, the reaction was filtered over celite. The solvent was removed *in vacuo*, and the pure product was obtained as a pink amorphous solid (903 mg, 96%), which was used without further purification in the next step. ¹H NMR (500 MHz, DMSO-*d*₆) δ 7.18–7.08 (m, 2H, ArH), 6.57–6.48 (m, 2H, ArH), 5.39 (s, 2H, NH₂), 5.25 (dd, *J* = 3.5, 1.0 Hz, 1H, glyco-H-4), 5.18 (dd, *J* = 9.7, 3.5 Hz, 1H, glyco-H-3), 4.93 (t, *J* = 9.9 Hz, 1H, glyco-H-2), 4.78 (d, *J* = 10.0 Hz, 1H, glyco-H-1), 4.21–4.13 (m, 1H, glyco-H-5), 4.11–3.93 (m, 2H, glyco-H-6), 2.09 (s, 3H, Ac-CH₃), 2.06 (s, 3H, Ac-CH₃), 2.00 (s, 3H, Ac-CH₃), 1.90 (s, 3H, Ac-CH₃). ¹³C NMR (126 MHz, DMSO-*d*₆) δ 169.93 (C=O), 169.84 (C=O), 169.46 (C=O), 169.17 (C=O), 149.42 (ArC), 135.15 (ArC), 115.20 (ArC), 114.07 (ArC), 86.07 (glyco-C-1), 73.25 (glyco-C-5), 71.20 (glyco-C-3), 67.62 (glyco-C-4), 67.24 (glyco-C-2), 61.66 (glyco-C-6), 20.63 (Ac-CH₃), 20.51 (Ac-CH₃), 20.40 (Ac-CH₃), 20.36 (Ac-CH₃). LR-MS: *m/z* = 456.2, [M + H]⁺.

p-(α-Azidoacetamido)phenyl 2,3,4,6-Tetra-O-acetyl-β-D-thiogalactopyranoside (7). **7** was synthesized starting from **6** in two

chemical steps in analogy to Casoni et al.:⁶⁶ Aniline **6** (300 mg, 0.66 mmol, 1 eq.) and triethylamine (140 μ L, 1.01 mmol, 1.6 eq.) were dissolved in 6 mL of dry DCM. The solution was cooled (0 °C), and bromoacetyl bromide (86 μ L, 0.99 mmol, 1.5 eq.) was added dropwise under vigorous stirring. The reaction was stirred for 1 h followed by TLC (PE:EtOAc, 7:3). After completion, the mixture was quenched with ice water. The organic phase was washed with aq. satd. NH_4Cl (3x), water (2x), and brine (1x) and dried over anhydrous Na_2SO_4 . After filtration, the solvent was removed *in vacuo* to yield the crude intermediate as an oil (370 mg), which was transformed according to general procedure ii. Product **7** was obtained as a white amorphous solid (283.2 mg, 80% over two steps). ^1H NMR in accordance with the literature⁶⁶ (500 MHz, CHCl_3 -*d*) δ 8.04 (s, 1H, Amide-NH), 7.52 (s, 4H, ArH), 5.41 (d, $J = 3.0$ Hz, 1H, glyco-H-4), 5.20 (t, $J = 9.9$ Hz, 1H, glyco-H-2), 5.04 (dd, $J = 9.9, 3.3$ Hz, 1H, glyco-H-3), 4.65 (d, $J = 10.0$ Hz, 1H, glyco-H-1), 4.18 (dd, $J = 11.3$ Hz, overlaps with 4.16, 1H, glyco-H-6), 4.16 (s, 2H, CH_2N_3), 4.11 (dd, $J = 11.3, 6.3$ Hz, 1H, glyco-H-6'), 3.92 (t, $J = 6.6$ Hz, 1H, glyco-H-5), 2.12 (s, 3H, Ac- CH_3), 2.10 (s, 3H, Ac- CH_3), 2.05 (s, 3H, Ac- CH_3), 1.97 (s, 3H, Ac- CH_3). ^{13}C NMR (126 MHz, CHCl_3 -*d*) δ 170.54 (C=O), 170.33 (C=O), 170.20 (C=O), 169.55 (C=O), 164.64 (C=O), 137.21 (ArC), 134.29 (ArC), 128.05 (ArC), 120.34 (ArC), 86.79 (glyco-C-1), 74.60 (glyco-C-5), 72.12 (glyco-C-3), 67.32 (glyco-C-4), 61.72 (glyco-C-2), 53.11 (glyco-C-6), 53.07 (CH_2N_3 , extracted from HSQC), 21.01 (Ac- CH_3), 20.85 (Ac- CH_3), 20.81 (Ac- CH_3), 20.73 (Ac- CH_3). LR-MS: $m/z = 539.1$, $[\text{M} + \text{H}]^+$.

p-(β -Azidopropamido)phenyl 2,3,4,6-Tetra-O-acetyl- β -D-thiogalactopyranoside (**8**). The title compound was synthesized starting from **6** (300 mg, 0.66 mmol, 1 eq.) according to general procedures i and ii and was obtained as a white amorphous solid over two chemical steps (316 mg, 87%). However, the elimination product could not be separated, resulting in a <10% contamination of the corresponding Michael-acceptor side product (quantified by ^1H NMR). ^1H NMR (500 MHz, CHCl_3 -*d*) δ 7.49 (s, 4H, ArH), 7.44 (s, 1H, NH), 6.44 (d, $J = 16.9$ Hz, 1H, $-\text{COCHCH}_2$, from impurity), 6.24 (dd, $J = 16.8, 10.3$ Hz, 1H, $-\text{COCHCH}-\text{H}$, from impurity), 5.80 (d, $J = 10.2$ Hz, 1H, $-\text{COCHCH}-\text{H}'$, from impurity), 5.40 (d, $J = 3.1$ Hz, 1H, glyco-H-4), 5.19 (t, $J = 9.9$ Hz, 1H, glyco-H-2), 5.03 (dd, $J = 9.9, 3.1$ Hz, 1H, glyco-H-3), 4.63 (d, $J = 9.9$ Hz, 1H, glyco-H-1), 4.17 (dd, $J = 11.3, 6.9$ Hz, 1H, glyco-H-6), 4.10 (dd, $J = 11.5, 6.3$ Hz, 1H, glyco-H-6'), 3.90 (t, $J = 6.5$ Hz, 1H, glyco-H-5), 3.72 (t, $J = 6.2$ Hz, 2H, COCH_2), 2.60 (t, $J = 6.2$ Hz, 2H, CH_2N_3), 2.11 (s, 3H, Ac- CH_3), 2.10 (s, 3H, Ac- CH_3), 2.05 (s, 3H, Ac- CH_3), 1.97 (s, 3H, Ac- CH_3). ^{13}C NMR (126 MHz, CHCl_3 -*d*) δ 170.45 (C=O), 170.25 (C=O), 170.10 (C=O), 169.48 (C=O), 168.22 (C=O), 137.92 (ArC), 134.23 (ArC), 127.27 (ArC), 120.14 (ArC), 86.78 (glyco-C-1), 74.43 (glyco-C-5), 72.00 (glyco-C-3), 67.24 (glyco-C-4), 67.20 (glyco-C-2), 61.58 (glyco-C-6), 47.24 ($\text{COCH}_2\text{CH}_2\text{N}_3$), 36.96 ($\text{COCH}_2\text{CH}_2\text{N}_3$), 20.88 (Ac- CH_3), 20.72 (Ac- CH_3), 20.67 (Ac- CH_3), 20.60 (Ac- CH_3). LR-MS: $m/z = 553.1$, $[\text{M} + \text{H}]^+$.

p-(γ -Azidobutyramido)phenyl 2,3,4,6-Tetra-O-acetyl- β -D-thiogalactopyranoside (**9**). The title compound was synthesized starting from **6** (300 mg, 0.66 mmol, 1 eq.) according to general procedures i and ii and was obtained as a white amorphous solid over two chemical steps (296 mg, 79%). ^1H NMR (500 MHz, CHCl_3 -*d*) δ 7.48 (s, 4H, Ar-H), 7.44 (s, 1H, NH), 5.40 (d, $J = 3.4$ Hz, 1H, glyco-H-4), 5.20 (t, $J = 9.9$ Hz, 1H, glyco-H-2), 5.02 (dd, $J = 10.0, 3.3$ Hz, 1H, glyco-H-3), 4.62 (d, $J = 9.9$ Hz, 1H, glyco-H-1), 4.17 (dd, $J = 11.3, 6.9$ Hz, 1H, glyco-H-6), 4.09 (dd, $J = 11.3, 6.3$ Hz, 1H, glyco-H-6'), 3.90 (t, $J = 6.6$ Hz, 1H, glyco-H-5), 3.41 (t, $J = 6.4$ Hz, 2H, COCH_2), 2.47 (t, $J = 7.1$ Hz, 2H, CH_2N_3), 2.12 (s, 3H, Ac- CH_3), 2.10 (s, 3H, Ac- CH_3), 2.04 (s, 3H, Ac- CH_3), 2.00 (t, $J = 6.8$ Hz, 2H, $-\text{CH}_2-$), 1.97 (s, 3H, Ac- CH_3). ^{13}C NMR (126 MHz, CHCl_3 -*d*) δ 170.57 (C=O), 170.35 (C=O), 170.26 (C=O), 170.21 (C=O), 169.61 (C=O), 138.25 (ArC), 134.31 (ArC), 127.14 (ArC), 120.11 (ArC), 86.95 (glyco-C-1), 74.52 (glyco-C-5), 72.10 (glyco-C-3), 67.36 (glyco-C-4), 67.32 (glyco-C-2), 61.68 (glyco-C-6), 50.78 (COCH_2), 34.26 (CH_2N_3), 24.66 (CH_2), 20.99 (Ac- CH_3), 20.82 (Ac- CH_3), 20.77 (Ac- CH_3), 20.71 (Ac- CH_3). LR-MS: $m/z = 567.1$, $[\text{M} + \text{H}]^+$.

p-(δ -Azidovaleryl-amido)phenyl 2,3,4,6-Tetra-O-acetyl- β -D-thiogalactopyranoside (**10**). The title compound was synthesized starting from **6** (300 mg, 0.66 mmol, 1 eq.) according to general procedures i and ii and was obtained as a white amorphous solid over two chemical steps (327 mg, 85%). ^1H NMR (500 MHz, CHCl_3 -*d*) δ 7.48 (s, 4H, Ar-H), 7.24 (s, 1H, NH), 5.40 (d, $J = 3.2$ Hz, 1H, glyco-H-4), 5.19 (t, $J = 9.9$ Hz, 1H, glyco-H-2), 5.03 (dd, $J = 9.9, 3.3$ Hz, 1H, glyco-H-3), 4.63 (d, $J = 10.0$ Hz, 1H, glyco-H-1), 4.17 (dd, $J = 11.3, 6.9$ Hz, 1H, glyco-H-6), 4.10 (dd, $J = 11.3, 6.3$ Hz, 1H, glyco-H-6'), 3.90 (t, $J = 6.6$ Hz, 1H, glyco-H-5), 3.34 (t, $J = 6.7$ Hz, 2H, $-\text{COCH}_2-$), 2.41 (t, $J = 7.3$ Hz, 2H, $-\text{CH}_2\text{N}_3$), 2.11 (s, 3H, Ac- CH_3), 2.10 (s, 3H, Ac- CH_3), 2.05 (s, 3H, Ac- CH_3), 1.97 (s, 3H, Ac- CH_3), 1.82 (p, $J = 7.4$ Hz, 2H, $-\text{CH}_2\text{CH}_2\text{N}_3$), 1.74–1.64 (p, 2H, $-\text{COCH}_2\text{CH}_2-$). ^{13}C NMR (126 MHz, CHCl_3 -*d*) δ 170.69 (C=O), 170.56 (C=O), 170.36 (C=O), 170.21 (C=O), 169.59 (C=O), 138.34 (ArC), 134.39 (ArC), 127.03 (ArC), 120.05 (ArC), 86.99 (glyco-C-1), 74.55 (glyco-C-5), 72.13 (glyco-C-3), 67.37 (glyco-C-4), 67.33 (glyco-C-2), 61.70 (glyco-C-6), 51.31 ($\text{CO}-\text{CH}_2-$), 37.07 ($-\text{CH}_2-\text{N}_3$), 28.43 ($-\text{COCH}_2\text{CH}_2-$), 22.75 ($-\text{CH}_2\text{CH}_2\text{N}_3$), 21.01 (Ac- CH_3), 20.85 (Ac- CH_3), 20.80 (Ac- CH_3), 20.72 (Ac- CH_3). LR-MS: $m/z = 581.2$, $[\text{M} + \text{H}]^+$.

p-(α -Azidoacetamido)phenyl- β -D-thiogalactopyranoside (**11**). The title compound was synthesized from **7** (275 mg, 0.51 mmol, 1 eq.) according to general procedure iii and was obtained as a white solid (142 mg, 75%). ^1H NMR (500 MHz, $\text{MeOH}-d_4$) δ 7.54 (s, 4H, ArH), 4.51 (d, $J = 9.7$ Hz, 1H, glyco-H-1), 4.01 (s, 2H, $-\text{CH}_2\text{N}_3$), 3.89 (d, $J = 3.2$ Hz, 1H, glyco-H-4), 3.76 (dd, $J = 11.5, 6.8$ Hz, 1H, glyco-H-6), 3.70 (dd, $J = 11.5, 5.2$ Hz, 1H, glyco-H-6'), 3.62–3.52 (m, 2H, glyco-H-2 + glyco-H-5), 3.49 (dd, $J = 9.2, 3.3$ Hz, 1H, glyco-H-3). ^{13}C NMR (126 MHz, $\text{MeOH}-d_4$) δ 168.47 (C=O), 138.61 (ArC), 133.58 (ArC), 130.91 (ArC), 121.59 (ArC), 90.50 (glyco-C-1), 80.61 (glyco-C-5), 76.30 (glyco-C-3), 70.93 (glyco-C-2), 70.40 (glyco-C-4), 62.60 (glyco-C-6), 53.26 ($-\text{CH}_2\text{N}_3$). HR-MS calcd $[\text{C}_{14}\text{H}_{17}\text{N}_4\text{O}_6\text{S}]^-$: 369.0874, found 369.0877.

p-(β -Azidopropamido)phenyl- β -D-thiogalactopyranoside (**12**). The title compound was synthesized from **8** (309 mg, 0.56 mmol, 1 eq.) according to general procedure iii and was obtained as a white solid (216 mg, 54%). ^1H NMR (500 MHz, $\text{MeOH}-d_4$) δ 7.53 (d, $J = 1.1$ Hz, 4H, ArH), 4.50 (d, $J = 9.6$ Hz, 1H, glyco-H-1), 3.88 (d, $J = 2.5$ Hz, 1H, glyco-H-4), 3.76 (dd, $J = 11.5, 6.8$ Hz, 1H, glyco-H-6), 3.70 (dd, $J = 11.5, 5.3$ Hz, 1H, glyco-H-6'), 3.64 (t, $J = 6.4$ Hz, 2H, $-\text{COCH}_2-$), 3.60–3.52 (m, 2H, glyco-H-2 + glyco-H-5), 3.48 (dd, $J = 9.2, 3.3$ Hz, 1H, glyco-H-3), 2.63 (t, $J = 6.4$ Hz, 2H, $-\text{CH}_2\text{N}_3$). ^{13}C NMR (126 MHz, $\text{MeOH}-d_4$) δ 171.27 (C=O), 139.20 (ArC), 133.68 (ArC), 130.38 (ArC), 121.39 (ArC), 90.59 (glyco-C-1), 80.61 (glyco-C-5), 76.33 (glyco-C-3), 70.93 (glyco-C-2), 70.43 (glyco-C-4), 62.63 (glyco-C-6), 48.43 ($-\text{COCH}_2-$), 37.08 ($-\text{CH}_2\text{N}_3$). HR-MS calcd $[\text{C}_{15}\text{H}_{19}\text{N}_4\text{O}_6\text{S}]^-$: 383.1031, found 383.1036.

p-(γ -Azidobutyramido)phenyl- β -D-thiogalactopyranoside (**13**). The title compound was synthesized from **9** (296 mg, 0.52 mmol, 1 eq.) according to general procedure iii and was obtained as a white solid in 81% yield. ^1H NMR (500 MHz, $\text{MeOH}-d_4$) δ 7.52 (s, 4H, Ar-H), 4.50 (d, $J = 9.6$ Hz, 1H, glyco-H-1), 3.88 (d, $J = 3.2$ Hz, 1H, glyco-H-4), 3.76 (dd, $J = 11.5, 6.8$ Hz, 1H, glyco-H-6), 3.70 (dd, $J = 11.5, 5.3$ Hz, 1H, glyco-H-6'), 3.61–3.52 (m, 2H, glyco-H-2 + glyco-H-5), 3.48 (dd, $J = 9.2, 3.3$ Hz, 1H, glyco-H-3), 3.39 (t, $J = 6.7$ Hz, 2H, $-\text{COCH}_2-$), 2.47 (t, $J = 7.3$ Hz, 2H, $-\text{CH}_2\text{N}_3$), 1.94 (p, $J = 7.0$ Hz, 2H, $-\text{CH}_2-$). ^{13}C NMR (126 MHz, $\text{MeOH}-d_4$) δ 173.37 (C=O), 139.37 (ArC), 133.70 (ArC), 130.21 (ArC), 121.38 (ArC), 90.62 (glyco-C-1), 80.62 (glyco-C-5), 76.34 (glyco-C-3), 70.94 (glyco-C-2), 70.43 (glyco-C-4), 62.63 (glyco-C-6), 51.92 ($-\text{COCH}_2-$), 34.73 ($-\text{CH}_2\text{N}_3$), 25.94 ($-\text{CH}_2-$). HR-MS calcd $[\text{C}_{16}\text{H}_{21}\text{N}_4\text{O}_6\text{S}]^-$: 397.1187, found 397.1189.

p-(δ -Azidovaleryl-amido)phenyl- β -D-thiogalactopyranoside (**14**). The title compound was synthesized from **10** (327 mg, 0.56 mmol) according to general procedure iii and was obtained as a white solid (235 mg, 84%). ^1H NMR (500 MHz, $\text{MeOH}-d_4$) δ 7.52 (s, 4H, ArH), 4.49 (d, $J = 9.6$ Hz, 1H, glyco-H-1), 3.88 (dd, $J = 3.3, 0.8$ Hz, 1H, glyco-H-4), 3.76 (dd, $J = 11.5, 6.8$ Hz, 1H, glyco-H-6), 3.70 (dd, $J = 11.5, 5.3$ Hz, 1H, glyco-H-6'), 3.62–3.50 (m, 2H, glyco-H-2 + glyco-

H-5), 3.48 (dd, $J = 9.2, 3.3$ Hz, 1H, glyco-H-3), 3.34 (t, $J = 6.7$ Hz, 2H, $-\text{COCH}_2-$), 2.40 (t, $J = 7.4$ Hz, 2H, $-\text{CH}_2\text{N}_3$), 1.82–1.72 (m, 2H, $-\text{CH}_2\text{CH}_2\text{N}_3$), 1.70–1.60 (m, 2H, $-\text{COCH}_2\text{CH}_2-$). ^{13}C NMR (126 MHz, MeOH- d_4) δ 174.06 (C=O), 139.39 (ArC), 133.72 (ArC), 130.18 (ArC), 121.37 (ArC), 90.62 (glyco-C-1), 80.62 (glyco-C-5), 76.34 (glyco-C-3), 70.94 (glyco-C-2), 70.43 (glyco-C-4), 62.63 (glyco-C-6), 52.16 ($-\text{COCH}_2-$), 37.27 ($-\text{CH}_2\text{N}_3$), 29.45 ($-\text{COCH}_2\text{CH}_2-$), 23.99 ($-\text{CH}_2\text{CH}_2\text{N}_3$). HR-MS calcd $[\text{C}_{17}\text{H}_{23}\text{N}_4\text{O}_6\text{S}]^-$: 411.1344, found 411.1350.

N-Propargyl-ciprofloxacin (20). The title compound was synthesized in analogy to McPherson et al.:⁷² Ciprofloxacin (500 mg, 1.5 mmol, 1 eq.) was dispersed in 10 mL of dry DMF together with Et₃N (310 μL , 2.25 mmol, 1.5 eq.) and propargyl bromide (250 μL , 2.25 mmol, 1.5 eq.). The mixture was stirred at 90 °C for 24 h, and further equivalents of Et₃N (309 μL , 2 mmol, 2 eq.) and propargyl bromide (250 μL , 2 mmol, 2 eq.) were added stepwise until the disappearance of the starting material, monitored by TLC (DCM:MeOH, 9:1). The reaction was poured on ice water. After filtration, the precipitate was redissolved and purified by MPLC (DCM:MeOH, 1–10%) to yield the title product as a beige amorphous solid (353 mg, 64%). ^1H NMR (500 MHz, CHCl₃- d) δ 14.99 (br s, 1H, COOH), 8.77 (s, 1H, ArH-2), 8.02 (d, $J = 13.0$ Hz, 1H, ArH-5), 7.37 (d, $J = 6.7$ Hz, 1H, ArH-8), 3.55 (br s, 1H, cPr-H), 3.43 (s, 2H, HCCCH₂-), 3.41 (br s, 4H, 2x piperazine-CH₂-), 2.84 (br s, 4H, 2x piperazine-CH₂'-), 2.33 (s, 1H, alkyne-H), 1.39 (d, $J = 6.3$ Hz, 2H, cPr-CH₂), 1.20 (br s, 2H, cPr-CH₂'). ^{13}C NMR (126 MHz, CHCl₃- d) δ 177.28 (C4=O), 167.17 (COOH), 153.82 (d, $J = 251.4$ Hz, cipro-C-6), 147.61 (cipro-C-2), 145.86 (d, $J = 10.1$ Hz, cipro-C-7), 139.21 (cipro-C-8a), 120.14 (d, $J = 7.6$ Hz, cipro-C-4a), 112.67 (d, $J = 23.4$ Hz, cipro-C-5), 108.35 (cipro-C-3), 105.04 (d, $J = 2.4$ Hz, cipro-C-8), 74.23 (HCCCH₂-), 51.52 (HCCCH₂-), 49.67 (piperazine), 46.95 (piperazine), 35.42 (cPr-CH), 8.39 (cPr-CH₂), $-\text{HCCCH}_2-$ (not observed). HR-MS calcd $[\text{C}_{20}\text{H}_{21}\text{FN}_3\text{O}_3]^+$: 370.1561, found 370.1552.

N-Butynyl-ciprofloxacin (21). Ciprofloxacin (500 mg, 1.5 mmol, 1 eq.) was dissolved in dry DMF and heated to 70 °C. Over 72 h, Et₃N (1512 μL , 10.5 mmol, 7 eq.) and 4-bromo-1-butyne (982 μL , 10.5 mmol, 7 eq.) were added portionwise in 1 eq. steps until the disappearance of the starting material, monitored by TLC (DCM:MeOH, 9:1). The reaction was poured on ice-cold water. After precipitation, the precipitate was purified by MPLC (DCM:MeOH, 1–10%) to yield the product as a beige amorphous solid (245 mg, 43%). ^1H NMR (500 MHz, DMSO- d_6) δ 15.22 (br s, 1H, COOH), 8.66 (s, 1H, ArH-2), 7.89 (d, $J = 13.3$ Hz, 1H, ArH-5), 7.56 (d, $J = 7.3$ Hz, 1H, ArH-8), 3.85–3.77 (br s, 1H, cPr-H), 3.32 (br s, 4H, 2x piperazine-CH₂-), 2.81 (s, 1H, HCCCH₂CH₂-), 2.64 (br s, 4H, piperazine-CH₂-), 2.56 (t, $J = 7.2$ Hz, 2H, RR'NCH₂CH₂CCH-), 2.38 (t, $J = 6.2$ Hz, 2H, RR'NCH₂CH₂CCH-), 1.31 (q, $J = 6.0$ Hz, 2H, cPr-CH₂-), 1.17 (br s, 2H, cPr-CH₂'-). ^{13}C NMR (126 MHz, DMSO- d_6) δ 176.40 (C4=O), 166.01 (COOH), 153.04 (d, $J = 249.4$ Hz, cipro-C-6), 148.05 (cipro-C-2), 145.22 (cipro-C-7), 139.20 (cipro-C-8a), 118.63 (cipro-C-4a), 110.94 (d, $J = 23.0$ Hz, cipro-C-5), 106.74 (cipro-C-3), 106.44 (cipro-C-8), 83.16 (HCCCH₂CH₂-), 71.87 (HCCCH₂CH₂-), 56.26 (HCCCH₂CH₂-), 51.98 (piperazine), 49.41 (piperazine), 49.38 (piperazine), 35.88 (cPr-CH), 16.19 (HCCCH₂CH₂-), 7.59 (cPr-CH₂). HR-MS calcd $[\text{C}_{21}\text{H}_{23}\text{FN}_3\text{O}_3]^+$: 384.1718, found 384.1711.

Gal-ciprofloxacin Conjugate 22 ($n = 1, m = 0$). The title compound was synthesized from **11** (20 mg, 0.054 mmol, 1 eq.) and **20** (40 mg, 0.108 mmol, 2 eq.) according to general procedure iv and was obtained as a beige amorphous solid (22 mg, 55%). ^1H NMR (500 MHz, DMSO- d_6) δ 15.22 (br s, 1H, COOH), 10.51 (s, 1H, $-\text{CONH}-$), 8.65 (s, 1H, cipro-ArH-2), 8.06 (s, 1H, triazole-H), 7.88 (d, $J = 13.3$ Hz, 1H, cipro-ArH-5), 7.55 (d, $J = 7.4$ Hz, 1H, cipro-ArH-8), 7.52 (d, $J = 8.6$ Hz, 2H, Phenyl-H), 7.43 (d, $J = 8.7$ Hz, 2H, Phenyl-H), 5.32 (s, 2H, $-\text{HNCO}-\text{CH}_2-$ triazole), 5.11 (br s, 1H, OH), 4.85 (br s, 1H, OH), 4.62 (br s, 1H, OH), 4.48 (d, $J = 9.4$ Hz, 1H, glyco-H-1), 4.44 (br s, 1H, OH), 3.81 (s, 1H, cPr-H), 3.70 (s, 2H, $-\text{triazole}-\text{CH}_2-\text{N}-\text{cipro}$), 3.69 (br s, 1H, glyco-H-4), 3.53–3.45 (m, 2H, glyco-H-6 + H-6'), 3.43 (glyco-H-2, extracted from HSQC), 3.38

(glyco-H-5, extracted from HSQC), 3.33 (glyco-H-3, extracted from HSQC), 3.33 (2x piperazine-CH₂, extracted from HSQC), 2.65 (s, 4H, 2x piperazine-CH₂), 1.31 (d, $J = 6.5$ Hz, 2H, cPr-CH₂), 1.17 (br s, 2H, cPr-CH₂'). ^{13}C NMR (126 MHz, DMSO- d_6) δ 176.41 (cipro-C4=O), 166.05 (COOH), 164.34 (C=O), 153.06 (d, $J = 249.3$ Hz, cipro-C-6), 148.03 (cipro-C-2), 145.23 (d, $J = 10.1$ Hz, cipro-C-7), 142.84 (triazole-C), 139.24 (cipro-C-8a), 137.09 (phenyl-C), 131.00 (phenyl-C), 129.46 (phenyl-C), 125.67 (triazole-CH), 119.60 (phenyl-C), 118.59 (d, $J = 7.5$ Hz, cipro-C-4a), 110.98 (d, $J = 23.4$ Hz, cipro-C-5), 106.75 (cipro-C-3), 106.43 (d, $J = 3.9$ Hz, cipro-C-8), 88.17 (glyco-C-1), 79.22 (glyco-C-5), 74.72 (glyco-C-3), 69.26 (glyco-C-2), 68.40 (glyco-C-4), 60.63 (glyco-C-6), 52.29 ($-\text{triazole}-\text{CH}_2-\text{N}-\text{cipro}$), 52.17 ($-\text{HNCO}-\text{CH}_2-$ triazole), 51.83 (piperazine), 49.40 (piperazine), 35.92 (cPr-CH), 7.61 (cPr-CH₂). HR-MS calcd $[\text{C}_{34}\text{H}_{39}\text{FN}_7\text{O}_9\text{S}]^+$: 740.2509, found 740.2500.

Gal-ciprofloxacin Conjugate 23 ($n = 1, m = 1$). The title compound was synthesized from **11** (20 mg, 0.054 mmol, 1 eq.) and **21** (41 mg, 0.108 mmol, 2 eq.) according to general procedure iv and was obtained as a beige amorphous solid (15 mg, 37%). ^1H NMR (500 MHz, DMSO- d_6) δ 15.23 (br s, 1H, COOH), 10.50 (s, 1, CONH), 8.66 (s, 1H, cipro-ArH-2), 7.94 (s, 1H, triazole-H), 7.90 (d, $J = 13.3$ Hz, 1H, cipro-ArH-5), 7.57 (d, $J = 6.6$ Hz, 1H, cipro-ArH-8), 7.52 (d, $J = 8.4$ Hz, 2H, Phenyl-H), 7.42 (d, $J = 8.7$ Hz, 2H, Phenyl-H'), 5.28 (s, 2H, $-\text{HNCO}-\text{CH}_2-$), 4.48 (d, $J = 9.4$ Hz, 1H, glyco-H-1), 3.82 (s, 1H, cPr-H), 3.69 (d, $J = 2.8$ Hz, 1H, glyco-H-4), 3.49 (glyco-H-6 + H-6', extracted from HSQC), 3.43 (glyco-H-2, extracted from HSQC), 3.38 (glyco-H-5, extracted from HSQC), 3.35 (2x piperazine-CH₂, extracted from HSQC), 3.33 (glyco-H-3, extracted from HSQC), 2.88 (t, $J = 7.5$ Hz, 2H, $-\text{triazole}-\text{CH}_2\text{CH}_2\text{NRR}'$), 2.68 (br s, 6H, 2x piperazine-CH₂ + $-\text{triazole}-\text{CH}_2\text{CH}_2\text{NRR}'$), 1.31 (d, $J = 6.0$ Hz, 2H, cPr-CH₂), 1.18 (br s, 2H, cPr-CH₂'). ^{13}C NMR (126 MHz, DMSO- d_6) δ 176.42 (cipro-C4=O), 166.06 (COOH), 164.39 (C=O), 153.09 (d, $J = 249.8$ Hz, cipro-C-6), 148.05 (cipro-C-2), 145.27 (d, $J = 9.9$ Hz, cipro-C-7), 144.96 (triazole-C), 139.26 (cipro-C-8a), 137.11 (phenyl-C), 131.00 (phenyl-C), 129.44 (phenyl-C), 124.00 (triazole-CH), 119.59 (phenyl-C), 118.58 (d, $J = 8.0$ Hz, cipro-C-4a), 110.99 (d, $J = 23.1$ Hz, cipro-C-5), 106.76 (cipro-C-3), 106.38 (d, $J = 3.1$ Hz, cipro-C-8), 88.17 (glyco-C-1), 79.21 (glyco-C-5), 74.72 (glyco-C-3), 69.25 (glyco-C-2), 68.39 (glyco-C-4), 60.63 (glyco-C-6), 57.29 (linker-CH₂), 52.27 (piperazine), 52.18 (linker-CH₂), 49.43 (piperazine), 35.92 (cPr-CH), 22.97 (linker-CH₂), 7.62 (cPr-CH₂). HR-MS calcd $[\text{C}_{35}\text{H}_{41}\text{FN}_7\text{O}_9\text{S}]^+$: 754.2665, found 754.2658.

Gal-ciprofloxacin Conjugate 24 ($n = 2, m = 0$). The title compound was synthesized from **12** (20 mg, 0.052 mmol, 1 eq.) and **20** (20 mg, 0.054 mmol, 1 eq.) according to general procedure iv and was obtained as a beige amorphous solid (26 mg, 66%). ^1H NMR (500 MHz, DMSO- d_6) δ 15.23 (br s, 1H, COOH), 10.09 (s, 1H, CONH), 8.66 (s, 1H, cipro-ArH-2), 7.97 (s, 1H, triazole-H), 7.90 (d, $J = 13.3$ Hz, 1H, cipro-ArH-5), 7.53 (d, $J = 7.4$ Hz, 1H, cipro-ArH-8), 7.48 (d, $J = 8.6$ Hz, 2H, phenyl-H), 7.37 (d, $J = 8.5$ Hz, 2H, phenyl-H'), 5.07 (br s, 1H, OH), 4.84 (br s, 1H, OH), 4.65 (t, $J = 6.6$ Hz, 2H, $-\text{NHCOCCH}_2-$), 4.60 (br s, 1H, OH), 4.43 (d, $J = 9.2$ Hz, 1H, glyco-H-1), 4.43 (br s, 1H, OH), 3.90–3.79 (br s, 1H, cPr-H), 3.67 (s, 1H, glyco-H-4), 3.64 (s, 2H, $-\text{triazole}-\text{CH}_2-\text{NRR}'$), 3.47 (glyco-H-6 + H-6', extracted from HSQC), 3.39 (glyco-H-2, extracted from HSQC), 3.35 (glyco-H-5, extracted from HSQC), 3.30 (glyco-H-3, extracted from HSQC), 3.29–3.25 (m, 4H, 2x piperazine-CH₂), 2.96 (t, $J = 6.6$ Hz, 2H, $-\text{NHCOCCH}_2-$), 2.61–2.57 (m, 4H, 2x piperazine-CH₂'), 1.34–1.25 (m, 2H, cPr-CH₂), 1.18–1.15 (m, 2H, cPr-CH₂'). ^{13}C NMR (126 MHz, DMSO- d_6) δ 176.43 (cipro-C4=O), 168.22 (COOH), 166.07 (C=O), 153.07 (d, $J = 250.0$ Hz, cipro-C-6), 148.07 (cipro-C-2), 145.23 (d, $J = 10.1$ Hz, cipro-C-7), 142.88 (triazole-C), 139.25 (cipro-C-8a), 137.65 (phenyl-C), 131.13 (phenyl-C), 128.70 (phenyl-C), 124.23 (triazole-CH), 119.48 (phenyl-C), 118.61 (d, $J = 7.5$ Hz, cipro-C-4a), 110.99 (d, $J = 22.9$ Hz, cipro-C-5), 106.77 (cipro-C-3), 106.40 (d, $J = 2.5$ Hz, cipro-C-8), 88.28 (glyco-H-1), 79.19 (glyco-H-5), 74.73 (glyco-H-3), 69.24 (glyco-H-2), 68.36 (glyco-H-4), 60.60 (glyco-H-6), 52.30 (linker-CH₂), 51.80 (piperazine), 49.39 (piperazine), 45.58 (linker-CH₂),

36.56 (linker-CH₂), 35.91 (cPr-CH), 7.61 (cPr-CH₂). HR-MS calcd [C₃₃H₄₁FN₇O₉S]⁺: 754.2665, found 754.2657.

Gal-ciprofloxacin Conjugate 25 (*n* = 2, *m* = 1). The title compound was synthesized from **12** (30 mg, 0.078 mmol, 1 eq.) and **21** (33 mg, 0.086 mmol, 1.1 eq.) according to general procedure iv as and was obtained as a beige amorphous solid (35 mg, 58%). ¹H NMR (500 MHz, DMSO-*d*₆) δ 15.23 (br s, 1H, COOH), 10.07 (s, 1H, CONH), 8.66 (s, 1H, cipro-ArH-2), 7.91 (d, *J* = 13.3 Hz, 1H, cipro-ArH-5), 7.87 (s, 1H, triazole-H), 7.55 (d, *J* = 7.3 Hz, 1H, cipro-ArH-8), 7.49 (d, *J* = 8.7 Hz, 2H, phenyl-H), 7.38 (d, *J* = 8.8 Hz, 2H, phenyl-H), 5.06 (br s, 1H, OH), 4.83 (br s, 1H, OH), 4.61 (t, *J* = 6.7 Hz, 2H, -NHCOCH₂CH₂- + OH), 4.43 (d, *J* = 9.3 Hz, 1H, glyco-H-1), 4.42 (s, 1H, OH), 3.83 (s, 1H, OH), 3.68 (s, 1H, glyco-H-4), 3.48 (ddd, *J* = 10.8, 6.5, 5.5 Hz, 2H), 3.40 (t, *J* = 6.3 Hz, 2H, glyco-H-2), 2.95 (t, *J* = 6.6 Hz, 2H, -NHCOCH₂CH₂-), 2.82 (t, *J* = 7.5 Hz, 2H, -triazole-CH₂CH₂NRR'), 2.65 (br s, 6H, 2x piperazine-CH₂ + -triazole-CH₂CH₂NRR'), 1.31 (q, *J* = 7.1 Hz, 2H, cPr-CH₂), 1.20–1.16 (m, 2H, cPr-CH₂). ¹³C NMR (126 MHz, DMSO-*d*₆) δ 176.37 (cipro-C4=O), 168.15 (C=O), 165.98 (COOH), 153.02 (d, *J* = 248.9 Hz, cipro-C-6), 148.02 (cipro-C-2), 145.16 (d, *J* = 10.5 Hz, cipro-C-7), 144.88 (cipro-C-7), 139.21 (cipro-C-8a), 137.65 (phenyl-C), 131.05 (phenyl-C), 128.66 (phenyl-C), 122.58 (triazole-CH), 119.38 (phenyl-C), 118.55 (d, *J* = 7.4 Hz, cipro-C-4a), 110.96 (d, *J* = 23.1 Hz, cipro-C-5), 106.73 (cipro-C-3), 106.32 (d, *J* = 3.8 Hz, cipro-C-8), 88.26 (glyco-C-1), 79.17 (glyco-C-5), 74.69 (glyco-C-3), 69.19 (glyco-C-2), 68.33 (glyco-C-4), 60.57 (glyco-C-6), 57.18 (linker-CH₂), 52.16 (piperazine), 49.35 (piperazine), 45.35 (linker-CH₂), 36.48 (linker-CH₂), 35.88 (cPr-CH), 22.87 (linker-CH₂), 7.58 (cPr-CH₂). HR-MS calcd [C₃₆H₄₃FN₇O₉S]⁺: 768.2822, found 768.2822.

Gal-ciprofloxacin Conjugate 26 (*n* = 3, *m* = 0). The title compound was synthesized from **13** (30 mg, 0.075 mmol, 1 eq.) and **20** (31 mg, 0.083 mmol, 1.1 eq.) according to general procedure iv and was obtained as a beige amorphous solid (30 mg, 52%). ¹H NMR (500 MHz, DMSO-*d*₆) δ 15.21 (br s, 1H, COOH), 9.96 (s, 1H, CONH), 8.65 (s, 1H, cipro-ArH-2), 8.06 (s, 1H, triazole-H), 7.89 (d, *J* = 13.3 Hz, 1H, cipro-ArH-5), 7.54 (d, *J* = 7.3 Hz, 1H, cipro-ArH-8), 7.51 (d, *J* = 8.6 Hz, 2H, phenyl-H), 7.39 (d, *J* = 8.8 Hz, 2H, phenyl-H), 5.06 (br s, 1H, OH), 4.84 (br s, 1H, OH), 4.60 (br s, 1H, OH), 4.44 (d, *J* = 9.4 Hz, 1H, glyco-H-1), 4.42 (OH, extracted from COSY), 4.41 (t, *J* = 6.9 Hz, 1H, -NHCOCH₂CH₂CH₂-), 3.81 (s, 1H, cPr-H), 3.68 (s, 1H, glyco-H-4), 3.66 (s, 2H, -triazole-CH₂-NRR'), 3.56–3.44 (m, 2H, glyco-H-6 + H-6'), 3.41 (t, *J* = 6.3 Hz, 1H, glyco-H-5), 3.37 (glyco-H-2, extracted from HSQC), 3.32 (glyco-H-3, extracted from HSQC), 3.32 (2x piperazine-CH₂, extracted from HSQC) 2.64 (br s, 4H, 2x piperazine-CH₂), 2.33 (t, *J* = 7.2 Hz, 2H, -NHCOCH₂CH₂CH₂-), 2.13 (tt, *J* = 7.1 Hz, 2H, -NHCOCH₂CH₂CH₂-), 1.33–1.27 (m, 2H, cPr-CH₂), 1.23–1.14 (br s, 2H, cPr-CH₂). ¹³C NMR (126 MHz, DMSO-*d*₆) δ 176.36 (cipro-C4=O), 170.11 (C=O), 165.96 (COOH), 153.01 (d, *J* = 249.7 Hz, cipro-C-6), 148.00 (cipro-C-2), 145.17 (d, *J* = 10.1 Hz, cipro-C-7), 143.11 (triazole-C), 139.19 (cipro-C-8a), 137.97 (phenyl-C), 131.15 (phenyl-C), 128.26 (phenyl-C), 123.81 (triazole-CH), 119.34 (phenyl-C), 118.56 (d, *J* = 7.5 Hz, cipro-C-4a), 110.94 (d, *J* = 23.1 Hz, cipro-C-5), 106.72 (cipro-C-3), 106.36 (d, *J* = 3.7 Hz, cipro-C-8), 88.34 (glyco-C-1), 79.17 (glyco-C-5), 74.70 (glyco-C-3), 69.20 (glyco-C-2), 68.34 (glyco-C-4), 60.58 (glyco-C-6), 52.41 (linker-CH₂), 51.87 (piperazine), 49.39 (piperazine), 48.84 (linker-CH₂), 35.85 (cPr-CH), 32.91 (linker-CH₂), 25.51 (linker-CH₂), 7.57 (cPr-CH₂). HR-MS calcd [C₃₆H₄₃FN₇O₉S]⁺: 768.2822, found 768.2815.

Gal-ciprofloxacin Conjugate 27 (*n* = 3, *m* = 1). The title compound was synthesized from **13** (30 mg, 0.075 mmol, 1 eq.) and **21** (32 mg, 0.083 mmol, 1.1 eq.) according to general procedure iv and was obtained as a beige amorphous solid (31 mg, 53%). ¹H NMR (500 MHz, DMSO-*d*₆) δ 15.22 (br s, 1H, COOH), 9.94 (s, 1H, CONH), 8.66 (s, 1H, cipro-ArH-2), 7.93 (s, 1H, triazole-H), 7.90 (d, *J* = 13.3 Hz, 1H, cipro-ArH-5), 7.56 (d, *J* = 7.2 Hz, 1H, cipro-ArH-8), 7.51 (d, *J* = 8.6 Hz, 2H, phenyl-H), 7.38 (d, *J* = 8.8 Hz, 2H, phenyl-H), 5.06 (br s, 1H, OH), 4.83 (br s, 1H, OH), 4.59 (br s, 1H, OH), 4.44 (d, *J* = 9.4 Hz, 1H, glyco-H-1), 4.42 (br s, 1H, OH), 4.38 (t, *J* =

6.8 Hz, 2H, -NHCOCH₂CH₂CH₂-), 3.82 (br s, 1H, cPr-H), 3.68 (s, 1H, glyco-H-4), 3.53–3.44 (m, 2H, glyco-H-6 + H-6'), 3.41 (t, *J* = 6.3 Hz, 1H, glyco-H-5), 3.37 (glyco-H-2, extracted from HSQC), 3.34 (2x piperazine-CH₂, extracted from HSQC), 3.32 (glyco-H-3) 2.84 (t, *J* = 7.6 Hz, 2H, -triazole-CH₂CH₂NRR'), 2.67 (br s, 6H, 2x piperazine-CH₂ + -triazole-CH₂CH₂NRR'), 2.31 (t, *J* = 7.3 Hz, 2H, -NHCOCH₂CH₂CH₂-), 2.11 (tt, *J* = 8.1, 7.5 Hz, 2H, -NHCOCH₂CH₂CH₂-), 1.36–1.28 (m, 2H, cPr-CH₂), 1.21–1.13 (m, 2H, cPr-CH₂). ¹³C NMR (126 MHz, DMSO-*d*₆) δ 176.37 (cipro-C4=O), 170.11 (CO), 165.97 (COOH), 153.03 (d, *J* = 249.5 Hz, cipro-C-6), 148.01 (cipro-C-2), 145.19 (d, *J* = 9.9 Hz, cipro-C-7), 145.05 (triazole-C), 139.20 (cipro-C-8a), 137.95 (phenyl-C), 131.12 (phenyl-C), 128.27 (phenyl-C), 122.21 (triazole-CH), 119.33 (phenyl-C), 118.56 (d, *J* = 8.0 Hz, cipro-C-4a), 110.94 (d, *J* = 23.1 Hz, cipro-C-5), 106.73 (cipro-C-3), 106.35 (d, *J* = 3.2 Hz, cipro-C-8), 88.33 (glyco-C-1), 79.17 (glyco-C-5), 74.70 (glyco-C-3), 69.20 (glyco-C-2), 68.34 (glyco-C-4), 60.58 (glyco-C-6), 57.21 (linker-CH₂), 52.19 (piperazine), 49.40 (piperazine), 48.74 (linker-CH₂), 35.87 (cPr-CH), 32.90 (linker-CH₂), 25.53 (linker-CH₂), 22.98 (linker-CH₂), 7.58 (cPr-CH₂). HR-MS calcd [C₃₇H₄₅FN₇O₉S]⁺: 782.2987, found 782.2965.

Gal-ciprofloxacin Conjugate 28 (*n* = 4, *m* = 0). The title compound was synthesized from **14** (30 mg, 0.073 mmol, 1 eq.) and **20** (30 mg, 0.08 mmol, 1.1 eq.) according to general procedure iv and was obtained as a beige amorphous solid (25 mg, 43%). ¹H NMR (500 MHz, DMSO-*d*₆) δ 15.21 (br s, 1H, COOH), 9.93 (s, 1H, CONH), 8.65 (s, 1H, cipro-ArH-2), 8.05 (s, 1H, triazole-H), 7.89 (d, *J* = 13.3 Hz, 1H, cipro-ArH-5), 7.54 (d, *J* = 7.3 Hz, 1H, cipro-ArH-8), 7.51 (d, *J* = 8.5 Hz, 2H, phenyl-H), 7.38 (d, *J* = 8.4 Hz, 2H, phenyl-H), 5.06 (br s, 1H, OH), 4.84 (br s, 1H, OH), 4.59 (br s, 1H, OH), 4.43 (d, *J* = 9.4 Hz, 2, glyco-H-1 + OH), 4.37 (t, *J* = 6.9 Hz, 2H, -NHCOCH₂CH₂CH₂CH₂-), 3.81 (s, 1H, cPr-H), 3.68 (br s, 1H, glyco-H-4), 3.65 (s, 2H, -triazole-CH₂CH₂NRR'), 3.56–3.44 (m, 2H, glyco-H-6 + H-6'), 3.41 (d, *J* = 6.0 Hz, 19H), 3.40 (glyco-H-5, extracted from HSQC), 3.37 (glyco-H-2, extracted from HSQC), 3.32 (2x piperazine-CH₂, extracted from HSQC), 2.63 (br s, 4H, 2x piperazine-CH₂'), 2.34 (t, *J* = 7.4 Hz, 2H, -NHCOCH₂CH₂CH₂CH₂-), 1.86 (tt, *J* = 7.1 Hz, 2H, -NHCOCH₂CH₂CH₂CH₂-), 1.55 (tt, *J* = 7.5 Hz, 2H, -NHCOCH₂CH₂CH₂CH₂-), 1.39–1.26 (m, 2H, cPr-CH₂), 1.22–1.12 (m, 2H, cPr-CH₂). ¹³C NMR (126 MHz, DMSO-*d*₆) δ 176.36 (cipro-C4=O), 170.82 (C=O), 165.96 (COOH), 153.01 (d, *J* = 249.9 Hz, cipro-C-6), 148.01 (cipro-C-2), 145.17 (d, *J* = 9.9 Hz, cipro-C-7), 143.02 (triazole-C), 139.19 (cipro-C-8a), 138.03 (phenyl-C), 131.15 (phenyl-C), 128.20 (phenyl-C), 123.77 (triazole-CH), 119.31 (phenyl-C), 118.56 (d, *J* = 7.8 Hz, cipro-C-4a), 110.94 (d, *J* = 23.2 Hz, cipro-C-5), 106.72 (cipro-C-3), 106.37 (d, *J* = 3.0 Hz, cipro-C-8), 88.35 (glyco-C-1), 79.17 (glyco-C-5), 74.69 (glyco-C-3), 69.20 (glyco-C-2), 68.33 (glyco-C-4), 60.57 (glyco-C-6), 52.40 (linker-CH₂), 51.86 (piperazine), 49.39 (piperazine), 49.03 (linker-CH₂), 35.85 (cPr-CH), 35.59 (linker-CH₂), 29.34 (linker-CH₂), 22.01 (linker-CH₂), 7.57 (cPr-CH₂). HR-MS calcd [C₃₇H₄₅FN₇O₉S]⁺: 782.2987, found 782.2972.

Gal-ciprofloxacin Conjugate 29 (*n* = 4, *m* = 1). The title compound was synthesized from **14** (30 mg, 0.073 mmol, 1 eq.) and **21** (56 mg, 0.146 mmol, 2 eq.) according to general procedure iv and was obtained as a beige amorphous solid (28 mg, 48%). ¹H NMR (500 MHz, DMSO-*d*₆) δ 15.23 (br s, 1H, COOH), 9.93 (s, 1H, CONH), 8.66 (s, 1H, cipro-ArH-2), 7.93–7.86 (m, 2H, triazole-H + cipro-ArH-5), 7.55 (d, *J* = 7.2 Hz, 1H, cipro-ArH-8), 7.50 (d, *J* = 8.6 Hz, 2H, phenyl-H), 7.37 (d, *J* = 8.6 Hz, 2H, phenyl-H'), 5.07 (br s, 1H, OH), 4.84 (br s, 1H, OH), 4.62 (br s, 1H, OH), 4.43 (d, *J* = 9.2 Hz, 2H, glyco-H-1 + OH), 4.34 (t, *J* = 6.9 Hz, 2H, -NHCOCH₂CH₂CH₂CH₂-), 3.81 (br s, 1H), 3.68 (s, 1H, glyco-H-4), 3.49 (glyco-H-6 + H-6', extracted from HSQC), 3.41 (glyco-H-5, extracted from HSQC), 3.37 (glyco-H-2, extracted from HSQC), 3.34 (2x piperazine-CH₂, extracted from HSQC), 3.32 (glyco-H-3, extracted from HSQC), 2.84 (t, *J* = 7.5 Hz, 2H, -triazole-CH₂CH₂NRR'), 2.67 (br s, 6H, 2x piperazine-CH₂ + -triazole-

$\text{CH}_2\text{-CH}_2\text{NRR}'$), 2.33 (t, $J = 7.3$ Hz, 2H, $-\text{NHCOCH}_2\text{CH}_2\text{CH}_2\text{CH}_2\text{-}$), 1.83 (tt, $J = 6.9$ Hz, 2H, $-\text{NHCOCH}_2\text{CH}_2\text{CH}_2\text{CH}_2\text{-}$), 1.54 (tt, $J = 7.4$ Hz, 2H, $-\text{NHCOCH}_2\text{CH}_2\text{CH}_2\text{CH}_2\text{-}$), 1.36–1.24 (m, 2H, cPr-CH_2), 1.25–1.06 (br s, 2H, cPr-CH_2). ^{13}C NMR (126 MHz, DMSO- d_6) δ 176.41 (cipro-C4=O), 170.89 (C=O), 166.04 (COOH), 153.07 (d, $J = 249.6$ Hz, cipro-C-6), 148.04 (cipro-C-2), 145.23 (d, $J = 9.9$ Hz, cipro-C-7), 144.99 (triazole-C), 139.24 (cipro-C-8a), 138.05 (phenyl-C), 131.19 (phenyl-C), 128.23 (phenyl-C), 122.23 (triazole-CH), 119.35 (phenyl-C), 118.58 (d, $J = 7.5$ Hz, cipro-C-4a), 110.98 (d, $J = 23.2$ Hz, cipro-C-5), 106.75 (cipro-C-3), 106.36 (d, $J = 3.0$ Hz, cipro-C-8), 88.37 (glyco-C-1), 79.19 (glyco-C-5), 74.72 (glyco-C-3), 69.24 (glyco-C-2), 68.38 (glyco-C-4), 60.62 (glyco-C-6), 57.25 (linker-CH $_2$), 52.21 (piperazine), 49.41 (piperazine), 49.00 (linker-CH $_2$), 35.90 (cPr-CH), 35.66 (linker-CH $_2$), 29.40 (linker-CH $_2$), 22.99 (linker-CH $_2$), 22.07 (linker-CH $_2$), 7.61 (cPr-CH $_2$). HR-MS calcd [$\text{C}_{37}\text{H}_{43}\text{FN}_7\text{O}_9\text{S}$] $^+$: 796.3135, found 796.3128.

5-(2'-Bromoethyl)thiophene-2-sulfonyl Chloride (16). 16 was synthesized in two chemical steps: thiopheneethanol 15 (1.0 mL, 9.0 mmol, 1 eq.) was dissolved in 40 mL of dry CH_2Cl_2 . The solution was cooled (0 °C), and a solution of PBr_3 (846 μL , 9.0 mmol, 1 eq.) in dry CH_2Cl_2 was added dropwise under vigorous stirring; the reaction was stirred for 1 h until full transformation, monitored by TLC (PE:EtOAc, 95:5). The reaction was quenched with ice water. The organic phase was washed with water (2x), aq. half satd. Na_2CO_3 (2x), and brine and dried over anhydrous Na_2SO_4 . The organic phase was reduced *in vacuo* and filtered over silica. After evaporation of the solvent *in vacuo* crude 2-(2'-bromoethyl)thiophene was obtained as a yellow oil (490 mg, 28%). ^1H NMR (500 MHz, CHCl_3 - d) δ 7.20 (dd, $J = 5.1, 1.2$ Hz, 1H, ArH-5), 6.97 (dd, $J = 5.1, 3.5$ Hz, 1H, ArH-4), 6.90 (dd, $J = 3.4, 1.0$ Hz, 1H, ArH-3), 3.58 (t, $J = 7.4$ Hz, 2H, $-\text{CH}_2\text{CH}_2\text{Br}$), 3.38 (t, $J = 7.5$ Hz, 2H, $-\text{CH}_2\text{CH}_2\text{Br}$). 2-(2'-Bromoethyl)thiophene (255 mg, 1.33 mmol, 1 eq.) was dissolved in 10 mL of dry CH_2Cl_2 , and the mixture was cooled (0 °C). HSO_3Cl (266 μL , 4 mmol, 3 eq.) was dissolved in 5 mL of dry CH_2Cl_2 and added dropwise to the starting material under vigorous stirring. The reaction was stirred 1 h until full transformation, monitored by TLC (PE:EtOAc, 95:5). The reaction was quenched with ice water. The aqueous phase was extracted with CH_2Cl_2 (3x). The combined organic phases were washed with half satd. brine (x) and brine (1x) and dried over anhydrous Na_2SO_4 . The solvent was evaporated *in vacuo* to obtain the crude product as a dark yellow oil (261 mg).

β -L-Fucopyranosyl-1-methylamine (17). β -L-Fucopyranosyl-1-nitromethane was synthesized according to Phiasivongsa et al.⁷³ with subsequent reduction to the amine as previously described in Sommer et al.⁴² NMR in agreement with literature data.⁴²

N - β -L-Fucopyranosylmethyl-2-(5-(2'-azidoethyl)thiophene)sulfonamide (19). β -L-Fucopyranosyl-1-methylamine (17, 128 mg, 0.60 mmol, 1 eq.) and K_2CO_3 (166 mg, 1.2 mmol, 2 eq.) were dispersed in 6 mL of dry DMF and cooled to 0 °C. Crude 2-chlorosulfonyl-5-(2'-bromoethyl)thiophene (261 mg, 0.90 mmol) was dissolved in 6 mL of dry DMF and added dropwise to the starting material under vigorous stirring. The reaction was stirred for 3 h until full conversion, as monitored by TLC (MeOH:EtOAc:aq. NH_4OH 25%, 4:4:2). After quenching with water, the aqueous phase was extracted with EtOAc (4x). The combined organic layers were washed with half satd. brine (3x) and brine (1x) and dried over anhydrous Na_2SO_4 . After filtration, the solvent was evaporated *in vacuo* and the crude material (191 mg) was dissolved in 10 mL of dry DMF. NaN_3 (143 mg, 2.2 mmol) was added, and the mixture was stirred for 3 h. After full transformation (monitored by HPLC-MS), the reaction was diluted with water and extracted with EtOAc (3x). The combined organic layers were washed with half satd. brine (3x) and satd. brine (1x) and dried over anhydrous Na_2SO_4 . After filtration, the solvent was evaporated *in vacuo*, and the product was purified by MPLC (DCM:MeOH, 1–11%) to yield the target compound as a white amorphous solid (141 mg, 60% after three chemical steps, 8% impurity of the corresponding alkyl chloride, determined by ^1H NMR). ^1H NMR (500 MHz, MeOH- d_4) δ 7.46 (d, $J = 3.8$ Hz, 1H, Ar-H), 6.97 (d, $J = 3.7$ Hz, 1H, Ar-H), 3.65–3.57 (m, 3H,

$-\text{CH}_2\text{CH}_2\text{N}_3 + \text{H-4}$), 3.50 (q, $J = 7.0$ Hz, 1H, H-5), 3.45–3.34 (m, 3H, $-\text{CH}_2\text{N-} + \text{H-2}$), 3.17 (td, $J = 9.1, 8.6, 2.4$ Hz, 1H, H-1), 3.12 (t, $J = 6.6$ Hz, 2H, $-\text{CH}_2\text{CH}_2\text{N}_3$), 3.06 (dd, $J = 12.9, 7.2$ Hz, 1H, $-\text{CH}_2\text{N-}$), 1.20 (d, $J = 6.5$ Hz, 3H, H-6). ^{13}C NMR (126 MHz, MeOH- d_4) δ 149.48 (Ar-C), 141.03 (Ar-C), 132.98 (Ar-C), 127.32 (Ar-C), 79.55 (glyco-C-2), 76.37 (glyco-C-3), 75.57 (glyco-C-5), 73.61 (glyco-C-4), 69.74 (glyco-C-1), 53.08 (glyco-C-2), 45.75 (linker-CH $_2$), 30.71 (linker-CH $_2$), 17.07 (glyco-C-6). HR-MS calcd [$\text{C}_{13}\text{H}_{19}\text{N}_4\text{O}_6\text{S}_2$] $^-$: 391.0751, found 391.0759.

Hybrid-Ciprofloxacin Conjugate 30 ($m = 0$). The title compound was synthesized from 19 (35 mg, 0.09 mmol, 1 eq.) and 20 (35 mg, 0.095 mmol, 1.1 eq.) according to general procedure iv and was obtained as a beige amorphous solid (30 mg, 44%). ^1H NMR (500 MHz, DMSO- d_6) δ 15.23 (br s, 1H, $-\text{COOH}$), 8.66 (s, 1H, cipro-H-2), 7.98 (s, 1H, triazole-H), 7.90 (d, $J = 13.3$ Hz, 1H, cipro-H-5), 7.66 (t, $J = 5.9$ Hz, 1H, $-\text{NH}_2\text{SO}_2-$), 7.55 (d, $J = 7.4$ Hz, 1H, cipro-H-8), 7.37 (d, $J = 3.7$ Hz, 1H, thienyl-H), 6.89 (d, $J = 3.8$ Hz, 1H, thienyl-H), 4.80 (br s, 1H, OH), 4.65 (t, $J = 6.7$ Hz, 1H, thiophene-CH $_2\text{CH}_2$ -triazole), 4.59 (br s, 1H, OH), 4.28 (d, $J = 5.5$ Hz, 1H, OH), 3.86–3.77 (m, 1H, cPr-H), 3.63 (s, 2H, triazole-CH $_2$ -NRR'), 3.47 (t, $J = 6.7$ Hz, 2H, thiophene-CH $_2\text{CH}_2$ -triazole), 3.39 (s, 1H, glyco-H-4), 3.37, 3.25–3.18 (m, 2H, $-\text{CH}_2\text{NHSO}_2-$ + glyco-H-3), 3.14 (t, $J = 9.3$ Hz, 1H, glyco-H-2), 3.01 (td, $J = 8.8, 2.3$ Hz, 1H, glyco-H-1), 2.73 (ddd, $J = 13.4, 8.4, 5.6$ Hz, 1H, $-\text{CH}_2\text{NHSO}_2-$), 2.59 (2.63–2.56 m, 4H, 2x piperazine-CH $_2$), 1.39–1.30 (m, 2H, cPr-CH $_2$), 1.20–1.14 (m, 4H, cPr-CH $_2$), 1.07 (d, $J = 6.4$ Hz, 3H, glyco-H-6). ^{13}C NMR (126 MHz, DMSO- d_6) δ 176.38 (cipro-C4=O), 165.98 (COOH), 153.02 (d, $J = 249.2$ Hz, cipro-C-6), 147.98 (cipro-C-2), 146.07 (Ar-C), 145.23 (d, $J = 10.1$ Hz, cipro-C-7), 143.18 (triazole-C), 139.65 (Ar-C), 139.23 (cipro-C-8a), 131.14 (Ar-C), 126.59 (Ar-C), 124.22 (triazole-CH), 118.56 (d, $J = 7.4$ Hz, cipro-C-4a), 110.95 (d, $J = 22.9$ Hz, cipro-C-5), 106.72 (cipro-C-3), 106.34 (d, $J = 2.6$ Hz, cipro-C-8), 78.24 (glyco-C-2), 74.64 (glyco-C-3), 73.64 (glyco-C-5), 71.56 (glyco-C-4), 68.30 (glyco-C-1), 52.41 (linker-CH $_2$), 51.88 (piperazine), 50.01 (linker-CH $_2$), 49.40 (piperazine), 44.74 (glyco-CH $_2$), 35.90 (cPr-CH), 29.97 (linker-CH $_2$), 16.93 (glyco-C-6), 7.57 (cPr-CH $_2$). HR-MS calcd [$\text{C}_{33}\text{H}_{41}\text{FN}_7\text{O}_9\text{S}_2$] $^+$: 762.2386, found 762.2382.

Hybrid-Ciprofloxacin Conjugate 31 ($m = 1$). The title compound was synthesized from 19 (56 mg, 0.14 mmol, 1 eq.) and 21 (59 mg, 0.15 mmol, 1.1 eq.) according to general procedure iv and was obtained as a beige amorphous solid (57 mg, 52%). ^1H NMR (500 MHz, DMSO- d_6) δ 15.23 (s, 1H, COOH), 8.67 (s, 1H, cipro-ArH-2), 7.93–7.89 (m, 2H, triazole-H + cipro-ArH-5), 7.68 (t, $J = 5.9$ Hz, 1H, $-\text{NHSO}_2-$), 7.58 (d, $J = 7.4$ Hz, 1H, cipro-ArH-8), 7.38 (d, $J = 3.7$ Hz, 1H, thienyl-H), 6.89 (d, $J = 3.8$ Hz, 1H, thienyl-H), 4.82 (br s, 1H, OH), 4.62 (t, $J = 6.9$ Hz, 2H, thiophene-CH $_2\text{CH}_2$ -triazole + OH), 4.29 (s, 1H, OH), 3.84 (s, 1H, cPr-H), 3.44 (t, $J = 6.9$ Hz, 2H, thiophene-CH $_2\text{CH}_2$ -triazole), 3.40 (s, 1H, glyco-H-4), 3.37 (1H, glyco-H-5, extracted from HSQC), 3.35 (4H, 2x piperazine-CH $_2$), 3.28–3.20 (m, 2H, $-\text{CH}_2\text{NSO}_2-$ + glyco-H-3), 3.15 (t, $J = 9.3$ Hz, 1H, glyco-H-2), 3.02 (td, $J = 8.8, 2.3$ Hz, 1H, glyco-H-1), 2.85 (t, $J = 7.5$ Hz, 2H, $-\text{triazole-CH}_2\text{CH}_2\text{NRR}'$), 2.74 (ddd, $J = 13.6, 8.4, 5.7$ Hz, 1H, $-\text{CH}_2\text{NSO}_2-$), 2.68 (br s, 6H, 2x piperazine-CH $_2$ + $-\text{triazole-CH}_2\text{CH}_2\text{NRR}'$), 1.91 (s, OH), 1.35–1.29 (m, 2H, cPr-CH $_2$), 1.22–1.16 (m, 2H, cPr-CH $_2$), 1.08 (d, $J = 6.4$ Hz, 3H, glyco-H-6). ^{13}C NMR (126 MHz, DMSO- d_6) δ 176.37 (cipro-C4=O), 165.97 (COOH), 153.03 (d, $J = 250.0$ Hz, cipro-C-6), 148.02 (cipro-C-2), 146.17 (Ar-C), 145.17 (d, $J = 10.4$ Hz, cipro-C-7), triazole-C not found, 139.66 (Ar-C), 139.21 (cipro-C-8a), 131.18 (Ar-C), 126.45 (Ar-C), 122.47 (triazole-CH), 118.57 (d, $J = 7.4$ Hz, cipro-C-4a), 110.95 (d, $J = 23.1$ Hz, cipro-C-5), 106.73 (cipro-C-3), 106.37 (d, $J = 2.5$ Hz, cipro-C-8), 78.24 (glyco-C-2), 74.65 (glyco-C-3), 73.63 (glyco-C-5), 71.57 (glyco-C-4), 68.31 (glyco-C-1), 57.16 (linker-CH $_2$), 52.15 (piperazine), 49.88 (linker-CH $_2$), 49.32 (piperazine), 44.74 (glyco-CH $_2$), 35.89 (cPr-CH), 29.99 (linker-CH $_2$), 22.87 (linker-CH $_2$), 16.93 (glyco-C-6), 7.59 (cPr-CH $_2$). HR-MS calcd [$\text{C}_{34}\text{H}_{43}\text{FN}_7\text{O}_9\text{S}_2$] $^+$: 776.2542, found 776.2538.

Competitive Binding Assays. *Lea* (According to Joachim et al.⁵⁸). A serial dilution of the test compounds was prepared in TBS/

Ca (8.0 g/L NaCl, 2.4 g/L Tris, 0.19 g/L KCl, 0.15 g/L CaCl₂·2H₂O), with 30% DMSO as a co-solvent. A concentrated solution of LecA was diluted in TBS/Ca together with the fluorescent reporter ligand (*N*-(fluorescein-5-yl)-*N'*-(β -D-(*m*-aminophenyl)-galactopyranosyl)thiocarbamide) to yield concentrations of 40 μ M and 20 nM, respectively. A 10 μ L solution of this mix was added to 10 μ L serial dilutions of the test compounds in a black 384-well microtiter plates (Greiner Bio-One, Germany, cat. no. 781900) in triplicate. After centrifugation (2680 rcf, 1 min, r.t.), the reactions were incubated for 30–60 min at r.t. in a humidity chamber. Fluorescence (excitation 485 nm, emission 535 nm) was measured in parallel and perpendicular to the excitation plane on a PheraStar FS plate reader (BMG Labtech GmbH, Germany). The measured intensities were reduced by the values of only LecA in TBS/Ca, and fluorescence polarization was calculated. The data were analyzed with the MARS Data Analysis Software (BMG Labtech GmbH, Germany) and fitted according to the four-parameter variable slope model. Bottom and top plateaus were fixed according to the control compounds in each assay (*p*-nitrophenyl)- β -D-galactoside), and the data was reanalyzed with these values fixed. A minimum of three independent measurements on three plates was performed for each inhibitor.

LecB (*LecB*_{PAO1} According to Hauck et al.⁴¹ and *LecB*_{PA14} According to Sommer et al.³³). A serial dilution of the test compounds was prepared in TBS/Ca, with 10% DMSO as a co-solvent. A concentrated solution of LecB PAO1 or PA14 was diluted in TBS/Ca together with the fluorescent reporter ligand (*N*-(fluorescein-5-yl)-*N'*-(α -L-fucopyranosyl ethylene)thiocarbamide) to yield concentrations of 300 nM and 20 nM, respectively. A 10 μ L solution of this mix was added to 10 μ L serial dilutions of the test compounds in a black 384-well microtiter plates (Greiner Bio-One, Germany, cat. no. 781900) in triplicate. After centrifugation (2680 rcf, 1 min, r.t.), the reactions were incubated for 4–8 h at r.t. in a humidity chamber. Fluorescence was measured and analyzed as for LecA. Bottom and top plateaus were fixed according to the control compound in each assay (*L*-fucose), and the data were reanalyzed with these values fixed. A minimum of three independent measurements on three plates was performed for each inhibitor.

Gyrase Supercoiling Inhibition. The assay was performed with the *E. coli* gyrase supercoiling kit (Inspiralis, Norwich, UK) according to the manufacturer's instructions. All pipetting steps before the reaction was started were performed on ice. A serial dilution of the test compounds was prepared in 5% DMSO in water. A mix of relaxed pBR322 DNA (5.5 μ g), 66 μ L assay buffer (5x), and 192.5 μ L water was prepared. 3 μ L of the dilution series (or 3 μ L 5% DMSO in water for control reactions) was added. 10 U gyrase (2 μ L, 5 U/ μ L) was diluted in 28 μ L dilution buffer. 3 μ L of the gyrase (1 U) solution was added to the reaction mixtures. For the negative control, 3 μ L of dilution buffer was added instead of the enzyme. The reaction was incubated for 30 min at 37 °C. The reactions were stopped by the addition of 30 μ L of STE-buffer (40% (m/v) sucrose, 100 mM Tris-HCl, pH 8, 10 mM EDTA, pH 8, 0.5 mg/mL bromophenol blue) and 30 μ L of CHCl₃/isoamyl alcohol (24:1) and vortexing. After centrifugation (17,600 rcf, 1 min, 4 °C), 50 μ L of the aqueous layer was loaded on an agarose gel (1%, Tris-EDTA-acetate buffer). The gel was run for 3 h at 85 V, and DNA was visualized afterward by staining with ethidium bromide. Agarose gels were digitalized using the E-box VX2 gel documentation instrument (Vilber, Eberhardzell, Germany). The fluorescence intensity of each supercoiled band was quantified using ImageJ (Version 1.52a, National Institute of Health, USA). The data were analyzed using GraphPad Prism (Version 6.0 h, GraphPad Software, USA) and fitted against inhibitor concentration according to the four-parameter variable slope model to determine IC₅₀ values. Bottom plateaus were fixed to 0. A minimum of three different experiments was performed for each inhibitor.

Bacterial Strain List. All microorganisms were obtained from the German Collection of Microorganisms and Cell Cultures (DSMZ) and the American Type Culture Collection (ATCC) or were part of our internal strain collection. The following strains were used: *Escherichia coli* DSM 1116 (source: Rolf Müller, HIPS), *Escherichia*

coli K12 MG1655 (source: Winfried Boos, Universität Konstanz), *Staphylococcus carnosus* DSM 20501 (source: Rolf Müller, HIPS), *Pseudomonas aeruginosa* PA14 wt (DSM 19882), *Pseudomonas aeruginosa* PAO1 wt (DSM 19880), *Pseudomonas aeruginosa* PA14 Δ lecA (Wagner et al., in preparation), and *Pseudomonas aeruginosa* PA14 Δ lecB (Wagner et al., in preparation).

Antibiotic Susceptibility (MIC Assay). The antibiotic activity of the synthesized conjugates was determined by broth microdilution assay based on the EUCAST guidelines, according to Wiegand, Hilpert, and Hancock.⁷⁴ Serial dilutions in sterile Müller-Hinton broth II (Fluka analytical, cat. no. 90922: 17.5 g/L casein acid hydrolysate, 3 g/L beef extract, 1.5 g/L starch, supplemented with 20–25 mg/L Ca²⁺ and 10–15 mg/L Mg²⁺, pH 7.3) of the conjugates 21–31 and 20 were prepared from 100 mM DMSO stocks (for ciprofloxacin (3), a 10 mM aq. stock of ciprofloxacin-HCl was used), in sterile 96-well plates, yielding a concentration range from 128 to 0.125 μ g/mL (12.8–0.0125 for ciprofloxacin). Bacterial strains were streaked on LB-agar plates (1% agar) from glycerol stocks and incubated at 37 °C overnight. Colonies were picked from plate and dispersed in fresh Müller-Hinton broth II (MHB II) to yield an OD₆₀₀ of 0.08–0.13. This dispersion was diluted 1:100 in fresh MHB II, which was then used for the assay to achieve a final inoculum of 5 \times 10⁵ CFU/mL. If indicated, PMBN was added to this inoculum at 2 μ g/mL. A 50 μ L inoculum was mixed with 50 μ L of the serial dilution in the corresponding well of the 96-well plate. The plates were incubated at 37 °C for 18–20 h in a humid incubator. Growth inhibition was assessed by visual inspection, and the given MIC values are the lowest concentration of the antibiotic at which there was no visible growth.

Biofilm Accumulation Assay. Bacterial precultures of *P. aeruginosa* PAO1 were prepared in 10 mL of LB and grown at 37 °C and 180 rpm overnight. The bacterial precultures were diluted in fresh LB to 50 mL and centrifuged (5925 rcf, 10 min, r.t.). The supernatant was discarded, and the pellet was resuspended and washed in 50 mL of fresh LB and centrifuged again (5925 rcf, 10 min, r.t.). The supernatant was discarded and the pellet was again resuspended in fresh LB to yield an OD₆₀₀ of 0.1. Then, 150 μ L of this inoculum were transferred to each well of a 96-well MBEC assay plate (SKU: 19113, Category: Well Base, Innovotech Inc., Canada). The outer wells were filled with 150 μ L of sterile LB as a control. Plates were incubated at 37 °C, 125 rpm, and 75% humidity for 24 h. Compound solutions (170 μ L, 200 μ M, 1% DMSO) in phosphate-buffered saline pH 7.4, supplemented with 100 μ M CaCl₂ (PBS/Ca) were dispensed in a 96-well plate (cat. no. 167008, Nunc MicroWell 96-Well Microplates, Thermo Scientific) in quintuplicate on plates. Each peg of the biofilm covered peg lid was washed in 200 μ L of PBS/Ca in a 96-well plate (Nunc) for 1 min at r.t. and then incubated with the compound solution for 5 or 10 min at 37 °C, 80 rpm under humid conditions. After the incubation step, the pegs were again washed with 200 μ L of PBS/Ca in a 96-well format for 30 s at r.t. and transferred to a last 96-well plate (Nunc) filled with 170 μ L PBS/Ca per well. The plate was sealed with parafilm and sonicated for 15 min using an ultrasound bath. A 100 μ L sample of each well was transferred to a vial and treated with 100 μ L of MeCN (spiked with 1.5 μ M diphenhydramine-HCl as an internal standard). After centrifugation (17,600 rcf, 10 min, 4 °C), the compound concentration in the supernatant was determined by LC-MS/MS. Fresh calibration curves for each compound were prepared in the same matrix for each experiment. In each assay, the accumulation factor relative to ciprofloxacin was determined. Statistical analysis (unpaired *t*-test) was performed using the GraphPad-Prism QuickCalcs online tool (<https://www.graphpad.com/quickcalcs/contMenu/>).

LC-MS/MS. LC-MS/MS analysis was performed on an Ultimate 3000 system (degasser, pump, autosampler, column compartment) equipped with a Nucleodur C18 Pyramid column (150 \times 2 mm, 3 μ m, Macherey-Nagel, Düren, Germany) coupled to a TSQ Quantum Access MAX (Thermo Fisher Scientific, Waltham MA) with the following gradient conditions: A, water (0.1% formic acid); B, acetonitrile (0.1% formic acid); flow 0.600 mL/min; 90% A for 1.0 min; 90–5% A in 0.7 min; 5% A for 1.8 min; equilibration at 90% A

for 1.0 min. MS was operated in positive SRM mode with the following mass transitions:

Diphenhydramin (IS): 256.04–164.90; 256.04–166.90.

Ciprofloxacin (3): 332.063–230.908; 332.063–244.968; spray voltage: 4001 V, vaporizer temperature: 420 °C, sheath gas pressure: 50 psi, ion sweep pressure: 2.5 psi, aux gas pressure: 30 psi, capillary temperature: 260 °C, tube lens offset: 97 V, skimmer offset: 0 V, collision pressure: 1.5 mTorr, collision energy: 36 eV (230.908), 23 eV (244.968).

(21): 740.140–559.933; 740.140–577.966; spray voltage: 3000 V, vaporizer temperature: 470 °C, sheath gas pressure: 60 psi, ion sweep pressure: 0 psi, aux gas pressure: 55 psi, capillary temperature: 296 °C, tube lens offset: 99 V, skimmer offset: 0 V, collision pressure: 1.5 mTorr, collision energy: 36 eV (559.933), 27 eV (577.966).

(29): 762.124–726.026; 762.124–744.061; spray voltage: 4500 V, vaporizer temperature: 223 °C, sheath gas pressure: 60 psi, ion sweep pressure: 0 psi, aux gas pressure: 55 psi, capillary temperature: 284 °C, tube lens offset: 99 V, skimmer offset: 0 V, collision pressure: 1.5 mTorr, collision energy: 33 eV (726.026), 29 eV (744.061).

Cytotoxicity (MTT Assay, According to Hauptenthal et al.⁷⁵). HEK293 or A549 cells (2×10^5 cells per well) were seeded in 24-well, flat-bottom plates. Culturing of cells, incubations, and OD measurements were performed as described with small modifications. Twenty-four hours after seeding the cells, the incubation was started by the addition of compounds in a final DMSO concentration of 1%. The living cell mass was determined after 48 h in a PHERAstar microplate reader (BMG Labtech, Ortenberg, Germany). Two independent measurements were performed for each compound.

Microsomal Stability. Microsomal stability was performed as previously described in Sommer et al.⁴⁴

Plasma Protein Binding. Plasma protein binding was measured with a rapid equilibrium dialysis assay plate (Thermo Fisher Scientific, Waltham MA). On one side of the membrane, 150 μ L of human plasma (seralab-BioIVT, West Sussex United Kingdom) and 150 μ L of PBS pH 7.4 (Gibco Thermo Fisher Scientific, Waltham MA) were added to the well; on the other side, 550 μ L of PBS was added to the well. The compound was added to a final concentration of 1 μ M to the plasma-containing well. The plate was closed and incubated in an orbital shaker at 37 °C for 6 h at 750 rpm. Samples of 10 μ L from each well were taken at 0, 5, and 6 h and mixed with 90 μ L of ice-cold acetonitrile with internal standard diphenhydramine (1 μ M). The concentration of compound in the supernatant was analyzed with LC-MS/MS. Plasma protein binding was calculated from the concentration difference between the wells. Five and 6 h samples were compared to ensure equilibrium. Warfarin was used as an assay control.

Human Plasma Stability. Compound stability in plasma was measured by incubation with plasma and LC-MS/MS quantification of the remaining compound. A 195 μ L solution of human plasma (seralab-BioIVT, West Sussex, United Kingdom) was incubated with 5 μ L of compound (40 μ M stock) at 37 °C for 0, 5, 60, and 150 min. Then, 800 μ L of ice-cold acetonitrile containing internal standard diphenhydramine (1 μ M) was added. The concentration of remaining compound in the supernatant was determined via LC-MS/MS measurement. Procaine was used as an activity control of plasma metabolism.

Cell Permeability. Permeability of the compound was assessed *in vitro* with Calu-3 HTB-55 cell line (ATCC). Cells were cultivated in minimum essential medium supplemented with Earle's salts, L-glutamine, 10% FCS, 1% non-essential amino acids (NEAA), and 1 mM sodium pyruvate. Passages between 35 and 55 were used, and the medium was changed every 2–3 days. For experiments, cells were harvested using Trypsin/EDTA and 1×10^5 cells seeded on Transwell inserts 3460. Cells were grown in an air–liquid interface beginning at day 3 and used for transport studies on days 11–13. TEER values exceeded 300 $\Omega \cdot \text{cm}^2$ before beginning transport studies. For experiments, Krebs-Ringer solution with 1% BSA was used and cells were accommodated to the buffer for at least 1 h with no decrease in TEER. Samples (200 μ L) were taken in regular intervals from the apical side (time intervals of 0, 20, 40, 60, 90, 120, 180, and 240 min)

and replenished with fresh buffer. TEER was monitored during the experiment, and epithelial barriers were considered compromised if the TEER fell below 300 $\Omega \cdot \text{cm}^2$ during 4 h of experiment duration. Fluorescein sodium salt and ciprofloxacin-HCl were used as a control. A 50 μ L sample was mixed with 150 μ L of ice-cold acetonitrile containing internal standard diphenhydramine (1 μ M), and the concentration of compound was analyzed with LC-MS/MS.

■ ASSOCIATED CONTENT

Supporting Information

The Supporting Information is available free of charge at <https://pubs.acs.org/doi/10.1021/acs.jmedchem.0c00856>.

¹H and ¹³C NMR spectra of new compounds; gyrase supercoiling inhibition assay gels; *P. aeruginosa* PAO1 biofilm accumulation raw data; lectin inhibition K_i values calculated from IC₅₀; antibiotic susceptibility in molar concentration; key compounds and intermediates as SMILES; purity of key compounds 11–14, 19–31 by HPLC-UV; and retention times and a representative chromatogram of conjugates 22–31 and ciprofloxacin (3) from slow gradient HPLC runs for lipophilicity comparison (PDF)

Molecular formula strings for all new compounds and key compounds (5–14, 16, and 19–31) (CSV)

■ AUTHOR INFORMATION

Corresponding Author

Alexander Titz – Chemical Biology of Carbohydrates (CBCH), Helmholtz Institute for Pharmaceutical Research Saarland (HIPS), Helmholtz Centre for Infection Research, D-66123 Saarbrücken, Germany; Deutsches Zentrum für Infektionsforschung (DZIF), Standort Hannover-Braunschweig, D-38124 Braunschweig, Germany; Department of Pharmacy and Department of Chemistry, Saarland University, D-66123 Saarbrücken, Germany; orcid.org/0000-0001-7408-5084; Phone: +49 681 99806 2500; Email: alexander.titz@helmholtz-hzi.de

Authors

Joscha Meiers – Chemical Biology of Carbohydrates (CBCH), Helmholtz Institute for Pharmaceutical Research Saarland (HIPS), Helmholtz Centre for Infection Research, D-66123 Saarbrücken, Germany; Deutsches Zentrum für Infektionsforschung (DZIF), Standort Hannover-Braunschweig, D-38124 Braunschweig, Germany; Department of Pharmacy and Department of Chemistry, Saarland University, D-66123 Saarbrücken, Germany

Eva Zahorska – Chemical Biology of Carbohydrates (CBCH), Helmholtz Institute for Pharmaceutical Research Saarland (HIPS), Helmholtz Centre for Infection Research, D-66123 Saarbrücken, Germany; Deutsches Zentrum für Infektionsforschung (DZIF), Standort Hannover-Braunschweig, D-38124 Braunschweig, Germany; Department of Pharmacy and Department of Chemistry, Saarland University, D-66123 Saarbrücken, Germany

Teresa Röhrig – Deutsches Zentrum für Infektionsforschung (DZIF), Standort Hannover-Braunschweig, D-38124 Braunschweig, Germany; Drug Design and Optimization (DDOP), Helmholtz Institute for Pharmaceutical Research Saarland (HIPS), Helmholtz Centre for Infection Research, D-66123 Saarbrücken, Germany

Dirk Hauck – Chemical Biology of Carbohydrates (CBCH), Helmholtz Institute for Pharmaceutical Research Saarland

(HIPS), Helmholtz Centre for Infection Research, D-66123 Saarbrücken, Germany; Deutsches Zentrum für Infektionsforschung (DZIF), Standort Hannover-Braunschweig, D-38124 Braunschweig, Germany

Stefanie Wagner – Chemical Biology of Carbohydrates (CBCH), Helmholtz Institute for Pharmaceutical Research Saarland (HIPS), Helmholtz Centre for Infection Research, D-66123 Saarbrücken, Germany; Deutsches Zentrum für Infektionsforschung (DZIF), Standort Hannover-Braunschweig, D-38124 Braunschweig, Germany

Complete contact information is available at:

<https://pubs.acs.org/10.1021/acs.jmedchem.0c00856>

Author Contributions

J.M. synthesized conjugates and individual building blocks. D.H. synthesized compound 17. J.M. and E.Z. performed lectin inhibition assays. J.M. performed gyrase supercoiling inhibition, antibiotic susceptibility, and biofilm accumulation assays. T.R. analyzed data for metabolic stability in human plasma, plasma protein binding, and acute cytotoxicity. S.W. provided conceptual advice and analyzed the data. J.M. and A.T. conceived the study. J.M. and A.T. wrote the paper with input from all coauthors.

Notes

The authors declare no competing financial interest.

ACKNOWLEDGMENTS

The authors are thankful to Prof. Dr. Rolf Müller and Dr. Jennifer Hermann (HIPS) for scientific discussions and for providing the bacterial strains *S. carnosus* DSM 20501 and *E. coli* DSM 1116. We are grateful to Dr. Thomas Ryckmans (F. Hoffmann la Roche, Basel) for metabolic stability assays against human liver microsomes and mouse liver microsomes, Tabea Wittmann and Dennis Jener (HIPS) for plasma stability, plasma protein binding, and cytotoxicity assays, and Justus Horstmann (HIPS) for cell permeation measurements. A.T. acknowledges financial support from the Helmholtz Association (VH-NG-934), the European Research Council (ERC Starting Grant, Sweetbullets), and DZIF.

LIST OF ABBREVIATIONS

XDR, extensively drug-resistant; WHO, World Health Organization; *P. aeruginosa*, *Pseudomonas aeruginosa*; MLM, mouse liver microsomes; HLM, human liver microsomes; PE, petroleum ether; CL_{MIC}, microsomal clearance; cPr, cyclopropyl; rcf, relative centrifugal force; LR-MS, low-resolution mass spectrometry

REFERENCES

(1) Rice, L. B. Federal funding for the study of antimicrobial resistance in nosocomial pathogens: no ESKAPE. *J. Infect. Dis.* **2008**, *197*, 1079–1081.

(2) Boucher, H. W.; Talbot, G. H.; Bradley, J. S.; Edwards, J. E.; Gilbert, D.; Rice, L. B.; Scheld, M.; Spellberg, B.; Bartlett, J. Bad bugs, no drugs: no ESKAPE! An update from the Infectious Diseases Society of America. *Clin. Infect. Dis.* **2009**, *48*, 1–12.

(3) Rice, L. B. Progress and challenges in implementing the research on ESKAPE pathogens. *Infect. Control Hosp. Epidemiol.* **2010**, *31*, S7–S10.

(4) Meynard, J.-L.; Barbut, F.; Guiguet, M.; Batissel, D.; Lalande, V.; Lesage, D.; Guiard-Schmid, J.-B.; Petit, J.-C.; Frottier, J.; Meyohas, M.-C. *Pseudomonas aeruginosa* infection in human immunodeficiency virus infected patients. *J. Infect.* **1999**, *38*, 176–181.

(5) Rizzi, E. B.; Schininà, V.; Bordi, E.; Buontempo, G.; Narciso, P.; Bibbolino, C. HIV-related bronchopulmonary infection by *Pseudomonas aeruginosa* in the HAART era: radiological findings. *Acta Radiol.* **2006**, *47*, 793–797.

(6) Bodey, G. P. *Pseudomonas aeruginosa* infections in cancer patients: have they gone away? *Curr. Opin. Infect. Dis.* **2001**, *14*, 403–407.

(7) Hauser, A. R.; Rello, J. *Severe infections caused by Pseudomonas aeruginosa*; Springer Science & Business Media: Boston, MA, 2012.

(8) Poole, K. *Pseudomonas aeruginosa*: resistance to the max. *Front. Microbiol.* **2011**, *2*, 65.

(9) WHO publishes list of bacteria for which new antibiotics are urgently needed; World Health Organization: Geneva, 2017 Available at: <https://www.who.int/news-room/detail/27-02-2017-who-publishes-list-of-bacteria-for-which-new-antibiotics-are-urgently-needed>. (accessed January 2020)

(10) Suci, P. A.; Mittelman, M. W.; Yu, F. P.; Geesey, G. G. Investigation of ciprofloxacin penetration into *Pseudomonas aeruginosa* biofilms. *Antimicrob. Agents Chemother.* **1994**, *38*, 2125–2133.

(11) Flemming, H.-C.; Wingender, J. The biofilm matrix. *Nat. Rev. Microbiol.* **2010**, *8*, 623–633.

(12) Davies, D. Understanding biofilm resistance to antibacterial agents. *Nat. Rev. Drug Discovery* **2003**, *2*, 114–122.

(13) Winzer, K.; Falconer, C.; Garber, N. C.; Diggle, S. P.; Camara, M.; Williams, P. The *Pseudomonas aeruginosa* lectins PA-IL and PA-III are controlled by quorum sensing and by RpoS. *J. Bacteriol.* **2000**, *182*, 6401–6411.

(14) Diggle, S. P.; Stacey, R. E.; Dodd, C.; Cámara, M.; Williams, P.; Winzer, K. The galactophilic lectin, LecA, contributes to biofilm development in *Pseudomonas aeruginosa*. *Environ. Microbiol.* **2006**, *8*, 1095–1104.

(15) Tielker, D.; Hacker, S.; Loris, R.; Strathmann, M.; Wingender, J.; Wilhelm, S.; Rosenau, F.; Jaeger, K.-E. *Pseudomonas aeruginosa* lectin LecB is located in the outer membrane and is involved in biofilm formation. *Microbiology* **2005**, *151*, 1313–1323.

(16) Gilboa-Garber, N. *Pseudomonas aeruginosa* lectins. *Methods Enzymol.* **1982**, *83*, 378–385.

(17) Gilboa-Garber, N.; Mizrahi, L.; Garber, N. Mannose-binding hemagglutinins in extracts of *Pseudomonas aeruginosa*. *Can. J. Biochem.* **1977**, *55*, 975–981.

(18) Gilboa-Garber, N. Purification and properties of hemagglutinin from *Pseudomonas aeruginosa* and its reaction with human blood cells. *Biochim. Biophys. Acta, Gen. Subj.* **1972**, *273*, 165–173.

(19) da Silva, D. P.; Matwchuk, M. L.; Townsend, D. O.; Reichhardt, C.; Lamba, D.; Wozniak, D. J.; Parsek, M. R. The *Pseudomonas aeruginosa* lectin LecB binds to the exopolysaccharide Psl and stabilizes the biofilm matrix. *Nat. Commun.* **2019**, *10*, 2183.

(20) Adam, E. C.; Mitchell, B. S.; Schumacher, D. U.; Grant, G.; Schumacher, U. *Pseudomonas aeruginosa* II lectin stops human ciliary beating: therapeutic implications of fucose. *Am. J. Respir. Crit. Care Med.* **1997**, *155*, 2102–2104.

(21) Landi, A.; Mari, M.; Kleiser, S.; Wolf, T.; Gretzmeier, C.; Wilhelm, I.; Kiritsi, D.; Thünaier, R.; Geiger, R.; Nyström, A.; Reggiori, F.; Claudinon, J.; Römer, W. *Pseudomonas aeruginosa* lectin LecB impairs keratinocyte fitness by abrogating growth factor signalling. *Life Sci. Alliance* **2019**, *2*, No. e201900422.

(22) Cott, C.; Thuenauer, R.; Landi, A.; Kühn, K.; Juillot, S.; Imberty, A.; Madl, J.; Eierhoff, T.; Römer, W. *Pseudomonas aeruginosa* lectin LecB inhibits tissue repair processes by triggering β -catenin degradation. *Biochim. Biophys. Acta, Mol. Cell Res.* **2016**, *1863*, 1106–1118.

(23) Wilhelm, I.; Levit-Zerdoun, E.; Jakob, J.; Villringer, S.; Frensch, M.; Übelhart, R.; Landi, A.; Müller, P.; Imberty, A.; Thuenauer, R.; Claudinon, J.; Jumaa, H.; Reth, M.; Eibel, H.; Hobeika, E.; Römer, W. Carbohydrate-dependent B cell activation by fucose-binding bacterial lectins. *Sci. Signaling* **2019**, *12*, No. ea07194.

(24) Zheng, S.; Eierhoff, T.; Aigal, S.; Brandel, A.; Thuenauer, R.; de Bentzmann, S.; Imberty, A.; Römer, W. The *Pseudomonas aeruginosa*

- lectin LecA triggers host cell signalling by glycosphingolipid-dependent phosphorylation of the adaptor protein CrkII. *Biochim. Biophys. Acta, Mol. Cell Res.* **2017**, *1864*, 1236–1245.
- (25) Eierhoff, T.; Bastian, B.; Thuenauer, R.; Madl, J.; Audfray, A.; Aigal, S.; Juillot, S.; Rydell, G. E.; Muller, S.; de Bentzmann, S.; Imberty, A.; Fleck, C.; Romer, W. A lipid zipper triggers bacterial invasion. *Proc. Natl. Acad. Sci. U. S. A.* **2014**, *111*, 12895–12900.
- (26) Boukerb, A. M.; Rousset, A.; Galanos, N.; Méar, J.-B.; Thépaut, M.; Grandjean, T.; Gillon, E.; Cecioni, S.; Abderrahmen, C.; Faure, K.; Redelberger, D.; Kipnis, E.; Desein, R.; Havet, S.; Darblade, B.; Matthews, S. E.; de Bentzmann, S.; Guéry, B.; Cournoyer, B.; Imberty, A.; Vidal, S. Antiadhesive properties of glycoclusters against *Pseudomonas aeruginosa* lung infection. *J. Med. Chem.* **2014**, *57*, 10275–10289.
- (27) Chemani, C.; Imberty, A.; de Bentzmann, S.; Pierre, M.; Wimmerová, M.; Guery, B. P.; Faure, K. Role of LecA and LecB lectins in *Pseudomonas aeruginosa*-induced lung injury and effect of carbohydrate ligands. *Infect. Immun.* **2009**, *77*, 2065–2075.
- (28) von Bismarck, P.; Schneppenheim, R.; Schumacher, U. Successful treatment of *Pseudomonas aeruginosa* respiratory tract infection with a sugar solution - a case report on a lectin based therapeutic principle. *Klin. Paediatr.* **2001**, *213*, 285–287.
- (29) Hauber, H.-P.; Schulz, M.; Pforte, A.; Mack, D.; Zabel, P.; Schumacher, U. Inhalation with fucose and galactose for treatment of *Pseudomonas aeruginosa* in cystic fibrosis patients. *Int. J. Med. Sci.* **2008**, *5*, 371–376.
- (30) Bucior, I.; Abbott, J.; Song, Y.; Matthey, M. A.; Engel, J. N. Sugar administration is an effective adjunctive therapy in the treatment of *Pseudomonas aeruginosa* pneumonia. *Am. J. Physiol.: Lung Cell. Mol. Physiol.* **2013**, *305*, L352–L363.
- (31) Klockgether, J.; Cramer, N.; Wiehlmann, L.; Davenport, C. F.; Tümmler, B. *Pseudomonas aeruginosa* genomic structure and diversity. *Front. Microbiol.* **2011**, *2*, 150.
- (32) Dötsch, A.; Schniederjans, M.; Khaledi, A.; Hornischer, K.; Schulz, S.; Bielecka, A.; Eckweiler, D.; Pohl, S.; Häussler, S. The *Pseudomonas aeruginosa* transcriptional landscape is shaped by environmental heterogeneity and genetic variation. *MBio* **2015**, *6*, No. e00749.
- (33) Sommer, R.; Wagner, S.; Varrot, A.; Nycholat, C. M.; Khaledi, A.; Häussler, S.; Paulson, J. C.; Imberty, A.; Titz, A. The virulence factor LecB varies in clinical isolates: consequences for ligand binding and drug discovery. *Chem. Sci.* **2016**, *7*, 4990–5001.
- (34) Boukerb, A. M.; Decor, A.; Ribun, S.; Tabaroni, R.; Rousset, A.; Commin, L.; Buff, S.; Doléans-Jordheim, A.; Vidal, S.; Varrot, A.; Imberty, A.; Cournoyer, B. Genomic rearrangements and functional diversification of lecA and lecB lectin-coding regions impacting the efficacy of glycomimetics directed against *Pseudomonas aeruginosa*. *Front. Microbiol.* **2016**, *7*, 811.
- (35) Varki, A.; Etzler, M. E.; Cummings, R. D.; Esko, J. D. Discovery and classification of glycan-binding proteins. In *Essentials of Glycobiology*; 2nd edition, Eds: Varki, A.; Cummings, R. D.; Esko, J. D.; Freeze, H. H.; Stanley, P.; Bertozzi, C. R.; Hart, G. W.; Etzler, M. E. Cold Spring Harbor Laboratory Press: 2009, Chapter 26. Available at: <http://www.ncbi.nlm.nih.gov/books/NBK1923/>.
- (36) Calvert, M. B.; Jumde, V. R.; Titz, A. Pathoblockers or antivirulence drugs as a new option for the treatment of bacterial infections. *Beilstein J. Org. Chem.* **2018**, *14*, 2607–2617.
- (37) Meiers, J.; Siebs, E.; Zahorska, E.; Titz, A. Lectin antagonists in infection, immunity, and inflammation. *Curr. Opin. Chem. Biol.* **2019**, *53*, 51–67.
- (38) Wagner, S.; Sommer, R.; Hinsberger, S.; Lu, C.; Hartmann, R. W.; Empting, M.; Titz, A. Novel strategies for the treatment of *Pseudomonas aeruginosa* infections. *J. Med. Chem.* **2016**, *59*, 5929–5969.
- (39) Cecioni, S.; Imberty, A.; Vidal, S. Glycomimetics versus multivalent glycoconjugates for the design of high affinity lectin ligands. *Chem. Rev.* **2015**, *115*, 525–561.
- (40) Bernardi, A.; Jiménez-Barbero, J.; Casnati, A.; De Castro, C.; Darbre, T.; Fieschi, F.; Finne, J.; Funken, H.; Jaeger, K.-E.; Lahmann, M.; Lindhorst, T. K.; Marradi, M.; Messner, P.; Molinaro, A.; Murphy, P. V.; Nativi, C.; Oscarson, S.; Penadés, S.; Peri, F.; Pieters, R. J.; Renaudet, O.; Reymond, J.-L.; Richichi, B.; Rojo, J.; Sansone, F.; Schäffer, C.; Turnbull, W. B.; Velasco-Torrijos, T.; Vidal, S.; Vincent, S.; Wennekes, T.; Zuilhof, H.; Imberty, A. Multivalent glycoconjugates as anti-pathogenic agents. *Chem. Soc. Rev.* **2013**, *42*, 4709–4727.
- (41) Hauck, D.; Joachim, I.; Frommeyer, B.; Varrot, A.; Philipp, B.; Möller, H. M.; Imberty, A.; Exner, T. E.; Titz, A. Discovery of two classes of potent glycomimetic inhibitors of *Pseudomonas aeruginosa* LecB with distinct binding modes. *ACS Chem. Biol.* **2013**, *8*, 1775–1784.
- (42) Sommer, R.; Exner, T. E.; Titz, A. A biophysical study with carbohydrate derivatives explains the molecular basis of monosaccharide selectivity of the *Pseudomonas aeruginosa* lectin LecB. *PLoS One* **2014**, *9*, No. e112822.
- (43) Sommer, R.; Hauck, D.; Varrot, A.; Wagner, S.; Audfray, A.; Prestel, A.; Möller, H. M.; Imberty, A.; Titz, A. Cinnamide derivatives of D-mannose as inhibitors of the bacterial virulence factor LecB from *Pseudomonas aeruginosa*. *ChemistryOpen* **2015**, *4*, 756–767.
- (44) Sommer, R.; Wagner, S.; Rox, K.; Varrot, A.; Hauck, D.; Wamhoff, E.-C.; Schreiber, J.; Ryckmans, T.; Brunner, T.; Rademacher, C.; Hartmann, R. W.; Brönstrup, M.; Imberty, A.; Titz, A. Glycomimetic, orally bioavailable LecB inhibitors block biofilm formation of *Pseudomonas aeruginosa*. *J. Am. Chem. Soc.* **2018**, *140*, 2537–2545.
- (45) Sommer, R.; Rox, K.; Wagner, S.; Hauck, D.; Henrikus, S. S.; Newsad, S.; Arnold, T.; Ryckmans, T.; Brönstrup, M.; Imberty, A.; Varrot, A.; Hartmann, R. W.; Titz, A. Anti-biofilm agents against *Pseudomonas aeruginosa*: a structure-activity relationship study of C-glycosidic LecB inhibitors. *J. Med. Chem.* **2019**, *62*, 9201–9216.
- (46) Cioci, G.; Mitchell, E. P.; Gautier, C.; Wimmerová, M.; Sudakevitz, D.; Pérez, S.; Gilboa-Garber, N.; Imberty, A. Structural basis of calcium and galactose recognition by the lectin PA-IL of *Pseudomonas aeruginosa*. *FEBS Lett.* **2003**, *555*, 297–301.
- (47) Wagner, S.; Hauck, D.; Hoffmann, M.; Sommer, R.; Joachim, I.; Müller, R.; Imberty, A.; Varrot, A.; Titz, A. Covalent lectin inhibition and application in bacterial biofilm imaging. *Angew. Chem., Int. Ed.* **2017**, *56*, 16559–16564.
- (48) Tanne, J. H. FDA adds ‘black box’ warning label to fluoroquinolone antibiotics. *BMJ* **2008**, *337*, a816.
- (49) Schwartz, R. S. Paul Ehrlich’s magic bullets. *N. Engl. J. Med.* **2004**, *350*, 1079–1080.
- (50) Barok, M.; Joensuu, H.; Isola, J. Trastuzumab emtansine: mechanisms of action and drug resistance. *Breast Cancer Res.* **2014**, *16*, 209.
- (51) Lehar, S. M.; Pillow, T.; Xu, M.; Staben, L.; Kajihara, K. K.; Vandlen, R.; DePalatis, L.; Raab, H.; Hazenbos, W. L.; Morisaki, J. H.; Kim, J.; Park, S.; Darwish, M.; Lee, B.-C.; Hernandez, H.; Loyet, K. M.; Lupardus, P.; Fong, R.; Yan, D.; Chalouni, C.; Luis, E.; Khalfin, Y.; Plise, E.; Cheong, J.; Lyssikatos, J. P.; Strandh, M.; Koefoed, K.; Andersen, P. S.; Flygare, J. A.; Tan, M. W.; Brown, E. J.; Mariathasan, S. Novel antibody-antibiotic conjugate eliminates intracellular *S. aureus*. *Nature* **2015**, *527*, 323–328.
- (52) Zhang, G.-F.; Liu, X.; Zhang, S.; Pan, B.; Liu, M.-L. Ciprofloxacin derivatives and their antibacterial activities. *Eur. J. Med. Chem.* **2018**, *146*, 599–612.
- (53) Klahn, P.; Brönstrup, M. Bifunctional antimicrobial conjugates and hybrid antimicrobials. *Nat. Prod. Rep.* **2017**, *34*, 832–885.
- (54) Milner, S. J.; Carrick, C. T.; Kerr, K. G.; Snelling, A. M.; Thomas, G. H.; Duhme-Klair, A.-K.; Routledge, A. Probing bacterial uptake of glycosylated ciprofloxacin conjugates. *ChemBioChem* **2014**, *15*, 466–471.
- (55) Howse, G. L.; Bovill, R. A.; Stephens, P. J.; Osborn, H. M. I. Synthesis and antibacterial profiles of targeted triclosan derivatives. *Eur. J. Med. Chem.* **2019**, *162*, 51–58.
- (56) Rodrigue, J.; Ganne, G.; Blanchard, B.; Saucier, C.; Giguère, D.; Shiao, T. C.; Varrot, A.; Imberty, A.; Roy, R. Aromatic thioglycoside inhibitors against the virulence factor LecA from *Pseudomonas aeruginosa*. *Org. Biomol. Chem.* **2013**, *11*, 6906–6918.

- (57) Kadam, R. U.; Garg, D.; Schwartz, J.; Visini, R.; Sattler, M.; Stocker, A.; Darbre, T.; Reymond, J.-L. CH- π 'T-shape' interaction with histidine explains binding of aromatic galactosides to Pseudomonas aeruginosa lectin LecA. *ACS Chem. Biol.* **2013**, *8*, 1925–1930.
- (58) Joachim, I.; Rikker, S.; Hauck, D.; Ponader, D.; Boden, S.; Sommer, R.; Hartmann, L.; Titz, A. Development and optimization of a competitive binding assay for the galactophilic low affinity lectin LecA from Pseudomonas aeruginosa. *Org. Biomol. Chem.* **2016**, *14*, 7933–7948.
- (59) Kadam, R. U.; Bergmann, M.; Hurley, M.; Garg, D.; Cacciarini, M.; Swiderska, M. A.; Nativi, C.; Sattler, M.; Smyth, A. R.; Williams, P.; Cámara, M.; Stocker, A.; Darbre, T.; Reymond, J.-L. A Glycopeptide dendrimer inhibitor of the galactose-specific lectin LecA and of Pseudomonas aeruginosa biofilms. *Angew. Chem., Int. Ed.* **2011**, *50*, 10631–10635.
- (60) Chu, D. T.; Fernandes, P. B. Structure-activity relationships of the fluoroquinolones. *Antimicrob. Agents Chemother.* **1989**, *33*, 131–135.
- (61) Gootz, T. D.; Brighty, K. E. Fluoroquinolone antibacterials: SAR, mechanism of action, resistance, and clinical aspects. *Med. Res. Rev.* **1996**, *16*, 433–486.
- (62) Idowu, T.; Schweizer, F. Ubiquitous nature of fluoroquinolones: the oscillation between antibacterial and anticancer activities. *Antibiotics* **2017**, *6*, 26.
- (63) Pham, T. D. M.; Ziora, Z. M.; Blaskovich, M. A. T. Quinolone antibiotics. *Med. Chem. Commun.* **2019**, *10*, 1719–1739.
- (64) Koga, H.; Itoh, A.; Murayama, S.; Suzue, S.; Irikura, T. Structure-activity relationships of antibacterial 6,7- and 7,8-disubstituted 1-alkyl-1,4-dihydro-4-oxoquinoline-3-carboxylic acids. *J. Med. Chem.* **1980**, *23*, 1358–1363.
- (65) Mustaev, A.; Malik, M.; Zhao, X.; Kurepina, N.; Luan, G.; Oppgaard, L. M.; Hiasa, H.; Marks, K. R.; Kerns, R. J.; Berger, J. M.; Drlica, K. Fluoroquinolone-gyrase-DNA complexes: two modes of drug binding. *J. Biol. Chem.* **2014**, *289*, 12300–12312.
- (66) Casoni, F.; Dupin, L.; Vergoten, G.; Meyer, A.; Ligeour, C.; Géhin, T.; Vidal, O.; Souteyrand, E.; Vasseur, J.-J.; Chevlot, Y.; Morvan, F. The influence of the aromatic aglycon of galactoclusters on the binding of LecA: a case study with O-phenyl, S-phenyl, O-benzyl, S-benzyl, O-biphenyl and O-naphthyl aglycons. *Org. Biomol. Chem.* **2014**, *12*, 9166–9179.
- (67) Richter, M. F.; Drown, B. S.; Riley, A. P.; Garcia, A.; Shirai, T.; Svec, R. L.; Hergenrother, P. J. Predictive compound accumulation rules yield a broad-spectrum antibiotic. *Nature* **2017**, *545*, 299–304.
- (68) O'Shea, R.; Moser, H. E. Physicochemical properties of antibacterial compounds: implications for drug discovery. *J. Med. Chem.* **2008**, *51*, 2871–2878.
- (69) Müsken, M.; Klimmek, K.; Sauer-Heilborn, A.; Donnert, M.; Sedlacek, L.; Suerbaum, S.; Häussler, S. Towards individualized diagnostics of biofilm-associated infections: a case study. *NPJ Biofilms Microbiomes* **2017**, *3*, 22.
- (70) Zięba, A.; Maślankiewicz, A.; Sitkowski, J. ^1H , ^{13}C and ^{15}N NMR spectra of ciprofloxacin. *Magn. Reson. Chem.* **2004**, *42*, 903–904.
- (71) Driguez, H.; Szeja, W. Facile synthesis of 1,2-trans-nitrophenyl-1-thioglycopyranosides. *Synthesis* **1994**, *1994*, 1413–1414.
- (72) McPherson, J. C., III; Runner, R.; Buxton, T. B.; Hartmann, J. F.; Farcasiu, D.; Bereczki, I.; Róth, E.; Tollas, S.; Ostorházi, E.; Rozgonyi, F.; Herczegh, P. Synthesis of osteotropic hydroxybisphosphonate derivatives of fluoroquinolone antibacterials. *Eur. J. Med. Chem.* **2012**, *47*, 615–618.
- (73) Phiasivongsa, P.; Samoshin, V. V.; Gross, P. H. Henry condensations with 4,6-O-benzylidenylated and non-protected D-glucose and L-fucose via DBU-catalysis. *Tetrahedron Lett.* **2003**, *44*, 5495–5498.
- (74) Wiegand, I.; Hilpert, K.; Hancock, R. E. W. Agar and broth dilution methods to determine the minimal inhibitory concentration (MIC) of antimicrobial substances. *Nat. Protoc.* **2008**, *3*, 163–175.
- (75) Hauptenthal, J.; Baehr, C.; Zeuzem, S.; Piiper, A. RNase A-like enzymes in serum inhibit the anti-neoplastic activity of siRNA targeting polo-like kinase 1. *Int. J. Cancer* **2007**, *121*, 206–210.

6.6 Curriculum vitae

Personal Information

Name: Eva Zahorska
Date of birth: 28.02.1992
Nationality: Slovak
Email: zahor.eva@gmail.com

Education

2017-present PhD candidate, Helmholtz Institute for Pharmaceutical Research Saarland and Saarland University, Saarbrücken, Germany
2014-2017 Joint master study program Biological Chemistry by the Johannes Kepler University (JKU), Linz, Austria and the University of South Bohemia (USB), Budweis, Czech Republic
2011-2014 Bachelor double degree program Biological Chemistry by the Johannes Kepler University (JKU), Linz, Austria and the University of South Bohemia (USB), Budweis, Czech Republic
2006-2011 Bilingual Gymnazium Milana Hodžu, Sučany, Slovak Republic (High school)

Scholarships

2016 Aktion Österreich-Tschechien, AÖCZ-Semesterstipendien by Austrian Agency for International Cooperation in Education and Research (OeAD-GmbH) and Centre for International Cooperation & Mobility (ICM) financed by BMWFW for a 3 months research project (part of Master thesis, Institute of Biophysics, JKU)
2015 Erasmus+ Program, Student mobility for studies awarded for 5 months

Languages

Slovak (native), English